

UNIVERSITÉ DE PARIS XI – U.F.R. DES SCIENCES D'ORSAY

Habilitation à Diriger des Recherches

Spécialité:

Sciences Physiques

présentée par

Samuel WALLON

Laboratoire de Physique Théorique,
Université de Paris-Sud, Bâtiment 210, 91405 Orsay cedex

Sujet:

**Hard exclusive processes in perturbative QCD:
from medium to asymptotical energies**

**Processus exclusifs durs en QCD perturbative:
des énergies modérées aux énergies asymptotiques**

Soutenue le 8 décembre 2009 devant le jury composé de

H. Sazdjian	Professeur à l'Université de Paris XI	Président
V. Braun	Professeur à l'Université de Regensburg	Rapporteur
K. Golec-Biernat	Professeur à l'Université de Cracovie	Rapporteur
R. Kirschner	Professeur à l'Université de Leipzig	Rapporteur
U. Ellwanger	Professeur à l'Université de Paris XI	
G. Korchemsky	Directeur de recherche à l'IPhT	

version du 8/12/09

Acknowledgements:

My first acknowledgements goes to Lech Szymanowski and Bernard Pire. Lech and myself met for the first time in 2001 in Krakow, and immediately we could find common scientific interests. By chance, his venue to Ecole Polytechnique soon after was the starting point of a very fruitful collaboration, and then friendship, to which Bernard was immediately associated. Although we met before, Bernard was considered to me as a “low energy” physicist, with the all (non-sense) prejudice associated to that... Hopefully for me, these starting discussions coincided to a time where I was trying to extend my activity in QCD in a wider range, and I soon realized that such a way of thinking was a bit narrow. Lech and I share a rather close culture based on first principle quantum field theory approaches and a common pleasure for long-term hard analytical computations relying on pencil, eraser, trash can, and a horizontal way of using paper in order to fit the long obtained expressions. With the more phenomenological interests of Bernard, in particular based on his bright physical sense and his knowledge of experiments, this led soon to very intense works, characterized by a somehow non quiet style of working, usually calling for rather thick doors. I am very pleased to express here the pleasure I have to meet them either at LPT or at Ecole Polytechnique on an almost everyday basis. Lech is a polyglot and a french culture lover. With Bernard, when stuck in front a problem, we thus always have a reason to talk about French culture, including politics, cheese and wine. This helped several times, including recently, to solve a given problem after such breaks, and lead us to celebrate good results around a (good) bottle of wine.

This rather emotional style of working, based on intensive arguing, met easily the style of Igor Anikin, which I saw for the first time in 2002. I am glad to Igor in particular for his fastidious style which we have both in common. Since shouting is the best way to prepare for tea time, which we all appreciate, one can again imagine the ultimate consequence of our common style, in which convincing all four of us at the same time is not an easy task.

This renewal of my activities more or less coincided with my arrival at LPT in 2001, where I could develop my own interests with excellent support, in one the most active particle physics group in France. In particular, I had the pleasure to meet there Michel Fontannaz, Dominique Schiff and Gregory Korchemsky, with whom I have had until now regular scientific exchanges from phenomenology to very formal developments. With Michel, Dominique and many other colleagues of the lab including Olivier Pene and Abdelhak Djouadi, I share a strong interest for scientific, non-sense scientific politics (in particular during recent times), and politics, and this can be an unlimited subject of discussion at lunch time. I also benefited from the very broad interests of Damir Becirevic, and from our both common pleasure for end-of-the-day chattering.

My interests for QCD à la BFKL was helped by a strong and long-term collaboration with Andrei Shuvaev, which started in DESY 13 years ago. This was at that time a kind of door for entering the strong although impenetrable russian knowledge, and I am strongly indebted to Andrei for this.

When meeting Lech in a café in Krakow, I simultaneously met Dmitri Ivanov, and it took more than 6 years before we were finally all three of us associated in a common project, with Igor and Bernard. This recent work, although very intense and demanding, has been one of my best experience in science, and I am indebted in all my friends for that.

In Ecole Polytechnique, while having lunch, I had the pleasure to have regular discussions with Claude Roiesnel. This led to a very pleasant collaboration on AdS/QCD correspondance in which I could see his high demanding standards, combining skill and rigour. We both exchanged and deepen a lot of our knowledge in group theory, calculus and curved spaces, in a pleasant atmosphere, again helped with an everyday tea. This has been further extended more recently by fresh blood, through the strong implication of Cyrille Marquet, whose interests both for formal aspects as well as phenomenology renewed our activity in the field, strongly helped by his great motivation combined with impressive skills, which I already noticed when he was following my lectures at the DEA of Theoretical Physics some years ago. I also thank Urko Reinosa, Tri Nang Pham and Georges Grunberg from Ecole Polytechnique, and Bachir Moussallam, Hagop Szadjian and the late Jan Stern from IPN, with whom I have had many discussions during the IPN/X regular seminar.

I would like also to thank Stephane Munier for regular discussions we had since he was a student in Saclay, in particular on saturation and related topics. I appreciate very much his broad interests and his independence.

During two years, I had the great pleasure to work with Florian Schwennsen. We had a very efficient collaboration, and I would like to thank him in particular for his impressive skills in dealing with non-trivial analytical computations and implementing them on the computer to extract phenomenological results. I have learnt a lot from him, leading me to leave a rather handcrafted style to reach a more professional way of dealing

with computers. Despite his very good skills for theoretical physics, he decided to leave physics, and I am sure he will be very successful in his future career.

It is with emotion that I now thank the late “Arthur” Dominique Vautherin, who was one of my first contact in physics, when still a student in Ecole Polytechnique. I remember how impressed I was by his personality when following his lectures, around 1991. We kept contact through years, and got again in close relationship after my PhD, in particular when starting my associate professor position. His optimistic style of life, combining strong humour with a tremendous brightness, was the basis of a strong leading scientist which I miss forever.

Through years, I had the opportunity to meet many people, from whom I benefited much, among those I should thank Al Mueller, for his impressive deepness combined with high pedagogical skills, from whom I took an enormous profit from a short one month visit in Columbia, while still a PhD student. I met there Yuri Kovchegov, playing both there with the dipole model.

I would like also to thank Lev Lipatov with whom I had many discussions through years, already starting in a small-x workshop in Cambridge when I was only a student, and where he was much available, both of us helped by a good glass of wine while standing on a typical english short-cut green grass. This was further settled in a more classical style in an almost private series of lectures he gave to our small group at LPTPE in Jussieu almost 10 years ago.

I am also indebted for the opportunity which Jochen Bartels gave me for spending a long period in Hambourg, at a time where the HERA community was particularly active. I met there Carlo Ewerz, with whom I kept contact during many years.

I would like also to thank many colleagues including first Yuri Dokshitzer, from which I learned much in a winter school in Gatchina and from a joined (with Al Mueller) series of lectures in Saclay, in particular the graphical language for practical $SU(n)$ computations, which as a drawer I appreciate so much, as well as Vladimir Braun, Stanley J. Brodsky, Etienne Burtin, Michel Davier, Markus Diehl, Nicole D’Hose, Samuel Friot, François Gelis, Krzysztof Golec-Biernat, Edmond Iancu, Roland Kirschner, Fabienne Kunne, Jean-Philippe Lansberg, Leszek Motyka, Dieter Müller, Roman Poeschl, François Richard, Franck Sabatié, Agustin Sabio Vera, Guy F. de Teramond, Oleg Teryaev, and the late Jan Kwiecinski. Special thanks for Christophe Royon and Laurent Schoeffel through which I had very close contact with experiment, and with whom it is always a pleasure to talk about anything including physics.

I want also to mention here Robi Peschanski and Henri Navelet, who guided me when starting my scientific activity as a PhD student. I still benefit from what I learned at that time based on the impressive analytical skills of Henri. He is among those (although he was not doing) who could be forced to use paper in a horizontal way when computing.

I would like also to thank Mathieu Segond, Mounir El Beiyad as well as all my students in DEAs and master degrees for questions, which step by step and years after years led to deepen my knowledge. Other students will for sure reduce my ignorance during coming years. It is frequently said that one only understand a piece of knowledge when being forced to tell it to somebody else, and I can testify that this is (un)fortunately probably true. Among former students, I have the pleasure to meet now everyday at LPT our young colleague Benoit Blossier, with whom I always have great pleasure to talk about any kind of subjects, including perturbative QCD, lattice QCD, politics and bicycle races.

I would like also to thank Philippe Boucaud and Jean-Pierre Leroy, as well as Olivier Brand-Foissac for their amazing availability when facing a terrific problems with my computer, and all my colleagues of the LPT for the nice, friendly and democratic atmosphere in the laboratory, now led by Henk Hilhorst. I am also indebted to our local support, in particular from Mireille Calvet.

I thank very much Vladimir Braun, Krzysztof Golec-Biernat and Roland Kirschner who accepted to refer on my manuscript, and Hagop Sazdjian, Ulrich Ellwanger (who already participated to my PhD committee) and Gregory Korchemsky, who accepted to be member of the committee.

I would like also to thank all my friends for support outside of physics, in particular while running during our traditionnal meeting on Wednesday lunch time, an activity which I recommend so much for cleaning up the brain, or to warm it up.

Finally, let me thank Claire, for her tender support through years, in particular during several very intense periods related either to research or to teaching activities when I was rather off of normal life. I thank all our little troupe made of Valentine, Juliette, Camille, Louis, which has grown up little by little, and help me so much when I passed through hard times. I would like to thank my parents Nicole and Michel for their continuous support and help through years, as well as Thérèse and Pierre, my parents-in-law.

à Claire

à Valentine, Camille, Juliette, Louis

à mes parents

Contents

I	Collinear Factorization in QCD	9
1	From inclusive to exclusive processes	11
1.1	Introduction	11
1.2	From DIS to DVCS	15
1.2.1	Kinematics of DVCS	15
1.2.2	DVCS and GPD	16
1.3	GPDs: some basics	19
1.3.1	Definitions	20
1.3.2	Elementary properties of GPDs	23
1.4	The illuminating example of ρ -electroproduction	27
1.4.1	ρ -meson production: from the wave function to the DA	27
1.4.2	ρ -meson production: factorization with a GPD and a DA	27
1.4.3	Chiral-even DA	28
1.4.4	Equations of motion	29
1.4.5	Collinear conformal invariance	29
1.4.6	Renormalization group equations	30
1.4.7	Selection rules and factorization status	31
1.4.8	Some solutions to factorization breaking?	31
1.4.9	Chiral-odd sector	33
1.5	Measurement of helicity-flip GPDs through a non-zero mixture of chiral-odd GPDs with chiral-odd ρ -meson	33
1.5.1	Kinematics	36
1.5.2	The Scattering Amplitude	38
1.5.3	Transversity GPD and Double Distribution	41
1.5.4	Unpolarized Differential Cross Section	43
1.5.5	Rates for JLab and COMPASS	45
2	Extensions and applications	49
2.1	GPD crossing $s \leftrightarrow t$: from DA to GDA	49
2.1.1	From GPDs to GDAs	49
2.1.2	Evolution equations	50
2.2	The photon GDAs	59
2.2.1	The $\gamma^* \gamma \rightarrow \gamma \gamma$ process in the threshold region	59
2.2.2	QCD factorization of the DVCS amplitude on the photon	62
2.2.3	The diphoton GDAs and their QCD evolution equations	65
2.3	Crossing $s \leftrightarrow u$: TDAs	69
2.4	An (almost) perturbative situation: $\gamma^* \gamma^* \rightarrow \rho_L^0 \rho_L^0$	71
2.4.1	Kinematics	72
2.4.2	The Born order amplitude	73
2.4.3	$\gamma_T^* \gamma_T^* \rightarrow \rho_L^0 \rho_L^0$ in the generalized Bjorken limit	77
2.4.4	$\gamma_L^* \gamma_L^* \rightarrow \rho_L^0 \rho_L^0$ in the generalized Bjorken limit	80
2.5	Exotic hybrid mesons	84
2.5.1	Quark model and spectroscopy	86

2.5.2	Hybrid meson distribution amplitude	87
2.5.3	Hybrid electroproduction	90
2.5.4	Study of hybrid mesons via the electroproduction of $\pi\eta$ pairs	94
2.5.5	Exotic hybrid meson production in $\gamma^*\gamma$ collisions	95
3	Light-Cone Collinear Factorization	99
3.1	Introduction	99
3.2	Factorization beyond leading twist	100
3.3	Parametrizations of vacuum-to-rho-meson matrix elements up to twist 3	102
3.3.1	LCCF parametrization	102
3.3.2	CCF parametrization	104
3.4	Equations of motion	105
3.5	Additional set of equations	107
3.5.1	Light-cone factorization direction arbitrariness	107
3.5.2	A minimal set of non-perturbative correlators	115
3.6	Dictionary	117
II	QCD in the Regge limit	121
4	Theoretical status	123
4.1	LL BFKL Pomeron	123
4.2	k_T factorization	126
4.3	The Odderon	130
4.4	LL BFKL Pomeron: limitations	130
4.5	Higher order corrections	131
4.6	Non-linear regime and saturation	133
4.6.1	Generalized Leading Log Approximation	133
4.6.2	Extended Generalized Leading Log Approximation and Color Glass Condensate	134
4.6.3	Saturation and geometrical scaling	135
4.7	Onium-onium scattering as a gold plated experiment: $\gamma^{(*)}\gamma^{(*)}$ at colliders	139
5	Inclusive and Exclusive tests of BFKL dynamics	141
5.1	Hadron-hadron colliders	141
5.1.1	Mueller-Navelet jets	143
5.1.2	Diffraction high energy double jet production	172
5.1.3	High p_T central jet production	173
5.2	HERA	173
5.2.1	DIS and diffractive DIS	174
5.2.2	Transverse energy flow	174
5.2.3	Energetic forward jet and π^0 production	174
5.2.4	Exclusive vector meson production	176
5.3	$\gamma^*\gamma^*$ at LEP2	180
6	Exclusive processes in the Regge limit beyond leading twist	183
6.1	Calculation based on the Light-Cone Collinear Factorization approach	185
6.1.1	$\gamma_L^* \rightarrow \rho_L$ transition as a recall	185
6.1.2	$\gamma_T^* \rightarrow \rho_T$ transition	186
6.2	Calculation based on the Covariant Collinear Factorization	192
6.3	Comparison of the two computations and discussion	196

7 Onium-onium scattering in $\gamma^{(*)}\gamma^{(*)}$ colliders	199
7.1 Sources of photons	199
7.1.1 Photon colliders: hadron and nucleus colliders	199
7.1.2 Photon colliders: $e \rightarrow \gamma$ conversion	200
7.2 ILC project	201
7.2.1 Reference Design Report for ILC	202
7.2.2 Detectors at ILC	203
7.3 $\gamma^*\gamma^* \rightarrow \text{hadrons}$ total cross-section	203
7.4 The $\gamma^*\gamma^* \rightarrow \rho_L^0 \rho_L^0$ exclusive process	204
7.4.1 Kinematics	206
7.4.2 Impact representation	208
7.4.3 Non-forward Born order differential cross-section for $\gamma_{L,T}^* \gamma_{L,T}^* \rightarrow \rho_L^0 \rho_L^0$	210
7.4.4 Non-forward Born order cross-section for $e^+e^- \rightarrow e^+e^- \rho_L^0 \rho_L^0$	218
7.4.5 Leading order BFKL resummation effects for the forward $\gamma_L^* \gamma_L^* \rightarrow \rho_L^0 \rho_L^0$ amplitude	225
7.4.6 Estimation of next to leading order effects	228
7.4.7 Summary and discussion	235
7.5 Hard Pomeron-Odderon interference effects in the production of $\pi^+\pi^-$ pairs in high energy $\gamma\gamma$ collisions	237
7.5.1 Introduction	237
7.5.2 Kinematics	239
7.5.3 Scattering amplitudes	240
7.5.4 Charge asymmetries and rates	242
7.5.5 Summary and prospects	246
 III Bibliography	 253

Introduction

QCD is the theory for strong interaction. In this manuscript, we will concentrate on the short distance dynamics of QCD, that is on the perturbative approach, which is applicable whenever one can show that a hard scale is available in the process under investigation.

The factorization between short distance and long distance dynamics of QCD has been studied since the very beginning of QCD. In the standard Operator Product Expansion, either for space-like (DIS) or for time-like processes (e^+e^- annihilation), one is able to justify this factorization, relying on the twist expansion in a fully controllable manner. This gives a systematic way of isolating long distance matrix elements from short distance coefficient functions. The physical observables are then expressed as convolution (in longitudinal momentum space) of these quantities, to be desentangled by suitable Mellin transformations. Given a renormalization scheme, these quantities satisfies renormalization group equations, and the corresponding anomalous dimensions have been computed to higher and higher orders, now up to 3 loops. The solution of these renormalization group equations can be expressed in Mellin space relying on the asymptotic freedom of QCD. This treatment provides a very efficient treatment, at the level of one percent typically, both for pure QCD studies and for studies of the electroweak sector of the standard model, where precision measurements requires clean evaluation of QCD effects.

Both experimentally and theoretically, efforts where first devoted to the study of inclusive observables, in particular to Deep Inelastic Scattering (DIS), which settled down the fact that QCD was the correct theory for strong interaction. The studies related to exclusive processes were mainly devoted to hadronic form factors and fixed angle elastic scattering, for which several tools were elaborated during pre-QCD times and then incorporating perturbative QCD developpements, combined with non-perturbative tools like QCD sum-rules.

Since a decade, interest for exclusive processes has been renewed. This was partially due to the possibility to access the detailed angular momentum content of the nucleon, after it has realized by Ji [1] that the quark orbital contribution could be extracted through Deep Virtual Compton Scattering. Since then, much effort have been devoted to exclusive processes, which began to be accessible in high resolution detectors at high luminosity accelerators (CEBAF, etc...). This gives the possibility to study the structure of hadron through the use of (virtual) photon probes, from pure diagonal observables (parton distributions) extended now more and more to non diagonal observables (Generalized Parton Distributions (GPDs), Generalized Distribution Amplitudes (GDAs), Transition Distribution Amplitudes (TDAs), etc...).

In a rather parallel way, and somehow independent approach for a long time, tremendous efforts were initiated in the sixties in order to understand the strong interaction in the very large center of mass energy limit (large s and fixed t Regge limit), and led to the introduction of the concept of Pomeron, and later on of Odderon. Such problems were addressed again almost immediately after QCD was settled down, within the framework of Quantum Field Theory, for observables for which perturbation theory could be trustable (excluding proton-(anti)proton cross-sections for example), leading to the seminal work of Balitski, Fadin, Kuraev and Lipatov (BFKL) [2-5] on the hard Pomeron. The starting of HERA in 1992 renewed the interest for these questions, and the so-called small- x_{Bj} physics (which corresponds to the large s limit à la Regge) started to be tested by H1 and ZEUS collaborations, in $e^\pm p$ DIS.

The natural question which was first adressed, apart from the formal interest of studying QCD in the Regge limit, was to know whether this was needed by the data, or asked in a pessimistic way, if standard renormalization group treatment could not be sufficient even at very low values of x_{Bj} . At the same time, HERA was considered to be the best place to see the onset of unitary corrections, which should manifest themselves through non-linear saturation effects, first emphasized in the comprehensive Gribov, Levin and Ryskin review [6]. In this spirit, the discovery of the geometrical scaling phenomenum in HERA data can most probably be considered as a

manifestations of saturation effects.

It has been realized that even with the very high statistics of HERA data, such a question of clearly seeing linear perturbative QCD evolution à la BFKL could not be answered based on inclusive data. This explains the increasing interest for exclusive processes when considering QCD in the Regge limit, making some bridge between the “low energy” community involved in GPD-like physics and the “high-energy” community involved in small- x_{Bj} physics. Meanwhile, it was also the reason why we got interested to exclusive processes, which at early time of HERA was considered to us as another world, rather low energy oriented, and (for unjustified but cultural reasons) not fascinating. Though, while used at first stage as a tool to investigate further the perturbative Regge dynamics, we soon realized that the study of hard exclusive processes was a very active field, with a strongly based starting-from-first-principle approach. This was the reason why we started, in a continuous way, to get strongly interested in both domain, trying to use and develop concepts and implementing phenomenological idea from one side to another one, and vice-versa.

This manuscript is thus a footprint of this activity (in a reversed historical perspective). The production of ρ -meson will one of our main Ariadne’s thread, which will be investigated through many aspects: twist 2 factorization within GPDs, GDAs, TDAs, factorization beyond leading twist in relationship with polarization effects, diffractive production in the perturbative Regge limit...

The manuscript starts by giving an (incomplete) overview of the collinear approach of hard exclusive processes, in Part. I.

In Chap. 1, we will review the basics of factorization of exclusive processes, at leading twist, from form-factors to DVCS. We will introduce the whole set of GPDs and discuss their basic properties. We will then turn to the extension of DVCS to hard electroproduction of vector mesons. As an application, we will show how one may access the GPD helicity-flip through a very exclusive process, which should however become soon accessible.

In Chap. 2, we will extend the collinear approach to less diagonal quantities than GPDs. First, we will elaborate on the properties of GDAs, for which we will present with some details the evolution equations and their solutions. We will illustrate the factorization of GDA in the case of the $\gamma\gamma^* \rightarrow \gamma\gamma$ exclusive process at threshold, for which we will exhibit an evolution equation with an anomalous contribution. Next, we will extend the notion of GPD to the case of an exchange of mesonic or baryonic quantum numbers in t -channel, leading to the introduction of TDAs. Both extensions will be then illustrated in the exclusive process $\gamma^*\gamma^* \rightarrow \rho_L\rho_L$, for which we exhibit factorizations involving a GDA or TDA depending on the energy and on the photon polarizations. Further, we will show how collinear factorization at dominant twist 2 provides a way to get access to hybrid exotic mesons, in electroproduction and in $\gamma\gamma^*$ collisions, with presumable high counting rates.

In Chap. 3, we will present a non-covariant scheme (Light-Cone Collinear Factorization) when dealing with factorization beyond leading twist, and show its equivalence with the Covariant Collinear Factorization at twist 3.

The developments of QCD based on the dynamics specific to the perturbative Regge limit will be presented in Part II.

In Chap. 4 we will review the theoretical status of QCD in the perturbative Regge limit, including BFKL Pomeron, Odderon, impact factor representation, higher order corrections and saturation effects.

In Chap. 5 the various tests of BFKL dynamics will be reviewed, in hadron-hadron collider, at HERA and at LEP2. This includes in particular our very recent complete NLLx study of Mueller Navelet jets.

In Chap. 6 we will show in detail how it is possible to use in a very efficient way the Light-Cone Collinear Factorization for the practical computation of the twist 3 $\gamma^* \rightarrow \rho_T$ impact factor.

The Chap. 7 will be devoted to studies the possibilities offered by $\gamma^{(*)}\gamma^{(*)}$ colliders for studying QCD in the perturbative Regge limit. In particular, we will give some basics on photon colliders and on ILC project. We will then concentrate on two situations. The first one deals with the diffractive production of ρ mesons in $\gamma^*\gamma^*$ collisions. The second one present a study of an exclusive observable sensitive to the Pomeron-Odderon interference, in order to find the elusive hard Odderon.

This manuscript will concentrate on perturbative QCD, only barely considering non-perturbative aspects when needed for phenomenology. We will try to be rather explicit when needed.

This manuscript is partially based on our own contributions (see publication list for related conferences proceedings):

Chap. 1: [W26]

Chap. 2: [W22], [W19], [W12, W13, W14, W18]

Chap. 3: [W25, W24]

Chap. 5: [W27]

Chap. 6: [W24]

Chap. 7: [W15, W16, W20], [W23]

Part I

Collinear Factorization in QCD

Chapter 1

From inclusive to exclusive processes

1.1 Introduction

Since a decade, a tremendous effort is being performed to extract exclusive data. They are now coming with increasing precision (DVCS, meson production, polarized experiments, ...) at moderate and high energy. During the same period, there have been much theoretical developments in hard exclusive processes, and the basis of collinear factorization were settled down, starting from the DIS and Distribution Amplitudes (DAs). The first investigation in the spirit of exclusive processes was the studies of form factors occurring in the hard reactions like $\gamma^* \pi \rightarrow \pi$ or $\gamma^* p \rightarrow p$. It was first shown that a counting rule [7, 8] could predict the scaling behaviour of the form factors for large Q^2 . Mainly relying on dimension analysis, they ultimately led to the microscopic description of the coupling of the hard photon probe to the constituent of the hadron, known since the end of the '60s as quarks, in the spirit of the parton model. In terms of Feynman diagram, the simplest possible

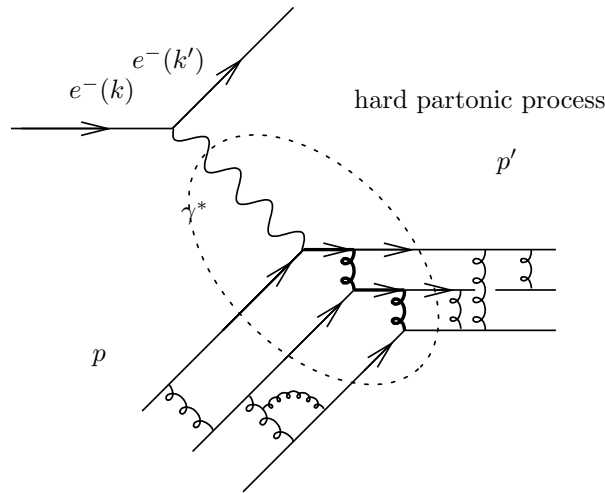
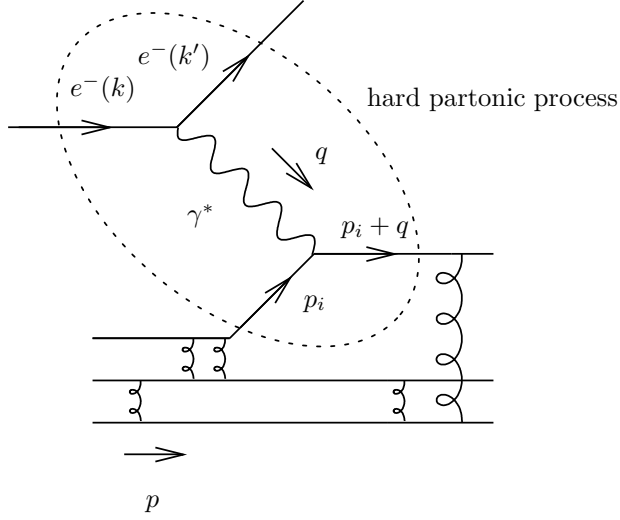


Figure 1.1: Parton model for describing a hadron form factor, in the elastic scattering $e^- p \rightarrow e^- p$. The dotted part corresponds to the hard part of the process. Bold line denotes hard propagators.

configuration describing the hard coupling of a hard photon (denoted hereafter as γ^* , with a virtuality Q^2) to a hadron which remains intact after the scattering is illustrated in Fig. 1.1. This can be justified for an hard process, when the virtuality of the hard photon probe is much higher than the any typical hadronization scale, relying on the fact that correction are suppressed by powers of the strong coupling, which is small due to asymptotic freedom. The main difference with the usual partonic description of Deep Inelastic Scattering (DIS), illustrated in Fig. 1.2 and the elastic case is due to the fact that the bound state, which for the illustrative example of the proton is to be understood as a $qq\bar{q}$ Fock state in the parton model, should remain intact while it scatters off the γ^* . Therefore, gluonic exchanges should occur in order that the partons “turns” and do not

Figure 1.2: Parton model for the Deep Inelastic Scattering $e^- p \rightarrow e^- X$.

fragment. This explains why, contrarily to the DIS case, for which scaling invariance occurs, the form factors dramatically falls off when Q^2 increases, due to the presence of hard propagators in the hard subprocess (bold line in Fig. 1.1).

This can be most easily understood when using the Breit frame. In the case of DIS, introducing the usual Bjorken variable

$$x_{Bj} = \frac{Q^2}{2p \cdot q} \quad (1.1)$$

the momentum of the photonic probe reads, in the Breit frame,

$$q = (0, 0_\perp, -2x_{Bj}P) = (0, 0_\perp, Q) \quad (1.2)$$

which means that the parton (of momentum xP with $x = x_{Bj}$) which is scattered by the photon faces a turn back of its momentum before and after the interaction:

$$\begin{array}{ccc} p_i = xp = (xP, 0_\perp, xP) & p_i + q = xp + q = (xP, 0_\perp, -xP) & \\ \longrightarrow & \longleftarrow & \\ \text{before scattering} & & \text{after scattering} \end{array} \quad (1.3)$$

In the peculiar case of elastic scattering, $x_{Bj} = 1$ and $\vec{q} = -2\vec{p}$. In the Breit frame, which is a peculiar infinite momentum frame, one can safely neglect any transverse momenta (their order of magnitude is typically the hadronization scale) with respect to the longitudinal momenta in the z direction (which is the direction of the boost when passing from the rest frame of the hadron to any infinite momentum frame). In the parton model, each incoming parton thus carries a longitudinal momentum $x_i p$ ($\sum x_i = 1$) while each outgoing partons have a longitudinal momentum $x'_i p'$ ($\sum x'_i = 1$).

Let us consider for a moment the hard part of Fig. 1.1. Each hard gluonic propagator contributes with a factor $\sim 1/Q^2$ while the fermionic propagators contributes with a typical factor $\sim 1/Q$. In order to get the scaling of the whole amplitude [9], assuming factorization between the long and the short distance dynamics, one may assume, like in the partonic model applied to DIS, that the fermions behaves as free particles before and after the hard interaction. This means technically that one can simply replace the incoming and outgoing fermions by their free spinors. Since the spinor of a massless fermion or equivalently a massive fermion in a large boosted frame is

$$u(p) \sim \sqrt{2E} \xi \quad (1.4)$$

where ξ is one of the 4 elementary spinors $(1, 0, 0, 0)$, $(0, 1, 0, 0)$, $(0, 0, 1, 0)$, $(0, 0, 0, 1)$, each incoming (outgoing) spinor contributes with a weight $\sim \sqrt{x_i |\vec{p}|}$ ($\sim \sqrt{x'_i |\vec{p}'|}$), or equivalently, $\sim \sqrt{Q}$ (except in the end-point regions

$x_i \rightarrow 0$ or $x'_i \rightarrow 0$ which we do not consider for the moment). Thus, in the case of the pion form factor, the elastic amplitude scales like $1/Q^3 (\sqrt{Q})^4 = 1/Q$. Turning back to the structure of the matrix element of the electromagnetic current for scalar particles, which reads

$$|\langle p' | J_\mu | p \rangle| \sim \frac{\text{const}}{Q} \sim \left| (p + p')_\mu \frac{\text{const}}{Q^2} \right| \quad (1.5)$$

one deduces that the pion form factor should scale like $1/Q^2$ for asymptotic Q .

The same counting rule applies to the baryonic case, giving a typical behaviour like $(1/Q^2)^2 (1/Q)^2 (\sqrt{Q})^6 \sim 1/Q^3$ and thus

$$|\langle B(p') | J_\mu | B(p) \rangle| \sim \frac{\text{const}}{Q^3} \sim \left| \bar{U}' \gamma_\mu U \frac{\text{const}}{Q^4} \right|, \quad (1.6)$$

where U and U' are baryonic spinors. From this one may deduce that the Sachs form factors should scale like $1/Q^4$.

More generally, considering the form factor of a hadron with n minimal constituents ($n = 2$ for a meson and $n = 3$ for a baryon), one immediately generalize the previous counting rules: the lowest order diagram involves $n - 1$ gluonic propagators ($1/Q^2$ contribution) to force the constituents to turn due to the γ^* scattering (which means that the corresponding Feynman diagram should be *connected*), with $n - 1$ fermionic propagators ($1/Q^2$ contribution). Each (anti)quark external line contributes with a factor \sqrt{q} , and an additional prefactor $1/Q$ should be added when relating the amplitude to the form factor definition. This finally leads to a contribution $1/Q^{2(n-1)} 1/Q^{(n-1)} Q^n 1/Q$ and thus to the counting rule

$$F_n(q^2) \simeq \frac{C}{(Q^2)^{n-1}}. \quad (1.7)$$

Note that this counting rule can be obtained by dimensional analysis, without referring to detailed structure of the hard part as we have done above. For further use, it is instructive to get the same result by using the Sudakov decomposition, or equivalently to use a light-cone basis. For any vector (v^0, v^1, v^2, v^3) one defines in the usual manner

$$\begin{aligned} x^+ &= \frac{1}{\sqrt{2}}(x^0 + x^3) \\ x^- &= \frac{1}{\sqrt{2}}(x^0 - x^3) \\ \underline{x} &= (x^2, x^3) \quad (\text{with euclidian metric}). \end{aligned} \quad (1.8)$$

The scalar product between two vectors v_1 and v_2 reads

$$v_1 \cdot v_2 = v_1^+ v_2^- + v_1^- v_2^+ - \underline{v}_1 \cdot \underline{v}_2 \quad (1.9)$$

The Sudakov basis is defined through the introduction of two light-cone vectors $p_{1(2)}$ (+(-) directions) with¹ $2 p_1 \cdot p_2 = s$. In the peculiar example discussed here, a natural choice is given by choosing $p_{2(1)}$ as the incoming (outgoing) hadron momentum, and $Q^2 = s$. Any momentum is then expanded as

$$k = \underset{+}{\alpha} p_1 + \underset{-}{\beta} p_2 + \underset{\perp}{k_\perp}, \quad (1.10)$$

examplifying the relationship with the light-cone coordinates. In particular the momentum square reads

$$k^2 = \alpha \beta s + k_\perp^2 = \alpha \beta s - \underline{k}^2 = 2k^+ k^- - \underline{k}^2. \quad (1.11)$$

Within this basis, the hard part of the form factor can be drawn as illustrated in Fig. 1.3. In this light-cone decomposition, external (on-shell) lines attached to the soft (non-perturbative) part carry momenta flying only along + or - directions, while due to the kink, an exchange of *both large* + and - is needed within the hard

¹In general applications s will play the role of a large parameter. Its relation with external kinematical parameters will depend on the specific process under consideration.

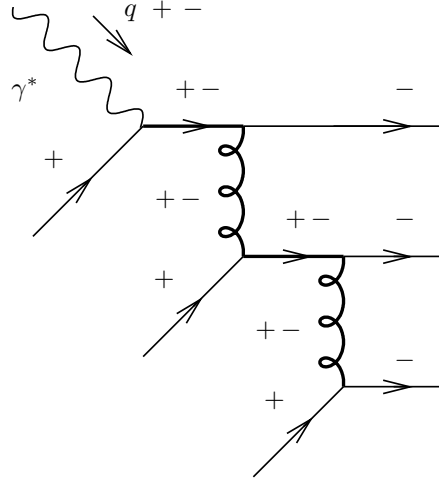


Figure 1.3: A typical contribution to the hard part of the hadron form factor. The + and - indicate the large light-cone momentum flowing along the corresponding lines. Bold line denotes hard propagators.

part. One can check on the example of Fig. 1.3 that the typical values of $\alpha\beta s$ is of the order of Q^2 , the hard scale, for any propagators entering the hard part. Such a diagrammatic analysis is at the heart of any proof of collinear factorization.

A similar analysis based on counting rules can be applied to large angle elastic scattering processes $h_a h_b \rightarrow h_a h_b$, i.e. in the regime where all s, t, u invariants are large [10], leading to a similar counting rule as the one obtained for the form factor. However, in this latter case, the analysis is complicated by contributions which are disconnected, when analysing the hard part from the point of view of Feynman diagrams [11], as illustrated in Fig. 1.4 for $\pi(p_1)\pi(p_2) \rightarrow \pi(p'_1)\pi(p'_2)$ scattering. The underlying assumptions is that there exist

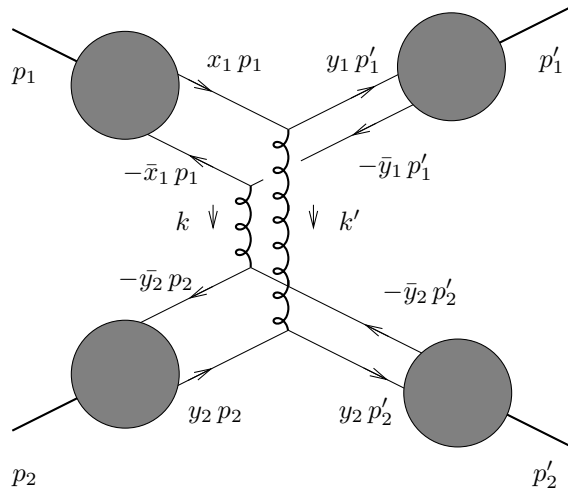


Figure 1.4: A typical contribution to large angle $\pi(p_1)\pi(p_2) \rightarrow \pi(p'_1)\pi(p'_2)$ scattering which is not governed by hard counting rule. The two bold gluon lines denotes hard propagators. The grey blobs symbolize vertices of non-perturbative nature.

peculiar configurations in the hadron bound state in which each constituent is assumed to carry a fraction of the momentum of the bound state, i.e. x and \bar{x} for the case of a meson (we denote $\bar{x} \equiv 1 - x$), with a negligible transverse momentum. Such configuration leads to an amplitude which dominates the pure hard configuration, when evaluating the loop momentum integral, which is dominated by a pinching. It means that when writing the diagram in a standard Feynman parameters representation (or equivalently in the Schwinger α representation) in order to analyze the loop momentum integration, the leading contribution when $s, t, u \rightarrow \infty$

is not dominated by end-point contributions of these parameters, as usual for hard part occurring in collinear factorization (as it would be the case e.g. in the form factor discussed above), but rather by configurations of these parameter inside their domain of variation (see the illuminating example of a scalar diagram discussed p.159 of Ref. [12]). Although these “pinched” contributions may be of importance for phenomenology, their contributions are expected to be suppressed by Sudakov effects (which suppresses configurations where internal constituent of hadrons are forced to be collinear) [13,14]. In practice, since this suppression only occurs in the asymptotical regime, large angle pp data [15] require a combination of both type of contributions [16–18]. Note that such a complication due to pinch singularities and Sudakov resummation effects does not occur as soon as the process involves at least one external photon [19]. We will not discuss further these type of contributions starting from now, except briefly in the case of photoproduction of mesons at HERA. For a rather comprehensive review of factorization before the more recent developments in DVCS and related process, see Ref. [20].

1.2 From DIS to DVCS

1.2.1 Kinematics of DVCS

We consider the Virtual Compton Scattering process:

$$\gamma^*(q) p(p) \rightarrow \gamma^*(q') p(p'). \quad (1.12)$$

This process includes in particular the Deep Virtual Compton Scattering (DVCS) process for which q^2 is large while the outgoing photon is on-shell. Another process which belong to this class is Timelike Compton Scattering (TCS), in which the incoming photon is on-shell while the produced one is timelike, corresponding to production of a pair of leptons. Finally, the more general case corresponds to the Double Deeply Virtual Compton Scattering (DDVCS), in which both the (spacelike) incoming photon and the (timelike) out-going one are far off-shell. Factorization is expected whenever at least one of the two scales $|q^2|$ and $|q'^2|$ are large, when the Mandelstam variable $s_{\gamma p}$ is large, with fixed $|q^2|/s_{\gamma p}$ and $|q'^2|/s_{\gamma p}$ ratios and fixed t (this should be contrasted with fixed angle scattering for which t is also asymptotically large). We define the transferred momentum by

$$\Delta = p' - p = q - q'. \quad (1.13)$$

As usual, one defines $Q^2 = -q^2$ and $Q'^2 = +q'^2$. The first scaling variable to be defined is the standard Bjorken variable

$$x_{bj} = \frac{Q^2}{2p \cdot q} = \frac{Q^2}{W^2 + Q^2 - M^2}. \quad (1.14)$$

The skewness ξ is defined in a covariant manner by

$$\xi = -\frac{(q - q') \cdot (q + q')}{(p + p') \cdot (q + q')}. \quad (1.15)$$

Expressing the various scalar product through the invariants $W^2 = (p + q)^2 = (p' + q')^2$ and $u = (p - q')^2 = (p' - q)^2$, combined with the relation $u + W^2 + t = -Q^2 + Q'^2 + 2M^2$ leads to

$$\xi = \frac{Q^2 + Q'^2}{2W^2 + Q^2 - Q'^2 - 2M^2 + t}. \quad (1.16)$$

Neglecting t with respect to Q^2 and/or Q'^2 and with respect to W^2 means that it is possible to choose two light-like vectors p_1 (+) and p_2 (-) such that the incoming and outgoing proton flies (almost) along p_2 , the proton receiving a kink Δ along p_2 and \perp directions only. The skewness can thus be written as

$$\xi \sim \frac{(p - p')_-(q + q')_+}{(p + p')_-(q + q')_+} = \frac{(p - p')_-}{(p + p')_-}. \quad (1.17)$$

Defining now the average momentum of the nucleons as

$$P = \frac{p + p'}{2} \quad (1.18)$$

which has two components, along $-$ and \perp directions, one can rewrite the $-$ components of p and p' in the convenient form

$$p_- = (1 + \xi) P_- \text{ and } p'_- = (1 - \xi) P_- , \quad (1.19)$$

while the $-$ component of Δ reads

$$\Delta_- = -2\xi P_- . \quad (1.20)$$

1.2.2 DVCS and GPD

We now consider the DVCS $\gamma^*(Q^2)p \rightarrow \gamma p$, which opened the way to the introduction of non-forward parton distributions, now called GPDs². This subprocess can be experimentally studied in the process $ep \rightarrow ep\gamma$. From Eq. (1.16) one deduces, since $Q'^2 = 0$, that

$$\xi = \frac{x_{Bj}}{2 - x_{Bj}} , \quad (1.21)$$

which relates the skewness to the usual x_{Bj} parameter. This shows in particular that at small- x_{Bj} , which is typical for HERA collider (H1, ZEUS experiments), skewness effects are presumably rather small, and were in particular overcome in the seminal paper [28] on diffractive electroproduction, which was devoted to HERA kinematics. We will not discuss here in detail the methods which have been developed [29] and are now used for extracting GPDs from DVCS studies³. Data on DVCS which support the factorization through GPD are now coming from HERA [30–35] and JLab [36–40] with increasing precision, allowing for detailed studies of GPDs. Further results are expected from COMPASS [41, 42]. For a very recent review on experimental results, see Ref. [43].

There are several ways to attack the problem of factorization of hard (inclusive of exclusive) processes. The first one, which we will mainly deal with in this manuscript, and which we briefly illustrated in the previous section, relies on the analysis of a given set of diagrams which are expected to dominate, which are then factorized in a hard and soft part. Then, considering diagrams which does not allow for factorization, one can practically show that they are suppressed in power of the hard scale Q . This is the basis of the classical hand-bag diagram analysis of DVCS [44] and of hard electroproduction of vector mesons [45].

In some cases, from this educated guess, one can infer a proof of factorization, for arbitrary diagrams, leading then to “factorization theorems”. The basic tool for such an analysis is an appropriate expansion in powers of the hard scale, like Q^2 for DVCS. In the Schwinger α representation, this large parameter appears as multiplied by α dependent terms in the argument of an oscillatory exponential. These terms are ratios of polynomials which are dependent of the topology of the given diagram. (see [46] p. 294 and [47] for details). The large Q^2 limit is thus dominated by diagrams for which this ratio vanishes. This leads to a systematic analysis of the amplitude as a convolution of “reduced” diagrams (hard part), convoluted with long-distance contributions. This the basis of the Radyushkin approach already used for the factorization of the pion form factor [48] and which lead to spectral properties of multiparton distributions functions [49, 50] - among which are Partons Distribution Functions (PDFs). This led to an all-order proof of factorization for DVCS and hard electroproduction of vector mesons in the seminal and pedagogical paper⁴ [51]. Another approach, this time in Feynman parameter representation (which is completely equivalent with Schwinger α representation by a simple rescaling of α -parameters) lead to an equivalent result for hard electroproduction of vector mesons, in the seminal work of Collins, Frankfurt and Strikman [52]. In this proof, the analysis relied on the Landau theory [53] of pinch singularities, in order to extract the dominant diagrams when carrying the expansion with respect to the large parameter (here Q^2), and in particular on the Coleman-Norton theorem [54] which gives a simple tool to classify the various soft contributions which may occur in terms of classical allowed trajectories. In both treatments, the non-trivial step is to prove that diagrams, which have a non factorizable topology are suppressed in the $1/Q$ power counting. This relies in particular on the Ward identities of QCD, which complicate the counting rules in comparison with scalar theories. Similar tools were used in the proof of factorization of DVCS of Refs. [55] and [56]. Any of these proofs relies on rather technical arguments with would need too much developments, and we thus refer to the quoted literature.

²For early reviews on GPDs, see Refs. [21, 22]. See Refs. [23, 24] for more recent reviews. Up-to-date reviews on models and data can be found in Refs. [25–27].

³See section 9 of [23] for a detailed review.

⁴One can find there a account of the main idea based on a detailed analysis of the box diagram in scalar field theory.

There exist actually others more formal proofs, which originate from DIS. Let us recall that DIS deals with the total $\gamma^*(Q^2)p \rightarrow X$ cross-section, which is related to the *forward* amplitude of the $\gamma^*(Q^2)p \rightarrow \gamma^*(Q^2)p$ process through the optical theorem. The factorization of the DIS cross-section can be formally proven based on the coordinate space Operator Product Expansion (OPE). It involves the convolution of a coefficient function (hard part) with the forward matrix element of a light-cone operator. Historically [57–60] this was proven and studied based on the relationship between moments of the structure functions and *local* light-cone operators, and using these sets of operators to perform an OPE. The structure function are reconstructed based on the knowledge of an infinite set of these moments. This is intrinsically due to the fact that the operator product expansion in the limit $x^2 \rightarrow 0$

$$J(x)J(0) = \sum_{n=0}^{\infty} C_n(x^2) x^{\mu_1} \cdots x^{\mu_n} O_{\mu_1 \cdots \mu_n}(0), \quad (1.22)$$

involves an infinite set of *local* light-cone operators and of Wilson coefficients (hereafter also called “hard part”). It turns out that the problem of resumming an infinite sum can be overcome by considering *non-local* light-cone operators. One of the practical advantage of considering such operators is that they satisfy renormalization group equations which leads, when considering specific matrix elements (forward hadron-hadron matrix elements for PDFs, non-forward hadron-hadron matrix elements for GPDs, vacuum-hadron matrix elements for DAs, etc...), to various sets of QCD evolution equations: Dokshitzer, Gribov-Lipatov, Altarelli-Parisi (DGLAP) [61–64] for PDFs and Efremov-Radyushkin, Brodsky-Lepage (ERBL) [48, 65, 66] for DAs. Non local OPE was investigated long before the more recent interest for DVCS [67, 68] (see also [69]), in particular in order to understand factorization of DIS and inclusive e^+e^- annihilation [70, 71]. Its use for DVCS and hard electroproduction lead to the classical approach of the Leipzig group [72].

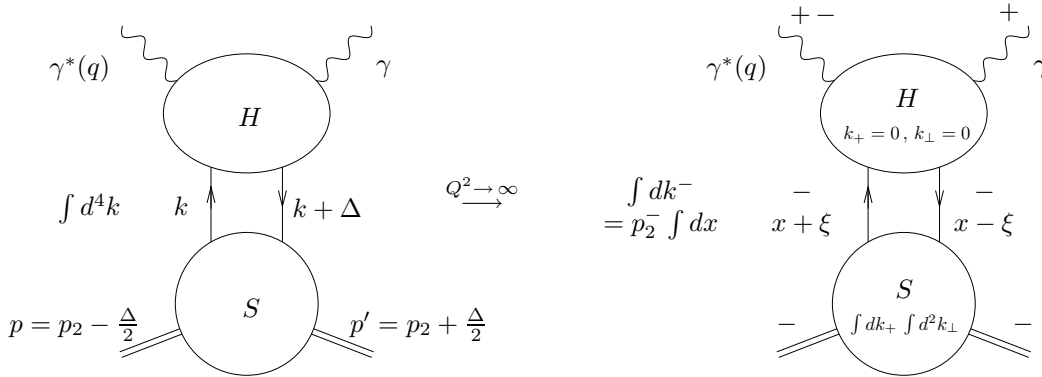


Figure 1.5: Momentum space factorization of the DVCS amplitude in the hard regime. The signs + and – indicate corresponding flows of large momentum components, with respect to which transverse components are neglected.

We will now explain how factorization of the DVCS amplitude in the large Q^2 limit occurs, without giving any argument of the reason why other non factorizable diagrams are suppressed, referring to the literature for proofs. The factorization follows two steps.

Factorization in momentum space

First, one should factorize the amplitude in coordinate or momentum space. We will deal here with the factorization in momentum space, which makes the connection with Feynman diagrams more direct. This can be set up more easily when using the Sudakov decomposition (1.10), this time with p_2 chosen in such a way that $P = \frac{1}{2}(p + p')$ (see Eq. (1.18)) reduces to p_2 in the limit of $P^2 \rightarrow 0$ we are interested in, i.e. the – part of P is identical to p_2 , and other components are unimportant from the point of view of factorization (it matters for the soft part, but not for the hard part). The vector p_1 is somehow arbitrary, and can be chosen in convenient way by relating it to the external kinematics, in such a way that

$$q = p_1 - \frac{Q^2}{2s} p_2. \quad (1.23)$$

This choice means that the outgoing photon satisfies

$$p_\gamma \sim p_1 - \Delta_\perp. \quad (1.24)$$

up to a term proportional to p_2 to satisfy the mass-shell condition. Another choice of kinematics is possible, by choosing p_1 to be along p_γ . This has to be kept in mind when we will implement a double factorization when replacing the produced photon par a vector meson, in which the second factorization goes along the p_V direction.

We will discuss in detail the arbitrariness related to the choice of p_1 in Chap. 3, for the case of exclusive hard processes beyond leading twist. We will for the moment restrict ourselves to the twist 2 dominant case. In the limit $Q^2 \rightarrow \infty$, the only component of the momentum k to be kept in the hard blob H is k_- . In particular, this means that the quark-antiquark pair entering H can be considered as being collinear, flying in the direction of the p_2 momentum. Therefore, the amplitude reads

$$\int d^4k S(k, k + \Delta) H(q, k, k + \Delta) = \int dk^- \int dk^+ d^2k_\perp S(k, k + \Delta) H(q, k^-, k^- + \Delta^-),$$

as illustrated in Fig. 1.5 with $p_2 = \frac{1}{2}(p + p')$, $\Delta = p' - p$. The fact that this approximation in the hard part leads to the dominant contribution in the $1/Q$ power counting can be checked explicitly in the case of the hand-bag diagram. This relies on exactly the same idea as the one used for the counting rule of Sec. 1.1: at twist 2 the hard part can be computed by keeping the dominant term in the Taylor expansion around the dominant light-cone momentum carried by the partons.

Factorization in the space of quantum numbers

Additionally to the infinite representations of the Lorentz group considered above, one should as well consider representation of finite dimensions, of spin 1/2 (quarks, antiquarks) and of spin 1 (gluons). At the same time, a factorization in color space is needed. In the specific case of the two partons (quark-antiquark) contribution, this means that one should factorize the amplitude in spinor space and in the fundamental representation of $SU(N)$. Both of these factorization can be achieved based on the Fierz identity (see [46] page 160). Let us recall that in 4 dimensions, there are 16 independent Dirac matrices

$$\begin{array}{ccccc} \Gamma_S & \Gamma_V^\mu & \Gamma_T^{\mu\nu} & \Gamma_A^\mu & \Gamma_P \\ I & \gamma^\mu & \sigma^{\mu\nu} = \frac{i}{2}[\gamma^\mu, \gamma^\nu] & \gamma^5 \gamma^\mu & i \gamma^5 \end{array} \quad (1.25)$$

Denoting⁵

$$\Gamma_\alpha \equiv (\Gamma^\alpha)^{-1}. \quad (1.26)$$

One readily gets that

$$\begin{aligned} (\gamma^\mu)^{-1} &= \gamma_\mu \equiv \Gamma_{V\mu}, & (\sigma^{\mu\nu})^{-1} &= \sigma_{\mu\nu} \equiv \Gamma_{T\mu\nu}, \\ (\gamma^5 \gamma^\mu)^{-1} &= \gamma_\mu \gamma^5 \equiv \Gamma_{A\mu}, & (i\gamma^5)^{-1} &= -i\gamma^5 \equiv \Gamma_P^{-1}. \end{aligned} \quad (1.27)$$

Since the hermitian conjugate of the matrices Γ^α is obtained through intertwining with the γ^0 matrix

$$\gamma^0 (\Gamma^\alpha)^\dagger \gamma^0 = \Gamma^\alpha$$

this immediately implies that $\bar{\Psi} \Gamma^\alpha \Psi$ are hermitian quantities. When considered as to non-local operators, these are the basic objects used for describing the soft part involved in the factorization of hard exclusive processes. From (1.27), one immediately gets the key relation

$$\text{Tr} \Gamma^\alpha \Gamma_\beta = 4\delta_\beta^\alpha. \quad (1.28)$$

from which one can identify the coefficients of the decomposition of any 4×4 matrix in the basis of Γ^α matrices

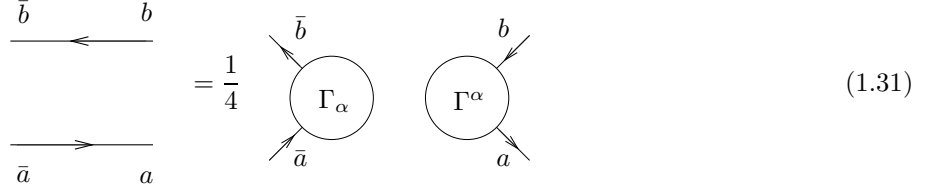
$$X = x_\alpha \Gamma^\alpha = \frac{1}{4} \Gamma^\alpha \text{Tr} (X \Gamma_\alpha) = \frac{1}{4} \Gamma_\alpha \text{Tr} (X \Gamma^\alpha), \quad (1.29)$$

⁵For γ^μ , this is compatible with the fact that $(\gamma^\mu)^{-1} = \gamma_\mu$, obtained when using the metric tensor $g_{\mu\nu}$.

from which one deduces the Fierz decomposition of the identity in the tensor product space (denoting bispinor indices with latine letters and labelling the Dirac matrices with greek letters)

$$\delta_{\bar{b}b} \delta_{a\bar{a}} = \frac{1}{4} \Gamma_{\alpha} \bar{\Gamma}_{\alpha} \Gamma_{ab}^{\alpha}. \quad (1.30)$$

This identity can be illustrated graphically as



$$= \frac{1}{4} \left(\text{Diagram 1} + \text{Diagram 2} \right) \quad (1.31)$$

The Fierz identity in color space goes along the same line, and a graphical rule can be given for practical use [73]. A graphical representation of generators of the Lie algebra of $SU(N)$ in the fundamental representation t_{ij}^a is given by



$$\equiv t_{ij}^a. \quad (1.32)$$

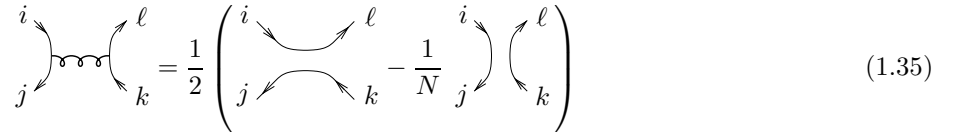
where the fundamental line carry an index to distinguish N and \bar{N} representations. Generators are conventionally normalized as

$$\text{Tr}(t^a t^b) = \frac{1}{2} \delta^{ab}. \quad (1.33)$$

This relation, similar to (1.28), enables to prove the Fierz identity

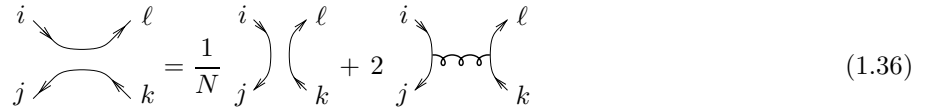
$$t_{ij}^a t_{kl}^a = \frac{1}{2} \left(\delta_{il} \delta_{jk} - \frac{1}{N} \delta_{ij} \delta_{kl} \right). \quad (1.34)$$

which is proven by expanding an arbitrary $N \times N$ hermitian matrix on the basis I and t^a ($a = 1, \dots, N^2 - 1$). This Fierz identity can be illustrated graphically as



$$= \frac{1}{2} \left(\text{Diagram 1} - \frac{1}{N} \text{Diagram 2} \right) \quad (1.35)$$

or equivalently, in the form to be used below,



$$= \frac{1}{N} \text{Diagram 1} + 2 \text{Diagram 2} \quad (1.36)$$

The Fierz identity in spinor and color space then shows that the DVCS amplitude completely factorizes, as illustrated for quark-antiquark exchange in Fig. 1.6. The above Fierz relations fixes the Feynman rules when computing the hard part, as we will illustrate in details in Chap.6 in the example of the $\gamma^* \rightarrow \rho$ impact factor. The final form of the factorized DVCS amplitude thus reads symbolically:

$$\mathcal{M} = \text{GPD} \otimes \text{Hard part}. \quad (1.37)$$

We will now present with some details the structure and properties of GPDs.

1.3 GPDs: some basics

We now define and review basic properties of GPDs. We will here adhere on the conventions of Ref. [23].

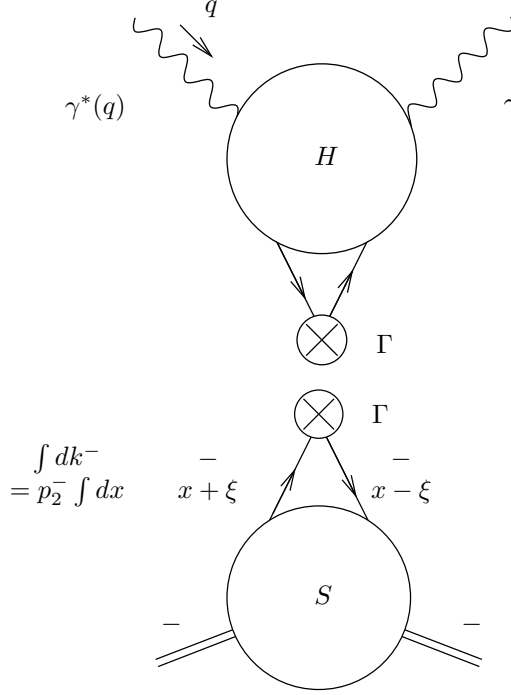


Figure 1.6: Factorization of the DVCS amplitude in the hard regime. The blob with a cross denote a set of Γ matrices. In the above (hard) part, the lines entering and exiting the crossed blob carry spinor and color indices but do not propagate any momentum. The corresponding momentum are on-shell. The whole momentum structure is contained in the blob H .

1.3.1 Definitions

Helicity non-flip GPDs

As explained above, the factorization of DVCS into a hard and a soft part naturally involves generalized parton distribution [1] which are defined through matrix elements of quark and gluons non-local operators with a light-like separation. We restrict ourselves for a moment to the GPDs in which the total transfer of helicity is zero. Using the conventions of Ji [74], the quarks GPDs are defined as⁶

$$\begin{aligned}
 F^q &= \frac{1}{2} \int \frac{dz^+}{2\pi} e^{ixP^-z^+} \langle p' | \bar{q}(-\frac{1}{2}z) \gamma^- q(\frac{1}{2}z) | p \rangle \Big|_{z^-=0, z_\perp=0} \\
 &= \frac{1}{2P^-} \left[H^q(x, \xi, t) \bar{u}(p') \gamma^- u(p) + E^q(x, \xi, t) \bar{u}(p') \frac{i\sigma^{-\alpha} \Delta_\alpha}{2m} u(p) \right], \\
 \tilde{F}^q &= \frac{1}{2} \int \frac{dz^+}{2\pi} e^{ixP^-z^+} \langle p' | \bar{q}(-\frac{1}{2}z) \gamma^- \gamma_5 q(\frac{1}{2}z) | p \rangle \Big|_{z^-=0, z_\perp=0} \\
 &= \frac{1}{2P^-} \left[\tilde{H}^q(x, \xi, t) \bar{u}(p') \gamma^- \gamma_5 u(p) + \tilde{E}^q(x, \xi, t) \bar{u}(p') \frac{\gamma_5 \Delta^-}{2m} u(p) \right]. \tag{1.38}
 \end{aligned}$$

The Lorentz invariance implies that the GPDs H^q , E^q , \tilde{H}^q , \tilde{E}^q only depend on the kinematical variables x , ξ , and t . Note in particular the fact that they thus do not depend on individual plus-momenta, but only on x and ξ which are minus-momentum *fractions*. This is due to the invariance of the above GPDs with respect to boost along the z -axis.

The above definitions are valid in the light-cone gauge $A^- = 0$. For arbitrary gauges a Wilson line

⁶We use non-standard labelling of large momentum in order to prepare our focus on electroproduction: thus P^- is large for the hadronic probe.

$[-\frac{1}{2}z^+, \frac{1}{2}z^+]$ should be included along a light-like path between the two fields at positions $-\frac{1}{2}z$ and $\frac{1}{2}z$, with

$$[z_1, z_2] = P \exp \left[ig \int_0^1 dt (z_1 - z_2)_\mu A^\mu(t z_1 + (1-t) z_2) \right], \quad (1.39)$$

defined in accordance with the convention

$$i \vec{D}_\mu = i \vec{\partial}_\mu + g A_\mu, \quad (1.40)$$

for the covariant derivative. This Wilson line ensure the gauge invariance. From a physical point of view, in the hand-bag factorized picture, this Wilson line in fact resums the infinite set of *longitudinally polarized gluon* exchanged between the fermion line joining the two photon vertices and the nucleon, which are not $1/Q$ suppressed. Any emission from the external lines joining the photon vertices to the nucleon compensate based on color neutrality, through unitarity arguments (see for example Ref. [9] p. 180 or Ref. [51]). This resummation has the nice feature to factorize completely from the hard part and can therefore be attributed to the non-perturbative correlators defining the GPDs. The same feature will occur for any non-perturbative correlators involved in collinear factorization. In a light-cone gauge, this Wilson line turns to unity, in agreement with the fact that gluon are only physically polarized in such gauges. Note that these non-suppressed gluons should not be confused with the exchange of transversally polarized gluons, which are $1/Q$ suppressed and which contribute starting from twist 3. Such twist 3 gluonic contributions will be considered with much details in Chap. 3 for DAs.

The distributions defined above have support in the interval $x \in [-1, 1]$, which can be separated three regions (see Fig. 1.7):

- for $x \in [\xi, 1]$ both momentum fractions $x + \xi$ and $x - \xi$ are positive; the distribution describes emission and reabsorption of a quark: this is the usual DGLAP region for quarks
- for $x \in [-\xi, \xi]$ one has $x + \xi \geq 0$ but $x - \xi \leq 0$. The second momentum fraction is now interpreted as belonging to a antiquark with momentum fraction $\xi - x$ emitted from the initial proton: this is the ERBL region in which the picture of a t -channel exchanged meson emerges
- for $x \in [-1, -\xi]$ both $x + \xi$ and $x - \xi$ are negative; one has emission and reabsorption of antiquarks with respective momentum fractions $\xi - x$ and $-\xi - x$: this is the usual DGLAP region for antiquarks

The interpretation of the 3 above regions in terms of density number operators [74–76] can be made explicit in the framework of light-cone quantization [77–80]. Note in particular that in the light-cone quantization, the fact that the support of GPD is $x \in [-1, 1]$ can be understood in an easy way, relying on similar arguments as for usual PDFs. Indeed, light-cone quantization (i.e. at fixed light-cone time z^- instead of fixed time z^0) involve intermediate states which should be on-shell (contrarily to usual quantization), with a positive light-cone energy k^+ . This energy being related the momentum along the P^- direction through the on-shell condition $k^+ = (m^2 + \underline{k}^2)/(2k^-)$, this implies when applying this constraint to all remnant in the emission of a parton by a hadron that $|x| \leq 1$.

Two peculiar limit are of special interest. The first one occurs when $\xi \rightarrow 0$, for which only the two DGLAP regions remain (including a possible non zero Δ_\perp). The second one is obtained when $\xi \rightarrow \pm 1$, for which the only remaining domain is the ERBL one.

The gluon GPDs are defined according to

$$\begin{aligned} F^g &= \frac{1}{P^-} \int \frac{dz^+}{2\pi} e^{ixP^- z^+} \langle p' | G^{-\mu}(-\frac{1}{2}z) G_\mu^-(\frac{1}{2}z) | p \rangle \Big|_{z^-=0, z_\perp=0} \\ &= \frac{1}{2P^-} \left[H^g(x, \xi, t) \bar{u}(p') \gamma^- u(p) + E^g(x, \xi, t) \bar{u}(p') \frac{i\sigma^{-\alpha} \Delta_\alpha}{2m} u(p) \right], \\ \tilde{F}^g &= -\frac{i}{P^-} \int \frac{dz^+}{2\pi} e^{ixP^- z^+} \langle p' | G^{-\mu}(-\frac{1}{2}z) \tilde{G}_\mu^-(\frac{1}{2}z) | p \rangle \Big|_{z^-=0, z_\perp=0} \\ &= \frac{1}{2P^-} \left[\tilde{H}^g(x, \xi, t) \bar{u}(p') \gamma^- \gamma_5 u(p) + \tilde{E}^g(x, \xi, t) \bar{u}(p') \frac{\gamma_5 \Delta^-}{2m} u(p) \right]. \end{aligned} \quad (1.41)$$

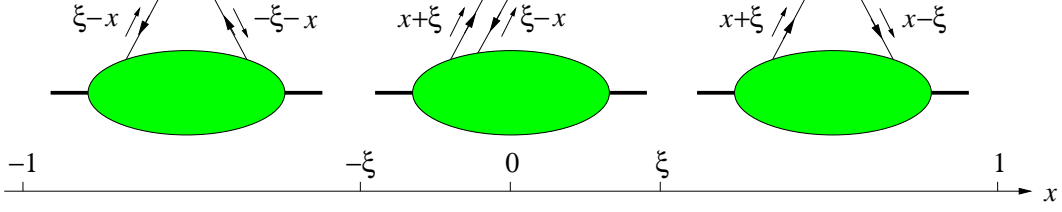


Figure 1.7: The parton interpretation of GPDs in the three x -intervals $[-1, -\xi]$, $[-\xi, \xi]$, and $[\xi, 1]$. Figure from Ref. [23].

Various equivalent parametrizations of GPDs have been introduced at the end of the '90s [51, 52, 75]. We refer to [51] and [75] for their comparison and for explicit dictionaries.

For completeness and further use when introducing GDAs, we now define analogous GPDs for pion. Due to the fixed parity of the pion, there are only 2 helicity non-flip GPDs, which reads

$$\begin{aligned} H_{\pi}^q(x, \xi, t) &= \frac{1}{2} \int \frac{dz^+}{2\pi} e^{ixP^-z^+} \langle \pi^+(p') | \bar{q}(-\frac{1}{2}z) \gamma^- q(\frac{1}{2}z) | \pi^+(p) \rangle \Big|_{z^-=0, z_{\perp}=0}, \\ H_{\pi}^g(x, \xi, t) &= \frac{1}{P^-} \int \frac{dz^+}{2\pi} e^{ixP^-z^+} \langle \pi^+(p') | G^{-\mu}(-\frac{1}{2}z) G_{\mu}^{-}(\frac{1}{2}z) | \pi^+(p) \rangle \Big|_{z^-=0, z_{\perp}=0}. \end{aligned} \quad (1.42)$$

Helicity flip GPDs

On top of the GPDs introduced above, one can introduce GPDs which describe the fact that the quarks exchange in t -channel may produce a transfert of one unit of helicity, and similarly for gluon which may produce a transfert of two units of helicity. In that situation, helicity is not anymore a suitable basis for these GPDs, and it is more convenient to deal with the notion of transversity, i.e. to deal with linearly polarized states instead of circularly one. In the quark case, one will therefore deal with the probability to find a quark with spin polarized along the spin of a polarized nucleon minus the probability to find it polarized oppositely. Thinking for a moment to the DGLAP picture in the quark sector (i.e. $\xi < x < 1$), since chirality = helicity for quarks, it is clear why the operators encountered in the definition of non-flip GPDs were chiral even (for example $\Delta q = q \uparrow - q \downarrow$ involve separately $q \uparrow$ ($q \downarrow$) for which the quark keep its + (resp. -) helicity during the scattering process). This situation should now be reversed, calling for chiral-odd operator matrix elements. This means that one should consider the following operators

$$\bar{q} \sigma^{-i} q, \quad \frac{1}{2} [G^{-i} G^{j-} + G^{-j} G^{i-}] - \frac{1}{2} g_T^{ij} G^{-\alpha} G_{\alpha}^{-}, \quad i, j = 1, 2 \quad (1.43)$$

Following [81], this leads to introduce 8 transversity GPDs⁷. For the quarks, they read

$$\begin{aligned} & \frac{1}{2} \int \frac{dz^+}{2\pi} e^{ixP^-z^+} \langle p' | \bar{q}(-\frac{1}{2}z) i\sigma^{-i} q(\frac{1}{2}z) | p \rangle \Big|_{z^-=0, z_{\perp}=0} \\ &= \frac{1}{2P^-} \bar{u}(p') \left[H_T^q i\sigma^{-i} + \tilde{H}_T^q \frac{P^- \Delta^i - \Delta^- P^i}{m^2} + E_T^q \frac{\gamma^- \Delta^i - \Delta^- \gamma^i}{2m} + \tilde{E}_T^q \frac{\gamma^- P^i - P^- \gamma^i}{m} \right] u(p), \end{aligned} \quad (1.44)$$

and similarly for gluons:

$$\begin{aligned} & \frac{1}{P^-} \int \frac{dz^+}{2\pi} e^{ixP^-z^+} \langle p' | S_{(ij)} G^{-i}(-\frac{1}{2}z) G^{j-}(\frac{1}{2}z) | p \rangle \Big|_{z^-=0, z_{\perp}=0} \\ &= S_{(ij)} \frac{1}{2P^-} \frac{P^- \Delta^j - \Delta^- P^j}{2mP^-} \\ & \times \bar{u}(p') \left[H_T^g i\sigma^{-i} + \tilde{H}_T^g \frac{P^- \Delta^i - \Delta^- P^i}{m^2} + E_T^g \frac{\gamma^+ \Delta^i - \Delta^- \gamma^i}{2m} + \tilde{E}_T^g \frac{\gamma^- P^i - P^- \gamma^i}{m} \right] u(p), \end{aligned} \quad (1.45)$$

⁷A first attempt in this direction, though uncomplete, can be found in [82].

where $S_{(\mu\nu)}$ denotes the standard symmetrization operator with removal of the trace (here in the two transverse dimensions). Note that the definition for quark distributions can be equivalently⁸ expressed in terms of $\sigma^{-\beta}\gamma_5 = +\frac{1}{2}i\epsilon^{-\beta\gamma\delta}\sigma_{\gamma\delta}$ and is given in [81].

An important property of helicity-flip distributions is that they evolve independently in the renormalization scale μ , i.e., quarks do not mix with gluons and vice versa. In particular, gluon transversity probes glue in the target which is “intrinsic” in the sense that it cannot be generated from quarks by the perturbative DGLAP parton splitting processes.

Before studying the elementary properties of GPDs, a comment is in order to relate the various non-local correlators with twist counting. In fact, the natural set of Γ matrices components (e.g. γ^-) occurring in these above correlators, due to the peculiar kinematics encountered in the large Q^2 limit, can be understood in a more formal way. Indeed the four-component fermion field ψ can be decomposed as the sum of two terms ψ_{\pm} , using the projection operators [77]

$$\psi = \psi_+ + \psi_-, \quad \psi_{\pm} \equiv \Pi^{\pm}\psi, \quad \Pi^{\pm} \equiv \frac{1}{2}\gamma^{\mp}\gamma^{\pm}. \quad (1.46)$$

These two terms ψ_{\pm} have the following light-cone spin:

$$\Sigma^{+-}\psi_{\mp} = \mp\frac{1}{2}\psi_{\mp}, \quad (1.47)$$

where $\Sigma^{\mu\nu} \equiv \frac{1}{4}[\gamma^{\mu}, \gamma^{\nu}]$ is the spin tensor. From the canonical dimension of the fermion field $[d] = 3/2$, one deduces that the ψ_- -component has a twist $\tau_q = 1$ since its spin is $s_q = 1/2$. Similarly, for the ψ_+ -component one finds $s_q = -1/2$ and thus $\tau_q = 2$. Therefore, only the ψ_- component enters a nonlocal operator of the minimal twist. In the literature, this component is usually referred as the “good component”, while the other one is the “bad” one. Using the chiral projection, one can additionally select definite helicity components. A similar treatment can be applied to the field strength tensor $F^{\mu\nu}$. This leads to a complete set of *non-local* operators (the presence of the Wilson line does not change the twist) which were used above when defining the quark and gluon GPDs. A pedagogical construction of these twist two operators based on this line of thought can be found in [24].

1.3.2 Elementary properties of GPDs

Reduction to PDFs

The above GPDs can be related to the usual PDFs: indeed, when considering the forward limit $p = p'$ and restricting ourselves to equal helicities for the initial and final state hadrons, the matrix elements in (1.38) and (1.41) reduce to the ones defining the ordinary spin independent or spin dependent densities $q(x)$, $\Delta q(x)$ for quarks and $g(x)$, $\Delta g(x)$ for gluons. In the case of the nucleon, introducing distribution with a support along $[-1, 1]$, this implies for quarks that

$$H^q(x, 0, 0) \equiv f^q(x) = q(x)\theta(x) - \bar{q}(-x)\theta(-x), \quad (1.48)$$

$$\tilde{H}^q(x, 0, 0) \equiv \Delta f^q(x) = \Delta q(x)\theta(x) + \Delta\bar{q}(-x)\theta(-x), \quad (1.49)$$

and similarly for gluons:

$$H^g(x, 0, 0) = xg(x)\theta(x) - xg(-x)\theta(-x), \quad (1.50)$$

$$\tilde{H}^g(x, 0, 0) = x\Delta g(x)\theta(x) + x\Delta g(-x)\theta(-x), \quad (1.51)$$

while there is no corresponding relations for the quark and gluon distributions E and \tilde{E} in the nucleon, since the equations which define them involve a factor Δ which vanishes in the forward limit.

Among the 8 transversity GPDs, H_T^q is the only one which survives in the forward limit, again due to prefactors proportional to Δ . The corresponding relation reads

$$H_T^q(x, 0, 0) \equiv \delta f^q(x) = \delta q(x)\theta(x) - \delta\bar{q}(-x)\theta(-x), \quad (1.52)$$

⁸Note that we use here and hereafter $\epsilon^{0123} = 1$ which differs with the convention of [81].

where $\delta q(x)$ (usually also denoted $h_1(x)$) is the quark transversity distribution, the only PDF which is not very well known experimentally (see [83] for a review on transversity, and [84] for a recent overview of the field.). This PDF was introduced in 1979 in a seminal paper of Ralston and Soper [85] on Drell-Yan with polarized beams. It was then rediscovered at the beginning of the '90s [86–88], and the possibilities to measure it in hadron-hadron or lepton-hadron collisions was investigated [89,90]. It turns out that Drell-Yan production with two transversely polarized hadrons is one of the most favourable reaction (through the study of double-spin transverse asymmetries) [85,91]. Another possibility relies on semi-inclusive DIS with unpolarized lepton beam and transversally polarized initial hadron, with two detected hadrons in the final state. The corresponding cross-section is sensitive to h_1 coupled with an interference fragmentation function (the Collins fragmentation function) [92–95]. The first measurement through this channel was obtained by the HERMES collaboration [96], and the COMPASS experiment recently also reported a transversity signal through this measurement [97]. Since the access to h_1 is very difficult, one may expect a hard day for the GPD case. We will discuss this within the case of exclusive processes later.

For pions, the following limits hold:

$$H_\pi^q(x, 0, 0) \equiv f_\pi^q(x) = q(x)\theta(x) - \bar{q}(-x)\theta(-x), \quad (1.53)$$

and similarly for gluons:

$$H_\pi^g(x, 0, 0) = xg(x)\theta(x) - xg(-x)\theta(-x). \quad (1.54)$$

Symmetry properties

Let us first consider the non-flip GPDs. From their definition through the non-local correlators (1.41), one readily obtains, after performing the replacement $x \rightarrow -x$, then using translation invariance on the obtained correlator, performing the change of variable $x^- \rightarrow -x^-$ and using the fact that A field commute on the light cone, that

$$H^g(-x, \xi, t) = H^g(x, \xi, t) \quad \text{and} \quad E^g(-x, \xi, t) = E^g(x, \xi, t) \quad (1.55)$$

$$\tilde{H}^g(-x, \xi, t) = -\tilde{H}^g(x, \xi, t) \quad \text{and} \quad \tilde{E}^g(-x, \xi, t) = -\tilde{E}^g(x, \xi, t). \quad (1.56)$$

The quark sector is more involved: since the quark is not its own antiparticle, the above series of transformation not not give any simple symmetry. One should additionally use the charge parity operator, denoted as \mathcal{C} when acting on the fields, and insert the identity in the form of $\mathcal{C}\mathcal{C}^{-1}$ inside these correlators. The transformation of the non-local operator can be obtained using the well-known transformation properties

$$\mathcal{C}\Psi(x)\mathcal{C}^\dagger = \eta_C C \bar{\Psi}^T(x) \quad \text{and} \quad \mathcal{C}\bar{\Psi}(x)\mathcal{C}^\dagger = \eta_C^* \Psi^T(x) C, \quad (1.57)$$

where $C = C^\dagger = C^{-1} = C^T = -C$ and $C\gamma_\mu C = -\gamma_\mu^T$. However, since the nucleon themselves have not a fixed C -parity, this does not give any simple relation. If the initial and final state would have a definite C -parity, denoted respectively as C_i and C_f , then one would get by comparing the correlator obtained after insertion of $\mathcal{C}\mathcal{C}^{-1}$ with the one obtained after using the above transformations which we performed for the gluon case that $H^q(-x, \xi, t) = -C_i C_f H^q(x, \xi, t) = -C H^q(x, \xi, t)$ where C is the C -parity in the t -channel. The same relation holds for E^q , while for \tilde{H}^q one gets⁹ $\tilde{H}^q(-x, \xi, t) = +C_i C_f \tilde{H}^q(x, \xi, t) = +C \tilde{H}^q(x, \xi, t)$, and similarly for \tilde{E}^q . It is thus natural to introduce GPDs corresponding to fixed C -parity in t -channel. For $C = +1$ in the t -channel, one thus defines

$$H^{q(+)}(x, \xi, t) = H^q(x, \xi, t) - H^q(-x, \xi, t), \quad (1.58)$$

$$\tilde{H}^{q(+)}(x, \xi, t) = \tilde{H}^q(x, \xi, t) + \tilde{H}^q(-x, \xi, t) \quad (1.59)$$

and similarly for E^q and \tilde{E}^q . These GPDs are usually called ‘‘singlet’’ (even when the flavour is fixed). In the forward limit they reduce to

$$H^{q(+)}(x, 0, 0) = [q(x) + \bar{q}(x)]\theta(x) - [q(-x) + \bar{q}(-x)]\theta(-x) \quad (1.60)$$

$$\tilde{H}^{q(+)}(x, 0, 0) = [\Delta q(x) + \Delta \bar{q}(x)]\theta(x) + [\Delta q(-x) + \Delta \bar{q}(-x)]\theta(-x), \quad (1.61)$$

⁹The sign differs due to an additional γ^5 matrix entering the non-local operator.

Similarly, one defines GPDs corresponding to $C = -1$ in the t -channel, called “nonsinglet” or “valence” GPDs, as

$$H^{q(-)}(x, \xi, t) = H^q(x, \xi, t) + H^q(-x, \xi, t), \quad (1.62)$$

$$\tilde{H}^{q(-)}(x, \xi, t) = \tilde{H}^q(x, \xi, t) - \tilde{H}^q(-x, \xi, t). \quad (1.63)$$

and similarly for E^q and \tilde{E}^q . In the forward limit one has

$$H^{q(-)}(x, 0, 0) = [q(x) - \bar{q}(x)] \theta(x) + [q(-x) - \bar{q}(-x)] \theta(-x) \quad (1.64)$$

$$\tilde{H}^{q(-)}(x, 0, 0) = [\Delta q(x) - \Delta \bar{q}(x)] \theta(x) - [\Delta q(-x) - \Delta \bar{q}(-x)] \theta(-x). \quad (1.65)$$

The GPDs (1.58, 1.59) can be extracted for example in the transition $\gamma^* \rightarrow V$ where V is a vector meson, and the GPDs (1.62, 1.63) can be measured through in the electroproduction of a pseudo scalar meson, as well as in the production of hybrid vector meson like 1^{-+} which will be discussed in Sec. 2.5. Of course, as we have seen above, for processes involving probes of fixed parity, like a π^0 , the only surviving GPD is the $C = +$ one.

The symmetry property with respect to ξ can be obtained when inserting the identity in the form $\mathcal{T} \mathcal{T}^{-1}$ where \mathcal{T} is the antiunitary operator which implements time reversal in the Hilbert space, therefore satisfying $\langle \mathcal{T} \phi | \mathcal{T} \psi \rangle = \langle \psi | \phi \rangle$. In practice, one should also combine this with the insertion of the identity in the form $\mathcal{P} \mathcal{P}^{-1}$ where \mathcal{P} is the unitary operator which implements parity. This is due to the fact that the light-cone coordinate z^+ combines time, which changes under time reversal, and the third coordinate, which is invariant, thus turning z^+ into $-z^-$. This mixing of z^+ and z^- coordinate is avoided when using P parity combined with T symmetry. This leads, for each of the 8 non-flip GPDs, to relations of the type¹⁰

$$H(x, -\xi, t) = H(x, \xi, t). \quad (1.66)$$

On the other hand, using hermiticity one gets from the matrix elements of the non-local operators that

$$\left[H(x, -\xi, t) \right]^* = H(x, \xi, t) \quad (1.67)$$

and similarly for E , \tilde{H} , \tilde{E} . Combined with (1.66), one therefore deduces from (1.67) that the non-flip GPDs are real valued functions. The same relations (1.66) and (1.67) hold for the pion GPDs H_π^q and H_π^g .

In the case of GPDs with helicity flip, the constraints obtained from time reversal invariance and hermiticity, for both quarks and gluons, are the following: for H_T , \tilde{H}_T and E_T , they read as (1.66) and (1.67), while for \tilde{E}_T (again both for quarks and gluons) an extra minus sign appears and one has

$$\tilde{E}_T(x, \xi, t) = -\tilde{E}_T(x, -\xi, t), \quad \left[\tilde{E}_T(x, \xi, t) \right]^* = -\tilde{E}_T(x, -\xi, t). \quad (1.68)$$

For pions, there is a direct relation between isospin and GPDs of given C -parity. It is standard to define the combinations

$$H^{u+d} = H^u + H^d \quad \text{and} \quad H^{u-d} = H^u - H^d \quad (1.69)$$

which enable one to define the isosinglet GPDs

$$H_{\pi^+}^{u+d} = H_{\pi^-}^{u+d} = H_{\pi^0}^{u+d} \quad (1.70)$$

and the isotriplet combinations

$$H_{\pi^+}^{u-d} = -H_{\pi^-}^{u-d}, \quad H_{\pi^0}^{u-d} = 0. \quad (1.71)$$

Since the gluon distributions are isosinglet, they are identical for the three pion states. The charge conjugation invariance is implemented as above by insertion inside the correlator of the identity in the form of $\mathcal{C}\mathcal{C}^{-1}$. Using the fact that C -parity exchanges π^+ and π^- states, and using isospin invariance (1.70) and (1.71) implies respectively that

$$H_{\pi^+}^{u+d}(x, \xi, t) = -H_{\pi^-}^{u+d}(-x, \xi, t), \quad \text{and} \quad H_{\pi^+}^{u-d}(x, \xi, t) = H_{\pi^-}^{u-d}(-x, \xi, t). \quad (1.72)$$

By comparison with (1.58) one thus deduces that the isosinglet sector corresponds to $C = +1$ while comparison with (1.58) shows that the isotriplet sector corresponds to $C = -1$.

¹⁰Note that time reversal makes an interchange of initial and final state; moreover exchange of p and p' means $\xi \rightarrow -\xi$.

Relation with local matrix elements and polynomiality

It turns out that the moments of order n of GPDs with respect to the variable x (i.e. integrals of GPDs multiplied by x^n over $x \in [-1, 1]$) are polynomials of the variable ξ of degree at most $n + 1$. The coefficient of these polynomials are the form factors appearing when decomposing the *local* twist 2 operators of usual DIS on the basis of P^μ and Δ^μ vectors. The highest degree term ξ^{n+1} only occurs in the $C = +$ sector, and called D -terms. We will not discuss in detail here the proof of this polynomiality condition, and will refer to Ref. [23] for a review on the various relations satisfied by the whole set of GPDs. We will study with much more details the corresponding relations in the crossed-case of GDA in Sec. 2.1.2.

Evolution equations

When writing the symbolic factorization formula (1.37), we have hidden the fact that a factorization scale should be introduced in order to separate long distance degrees of freedom, belonging to the GPDs, from the short distance one, which belong to the hard part. From the technical point of view, such a scale is required by the UV divergencies. Indeed, GPDs are defined as matrix element of non-local twist 2 operators, according to Eqs. (1.38, 1.41, 1.44, 1.45). The matrix elements diverges in the UV limit $z^2 \rightarrow 0$, calling for a renormalization. This is done at the scale μ_F^2 . From the point of view of the hard part, this factorization scale is required by collinear divergencies appearing due to the fact that the quarks and gluons are on the mass-shell. The renormalization of these IR collinear divergencies is performed at this scale μ_F^2 . Additionally, when computed at a given order in perturbation theory, the hard part faces UV divergencies, calling for an additional renormalization, at a scale μ_R^2 . This implies a residual dependency over μ_R^2 for the whole amplitude at given order of perturbation theory. On the other hand, order by order in perturbation theory, the amplitude is independent of the factorization scale μ_F^2 .

The fact that the amplitude is μ_F^2 -independent and that the hard part is μ_R^2 -independent implies evolution equations. For the forward case, i.e. $\xi = 0$, these are the DGLAP equations [61, 63, 64] (these equations are valid for arbitrary value of Δ_\perp) for usual PDFs. In the spirit of the above meaning of μ_F^2 , these equations were obtained based on various methods. The partonic approach relies on the computation of logarithmic divergent diagrams occurring due to the mass-singularities of the hard part. See Ref. [98] for a comprehensive review of this method. The historical operator approach, based on the renormalisation of matrix element of light-cone local operators, i.e. of Mellin moment of structure functions, was obtained in Refs. [59, 60, 99]. The implementation of the μ_R^2 -independence of the Wilson coefficients led equivalently to these evolution equation. The approach based on the renormalization of *non-local* operators was developed by the Leipzig group [100–103] and by the Gatchina group [104, 105], and first lead to recover the known DGLAP result without appealing to matrix elements nor local operators.

In the non-forward case, the evolution equation combines the two limiting kernel: DGLAP, for $\xi \rightarrow 0$ and ERBL [48, 65, 66] kernel, for $\xi \rightarrow \pm 1$, corresponding to the physical limit of the exchange of a meson in t -channel. This equation was obtained either using old-fashioned perturbation theory on the light-cone, in the light-cone gauge [66] or based on the analysis of the renormalization of local operators [48]. The general kernel was obtained early in Refs. [106, 107], based on a momentum space computation. The first form of the LLQ kernel obtained within the context of GPDs was given in Refs. [72, 108] of the Leipzig group, based on the renormalization of the non-local light-ray operators, in coordinate space. It was also reconsidered and recomputed in Ref. [109], as well as in Refs. [51] and [110]. Other proofs based on the renormalization of light-ray operators can be found in Refs. [111] and [112, 113]. In Ref. [51, 114], the evolution kernel for *double distributions* is computed.

Based on the support properties of the kernel, and on the fact that the ERBL kernel, when Fourier transform, has a unique analytical continuation, which is the Fourier transform of the kernel for light-ray operators [72], a check of the consistency between the NLLQ ERBL kernel, computed in Refs. [115–118], and the NLLQ DGLAP kernel [119–121] was performed, when taking appropriate matrix elements.

The NLLQ kernel was then obtained in Refs. [122–127], based on conformal field theory as well as the continuation discussed above, starting from the pure ERBL kernel. See Ref. [128] for a simple introduction to conformal symmetry method (applied there to the Next-to-Next-to-Leading hard contribution to the photon-to-pion form factor).

We will not give here the explicit expression of these evolution equations. We refer to Ref. [24] for explicit expressions. For a detailed and pedagogical construction of the LLQ kernel in coordinate space, see Ap. G-5

of Ref. [24], and for the corresponding construction in momentum space, which was first used in the pionering but hard to read Refs. [106, 107], see Ap. G-6 of Ref. [24].

1.4 The illuminating example of ρ -electroproduction

1.4.1 ρ -meson production: from the wave function to the DA

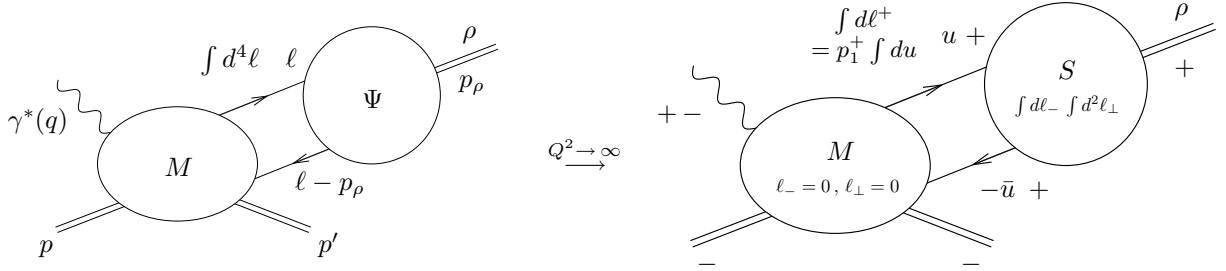


Figure 1.8: Factorization of the amplitude of hard ρ -electroproduction.

We now replace the produced photon by a ρ -meson, described in QCD by its wave function Ψ which reduces in hard processes to its Distribution Amplitude. Following the same line of thinking as for GPDs (actually DAs where introduced long before GPDs, for form factor studies, see Sec. 1.1. We here follow a non-historical presentation, more convenient from a pedagogical point of view), this DA should be defined by integrating over the ℓ^- momentum as well as over the ℓ_\perp momentum, the hard part on which it will be connected by collinear partons being only ℓ^+ -dependent. This DA is defined thus as [129–133]

$$\Phi(u, \mu_F^2) = \int d\ell^- \int_{|\ell_\perp^2| < \mu_F^2} d^2\ell_\perp \Psi(\ell, \ell - p_\rho). \quad (1.73)$$

As for DVCS, in the limit $Q^2 \rightarrow \infty$, the amplitude of diffractive electroproduction of a ρ -meson can be written as

$$\int d^4\ell M(q, \ell, \ell - p_\rho) \Psi(\ell, \ell - p_\rho) = \int d\ell^+ M(q, \ell^+, \ell^+ - p_\rho^+) \int_{|\ell_\perp^2| < \mu_F^2} d\ell^- \int d^2\ell_\perp \Psi(\ell, \ell - p_\rho) \quad (1.74)$$

(see Fig. 1.8). Here $1/\mu_F$ give the typical scale down to which the transverse degrees of freedom are integrated out in the wave function, thus fixing the typical resolution. It is related to the non-local matrix element $\langle 0 | \bar{u}(z) \gamma_\mu d(-z) | \rho^-(P, \lambda) \rangle$ by Fourier transform (detailed expression are given in next sections) with respect to the longitudinal $-$ coordinate (conjugated to the longitudinal $+$ momentum) of the quark-antiquark fields, at zero $+$ coordinate and (almost) zero transverse coordinate. The reason why is it only almost at zero transverse coordinate is the same as for GPDs: it lays on the fact that this correlator of a non-local operator faces UV divergencies when $z^2 \rightarrow 0$ which are regularized at the renormalization scale μ_F^2 . Physically, the scale μ_F^2 sets the boundary between the low and the high-energy part in the process, the short distance modes belonging to the probe, i.e. to the hard part, while the long distance one belongs to the DA. Note that the “hard” part itself can also contain long-distance effects, as we discuss next, due to other hadronic states which participate to the process, like in meson electroproduction. However these hadronic states are assumed to be well separated from the rho by a proper choice of the kinematics, in particular fixed ratio W^2/Q^2 in order to avoid the region were a resonance could occur between final states, through long-distance effects, which would spoil the perturbative approach.

1.4.2 ρ -meson production: factorization with a GPD and a DA

The description of hard exclusive processes involving the production of a meson was initiated in [28], in the special limit of HERA kinematics (small- x_{Bj} region, i.e. small ξ limit, see Part. II) for which the t -channel exchange is dominated by gluons. For general x_{Bj} , a first description was provided in Ref. [134], including the

effect of GPDs and describing the production of the meson through a dipole approach, i.e. a quark-antiquark pair in coordinate space. A proof of factorization at the leading twist 2 and at any order in perturbation was then given in Ref. [52], and shortly after in [51] (see the above discussion in Sec. 1.2.2).

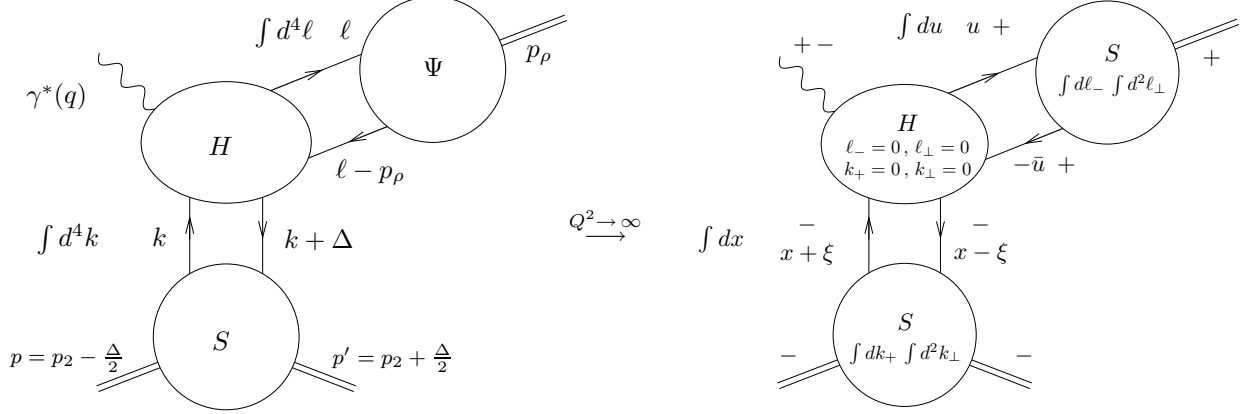


Figure 1.9: Full factorization of the amplitude of hard electroproduction of a ρ -meson.

Combining the previous factorizations involving a DA (see Sec. 1.4.1) and GPDs (see Sec. 1.2.2), one can describe the hard electroproduction of a ρ -meson in a fully factorized form involving a GPD and a DA, as illustrated in Fig. 1.9. The corresponding amplitude reads

$$\int d^4k d^4\ell S(k, k + \Delta) H(q, k, k + \Delta) \Psi(\ell, \ell - p_\rho) = \int dk^- dl^+ \quad (1.75)$$

$$\times \int dk^+ \int_{|k_\perp^2| < \mu_{F_2}^2} d^2k_\perp S(k, k + \Delta) H(q; k^-, k^- + \Delta^-; \ell^+, \ell^+ - p_\rho^+) \int dl^- \int_{|\ell_\perp^2| < \mu_{F_1}^2} d^2\ell_\perp \Psi(\ell, \ell - p_\rho).$$

GPD $F(x, \xi, t, \mu_{F_2}^2)$ Hard part $T(x/\xi, u, \mu_{F_1}^2, \mu_{F_2}^2)$ DA $\Phi(u, \mu_{F_1}^2)$

where we have assumed that a suitable Sudakov basis has been chosen, in such a way that the ρ -meson flies along the $+$ direction, while the t -channel momentum is along the $-$ and the transverse direction. In such a basis, which differs from the one used for DVCS (where no emphasis was put on the momentum of the produced photon), the virtual photon has now components along the $+$, $-$ and transverse directions.

1.4.3 Chiral-even DA

As discussed above, DAs are obtained from wave functions through $\int dl^- \int d^2\ell_\perp$ integration, and thus related to non-local correlators between fields separated by a light-like distance z (along p_2 , conjugated to the $+$ direction by Fourier transformation). The vector correlator reads [135–137]

$$\langle 0 | \bar{u}(z) \gamma_\mu d(-z) | \rho^-(P, \lambda) \rangle = f_\rho m_\rho \left[p_\mu \frac{e^{(\lambda)} \cdot z}{p \cdot z} \int_0^1 du e^{i(u-\bar{u})p \cdot z} \phi_\parallel(u, \mu_F^2) \right. \\ \left. + e_{\perp\mu}^{(\lambda)} \int_0^1 du e^{i(u-\bar{u})p \cdot z} g_\perp^{(v)}(u, \mu_F^2) - \frac{1}{2} z_\mu \frac{e^{(\lambda)} \cdot z}{(p \cdot z)^2} m_\rho^2 \int_0^1 du e^{i(u-\bar{u})p \cdot z} g_3(u, \mu_F^2) \right] \quad (1.76)$$

where ϕ_\parallel , $g_\perp^{(v)}$, g_3 are DAs respectively of twist 2, 3 and 4, with $p = p_1$, $P = p_\rho$.

Correspondingly, the axial correlator calls for the introduction of a twist 3 DA, as [135–137]

$$\langle 0 | \bar{u}(z) \gamma_\mu \gamma_5 d(-z) | \rho^-(P, \lambda) \rangle = \frac{1}{2} \left[f_\rho - f_\rho^T \frac{m_u + m_d}{m_\rho} \right] m_\rho \epsilon_\mu^{\nu\alpha\beta} e_{\perp\nu}^{(\lambda)} p_\alpha z_\beta \int_0^1 du e^{i\xi p \cdot z} g_\perp^{(a)}(u, \mu_F^2), \quad (1.77)$$

the normalization being fixed from the local limit:

$$\langle 0 | \bar{u}(0) \gamma_\mu d(0) | \rho^-(P, \lambda) \rangle = f_\rho m_\rho e_\mu^{(\lambda)}, \quad \langle 0 | \bar{u}(0) \sigma_{\mu\nu} d(0) | \rho^-(P, \lambda) \rangle = i f_\rho^T (e_\mu^{(\lambda)} P_\nu - e_\nu^{(\lambda)} P_\mu). \quad (1.78)$$

All four functions $\phi = \{\phi_{\parallel}, g_{\perp}^{(v)}, g_{\perp}^{(a)}, g_3\}$ are normalized as

$$\int_0^1 du \phi(u) = 1.$$

A simple way to understand this twist counting relies on the fact that when using an infinite momentum frame, e.g. the Breit frame (1.3), the only component of p is the $+$ component, of order Q , while $p \cdot z \sim 1$ implies that $z \sim 1/Q$. The polarization vector scales like $e^{(\lambda)} \cdot z \sim 1$ and $e_{\perp}^{(\lambda)} \sim 1$. This is enough to obtain the above indicated twist counting. From the point of view of Feynman diagrams, this can be checked by inspection when combining hard parts with the above DAs and extracting the corresponding Q -scaling. This will be explicitly illustrated in our computation of the twist 3 $\gamma^* \rightarrow \rho_T$ impact factor in Chap. 6. We refer to Ref. [138] for analogous definitions of the pseudo-scalar mesons DAs.

1.4.4 Equations of motion

Dirac equation leads to

$$\langle i(\overrightarrow{\mathcal{D}}(0)\psi(0))_{\alpha} \bar{\psi}_{\beta}(z) \rangle = 0 \quad (1.79)$$

where the covariant derivative is defined in Eq. (1.40). After applying the Fierz decomposition to 2 and 3-parton correlators, the Dirac equation implies Equations Of Motion (EOM) relating the various 2 and 3-body DAs (see Sec. 1.4.8 for the definition of 3-parton DAs), which are therefore not independent. We will rely on this method in Sec. 3.4 when dealing with factorization beyond leading twist in the Light-Cone Collinear Factorization.

In fact, another way of obtaining these equations relies on exact operator identities between non-local operators (see Refs. [105, 139, 140]). The corresponding matrix elements of the various terms arising in these identities lead to integral relations between 2 and 3 partons DAs. We refer to Ref. [136] for the use of this method.

1.4.5 Collinear conformal invariance

The use of conformal invariance in physics turn back to the beginning of XXth century, when it was noticed by Cunningham and by Bateman that Maxwell equations are conformal invariant. It was then mainly used within the context of scaling violation of quantum field theories, in particular for the study of second order phase transition, starting from the 60s. In the special case of two dimensional theories, this initiated the developpement of a whole branch of mathematical physics. In QCD, the interest for conformal invariance has been much recent, mainly starting with the study of DAs and of their evolution equations [48, 66]. We will only give here some very basic informations and refer to [141] for a comprehensive review, including the use of conformal invariance for the above mention computation of NLLQ kernels.

The full conformal group $SO(4, 2)$ is defined as transformations which only change the scale of the metric, and has 15 generators. In the limit $Q^2 \rightarrow \infty$, hadron states are replaced by a bunch of partons that are collinear to p_1 , which thus lives along p_2 , implying that z is the only remaining variable. The transformations which map the light-ray in the p_2 direction into itself is the collinear subgroup of the full conformal group $SO(4, 2)$, that is $SL(2, \mathbb{R})$, made of translations $z \rightarrow z + c$, dilatations $z \rightarrow \lambda z$ and special conformal transformations $z \rightarrow z' = z/(1 + 2az)$. The Lie algebra of $SL(2, \mathbb{R})$ is $O(2, 1)$.

In fact, starting from the full conformal group $SO(4, 2)$, there are two generators whose action on the light-ray z is a dilatation: the dilatation D and the Lorentz rotation M_{+-} leave the light-ray invariant, acting on z as dilatations. It is possible to combine these two generators in order to get an operator $i/2(D - M_{+-})$ which behaves like the identity on the p_2 axis: it is the collinear-twist operator. The remaining combination $i/2(D + M_{+-})$ combined with the generators of translations on the p_2 axis and of special conformal transformations on the p_2 axis then realize a representation of the Lie algebra of the above mentioned $SL(2, \mathbb{R})$ group. Note that another conformal symmetry appears in high-energy QCD: it is the global 2-dimensional transverse conformal symmetry of QCD in the perturbative Regge limit. In that case the group is $SL(2, \mathbb{C})$ (see Sec. 4.6.1).

Interestingly, the light-cone operators which enters the definition of DAs can be expressed in terms of a basis of conformal operators. Since conformal transformations commute with exact EOM (they are not renormalized), EOM can be solved exactly (with an expansion in terms of the conformal spin $n + 2$). For example the twist 2

DA for ρ_L can be expressed, for unpredicted $a_n^\parallel(\mu)$, as [140, 142]

$$\phi_\parallel(u, \mu_0) = 6 u \bar{u} \sum_{n=0}^{\infty} a_n^\parallel(\mu) C_n^{3/2}(u - \bar{u}) \quad C_n^{3/2} = \text{ Gegenbauer polynomial.} \quad (1.80)$$

An elementary proof of this expansion is given in the appendix B of Ref. [9] as well as in the appendix of Ref. [143]. We will recover in a pedestrian way this structure when studying Generalized Distribution Amplitudes in Sec. 2.1. The coefficients of the expansion (1.80) are not prescribed by pQCD. They can be obtained for example based on QCD sum rules [144] applied to the non-local correlators which define the DAs [145–147] or any non-perturbative approach, like the lattice [148–150]. We refer to the Ref. [151] for a very recent overview of the shape of the pion DA based on various models, which is beyond the scope of this manuscript. For a recent review of lattice results on hadronic observable, see Ref. [152].

1.4.6 Renormalization group equations

In a similar way as we have discussed above the μ_F^2 dependency for the factorization of the DVCS amplitude, the factorization (1.74) or (1.75) of the process in term of a DA, which symbolically reads

$$\mathcal{M}(Q^2) = \Phi^*(x, \mu_F^2) \otimes T_H(x, Q^2, \mu_F^2), \quad (1.81)$$

also involves an arbitrary factorization scale μ_F^2 . This arbitrariness leads to the ERBL equation [48, 65, 66] for the DA $\Phi(u, \mu_F^2)$:

$$\mu_F^2 \frac{\partial}{\partial \mu_F^2} \Phi(x, \mu_F^2) = V(x, u, \mu_F^2) \otimes \Phi(u, \mu_F^2).$$

The explicit form of the kernel can be obtained in various ways. The first point of view relies on the fact that the hard part satisfies the analogous equation

$$\mu_F^2 \frac{\partial}{\partial \mu_F^2} T_H(x, Q^2, \mu_F^2) = -V(x, u, \mu_F^2) \otimes T_H(u, Q^2, \mu_F^2).$$

based on the fact that the whole amplitude should not depend on the factorization scale. The computation of V relies on the analysis of the IR singularities of the hard part T_H , occurring when the regulator μ_F^2 vanishes. Indeed, two kinds of IR singularities may occur in QCD (or in QED): the soft singularities, and the collinear singularities. Except for the $|_+$ prescription of the obtained kernel, we will not be concerned by the first type of singularities here. These kind of singularities are responsible for BFKL dynamics at small- x , see Chap. 4. On the other hand, the collinear singularities are responsible for logarithmic contributions of the type $\alpha_s \ln Q^2/\mu_F^2$. This is the essence of the DGLAP approach for DIS structure functions, which sums up the whole series of terms like $\sum_n (\alpha_s \ln Q^2/\mu_F^2)^n$, corresponding to ladder-like diagrams in a physical gauge [66, 98]. Another point of view relies on the fact that the hard part diverges in the UV, and is therefore calling for a renormalization procedure. The introduction of an arbitrary renormalization scale μ_R^2 in order to implement this renormalization of the hard matrix element leads to renormalization group equations equivalent to Eq. (1.82), this time for the Wilson coefficients.

The renormalization group equation can be solved based on the conformal invariance discussed above in Sec. 1.4.5. Since the LLQ renormalization of the conformal operators is diagonal in the conformal spin (counterterms are tree level at this accuracy and they thus respect the conformal symmetry of the classical theory), this implies that

$$\phi_\parallel(u, \mu) = 6 u \bar{u} \sum_{n=0}^{\infty} a_n^\parallel(\mu_0) \left(\frac{\alpha_s(\mu)}{\alpha_s(\mu_0)} \right)^{2\gamma_n^{(0)}/\beta_0} C_n^{3/2}(u - \bar{u}) \xrightarrow{\mu \rightarrow \infty} 6 u \bar{u} \text{ asymptotic DA} \quad (1.82)$$

with the anomalous dimensions

$$\gamma_n^{(0)} = C_F \left(\frac{1}{2} - \frac{1}{(n+1)(n+2)} + 2 \sum_{m=2}^{n+1} \frac{1}{m} \right). \quad (1.83)$$

At NLLQ conformal symmetry is broken; studying conformal anomalies provides the NLLQ anomalous dimensions and the corresponding ERBL kernels [122–127].

A convenient choice of renormalization and factorization scale is provided by $\mu_R^2 = \mu_F^2 = Q^2$. One should however keep in mind that in any hard process, the choice of the renormalization scale μ_R^2 , although arbitrary, is of practical importance when dealing with a fixed order computation (which is always the case in practice, since no all-order are known!) and that this dependency corresponds to higher order contributions which one may want to minimize. Various approaches have been proposed in the literature: the Principle of Minimal Sensitivity (PMS) [153, 154], the principle of Fastest Apparent Convergence (FAC) [155–157] and the Brodsky-Lepage-Mackenzie (BLM) [158] scheme. We end this discussion with the fact that the doubly factorized amplitude (1.75) involves two factorization scales, which are independent and arbitrary, and that the hard part involves a renormalization scale μ_R^2 . Again, a convenient choice is to consider $\mu_{F_1}^2 = \mu_{F_2}^2 = \mu_R^2 = Q^2$. See [159] for a clear and pedagogical discussion of the rôle of the factorization and renormalization scale in hard processes (illustrated there for the pion transition form factor $F_{\gamma\pi}$).

1.4.7 Selection rules and factorization status

The selection rule for the meson electroproduction can be obtained in a simple manner. Since for a massless particle chirality = + (resp. -) helicity for a (anti)particle and based on the fact that QED and QCD vertices are chiral even (no chirality flip during the interaction), one deduces¹¹ that the total helicity of a $q\bar{q}$ pair produced by a γ^* should be 0. Therefore, the helicity of the γ^* equals the z projection of the $q\bar{q}$ angular momentum $L_z^{q\bar{q}}$. In the pure collinear limit (i.e. twist 2), the $q\bar{q}$ does not carry any angular momentum: $L_z^{q\bar{q}} = 0$. Thus the γ^* is longitudinally polarized. Additionally, at $t = 0$ there is no source of orbital momentum from the proton coupling, which implies that the helicity of the meson and of the photon should be identical. In the collinear factorization approach, the extension to $t \neq 0$ changes nothing from the hard part side, as we have seen above in our description of the factorization theorem, the only dependence with respect to t being encoded in the non-perturbative correlator which defines the GPDs. This implies that the above selection rule remains true. Thus, only 2 transitions are possible (this is the so-called s -channel helicity conservation (SCHC)): $\gamma_L^* \rightarrow \rho_L$, for which QCD factorization holds at $t=2$ at any order (i.e. LL, NLL, etc...) [52] and $\gamma_T^* \rightarrow \rho_T$, corresponding to twist $t = 3$ at the amplitude level, for which QCD factorization is not proven. In fact an explicit computation of the ρ_T electroproduction [160] at leading order shows that the hard part has *end-point singularities* like

$$\int_0^1 \frac{du}{u} \quad \text{and} \quad \int_0^1 \frac{du}{1-u} \quad (1.84)$$

occurring when the momentum fraction carried by the quark or the anti-quark vanishes.

1.4.8 Some solutions to factorization breaking?

In order to extend the factorization theorem at higher twist, as well as to improve the phenomenological description of hard exclusive processes at moderate values of the hard scale, several solutions have been proposed.

DAs with higher number of partons

One may add contributions of 3-parton DAs [136, 137] for ρ_T [161, 162] (of dominant twist equal 3 for ρ_T). Denoting the field strength by $G_{\mu\nu} = \partial_\mu A_\nu - \partial_\nu A_\mu - g[A_\mu, A_\nu]$, the chiral-even three-particle DAs of ρ reads [136, 137]

$$\begin{aligned} \langle 0 | \bar{u}(z) g \tilde{G}_{\mu\nu}(vz) \gamma_\alpha \gamma_5 d(-z) | \rho^-(P, \lambda) \rangle &= f_{3\rho}^A m_\rho p_\alpha [p_\nu e_{\perp\mu}^{(\lambda)} - p_\mu e_{\perp\nu}^{(\lambda)}] \mathcal{A}(v, pz) \\ + f_{3\rho}^A m_\rho^3 \frac{e^{(\lambda)} \cdot z}{pz} [p_\mu g_{\alpha\nu}^\perp - p_\nu g_{\alpha\mu}^\perp] \tilde{\Phi}(v, pz) &+ f_{3\rho}^A m_\rho^3 \frac{e^{(\lambda)} \cdot z}{(pz)^2} p_\alpha [p_\mu z_\nu - p_\nu z_\mu] \tilde{\Psi}(v, pz) \end{aligned} \quad (1.85)$$

¹¹This is the same reason which explains the vanishing of F_L in DIS.

and

$$\begin{aligned} \langle 0 | \bar{u}(z) g G_{\mu\nu}(vz) i\gamma_\alpha d(-z) | \rho^-(P) \rangle &= f_{3\rho}^V m_\rho p_\alpha [p_\nu e_{\perp\mu}^{(\lambda)} - p_\mu e_{\perp\nu}^{(\lambda)}] \mathcal{V}(v, pz) \\ &+ f_{3\rho}^V m_\rho^3 \frac{e^{(\lambda)} \cdot z}{pz} [p_\mu g_{\alpha\nu}^\perp - p_\nu g_{\alpha\mu}^\perp] \Phi(v, pz) + f_{3\rho}^V m_\rho^3 \frac{e^{(\lambda)} \cdot z}{(pz)^2} p_\alpha [p_\mu z_\nu - p_\nu z_\mu] \Psi(v, pz). \end{aligned} \quad (1.86)$$

Among these DA, \mathcal{A} and \mathcal{V} contribute to twist 3 while $\tilde{\Phi}$, $\tilde{\Psi}$, Φ , Ψ contribute to twist 4. Note that we use here the usual notation when dealing with the Fourier transform

$$\mathcal{A}(v, pz) = \int D\alpha e^{-ipz(\alpha_u - \alpha_d + v\alpha_g)} A(\underline{\alpha})$$

and similarly for \mathcal{V} . $\underline{\alpha}$ is the set of three momentum fractions: $\underline{\alpha} = \{\alpha_d, \alpha_u, \alpha_g\}$ The integration measure is defined as

$$\int D\underline{\alpha} \equiv \int_0^1 d\alpha_d \int_0^1 d\alpha_u \int_0^1 d\alpha_g \delta(1 - \sum \alpha_i). \quad (1.87)$$

This in fact does not solve the problem, while reducing the level of divergency, but is needed for consistency.

Sudakov resummation and Improved Collinear Approximation

On top of the potential end-point singularities discussed above, phenomenologically the use of simple asymptotical DAs lead usually to a too small ERL contribution in hard exclusive processes, a situation which is not improved by NLO corrections. It was suggested by Chernyak and Zhitnitsky [9] to use DAs which would be mostly concentrated close to the end point, and not identical to the asymptotical DA, a solution which indeed improve very much the description of the data, for example of the pion form factor. However, since close to the end-point one may face theoretical inconsistencies when justifying the factorization, Li and Sterman [163] then introduced an Improved Collinear Approximation (ICA). They suggested to keep a transverse ℓ_\perp dependency in the q , \bar{q} momenta. Soft and collinear gluon exchange between the valence quarks are responsible for large double-logarithmic effects which exponentiate. The corresponding study is made easier when using the impact parameter space b_\perp conjugated to ℓ_\perp , leading to the Sudakov factor

$$\exp[-S(u, b, Q)], \quad (1.88)$$

a factor already involved in previous studies of elastic hadron-hadron scattering at fixed angle [164]. S diverges when $b_\perp \sim O(1/\Lambda_{QCD})$ (large transverse separation, i.e. small transverse momenta) or small fraction $u \sim O(\Lambda_{QCD}/Q)$. This thus regularizes potential end-point singularities, even when using non asymptotical DAs. See Ref. [165] for a detailed and pedagogical discussion in the case of the $\gamma\gamma^* \rightarrow \pi^0$ form factors. These Sudakov effects have been implemented outside of pure QCD processes, in particular for the study of semi-leptonic $B \rightarrow \pi$ decay [166]. In this ICA, a dependency of the hard part with respect to the partons transverse momenta is kept. This suggested Jakob and Kroll to keep such a dependency also inside the wave function of the produced meson. This was implemented in the form of a an ad-hoc non-perturbative gaussian ansatz [167]

$$\exp[-a^2 |k_\perp^2| / (u\bar{u})], \quad (1.89)$$

and other similar ansätze, which give back the usual asymptotic DA $6u\bar{u}$ when integrating over k_\perp . These gaussian ansätze combined with the perturbative Sudakov resummation tail effect were then implemented for various phenomenological studies like the pion form factor [167], the meson-photon form factor [168, 169]. The phenomenological description of the pion form factor is then improved, but is still below the data, even with the Chernyak and Zhitnitsky model. For other observables for which one really faces a end-point singularity, like the above example of ρ_T -electroproduction, the same approach seems to allow for a consistent treatment, and at least to interesting models [170–173] which can describe the meson electroproduction data, in particular the HERA data at small- x_{Bj} which will be discussed in Sec. 5.2.4.

We will see in Chap. 6 that at small x_{Bj} , relying on the k_T -factorization, the off-mass-shellness of the t -channel gluons can serve as a regulator, preventing from facing end-point singularities.

1.4.9 Chiral-odd sector

The \pm chiralities are defined by the decomposition

$$q_{\pm}(z) \equiv \frac{1}{2}(1 \pm \gamma^5)q(z) \quad \text{with} \quad q(z) = q_+(z) + q_-(z), \quad (1.90)$$

implying that

$$\bar{q}_{\pm}(z)\gamma^{\mu}q_{\pm}(-z) \quad \text{or} \quad \bar{q}_{\pm}(z)\gamma^{\mu}\gamma^5q_{\pm}(-z) \quad (1.91)$$

conserve chirality (chiral-even) while

$$\bar{q}_{\pm}(z) \cdot 1 \cdot q_{\mp}(-z), \quad \bar{q}_{\pm}(z) \cdot \gamma^5 \cdot q_{\mp}(-z) \quad \text{or} \quad \bar{q}_{\pm}(z)[\gamma^{\mu}, \gamma^{\nu}]q_{\mp}(-z) \quad (1.92)$$

change chirality (chiral-odd). The production of a transverse ρ is dominated by its twist 2 chiral-odd DA, as expected from the selection rule of Sec. 1.4.7. Defining as usual

$$\sigma_{\mu\nu} \equiv \frac{i}{2}[\gamma_{\mu}, \gamma_{\nu}], \quad (1.93)$$

the chiral-odd ρ -DAs read [135–137]

$$\begin{aligned} \langle 0|\bar{u}(z)\sigma_{\mu\nu}d(-z)|\rho^-(P, \lambda)\rangle &= if_{\rho}^T \left[(e_{\perp\mu}^{(\lambda)}p_{\nu} - e_{\perp\nu}^{(\lambda)}p_{\mu}) \int_0^1 du e^{i(2u-1)p \cdot z} \phi_{\perp}(u, \mu^2) \right. \\ &+ (p_{\mu}z_{\nu} - p_{\nu}z_{\mu}) \frac{e^{(\lambda)} \cdot z}{(p \cdot z)^2} m_{\rho}^2 \int_0^1 du e^{i(2u-1)p \cdot z} h_{\parallel}^{(t)}(u, \mu^2) + \frac{1}{2}(e_{\perp\mu}^{(\lambda)}z_{\nu} - e_{\perp\nu}^{(\lambda)}z_{\mu}) \frac{m_{\rho}^2}{p \cdot z} \int_0^1 du e^{i(2u-1)p \cdot z} h_3(u, \mu^2) \left. \right] \end{aligned} \quad (1.94)$$

and

$$\langle 0|\bar{u}(z)d(-z)|\rho^-(P, \lambda)\rangle = -i \left(f_{\rho}^T - f_{\rho} \frac{m_u + m_d}{m_{\rho}} \right) (e^{(\lambda)} \cdot z) m_{\rho}^2 \int_0^1 du e^{i(2u-1)p \cdot z} h_{\parallel}^{(s)}(u, \mu^2). \quad (1.95)$$

The DA ϕ_{\perp} of ρ_T is of twist-2, while $h_{\parallel}^{(s)}$ and $h_{\parallel}^{(t)}$ of ρ_L are twist-3. Finally, h_3 of ρ_T is of twist-4. These DAs $\phi = \{\phi_{\perp}, h_{\parallel}^{(s)}, h_{\parallel}^{(t)}, h_3\}$ are normalized to $\int_0^1 du \phi(u) = 1$.

The 3-partons chiral-odd reads (we refer to Refs. [136, 137] for complete formula)

$$\begin{aligned} \langle 0|\bar{u}(z)\sigma_{\alpha\beta}gG_{\mu\nu}(vz)d(-z)|\rho^-(P, \lambda)\rangle \\ = f_{\rho}^T m_{\rho}^2 \frac{e^{(\lambda)} \cdot z}{2(p \cdot z)} [p_{\alpha}p_{\mu}g_{\beta\nu}^{\perp} - p_{\beta}p_{\mu}g_{\alpha\nu}^{\perp} - p_{\alpha}p_{\nu}g_{\beta\mu}^{\perp} + p_{\beta}p_{\nu}g_{\alpha\mu}^{\perp}] \mathcal{T}(v, pz) + 4 \text{ DAs involving } \rho_T \end{aligned} \quad (1.96)$$

where \mathcal{T} of ρ_L is of twist 3 while the 4 DA of ρ_T are of twist 4. Other 3-partons DAs are defined through the remaining 3-partons correlators as

$$\begin{aligned} \langle 0|\bar{u}(z)gG_{\mu\nu}(vz)d(-z)|\rho^-(P, \lambda)\rangle &= if_{\rho}^T m_{\rho}^2 [e_{\perp\mu}^{(\lambda)}p_{\nu} - e_{\perp\nu}^{(\lambda)}p_{\mu}] S(v, pz) \\ \langle 0|\bar{u}(z)ig\tilde{G}_{\mu\nu}(vz)\gamma_5d(-z)|\rho^-(P, \lambda)\rangle &= if_{\rho}^T m_{\rho}^2 [e_{\perp\mu}^{(\lambda)}p_{\nu} - e_{\perp\nu}^{(\lambda)}p_{\mu}] \tilde{S}(v, pz) \end{aligned} \quad (1.97)$$

where S and \tilde{S} of ρ_T are of twist 4.

1.5 Measurement of helicity-flip GPDs through a non-zero mixture of chiral-odd GPDs with chiral-odd ρ -meson

Based on [W26], to be submitted. See [W57] for a preliminary version as conference proceedings.

Transversity quark distributions in the nucleon remain among the most unknown leading twist hadronic observables. This is mostly due to their chiral odd character which enforces their decoupling in most hard

amplitudes. As we shortly reviewed in Sec. 1.3.2, after the pioneering studies [85–87,89], much work [83,84,174] has been devoted to the exploration of many channels but experimental difficulties have challenged the most promising ones.

Access to the chiral-odd transversity generalized parton distributions [81], noted H_T , E_T , \tilde{H}_T , \tilde{E}_T (see Sec. 1.3.1), has however turned out to be even more challenging [175,176] than the usual transversity distributions : one photon or one meson electroproduction leading twist amplitudes are insensitive to transversity GPDs. Indeed, since QED and QCD are chiral even, chiral-odd objects can only appear in pairs. The amplitude of ρ_T electroproduction on linearly polarized N vanishes at leading twist 2, as illustrated in Fig. 1.10 at Born order [175]: a single gluon exchange between hard lines is not enough to prevent the vanishing of the Dirac trace $\gamma^\alpha [\gamma^\mu, \gamma^\nu] \gamma_\alpha = 0$. This vanishing remains valid at all order [176].

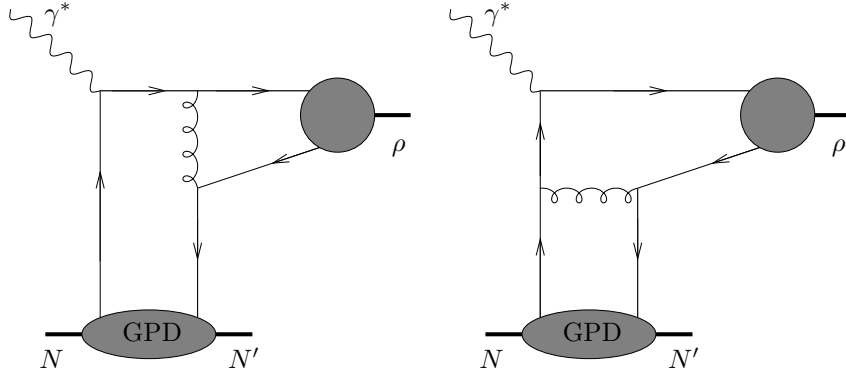


Figure 1.10: Two contributions to the amplitude of hard ρ_T -electroproduction at Born order.

A possible way out is to consider higher twist contributions to these amplitudes [177,178], which however are beyond the factorization proofs and often plagued with end-point singularities. The strategy which we follow here, as initiated in Refs. [179,180], is to study the leading twist contribution to processes where more mesons are present in the final state; the hard scale which allows to probe the short distance structure of the nucleon is now the invariant mass of the meson pair, related to the large transverse momentum transmitted to each final meson. In the example developed previously [179,180], the process under study was the high energy photo(or electro) diffractive production of two vector mesons, the hard probe being the virtual "Pomeron" exchange (and the hard scale was the virtuality of this pomeron), in analogy with the virtual photon exchange occurring in the deep electroproduction of a meson. A similar strategy has also been advocated recently in Ref. [181] to enlarge the number of processes which could be used to extract information on chiral-even GPDs.

The process we study here

$$\gamma + N \rightarrow \pi^+ + \rho_T^0 + N', \quad (1.98)$$

is a priori sensitive to chiral-odd GPDs because of the chiral-odd character of the leading twist distribution amplitude of the transversally polarized ρ meson. Its detailed study should not present major difficulties to modern detectors such as those developed for the 12 GeV upgrade of Jlab or for the Compass experiment at CERN. The estimated rate depends of course much on the magnitude of the chiral-odd generalized parton distributions. Not much is known about them, but model calculations have been developed in [180] for the ERBL part and in Refs. [182–186]; moreover, a few moments have been computed on the lattice [187,188]. To supplement this and use the recent phenomenological knowledge acquired on the transversity quark distributions through single inclusive deep inelastic data, we will propose a parametrization of the (dominant) transversity GPD H_T^q based on the concept of double distributions.

Let us now explain how we factorize the amplitude of this process and what is the rationale of this extension of the existing factorization proofs in the framework of QCD. The basis of our argument is two-folded.

- We use the now classical proof of the factorization of exclusive scattering at fixed angle and large energy [133], on which we briefly commented in Sec. 1.1. The amplitude for the process $\gamma + \pi \rightarrow \pi + \rho$ is written as the convolution of mesonic distribution amplitudes and a hard scattering subprocess amplitude $\gamma + (q + \bar{q}) \rightarrow (q + \bar{q}) + (q + \bar{q})$ with the meson states replaced by collinear quark-antiquark pairs. This is

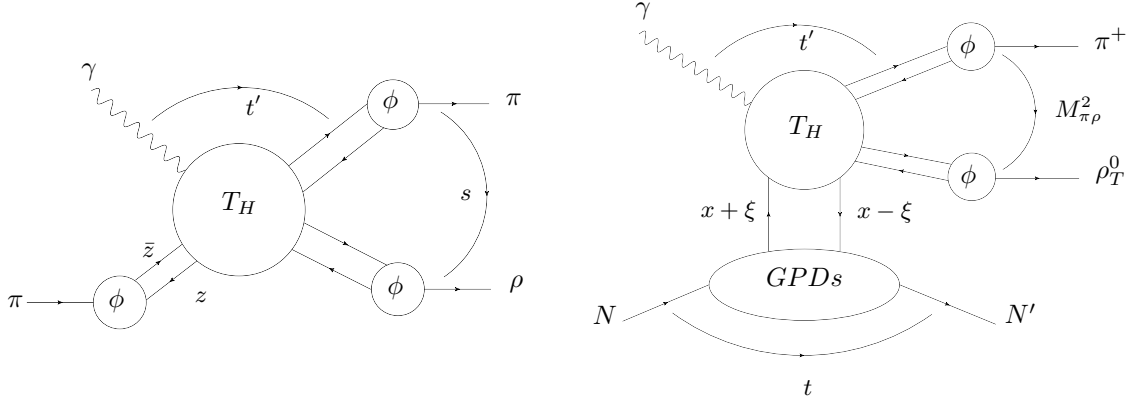


Figure 1.11: a (left): Factorization of the amplitude for the process $\gamma + \pi \rightarrow \pi + \rho$ at large s and fixed angle (i.e. fixed ratio t'/s); b (right): replacing one DA by a GPD leads to the factorization of the amplitude for $\gamma + N \rightarrow \pi + \rho + N'$ at large $M_{\pi\rho}^2$.

described in Fig. 1.11a. The absence of any pinch singularities (which is the weak point of the proof for the generic case $A + B \rightarrow C + D$) has been proven in the case of interest here [19].

- We extract from the factorization procedure of the deeply virtual Compton scattering amplitude near the forward region the right to replace in Fig. 1.11a the lower left meson distribution amplitude by a $N \rightarrow N'$ GPD, and thus get Fig. 1.11b. Indeed the same collinear factorization property bases the validity of the leading twist approximation which either replaces the meson wave function by its distribution amplitude or the $N \rightarrow N'$ transition to its GPDs. A slight difference is that light cone fractions ($z, 1 - z$) leaving the DA are positive, but the corresponding fractions ($x + \xi, \xi - x$) may be positive or negative in the case of the GPD. The calculation will show that this difference does not ruin the factorization property, at least at the order that we are working here.

One may adopt another point of view based on an analogy with the timelike Compton scattering

$$\gamma N \rightarrow \gamma^* N' \rightarrow \mu^+ \mu^- N', \quad (1.99)$$

where the lepton pair has a large squared invariant mass Q^2 , is instructive. This process has been thoroughly discussed [72, 189] in the framework of the factorization of GPDs, and it has been proven that its amplitude was quite similar to the deeply virtual Compton scattering one, being dominated at lowest order by the handbag diagram amplitude convoluted with generalized quark distributions in the nucleon. There is no ambiguity in this case for the definition of the hard scale, the photon virtuality Q being the only scale present. Although the meson pair in process (1.98) has a more complex momentum flow, we feel justified to draw on this analogy to ascribe the role of the hard scale to the meson pair invariant squared mass. However, to describe the final state mesons by their distribution amplitudes (DAs), one needs in addition a large transverse momentum (and thus large Mandelstam t' , see Fig. 1.11b). Practically, we consider kinematics in which $|u'| \sim |t'| \sim |p_T^2| \sim M_{\pi\rho}^2$. We cannot prove, at the level of our study, that $M_{\pi\rho}^2$ is the most adequate hard scale. Indeed, applying a definite strategy to define a factorization scale requires at least a next to leading (in the strong coupling) analysis [W14, 190] and this is clearly a major work to be undertaken.

For both point of view, in order for the factorization of a partonic amplitude to be valid, and the leading twist calculation to be sufficient, one should avoid the dangerous kinematical regions where a small momentum transfer is exchanged in the upper blob, namely small $t' = (p_\pi - p_\gamma)^2$ or small $u' = (p_\rho - p_\gamma)^2$, and the regions where strong interactions between two hadrons in the final state are non-perturbative, namely where one of the invariant masses $(p_\pi + p_{N'})^2, (p_\rho + p_{N'})^2, (p_\pi + p_\rho)^2$ is in the resonance region. We will discuss the necessary minimal cuts to be applied to data before any attempt to extract the chiral odd GPDs. However, although the ultimate proof of the validity of the factorization scheme proposed in this paper is based on comparison of the predictions with experimental data, on the theoretical side it requires to go beyond Born approximation considered here which is beyond the scope of the present work.

In this study, we will concentrate and provide results on the unpolarized differential cross section in the kinematics of two specific experiments : Hall A/B and Hall D at JLab where $S_{\gamma N} \sim 20 \text{ GeV}^2$ and Compass at CERN where $S_{\gamma N} \sim 200 \text{ GeV}^2$

As a final remark in this introduction, let us stress that our discussion applies as well to the case of electroproduction where a moderate virtuality of the initial photon may help to access the perturbative domain with a lower value of the hard scale $M_{\pi\rho}$. It is only a matter of further technical complications to extend our computation to that cas.

1.5.1 Kinematics

We study the exclusive photoproduction of a transversely polarized vector meson and a pion on a polarized or unpolarized proton target

$$\gamma(q) + N(p_1, \lambda) \rightarrow \pi(p_\pi) + \rho_T(p_\rho) + N'(p_2, \lambda'), \quad (1.100)$$

in the kinematical regime of large invariant mass $M_{\pi\rho}$ of the final meson pair and small momentum transfer $t = (p_1 - p_2)^2$ between the initial and the final nucleons. Roughly speaking, these kinematics mean a moderate to large, and approximately opposite, transverse momentum of each meson. Our conventions are the following. We decompose momenta on a Sudakov basis as ¹²

$$k^\mu = a n^\mu + b p^\mu + k_\perp^\mu, \quad (1.101)$$

with p and n the light-cone vectors

$$p^\mu = \frac{\sqrt{s}}{2}(1, 0, 0, 1) \quad n^\mu = \frac{\sqrt{s}}{2}(1, 0, 0, -1) \quad p \cdot n = \frac{s}{2}, \quad (1.102)$$

and

$$k_\perp^\mu = (0, k^x, k^y, 0), \quad k_\perp^2 = -\vec{k}_t^2. \quad (1.103)$$

The particle momenta read

$$p_1^\mu = (1 + \xi) p^\mu + \frac{M^2}{s(1 + \xi)} n^\mu, \quad p_2^\mu = (1 - \xi) p^\mu + \frac{M^2 + \vec{\Delta}_t^2}{s(1 - \xi)} n^\mu + \Delta_\perp^\mu, \quad q^\mu = n^\mu, \quad (1.104)$$

$$\begin{aligned} p_\pi^\mu &= \alpha n^\mu + \frac{(\vec{p}_t - \vec{\Delta}_t/2)^2 + m_\pi^2}{\alpha s} p^\mu + p_\perp^\mu - \frac{\Delta_\perp^\mu}{2}, \\ p_\rho^\mu &= \alpha_\rho n^\mu + \frac{(\vec{p}_t + \vec{\Delta}_t/2)^2 + m_\rho^2}{\alpha_\rho s} p^\mu - p_\perp^\mu - \frac{\Delta_\perp^\mu}{2}, \end{aligned} \quad (1.105)$$

with $\bar{\alpha} = 1 - \alpha$ and M, m_π, m_ρ the masses of the nucleon, the pion and the ρ meson. From these kinematical relations it follows

$$2\xi = \frac{(\vec{p}_t - \frac{1}{2}\vec{\Delta}_t)^2 + m_\pi^2}{s\alpha} + \frac{(\vec{p}_t + \frac{1}{2}\vec{\Delta}_t)^2 + m_\rho^2}{s\alpha_\rho} \quad (1.106)$$

and

$$1 - \alpha - \alpha_\rho = \frac{2\xi M^2}{s(1 - \xi^2)} + \frac{\vec{\Delta}_t^2}{s(1 - \xi)}. \quad (1.107)$$

The total center-of-mass energy squared of the γ -N system is

$$S_{\gamma N} = (q + p_1)^2 = (1 + \xi)s + M^2. \quad (1.108)$$

¹²The convention used here differs from other chapters. The momentum of the nucleon is along the + direction, while the photon has a momentum along - direction. We here denote as \vec{k}_t any euclidian two-dimensional vector.

ξ is the skewness parameter which can be written in terms of the τ variable used in lepton pair production, as

$$\xi = \frac{\tau}{2 - \tau} \quad , \quad \tau = \frac{M_{\pi\rho}^2 - t}{S_{\gamma N} - M^2} . \quad (1.109)$$

On the nucleon side, the transferred squared momentum is

$$t = (p_2 - p_1)^2 = -\frac{1 + \xi}{1 - \xi} \vec{\Delta}_t^2 - \frac{4\xi^2 M^2}{1 - \xi^2} . \quad (1.110)$$

The other various Mandelstam invariants read

$$s' = (p_\pi + p_\rho)^2 = M_{\pi\rho}^2 = 2\xi s \left(1 - \frac{2\xi M^2}{s(1 - \xi^2)} \right) - \vec{\Delta}_t^2 \frac{1 + \xi}{1 - \xi} , \quad (1.111)$$

$$-t' = -(p_\pi - q)^2 = \frac{(\vec{p}_t - \vec{\Delta}_t/2)^2 + \bar{\alpha} m_\pi^2}{\alpha} , \quad (1.112)$$

$$-u' = -(p_\rho - q)^2 = \frac{(\vec{p}_t + \vec{\Delta}_t/2)^2 + (1 - \alpha_\rho) m_\rho^2}{\alpha_\rho} .$$

and

$$M_{\pi N'}^2 = s \left(1 - \xi + \frac{(\vec{p}_t - \vec{\Delta}_t/2)^2 + m_\pi^2}{s\alpha} \right) \left(\alpha + \frac{M^2 + \vec{\Delta}_t^2}{s(1 - \xi)} \right) - \left(\vec{p}_t + \frac{1}{2} \vec{\Delta}_t \right)^2 , \quad (1.113)$$

$$M_{\rho N'}^2 = s \left(1 - \xi + \frac{(\vec{p}_t + \vec{\Delta}_t/2)^2 + m_\rho^2}{s\alpha_\rho} \right) \left(\alpha_\rho + \frac{M^2 + \vec{\Delta}_t^2}{s(1 - \xi)} \right) - \left(\vec{p}_t - \frac{1}{2} \vec{\Delta}_t \right)^2 . \quad (1.114)$$

The hard scale $M_{\pi\rho}^2$ is the invariant squared mass of the (π^+, ρ^0) system. The leading twist calculation of the hard part only involves the approximated kinematics in the generalized Bjorken limit: neglecting $\vec{\Delta}_\perp$ in front of \vec{p}_\perp as well as hadronic masses, it amounts to

$$M_{\pi\rho}^2 \approx \frac{\vec{p}_t^2}{\alpha \bar{\alpha}} . \quad (1.115)$$

$$\alpha_\rho \approx 1 - \alpha \equiv \bar{\alpha} \quad (1.116)$$

$$\tau \approx \frac{M_{\pi\rho}^2}{S_{\gamma N} - M^2} \quad (1.117)$$

$$-t' \approx \bar{\alpha} M_{\pi\rho}^2 \quad \text{and} \quad -u' \approx \alpha M_{\pi\rho}^2 . \quad (1.118)$$

The typical cuts that one should apply are $-t', -u' > \Lambda^2$ and $M_{\pi N'}^2 = (p_\pi + p_{N'})^2 > M_R^2$, $M_{\rho N'}^2 = (p_\rho + p_{N'})^2 > M_R^2$ where $\Lambda \gg \Lambda_{QCD}$ and M_R is a typical baryonic resonance mass. This amounts to cuts in α and $\bar{\alpha}$ at fixed $M_{\pi\rho}^2$, which are easily translated in terms of u' at fixed $M_{\pi\rho}^2$. These conditions boil down to a safe kinematical domain $(-u')_{min} \leq -u' \leq (-u')_{max}$ which we will discuss in more details in Section 5.

The squared invariant masses (1.113) and (1.114) can be approximated when neglecting m_π^2 , m_ρ^2 and $\vec{\Delta}_t^2$ by

$$M_{\pi N'}^2 \approx s \alpha (1 - \xi) - \vec{p}_t \cdot \vec{\Delta}_t + M^2 . \quad (1.119)$$

and

$$M_{\rho N'}^2 \approx s \bar{\alpha} (1 - \xi) + \vec{p}_t \cdot \vec{\Delta}_t + M^2 . \quad (1.120)$$

The lowest value of $M_{\pi N'}^2$ is obtained when \vec{p}_t and $\vec{\Delta}_t$ are parallel, and can be estimated as a function of u' as

$$M_{\pi N'}^2 \gtrsim -u' \left[\frac{S_{\gamma N}}{M_{\pi\rho}^2} \frac{1 - \xi}{1 + \xi} - 2 \frac{|\vec{\Delta}_t|}{|\vec{p}_t|} \right] + M^2 , \quad (1.121)$$

and a similar equation for $M_{\rho N'}^2$. One can show that this relation (and the similar one for $M_{\pi N'}^2$) implies that the absence of resonance is automatically satisfied in the region of phase space which dominates the cross-section, as soon as the constraints on u' and t' in order to have factorization are satisfied.

In the following, we will choose as kinematical independent variables $t, u', M_{\pi\rho}^2$.

1.5.2 The Scattering Amplitude

We now concentrate on the specific process

$$\gamma(q) + p(p_1, \lambda) \rightarrow \pi^+(p_\pi) + \rho_T^0(p_\rho) + n(p_2, \lambda'). \quad (1.122)$$

Let us start by recalling the non-perturbative quantities which enter the scattering amplitude of our process (1.122). The transversity generalized parton distribution of a parton q (here $q = u, d$) in the nucleon target at zero momentum transfer is defined, in agreement with Eq. (1.44), by

$$\begin{aligned} & \langle n(p_2), \lambda' | \bar{d} \left(-\frac{y}{2} \right) \sigma^{+j} \gamma^5 u \left(\frac{y}{2} \right) | p(p_1), \lambda \rangle \\ &= \bar{u}(p_2, \lambda') \sigma^{+j} \gamma^5 u(p_1, \lambda) \int_{-1}^1 dx e^{-\frac{i}{2}x(p_1^+ + p_2^+)y^-} H_T^{ud}(x, \xi, t), \end{aligned} \quad (1.123)$$

where λ and λ' are the light-cone helicities of the nucleons p and n . Here H_T^{ud} is the flavor non-diagonal GPD [191] which can be expressed in terms of diagonal ones as

$$H_T^{ud} = H_T^u - H_T^d. \quad (1.124)$$

The chiral-odd light-cone DA for the transversely polarized meson vector ρ_T^0 , is defined, in leading twist 2, by the matrix element (1.94) which reads here, for the ρ^0 ,

$$\langle 0 | \bar{u}(0) \sigma^{\mu\nu} u(x) | \rho^0(p, \epsilon_\pm) \rangle = \frac{i}{\sqrt{2}} (\epsilon_\pm^\mu(p) p^\nu - \epsilon_\pm^\nu(p) p^\mu) f_\rho^\perp \int_0^1 du e^{-iup \cdot x} \phi_\perp(u) \quad (1.125)$$

where $\epsilon_\pm^\mu(p_\rho)$ is the ρ -meson transverse polarization and with $f_\rho^\perp = 160$ MeV.

The light-cone DA for the pion π^+ is defined, in leading twist 2, by the matrix element (see for example [138])

$$\langle 0 | \bar{d}(z) \gamma^\mu \gamma^5 u(-z) | \pi^+(p) \rangle = ip^\mu f_\pi \int_0^1 du e^{-i(2u-1)p \cdot z} \phi_\pi(u) \quad (1.126)$$

with $f_\pi = 131$ MeV. In our calculations, we use the asymptotic form of these DAs : $\phi_\pi(u) = \phi_\perp(u) = 6u\bar{u}$.

We now pass to the computation of the scattering amplitude of the process (1.122). As the order of magnitude of the hard scale is greater than GeV^2 , it is possible to study it in the framework of QCD factorization, where the invariant squared mass of the (π^+, ρ^0) system $M_{\pi\rho}^2$ is taken as the factorization scale.

The amplitude gets contributions from each $E_T, H_T, \tilde{E}_T, \tilde{H}_T$. However, all of them but H_T are accompanied by kinematical factors which vanish at $\vec{\Delta}_t = 0$. The contribution proportional to H_T is thus dominant in the small t domain which we are interested in. We will thus restrict our study to this contribution, so that the whole t -dependence will come from the t -dependence of H_T , as we model in Sec. 1.5.3. The interesting extension of considering each of the four transversity GPDs - in particular with respect to the impact picture of the parton content of the nucleon [192–197] - is left for further work.

Note that within the collinear framework, the hard part is computed with $\vec{\Delta}_t = 0$.

Thus we write the scattering amplitude of the process (1.122) in the factorized form :

$$\mathcal{A}(t, M_{\pi\rho}^2, p_T) = \frac{1}{\sqrt{2}} \int_{-1}^1 dx \int_0^1 dv \int_0^1 dz (T^u(x, v, z) - T^d(x, v, z)) H_T^{ud}(x, \xi, t) \Phi_\pi(z) \Phi_\perp(v), \quad (1.127)$$

where T^u and T^d are the hard parts of the amplitude where the photon couples respectively to a u -quark (Fig. 1.12a) and to a d -quark (Fig. 1.12b). This decomposition, with the $\frac{1}{\sqrt{2}}$ prefactor, takes already into account that the ρ^0 -meson is described as $\frac{u\bar{u} - d\bar{d}}{\sqrt{2}}$.

For this process, one has two kinds of Feynman diagrams: some without (Fig. 1.12) and some with a 3-gluon vertex (Fig. 1.13). In both cases, an interesting symmetry allows to deduce the contribution of some diagrams from other ones. This is exemplified in Fig. 1.12. The transformation rules

$$x \rightarrow -x \quad u \rightarrow \bar{u} \quad v \rightarrow \bar{v} \quad e_u \rightarrow e_d \quad (1.128)$$

1.5. MEASUREMENT OF HELICITY-FLIP GPDs THROUGH A NON-ZERO MIXTURE OF CHIRAL-ODD GPDs WITH

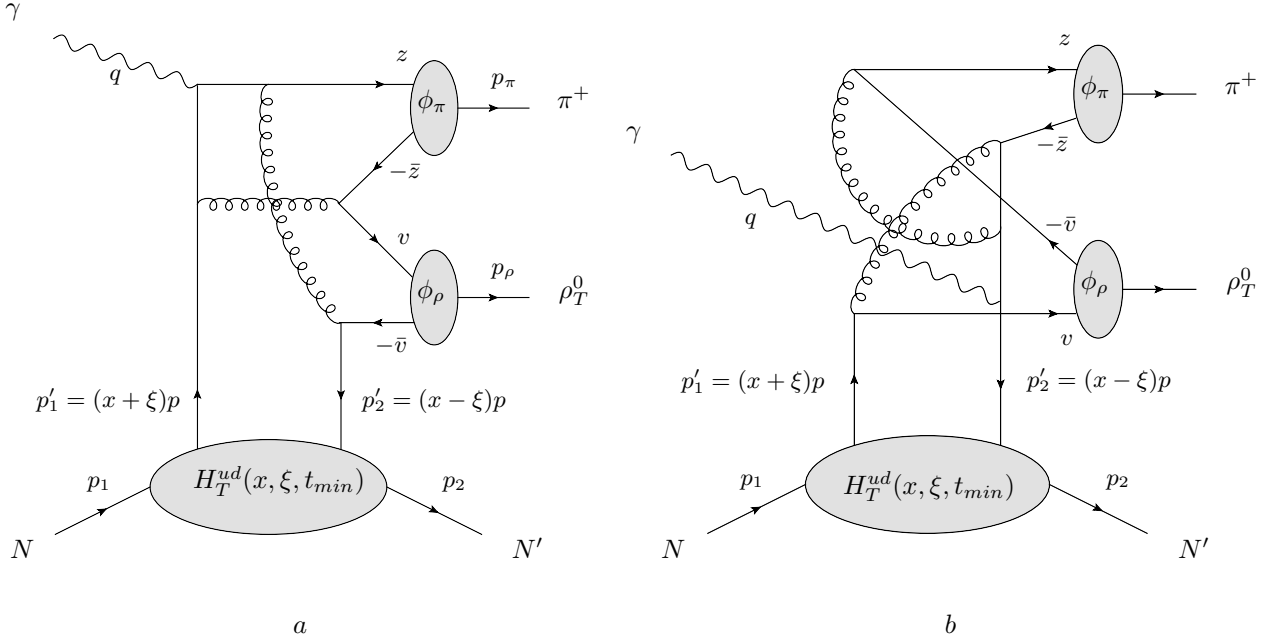


Figure 1.12: Two representative diagrams with a photon u -quark coupling (a) and with a photon d -quark coupling (b).

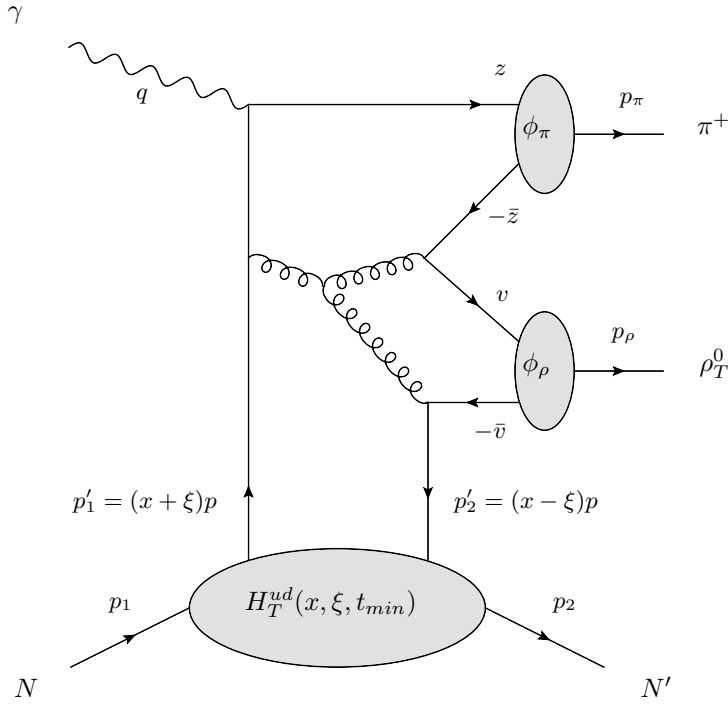


Figure 1.13: Representative diagram with a 3 gluon vertex.

relate the hard amplitude of Fig. 1.12b to the one of Fig. 1.12a. This reduces our task to the calculation of half the 62 diagrams involved in the process.

Let us sketch the main steps of the calculation on the specific example of the diagram of Fig.1.12a, in the

Feynman gauge. Using the usual notation $\not{k} = k_\mu \gamma^\mu$, the amplitude reads:

$$\begin{aligned} T_{2a}^u(x, v, z) &= Tr[(if_\pi \not{p}_\pi \gamma^5)(-ig\gamma^\mu)\not{F}(p'_2 + \bar{v}p_\rho + zp_\pi)(ie_u \not{\epsilon}(q))\not{F}(p'_1 - vp_\rho - \bar{z}p_\pi) \\ &\quad (-ig\gamma^\nu)(\sigma^{\alpha\beta} \gamma^5)(-ig\gamma_\mu)(2i\sigma^{\sigma\rho p_\rho} f_\rho^\perp)(-ig\gamma_\nu)] \\ &\times Tr_C[t^a t^b t^a t^b] \frac{1}{(8N_c)^2} \frac{1}{4N_c} G(p'_2 + \bar{v}p_\rho) G(vp_\rho + \bar{z}p_\pi), \end{aligned} \quad (1.129)$$

where the fermion propagator is (we put all quark masses to zero) :

$$i\not{F}(k) = \frac{i\not{k}}{k^2 + i\epsilon}, \quad (1.130)$$

and

$$-ig^{\mu\nu} G(k) = \frac{-ig^{\mu\nu}}{k^2 + i\epsilon} \quad (1.131)$$

is the gluonic propagator. Tr_C is the trace over color indices and the factors $\frac{1}{(8N_c)^2}$ and $\frac{1}{4N_c}$ come from Fierz decompositions. The corresponding expression for the diagram 1.12b

$$\begin{aligned} T_{2b}^d(x, v, z) &= Tr[(if_\pi \not{p}_\pi \gamma^5)(-ig\gamma^\mu)(2i\sigma^{\sigma\rho p_\rho} f_\rho^\perp)(-ig\gamma^\nu)(\sigma^{\alpha\beta} \gamma^5) \\ &\quad (-ig\gamma_\mu)\not{F}(p'_2 + \bar{v}p_\rho + zp_\pi)(ie_d \not{\epsilon}(q))\not{F}(p'_1 - vp_\rho - \bar{z}p_\pi)(-ig\gamma_\nu)] \\ &\times Tr_C[t^a t^b t^a t^b] \frac{1}{(8N_c)^2} \frac{1}{4N_c} G(-p'_1 + vp_\rho) G(-\bar{v}p_\rho - zp_\pi), \end{aligned} \quad (1.132)$$

justifies the symmetry we quote a few lines above. Thus the hard part of the diagram 1.12a is proportional to

$$T_{2a}^u \propto \frac{1}{[(p'_2 + \bar{v}p_\rho + zp_\pi)^2 + i\epsilon][(p'_1 - vp_\rho - \bar{z}p_\pi)^2 + i\epsilon][(p'_2 + \bar{v}p_\rho)^2 + i\epsilon][(vp_\rho + \bar{z}p_\pi)^2 + i\epsilon]} \quad (1.133)$$

and the $i\epsilon$ prescription in the 4 propagators leads to the fact that the scattering amplitude gets both a real and an imaginary parts. Integrations over v and z have been done analytically whereas numerical methods are used for the integration over x (cf Appendix).

Lorentz invariance and the linearity of the amplitude with respect to the polarization vectors and with respect to the nucleons' spinors allow us to write the amplitude as:

$$\begin{aligned} \mathcal{A} &= (\epsilon_\pm^*(p_\rho) \cdot N_{\lambda_1 \lambda_2}^\perp)(\epsilon_{\gamma\perp} \cdot p_T) A' + (\epsilon_\pm^*(p_\rho) \cdot \epsilon_{\gamma\perp})(N_{\lambda_1 \lambda_2}^\perp \cdot p_T) B' \\ &+ (\epsilon_\pm^*(p_\rho) \cdot p_T)(N_{\lambda_1 \lambda_2}^\perp \cdot \epsilon_{\gamma\perp}) C' + (\epsilon_\pm^*(p_\rho) \cdot p_T)(N_{\lambda_1 \lambda_2}^\perp \cdot p_T)(\epsilon_{\gamma\perp} \cdot p_T) D' \\ &+ (\epsilon_\pm^*(p_\rho) \cdot p)(N_{\lambda_1 \lambda_2}^\perp \cdot \epsilon_{\gamma\perp}) E' + (\epsilon_\pm^*(p_\rho) \cdot p)(N_{\lambda_1 \lambda_2}^\perp \cdot p_T)(\epsilon_{\gamma\perp} \cdot p_T) F' \end{aligned} \quad (1.134)$$

where A', B', C', D', E', F' are scalar functions of s, ξ, α and $M_{\pi\rho}^2$,

$$\epsilon_\pm^\mu(p_\rho) = \left(\frac{\vec{p}_\rho \cdot \vec{e}_\pm}{m_\rho}, \vec{e}_\pm + \frac{\vec{p}_\rho \cdot \vec{e}_\pm}{m_\rho(E_\rho + m_\rho)} \vec{p}_\rho \right) \quad (1.135)$$

is the transverse polarization of the vector meson ρ , with $\vec{e}_\pm = -\frac{1}{\sqrt{2}}(\pm 1, i, 0)$, $\epsilon_{\gamma\perp}^\mu$ the transverse polarization of the on-shell photon and

$$N_{\lambda_1 \lambda_2}^{\perp\mu} = \frac{2i}{p \cdot n} g_\perp^{\mu\nu} \bar{u}(p_2, \lambda_2) \not{n} \gamma_\nu \gamma^5 u(p_1, \lambda_1) \quad (1.136)$$

is the spinor dependent part which expresses the nucleon helicity flip with $g_\perp^{\mu\nu} = \text{diag}(0, -1, -1, 0)$. To be more precise, the expression of this 2-dimensional transverse vector reads

$$N_{+\hat{x}, +\hat{x}}^{\perp\mu} = -4i\sqrt{1 - \xi^2}(0, 1, 0, 0) \quad N_{-\hat{x}, +\hat{x}}^{\perp\mu} = 4\sqrt{1 - \xi^2}(0, 0, 1, 0) \quad (1.137)$$

$$N_{+\hat{x}, -\hat{x}}^{\perp\mu} = -4\sqrt{1 - \xi^2}(0, 0, 1, 0) \quad N_{-\hat{x}, -\hat{x}}^{\perp\mu} = 4i\sqrt{1 - \xi^2}(0, 1, 0, 0), \quad (1.138)$$

assuming that these nucleons are polarized along the \hat{x} axis.

Since the DA of ρ_T^0 (see below) introduces the factor $\epsilon_{\pm}^{\mu}(p_{\rho})p_{\rho}^{\nu} - \epsilon_{\pm}^{\nu}(p_{\rho})p_{\rho}^{\mu}$, any term proportional to p_{ρ}^{μ} in its polarisation does not contribute to the amplitude. One may then replace

$$\begin{aligned}\epsilon_{\pm}^{\mu}(p_{\rho}) &\Rightarrow 2\bar{\alpha}\frac{\vec{p}_t \cdot \vec{e}_{\pm}}{\bar{\alpha}^2 s + \vec{p}_t^2}(p^{\mu} + n^{\mu}) + (0, \vec{e}_{\pm}) \\ &\Rightarrow 2\bar{\alpha}\frac{\vec{p}_t \cdot \vec{e}_{\pm}}{\bar{\alpha}^2 s + \vec{p}_t^2}\left[1 - \frac{\vec{p}_t^2}{\bar{\alpha}^2 s}\right]p^{\mu} + 2\frac{\vec{p}_t \cdot \vec{e}_{\pm}}{\bar{\alpha}^2 s + \vec{p}_t^2}p_T^{\mu} + (0, \vec{e}_{\pm}).\end{aligned}\quad (1.139)$$

Consequently, the amplitude of this process can be simplified as

$$\begin{aligned}\mathcal{A} &= (\vec{N}_t \cdot \vec{e}_{\pm}^*)(\vec{p}_t \cdot \vec{e}_{\gamma t})A + (\vec{N}_t \cdot \vec{e}_{\gamma t})(\vec{p}_t \cdot \vec{e}_{\pm}^*)B \\ &+ (\vec{N}_t \cdot \vec{p}_t)(\vec{e}_{\gamma t} \cdot \vec{e}_{\pm}^*)C + (\vec{N}_t \cdot \vec{p}_t)(\vec{p}_t \cdot \vec{e}_{\gamma t})(\vec{p}_t \cdot \vec{e}_{\pm}^*)D\end{aligned}\quad (1.140)$$

where A, B, C, D are also scalar functions of s, ξ, α and $M_{\pi\rho}^2$.

1.5.3 Transversity GPD and Double Distribution

In order to get an estimate of the differential cross section of this process, we need to propose a model for the transversity GPD $H_T^q(x, \xi, t=0)$ ($q = u, d$). Contrary to what Enberg *et al.* have done [180], here we must get a parametrization in both ERBL ($[-\xi; \xi]$) and DGLAP ($[-1; -\xi] \cup [\xi; 1]$) domains.

We use the standard description of GPDs in terms of double distributions [51, 114]

$$H_T^q(x, \xi, t=0) = \int_{\Omega} d\beta d\alpha \delta(\beta + \xi\alpha - x) f_T^q(\beta, \alpha, t=0), \quad (1.141)$$

where f_T^q is the quark transversity double distribution and $\Omega = \{|\beta| + |\alpha| \leq 1\}$ is its support domain. Moreover we may add a D-term contribution, which is necessary to be completely general while fulfilling the polynomiality constraints. Since adding a D-term is quite arbitrary and unconstrained, we do not include it in our parametrization. We thus propose a simple model for these GPDs, by writing f_T^q in the form

$$f_T^q(\beta, \alpha, t=0) = \Pi(\beta, \alpha)\delta q(\beta)\Theta(\beta) - \Pi(-\beta, \alpha)\delta\bar{q}(-\beta)\Theta(-\beta), \quad (1.142)$$

where $\Pi(\beta, \alpha) = \frac{3}{4}\frac{(1-\beta)^2 - \alpha^2}{(1-\beta)^3}$ is a profile function and $\delta q, \delta\bar{q}$ are the quark and antiquark transversity parton distribution functions (PDF). The transversity GPD H_T^q thus reads

$$\begin{aligned}H_T^q(x, \xi, t=0) &= \Theta(x > \xi) \int_{\frac{-1+x}{1+\xi}}^{\frac{1-x}{1-\xi}} dy \frac{3}{4} \frac{(1-x+\xi y)^2 - y^2}{(1-x+\xi y)^3} \delta q(x-\xi y) \\ &+ \Theta(\xi > x > -\xi) \left[\int_{\frac{-1+x}{1+\xi}}^{\frac{x}{\xi}} dy \frac{3}{4} \frac{(1-x+\xi y)^2 - y^2}{(1-x+\xi y)^3} \delta q(x-\xi y) \right. \\ &\quad \left. - \int_{\frac{x}{\xi}}^{\frac{1+x}{1+\xi}} dy \frac{3}{4} \frac{(1+x-\xi y)^2 - y^2}{(1+x-\xi y)^3} \delta\bar{q}(-x+\xi y) \right] \\ &- \Theta(-\xi > x) \int_{\frac{-1+x}{1-\xi}}^{\frac{1+x}{1+\xi}} dy \frac{3}{4} \frac{(1+x-\xi y)^2 - y^2}{(1+x-\xi y)^3} \delta\bar{q}(-x+\xi y).\end{aligned}\quad (1.143)$$

For the transversity PDFs δq and $\delta\bar{q}$, we use the parametrization proposed by Anselmino *et al.* [198]

$$\delta u(x) = 7.5 \cdot 0.5(1-x)^5(xu(x) + x\Delta u(x)), \quad (1.144)$$

$$\delta\bar{u}(x) = 7.5 \cdot 0.5(1-x)^5(x\bar{u}(x) + x\Delta\bar{u}(x)), \quad (1.145)$$

$$\delta d(x) = 7.5 \cdot (-0.6)(1-x)^5(xd(x) + x\Delta d(x)), \quad (1.146)$$

$$\delta\bar{d}(x) = 7.5 \cdot (-0.6)(1-x)^5(x\bar{d}(x) + x\Delta\bar{d}(x)), \quad (1.147)$$

where the helicity-dependent PDFs $\Delta q(x)$, $\Delta \bar{q}(x)$ are parametrized with the help of the unpolarized PDFs $q(x)$ and $\bar{q}(x)$ by [199]

$$\Delta u(x) = \sqrt{x} u(x), \quad (1.148)$$

$$\Delta \bar{u}(x) = -0.3 x^{0.4} \bar{u}(x), \quad (1.149)$$

$$\Delta d(x) = -0.7 \sqrt{x} d(x), \quad (1.150)$$

$$\Delta \bar{d}(x) = -0.3 x^{0.4} \bar{d}(x), \quad (1.151)$$

and the PDFs $q(x)$, $\bar{q}(x)$ come from GRV parametrizations [200]. All these PDFs are calculated at the energy scale $\mu^2 = 10 \text{ GeV}^2$. Fig.1.14 represents $H_T^u(x, \xi, t = 0)$ and $H_T^d(x, \xi, t = 0)$, respectively, for different values of ξ , which are determined through (1.109) for $S_{\gamma N} = 20 \text{ GeV}^2$ of JLab and for $M_{\pi\rho}^2$ equal 2, 4, 6 GeV^2 . Similarly, Fig.1.15 represents $H_T^u(x, \xi, t = 0)$ and $H_T^d(x, \xi, t = 0)$, respectively, for different values of ξ , which are determined through (1.109) for $S_{\gamma N} = 200 \text{ GeV}^2$ of Compass and for $M_{\pi\rho}^2$ equal 2, 4, 6 GeV^2 .

These two GPDs show some common features like a peak when x is near $\pm\xi$, their order of magnitude and the fact that they both tend to zero when x tends to ± 1 . The main difference is their opposite sign. The restricted analysis of Ref. [180] based on a meson exchange is insufficient for this study since it only gives us the transversity GPDs in the ERBL region. The MIT bag model inspired method of Ref. [182] underestimates the value of $H_T(x, \xi)$ in the ERBL domain because this model does not take into account antiquark degrees of freedom. One can notice that these GPDs have the same order of magnitude but some differences with other models like light-front constituent quark models [183, 184], principally due to the fact that in [183, 184], parametrizations have been done at $\mu^2 \sim 0.1 \text{ GeV}^2$ whereas our model is calculated at $\mu^2 \sim 10 \text{ GeV}^2$. Other model-studies have been developed in the chiral quark soliton model and a QED-based overlap representation [185, 186].

The t -dependence of these chiral-odd GPDs is related to the impact picture of the parton content of the nucleon [192–197]. We use here the simple multiplicative ansatz

$$H_T^q(x, \xi, t) = H_T^q(x, \xi, t = 0) F_H(t) \quad (1.152)$$

where

$$F_H(t) = \frac{C^2}{(t - C)^2} \quad (1.153)$$

is a standard dipole form factor with $C = .71 \text{ GeV}^2$.

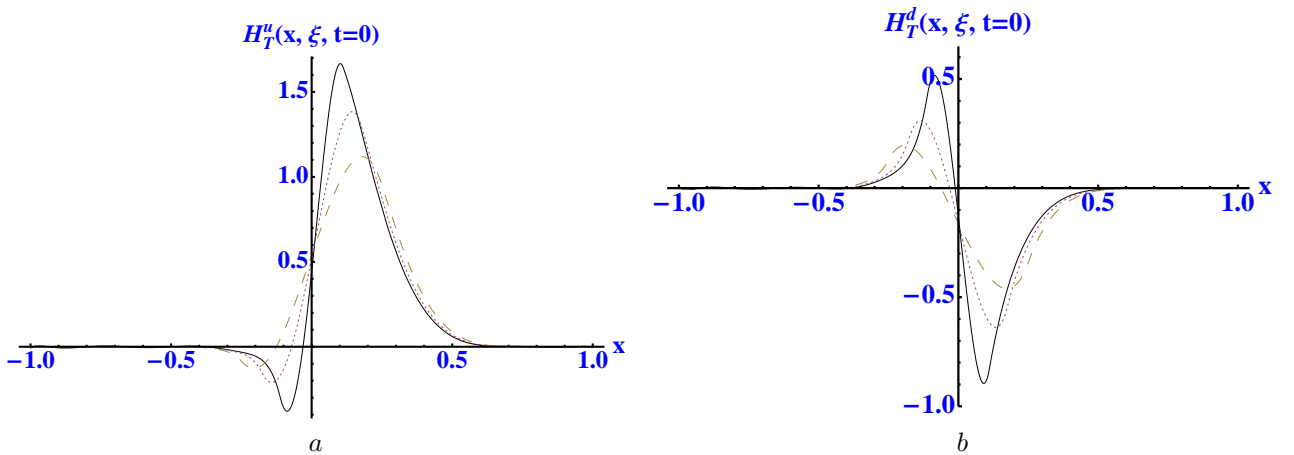


Figure 1.14: Transversity GPD $H_T^u(x, \xi, t = 0)$ (a) and $H_T^d(x, \xi, t = 0)$ (b) of the nucleon for $\xi = .111$ (solid line), $\xi = .176$ (dotted line), $\xi = .25$ (dashed line), corresponding respectively to $M_{\pi\rho}^2/S_{\gamma N}$ equal to 4/20, 6/20 and 8/20.

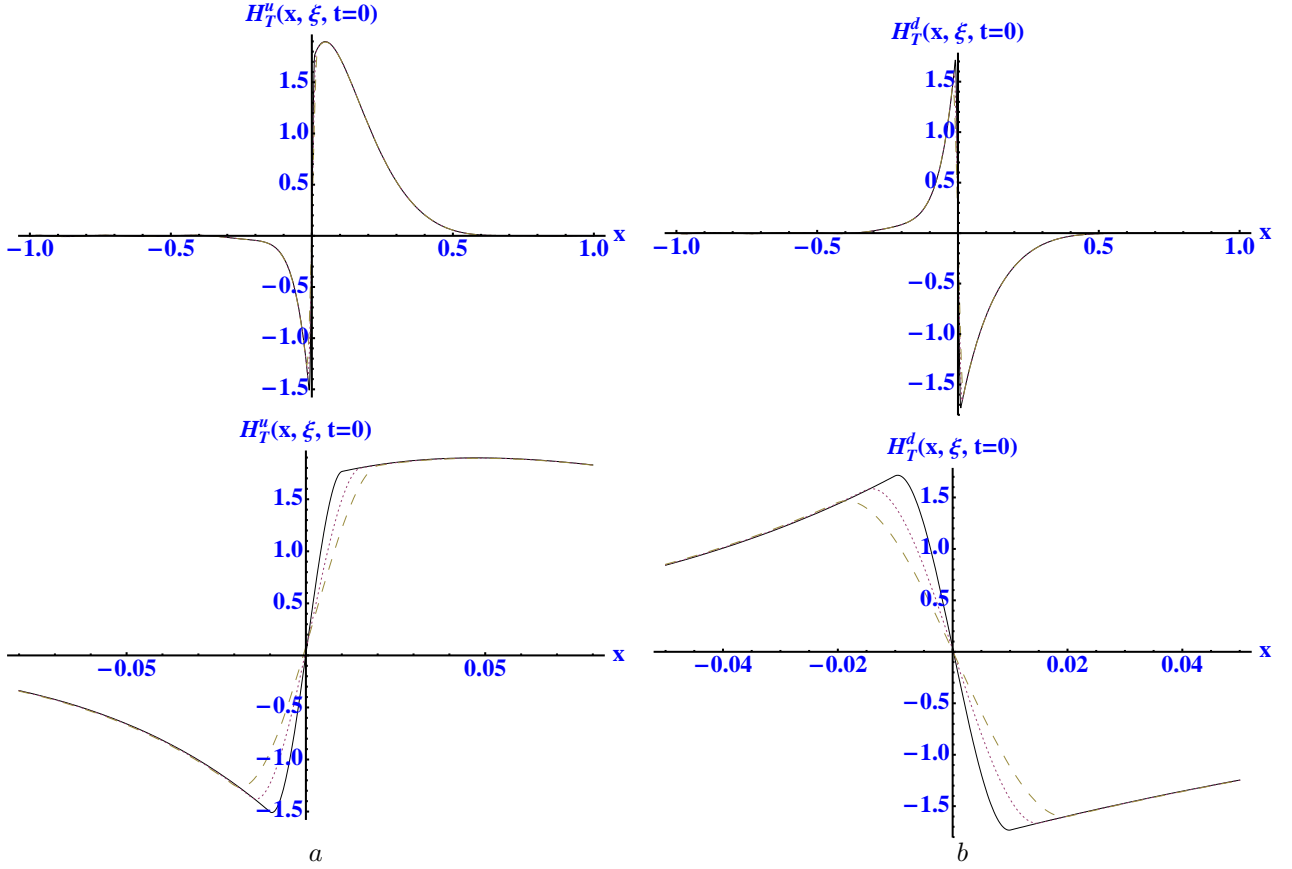


Figure 1.15: Transversity GPD $H_T^u(x, \xi, t=0)$ (a) and $H_T^d(x, \xi, t=0)$ (b) of the nucleon for $\xi = .01$ (solid line), $\xi = .015$ (dotted line), $\xi = .02$ (dashed line), corresponding respectively to $M_{\pi\rho}^2/S_{\gamma N}$ equal to $4/200$, $6/200$ and $8/200$.

1.5.4 Unpolarized Differential Cross Section

Starting with the expression of the scattering amplitude (1.140) we now calculate the amplitude squared for the unpolarized process

$$|\mathcal{M}|^2 = \left(\frac{1}{2}\right) \left(\frac{1}{2}\right) \sum_{\lambda_1 \lambda_2} \mathcal{A} \mathcal{A}^* \quad (1.154)$$

It can seem odd to study the chiral-odd quark content of the nucleon by calculating the cross section of an unpolarized scattering but it is enough for now in order to reach this unknown structure. Of course it is possible to consider the polarized one by producing the spin density matrix, which will be done in a future work.

We now present our preliminary results on the cross-section as a function of t , $M_{\pi\rho}^2$, $-u'$ which reads

$$\left. \frac{d\sigma}{dt du' dM_{\pi\rho}^2} \right|_{t=t_{min}} = \frac{|\mathcal{M}|^2}{32 S_{\gamma N}^2 M_{\pi\rho}^2 (2\pi)^3}. \quad (1.155)$$

Let us first discuss the u' dependence at fixed $M_{\pi\rho}^2$ and at $t = t_{min}$. We show, in Figs. 1.16 and 1.17, respectively, the differential cross section (1.155) as a function of $|u'|$ for $M_{\pi\rho}^2 = 6 \text{ GeV}^2$ fixed at $S_{\gamma N} = 20 \text{ GeV}^2$ i.e. $\xi = 0.176$ and at $S_{\gamma N} = 200 \text{ GeV}^2$ i.e. $\xi = 0.015$.

The physical region over $|u'|$ is contained between $-u'_{min}$ and $-u'_{max}$ due to the typical cuts $-t', -u' > \Lambda^2 = 1 \text{ GeV}^2$. Here a table where is written the minimal and maximal values of $-u'$ with respect to $M_{\pi\rho}^2$:

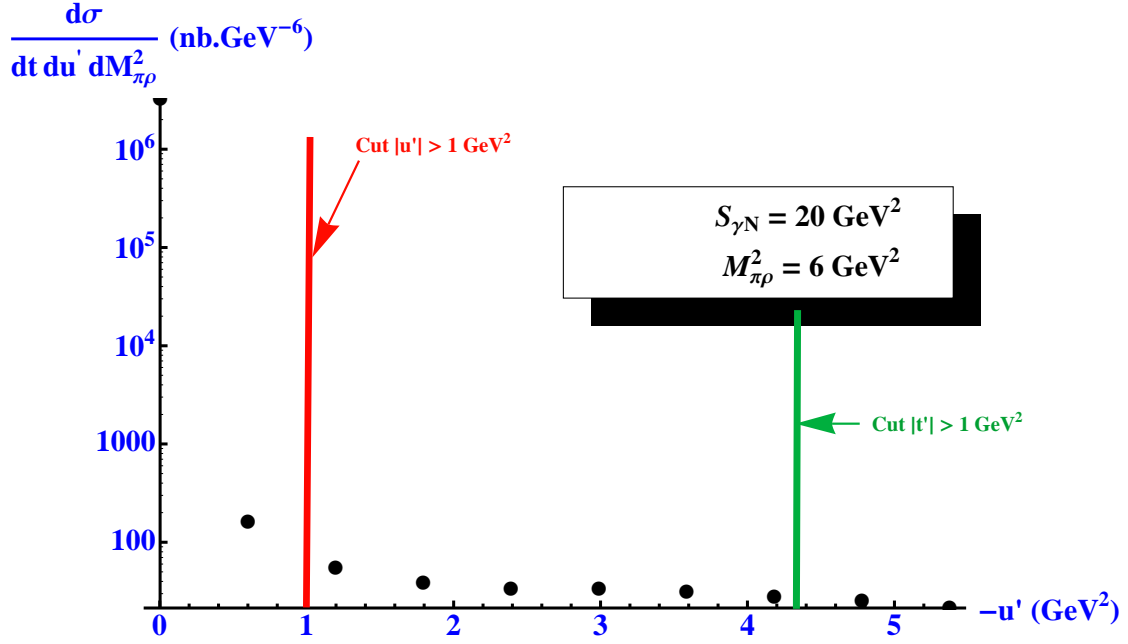


Figure 1.16: Variation of the differential cross section (1.155) ($\text{nb} \cdot \text{GeV}^{-6}$) with respect to $|u'|$ at $M_{\pi\rho}^2 = 6 \text{ GeV}^2$, $S_{\gamma N} = 20 \text{ GeV}^2$ and $\xi = 0.176$.

$M_{\pi\rho}^2$ (GeV^2)	$-u'_{min}$ (GeV^2)	$-u'_{max}$ (GeV^2)
2	1	0.378
3	1	1.378
4	1	2.378
5	1	3.378
6	1	4.378
7	1	5.378
8	1	6.378

One can notice that $-u'_{max}$ does not depend on $S_{\gamma N}$ and that for $M_{\pi\rho}^2 = 2 \text{ GeV}^2$ those cuts induce no physical region, hence an impossibility to get any measurement for this value of the hard scale.

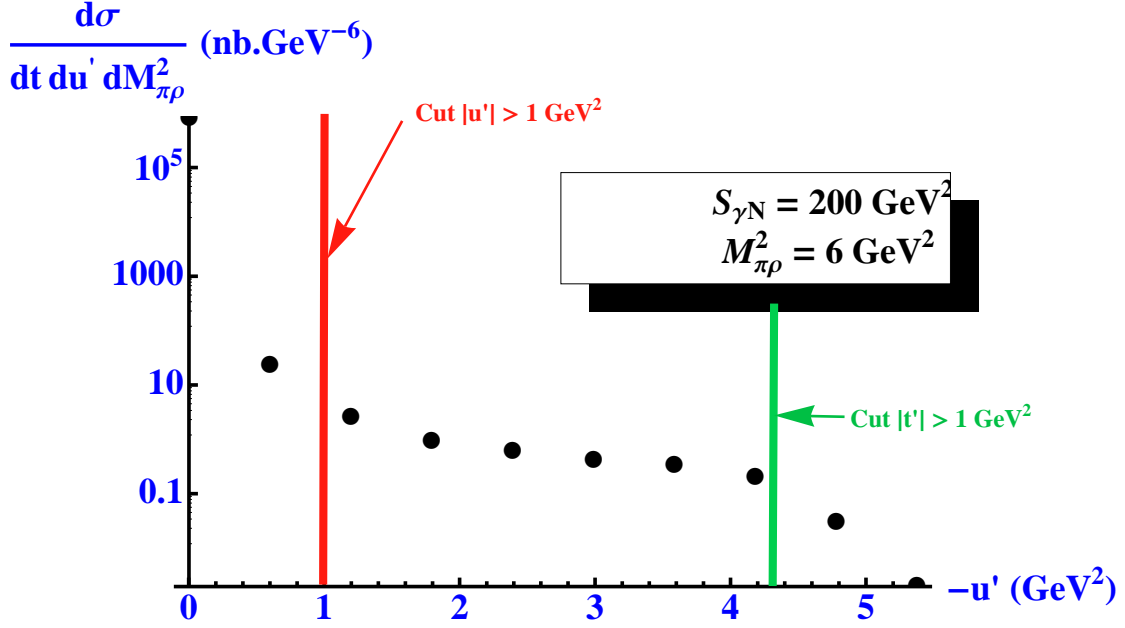


Figure 1.17: Variation of the differential cross section (1.155) (nb.GeV⁻⁶) with respect to $|u'|$ at $M_{\pi\rho}^2 = 6 \text{ GeV}^2$, $S_{\gamma N} = 200 \text{ GeV}^2$ and $\xi = 0.015$.

In Figs.1.18 and 1.19, we show the $M_{\pi\rho}^2$ dependence of the differential cross section when integrating over u' in the range $|u'|, |t'| > \Lambda^2$, with $\Lambda = 1 \text{ GeV}$,

$$\left. \frac{d\sigma}{dt dM_{\pi\rho}^2} \right|_{t=t_{min}} = \int_{u'_{min}}^{u'_{max}} du' \left. \frac{d\sigma}{dt du' dM_{\pi\rho}^2} \right|_{t=t_{min}} \quad (1.156)$$

which quantifies the feasibility of the measurement that we propose. We plot it for both medium (JLab at $S_{\gamma N} = 20 \text{ GeV}^2$) and high energy (Compass at $S_{\gamma N} = 200 \text{ GeV}^2$).

1.5.5 Rates for JLab and COMPASS

To get an experimental rate, we, at first, integrate $\left. \frac{d\sigma}{dt dM_{\pi\rho}^2} \right|_{t=t_{min}}$ over $M_{\pi\rho}^2 \in [3 \text{ GeV}^2, 8 \text{ GeV}^2]$, then multiply the result by $F_H^2(t)/F_H^2(t_{min})$, to recover the t -dependence, and integrate it over a moderate t -range such as $[-0.01 \text{ GeV}^2, -0.001 \text{ GeV}^2]$. We finally obtain the following total cross sections for the photoproduction of a $\pi\rho_T$ pair :

$$\sigma_{\gamma N \rightarrow \pi^+ \rho_T^0 N'}(S_{\gamma N} = 20 \text{ GeV}^2) \simeq 860 \text{ nb} \quad \sigma_{\gamma N \rightarrow \pi^+ \rho_T^0 N'}(S_{\gamma N} = 200 \text{ GeV}^2) \simeq 11 \text{ nb}. \quad (1.157)$$

Thus, one can get an estimate for the experimental rate R_{JLab}^D at JLab Hall D (12 GeV) by

$$\begin{aligned} R_{JLab}^D &= \sigma_{\gamma N \rightarrow \pi^+ \rho_T^0 N'}(S_{\gamma N} = 20 \text{ GeV}^2) \times N_\gamma \times N_p \\ &= 110 \text{ events} \cdot \text{s}^{-1} \end{aligned} \quad (1.158)$$

where $N_\gamma \sim 10^8$ photons/s is the photon flux (for tagged photons at 9 GeV) and $N_p = 1.27 \text{ b}^{-1}$ is the number of protons per surface in the target (liquid hydrogen of 30 cm), assuming that the efficiency of the detector is at 100%.

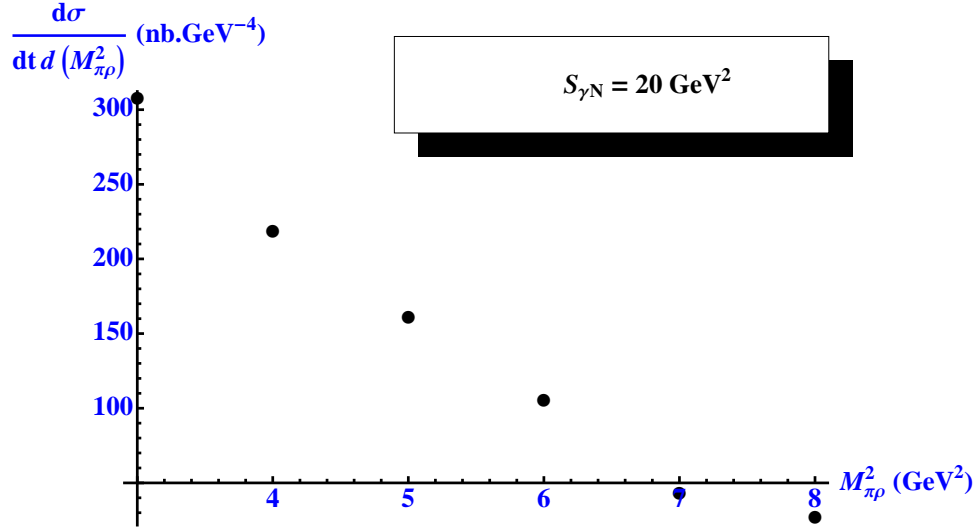


Figure 1.18: $M_{\pi\rho}^2$ dependence of the differential cross section (1.156) (nb.GeV⁻⁴) at $S_{\gamma N} = 20$ GeV²

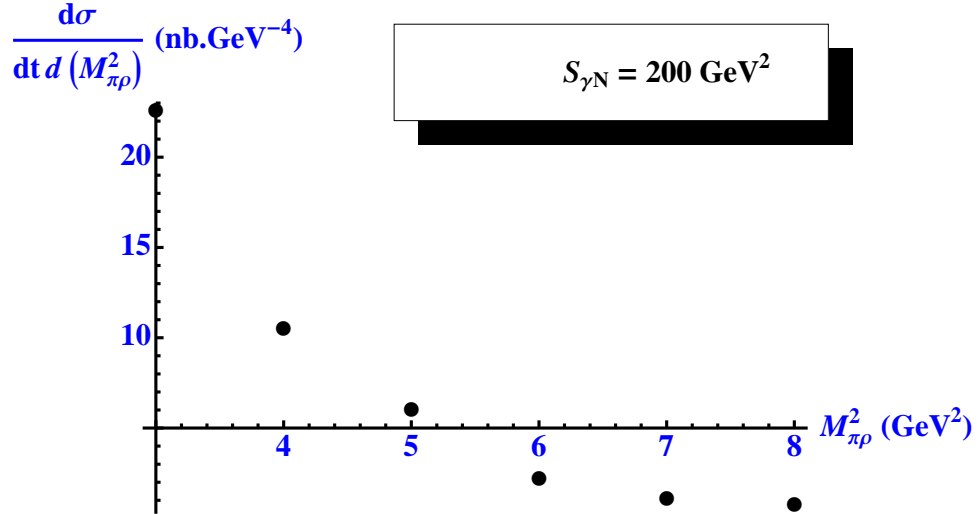


Figure 1.19: $M_{\pi\rho}^2$ dependence of the differential cross section (1.156) (nb.GeV⁻⁴) at $S_{\gamma N} = 200$ GeV²

It is possible to relate the total cross section of our process to the leptonproduction $l + N \rightarrow l + \pi^+ + \rho_T^0 + N'$ studied at the Compass experiment ($l = \mu$) and at JLab Hall A/B ($l = e^-$) by

$$\sigma(lN \rightarrow l\pi^+\rho_T^0N') = \iint dQ^2 d\nu \Gamma_T^l(Q^2, \nu) \sigma_{\gamma^*N \rightarrow \pi^+\rho_T^0N'}(Q^2, \nu) \quad (1.159)$$

1.5. MEASUREMENT OF HELICITY-FLIP GPDs THROUGH A NON-ZERO MIXTURE OF CHIRAL-ODD GPDs WITH

where

$$\Gamma_T^l(Q^2, \nu) = \frac{\alpha}{2\pi Q^2 \nu^2} \left(\nu - \frac{Q^2}{2M^2} \right) \left[\left(\frac{\nu}{E_l} \right)^2 \left(1 - 2 \frac{m_l^2}{Q^2} \right) + \left(1 - \frac{\nu}{E_l} - \frac{Q^2}{4E_l^2} \right) \frac{2}{1 + \frac{Q^2}{\nu^2}} \right] \quad (1.160)$$

is the flux of transverse virtual photon, with the fine structure constant $\alpha = 1/137$ and E_l the lepton energy (in the laboratory frame), and where we assume that

$$\sigma_{\gamma^* N \rightarrow \pi^+ \rho_T^0 N'}(Q^2, \nu) \simeq \sigma_{\gamma N \rightarrow \pi^+ \rho_T^0 N'}(Q^2 = 0, \nu = \frac{S_{\gamma N} - M^2}{2M}) \quad (1.161)$$

Consequently, the total cross section of the electroproduction at JLab Hall A/B ($E_e = 11$ GeV) is

$$\sigma(e^- N \rightarrow e^- \pi^+ \rho_T^0 N') \simeq \sigma_{\gamma N \rightarrow \pi^+ \rho_T^0 N'}(Q^2 = 0, \nu = 10 \text{ GeV}) \int_{2 \cdot 10^{-6}}^1 dQ^2 \int_4^6 d\nu \Gamma_T(Q^2, \nu) \quad (1.162)$$

with

$$\sigma_{\gamma N \rightarrow \pi^+ \rho_T^0 N'}(Q^2 = 0, \nu = 5 \text{ GeV}) \simeq \sigma_{\gamma N \rightarrow \pi^+ \rho_T^0 N'}(S_{\gamma N} = 10 \text{ GeV}^2) \simeq 20 \mu\text{b} \quad (1.163)$$

and an estimate of the experimental rate $R_{JLab}^{A/B}$

$$\begin{aligned} R_{JLab}^{A/B} &= \sigma(e^- N \rightarrow e^- \pi^+ \rho_T^0 N') \times \mathcal{L}_{JLab}^{A/B} \\ &= 3.5 \cdot 10^3 \text{ events} \cdot \text{s}^{-1} \end{aligned} \quad (1.164)$$

where $\mathcal{L}_{JLab}^{A/B} = 10^{35} \text{ cm}^{-2} \cdot \text{s}^{-1}$ is the luminosity for the electron beam.

The total cross section of the muon-production at Compass is

$$\sigma(\mu N \rightarrow \mu \pi^+ \rho_T^0 N') \simeq \sigma_{\gamma N \rightarrow \pi^+ \rho_T^0 N'}(Q^2 = 0, \nu = 100 \text{ GeV}) \int_{0.02}^1 dQ^2 \int_{56}^{144} d\nu \Gamma_T(Q^2, \nu) \quad (1.165)$$

with

$$\sigma_{\gamma N \rightarrow \pi^+ \rho_T^0 N'}(Q^2 = 0, \nu = 100 \text{ GeV}) \simeq \sigma_{\gamma N \rightarrow \pi^+ \rho_T^0 N'}(S_{\gamma N} = 200 \text{ GeV}^2) \quad (1.166)$$

and an estimate of the experimental rate $R_{Compass}$

$$\begin{aligned} R_{Compass} &= \sigma(\mu N \rightarrow \mu \pi^+ \rho_T^0 N') \times \mathcal{L}_{Compass} \times 15\% \\ &= 2 \cdot 10^{-3} \text{ events} \cdot \text{s}^{-1} \end{aligned} \quad (1.167)$$

where $\mathcal{L}_{Compass} = 2.5 \cdot 10^{32} \text{ cm}^{-2} \cdot \text{s}^{-1}$ is the luminosity for the muon beam in Compass and 15% expresses the efficiency of the detector.

According to these results, one can conclude that the photoproduction of a transversally polarized vector meson on a nucleon target is a very good way to reach informations on the generalized chiral-odd quark content of the proton. Indeed, if the JLab CLAS-12 upgrade gets the luminosity experimentalists expect ($\mathcal{L} \sim 10^{35} \text{ cm}^2 \cdot \text{s}^{-1}$), one must reach very high statistics per year to extract transversity GPD and measure it with a rather good precision, without demanding a polarization of the nucleon. This study thus clearly prove the feasibility of the experiment at JLab. For COMPASS, the situation is unfortunately not so favorable.

Having proven the feasibility at JLab, the next stage is of course to get more reliable precision in our prediction. This can be obtained in several ways. First, our model for this GPD H_T^q could be improved by adding, for instance, the D-term which gives a complete parametrization by double distribution. Next, one could think about extending this study to the polarized process, by calculating some observables like the spin density matrix of the vector meson. Further, the extension to the case of electroproduction can be done. Last, a interesting comparison could be obtain with respect to the photoproduction of longitudinally polarized ρ -mesons through non-flip GPDs, which are expected to dominate the cross-section.

Appendix

The explicit calculation of the trace for the diagram 1.12b gives

$$\begin{aligned}
T_{2b}^d(x, v, z) &= \frac{iC_{Fed}f_\rho^\perp f_\pi g^4 \bar{z}}{32N_C^3 s^2 \bar{\alpha} [x - \xi - i\epsilon][x + \xi - i\epsilon]} \\
&\times \frac{\left[(\vec{N}_t \cdot \vec{\sigma}_{\rho t}^*) (\vec{p}_t \cdot \vec{e}_{\gamma t}) - (\vec{N}_t \cdot \vec{p}_t) (\vec{e}_{\gamma t} \cdot \vec{\sigma}_{\rho t}^*) + \frac{2\alpha\xi - \bar{\alpha}}{2\alpha\xi + \bar{\alpha}} (\vec{N}_t \cdot \vec{e}_{\gamma t}) (\vec{p}_t \cdot \vec{\sigma}_{\rho t}^*) \right]}{zv\bar{v}[(\alpha\bar{z} + \bar{\alpha}v)(x + \xi - i\epsilon) - 2\xi\bar{z}v]}
\end{aligned} \tag{1.168}$$

One can already notice that the hard part of this diagram depends on x only via two expressions $x - \xi - i\epsilon$ and $x + \xi - i\epsilon$. This contribution should then be integrated over v and z , the integral with respect to x requiring a specific model for GPDs, see Eq.(1.127). The choice of a specific order of integration over v involving the DA of ρ or z involving the pion DA does not lead to any simplifications. We choose to integrate first over v . This first integration is rather straightforward. The second integration is more involved because of the presence of $i\epsilon$ terms inside the integrand, and in particular as an argument of logarithmic function, leading in the final result to appearance of imaginary parts. For example, it requires to evaluate integrals of the type

$$\int_0^1 dz \frac{1}{2\xi z - \bar{\alpha}X} \log \left[\frac{\alpha X z}{\bar{\alpha}X + z(\alpha X - 2\xi)} \right] \tag{1.169}$$

where $X = x - \xi + i\epsilon$ contains all dependence of the integrand on $i\epsilon$.

Nevertheless, since we have rewritten the x -dependence of propagators with the new variable X , it is possible to calculate this integral analytically without any problem. Thus the expression (1.169) gives

$$\frac{\pi^2}{12\xi} + \frac{1}{2\xi} \text{Li}_2 \left[\left(1 - \frac{2\xi}{\alpha X} \right) \left(1 - \frac{2\xi}{\bar{\alpha}X} \right) \right] - \frac{1}{2\xi} \text{Li}_2 \left[1 - \frac{2\xi}{\alpha X} \right] - \frac{1}{2\xi} \text{Li}_2 \left[1 - \frac{2\xi}{\bar{\alpha}X} \right]. \tag{1.170}$$

The final result for each particular diagram is rather lengthy, and because of that we do not present explicit final results for scalar functions A, B, C, D of (1.140). The final integration over x with any transversity GPD is done numerically.

Chapter 2

Extensions and applications

2.1 GPD crossing $s \leftrightarrow t$: from DA to GDA

2.1.1 From GPDs to GDAs

In the generic situation investigated in chapter 1, we have dealt with DVCS $\gamma^*(Q^2)p \rightarrow \gamma p$ in the regime where Q^2 and s were both large (with respect to Λ_{QCD}^2), with a fixed ratio, and with t fixed. The reaction $\gamma^*(Q^2)\pi \rightarrow \gamma\pi$ can be treated along the same line of thought. It is however possible to consider this last process in the cross-channel, i.e. $\gamma^*\gamma \rightarrow \pi\pi$, asking now for a large $Q^2 \gg \Lambda_{QCD}^2$ value and a small s value, i.e., due to the constraint $s + t + u = -Q^2 + M^2 + 2m_\pi^2$, to study the limit $t \gg \Lambda_{QCD}^2$. As shown formally in [72] by considering the light-cone limit of the non-local twist 2 operators, and then investigated in [201, 202] by similarity with DVCS, this process indeed factorizes, involving an hard part describing the process $\gamma^*\gamma \rightarrow q\bar{q}$ with collinear and on-shell produced quark, and a soft part describing the production of the $\pi\pi$ pair from a $q\bar{q}$. This last part was called Generalized Distribution Amplitude (GDA).

As discussed in chapter 1, the non-perturbative matrix elements occurring in DVCS are GPDs defined in the pion case as [203]

$$H_q(x, \xi, t) = \frac{1}{2} \int \frac{dz^-}{2\pi} e^{ix(P^+z^-)} \langle \pi^+(p') | \bar{q}(-z^-/2) \gamma^+ q(z^-/2) | \pi^-(p) \rangle \quad (2.1)$$

where we have made an interchange of notation between $+$ and $-$ components with respect to Sec.1.3 to make the comparison with GDA easier. Here, as usual $P = (p + p')/2$, which is thus now along $+$.

In a similar way, in the crossed-channel investigated now, the GDAs for quarks and gluons are defined respectively, in $A^+ = 0$ gauge:

$$\Phi_q(z, \zeta, W^2) = \int \frac{dx^-}{2\pi} e^{-iz(P^+x^-)} \langle \pi^+(p) \pi^-(p') | \bar{q}(x^-) \gamma^+ q(0) | 0 \rangle, \quad (2.2)$$

$$\begin{aligned} \Phi_g(z, \zeta, W^2) &= \frac{1}{P^+} \int \frac{dx^-}{2\pi} e^{-iz(P^+x^-)} \langle \pi^+(p) \pi^-(p') | F^{+\mu}(x^-) F_\mu^+(0) | 0 \rangle, \\ &= z(1-z)P^+ \int \frac{dx^-}{2\pi} e^{-iz(P^+x^-)} \langle \pi^+(p) \pi^-(p') | A^\mu(x^-) A_\mu(0) | 0 \rangle, \end{aligned} \quad (2.3)$$

with

$$\zeta = \frac{p_+}{p_+ + p'_+}. \quad (2.4)$$

Let us see how to pass from GDA to GPD in terms of kinematical variables. This is done by crossing of the final state $\pi^-(p')$ to an initial state $\pi^+(-p')$ and then by the replacement

$$\begin{array}{ccc} GDA & & GPD \\ -p' & \longrightarrow & p \\ p & \longrightarrow & p' \end{array} \quad (2.5)$$

from which one can check that under the replacement (2.5), the relative fraction of longitudinal momenta $1 - 2\zeta$ becomes

$$1 - 2\zeta = \frac{p'_+ - p_+}{p_+ + p'_+} \longrightarrow \frac{p_+ + p'_+}{p_+ - p'_+} = \frac{1}{\xi} \quad (2.6)$$

while the internal z variable transforms according to the argument of the Fourier transform

$$(2z - 1)(p_+ + p'_+) \frac{x^-}{2} \longrightarrow (2z - 1)(p'_+ - p_+) \frac{x^-}{2} = (2z - 1) \frac{p'_+ - p_+}{p'_+ + p_+} \frac{p'_+ + p_+}{2} x^- \quad (2.7)$$

which thus implies that

$$1 - 2z \longrightarrow \frac{x}{\xi}. \quad (2.8)$$

From the form of the non-local correlator (2.3), one readily obtains, after performing the replacement $z \rightarrow 1 - z$, then using translation invariance on the obtained correlator, performing the change of variable $x^- \rightarrow -x^-$ and the fact that A field commute on the light cone, that

$$\Phi_g(z, \zeta, W^2) = \Phi_g(1 - z, \zeta, W^2). \quad (2.9)$$

C -invariance leads to the identity

$$\Phi_g(z, 1 - \zeta, W^2) = \Phi_g(z, \zeta, W^2), \quad (2.10)$$

which is easily obtained after inserting the C operator in the correlator (2.3).

The quark case is more involved, since one needs to combine the two above transformations and to compare the obtained correlators in order to get symmetrical properties. One gets from the well-known transformation properties (2.11)

$$C \Psi(x) C^\dagger = \eta_C C \bar{\Psi}^T(x) \quad \text{and} \quad C \bar{\Psi}(x) C^\dagger = \eta_C^* \Psi^T(x) C,$$

where $C = C^\dagger = C^{-1} = C^T = -C$ and $C \gamma_\mu C = -\gamma_\mu^T$ the relations

$$\Phi_q(1 - z, \zeta, W^2) = -C \Phi_q(z, \zeta, W^2) = -\Phi_q(z, 1 - \zeta, W^2), \quad (2.11)$$

where $C = \pm$ denote in this last equation the C -parity quantum number of the two-pion state. For further use, we note that based on the fact that the isoscalar state $I = 0$ is a symmetrical combination of π^+ and π^- while the isovector state $I = 1$ is an antisymmetrical combination of π^+ and π^- , the C -even state (denoted Φ^+) corresponds to the isoscalar state while the C -odd state (denoted Φ^-) corresponds to the isovector combination. In the present case, due to the initial $C = +$ state, we are of course restricted to the case of Φ^+ , which we here after denote Φ for simplicity.

2.1.2 Evolution equations

ERBL evolution kernel

As discussed in Sec.1.4.6, non-perturbative correlators involved in hard processes satisfy evolution equation due to the arbitrariness of the factorization scale μ_F .

We here present the evolution of the distributions for gluons and of quarks in the singlet combination of n_f flavors and adhere to the approach and notations of [202], where the evolution kernel involved in the renormalization group equation due to the factorization scale arbitrariness was obtained in axial gauge $A^+ = 0$, based on the computation of collinear singular diagrams, when dressing the hard part at one loop. This was done following the approach of Refs. [204] and [205]. Another approach, as explained in Chap. 1, relies on the renormalization group equations for non-local operators [105].

As in intermediate step, one introduces the auxiliary functions

$$z\bar{z} f_Q(z) = \sum_{q=1}^{n_f} \Phi_q(z), \quad (2.12)$$

$$z^2 \bar{z}^2 f_G(z) = \Phi_g(z). \quad (2.13)$$

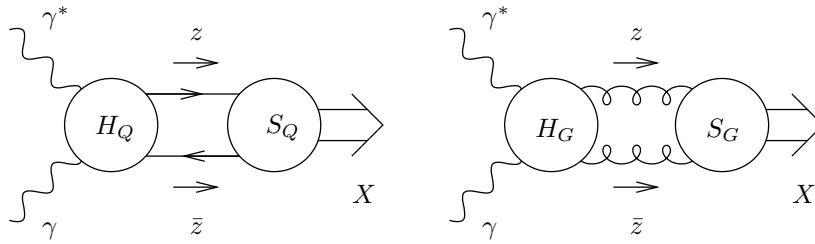


Figure 2.1: The scattering amplitude in the factorized form $H \otimes f$, where f denotes the soft matrix elements and H is the hard coefficient. X is a given system of bound states (single hadron state in the case of a DA, two hadron state or three hadron state in the case of a GDA).

The dependence with respect to the factorization scale is controlled by the usual ξ parameter [61,62] involved for example in the DGLAP evolution equation, arising from the β -function of QCD, which reads¹

$$\xi(\mu^2, \mu_0^2) = \frac{2}{\beta_0} \ln \left(\frac{\alpha_S(\mu_0^2)}{\alpha_S(\mu^2)} \right), \quad (2.14)$$

where α_S is the one-loop running coupling and $\beta_0 = 11 - 2n_f/3$. ξ is analogous to a time variable describing the evolution from the scale μ_0 to the scale μ . The evolution equation takes the form

$$\frac{\partial}{\partial \xi} f(z, \xi) = \int_0^1 du V(z, u) f(u, \xi) \equiv V \otimes f, \quad (2.15)$$

where f is a two-component vector due to quark-gluon mixing, which reads

$$f = \begin{pmatrix} f_Q \\ f_G \end{pmatrix}, \quad (2.16)$$

and V is the 2×2 matrix kernel

$$V = \begin{pmatrix} V_{QQ} & V_{QG} \\ V_{GQ} & V_{GG} \end{pmatrix}. \quad (2.17)$$

In axial gauge, contrarily to the covariant gauge case, the one-loop corrections to the hard coefficient H are obtained by insertion of diagrams of the type illustrated in Fig. 2.2 between the hard part H and the soft part f , leading a ladder-like structure of the same type as the one encountered in the computation of the familiar DGLAP evolution kernel in planar gauge [98]. To get the whole one-loop corrections this should be supplemented with (renormalized) self-energy insertions on each line connecting H to f . These corrections thus have the symbolic form $H \otimes \xi V \otimes f$. Now, instead of considering the evolution kernel as acting on the hard part, as was done during the practical stages of the computation, it may be viewed as acting on the soft part, again exactly in same spirit as for inclusive quantities [98]. This thus leads to the following evolution equation

$$f^{(1)}(z) = f^{(0)}(z) + \xi \int_0^1 du V(z, u) f^{(0)}(u). \quad (2.18)$$

The diagrams involve an integration with respect to the loop momentum k . The integration with respect to k^- is done using standard Cauchy method, closing around relevant pole in the complex plane. In the one-loop approximation, the collinear singularities are responsible for contribution of the type $1/k_\perp^2$ which, after taking into account the fact that the coupling α_s is to be taken at the scale k_\perp^2 ,²

$$\int_{\mu_0^2}^{\mu^2} \frac{d\kappa_T^2}{\kappa_T^2} \frac{\alpha_S(\kappa_T^2)}{2\pi}, \quad (2.19)$$

¹Note that this notation may differ depending on the author: $\xi_{[here]} = \xi [202] = 2 \xi [98]$, which should be taken into account in the proper definition of the evolution kernel.

²Note that the problem of fixing scale at which the coupling should be taken has been investigated in [98] from the point of view of perturbation theory. The proof is very tricky, and as far as we know was not investigated at higher loop level [206]. On the contrary, the scale fixing for the running coupling is given for free in the language of operator product expansion combined with renormalization group analysis.

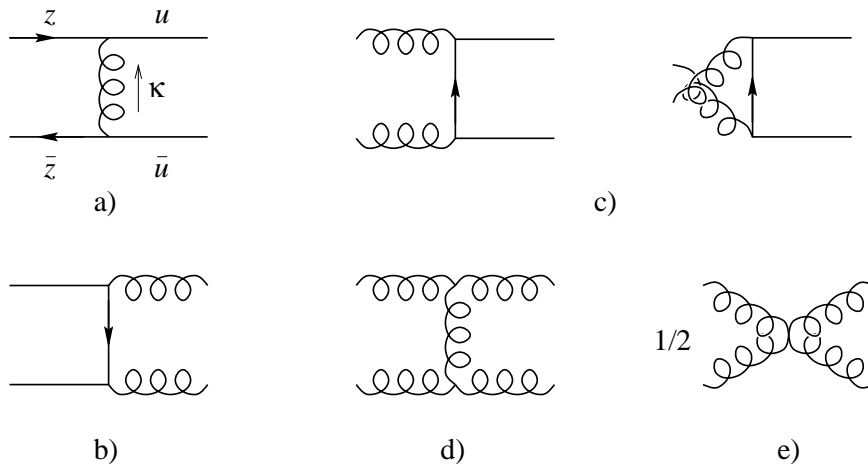


Figure 2.2: One-loop insertions, to be supplemented by self-energy insertions on every line appearing in Fig. 2.1. The sum of all insertions gives the evolution kernel ξV . We remark that the one-loop graph (e) must be multiplied by 1/2 to avoid double counting. u and z denote light cone plus momentum fractions, and κ the loop four-momentum.

relying on the fact that the k_{\perp}^2 momentum is assumed to be larger than the IR cut-off μ_0^2 provided by the soft part, and smaller than the UV regulator μ^2 coming from the hard part. This contribution equals the “time” variable $\xi(\mu^2, \mu_0^2)$ defined by Eq.(2.14). The next step is to note, in the spirit of all-order renormalization group analysis, that this one loop contribution should resummed, since the large logarithm of the ratio of the two scales μ^2/μ_0^2 may compensate the smallness of the coupling. This means that one should rather consider the infinite set of ladder-like diagrams instead of one single rung, exactly in the same spirit as for DGLAP equation [98], which at the level of the whole $\gamma^*\gamma \rightarrow X$ process means that one should consider $\sum_n (\alpha_s \ln Q^2/\mu_0^2)^n$ instead of a single $\alpha_s \ln Q^2/\mu_0^2$ one-loop contribution.

At this stage, before proceeding, one should note that the analysis can be performed in a non-physical gauge, like the covariant gauge. This makes the evaluation of the leading logarithmic contribution much more involved. Indeed, it is known that in covariant gauge, a non-ladder like diagram provides a contribution of double-logarithmic type, $\sim \alpha_s \ln^2 Q^2/\mu_0^2$. It turns out that the whole series $\sum_n (\alpha_s \ln^2 Q^2/\mu_0^2)^n$ cancels, when considering a colourless bound state [207]. By direct inspection at a given order of perturbation theory, one can prove that is true for all terms like $\sim \alpha_s^n \ln^m Q^2/\mu_0^2$ with $2n \geq m > n$, in agreement with the expectation of the operator product extension analysis. Such a tedious analysis is much simplified when using planar gauges [98], in which the logarithmic contribution are ladder like, and are of the type expected by the operator product extension analysis. The first use of physical gauge for exclusive processes is due to the work of Brodsky and Lepage [66, 133, 208], who computed the evolution kernel for DAs in the language of perturbation theory on the light cone (also called light-front perturbation theory, or old fashioned perturbation theory), using an axial gauge. It is only in such physical gauges that evolution equations have a natural partonic interpretation.

Assuming now that the logarithmic analysis has been performed, in whatever gauge, the resummed evolution is a Bethe-Salpeter equation, where the kernel is the one-loop kernel (this generalizes to higher loop order). This means simply that in Eq. (2.18), one should just remove the index (1) in l.h.s and the index (0) in the second term of the r.h.s, giving thus

$$f(z) = f^{(0)}(z) + \xi \int_0^1 du V(z, u) f(u). \quad (2.20)$$

which is equivalent to the expected form (2.15).

The integration over k^+ may be reexpressed as an integral over the incoming light cone fraction u , denoted above as a convolution \otimes . In this collinear approach, the obtained evolution kernels act only in z space, and

describe the change of light cone fractions from u to z . They reads

$$\begin{aligned}
V_{QQ}(z, u) &= C_F \left[\theta(z-u) \frac{u}{z} \left(1 + \frac{1}{z-u} \Big|_+ \right) + \{u \leftrightarrow \bar{u}, z \leftrightarrow \bar{z}\} \right], \\
V_{QG}(z, u) &= 2n_f T_F \left[\theta(z-u) \frac{u}{z} (2z-u) - \{u \leftrightarrow \bar{u}, z \leftrightarrow \bar{z}\} \right], \\
V_{GQ}(z, u) &= \frac{C_F}{z\bar{z}} \left[\theta(z-u) \frac{u}{z} (\bar{z}-2\bar{u}) - \{u \leftrightarrow \bar{u}, z \leftrightarrow \bar{z}\} \right], \\
V_{GG}(z, u) &= \frac{C_A}{z\bar{z}} \left[\theta(z-u) \left(u\bar{u} \frac{1}{z-u} \Big|_+ - u\bar{u} - \frac{u}{2z} [(2z-1)^2 + (2u-1)^2] \right) \right. \\
&\quad \left. + \{u \leftrightarrow \bar{u}, z \leftrightarrow \bar{z}\} - \frac{2}{3} n_f T_F \delta(u-z) \right], \tag{2.21}
\end{aligned}$$

where the color factors are $C_F = 4/3$, $T_F = 1/2$ and $C_A = 3$. The subscript $+$ denotes the usual $+$ distributions, which act on a given test function f as

$$\int_0^1 da \left[\frac{1}{a} \right]_+ f(a) = \int_0^1 da \frac{f(a) - f(0)}{a}. \tag{2.22}$$

The kernels (2.21) are the remaining finite parts after the cancellation of infrared divergences between graph (a), resp. (d), and quark self-energy, resp. gluon self-energy insertions, in the same way as the DGLAP kernel is obtained. These singularities of the real diagrams arises when the momentum of the emitted vector particle (here a gluon) drawn vertically in Fig. 2.2 tends to zero, and as usual are compensated by virtual correction (here the self-energy insertions). These self-energy corrections are related to parton splitting

$$\begin{aligned}
f_Q^{(1)}(z) \Big|_{SE} &= \left[1 - \xi \int dx P_{QQ}(x) \right] f_Q^{(0)}(z) = \left[1 - \xi \int dx P_{GQ}(x) \right] f_Q^{(0)}(z) \\
f_G^{(1)}(z) \Big|_{SE} &= \left[1 - \xi \int dx \left(\frac{1}{2} P_{GG}(x) + n_f P_{QG}(x) \right) \right] f_G^{(0)}(z), \tag{2.23}
\end{aligned}$$

with the unregularized DGLAP splitting functions

$$\begin{aligned}
P_{QQ}(x) &= C_F \frac{1+x^2}{1-x}, \\
P_{QG}(x) &= T_F [x^2 + (1-x)^2], \\
P_{GQ}(x) &= C_F \frac{1+(1-x)^2}{x}, \\
P_{GG}(x) &= 2C_A \left[\frac{x}{1-x} + \frac{1-x}{x} + x(1-x) \right]. \tag{2.24}
\end{aligned}$$

Indeed, a given virtual correction can be seen as the probability of non-emission of the given final state during the “time” ξ , which is just 1 minus the probability of emission, given by the splitting function multiplied by the time ξ .

Solution

We will now study the solution of the evolution equation (2.15). This can be done in two ways: either directly, using orthogonal polynomials, as will do now, or using the hidden conformal symmetry. The solution can be provided for arbitrary values of C . For future applications to $\gamma^* \gamma \rightarrow \gamma \gamma$ and $\gamma^* \gamma \rightarrow H$ ($H = 1^-$, see Sec.2.5), it will be enough for us to consider the case $C = +$ appearing in the process $\gamma^* \gamma \rightarrow \pi \pi$ from which we started. The case $C = -$ will be used when playing with Pomeron/Odderon interference in Sec. 7.5.

In the direct way, one is looking for solutions of the form

$$f(z, \xi) = f(z) e^{-\gamma \xi}. \tag{2.25}$$

Introducing the natural set of variables $y = 2u - 1$ and $x = 2z - 1$ which are the relative momentum fraction of the bound state³, we study the action of the matrix kernel V acting on the states

$$f_Q^{(0)} = \begin{pmatrix} x^n \\ 0 \end{pmatrix}, \quad f_G^{(0)} = \begin{pmatrix} 0 \\ x^{n-1} \end{pmatrix}, \quad (2.26)$$

where n should be an odd integer due to the symmetry properties (2.11) and (2.9). One gets

$$\begin{aligned} V_{QQ} \otimes y^n &= -\gamma_{QQ}(n) x^n + O(x^{n-2}), & V_{QG} \otimes y^{n-1} &= -\gamma_{QG}(n) x^n + O(x^{n-2}), \\ V_{GQ} \otimes y^n &= -\gamma_{GQ}(n) x^{n-1} + O(x^{n-3}), & V_{GG} \otimes y^{n-1} &= -\gamma_{GG}(n) x^{n-1} + O(x^{n-3}), \end{aligned} \quad (2.27)$$

with the anomalous dimensions

$$\gamma_{QQ}(n) = C_F \left(\frac{1}{2} - \frac{1}{(n+1)(n+2)} + 2 \sum_{k=2}^{n+1} \frac{1}{k} \right), \quad (2.28)$$

$$\gamma_{QG}(n) = -n_f T_F \frac{n^2 + 3n + 4}{n(n+1)(n+2)}, \quad (2.29)$$

$$\gamma_{GQ}(n) = -2C_F \frac{n^2 + 3n + 4}{(n+1)(n+2)(n+3)}, \quad (2.30)$$

$$\gamma_{GG}(n) = C_A \left(\frac{1}{6} - \frac{2}{n(n+1)} - \frac{2}{(n+2)(n+3)} + 2 \sum_{k=2}^{n+1} \frac{1}{k} \right) + \frac{2}{3} n_f T_F \quad (2.31)$$

which are identical to the celebrated anomalous dimensions of the flavour singlet operators. This is of course not accidental and is related to the fact that the anomalous dimensions remain unchanged in the local limit, in which the anomalous dimensions coincide with the one of form factors (see Sec. 2.1.2).

We therefore deduce from (2.27) that the space of solutions with $n \leq n_0$ is stable when applying the kernel V . One can thus look for polynomials $p_n(x)$ and $q_{n-1}(x)$ satisfying

$$V_{QQ} \otimes p_n = -\gamma_{QQ}(n) p_n, \quad (2.32)$$

$$V_{QG} \otimes q_{n-1} = -\gamma_{QG}(n) p_n, \quad (2.33)$$

$$V_{GQ} \otimes p_n = -\gamma_{GQ}(n) q_{n-1}, \quad (2.34)$$

$$V_{GG} \otimes q_{n-1} = -\gamma_{GG}(n) q_{n-1}. \quad (2.35)$$

Based on the theory of orthogonal polynomials, the complete identification can be performed relying on the interval of definition of the system of polynomials we are looking for and on the weight with respect to which these polynomial are orthogonal among themselves.

The weight can be obtained as follows, relying on the symetries of the evolution kernels:

$$(1-x^2) V_{QQ}(x, y) = (1-y^2) V_{QQ}(y, x), \quad (2.36)$$

$$2C_F(1-x^2) V_{QG}(x, y) = n_f T_F (1-y^2)^2 V_{GQ}(y, x), \quad (2.37)$$

$$(1-x^2)^2 V_{GG}(x, y) = (1-y^2)^2 V_{GG}(y, x). \quad (2.38)$$

For a given couple of integer numbers n, m , Eq.(2.32) implies that

$$\begin{aligned} \int_{-1}^1 dx (1-x^2) p_n(x) p_m(x) &= -\frac{1}{\gamma_{QQ}(n)} \int_{-1}^1 dx \int_{-1}^1 dy V_{QQ}(x, y) p_n(y) p_m(x) (1-x^2) \\ &= -\frac{1}{\gamma_{QQ}(n)} \int_{-1}^1 dx \int_{-1}^1 dy V_{QQ}(y, x) p_n(y) p_m(x) (1-y^2) \\ &= \frac{\gamma_{QQ}(m)}{\gamma_{QQ}(n)} \int_{-1}^1 dy p_n(y) p_m(y) (1-y^2) \end{aligned} \quad (2.39)$$

³One may find the notations ζ [9] or ξ [135–137] for y in the litterature.

after using the property (2.36). This shows that for $n \neq m$, p_n and p_m are orthogonal with the weight $1 - x^2$. Analogously, using Eq.(2.38), one easily gets that q_{n-1} and q_{m-1} are orthogonal with the weight $(1 - x^2)^2$. Thus, p_n is proportional to the Gegenbauer polynomials $C_n^{(3/2)}(x)$ while q_{n-1} is proportional to the Gegenbauer polynomials $C_{n-1}^{(5/2)}(x)$. Indeed, Gegenbauer polynomials C_n^ν [209] are defined in such a way that

$$p_n(x) = 2^\nu \Gamma(\nu) \left[\frac{n!(n+\nu)}{2\pi \Gamma(n+2\nu)} \right]^{\frac{1}{2}} C_n^\nu(x) \quad (2.40)$$

where $p_n(x)$ are orthonormal basis with weight $(1 - x^2)^{\nu - \frac{1}{2}}$. The last step is to check that the symmetry relation (2.37) is compatible with this identification. This requires to fix accurately the normalization of p_n and q_{n-1} . This is done by using the mixing of p_n and q_{m-1} , according to

$$\begin{aligned} \int_{-1}^1 dx (1 - x^2)^2 q_{m-1}(x) q_{n-1}(x) &= -\frac{1}{\gamma_{GQ}(n)} \int_{-1}^1 dx \int_{-1}^1 dy V_{GQ}(x, y) q_{m-1}(x) p_n(y) (1 - x^2)^2 \\ &= -\frac{2 C_F}{n_f T_F} \frac{1}{\gamma_{GQ}(n)} \int_{-1}^1 dx \int_{-1}^1 dy V_{QG}(y, x) q_{m-1}(x) p_n(y) (1 - y^2) \\ &= \frac{2 C_F}{n_f T_F} \frac{\gamma_{QG}(n)}{\gamma_{GQ}(n)} \int_{-1}^1 dy p_m(y) p_n(y) (1 - y^2) = \frac{n+3}{n} \int_{-1}^1 dy p_m(y) p_n(y) (1 - y^2) \end{aligned} \quad (2.41)$$

after using the explicit form of the anomalous dimensions (2.30, 2.29). Now, according to Eq.(2.40),

$$\|C_{n-1}^{5/2}\|^2 = \frac{n(n+3)}{9} \|C_n^{3/2}\|^2, \quad (2.42)$$

and thus one can identify p_n with $C_n^{(3/2)}(x)$ and (q_{n-1}) with $C_{n-1}^{(5/2)}(x)$ provided that one makes the redefinition

$$\gamma_{QG}(n) \rightarrow \gamma'_{QG}(n) = \frac{n}{3} \gamma_{QG}(n), \quad \gamma_{GQ}(n) \rightarrow \gamma'_{GQ}(n) = \frac{3}{n} \gamma_{GQ}(n) \quad (2.43)$$

in such a way that

$$\frac{\gamma'_{QG}(n)}{\gamma'_{GQ}(n)} = \frac{n(n+3)}{9}$$

in accordance to the ratio (2.42) of the squared norms.

To get an explicit solution, one needs to diagonalize the 2×2 anomalous dimension matrices, in the same way as for DGLAP equation [98]. The eigenvalues are

$$\Gamma_n^{(\pm)} = \frac{1}{2} \left[\gamma_{QQ}(n) + \gamma_{GG}(n) \pm \sqrt{[\gamma_{QQ}(n) - \gamma_{GG}(n)]^2 + 4\gamma'_{QG}(n)\gamma'_{GQ}(n)} \right], \quad (2.44)$$

with the corresponding eigenvectors

$$v_n^{(\pm)}(x) = \begin{pmatrix} C_n^{(3/2)}(x) \\ g_n^{(\pm)} C_{n-1}^{(5/2)}(x) \end{pmatrix}, \quad (2.45)$$

where

$$g_n^{(\pm)} = \frac{\Gamma_n^{(\pm)} - \gamma_{QQ}(n)}{\gamma'_{GQ}(n)}. \quad (2.46)$$

The general C even solution of Eq. (2.15) may then be written as

$$f(x, \xi) = \sum_{\text{odd } n} \left\{ A_n^{(+)} v_n^{(+)}(x) e^{-\Gamma_n^{(+)} \xi} + A_n^{(-)} v_n^{(-)}(x) e^{-\Gamma_n^{(-)} \xi} \right\} \quad (2.47)$$

with integration constants $A_n^{(\pm)}$.

The solution for the GDAs Φ_q and Φ_g thus reads

$$\begin{aligned} \sum_{q=1}^{n_f} \Phi_q^+(z, \mu^2) &= z(1-z) \sum_{\text{odd } n} A_n(\mu^2) C_n^{(3/2)}(2z-1), \\ \Phi_g(z, \mu^2) &= z^2(1-z)^2 \sum_{\text{odd } n} A'_n(\mu^2) C_{n-1}^{(5/2)}(2z-1), \end{aligned} \quad (2.48)$$

with

$$A_n(\mu^2) = A_n^{(+)} \left(\frac{\alpha_S(\mu^2)}{\alpha_S(\mu_0^2)} \right)^{K_n^{(+)}} + A_n^{(-)} \left(\frac{\alpha_S(\mu^2)}{\alpha_S(\mu_0^2)} \right)^{K_n^{(-)}}, \quad (2.49)$$

$$A'_n(\mu^2) = g_n^{(+)} A_n^{(+)} \left(\frac{\alpha_S(\mu^2)}{\alpha_S(\mu_0^2)} \right)^{K_n^{(+)}} + g_n^{(-)} A_n^{(-)} \left(\frac{\alpha_S(\mu^2)}{\alpha_S(\mu_0^2)} \right)^{K_n^{(-)}}. \quad (2.50)$$

In these expressions, all the exponents $K_n^{(\pm)} = 2\Gamma_n^{(\pm)}/\beta_1$ are positive except for $K_1^{(-)} = 0$. Therefore, in the asymptotical regime $\mu \rightarrow \infty$, $A_1^{(-)}$ will be the only term to be kept.

Relation with local matrix elements and polynomiality

Up to now, all what we have said in this section applies to any DA, since the only internal variable involved in the above description is the relative $q - \bar{q}$ momentum fraction, which has to do with the splitting of the hard part into a $q - \bar{q}$ pair. The second variable which is involved is the factorization scale, which governs the QCD evolution. The GDA gets involved when specifying that the final state is actually not a single bound state, but a pair or a triplet⁴ of bound states. In collinear factorization, restricting to the case of a hadron pair GDA, e.g. $\pi\pi$ pair, this means the introduction of a second longitudinal variable, denoted hereafter as ζ , which encodes the fraction of longitudinal momentum carried by one of the hadron in the pair. This dependency is hidden in the coefficients $A_n^{(+)}$ and $A_n^{(-)}$, which are also dependent of the Mandelstam variable W^2 .

Based on the relationship between z -moments of the GDAs and matrix elements of local operators, one can show that the ζ -dependency with respect to ζ is polynomial. Indeed, let us consider the moments of the quark GDA (2.2). Defining $\partial^+ = \partial/\partial x^-$, it reads

$$\begin{aligned} \int_0^1 dz z^n \Phi_q(z) &= \int \frac{dx^-}{2\pi} \int dz z^n e^{-iz(P^+x^-)} \langle \pi(p)\pi(p') | \bar{q}(x^-) \gamma^+ q(0) | 0 \rangle \\ &= \frac{1}{(P^+)^n} \int \frac{dx^-}{2\pi} \left(i \frac{\partial}{\partial x^-} \right)^n \left[\int dz e^{-iz(P^+x^-)} \langle \pi(p)\pi(p') | \bar{q}(x^-) \gamma^+ q(0) | 0 \rangle \right] \\ &= \frac{1}{(P^+)^{n+1}} \int dx^- \delta(x^-) (-i\partial^+)^n \langle \pi(p)\pi(p') | \bar{q}(x^-) \gamma^+ q(0) | 0 \rangle \\ &= \frac{1}{(P^+)^{n+1}} \left[(-i\partial^+)^n \langle \pi(p)\pi(p') | \bar{q}(x) \gamma^+ q(0) | 0 \rangle \right]_{x=0}, \end{aligned} \quad (2.51)$$

where the third line is obtained after integrating by part, and similarly for the gluonic operators:

$$\int_0^1 dz z^{n-1} \Phi_g(z) = \frac{1}{(P^+)^{n+1}} \left[(-i\partial^+)^{n-1} \langle \pi(p)\pi(p') | F^{+\mu}(x) F_{\mu}^+(0) | 0 \rangle \right]_{x=0}. \quad (2.52)$$

The next step is similar to the usual treatment of matrix elements of twist 2 operators in DIS (except for the non-forward nature of the matrix elements considered here): the above local matrix elements are the $+$ -components of tensors which one can decompose on the available set of vectors or tensors, i.e. the metric $g^{\mu\nu}$, the vectors $(p+p')^\mu$ and $(p-p')^\mu$. Identifying now the $+$ components of these vectors, $(p+p')^+ = P^+$ and $(p-p')^+ = (2\zeta-1)P^+$ ($g^{++} = 0$), the r.h.s of Eqs.(2.51, 2.52) are explicitly polynomials in $2\zeta-1$ with degree at most $n+1$. The expansion (2.48) explicitly show that the coefficients A_n and A'_n are respectively the

⁴Generalization from $\pi\pi$ to $\pi\pi\pi$ was discussed in [210].

Gegenbauer moments of the GDAs $\sum_q \Phi_q$ and Φ_g , with their corresponding weights. Thus, since the degrees of $C_n^{(3/2)}(x)$ and $C_{n-1}^{(5/2)}(x)$ are respectively n and $n-1$, the above reasoning for the power moments, which we considered in Eqs.(2.51, 2.52) of the GDAs, applies also for the coefficients A_n and A'_n , showing that they are themselves polynomials in $2\zeta - 1$ with degree at most $n+1$.

In order to perform easily the angular analysis of the pion pair, it is convenient to use Legendre polynomials when expanding these coefficients. Using the notations of [203], it reads

$$A_n(\zeta, W^2) = 6 n_f \sum_{\text{even } l}^{n+1} B_{nl}(W^2) P_l(2\zeta - 1). \quad (2.53)$$

A similar expansion can be performed for A'_n , introducing coefficients B'_{nl} .

The C -invariance properties (2.11) and (2.10) govern the ζ symmetry and restrict l to even integers in the C -even sector we are investigating.

The expansion Eq.(2.53) leads to a complete separation of variables μ and W^2 on one side (coefficients B_{nl} and B'_{nl}), and ζ on the other hand (Legendre polynomials). This implies interesting properties of these coefficients B_{nl} and B'_{nl} . First, the expansion coefficients B_{nl} being linear combinations of the local operator matrix elements in Eq.(2.51, 2.52), they are analytic functions of W^2 . This allows one to relate them to the moments of parton distribution of the pion when W^2 becomes zero or spacelike. Second, for each fixed value of n , A_n (A'_n) are linear combination of B_{nl} (resp. B'_{nl}), showing that the factorization scale dependence of Eqs.(2.49, 2.50) leads to the same dependency for B_{nl} (resp. B'_{nl}), which reads for of the B_{nl} coefficients

$$B_{nl}(W^2, \mu^2) = B_{nl}^{(+)}(W^2) \left(\frac{\alpha_S(\mu^2)}{\alpha_S(\mu_0^2)} \right)^{K_n^{(+)}} + B_{nl}^{(-)}(W^2) \left(\frac{\alpha_S(\mu^2)}{\alpha_S(\mu_0^2)} \right)^{K_n^{(-)}}. \quad (2.54)$$

A similar equation for B'_{nl} can be written, involving the factors $g_n^{(\pm)}$. For further use within our study of hybrid production with $\pi\eta$ decay, let us explicitly display, in the limit $\mu \rightarrow \infty$, the asymptotic form of the GDAs, which reads

$$\sum_{q=1}^{n_f} \Phi_q^+(z, \zeta, W^2) = 18 n_f z(1-z)(2z-1) \left[B_{10}^{(-)}(W^2) + B_{12}^{(-)}(W^2) P_2(2\zeta - 1) \right], \quad (2.55)$$

$$\Phi_g(z, \zeta, W) = 48 z^2(1-z)^2 \left[B_{10}^{(-)}(W^2) + B_{12}^{(-)}(W^2) P_2(2\zeta - 1) \right], \quad (2.56)$$

where $P_2(2\zeta - 1) = 1 - 6\zeta(1 - \zeta)$. We note that $B_{10}^{(-)}$ and $B_{12}^{(-)}$ are μ_0 independent due to the vanishing of $K_1^{(-)} = 0$.

For further use in the case of the C -odd $\pi^+\pi^-$ GDA, when studying interference between Odderon and Pomeron in Sec. 7.5, we shortly provide similar expression for the $C = -$ sector:

$$\Phi^{q(-)}(z, \zeta, s; \mu^2) = 6z(1-z) \sum_{\substack{n=0 \\ \text{even}}}^{\infty} \sum_{\substack{l=1 \\ \text{odd}}}^{n+1} B_{nl}^q(s, \mu^2) C_n^{3/2}(2z-1) P_l(2\zeta - 1) \quad (2.57)$$

where now n is restricted to be even and l to be odd due to the symmetry properties (2.11). Since in the C -odd sector there is no mixing with gluon, one has simply a multiplicative renormalization of the coefficients B_{nl}^q which thus evolve as

$$B_{nl}^q(W^2, \mu^2) = B_{nl}^q(W^2, \mu_0^2) \left(\frac{\alpha_s(\mu^2)}{\alpha_s(\mu_0^2)} \right)^{2\gamma_{\text{QCD}}(n)/\beta_0} \quad \text{for even } n \quad (2.58)$$

which is the same as the evolution of the DA for a single C -odd ρ or π [48, 66], with the anomalous dimension (1.83). Note that a C -even DA satisfies the same evolution equation (2.58), this time with n odd.

Polar angle distribution

The last step in order to relate the previous expansion of the GDAs is to relate ζ with the external kinematical variables.

In the CMS for the pion pair, denoting θ as the polar angle of the pion 1 with respect to the z axis, the momentum of the pions reads

$$p_{\pi_1} = (\sqrt{|\vec{p}| + m_\pi^2}, |\vec{p}| \sin \theta \vec{u}_\phi, |\vec{p}| \cos \theta) \quad \text{and} \quad p_{\pi_2} = (\sqrt{|\vec{p}| + m_\pi^2}, -|\vec{p}| \sin \theta \vec{u}_\phi, -|\vec{p}| \cos \theta), \quad (2.59)$$

or equivalently, in the light-cone basis $(+, -, \perp)$,

$$\begin{aligned} p_{\pi_1} &= \left(\frac{\sqrt{|\vec{p}| + m_\pi^2} + |\vec{p}| \cos \theta}{\sqrt{2}}, \frac{\sqrt{|\vec{p}| + m_\pi^2} - |\vec{p}| \cos \theta}{\sqrt{2}}, |\vec{p}| \sin \theta \vec{u}_\phi \right), \\ p_{\pi_2} &= \left(\frac{\sqrt{|\vec{p}| + m_\pi^2} - |\vec{p}| \cos \theta}{\sqrt{2}}, \frac{\sqrt{|\vec{p}| + m_\pi^2} + |\vec{p}| \cos \theta}{\sqrt{2}}, -|\vec{p}| \sin \theta \vec{u}_\phi \right), \end{aligned} \quad (2.60)$$

the total momentum of the pair being, in the CMS and in the light-cone basis

$$P = \frac{1}{\sqrt{2}}(m_{\pi\pi}, m_{\pi\pi}, 0_\perp). \quad (2.61)$$

From the definition of the $+$ momentum fraction of the pion 1,

$$\zeta = \frac{p_{\pi_1}^+}{P^+}, \quad (2.62)$$

it thus follows that the *relative* $+$ momentum fraction is

$$2\zeta - 1 = 2 \cos \theta \frac{|\vec{p}|}{m_{\pi\pi}} = \beta \cos \theta, \quad (2.63)$$

where $\beta = |\vec{p}|/E_\pi$ is the velocity of each pion in the CMS. This relation can be extended in the case of a GDA with final hadron states of different masses, e.g. in Sec. 2.5, when dealing with the hybrid decay $H \rightarrow \pi \eta$.

Thus, the expansion in Legendre polynomials of $1 - 2\zeta$ can be replaced by an expansion in Legendre polynomials of $\cos \theta$, making thus contact with the usual partial wave expansion. Since on one hand the involved Legendre polynomials are of even degrees, and on the other hand knowing that a Legendre polynomial of a degree of given parity (here even) only contains monomials of the same parity, this expansion can be recast in the form

$$\sum_{q=1}^{n_f} \Phi_q^+ = 6n_f z(1-z) \sum_{\substack{n=1 \\ \text{odd}}}^{\infty} \sum_{\substack{l=0 \\ \text{even}}}^{n+1} \tilde{B}_{nl}(W^2) C_n^{(3/2)}(2z-1) P_l(\cos \theta) \quad (2.64)$$

for quarks, where the coefficients $\tilde{B}_{nl}(W^2)$ are linear combinations of the type

$$\tilde{B}_{nl} = \beta^l [B_{nl} + c_{l,l+2} B_{n,l+2} + \dots + c_{l,n+1} B_{n,n+1}] \quad (2.65)$$

with polynomials $c_{l,\nu}$ in β^2 . As explain above, in the asymptotic limit $\mu \rightarrow \infty$ we restrict ourselves to $n = 1$ in the Gegenbauer expansion, which therefore leads to a partial wave expansion which only contains an S - and a D -wave:

$$\begin{aligned} \sum_{q=1}^{n_f} \Phi_q^+ &= 18n_f z(1-z)(2z-1) [B_{10}(W^2) + B_{12}(W^2) P_2(2\zeta-1)] \\ &= 18n_f z(1-z)(2z-1) [\tilde{B}_{10}(W^2) + \tilde{B}_{12}(W^2) P_2(\cos \theta)] \end{aligned} \quad (2.66)$$

with

$$\begin{aligned} \tilde{B}_{10}(W^2) &= B_{10}(W^2) - \frac{1-\beta^2}{2} B_{12}(W^2), \\ \tilde{B}_{12}(W^2) &= \beta^2 B_{12}(W^2). \end{aligned} \quad (2.67)$$

2.2 The photon GDAs

Based on [W22]

In this section, we illustrate the concept of GDA by calculating the leading order diphoton GDAs. This relies on the computation of the amplitude of the process $\gamma^*\gamma \rightarrow \gamma\gamma$ in the low energy and high photon virtuality region at the Born order and in the leading logarithmic approximation. As in the case of the anomalous photon structure functions, the $\gamma\gamma$ generalized distribution amplitudes exhibit a characteristic $\ln Q^2$ behaviour and obey inhomogeneous QCD evolution equations [W22, W46, W49].

The photon is a much interesting object for QCD studies. Its pointlike coupling to quarks enables to calculate perturbatively part of its wave function. In the case of a virtual photon, this perturbative part is leading at large virtuality; a twist expansion generates non-leading components of the photon distribution amplitude [139, 211, 212], from which the lowest order one is chiral-odd (like for a transversally polarized ρ -meson, in accordance with Vector Meson Dominance) and proportional to the magnetic susceptibility of the vacuum. The construction of the photon DA relies on the background field method (for a review see [213]) in order to separate the point-like, i.e. electromagnetic component, from its hadronic one. This photon DA is at the moment unknown experimentally, although several propositions have been made to measure it [174, 214]. The study of the two photon state is kinematically richer and is thus a most welcome theoretical laboratory for the study of exclusive hard reactions. It will illustrate the concept of GDA developed in the previous section.

The parton content of the photon (for a review see [215]) has been the subject of many studies since the seminal paper by Witten [216] which lead to the concept of photon structure functions with evolution equations involving an inhomogeneous term due to the point-like coupling of the photon, which has no counterpart in the case of the proton structure functions. Their key point which explains the appearance of this anomalous contribution is the fact that the photon plays two dual roles in the analysis: on one side it is an external state, and on the other side it is a dynamical degree of freedom, like the quark of the gluon.

The notion of anomalous parton distribution in a photon can be extended to the case of GPDs, leading to a factorized description of the DVCS on a photon [217], $\gamma^*(q)\gamma \rightarrow \gamma\gamma$, in the regime discussed in Sec.1.2.2, i.e. at large energy and small hadronic momentum transfer but large photon virtuality ($Q^2 = -q^2$).

The two meson GDAs [218–220] is a natural extension of GDA for a pion pair studied in Sec.2.1. In the same way, they describe the coupling of a quark-antiquark (or gluon-gluon) pair to a pair of mesons, and are related by crossing to the meson GPDs. Analogously, the two photon generalized distribution amplitudes (GDAs) which describes the coupling of a quark antiquark (or gluon-gluon) pair to a pair of photons, are related by crossing to the photon GPDs.

Our starting point is the scattering amplitude of the $\gamma^*(q)\gamma \rightarrow \gamma\gamma$ process in the near threshold kinematics, namely at small s and large $-t \sim Q^2$, at large Q^2 in the leading order of the electromagnetic coupling. Our motivation here is essentially formal, since the measurement of this GDA would be presumably very hard: the quantum number of this channel is the same as the one of pseudoscalar neutral mesons production, decaying in a pair of photon, e.g. $\pi^0 \rightarrow \gamma\gamma$ which dominates the counting rates of our purely electromagnetic process.

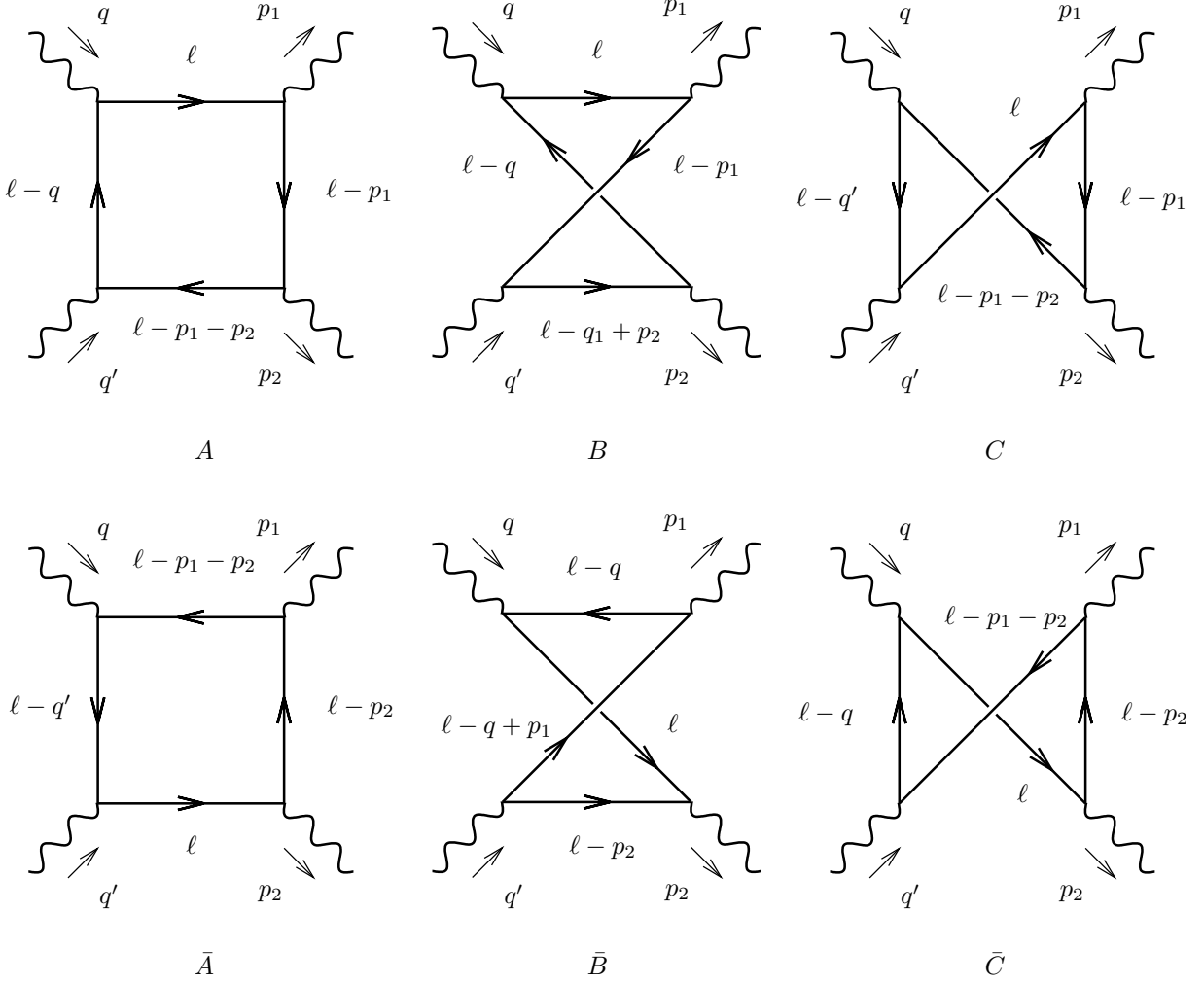
2.2.1 The $\gamma^*\gamma \rightarrow \gamma\gamma$ process in the threshold region

Let us consider the two photon production occurring in Compton scattering on a photon target

$$\gamma^*(q)\gamma(q') \rightarrow \gamma(p_1)\gamma(p_2). \quad (2.68)$$

It involves, at leading order in α_{em} , and zeroth order in α_S the six Feynman diagrams of Fig. 2.3 with quarks in the loop. The pure QED content of this amplitude, involving a lepton in the loop, can be straightforwardly be obtained from the results below, and will not be considered here.

We restrict ourselves to the threshold kinematics where $W^2 = (p_1 + p_2)^2 = 0$, although the factorization in terms of GDAs could be straightforwardly extended to the situation where $0 \neq W^2 \ll -t$. This simplifies greatly the tensorial structure of the amplitude while still preserving the richness of the skewedness (ζ) dependence of GDAs, but would not allow any impact parameter interpretation of the GDAs [218–220]. We use the following

Figure 2.3: The 6 Born order diagrams for $\gamma^* \gamma \rightarrow \gamma \gamma$

kinematics:

$$\begin{aligned}
 q &= p - \frac{Q^2}{s} n, & q' &= \frac{Q^2}{s} n, \\
 p_1 &= \zeta p, & p_2 &= \bar{\zeta} p,
 \end{aligned} \tag{2.69}$$

where p and n are two light-cone Sudakov vectors with $2p \cdot n = s$. The momentum ℓ in the quark loop is parametrized as

$$\ell^\mu = z p^\mu + \beta n^\mu + \ell_\perp. \tag{2.70}$$

The process involves one virtual and three real photons and its amplitude can be written as

$$A = \epsilon_\mu \epsilon'_\nu \epsilon_{1\alpha}^* \epsilon_{2\beta}^* T^{\mu\nu\alpha\beta}, \tag{2.71}$$

where in our (forward) kinematics the four photon polarization vectors $\epsilon(q)$, $\epsilon'(q')$, $\epsilon_1(p_1)$ and $\epsilon_2(p_2)$ are transverse with respect to the Sudakov vectors p and n .

The tensorial decomposition of $T^{\mu\nu\alpha\beta}$ reads [221]

$$T^{\mu\nu\alpha\beta}(W=0) = \frac{1}{4} g_\perp^{\mu\nu} g_\perp^{\alpha\beta} W_1 + \frac{1}{8} \left(g_\perp^{\mu\alpha} g_\perp^{\nu\beta} + g_\perp^{\nu\alpha} g_\perp^{\mu\beta} - g_\perp^{\mu\nu} g_\perp^{\alpha\beta} \right) W_2 + \frac{1}{4} \left(g_\perp^{\mu\alpha} g_\perp^{\nu\beta} - g_\perp^{\mu\beta} g_\perp^{\alpha\nu} \right) W_3, \tag{2.72}$$

and it involves three scalar functions W_i , $i = 1, 2, 3$.

The integration over ℓ is performed as usual within the Sudakov representation, using

$$d^4\ell = \frac{s}{2} dz d\beta d^2\ell_\perp \rightarrow \frac{\pi s}{2} dz d\beta d\ell^2. \quad (2.73)$$

Our goal here is to exhibit a factorization of a hard part convoluted with a GDA, thus involving an integration in the z variable. This means that our expressions should not be computed completely, but rather left unintegrated with respect to z . In all the following calculations, the mass of the quark will play the role of an infrared regulator. The calculation of each of the six diagrams goes along the same line, and for illustration we only detail the calculations for the diagram A. One gets for W_1^A

$$W_1^A = -i \frac{se_q^4 N_C}{32\pi^3} \int \frac{dz d\beta d\ell^2 \text{Tr} A_1}{[(\ell - q)^2 - m^2 + i\eta][(\ell - p_1)^2 - m^2 + i\eta](\ell^2 - m^2 + i\eta)[(\ell - q - q')^2 - m^2 + i\eta]}, \quad (2.74)$$

where $\text{Tr} A_1 = \text{Tr}[\gamma_\perp^\mu(\ell - \not{q} + m)\gamma_\perp^\mu(\ell - \not{p}_1 - \not{p}_2 + m)\gamma_\perp^\alpha(\ell - \not{p}_1 + m)\gamma_\perp^\alpha(\ell + m)]$ and Tr means the trace over spinorial indices.

The integration over β is done using the Cauchy theorem (a straightforward analysis shows that each diagram separately converges when $\beta \rightarrow \pm\infty$). The propagators induce poles in the complex β -plane with values

$$\begin{aligned} \beta_1 &= \frac{\ell^2 + m^2 - i\eta}{zs}, & \beta_2 &= \frac{\ell^2 + m^2 - i\eta}{(z - \zeta)s}, \\ \beta_3 &= -\frac{\ell^2 + m^2 + \bar{z}Q^2 - i\eta}{\bar{z}s}, & \beta_4 &= -\frac{\ell^2 + m^2 - i\eta}{\bar{z}s}. \end{aligned} \quad (2.75)$$

Since the four poles lie all below the real axis for $z > 1$ and lie all above the real axis for $z < 0$, the only region where the amplitude may not vanish is $1 > z > 0$. One identifies two different regions:

- the region where $\zeta < z < 1$, for which one may close the contour in the lower half plane and get the contribution of the poles β_1 and β_2 ,
- the region where $0 < z < \zeta$, for which one may close the contour in the lower half plane and take the contribution of the pole β_1 .

The β integration thus leads to

$$I^{A_1} = -2i\pi \int_\zeta^1 dz \int d\ell^2 \left(\frac{\text{Tr} A_1(\beta = \beta_1)}{DA_{\beta_1}} + \frac{\text{Tr} A_1(\beta = \beta_2)}{DA_{\beta_2}} \right) - 2i\pi \int_0^\zeta dz \int d\ell^2 \frac{\text{Tr} A_1(\beta = \beta_1)}{DA_{\beta_1}}, \quad (2.76)$$

where DA_{β_i} denote the value of the product of propagators at the pole β_i .

To go further, one should disentangle UV and IR divergencies. In the leading logarithmic approximation we are interested in, the trace $\text{Tr} A_1$ may be simplified by taking the limit $m^2 \rightarrow 0$. Of course one should keep $m^2 \neq 0$ in the denominators, since it regulates IR divergencies. When considering each of the six diagrams separately, each integral over \mathbf{l}^2 in Eq.(2.76) is UV divergent. However, it is a well-known classical result of QED that the sum of integrals corresponding to the six diagrams of Fig. 2.3 is UV finite based on QED gauge invariance (see of example p 321 of Ref. [222]), so we separate UV divergent terms of each diagram in an algebraic way, and we show that the UV finiteness appears for the sum of diagrams A, B and C and for the sum of diagrams D, E and F separately.

The traces are clearly simple polynomials in ℓ^2 , which may be written as $\text{Tr} A_1(\beta = \beta_i) \sim \alpha_i \ell^4 + \gamma_i Q^2 \ell^2 + \delta_i Q^4$, where α_i , γ_i and δ_i are dimensionless functions of z and ζ . Power counting in ℓ^2 shows that the $\alpha_i \ell^4$ term in these integrals is ultraviolet divergent, since DA_{β_i} behaves as ℓ^6 . Our aim is to recover the UV finiteness of the sum of diagrams before performing the integration over z . This cancellation of UV divergences occurs separately in each interval $z \in [0, \zeta]$ and $z \in [\zeta, 1]$. For illustration, we consider the interval $[0, \zeta]$, which corresponds to the second term in the r.h.s of Eq.(2.76). The UV divergent part of I^{A_1} in this interval has the form :

$$-2i\pi \int_0^\zeta dz \int \frac{d\ell^2}{\ell^2} a_1^{div}(z, \zeta), \quad (2.77)$$

where a_1^{div} is a definite function of z and ζ . The contributions from diagrams B and C lead to similar equations as Eq.(2.77) with a_1^{div} replaced respectively by b_1^{div} and c_1^{div} . The cancellation of UV divergences in the sum of A, B and C diagrams is manifest through the fact that $a_1^{div} + b_1^{div} + c_1^{div} = 0$.

The technical key point is now to extract the convergent UV part of the second term of Eq.(2.76) by adding and subtracting a simple term which reproduces the same UV divergence, without spoiling the IR convergency. This can be done in the form

$$\begin{aligned} I_{div}^{A_1} &= -2i\pi \int_0^\zeta dz \int d\underline{\ell}^2 \left(\frac{Tr A_1(\beta = \beta_1)}{DA_{\beta_1}} - \frac{\underline{\ell}^4}{(\underline{\ell}^2 + m^2)^3} a_1^{div}(z, \zeta) \right) \\ &- 2i\pi \int_0^\zeta dz \int d\underline{\ell}^2 \frac{\underline{\ell}^4}{(\underline{\ell}^2 + m^2)^3} a_1^{div}(z, \zeta) \end{aligned} \quad (2.78)$$

The first term in Eq.(2.78) is thus both UV and IR finite and can be computed analytically. Since the second term in Eq.(2.78) cancels out when summing diagrams A, B and C, we do not need to compute it. The same procedure is applied to the contribution coming from the interval $z \in [\zeta, 1]$. Finally, the contributions from the diagrams D, E and F are considered in the same way⁵.

This leads to following result of our calculation of the amplitude W_1 , in the leading log Q^2 approximation:

$$\begin{aligned} W_1 &= \frac{e_q^4 N_C}{2\pi^2} \int_0^1 dz (2z - 1) \left[\frac{2z - \zeta}{z\bar{\zeta}} \theta(z - \zeta) + \frac{2z - 1 - \zeta}{\bar{z}\zeta} \theta(\zeta - z) \right. \\ &+ \left. \frac{2z - \bar{\zeta}}{z\zeta} \theta(z - \bar{\zeta}) + \frac{2z - 1 - \bar{\zeta}}{\bar{z}\bar{\zeta}} \theta(\bar{\zeta} - z) \right] \log \frac{m^2}{Q^2}. \end{aligned} \quad (2.79)$$

The amplitudes W_2 and W_3 are calculated in the same way and we get

$$W_2 = 0 \quad (2.80)$$

and

$$\begin{aligned} W_3 &= -\frac{e_q^4 N_C}{2\pi^2} \int_0^1 dz \left[\frac{\zeta}{z\bar{\zeta}} \theta(z - \zeta) - \frac{\bar{\zeta}}{\bar{z}\zeta} \theta(\zeta - z) \right. \\ &- \left. \frac{\bar{\zeta}}{z\zeta} \theta(z - \bar{\zeta}) + \frac{\zeta}{\bar{z}\bar{\zeta}} \theta(\bar{\zeta} - z) \right] \log \frac{m^2}{Q^2}. \end{aligned} \quad (2.81)$$

2.2.2 QCD factorization of the DVCS amplitude on the photon

Our aim is now to interpret the results (2.79) and (2.81) from the point of view of QCD factorization based on the operator product expansion, yet still in the zeroth order of the QCD coupling constant and in the leading logarithmic approximation. The crucial point is to note that the final contribution to this amplitude involves mixing of operators constructed from quark fields with operators constructed from photon fields [216]. This mixing can be understood by denoting the integrands of Eq.(2.79) and Eq.(2.81) by $\mathcal{F}(z, \zeta) \log \frac{m^2}{Q^2}$ and rewriting them by using the obvious identity

$$\mathcal{F}(z, \zeta) \log \frac{m^2}{Q^2} = \mathcal{F}(z, \zeta) \log \frac{m^2}{M_F^2} + \mathcal{F}(z, \zeta) \log \frac{M_F^2}{Q^2}, \quad (2.82)$$

where M_F corresponds to an arbitrary QCD factorization scale. As will be shown below the first term with $\log \frac{m^2}{M_F^2}$ may be identified with the quark GDA of the photon, whereas the second term with $\log \frac{M_F^2}{Q^2}$ corresponds to the so-called photon GDA of the photon, coming from the matrix element of the correlator field from photonic fields which contributes at the same order in α_{em} as the quark correlator to the scattering amplitude. The choice $M_F^2 = Q^2$ will allow to express the amplitude only in terms of the quark-antiquark fragmentation into two photons.

⁵This set of transformations can be implemented in an automatic way using for example MATHEMATICA, and allows for an automatic treatment of the resulting integrals.

We first consider two quark non local correlators on the light cone and their matrix elements between the vacuum and a diphoton state which define the diphoton GDAs Φ_1, Φ_3 :

$$F^q = \int \frac{dy}{2\pi} e^{i(2z-1)\frac{y}{2}} \langle \gamma(p_1) \gamma(p_2) | \bar{q}(-\frac{y}{2}N) \gamma \cdot N q(\frac{y}{2}N) | 0 \rangle = \frac{1}{2} g_{\perp}^{\mu\nu} \epsilon_{\mu}^*(p_1) \epsilon_{\nu}^*(p_2) \Phi_1(z, \zeta, 0) \quad (2.83)$$

and

$$\tilde{F}^q = \int \frac{dy}{2\pi} e^{i(2z-1)\frac{y}{2}} \langle \gamma(p_1) \gamma(p_2) | \bar{q}(-\frac{y}{2}N) \gamma \cdot N \gamma^5 q(\frac{y}{2}N) | 0 \rangle = -\frac{i}{2} \epsilon^{\mu\nu\rho N} \epsilon_{\mu}^*(p_1) \epsilon_{\nu}^*(p_2) \Phi_3(z, \zeta, 0), \quad (2.84)$$

where we note $N = n/n \cdot p$, $\epsilon^{\mu\nu\rho N} = \epsilon^{\mu\nu\alpha\beta} p_{\alpha} N_{\beta}$, with $\epsilon^{0123} = 1$, and where we did not write explicitly, for simplicity of notation, neither the electromagnetic nor the gluonic Wilson lines. We will also define the matrix elements of photonic correlators

$$F^{\gamma} = \int \frac{dy}{2\pi} e^{i(2z-1)\frac{y}{2}} \langle \gamma(p_1) \gamma(p_2) | F^{N\mu}(-\frac{y}{2}N) F_{\mu}^N(\frac{y}{2}N) | 0 \rangle \quad (2.85)$$

and

$$\tilde{F}^{\gamma} = \int \frac{dy}{2\pi} e^{i(2z-1)\frac{y}{2}} \langle \gamma(p_1) \gamma(p_2) | F^{N\mu}(-\frac{y}{2}N) \tilde{F}_{\mu}^N(\frac{y}{2}N) | 0 \rangle, \quad (2.86)$$

where $F^{N\mu} = N_{\nu} F^{\nu\mu}$ and $\tilde{F}^{\mu\nu} = \frac{1}{2} \epsilon^{\mu\nu\rho\sigma} F_{\rho\sigma}$, which mix with correlators (2.83) and (2.84), but contrarily to the quark correlator matrix element, are non zero at order α_{em}^0 [216].

The quark correlator matrix elements, calculated in the lowest order of α_{em} and α_S , suffer from ultraviolet divergences, which we regulate through the usual dimensional regularization procedure, with $d = 4 + 2\epsilon$. We obtain (with $\frac{1}{\bar{\epsilon}} = \frac{1}{\epsilon} + \gamma_E - \log 4\pi$)

$$F^q = -\frac{N_C e_q^2}{4\pi^2} g_T^{\mu\nu} \epsilon_{\mu}^*(p_1) \epsilon_{\nu}^*(p_2) \left[\frac{1}{\bar{\epsilon}} + \log m^2 \right] F(z, \zeta), \quad (2.87)$$

with

$$F(z, \zeta) = \frac{\bar{z}(2z - \zeta)}{\bar{\zeta}} \theta(z - \zeta) + \frac{\bar{z}(2z - \bar{\zeta})}{\zeta} \theta(z - \bar{\zeta}) + \frac{z(2z - 1 - \zeta)}{\zeta} \theta(\zeta - z) + \frac{z(2z - 1 - \bar{\zeta})}{\bar{\zeta}} \theta(\bar{\zeta} - z) \quad (2.88)$$

for the $\mu \leftrightarrow \nu$ symmetric (polarization averaged) part. The corresponding results for the antisymmetric (polarized) part read

$$\tilde{F}^q = -\frac{N_C e_q^2}{4\pi^2} (-i \epsilon^{\mu\nu\rho N}) \epsilon_{\mu}^*(p_1) \epsilon_{\nu}^*(p_2) \left[\frac{1}{\bar{\epsilon}} + \log m^2 \right] \tilde{F}(z, \zeta), \quad (2.89)$$

with

$$\tilde{F}(z, \zeta) = \frac{\bar{z}\zeta}{\bar{\zeta}} \theta(z - \zeta) - \frac{\bar{z}\bar{\zeta}}{\zeta} \theta(z - \bar{\zeta}) - \frac{z\bar{\zeta}}{\zeta} \theta(\zeta - z) + \frac{z\zeta}{\bar{\zeta}} \theta(\bar{\zeta} - z). \quad (2.90)$$

Let us stress again that here we concentrate only on the leading logarithmic behaviour and thus focus on the divergent parts and their associated logarithmic functions. The ultraviolet divergent parts are removed through the renormalization procedure (see for example [223]) involving quark and photon correlators (O^q, O^{γ}) corresponding to one of the two following pairs

$$(\bar{q}(-\frac{y}{2}N) \gamma \cdot N q(\frac{y}{2}N), F^{N\mu}(-\frac{y}{2}N) F_{\mu}^N(\frac{y}{2}N)), \quad (2.91)$$

or

$$(\bar{q}(-\frac{y}{2}N) \gamma \cdot N \gamma^5 q(\frac{y}{2}N), F^{N\mu}(-\frac{y}{2}N) \tilde{F}_{\mu}^N(\frac{y}{2}N)). \quad (2.92)$$

The renormalized operators are defined as:

$$\begin{pmatrix} O^q \\ O^{\gamma} \end{pmatrix}_R = \begin{pmatrix} Z_{qq} & Z_{q\gamma} \\ Z_{\gamma q} & Z_{\gamma\gamma} \end{pmatrix} \begin{pmatrix} O^q \\ O^{\gamma} \end{pmatrix}. \quad (2.93)$$

The matrix element of the renormalized quark-quark correlator is thus equal to

$$\langle \gamma(p_1)\gamma(p_2)|O_R^q|0 \rangle = Z_{qq} \langle \gamma(p_1)\gamma(p_2)|O^q|0 \rangle + Z_{q\gamma} \langle \gamma(p_1)\gamma(p_2)|O^\gamma|0 \rangle, \quad (2.94)$$

with $Z_{qq} = 1 + \mathcal{O}\left(\frac{e^2}{\epsilon}\right)$. Since the matrix element $\langle \gamma(p_1)\gamma(p_2)|O^q|0 \rangle$ contains a UV divergence (see Eqs.(2.87), (2.89)) and since $\langle \gamma(p_1)\gamma(p_2)|O^\gamma|0 \rangle$ is UV finite and of order α_{em}^0 , one can absorb this divergence into the renormalization constant $Z_{q\gamma}$. The normalization of the renormalized correlator is fixed with the help of the renormalization condition which is chosen as

$$\langle \gamma(p_1)\gamma(p_2)|O_R^q|0 \rangle = 0 \quad \text{at} \quad M_R = m. \quad (2.95)$$

In this way the renormalized GDA with vector correlator is equal to

$$F_R^q = -\frac{N_C e_q^2}{4\pi^2} g_T^{\mu\nu} \epsilon_\mu^*(p_1) \epsilon_\nu^*(p_2) \log \frac{m^2}{M_R^2} F(z, \zeta) \quad (2.96)$$

and we have a similar result for the renormalized GDA with axial correlator

$$\tilde{F}_R^q = -\frac{N_C e_q^2}{4\pi^2} (-i\epsilon^{\mu\nu\rho N}) \epsilon_\mu^*(p_1) \epsilon_\nu^*(p_2) \log \frac{m^2}{M_R^2} \tilde{F}(z, \zeta). \quad (2.97)$$

As we want to use the QCD factorization formula, which correspond to the factorization scale M_F , we identify now the renormalization scale M_R with M_F ,

$$M_R = M_F. \quad (2.98)$$

Eqs. (2.96, 2.97) together with Eqs (2.88, 2.90) permit us to write the expressions of the diphoton generalized distribution amplitudes:

$$\Phi_1^q(z, \zeta, 0) = -\frac{N_C e_q^2}{2\pi^2} \log \frac{m^2}{M_F^2} F(z, \zeta), \quad (2.99)$$

$$\Phi_3^q(z, \zeta, 0) = -\frac{N_C e_q^2}{2\pi^2} \log \frac{m^2}{M_F^2} \tilde{F}(z, \zeta). \quad (2.100)$$

Now we are able to write the quark contribution to the $\gamma^*\gamma \rightarrow \gamma\gamma$ amplitude at threshold as a convolution of coefficient functions and GDAs $\Phi_i^q(z, \zeta, 0)$

$$W_1^q = \int_0^1 dz C_V^q(z) \Phi_1^q(z, \zeta, 0), \quad W_3^q = \int_0^1 dz C_A^q(z) \Phi_3^q(z, \zeta, 0), \quad (2.101)$$

where the Born order coefficient functions $C_{V/A}^q$ attached to the quark-antiquark symmetric and antisymmetric correlators are equal to:

$$C_V^q = e_q^2 \left(\frac{1}{z} - \frac{1}{\bar{z}} \right), \quad C_A^q = e_q^2 \left(\frac{1}{z} + \frac{1}{\bar{z}} \right). \quad (2.102)$$

We recover in that way the $\ln \frac{m^2}{M_F^2}$ term in the right hand side of Eq.(2.82). The photon operator contribution involves a new coefficient function of order α_{em}^2 calculated at the factorization scale M_F , which plays the role of the infrared cutoff. This function is convoluted with the photonic correlators $F^{N\mu}(-\frac{y}{2}N)F_\mu^N(\frac{y}{2}N)$ and $F^{N\mu}(-\frac{y}{2}N)\tilde{F}_\mu^N(\frac{y}{2}N)$ (cf Eqs.(2.85, 2.86)) which are of order α_{em}^0 . These convolutions have the same expressions as those in Sec. 2.2.1 (Eqs.(2.79, 2.81)) with the quark mass replaced by the factorization scale, $m \rightarrow M_F$. In this way, we recover the second term in the right hand side of Eq.(2.82). This equation in fact reflects the independence of the scattering amplitude on the choice of the scale M_F , which is controlled by the renormalization group equation.

The factorization scale M_F^2 can be chosen in any convenient way. The choice $M_F^2 = Q^2$ kills the logarithmic terms coming from the contribution of photonic GDAs, so that the scattering amplitude is written (at least in the leading logarithmic approximation) solely in terms of the quark correlators. With $M_F^2 = Q^2$ we interpret

this process within the parton model (see e.g. [224], [217] for an analogous interpretation of parton distributions inside the photon).

Before ending this section, it is interesting to connect our factorized structure with the initial direct computation based on the 6 diagrams of Fig. 2.3. Among these 6 diagrams, the diagrams B and \bar{B} do not have the topology of factorizable diagrams at twist 2, since one cannot isolate a left part from a right part by just cutting two lines, a fact which may seem at odd with our obtained factorized result. It turns out that a careful analysis shows that these (laying) cat-ears diagrams in fact only contribute for regulating UV divergencies. They do not contribute to the leading logarithmic finite part which lead to the definition of the GDA. This is thus consistent with a diagrammatic analysis of factorization involving a quark-antiquark exchange in the s -channel, within a hand-bag diagram interpretation.

2.2.3 The diphoton GDAs and their QCD evolution equations

We have thus demonstrated that it is legitimate to define the Born order diphoton GDAs at zero W and at $M_F = Q$ as

$$\begin{aligned} \Phi_1^q(z, \zeta, 0) &= \frac{N_C e_q^2}{2\pi^2} \log \frac{Q^2}{m^2} \left[\frac{\bar{z}(2z - \zeta)}{\bar{\zeta}} \theta(z - \zeta) + \frac{\bar{z}(2z - \bar{\zeta})}{\zeta} \theta(z - \bar{\zeta}) \right. \\ &\quad \left. + \frac{z(2z - 1 - \zeta)}{\zeta} \theta(\zeta - z) + \frac{z(2z - 1 - \bar{\zeta})}{\bar{\zeta}} \theta(\bar{\zeta} - z) \right] \end{aligned} \quad (2.103)$$

and

$$\begin{aligned} \Phi_3^q(z, \zeta, 0) &= \frac{N_C e_q^2}{2\pi^2} \log \frac{Q^2}{m^2} \left[\frac{\bar{z}\zeta}{\bar{\zeta}} \theta(z - \zeta) - \frac{\bar{z}\bar{\zeta}}{\zeta} \theta(z - \bar{\zeta}) \right. \\ &\quad \left. - \frac{z\bar{\zeta}}{\zeta} \theta(\zeta - z) + \frac{z\zeta}{\bar{\zeta}} \theta(\bar{\zeta} - z) \right]. \end{aligned} \quad (2.104)$$

Since we focus on the leading logarithmic contribution, we only obtain the *anomalous* part of these GDAs. Their z - and ζ -dependence are shown on Figs. 2.4 and 2.5.

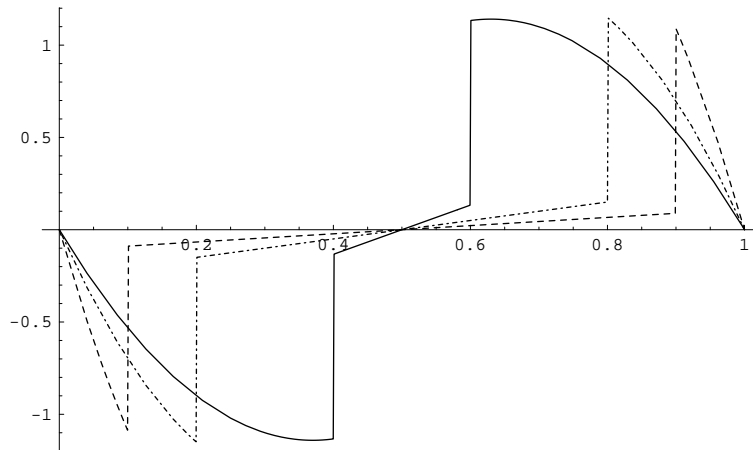


Figure 2.4: The unpolarized anomalous diphoton GDA $\Phi_1^q 2\pi^2 / (N_C e_q^2 \log(Q^2/m^2))$ at Born order and at threshold for $\zeta = 0.1$ (dashed), 0.2 (dash-dotted), 0.4 (solid).

Note that $\Phi_i^q(z, \zeta, 0)$ GDAs are discontinuous functions of z at the points $z = \zeta$ and $z = \bar{\zeta}$. Nevertheless,

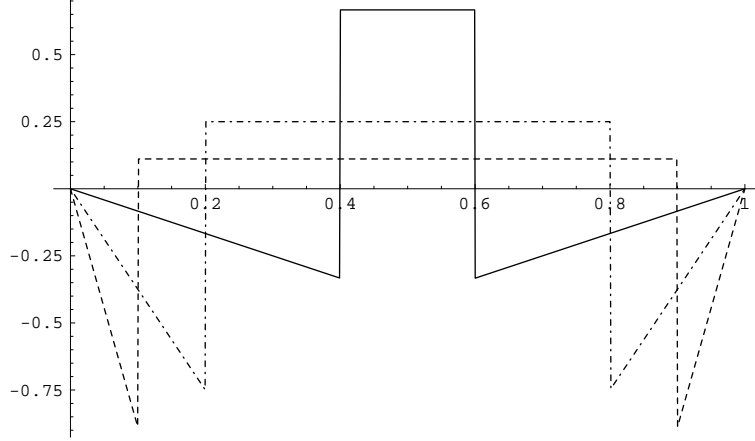


Figure 2.5: The polarized anomalous diphoton GDA $\Phi_3^q 2\pi^2/(N_C e_q^2 \log(Q^2/m^2))$ at Born order and for $\zeta = 0.1$ (dashed), 0.2 (dash-dotted), 0.4 (solid).

these GDAs still verify the property of polynomiality discussed in Sec.2.1.2:

$$\int_0^1 dz (2z-1)^n \Phi_1^q(z, \zeta) = \sum_{k=0}^{n+1} a_k \zeta^k, \quad (2.105)$$

$$\int_0^1 dz (2z-1)^n \Phi_3^q(z, \zeta) = \sum_{k=0}^{n+1} \tilde{a}_k \zeta^k. \quad (2.106)$$

As we have two photons in the final state, the only non vanishing correlators are the C-even one, i.e. the singlet sector of the GDAs which correspond to the combinations of operators $\frac{1}{2}(O^q(x_1, x_2) - O^q(x_2, x_1))$ and $\frac{1}{2}(\tilde{O}^q(x_1, x_2) + \tilde{O}^q(x_2, x_1))$. This singlet sector means for the GDAs Φ_i^q the combinations $\Phi_+^q(z, \zeta, 0) = \frac{1}{2}(\Phi_1^q(z, \zeta, 0) - \Phi_1^q(\bar{z}, \zeta, 0))$ and $\tilde{\Phi}_+^q(z, \zeta, 0) = \frac{1}{2}(\Phi_3^q(z, \zeta, 0) + \Phi_3^q(\bar{z}, \zeta, 0))$, which respectively simplifies into

$$\Phi_+^q(z, \zeta, 0) = \Phi_1^q(z, \zeta, 0) \quad (2.107)$$

and

$$\tilde{\Phi}_+^q(z, \zeta, 0) = \Phi_3^q(z, \zeta, 0). \quad (2.108)$$

One can indeed check on Eqs.(2.103) that

$$\Phi_1(1-z, \zeta) = -C \Phi_1(z, \zeta) = -\Phi_1(z, 1-\zeta), \quad (2.109)$$

with here $C = +$, consistently with (2.11) based on the C -parity properties of the correlator (2.2) of the same non-local operator also entering in Eq.(2.83). On top of the correlators encountered there for the pion case, we now use a non-local correlator (2.84) involving an additional γ^5 matrix, for which

$$\Phi_3(1-z, \zeta) = +C \Phi_3(z, \zeta) = -\Phi_3(z, 1-\zeta), \quad (2.110)$$

with again here $C = +$. This symmetry can be readily check on our result (2.104).

Now, from the point of view of flavor decomposition, we can distinguish either the singlet sector

$$\Phi_+^S \propto \sum_{q=1}^{N_f} \Phi_+^q, \quad \tilde{\Phi}_+^S \propto \sum_{q=1}^{N_f} \tilde{\Phi}_+^q, \quad (2.111)$$

or the non-singlet sector

$$\Phi_+^{NS} = \Phi_+^q - \Phi_+^{q'}, \quad \tilde{\Phi}_+^{NS} = \tilde{\Phi}_+^q - \tilde{\Phi}_+^{q'}, \quad (2.112)$$

where q and q' are two different quark flavors.

Let us illustrate the effect of evolution in the simplest, i.e. without mixing with gluons, case of non-singlet and vector GDA Φ_+^{NS} .

Switching on QCD, the non-singlet and vector sector of diphoton GDAs evolves according to the ERBL evolution equation [48, 65, 66] modified by the presence of the anomalous part (2.103)

$$Q^2 \frac{d}{dQ^2} \Phi_+^{NS}(z, \zeta, Q^2) = \frac{\alpha_s(Q^2)}{2\pi} \int_0^1 du V_{NS}(z, u, Q^2) \Phi_+^{NS}(u, \zeta, Q^2) + (e_q^2 - e_{q'}^2) f_1'(z, \zeta), \quad (2.113)$$

with $\Phi_+^{NS}(z, \zeta, Q^2) = z(1-z)\Phi_+^{NS}(z, \zeta, Q^2)$ and $f_1(z, \zeta) = z(1-z)f_1'(z, \zeta)$. Here $f_1(z, \zeta)$ is defined by the r.h.s. of Eqs.(2.103), as the corresponding functions which multiply $e_q^2 \ln Q^2/m^2$. The QCD kernel V_{NS} is given by (2.21)⁶. Note that the homogeneous part of Eq.(2.113) is equivalent to Eq.(2.15) in the limit $Q^2 \gg m^2$ we are considering here, since from Eq.(2.14) one has

$$\xi(Q^2, m^2) = \frac{2}{\beta_0} \ln \left[1 + \frac{\beta_0}{4\pi} \ln \frac{Q^2}{m^2} \right] \sim \frac{2}{\beta_0} \ln \ln \frac{Q^2}{m^2} + cst. \quad (2.114)$$

As shown in Sec.2.1.2, the kernel V_{NS} is diagonalized in the basis spanned by Gegenbauer polynomials $C_p^{(3/2)}(x)$. This property permits us to write the solution of the equation (2.113) as

$$\Phi_+^{NS}(z, \zeta, Q^2) = z(1-z) \sum_{p \text{ odd}}^{\infty} \left[A_p \left[\log \frac{Q^2}{m^2} \right]^{-6 \frac{\gamma_{qq}(p)}{33-2N_f}} + (e_q^2 - e_{q'}^2) \log \frac{Q^2}{m^2} \frac{f_p'(\zeta)}{1 + 6 \frac{\gamma_{qq}(p)}{33-2N_f}} \right] C_p^{(3/2)}(2z-1), \quad (2.115)$$

where A_p are integration constants, N_f is the number of flavors, $\gamma_{qq}(p)$ are the usual anomalous dimensions (2.28) and the coefficients $f_p'(\zeta)$ are projection of $f_1'(z, \zeta)$ on appropriate $C_p^{(3/2)}$ polynomials

$$f_p'(\zeta) = \frac{4(2p+3)}{(p+1)(p+2)} \int_0^1 dz z \bar{z} f_1'(z, \zeta) C_p^{(3/2)}(2z-1). \quad (2.116)$$

The expressions for $f_p'(\zeta)$ are lengthy, involving hypergeometric functions, and their explicit expression is not illuminating. For large Q^2 , the solution (2.115), at the leading logarithm level, reads

$$\Phi_+^{NS}(z, \zeta, Q^2) \simeq (e_q^2 - e_{q'}^2) \log \frac{Q^2}{m^2} z \bar{z} \sum_{p \text{ odd}}^{\infty} \frac{f_p'(\zeta)}{1 + 6 \frac{\gamma_{qq}(p)}{33-2N_f}} C_p^{(3/2)}(2z-1). \quad (2.117)$$

Due to the non-trivial form of $f_p'(\zeta)$, it was not possible to obtain a resummed form of (2.117), and not even of the asymptotics of the large p terms.

The formula (2.117) shows the known result that the anomalous part of GDAs dominates at large Q^2 . The z, ζ dependences of Φ_1^q are nevertheless modified by strong interaction, due to the presence of the denominator $1 + 6 \frac{\gamma_{qq}(p)}{33-2N_f}$. The result of this method, for $N_f = 2$, is shown in Fig. 2.6. The procedure of decomposing a GDA into series of Gegenbauer polynomials ensures a good numerical description of both the unevolved GDA and the one with the evolution taken into account, except in the regions z close to ζ and $1 - \zeta$. This is technically due to the well known fact that theta function are very badly described by series of polynomials, thus creating spurious oscillations around the points where theta functions changes from 0 to 1, at $z = \zeta$ and $z = 1 - \zeta$. Fig. 2.6 was obtained after combining the sum of 41 (201) contributions of Gegenbauer polynomials for the regions $0 < z < \zeta$ and $1 - \zeta < z < 1$ ($\zeta < z < 1 - \zeta$). Such a choice for the regions $0 < z < \zeta$ and $1 - \zeta < z < 1$ is motivated by numerical instabilities of the Gegenbauer series (2.117) when z is close to 0 and 1, which requires to truncate the series at a moderate number of terms (41 terms), which nevertheless leads to a good stability of results. These numerical instabilities are due to the fact that, as soon as z deviates from 0 or 1, $f_p'(\zeta)$ (Eq.(2.116)) becomes very large with ζ fixed and p larger than 50. This is in contrast with the region $\zeta < z < 1 - \zeta$ where a very good stability of the results is achieved when summing a very high number of terms (we took 201 terms: taking more terms would then generate huge instabilities in the vicinity of ζ and $1 - \zeta$).

⁶Note that with respect to Ref.[W22] the notation for V_{NS} is changed, by a permutation of the arguments z and u and by factorizing the factor $\alpha_s(Q^2)/(2\pi)$.

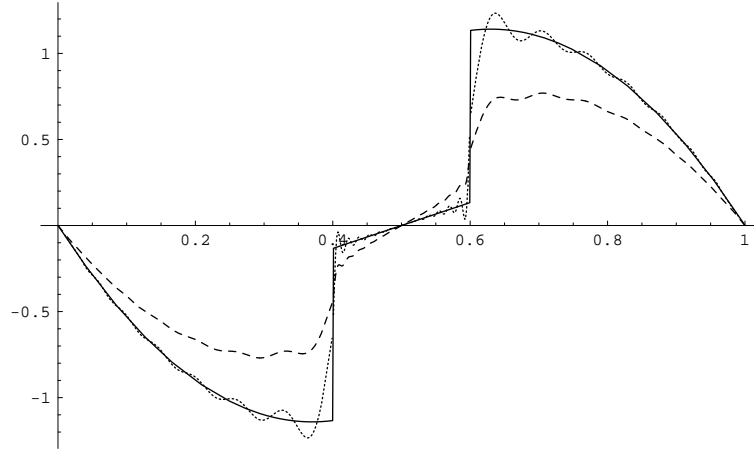


Figure 2.6: The bare (solid line) and the QCD evolved (dashed line) non-singlet and vector sector of diphoton GDA at large Q^2 $\Phi_+^{NS}/((e_q'^2 - e_q^2) \log(Q^2/m^2))$ (see Eq.(2.117)) for $\zeta = 0.2$. The dotted line is the truncated (see text) Gegenbauer expansion of the bare GDA.

As can be seen from Fig. 2.6, QCD evolution affects the form of the GDA in the whole z range. In practice, one cannot trust the truncated Gegenbauer expansion near the discontinuity points. To obtain a trustable behaviour of the evolved GDA around $z = \zeta$ and $z = \bar{\zeta}$, one has to sum in Eq.(2.117) the infinite series involving Gegenbauer polynomials, which is a non trivial task. Because of that, one could think about a method based on direct iteration of the non-homogeneous equation (2.113), keeping only the leading terms at large Q^2 . In particular, we have solved the evolution equation (2.113, 2.21) in the vicinity of singularity points $z = \zeta, 1 - \zeta$. Because of the antisymmetry of the GDA (2.103), let us concentrate our discussion on the form of the evolved GDA around the singular point $z = \zeta$. The iteration of the kernel (2.113) generates leading terms of the form $K^n \ln^n(\zeta - z)$ for $z \rightarrow \zeta^-$ and $K^n \ln^n(z - \zeta)$ for $z \rightarrow \zeta^+$, which we resummed. The details of the

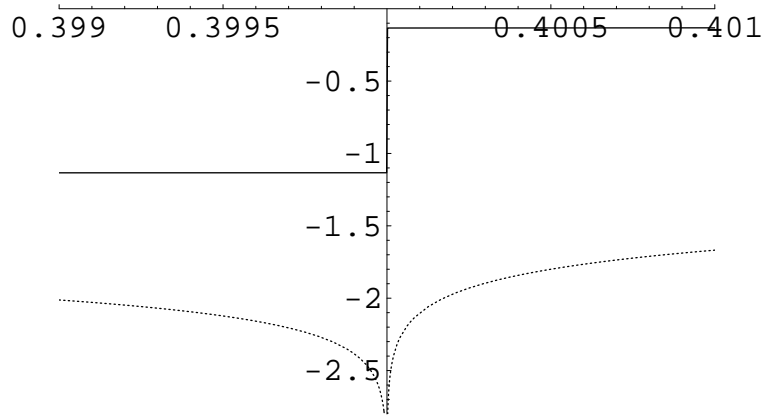


Figure 2.7: The behaviour of the evolved GDA from the leading logarithmic resummations (2.118, 2.119) in the vicinity of the discontinuity point $z = \zeta$, for the case $\zeta = .4$ (dotted curve). The Born GDA is given for reference as the solid line.

method can be found in the Appendix of Ref. [22]. The key point there is to approximate correctly the kernel without spoiling the series which should be resummed. Physically, this series corresponds to the resummation of soft gluons exchanged between quark-antiquark lines, when iterating the ERBL kernel on the bare GDA. The

result of this resummation is

$$\Phi_+^{NS}(z \rightarrow \zeta^-, \zeta) = \frac{1}{2} (e_q^2 - e_{q'}^2) \log \frac{Q^2}{m^2} \left[\frac{4\zeta^2 - \zeta - 1}{\bar{\zeta}} (1 - K \ln(\zeta - z)) + \frac{1}{1 - K \ln(\zeta - z)} \right] \quad (2.118)$$

and

$$\Phi_+^{NS}(z \rightarrow \zeta^+, \zeta) = \frac{1}{2} (e_q^2 - e_{q'}^2) \log \frac{Q^2}{m^2} \left[\frac{4\zeta^2 - \zeta - 1}{\bar{\zeta}} (1 - K \ln(z - \zeta)) - \frac{1}{1 - K \ln(z - \zeta)} \right], \quad (2.119)$$

where $K = 6C_F/(11N_C - 2N_f)$. We display in Fig. 2.7 the asymptotic resummation given by Eqs.(2.118,2.119). As mentioned above, the resummation of logarithmic contribution is required in the regions $K \log |z - \zeta| \gtrsim 1$ and $K \log |z - \bar{\zeta}| \gtrsim 1$, which in our case ($K = 8/29$) corresponds to $|z - \zeta|, |z - \bar{\zeta}| \lesssim 3 \cdot 10^{-2}$. In practice, subleading contributions are non negligible in a larger domain in z around ζ and $\bar{\zeta}$, and prevent us from getting trustable numerical results based on this iterative method. This is due to the numerically large values of K .

One can check that this iterative method stabilizes only when applied for unphysically small values of K (typically $\lesssim .03$). In that case, we could verify numerically the efficiency of our resummation.

Note that these singularities of the GDA at $z = \zeta$ and $z = 1 - \zeta$ does not affect the DVCS amplitude (2.101) since they are integrable singularities⁷. The study of these singularities is however important since the photon GDA is a universal object which is process independent.

We have thus derived the leading amplitude of the DVCS (polarization averaged or polarized) process on a photon target at threshold. We have shown that the amplitude coefficients W_i^q factorize in the forms shown in Eq.(2.101), irrespectively of the fact that the handbag diagram interpretation appears only *after* cancellation of UV divergencies in the scattering amplitude. We have shown that the objects $\Phi_i^q(z, \zeta, 0)$ are matrix elements of non-local quark operators on the light cone, and that they have an anomalous component which is proportional to $\log(Q^2/m^2)$. They thus have all the properties attached to generalized distribution amplitudes, and they obey *non-homogeneous* ERBL evolution equations. This new type of evolution equations is an interesting playground to study the effects of gluon radiation on a non diagonal object such as a GDA.

2.3 Crossing $s \leftrightarrow u$: TDAs

In the same spirit of the crossing $s \leftrightarrow t$ which lead from the GPD to the GDA, one can investigate the crossing $t \leftrightarrow u$. GPDs occurs in DVCS in the small scattering angle regime. Similarly, the study of DVCS in the regime where the scattering angle is around π corresponds to the small u limit, for s fixed. This regime leads naturally to the introduction of the concept of Transition Distribution Amplitude (TDA), obtained by analytic continuation from GPD by $t \leftrightarrow u$ crossing [225,226], as illustrated in Fig. 2.8. Consider a process of the type

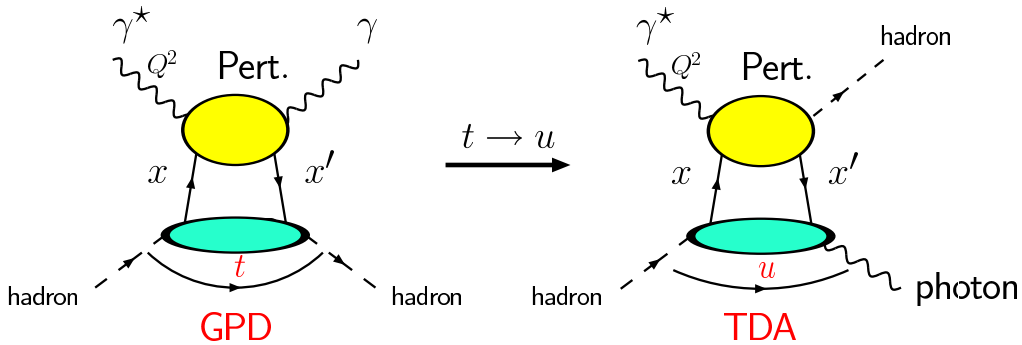


Figure 2.8: Passing from GPD to TDA, illustrated here for the pion case.

$ab \rightarrow cd$, where a is for illustration a hard γ^* , and other particles are on-shell (and neglecting masses) (see the conventions of Fig. 2.9), e.g. $\gamma^* \pi \rightarrow \gamma \pi$. In particular the process $\gamma^* p \rightarrow p \gamma$ in the backward regime should be studied a JLab in the near future [227].

⁷The coefficient function C_V^q (2.102) is regular. This would remain true after taking into account its QCD evolution.

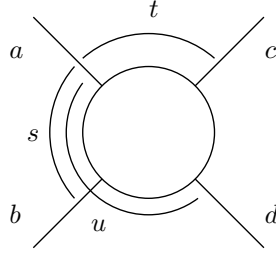
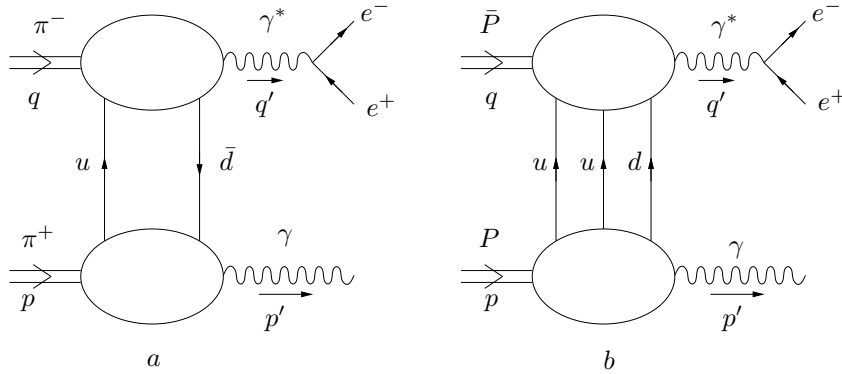


Figure 2.9: Mandelstam variables.

Figure 2.10: The factorization of the annihilation process $\bar{H} H \rightarrow \gamma^* \gamma$ into a hard subprocess (upper blob) and a transition distribution amplitude (lower blob) for the meson case (a) and the baryon case (b). Figure taken from Ref. [226].

One can construct a Sudakov basis from the momentum of particle b (p_2) and through the expansion of the momentum of the hard photon a as $q = p_1 - Q^2/s p_2$ which thus defines p_1 . In that frame, in the kinematics we are considering now, the particle c almost flies along p_2 . A similar analysis as the one leading to the introduction of GPDs from DVCS, for which d would fly almost along p_2 , shows that one can expect a factorization between a hard coefficient function, describing the transition $\gamma^* \rightarrow c$ in a perturbative manner, and a TDA, which describes the non-perturbative transition $b \rightarrow d$. The main difference with the GPDs lies on the fact that the TDA is not anymore diagonal in the quantum numbers, since there is now a non-trivial exchange of quantum numbers in the t -channel. A natural generalisation of the process $\gamma^* N \rightarrow \gamma N$ is obtained when replacing the produced photon by a pion, through its corresponding DA [228].

From this direct connection with GPDs from $t \leftrightarrow u$ crossing, used as a starting example, one can further apply the notion of TDA for other processes related by the additional crossing $s \leftrightarrow u$. For example, in the case where c is a hard time-like photon (seen as a lepton-antilepton pair) providing the hard scale, one can consider the annihilation processes $\pi^- \pi^+ \rightarrow \gamma^* \gamma$ or $\bar{p} p \rightarrow \gamma^* \gamma$ in the near forward regime (see Fig. 2.10). This process is expected to be studied at PANDA [229] and was studied in detail in Ref. [230]. The related process $\gamma^* \gamma \rightarrow \pi^- \pi^+$ at small t was investigated in Ref. [231]. In these processes, the quantum number which are exchanged in the t -channel are respectively the one of a pion and of a proton. The computation of the hard part for these two processes goes along the same line as the one for the hard part of the DVCS, after projecting the t -channel state on appropriate quantum numbers. In the case of the process $\bar{p} p \rightarrow \gamma^* \gamma$, instead of the $\langle p | u(z_1) u(z_2) d(z_3) | p \rangle$ matrix element, diagonal in baryonic quantum numbers, one introduces the matrix element $\langle \gamma | u(z_1) u(z_2) d(z_3) | p \rangle$ of a non-local operator which carries a baryonic quantum numbers. The hard part describes the perturbative $\bar{q} q \bar{q} q \rightarrow \gamma^*$ transition, which should be convoluted with the antiproton DA to describe the $\bar{p} q q q \rightarrow \gamma^*$ transition. A similar analysis [226] can be carried for the process $\bar{p} p \rightarrow \gamma^* \pi$, involving this time the TDA defined through $\langle \pi | u(z_1) u(z_2) d(z_3) | p \rangle$ matrix elements, as illustrated in Fig. 2.11.

Before illustrating the appearance of TDA in a specific perturbative example, we end this section by noting the fact that TDA satisfy QCD evolution equation of the same type as the one for GPDs.

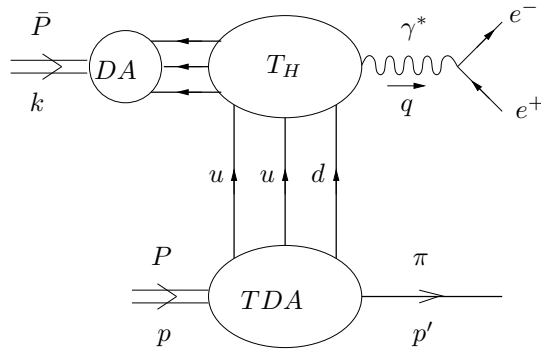


Figure 2.11: The factorization of the annihilation process $\bar{p} p \rightarrow \gamma^* \pi$ into the antiproton distribution amplitude (DA), the hard subprocess amplitude (T_H) and a baryon \rightarrow meson transition distribution amplitude (TDA). Figure taken from Ref. [225].

2.4 An (almost) perturbative situation: $\gamma^* \gamma^* \rightarrow \rho_L^0 \rho_L^0$

Based on [W19]

We will now consider an (almost) perturbative situation where one may describe the same process in a factorized form involving a GDA or a TDA, depending on the kinematical regime and on the polarization of the states [W19, W43, W44, W40]. We consider the process

$$\gamma^*(Q_1^2) \gamma^*(Q_2^2) \rightarrow \rho_L^0 \rho_L^0. \quad (2.120)$$

Our study was motivated by several reasons. First, based on our investigations of this process in the perturbative Regge limit, see Sec. 7.4, the present study at Born order is a way to control precisely the contribution of quark exchange with respect to gluon exchange, which dominates at large W^2 , although suppressed in the power counting of α_s . Second, due to presence of several scales (Q_1^2 , Q_2^2 and W^2) in this process, it is a very interesting process for factorization studies.

We will show by a Born order analysis that the scattering amplitude simultaneously factorizes in two quite different ways: the part with transverse photons is described by the QCD factorization formula involving the generalized distribution amplitude of two final ρ mesons, whereas the part with longitudinally polarized photons takes the QCD factorized form with the $\gamma_L^* \rightarrow \rho_L^0$ transition distribution amplitude. In this peculiar example which is almost perturbative, we will compute perturbative expressions for these GDA and TDA, which, as we saw in previous sections, are in general, non-perturbative functions, in terms of the ρ -meson distribution amplitude.

Note that we focus here on the peculiar case of transversally produced ρ -meson to avoid any complication due to higher twist contributions which one should then consider. Therefore, our treatment will exhibit a factorization at twist 2 level.

The contribution which we will investigate now is based on quark exchange. At high energy, in the Regge limit which we will investigate later in Sec. 7.4, gluonic exchange in t -channel would dominate, and large logarithms of s could compensate the higher power in α_s . We will not be concerned here by this regime, although the present study will provide us some typical cuts on the kinematical regime in which one or another dynamics is applicable.

The Born order contribution with quark exchanges is described by the same set of diagrams which contribute to the scattering of real photons producing pions, e.g. $\gamma\gamma \rightarrow \pi^+\pi^-$, at large momentum transfer, studied long ago by Brodsky and Lepage [10] in the framework of the factorized form of exclusive processes at fixed angle [48, 65, 66], in which mesons are described by their light-cone distribution amplitudes (DAs). This is illustrated in Fig. 7.11. In this sense our present study can be seen as a complement of Ref. [10] for the case of the scattering with virtual photons, i.e. with both, transverse and longitudinal polarizations, and in the forward kinematics. A similar analysis was carried in Ref. [232] for the process $\gamma_T^* \gamma_T^* \rightarrow \pi^+\pi^-$, in the regime $s, -t, -u \gg \Lambda_{QCD}^2$, for which a factorization involving a GDA could occur, and where the GDA could be

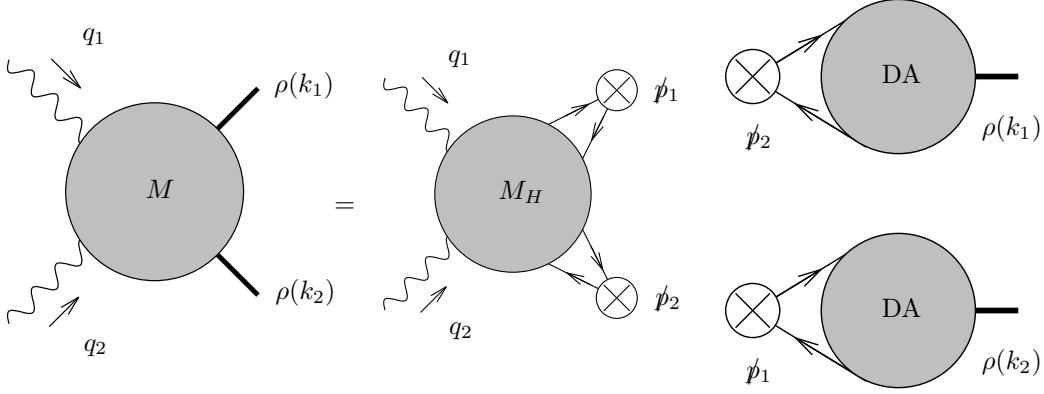


Figure 2.12: The amplitude of the process $\gamma^*(Q_1)\gamma^*(Q_2) \rightarrow \rho_L^0(k_1)\rho_L^0(k_2)$ in the collinear factorization.

computed in terms of the pion DAs. Since we will deal with longitudinally polarized ρ -meson, our results for the transition $\gamma_T^* \gamma_T \rightarrow \rho_L^0 \rho_L^0$, will be rather similar when considering the same peculiar kinematical regime.

In our case, the virtualities $Q_i^2 = -q_i^2$, $i = 1, 2$, supply the hard scale to the process (2.120) which justifies the use of the QCD collinear factorization methods and the description of ρ mesons by means of their distribution amplitudes.

2.4.1 Kinematics

As usual, we rely on a Sudakov basis (defined through p_1 and p_2 with $2p_1 \cdot p_2 = s$), in such a way that the two incoming virtual photon would fly along p_1 and p_2 if they would be on-shell. In the forward regime that we are investigating, there is no transverse momentum and therefore no complicated tensorial structures can occur. This is however only a technical simplification, and the approach would be very similar in the non-forward case. The photon momenta thus reads

$$q_1 = p_1 - \frac{Q_1^2}{s} p_2 \quad q_2 = p_2 - \frac{Q_2^2}{s} p_1, \quad (2.121)$$

and neglecting the meson masses, their momenta reads

$$k_1 = \left(1 - \frac{Q_2^2}{s}\right) p_1 \quad k_2 = \left(1 - \frac{Q_1^2}{s}\right) p_2. \quad (2.122)$$

The positivity of energy of produced ρ 's requires that $s \geq Q_i^2$. The usual invariant W^2 is defined as

$$W^2 = (q_1 + q_2)^2 = (k_1 + k_2)^2 = s \left(1 - \frac{Q_1^2}{s}\right) \left(1 - \frac{Q_2^2}{s}\right), \quad (2.123)$$

or

$$s = \frac{1}{2} [Q_1^2 + Q_2^2 + W^2 + \lambda(Q_1^2, Q_2^2, -W^2)], \quad (2.124)$$

with $\lambda(x, y, z) \equiv \sqrt{x^2 + y^2 + z^2 - 2xy - 2xz - 2zy}$, while the minimum squared momentum transfer is

$$t_{min} = (q_2 - k_2)^2 = (q_1 + k_1)^2 = -\frac{Q_1^2 Q_2^2}{s}. \quad (2.125)$$

We note that, contrarily to the large angle case where all Mandelstam invariants were assumed to be large, as studied in Ref. [10], here t_{min} may not be large with respect to Λ_{QCD}^2 depending on the respective values of Q_1^2 , Q_2^2 and W^2 . The above kinematics is written in a form which seems compatible with a TDA type of factorization (“upper” and “lower” meson flies along two different light-cone directions) and not to a GDA factorization. We will see below that this is just an artefact of our treatment restricted to the forward case, which in fact does not prevent a GDA-type of factorization.

2.4.2 The Born order amplitude

The scattering amplitude \mathcal{A} of the process (2.120) can be written in the form

$$\mathcal{A} = T^{\mu\nu} \epsilon_\mu(q_1) \epsilon_\nu(q_2), \quad (2.126)$$

where the tensor $T^{\mu\nu}$ has in the above kinematics a simple decomposition which is consistent with Lorentz covariance and electromagnetic gauge invariance

$$T^{\mu\nu} = \frac{1}{2} g_T^{\mu\nu} (T^{\alpha\beta} g_{T\alpha\beta}) + (p_1^\mu + \frac{Q_1^2}{s} p_2^\mu)(p_2^\nu + \frac{Q_2^2}{s} p_1^\nu) \frac{4}{s^2} (T^{\alpha\beta} p_{2\alpha} p_{1\beta}), \quad (2.127)$$

and where the transverse projector reads $g_T^{\mu\nu} = g^{\mu\nu} - (p_1^\mu p_2^\nu + p_1^\nu p_2^\mu)/(p_1 \cdot p_2)$. The first term on the rhs of Eq. (2.127) contributes in the case of transversely polarized photons, the second one for longitudinally polarized virtual photons. The longitudinally polarized ρ^0 -meson DA $\phi(z)$ is defined from the non-local correlator (1.76). Taking into account the ρ^0 -wave function, it reads

$$\langle \rho_L^0(k) | \bar{q}(x) \gamma^\mu q(0) | 0 \rangle = \frac{f_\rho}{\sqrt{2}} k^\mu \int_0^1 dz e^{iz(kx)} \phi(z), \quad \text{for } q = u, d, \quad (2.128)$$

proportional to the coupling constant f_ρ , and where as usual for simplicity of notation we omit the Wilson line.

The Born order contribution to the amplitude (2.126) is calculated in a similar way as in the classical work of Brodsky-Lepage [10] but in very different kinematics. In our case the virtualities of photons supply the hard scale, and not the transverse momentum transfer. Within the collinear approximation, the momenta of the quarks and antiquarks which constitute the ρ -mesons can be written as

$$\begin{aligned} \ell_1 &\sim z_1 k_1, & \ell_2 &\sim z_2 k_2 \\ \tilde{\ell}_1 &\sim \bar{z}_1 k_1, & \tilde{\ell}_2 &\sim \bar{z}_2 k_2. \end{aligned} \quad (2.129)$$

There are 20 possible diagrams, which can be organized into two classes. The first class corresponds to the diagrams where the two virtual photons couple to two different quark lines, leading to 8 different diagrams, as illustrated in Fig. 2.13. The second class of diagrams corresponds to the one where the two virtual photons are coupled to the same quark line, resulting into 12 different contributions, as illustrated in Fig. 2.14.

We first focus on the case of longitudinally polarized photon. Their polarization read

$$\epsilon_{\parallel}(q_1) = \frac{1}{Q_1} q_1 + \frac{2Q_1}{s} p_2 \quad \text{and} \quad \epsilon_{\parallel}(q_2) = \frac{1}{Q_2} q_2 + \frac{2Q_2}{s} p_1. \quad (2.130)$$

Due to the gauge invariance of the total amplitude, when computing each Feynman diagrams, one can make use of the fact that the longitudinal polarization of photon 1 (resp. 2) can be effectively considered as proportional to p_2 (resp. p_1), in accordance with the structure of the second term of Eq.(2.127). One then readily sees that in the kinematics we are investigating, the only diagrams which are non zero in the Feynman gauge are the diagrams $(1b) \otimes (2a)$, $(3a) \otimes (4b)$ on the one hand, and $(s2)$, $(s2')$ on the other hand, leading to the 4 diagrams illustrated in Fig. 2.15.

Second, for transversally polarized virtual photons, described by the first term in Eq.(2.127), one needs to contract the two polarization indices through the two dimensional identity tensor $g_{\mu\nu}^T$. The four non vanishing graphs corresponding to the coupling of the photons to different quark lines are $(1a) \otimes (2b)$, $(1b) \otimes (2a)$, $(3a) \otimes (4b)$ and $(3b) \otimes (4a)$. When considering the graphs corresponding to the coupling of the photons to the same quark line, the above mentioned contraction kills the graphs $(s2)$, $(s2')$ and $(s5)$, $(s5')$, that is the graphs where the gluon is emitted from the quark connecting the two virtual photons. In this second class of diagrams, 8 diagrams thus remain. The whole set of twelve diagrams to be computed is shown in Fig. 2.16.

It should be noted that in the peculiar kinematics which is chosen here, the only diagrams which contribute both to the longitudinal and to the transverse virtual photon cases are $(1b) \otimes (2a)$, $(3a) \otimes (4b)$, that is the two first diagrams of Fig. 2.15 and Fig. 2.16.

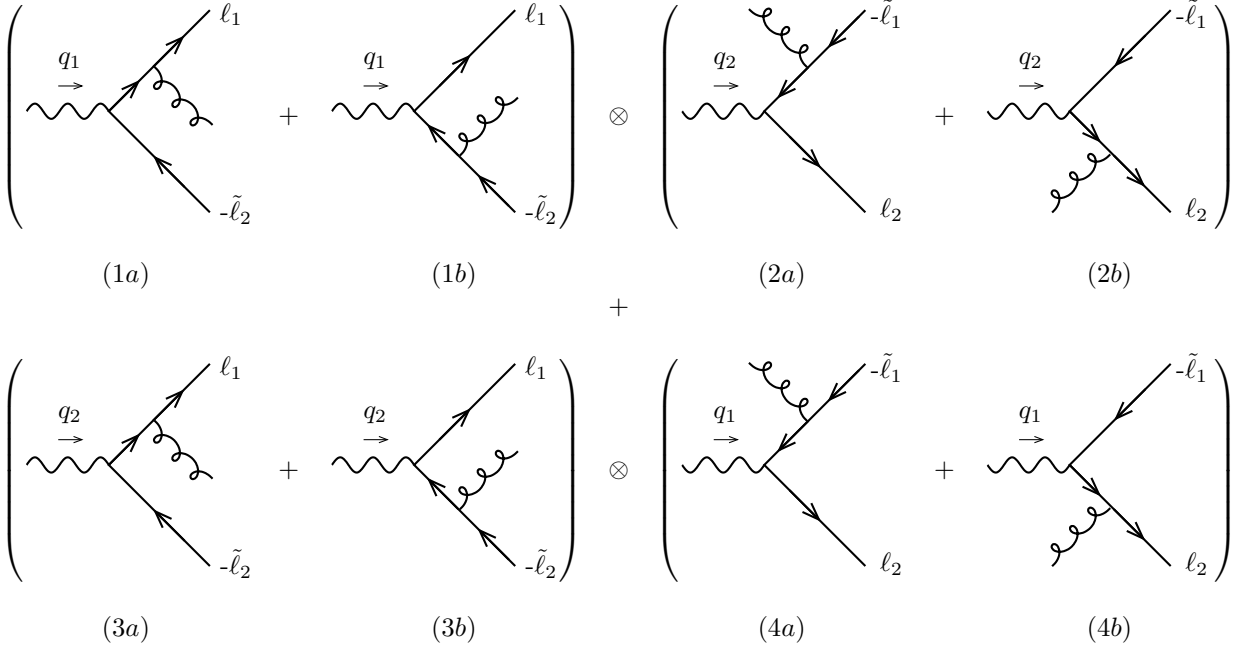


Figure 2.13: Feynman diagrams contributing to M_H , in which the virtual photons couple to different quark lines.

Our final result for the scalar components of the scattering amplitude (2.127) reads :

$$T^{\alpha\beta} g_{T\alpha\beta} = -\frac{e^2(Q_u^2 + Q_d^2)g^2 C_F f_\rho^2}{4N_c s} \int_0^1 dz_1 dz_2 \phi(z_1) \phi(z_2) \quad (2.131)$$

$$\times \left\{ 2 \left(1 - \frac{Q_2^2}{s}\right) \left(1 - \frac{Q_1^2}{s}\right) \left[\frac{1}{(z_2 + \bar{z}_2 \frac{Q_1^2}{s})^2 (z_1 + \bar{z}_1 \frac{Q_2^2}{s})^2} + \frac{1}{(\bar{z}_2 + z_2 \frac{Q_1^2}{s})^2 (\bar{z}_1 + z_1 \frac{Q_2^2}{s})^2} \right] + \left(\frac{1}{\bar{z}_2 z_1} - \frac{1}{\bar{z}_1 z_2} \right) \left[\frac{1}{1 - \frac{Q_2^2}{s}} \left(\frac{1}{\bar{z}_2 + z_2 \frac{Q_1^2}{s}} - \frac{1}{z_2 + \bar{z}_2 \frac{Q_1^2}{s}} \right) - \frac{1}{1 - \frac{Q_1^2}{s}} \left(\frac{1}{\bar{z}_1 + z_1 \frac{Q_2^2}{s}} - \frac{1}{z_1 + \bar{z}_1 \frac{Q_2^2}{s}} \right) \right] \right\}$$

$$T^{\alpha\beta} p_{2\alpha} p_{1\beta} = -\frac{s^2 f_\rho^2 C_F e^2 g^2 (Q_u^2 + Q_d^2)}{8N_c Q_1^2 Q_2^2} \int_0^1 dz_1 dz_2 \phi(z_1) \phi(z_2) \quad (2.132)$$

$$\times \left\{ \frac{(1 - \frac{Q_1^2}{s})(1 - \frac{Q_2^2}{s})}{(z_1 + \bar{z}_1 \frac{Q_2^2}{s})(z_2 + \bar{z}_2 \frac{Q_1^2}{s})} + \frac{(1 - \frac{Q_1^2}{s})(1 - \frac{Q_2^2}{s})}{(\bar{z}_1 + z_1 \frac{Q_2^2}{s})(\bar{z}_2 + z_2 \frac{Q_1^2}{s})} + \frac{1}{z_2 \bar{z}_1} + \frac{1}{z_1 \bar{z}_2} \right\},$$

where $Q_u = 2/3$ ($Q_d = -1/3$) denote the charge of the quark u (d).

The above results are obtained for arbitrary values of the photon virtualities Q_i . A closer look into formulas (2.126-2.132) leads to the conclusion that all integrals over quarks momentum fractions z_i are convergent due to the non-zero values of Q_i . Further inspection of the amplitudes (2.126-2.132) reveals that the transverse photon part has a behaviour like $1/W^2$ while the longitudinal photon part behaves like $1/(Q_1 Q_2)$. We will correspondingly now distinguish two regions:

- (a) the region where the squared invariant mass of the two rho's W^2 is much smaller than the largest photon virtualities, namely $Q_1^2 \gg W^2$ (or $Q_2^2 \gg W^2$), with Q_1 and Q_2 being not parametrically close. This will lead to a factorization regime involving a two- ρ GDA.

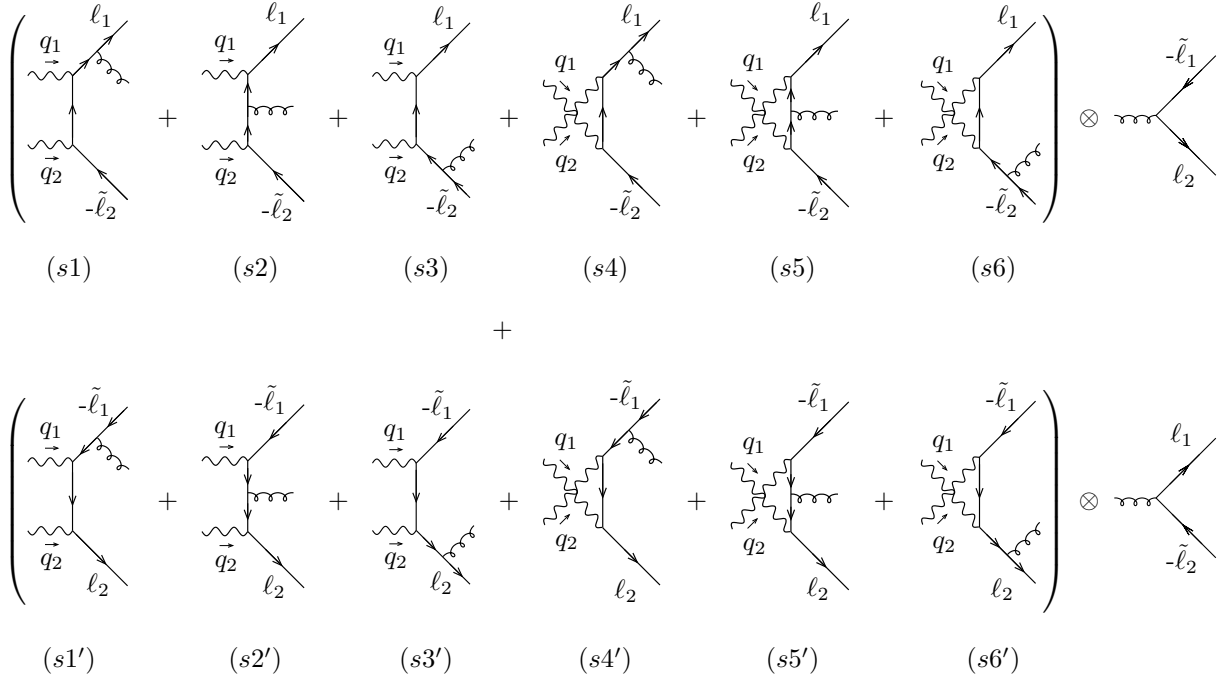


Figure 2.14: Feynman diagrams contributing to M_H , in which the virtual photons couple to a single quark line.

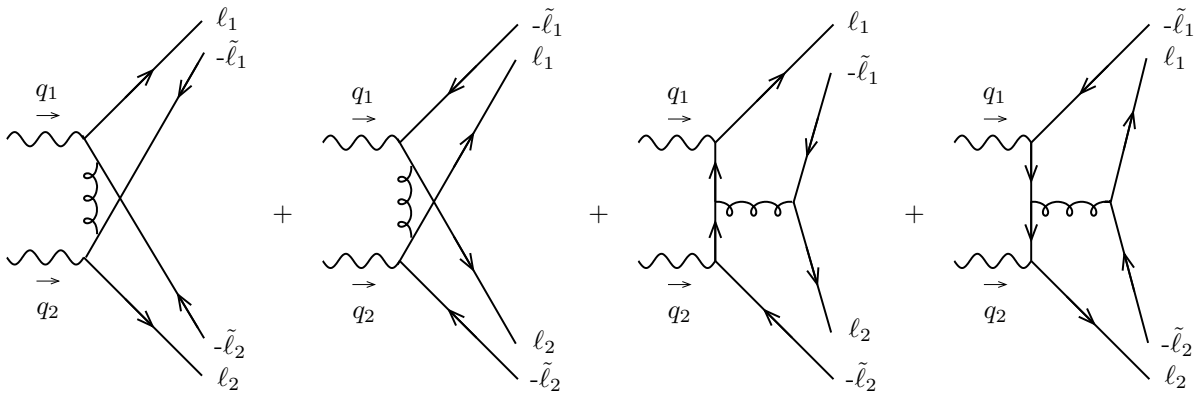
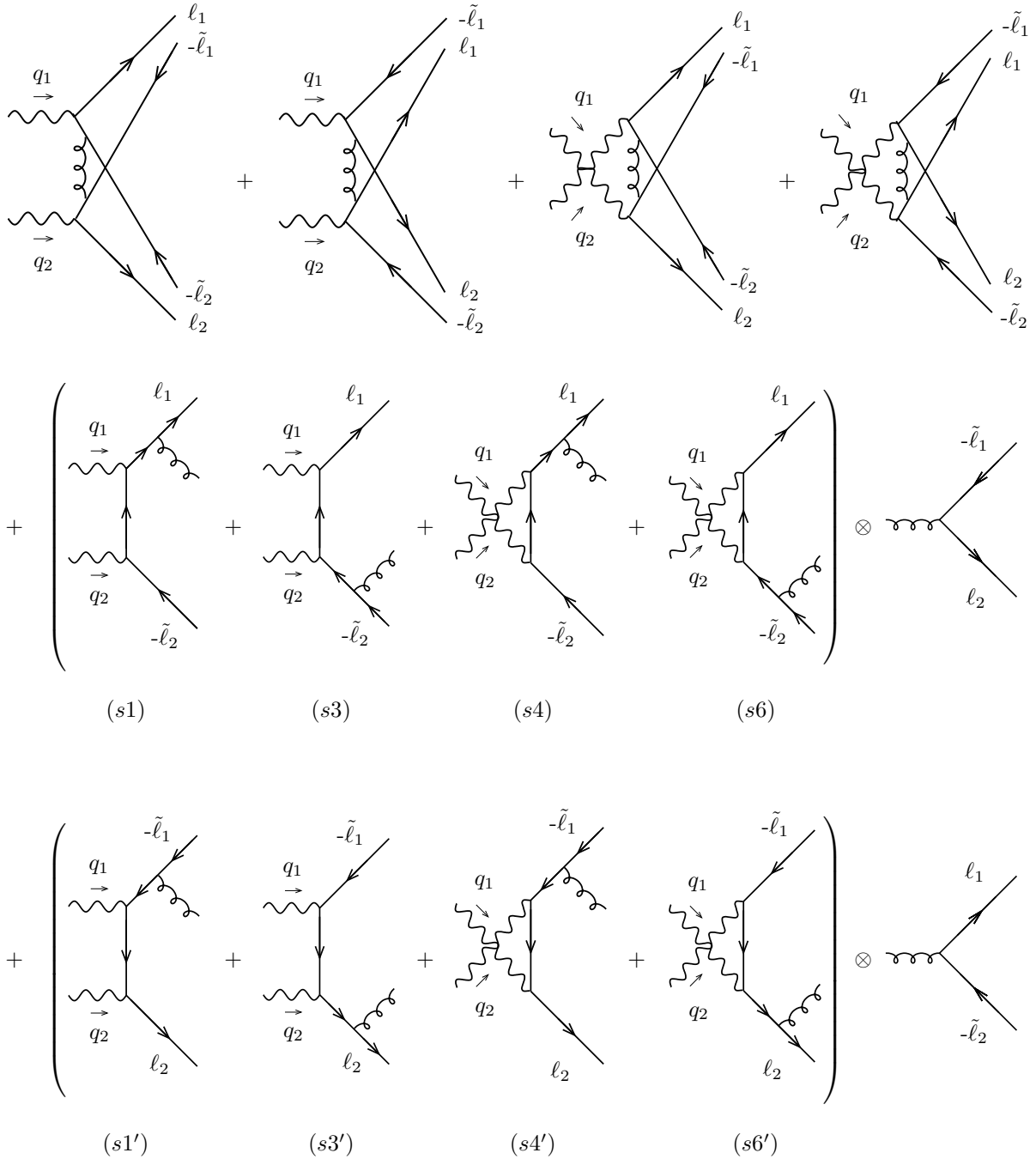


Figure 2.15: Feynman diagrams contributing to M_H in the case of longitudinally polarized virtual photons.

Figure 2.16: Feynman diagrams contributing to M_H in the case of transversally polarized virtual photons.

- (b) the region where photon virtualities are strongly ordered, that is $Q_1^2 \gg Q_2^2$ (or $Q_2^2 \gg Q_1^2$). This will lead to a factorization regime involving a $\gamma^* \rightarrow \rho$ TDA.

2.4.3 $\gamma_T^* \gamma_T^* \rightarrow \rho_L^0 \rho_L^0$ in the generalized Bjorken limit

We first focus on the region where the scattering energy W is small in comparison with the highest photon virtuality, arbitrarily chosen to be Q_1

$$\frac{W^2}{Q_1^2} = \frac{s}{Q_1^2} \left(1 - \frac{Q_1^2}{s}\right) \left(1 - \frac{Q_2^2}{s}\right) \approx 1 - \frac{Q_1^2}{s} \ll 1, \quad (2.133)$$

which leads to the kinematical conditions very close to the ones considered in Sec.2.1 when discussing the factorization of $\gamma_T^* \gamma_T \rightarrow \pi\pi$ near threshold in terms of a perturbatively calculable coefficient function convoluted with a GDA, or in Sec.2.2 when considering $\gamma_T^* \gamma_T \rightarrow \gamma\gamma$ at threshold. We will recover a similar type of factorization with a GDA of the expression (2.131) also in the case of our process (2.120), as illustrated in Fig. 2.17, provided Q_1 and Q_2 are not parametrically close (we shall come back to the peculiar case $Q_1 = Q_2$

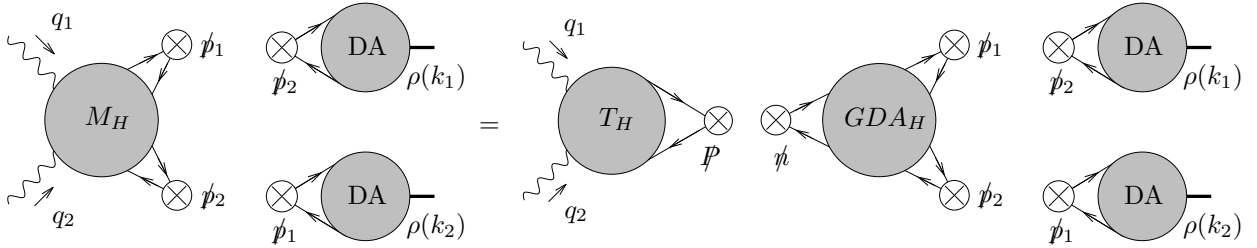


Figure 2.17: Factorisation of the amplitude in terms of a GDA.

at the end of this section), i.e.

$$1 - \frac{Q_1^2}{s} \ll 1 - \frac{Q_2^2}{s}. \quad (2.134)$$

Indeed, in the scaling limit (2.133) with (2.134), the contribution of the four cats-ears diagrams (i.e. the first line of Fig. 2.16), which corresponds to the second line of (2.131), is subdominant and the dominant contribution is given by the last term in (2.131), i.e.

$$T^{\alpha\beta} g_{T\alpha\beta} \approx \frac{e^2(Q_u^2 + Q_d^2) g^2 C_F f_\rho^2}{4 N_c W^2} \int_0^1 dz_1 dz_2 \phi(z_1) \phi(z_2) \quad (2.135)$$

$$\left(\frac{1}{\bar{z}_2 z_1} - \frac{1}{\bar{z}_1 z_2} \right) \left(\frac{1}{\bar{z}_1 + z_1 \frac{Q_2^2}{s}} - \frac{1}{z_1 + \bar{z}_1 \frac{Q_2^2}{s}} \right).$$

The virtuality Q_2 plays in the expression (2.135) the role of a regulator of the end-point singularities. Before recovering each factor of the factorized equation (2.135) by a direct calculation, let us discuss the physics which is behind. In Fig. 2.16, the diagrams which contribute in the scaling region (2.133) with (2.134) are (s3), (s3') and (s6), (s6').

The sum of these four diagrams factorizes into a hard part convoluted with a soft (but still perturbative) part.

This result can be understood diagrammatically by investigating the typical virtualities of the hard quark connecting the two virtual photons (denoted as p_H^2), and the virtuality of the quark connecting the emitted

gluon to the virtual photon (denoted as p_S^2). One gets, for the 8 non-vanishing diagrams,

$$(s1) \quad p_H^2 = z_2 W^2 \quad p_S^2 = -Q_2^2 \left(z_2 + \bar{z}_2 \frac{Q_1^2}{s} \right) \quad (2.136)$$

$$(s3) \quad p_H^2 = \bar{z}_1 W^2 \quad p_S^2 = -Q_1^2 \left(\bar{z}_1 + z_1 \frac{Q_2^2}{s} \right) \quad (2.137)$$

$$(s4) \quad p_H^2 = z_2 W^2 \quad p_S^2 = -s \left(\bar{z}_2 + z_2 \frac{Q_1^2}{s} \right) \quad (2.138)$$

$$(s6) \quad p_H^2 = \bar{z}_1 W^2 \quad p_S^2 = -s \left(z_1 + \bar{z}_1 \frac{Q_2^2}{s} \right) \quad (2.139)$$

$$(s1') \quad p_H^2 = \bar{z}_2 W^2 \quad p_S^2 = -Q_2^2 \left(\bar{z}_2 + z_2 \frac{Q_1^2}{s} \right) \quad (2.140)$$

$$(s3') \quad p_H^2 = z_1 W^2 \quad p_S^2 = -Q_1^2 \left(z_1 + \bar{z}_1 \frac{Q_2^2}{s} \right) \quad (2.141)$$

$$(s4') \quad p_H^2 = \bar{z}_2 W^2 \quad p_S^2 = -s \left(z_2 + \bar{z}_2 \frac{Q_1^2}{s} \right) \quad (2.142)$$

$$(s6') \quad p_H^2 = z_1 W^2 \quad p_S^2 = -s \left(\bar{z}_1 + z_1 \frac{Q_2^2}{s} \right). \quad (2.143)$$

The gluon propagator has a virtuality $p_G^2 = s \bar{z}_1 z_2 \left(1 - \frac{Q_2^2}{s} \right) \left(1 - \frac{Q_1^2}{s} \right) \sim \bar{z}_1 z_2 W^2$ for diagrams (s1), (s3), (s4), (s6) and $p_G^2 = s \bar{z}_2 z_1 \left(1 - \frac{Q_2^2}{s} \right) \left(1 - \frac{Q_1^2}{s} \right) \sim z_1 \bar{z}_2 W^2$ for diagrams (s1'), (s3'), (s4'), (s6'). A careful analysis of the numerators of these diagrams shows that under the constraint (2.134), the diagrams (s3), (s3') and (s6), (s6') dominates with respect to the 4 other ones (this is an artefact of our forward kinematics which force us to insert this additional constraint in order to get a GDA factorization). Then, comparing the typical virtuality of the hard quark connecting the two virtual photons with the one of the quark connecting the emitted gluon to the virtual photon and of the gluon, one can see that the first one is of order of Q_1^2 for graphs (s3), (s3') and s for graphs (s6), (s6'), while the later ones are of the order of W^2 , which is negligible in the scaling region with respect to Q_1^2 and s . This justifies the expected factorization between a short distance coefficient function and a soft part (although still perturbative in our case) which will be part of a double ρ GDA.

Let us now recall the definition of the leading twist GDA for ρ_L^0 pair. We introduce the vector $P = k_1 + k_2 \approx p_1$, whereas the field coordinates are the ray-vectors along the light-cone direction $n^\mu = p_2^\mu / (p_1 \cdot p_2)$. In our peculiar kinematics the usual variable $\zeta = (k_1 n) / (P n)$ characterizing the GDA equals $\zeta \approx 1$. Thus we define the GDA of the ρ_L^0 pair $\Phi_q(z, \zeta, W^2)$ by the formula

$$\begin{aligned} & \langle \rho_L^0(k_1) \rho_L^0(k_2) | \bar{q}(-\alpha n/2) \not{n} \left[\int_{-\frac{\alpha}{2}}^{\frac{\alpha}{2}} dy n_\nu A^\nu(y) \right] q(\alpha n/2) | 0 \rangle \\ &= \int_0^1 dz e^{-i(2z-1)\alpha(nP)/2} \Phi^{\rho_L \rho_L}(z, \zeta, W^2), \quad q = u, d. \end{aligned} \quad (2.144)$$

in the similar way as for the two pions GDA (2.2).

Now we calculate the GDA $\Phi_q(z, \zeta, W^2)$ in the Born order of the perturbation theory. First we show that the gluonic Wilson line does not give a contribution in our kinematics. For that expand the Wilson line and the S-matrix operator with quark-gluon interaction in (2.144) at the first order in g . We obtain (up to an irrelevant multiplicative factor)

$$n_\mu g^2 \int d^4 v \langle \rho_L^0(k_1) \rho_L^0(k_2) | T[\bar{q}(-\alpha n/2) \gamma^\mu \left[\int_{-\frac{\alpha}{2}}^{\frac{\alpha}{2}} dy n_\nu A^\nu(y) \right] q(\alpha n/2) \bar{q}(v) \not{A}(v) q(v) | 0 \rangle \quad (2.145)$$

After applying the Fierz identity and ordering quark operators into two non-local correlators defining DA of ρ -mesons we obtain

$$n_\mu \langle \rho_L^0(k_1) | \bar{q}(-\alpha n/2) \gamma^\delta q(v) | 0 \rangle \langle \rho_L^0(k_2) | \bar{q}(v) \gamma^\sigma q(\alpha n/2) | 0 \rangle \text{Tr}[\gamma^\delta \gamma^\mu \gamma^\sigma \gamma^\beta] n_\beta + (k_1 \leftrightarrow k_2), \quad (2.146)$$

where we omitted the gluon propagator coming from the contraction of the two gauge fields. The original Wilson line results at this order in the presence of the vector n_β in the above expression. The only nonvanishing contribution at leading twist takes the form

$$\langle \rho_L^0(k_1) | \bar{q}(-\alpha n/2) \not{n} q(v) | 0 \rangle \langle \rho_L^0(k_2) | \bar{q}(v) \not{n} q(\alpha n/2) | 0 \rangle \text{Tr}[\not{n}_1 \not{n} \not{n}_1 \not{n}] + (k_1 \leftrightarrow k_2). \quad (2.147)$$

This is illustrated in Fig. 2.18. It equals zero since in our kinematics one of the matrix elements defining the

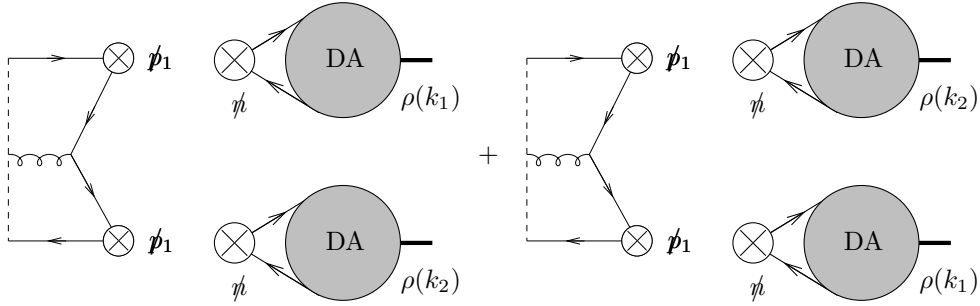


Figure 2.18: Wilson line contribution to the GDA, expressed as a convolution of a hard part with the DAs. In each diagram, the right blobs with a cross symbolize non-local $\bar{q} \not{n} q$ operators, arising from Fierz decomposition, while the left one are Γ matrices arising from Fierz decomposition when factorizing the ρ -DAs.

DA of the ρ -meson vanishes.

The remaining contributions to the correlator in (2.144) at order g^2 are illustrated in Fig. 2.19. It leads to

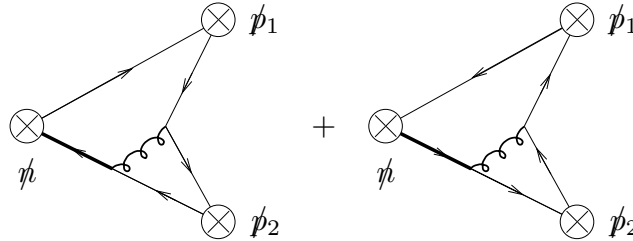


Figure 2.19: Non vanishing contributions to the hard part of the GDA at Born order. The quark and gluon bold lines correspond to propagators while the thin line indicates the spinorial content. In each diagram, the left blob with a cross symbolizes a non-local $\bar{q} \not{n} q$ operator, arising from Fierz decomposition, while the right one are Γ matrices arising from Fierz decomposition when factorizing the ρ -DAs.

the result

$$\Phi^{\rho_L \rho_L}(z, \zeta \approx 1, W^2) = -\frac{f_\rho^2 g^2 C_F}{2 N_c W^2} \int_0^1 dz_2 \phi(z) \phi(z_2) \left[\frac{1}{z \bar{z}_2} - \frac{1}{\bar{z} z_2} \right]. \quad (2.148)$$

The hard part T_H of the amplitude corresponds to the diagrams shown in Fig. 2.20. In the case of a quark of a given flavour it equals

$$T_H(z) = -4 e^2 N_c Q_q^2 \left(\frac{1}{\bar{z} + z \frac{Q_s^2}{s}} - \frac{1}{z + \bar{z} \frac{Q_s^2}{s}} \right) \quad (2.149)$$

The Eqs. (2.148, 2.149) taken together with the flavour structure of ρ^0 permit to write (2.135) in the form

$$T^{\alpha\beta} g_{T\alpha\beta} = \frac{e^2}{2} (Q_u^2 + Q_d^2) \int_0^1 dz \left(\frac{1}{\bar{z} + z \frac{Q_s^2}{s}} - \frac{1}{z + \bar{z} \frac{Q_s^2}{s}} \right) \Phi^{\rho_L \rho_L}(z, \zeta \approx 1, W^2), \quad (2.150)$$

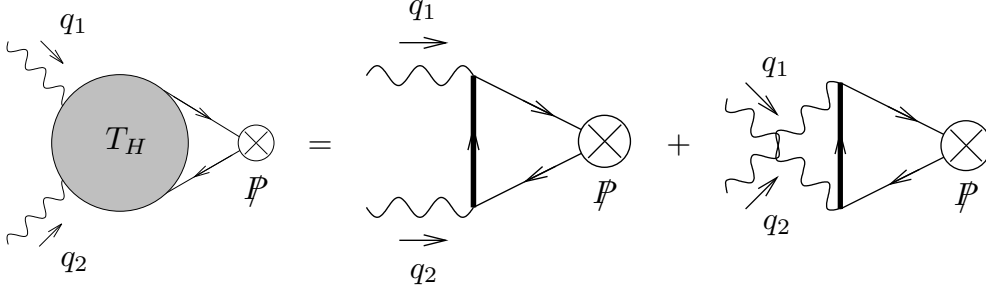


Figure 2.20: Expansion of the hard part T_H at g^2 order. In each diagram, the bold line correspond to a quark propagator, while the thin line denote the spinorial structure. The blobs with a cross are Γ matrices arising from Fierz expansion after factorization of the GDA.

which shows the factorization of $T^{\alpha\beta}g_{T\alpha\beta}$ into a hard part and a GDA. The Eq. (2.150) is the limiting case for $\zeta \rightarrow 1$ of the original equation derived in Ref. [72].

The peculiar case of parametrically close photon virtualities deserves particular attention. In this case, there are subtle problems for defining the light-cone vector P since the two outgoing mesons should be now treated in an almost symmetric way. In order to circumvent this difficulty, it is useful to start from the factorized formula (2.150) in the kinematical domain (2.133), assuming $Q_1 > Q_2$. Let us continue (2.150) in Q_2 up to $Q_2 = Q_1$. To control this continuation, one should restore the Q_1^2 and Q_2^2 dependence, encoded in ζ and W^2 through $W^2/\zeta = s(1 - Q_1^2/s)$, as

$$\Phi^{\rho_L\rho_L}(z, \zeta, W^2) = -\frac{f_\rho^2 g^2 C_F \zeta}{2N_c W^2} \int_0^1 dz_2 \phi(z) \phi(z_2) \left[\frac{1}{z\bar{z}_2} - \frac{1}{\bar{z}z_2} \right]. \quad (2.151)$$

The hard part in (2.150) is proportional to $1 - Q_2^2/s$. This factor $1 - Q_2^2/s$, now of the order of $1 - Q_1^2/s$, starts to play the role of a suppression factor. The amplitude (2.150) which is proportional to $\frac{1}{s} \frac{1 - Q_2^2/s}{1 - Q_1^2/s}$, now behaves as $1/s \sim 1/Q^2$. In the leading twist approximation, this factorized result vanishes. This observation is confirmed by the result (2.131) of the direct calculation. Indeed, in the case $Q_1 = Q_2 = Q$, the magnifying factor $1/(1 - Q^2/s)$ in the two terms of the last line of (2.131) is not present anymore. Thus, the resulting amplitude should be considered as a higher twist contribution.

Let us finally note that in general GDAs are complex functions. In our case, i.e. in the Born approximation, the hard part (2.149) and the GDA (2.148) are real quantities. This is due to the use of the real DA of rho mesons and to the absence of the s -channel cut of hard diagrams in the Born approximation. The situation will be changed by inclusion of radiative corrections which can result in the appearance of an imaginary part of the scattering amplitude. Similar properties, namely the reality of the perturbative GDA are discussed also in Ref. [232], dealing with different kinematics.

2.4.4 $\gamma_L^* \gamma_L^* \rightarrow \rho_L^0 \rho_L^0$ in the generalized Bjorken limit

To analyse the case of longitudinally polarized photon scattering, let us now turn to another interesting limiting case where

$$Q_1^2 \gg Q_2^2. \quad (2.152)$$

This is the regime which we have investigated in Sec.2.3. In this limit, the amplitude with initial longitudinally polarized photons should factorize as the convolution of a perturbatively calculable coefficient function and a $\gamma \rightarrow \rho$ TDA defined from the non-local quark correlator

$$\int \frac{dz^-}{2\pi} e^{-ixP^+z^-} \langle \rho(p_2) | \bar{q}(-z^-/2) \gamma^+ q(z^-/2) | \gamma(q_2) \rangle. \quad (2.153)$$

We use the same notation for the TDA as for GPDs and thus write

$$\begin{aligned} q_1 &= \frac{1}{1+\xi} n_1 - 2\xi n_2, & k_1 &= \frac{1 - \frac{Q_2^2}{s}}{1+\xi} n_1 \\ q_2 &= -\frac{Q_2^2}{(1+\xi)s} n_1 + (1+\xi) n_2, & k_2 &= (1-\xi) n_2, \end{aligned} \quad (2.154)$$

where ξ is the skewedness parameter which equals $\xi = Q_1^2/(2s - Q_1^2)$ (see also the formula (2.124) which relates s with the total scattering energy W) and the new n_i Sudakov light-cone vectors are related to the p_i 's as

$$p_1 = \frac{1}{1+\xi} n_1, \quad p_2 = (1+\xi) n_2, \quad (2.155)$$

with $p_1 \cdot p_2 = n_1 \cdot n_2 = s/2$. As for GPDs, we introduce the average ‘‘target’’ momentum P and the momentum transfer Δ

$$P = \frac{1}{2}(q_2 + k_2), \quad \Delta = k_2 - q_2. \quad (2.156)$$

We still restrict our study to the strictly forward case with $t = t_{min} = -2\xi Q_2^2/(1+\xi)$.

In the region defined by Eq. (2.152) we can put $Q_2 = 0$ inside $\{\dots\}$ in the expression in Eq. (2.132), which results, in this approximation, in the formula:

$$\begin{aligned} &\int_0^1 dz_1 dz_2 \phi(z_1) \phi(z_2) \{\dots\} \\ &= \int_0^1 dz_1 dz_2 \phi(z_1) \phi(z_2) \left\{ \frac{(1-\xi)}{\bar{z}_1[\bar{z}_2(1+\xi) + 2\xi z_2]} + \frac{(1-\xi)}{z_1[z_2(1+\xi) + 2\xi \bar{z}_2]} + \frac{1}{z_2 \bar{z}_1} + \frac{1}{z_1 \bar{z}_2} \right\}. \end{aligned} \quad (2.157)$$

The terms in the $\{\dots\}$ are ordered in accordance with diagrams shown in Fig. 2.15. Each of these 4 diagrams contributes, in accordance with their topology which allows for a factorization of TDA type.

Now our aim is precisely to rewrite Eq. (2.157) in a form corresponding to the QCD factorization with a TDA, as illustrated in Fig. 2.21.

For that we look more closely into diagrams contributing to each of the four terms in (2.157) from the point of view of such a factorization. For example, the second term in (2.157), corresponding to the second diagram shown in Fig. 2.15, suggests the introduction of the new variable x , defined through $z_2 = (x - \xi)/(1 - \xi)$, with $x \in [\xi, 1]$, which results in the equality

$$\int_0^1 dz_2 \frac{\phi(z_2)(1-\xi)}{z_1[z_2(1+\xi) + 2\xi \bar{z}_2]} = \int_{\xi}^1 dx \frac{\phi\left(\frac{x-\xi}{1-\xi}\right)}{z_1(x+\xi)}, \quad (2.158)$$

i.e. which corresponds to a part of the contribution from the DGLAP integration region of the amplitude with a factorized TDA. A similar analysis of all remaining terms permits to represent Eq. (2.157) in the form

$$\begin{aligned} &\int_0^1 dz_1 dz_2 \phi(z_1) \phi(z_2) \{\dots\} \\ &= \int_{-1}^1 dx \int_0^1 dz_1 \phi(z_1) \left(\frac{1}{\bar{z}_1(x-\xi)} + \frac{1}{z_1(x+\xi)} \right) \\ &\quad \times \left[\Theta(1 \geq x \geq \xi) \phi\left(\frac{x-\xi}{1-\xi}\right) - \Theta(-\xi \geq x \geq -1) \phi\left(\frac{1+x}{1-\xi}\right) \right], \end{aligned} \quad (2.159)$$

with the step function $\Theta(a \geq x \geq b) = \Theta(a-x)\Theta(x-b)$. This factorized expression suggests the identification of

$$\int_0^1 dz_1 \phi(z_1) \left(\frac{1}{\bar{z}_1(x-\xi)} + \frac{1}{z_1(x+\xi)} \right) \quad (2.160)$$

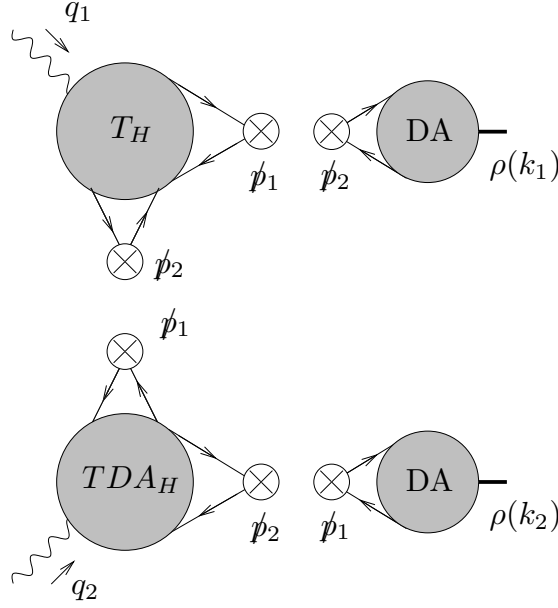


Figure 2.21: Factorization of the amplitude in terms of a TDA. In the left of each DA blob, the crossed-blobs are non-local operators with indicated Fierz structure. In the right of each left T_H and TDA_H blobs, the crossed-blobs are Fierz Γ matrices, with the indicated structure. At the bottom of the T_H blob, the crossed-blob is a Fierz Γ matrix, while at the top of the TDA_H blob, the crossed-blob is a non-local operator with indicated Fierz structure.

as the coefficient function T_H (up to a multiplicative factor), and of

$$T(x, \xi, t_{min}) \equiv N_c \left[\Theta(1 \geq x \geq \xi) \phi \left(\frac{x - \xi}{1 - \xi} \right) - \Theta(-\xi \geq x \geq -1) \phi \left(\frac{1 + x}{1 - \xi} \right) \right] \quad (2.161)$$

as the $\gamma_L^* \rightarrow \rho_L$ TDA.

To justify this interpretation we start from the hard part $T_H(z_1, x)$ of the scattering amplitude, which appears in Fig. 2.21, as illustrated at order g^2 in Fig. 2.22. It equals, for a meson built from a quark with a single flavour,

$$T_H(z_1, x) = -i f_\rho g^2 e Q_q \frac{C_F \phi(z_1)}{2 N_c Q_1^2} \epsilon^\mu(q_1) \left(2\xi n_{2\mu} + \frac{1}{1 + \xi} n_{1\mu} \right) \times \left[\frac{1}{z_1(x + \xi - i\epsilon)} + \frac{1}{\bar{z}_1(x - \xi + i\epsilon)} \right], \quad (2.162)$$

and obviously coincides with the hard part of the ρ -meson electroproduction amplitude. The tensorial structure $2\xi n_2^\mu + \frac{1}{1 + \xi} n_1^\mu = p_1^\mu + Q_1^2/s p_1^\mu$ coincides again with the one present in Eq.(2.127) when performing the direct calculation.

Passing to the TDA, let us consider the definition of $\gamma_L^*(q_2) \rightarrow \rho_L^q(k_2)$ TDA, $T(x, \xi, t_{min})$, in which we assume that the meson is built from a quark with a single flavour, $\rho_L^q(k_2) = \bar{q}q$. The vector $P = 1/2(q_2 + k_2) \approx n_2$ in our kinematics, and the ray-vector of coordinates is oriented along the light-cone vector $n = n_1/(n_1 \cdot n_2)$. The non-local correlator defining the TDA is given by the formula

$$\int \frac{dz^-}{2\pi} e^{ix(P \cdot z)} \langle \rho_L^q(k_2) | \bar{q}(-z/2) \hat{n} e^{-ieQ_q \int_{z/2}^{-z/2} dy_\mu A^\mu(y)} q(z/2) | \gamma^*(q_2) \rangle = \frac{e Q_q f_\rho}{P^+} \frac{2}{Q_2^2} \epsilon_\nu(q_2) \left((1 + \xi) n_2^\nu + \frac{Q_2^2}{s(1 + \xi)} n_1^\nu \right) T(x, \xi, t_{min}), \quad (2.163)$$

in which we explicitly show the electromagnetic Wilson-line assuring the abelian gauge invariance of the non-local operator. On the contrary, for simplicity of notation, we omit the Wilson line required by the non-abelian QCD

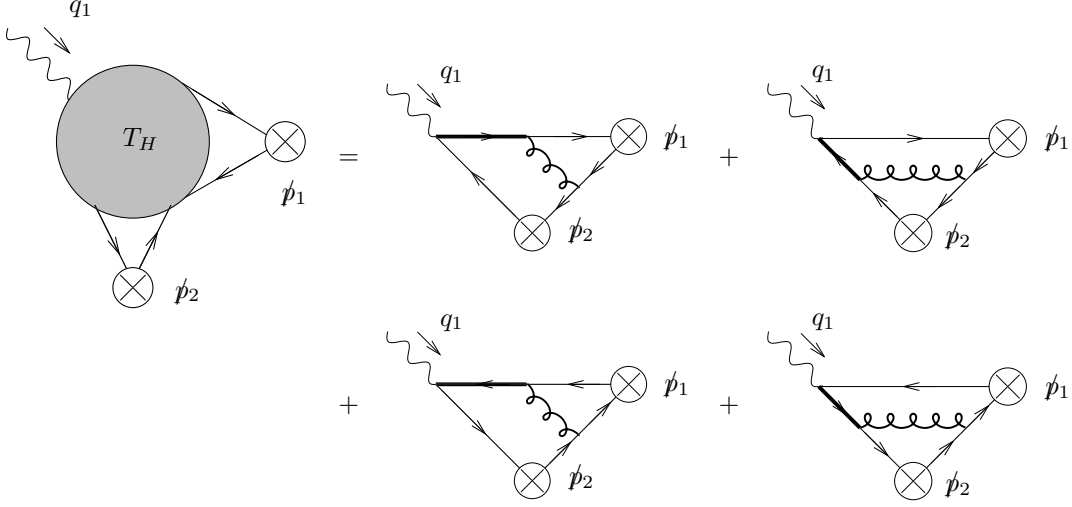


Figure 2.22: The hard part T_H at order g^2 . Bold quark and gluon lines are hard propagators. Thin line are spinor lines. For each diagram, the right crossed-blob is a given Γ matrix arising from Fierz expansion when factorizing the DA, and the bottom crossed-blob is a given non-local operator of given Fierz type.

invariance since it does not play any role in this case. Note also that the factor $(1+\xi)n_2^\nu + \frac{Q_s^2}{s(1+\xi)}n_1^\nu = p_2^\nu + \frac{Q_s^2}{s}p_1^\nu$ corresponds to a part of the tensorial structure of the second term in Eq. (2.127).

Now, the simple perturbative calculation of the matrix element in (2.163) in the lowest order in the electromagnetic coupling constant e leads to the expression for $T(x, \xi, t_{min})$ given by Eq. (2.161). The contributing diagrams are drawn in Fig. 2.23. In particular, the contribution to the rhs of (2.163) proportional to the vec-

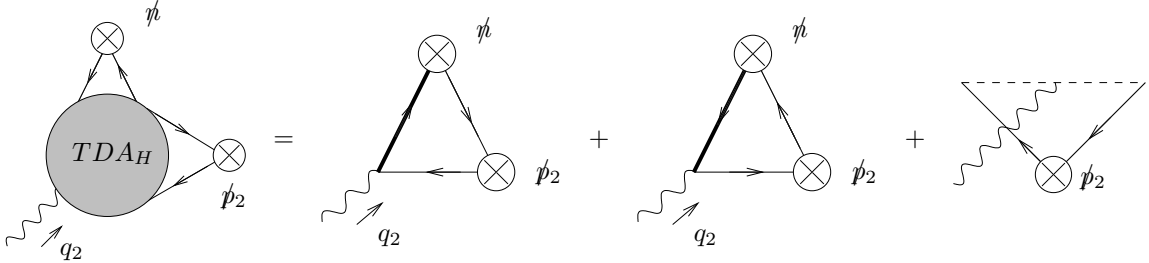


Figure 2.23: The hard part of the TDA at order $e Q_q$. In each diagram, the lower crossed-blob denotes a given Γ matrix arising from Fierz expansion. The bold lines are hard quark propagators, while the thin lines only carry spinor indices. The upper crossed-blob denotes non-local operators with given Fierz structure. The dotted line is a QED Wilson line.

tor n_1^ν (or p_1^ν) corresponds to the contribution coming from the expansion of the electromagnetic Wilson line, illustrated by the last diagram in Fig. 2.23.

Putting all factors together and restoring the flavour structure of the ρ^0 , we obtain the factorized form involving a TDA, of the expression $T^{\alpha\beta} p_{2\alpha} p_{1\beta}$ in Eq. (2.132) as

$$T^{\alpha\beta} p_{2\alpha} p_{1\beta} = -if_\rho^2 e^2 (Q_u^2 + Q_d^2) g^2 \frac{C_F}{8N_c} \int_{-1}^1 dx \int_0^1 dz_1 \left[\frac{1}{\bar{z}_1(x-\xi)} + \frac{1}{z_1(x+\xi)} \right] T(x, \xi, t_{min}). \quad (2.164)$$

Note that in this perturbative analysis, only the DGLAP part of the TDA, with $1 \geq |x| \geq \xi$, contributes. This is a consequence of the support properties of the ρ -meson distribution amplitude. From a diagrammatic point of view, this can be easily understood from the analysis of Fig. 2.15, where one can readily check, from the momentum flow of each quark and antiquark which makes each of the two ρ -meson, that the quark and

antiquark in the t -channel can always be interpreted in accordance with the two DGLAP regions for quarks or antiquarks, as we have seen p21.

Finally a few remarks are in order. Firstly let us note that our choice of the ordering of virtualities $Q_1^2 \gg Q_2^2$ is a quite arbitrary one. Equally well we could assume the opposite condition, i.e. $Q_1^2 \ll Q_2^2$. In this case one gets of course again the QCD factorization with a TDA but this time describing the transition $\gamma^*(q_1) \rightarrow \rho_L^0(k_1)$. In view of this observation one can conclude that both the polarizations of participating particles and also the kinematical conditions like the ordering of virtualities determine a TDA-type of factorization.

Secondly let us note that the restriction to the DGLAP region in our TDA is related to a description of the ρ -mesons by their DAs and by the limitation to the Born approximation. The calculations of our process beyond the Born approximation would lead to the factorization of the obtained result into the corrected hard part which includes effects of radiative contributions and a modified TDA absorbing - by using the DGLAP-ERBL evolution equations - the infrared and collinear divergences caused by these radiative corrections. The evolution governed by these evolution equations do in fact connect the DGLAP region, both with the ERBL and the DGLAP region, as discussed e.g. in Ref. [51].

We have thus shown that the direct calculation of the scattering amplitude of (2.120) at Born level factorizes in the two regimes: (a) the region where the squared invariant mass of the two rho's W^2 is much smaller than the largest photon virtualities, namely $Q_1^2 \gg W^2$ (or $Q_2^2 \gg W^2$), with Q_1 and Q_2 being not parametrically close, and (b) the region where photon virtualities are strongly ordered, that is $Q_1^2 \gg Q_2^2$ (or $Q_2^2 \gg Q_1^2$). In the region (a) the amplitude with transverse photons factorizes in a hard subprocess and a GDA, up to corrections of order W^2/Q_1^2 (resp. W^2/Q_2^2). In the region (b) the amplitude with longitudinal photons factorizes in a hard subprocess and a TDA, up to corrections of order Q_2^2/Q_1^2 (resp. Q_1^2/Q_2^2). This is illustrated in Fig. 2.24. We have also shown that the polarization states of the photons dictate either the factorization involving a GDA or involving a TDA. Usually these two types of factorizations are applied to two different kinematical regimes. These two domains have here a non empty intersection, in which we get two factorisation formulas for both polarizations of the photons, $\gamma_T^* \gamma_T^* \rightarrow \rho_L \rho_L$ and $\gamma_L^* \gamma_L^* \rightarrow \rho_L \rho_L$, as shown in Fig. 2.24. Fig. 2.24 illustrates also that the collinear QCD factorization with GDA or TDA is not demonstrated by our analysis in the limited region where the virtualities Q_i^2 are parametrically close, but vanishes at dominant twist⁸. In this figure, the different domains where the transverse or longitudinal amplitudes dominates are displayed. Finally, Fig. 2.24 shows the perturbative Regge domain, corresponding to the large W^2 limit, to be studied in Sec. 7.4.

Our analysis is restricted to the case of longitudinally polarized ρ^0 -mesons. In this way we have avoided the potential problems due to the breaking of QCD factorization with GDA or TDA at the end-point region of the distribution amplitudes of transversally polarized vector mesons, to be discussed in Chap. 3. The problem of obtaining a factorized formula with GDA or TDA in this case is open.

Although we have restricted ourselves, for simplicity, to the forward kinematics, similar results may be obtained in a more general case. These results involving neutral ρ^0 -mesons can be generalized to the case of the production of a $(\rho^+ \rho^-)$ -meson pair. On the theoretical side, in order to preserve the electromagnetic gauge invariance of the TDA $\gamma^* \rightarrow \rho^\pm$, one should modify the definition of the non-local correlator (2.163). This may be done by applying the Mandelstam approach [233], i.e. by replacing the electromagnetically gauge invariant correlator (2.163) by the product of two effective electromagnetically gauge invariant quark fields

$$q(z) \exp(i e_q \int_z^\infty dy n_\mu A^\mu(y)).$$

2.5 Exotic hybrid mesons

Based on [W12, W13, W14, W18]

In QCD, hadrons are bound states described in terms of quarks, anti-quarks and gluons. The usual, well-known, mesons are supposed to contain quarks and anti-quarks as valence degrees of freedom. These valence degrees of freedom define the charge and other quantum numbers of corresponding hadrons, while the sea configurations do not change the quantum numbers. On the other hand, gluons carry the interaction, and do not participate in the quantum number content of the hadron. They only appear when considering higher

⁸We thanks M. Diehl for pointing out this to us.

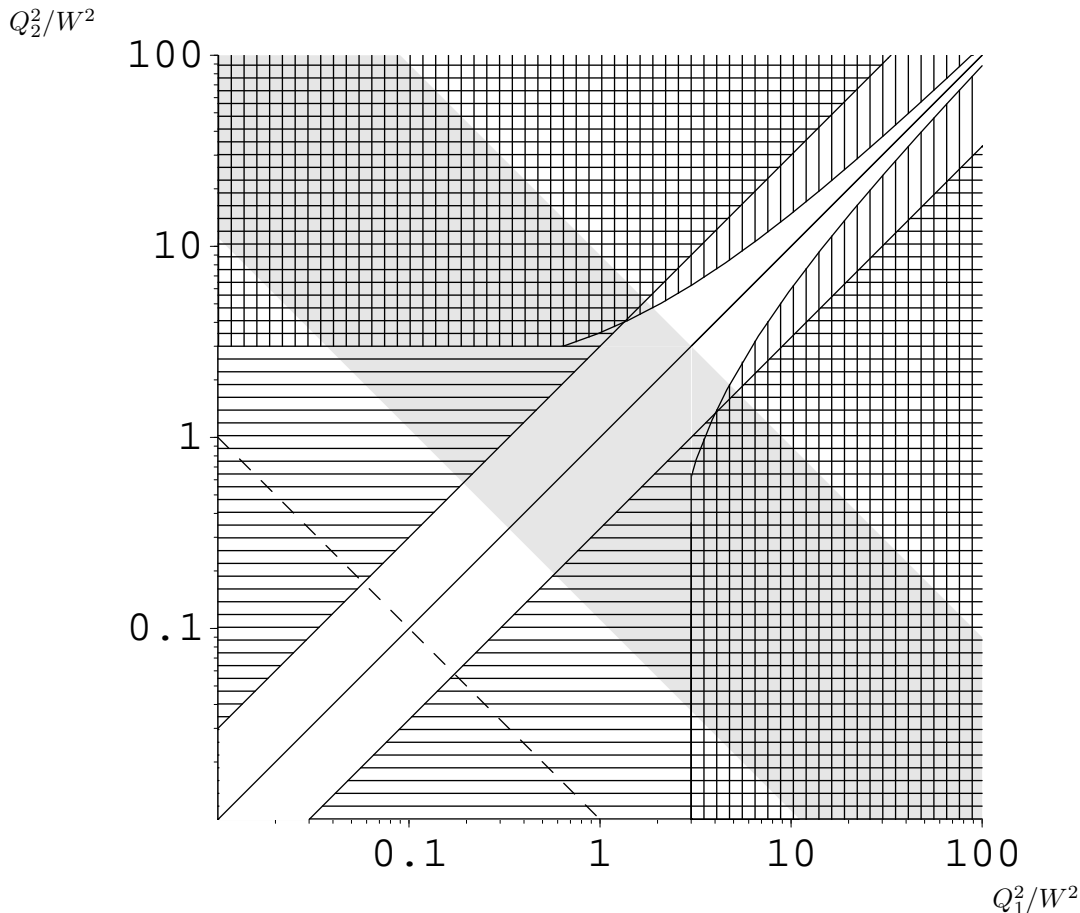


Figure 2.24: Different kinematical regions. In the domain (1), denoted with vertical lines, the QCD factorization with a GDA is justified. This region is the union of two disconnected domains: the lower right one is given by the conditions $1 - Q_2^2/s \geq c(1 - Q_1^2/s)$ and $Q_1^2/W^2 \geq c$ while the upper left one is given by $1 - Q_1^2/s \geq c(1 - Q_2^2/s)$ and $Q_2^2/W^2 \geq c$, c being arbitrary large. In the domain (2), denoted with horizontal lines, the QCD factorization with a TDA is justified. It corresponds to $Q_1^2/Q_2^2 \geq c$ or $Q_1^2/Q_2^2 \leq 1/c$. In the intersecting domain, both factorizations are valid. In the region without any lines, no factorization neither in terms of GDA nor TDA is established; however, inside this region, in the upper part which is limited by two converging line the amplitude is zero at dominant twist. For illustration, we choose $c = 3$. The grey band represents the domain where the Born order amplitudes with transverse and longitudinal photon, calculated directly, have comparable magnitudes. In the upper (lower) corner the transverse (resp. longitudinal) polarizations give dominant contribution. Below the dashed line is the perturbative Regge domain.

order Fock states in the infinite tower of states describing the hadron, on the same footing as sea quark and antiquarks.

However, QCD does not prohibit the existence of explicit gluonic degrees of freedom in the form of a vibrating flux tube, for instance. Indeed, the only severe constraint which must be fulfilled is the color neutrality of the state, which is one the pillar of QCD. This can be satisfied in various situations outside of the usual meson $q\bar{q}$ and baryons qqq quark-model description. This includes the states where the $q\bar{q}g$ and gg configurations in Fock space are dominating, respectively called hybrids and glueballs, and are of fundamental importance to understand the dynamics of quark confinement and the nonperturbative sector of quantum chromodynamics [234–240].

Let us now consider the specific case of hard processes, which allows to apply perturbative QCD. As we have seen above, any description of hard exclusive process involves matrix elements of *non-local* light-cone operators. The gluonic degrees of freedom are hidden, even when considering twist 2 operators, in the path-

ordered gluonic exponential which connect the fermionic fields and make these operators gauge invariant. This thus opens the way to the description of the production of states which are outside the usual quark model (called exotic particles). We will now specifically consider the case of hard electroproduction of an isotriplet exotic hybrid meson $J^{PC} = 1^{-+}$, for which we proved [W12, W13] that the corresponding amplitude has a non-vanishing twist 2 component, leading to non-suppressed rates at large Q^2 . On top of the theoretical interest for such states, our motivation is also based on the fact that there exist candidates for such states, like $\pi_1(1400)$ and $\pi_1(1600)$, and evidence for a $\pi_1(2015)$ has been reported. In particular, we made some phenomenological investigation [W13, W18] based on the fact that the $\pi_1(1400)$ was seen mostly through its $\pi\eta$ decay mode, as investigated by the Brookhaven collaboration E852 [241, 242].

2.5.1 Quark model and spectroscopy

Let us first recall basics about the quark model. In this model the hadrons, mesons and baryons, are bound states of quark-antiquark or three-quarks systems. We consider the mesons, *i.e.* the quark-antiquark systems. Their total angular momentum results from the summation of spin S and orbital L angular momenta of quarks. Neglecting any spin-orbital interaction, the quantum numbers S and L may be considered as additional quantum numbers for the classification of hadron states. Therefore, the eigenvalues of the squares of the angular momenta read:

$$\begin{aligned} \mathbf{J}^2 &= J(J+1) \quad \mathbf{S}^2 = S(S+1) \quad \mathbf{L}^2 = L(L+1), \\ \mathbf{J} &= \mathbf{S} + \mathbf{L}, \end{aligned} \tag{2.165}$$

where the number L may take all positive integer values (including zero). The meson octets correspond to the case where $S = 0, 1$. For given values of S and L , the total angular momentum J can take the values

$$J = S + L, S + L - 1, \dots, |S - L|. \tag{2.166}$$

The values S and L are related to the C - and P -parity of the quark-antiquark system in the form:

$$C = (-)^{L+S}, \quad P = (-)^{L+1}. \tag{2.167}$$

Consequently, in the quark model, the quantum numbers S, L, J, P, C and the relations between them (2.166), (2.167) leads to the following classification of the meson states:

- $S = 0, L = J$:

$$J^{PC} = 0^{-+}, 1^{+-}, 2^{-+}, 3^{+-}, \dots \tag{2.168}$$

- $S = 1, L = 0, J = 1$:

$$J^{PC} = 1^{--} \tag{2.169}$$

- $S = 1, L = 1, J = 2, 1, 0$:

$$J^{PC} = 0^{++}, 1^{++}, 2^{++} \tag{2.170}$$

- $S = 1, L = 2, J = 3, 2, 1$:

$$J^{PC} = 1^{--}, 2^{--}, 3^{--} \tag{2.171}$$

and so on. From this, one can see explicitly that the mesons with $J^{PC} = 0^{--}, 0^{+-}, 1^{-+}, \dots$ are forbidden. However, as sketch above, such mesons may be described beyond the quark model, by adding an extra degree of freedom (a gluon, for instance) to get the needed quantum numbers, as discussed for instance in Ref. [243, 244]. We will now consider this in the context of hard processes.

2.5.2 Hybrid meson distribution amplitude

After this recall about the fact that 1^{-+} is forbidden in the quark model and that non-local quark twist 2 operators necessarily involve gluon operators due to color gauge invariance, thus opening the way to the description of states outside the quark model but still within a non-suppressed scaling, it remains to be proven that this is practically possible, both in a qualitative and quantitative way.

Quantum numbers

The first key problem is whether this gluon admixture allows this quark matrix element to have exotic quantum numbers such as $J^{PC} = 1^{-+}$. Let us define, as usual, the meson distribution amplitude through the Fourier transformed correlator taken at $z^2 = 0$,

$$\begin{aligned} \langle H(p, \lambda) | \bar{\psi}(-z/2) \gamma_\mu [-z/2; z/2] \psi(z/2) | 0 \rangle = \\ i f_H M_H \left[\left(e_\mu^{(\lambda)} - p_\mu \frac{e^{(\lambda)} \cdot z}{p \cdot z} \right) \int_0^1 dy e^{i(\bar{y}-y)p \cdot z/2} \phi_T^H(y) \right. \\ \left. + p_\mu \frac{e^{(\lambda)} \cdot z}{p \cdot z} \int_0^1 dy e^{i(\bar{y}-y)p \cdot z/2} \phi_L^H(y) \right], \end{aligned} \quad (2.172)$$

where $\bar{y} = 1 - y$; f_H denotes a dimensionful coupling constant for the hybrid meson, so that the distribution amplitude ϕ^H is dimensionless, following the convention of the previous chapter. f_H is the analog of f_π or f_ρ . Its normalization will be discussed in a second step.

For the longitudinal polarization case (neglecting mass effects),

$$e_\mu^{(0)} = \frac{e^{(0)} \cdot z}{p \cdot z} p_\mu$$

only ϕ_L^H contributes, so that our correlator reads

$$\langle H(p, 0) | \bar{\psi}(-z/2) \gamma_\mu [-z/2; z/2] \psi(z/2) | 0 \rangle = i f_H M_H e_\mu^{(0)} \int_0^1 dy e^{i(\bar{y}-y)p \cdot z/2} \phi_L^H(y). \quad (2.173)$$

As discussed in Sec. 1.3.1, Eqs. (2.172) and (2.173) involve a path-ordered gluonic exponential along the straight line connecting the initial and final points $[z_1; z_2]$ which provides the gauge invariance for our bilocal operator. It equals unity in a light-like (axial) gauge. In the following we will only consider the case of a longitudinally polarized H and we will therefore omit the index L from the hybrid meson distribution amplitude.

Let us now prove that it is possible to describe in this way an exotic $J = 1$ meson state with quantum numbers $PC = -+$. Let us first consider the charge conjugation invariance. Inserting the charge conjugation operator \mathcal{C} inside our correlator (2.173), one can immediately deduce for the neutral member of the isotriplet H^0 (with the flavour structure $1/\sqrt{2}(\bar{u}u - \bar{d}d)$ analogous to the ρ^0) that the parameterizing function ϕ^H is antisymmetric, *i.e.*

$$\phi^H(y) = -\phi^H(1-y). \quad (2.174)$$

This is at odd with the DA symmetrical property that one would get in the more familiar case of the ρ -meson, which has $C = -$.

Isospin invariance and G-parity imply the same relation for charged hybrids. The property (2.174) is in agreement with the case of the C -even two pion GDA discussed in Eq. (2.11). In particular, the antisymmetric property implies

$$\int_0^1 dy \phi^H(y) = 0. \quad (2.175)$$

We now consider the remaining quantum number, the parity. Since the UV singularities only occur in the hard part, one can Taylor expand the left hand side of (2.172), which does not contain any singularities in z . We thus rewrite the hybrid-to-vacuum matrix element in the form

$$\begin{aligned} \langle H(p, \lambda) | \bar{\psi}(-z/2) \gamma_\mu [-z/2; z/2] \psi(z/2) | 0 \rangle = \\ \sum_{n \text{ odd}} \frac{1}{n!} z_{\mu_1} \dots z_{\mu_n} \langle H(p, \lambda) | \bar{\psi}(0) \gamma_\mu \overleftrightarrow{D}_{\mu_1} \dots \overleftrightarrow{D}_{\mu_n} \psi(0) | 0 \rangle, \end{aligned} \quad (2.176)$$

where D_μ is the usual covariant derivative and

$$\overleftrightarrow{D}_\mu = \frac{1}{2} (\overrightarrow{D}_\mu - \overleftarrow{D}_\mu). \quad (2.177)$$

Due to the positive charge parity of H^0 , see (2.174), only odd terms in (2.176) do contribute. The simplest case is provided by the $n = 1$ twist 2 operator

$$\mathcal{R}_{\mu\nu} = S_{(\mu\nu)} \bar{\psi}(0) \gamma_\mu \overleftrightarrow{D}_\nu \psi(0), \quad (2.178)$$

where $S_{(\mu\nu)}$ denotes the standard symmetrization operator

$$S_{(\mu\nu)} T_{\mu\nu} = \frac{1}{2} (T_{\mu\nu} + T_{\nu\mu}).$$

Note that the removal of the trace is here automatically implied due to the Dirac equation satisfied by the fields. $\mathcal{R}_{\mu\nu}$ is proportional to the quark energy-momentum tensor⁹, *i.e.* $\mathcal{R}_{\mu\nu} = -i \Theta_{\mu\nu}$. Its matrix element of interest is

$$\langle H(p, \lambda) | \mathcal{R}_{\mu\nu} | 0 \rangle = \frac{1}{2} f_H M_H S_{(\mu\nu)} e_\mu^{(\lambda)} p_\nu \int_0^1 dy (1-2y) \phi^H(y), \quad (2.179)$$

Note that it is the symmetry in $\mu\nu$ of the energy momentum tensor which selects the twist-2 function, since the spin of the operator equals 2, while its dimension equals 4.

To determine the parity one should treat the meson polarization with some care. Indeed the equation $e_{L\mu} \sim p_\mu/M_H$ holds for a *fast* longitudinally polarized vector meson. But we know that the meson is an eigenstate of the parity operator P only in its *rest* frame. In this frame p_μ has only a zeroth component, while e_μ has a vanishing zeroth component. One need thus to study the parity transformation of \mathcal{R}_{0k} . This can be readily done by evaluating $\mathcal{P} \mathcal{R}_{0k} \mathcal{P}^\dagger$, using the well know properties of Dirac field under \mathcal{P} (with $|\eta_P| = 1$)

$$\mathcal{P} \Psi(x) \mathcal{P}^\dagger = \eta_P \gamma^0 \Psi(\tilde{x}) \quad \text{and} \quad \mathcal{P} \bar{\Psi}(x) \mathcal{P}^\dagger = \eta_P^* \bar{\Psi}(\tilde{x}) \gamma^0, \quad (2.180)$$

where $\tilde{x} = (x^0, -\vec{x})$ for $x = (x^0, \vec{x})$, and the corresponding transformation of the field A^μ :

$$\mathcal{P} A^\mu(x) \mathcal{P}^\dagger = A_\mu(\tilde{x}) \quad (2.181)$$

and leads, for $k = 1, 2, 3$, to

$$P \left(S_{(k0)} \bar{\psi}(0) \gamma_k \overleftrightarrow{D}_0 \psi(0) \right) = -, \quad (2.182)$$

where we have used the fact that $\gamma^0 \gamma_k \gamma^0 = -\gamma_k$ for $k = 1, 2, 3$. This ends the proof that the non-local matrix element (2.173) may describe an exotic hybrid meson and that its light-cone distribution amplitude is a leading twist quantity with vanishing first moment (2.174).

⁹See for example [24] appendix E for explicit expressions.

Normalization

After showing that the hybrid meson $J^{PC} = 1^{-+}$ can be produced at twist two level, we now show that the electroproduction amplitude has an order of magnitude comparable with ρ -electroproduction. The key point is to evaluate the magnitude of the non-perturbative coupling f_H . For this purpose, we will rely on the appearance of the quark energy-momentum tensor in the infinite set of local operators in Eq.(2.176).

The non-zero matrix element of the quark energy-momentum tensor between vacuum and exotic meson state was explored long ago [245]. It may be related, by making use of the equations of motion, to the matrix element of quark-gluon operator and estimated with the help of the techniques of QCD sum rules [246,247], which allows to fix the coupling constant, f_H . It turns out that one of the solutions corresponds to a resonance with mass around 1.4 GeV, which is the order of magnitude of the $\pi_1(1400)$ candidate, and the coupling constant at this scale is ¹⁰

$$f_H \approx 50 \text{ MeV} . \quad (2.183)$$

Note that the same exotic quantum numbers (except isospin) were found [243,244] for the gluonic energy momentum tensor (attributed therefore to the gluonium). It was noticed there that energy momentum conservation leads to a zero coupling of the operator to such an exotic state. This argument would be applicable in our case for the isosinglet combination, if the quark gluon interaction, leading to the non-conservation of both quark and gluon energy momentum tensor (while the sum is conserved), is assumed to be negligible. However, there is no reason to expect it to be applicable to isovector combinations or to each quark flavour separately. In addition, even for isosinglet combination (including the pure gluonium case), this argument is no more applicable to the local operators of higher spin ($n = 3, 5, \dots$) which appear in Eq.(2.176). Indeed, since these local operators involve extra covariant derivatives,

$$\langle H(p, 0) | \mathcal{R}_{\mu\nu_1 \dots \nu_n} | 0 \rangle = i^{n+1} f_H M_H S_{(\mu\nu_1 \dots \nu_n)} e_{\mu}^{(0)} p_{\nu_1} \dots p_{\nu_n} \int_0^1 dy \left(y - \frac{1}{2} \right)^n \phi^H(y) , \quad (2.184)$$

although they preserves all the quantum numbers, and lead to a non zero vacuum-to-hybrid matrix element (before addressing the question of its prefactor), the argument based on the conservation of the operator is not anymore valid, as it is not the energy-momentum tensor anymore, and thus prevent the vanishing of the coupling based on simple symmetry arguments.

In summary, the hybrid light-cone distribution amplitude is a leading twist quantity which should have a vanishing first moment (2.174) because of the antisymmetry. This distribution amplitude obeys usual evolution equations [48, 65, 66] and has an asymptotic limit [204]

$$\Phi_{as}^H = 30 y (1 - y) (1 - 2y) \quad (2.185)$$

with assumed normalization of the distribution amplitude $\phi^H(y)$ as

$$\int_0^1 dy (1 - 2y) \phi^H(y) = 1 . \quad (2.186)$$

As for any form factor, the coupling constant f_H satisfies renormalization group evolution equations, given by the formula (the hybrid DA evolves like a flavor non-singlet GDA, but for the value $C = +$, which constraints n to be odd, see (2.58) and the comment after that equation)

$$f_H(Q^2) = f_H \left(\frac{\alpha_S(Q^2)}{\alpha_S(M_H^2)} \right)^{K_1} \quad K_1 = \frac{2\gamma_{QQ}(1)}{\beta_0} , \quad (2.187)$$

where the QQ anomalous dimension is given by Eq. (2.28), i.e.

$$\gamma_{QQ}(n) = C_F \left(\frac{1}{2} - \frac{1}{(n+1)(n+2)} + 2 \sum_{k=2}^{n+1} \frac{1}{k} \right) , \quad (2.188)$$

¹⁰our f_H corresponds to $2\sqrt{2}f_R$ in the notations of Ref. [246,247].

and thus $\gamma_{QQ}(1) = 16/9$ and where the one loop β function reads $\beta_0 = 11 - 2n_f/3$ (in the notation of Eq.(2.188), $n = 1$ corresponds to the energy-momentum tensor). Since the exponent K_1 is a small positive number which drives slowly to zero the coupling constant $f_H(Q^2)$, while experiments are likely to be feasible at moderate values of Q^2 , we neglect this evolution and in the following estimate we use the value from Eq. (2.183).

2.5.3 Hybrid electroproduction

We now study the exotic hybrid meson by means of its deep exclusive electroproduction, *i.e.*

$$e(k_1) + N(p) \rightarrow e(k_2) + H(p_H) + N(p'), \quad (2.189)$$

through the subprocess:

$$\gamma_L^*(q) + N(p) \rightarrow H_L(p_H) + N(p') \quad (2.190)$$

when the baryon is scattered at small angle. Relying on the collinear factorization theorem for hard exclusive electroproduction of a vector meson discussed in Sec. 1.4, the corresponding amplitude reads, at leading twist and when $-t \ll Q^2$ as

$$\mathcal{A} = \int_0^1 dz \int_{-1}^1 dx \Phi_H(z, \mu_F^2, \mu_R^2) H(x, z, Q^2, \mu_F^2, \mu_R^2) F(x, \mu_F^2, \mu_R^2) \equiv \Phi_H \otimes H \otimes F, \quad (2.191)$$

where the parameters μ_F^2 and μ_R^2 are the factorization and renormalization scales, respectively. We adopt the standard convention that $\mu_F = \mu_R$. In Eq.(2.191), H is the hard part of amplitude which is controlled by perturbative QCD. The hybrid meson DA Φ_H describes the transition from the partons to the meson, and F denotes generalized parton distributions which are related to nonperturbative matrix elements of bilocal operators between different hadronic states, has explained in Sec. 1.3. One typical diagram corresponding to the factorized amplitude (2.191) is illustrated in Fig. 2.25.

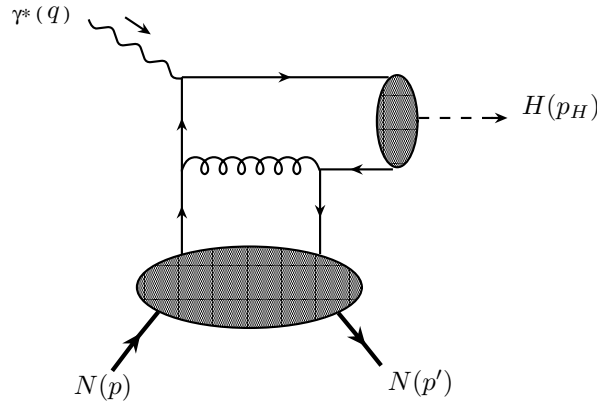


Figure 2.25: Typical diagram describing the electroproduction of a meson at lowest order. The grey blobs are non-perturbative matrix elements, namely the meson distribution amplitude and the nucleon generalized parton distribution

The calculation of the production amplitude, at leading order in α_s , is now straightforward and leads to an expression completely similar to the one for the production of longitudinally polarized vector meson, except for the C -parity which enforces the coupling to a $C = -$ GPD, while ρ -electroproduction involves a $C = +$ GPD.

We estimate the ratio of hybrid to ρ electroproduction cross-sections through their Born order expression and obtain, denoting as $M^{(\pm)}$ a meson of C -parity \mp (we label the DAs through their symmetrical properties):

$$\mathcal{A}_{\gamma_L^* p \rightarrow M_L^{(\pm)0} p} = \frac{e\pi\alpha_s f_H C_F}{\sqrt{2} N_c Q} \left[e_u \mathcal{H}_{uu}^\pm - e_d \mathcal{H}_{dd}^\pm \right] \mathcal{V}^{(M,\pm)}, \quad (2.192)$$

where

$$\mathcal{H}_{ff}^\pm = \frac{1}{P^-} \int_{-1}^1 dx \left[\bar{u}(p_2) \gamma^- u(p_1) H_{ff}(x, \xi) + \bar{u}(p_2) \frac{i\sigma_{-\alpha} \Delta^\alpha}{2M} u(p_1) E_{ff}(x, \xi) \right] \left[\frac{1}{x + \xi - i\epsilon} \pm \frac{1}{x - \xi + i\epsilon} \right], \quad (2.193)$$

and

$$\mathcal{V}^{(M,\pm)} = \int_0^1 dy \phi^M(y) \left[\frac{1}{y} \pm \frac{1}{1-y} \right]. \quad (2.194)$$

Here H and E are the quark non-flip GPDs defined by Eq. (1.38). Note that the simple pole in y in (2.192) does not lead to any infrared divergency since the function $\phi^H(y)$ is expected to vanish, as usual, when the fraction y goes to zero or unity. The symmetry properties of the hard part (i.e. of the product of the second bracket of Eq. (2.193) with Eq. (2.194)) are in accordance with the C -parity of the produced mesonic state and of the t -channel state: for the hybrid $C = +$, the DA is odd, as the hard part, under $y \leftrightarrow \bar{y}$ while the GPD $C = -$ is even under $x \leftrightarrow -x$, in accordance with Eq. (1.62) ("non-singlet", i.e. $q - \bar{q}$ combination of quark distributions). The symmetry are opposite for the ρ -meson, involving the "singlet", i.e. $q + \bar{q}$, combination.

A full phenomenological study of hybrid electroproduction was performed in Ref. [W13]. We here only summarize our main results. The order of magnitude of hybrid electroproduction may be easily deduced through a direct comparison with ρ meson electroproduction amplitude [22]. We thus estimate that the ratio of hybrid and ρ electroproduction cross-sections is:

$$\frac{d\sigma^H(Q^2, x_B, t)}{d\sigma^\rho(Q^2, x_B, t)} = \left| \frac{f_H (e_u \mathcal{H}_{uu}^- - e_d \mathcal{H}_{dd}^-) \mathcal{V}^{(H,-)}}{f_\rho (e_u \mathcal{H}_{uu}^+ - e_d \mathcal{H}_{dd}^+) \mathcal{V}^{(\rho,+)}} \right|^2, \quad (2.195)$$

with $f_\rho = 216 \text{ MeV}$.

If we neglect the antiquarks contribution, i.e. if we restrict the x -integral to $[0, 1]$, one sees that the imaginary parts of the amplitudes for both meson electroproduction are equal in magnitude up to the factor \mathcal{V}^M . The ratio of the real parts depend much on the model used for guessing the generalized parton distributions. Since the imaginary part dominates in some kinematics, it is not unreasonable as a first estimate of the ratio of the cross sections, to assume that the full amplitude ratio is driven by the same quantity. Using the asymptotic forms for the hybrid and ρ mesons distribution amplitudes, which for the ρ -meson case is supported by QCD sum rule [135, 248], we thus estimate that :

$$\frac{d\sigma^H(Q^2, x_B, t)}{d\sigma^\rho(Q^2, x_B, t)} \approx \left(\frac{5f_H}{3f_\rho} \right)^2 \approx 0.15. \quad (2.196)$$

In Ref. [W13], we did some more precise predictions, using the standard description of GPDs in terms of double distributions [51, 114]. We also investigated the dependency on the renormalization scale μ_R^2 . We considered two possibilities, in order to study the uncertainties when fixing the renormalization scale: the first one, in a "default" way, is just the natural scale $\mu_R^2 = Q^2$. The second one is based on the BLM scheme [158], for which we made some devoted studies in Ref. [W14]. We argued in particular in Ref. [W14] that when applying the BLM method to fix μ_R^2 , one fails to fix one single scale, since the amplitude has both real and imaginary parts, thus leading to two different scales.

Furthermore, in both H and ρ cases, one faces a singularity when extracting the BLM scale through the real part of the imaginary amplitude for certain value of ξ . Such a problem does not occur for π -electroproduction. We thus suggested and implemented the BLM scheme at the level of the cross-sections ¹¹.

The resulting differential cross sections for hybrid meson and ρ meson (quark contribution only) production are shown on Fig. 2.26 for $x_B = 0.18$ and 0.33 , using the above mentioned naive scale fixing. The BLM

¹¹Note that this stimulated further studies on BLM scheme within exclusive processes in Ref. [190].

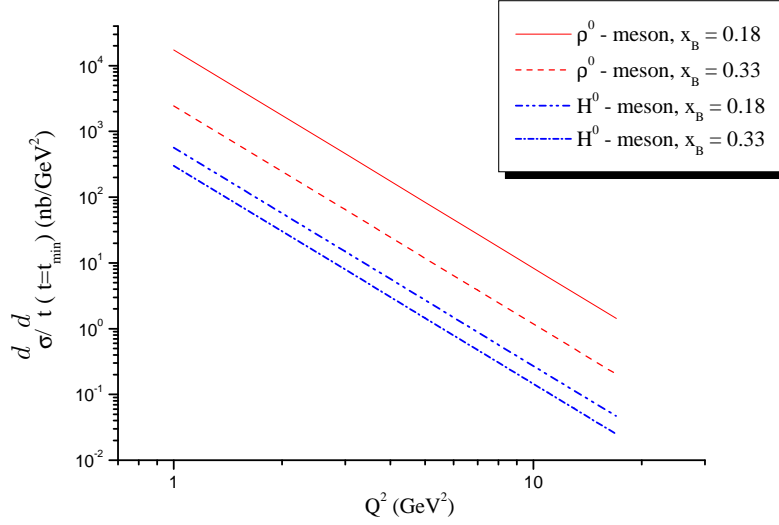


Figure 2.26: Differential cross section for ρ and hybrid meson production with the naive choice of the renormalization scale and different x_B .

procedure, implemented at the level of the cross-section according to Ref. [W14], leads to the following values of the renormalization scales:

$$\begin{aligned}\mu_R^2 &= e^{-4.9} Q^2, & \text{for } \rho \text{ meson,} \\ \mu_R^2 &= e^{-5.13} Q^2, & \text{for } H \text{ meson.}\end{aligned}\quad (2.197)$$

for the case $\xi = 0.2$ (or $x_B \approx 0.33$), and

$$\begin{aligned}\mu_R^2 &= e^{-4.68} Q^2, & \text{for } \rho \text{ meson,} \\ \mu_R^2 &= e^{-5.0} Q^2, & \text{for } H \text{ meson.}\end{aligned}\quad (2.198)$$

for the case $\xi = 0.1$ (or $x_B \approx 0.18$).

Note that, taking into account the D-terms, the ρ meson BLM scale is slightly diminished. For instance, in the case $x_B \approx 0.33$ we have

$$\mu_R^2 = e^{-5.4} Q^2. \quad (2.199)$$

These renormalization scales have rather small magnitudes. This has a tendency to enlarge the cross sections but may endanger the validity of the perturbative approach. However, it is possible that the coupling constant α_s stays below unity and the perturbative theory does not suffer from the IR divergencies. We use the Shirkov and Solovtsov's ansatz [249] for the analytic running coupling constant.

The role of power corrections was investigated in Ref. [170], due to the intrinsic transverse momentum of partons (the kinematical higher twist). In that approach the inclusion of the intrinsic transverse momentum dependence results in a rather strong effect on the differential cross-section before the scaling regime is achieved. In Ref. [170], the renormalization scale μ_R^2 is defined by the gluon virtuality so that the scale is a function of parton fractions flowing into the corresponding gluon propagator.

On Fig. 2.27, we present our results for the differential cross section of the hybrid meson electroproduction compared to the ρ meson electroproduction, using the BLM scales. We can see that the hybrid cross section is rather sizeable in comparison with the corresponding ρ meson cross section. We also show the results obtained in Ref. [170] for the ρ meson electroproduction. We see that in the region $Q^2 \sim 5 - 10 \text{ GeV}^2$ the size of the ρ meson cross section obtained with the inclusion of transverse momentum effects is very close to the analogous

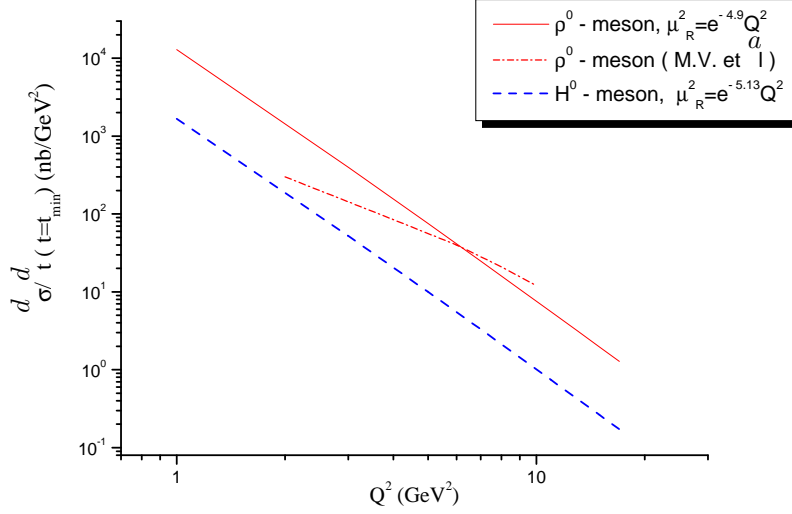


Figure 2.27: Differential cross-section for exotic hybrid meson electroproduction (dashed line) with $\mu_R^2 = e^{-5.13}Q^2$ compared with the quark contribution to ρ^0 electroproduction (solid line) with $\mu_R^2 = e^{-4.9}Q^2$, as a function of Q^2 , for $x_B \approx 0.33$. The dash-dotted line is the result of Vanderhaegen et al [170] for ρ electroproduction.

x_B	0.33				0.18			
Q^2 (GeV ²)	3.0	7.0	11.0	17.0	3.0	7.0	11.0	17.0
$\mu_R^2 = Q^2$	0.123	0.123	0.123	0.123	0.0325	0.0326	0.0326	0.0326
$\mu_R^2 = \mu_{BLM}^2$	0.131	0.133	0.133	0.134	0.0356	0.0362	0.0365	0.0367

Table 2.1: Ratio $d\sigma^H : d\sigma^\rho$ for both the naive and BLM scales and for the different values of x_B .

cross section computed with the BLM scale and without the intrinsic transverse momentum dependence. On the other hand, for higher values of Q^2 the leading order amplitude computed with the BLM scale fixing is falling faster than the corresponding amplitude derived in Ref. [170], whereas for smaller values of Q^2 it is larger than that prediction. We do not want to claim here that kinematical higher twist contributions have no effects at low values of Q^2 but rather that a rather strong effect on the Q^2 dependence of the cross sections may be dictated by another mechanism which is much more controllable since it depends on the estimate of higher order perturbative contributions.

All this shows that the scale fixing ambiguities lead to a non negligible theoretical uncertainty on the absolute value of cross sections. It is important however to understand that most of this uncertainty does not apply to ratios of cross sections, and in particular to the most interesting ratio $d\sigma^H : d\sigma^\rho$, which measures the expected cross section for hybrid production with respect to the well measured and large cross section for ρ meson production. Indeed, as shown on Table 2.1, this ratio is very insensitive to the scale fixing procedure. Moreover it is not small when x_B is large enough and almost Q^2 independent. The decreasing value of the ratio when x_B diminishes comes from the relative sign of the two terms contributing in Eq. (2.192), *i.e.* when $\xi \rightarrow 0$ the structure \mathcal{H}^- goes to zero too. Exotic hybrid meson can be therefore electroproduced in an experimentally feasible way in actual experiments at JLAB, HERMES or Compass. Their study in high statistics experiments at JLAB should be fruitful. The signal may be discovered through a missing mass measurement provided the

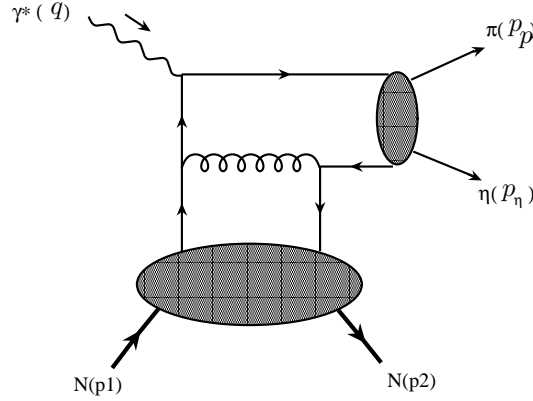


Figure 2.28: Typical diagram describing the electroproduction of $\pi\eta$ pair. The higher and lower blobs represent the GDAs and GPDs, respectively.

recoil proton energy-momentum is well measured. This allows to study all decay channels of these poorly known states.

2.5.4 Study of hybrid mesons via the electroproduction of $\pi\eta$ pairs

In the case where there is no recoil detector which allows to identify the hybrid production events through a missing mass reconstruction, one will have to base an identification process through the possible decay products of the hybrid meson H^0 . Since the particle $\pi_1(1400)$ has a dominant $\pi\eta$ decay mode [241,242], we now proceed to the description of the process

$$e(k_1) + N(p_1) \rightarrow e(k_2) + \pi^0(p_\pi) + \eta(p_\eta) + N(p_2) \quad (2.200)$$

or

$$\gamma^*(q) + N(p_1) \rightarrow \pi^0(p_\pi) + \eta(p_\eta) + N(p_2). \quad (2.201)$$

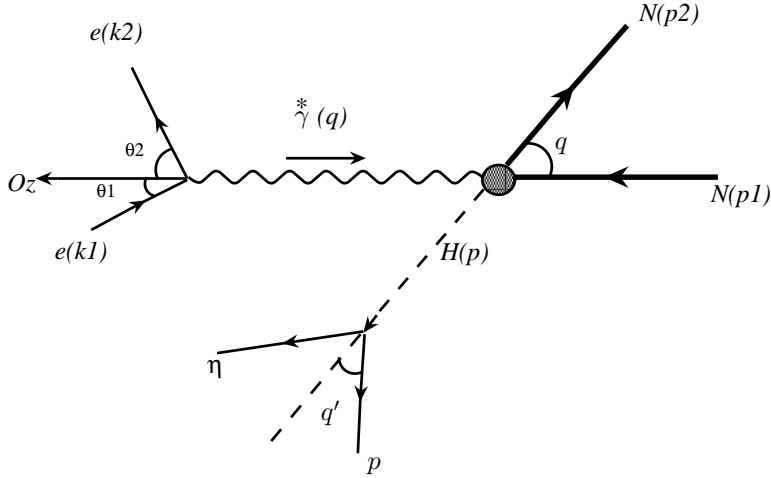
The formalism of GDAs, which we have presented in Ref. 2.1, allows one to compute the amplitude through a factorization illustrated in Fig. 2.28. The $\pi\eta$ GDA as a form of the type (2.55). We refer to Ref. [W13] for the detailed analysis of the $\pi\eta$ GDA and the computation of the amplitude.

Since the mass region around 1400 MeV is dominated by the strong $a_2(1329)$ (2^{++}) resonance [241,242], it is therefore natural to look for the interference of the amplitudes of hybrid and a_2 production, which is linear, rather than quadratic in the hybrid electroproduction amplitude. In our case, since the hybrid production amplitude may be rather small with respect to a continuous background, we propose [W13] to use the supposedly large amplitude for a_2 electroproduction as a magnifying lens to unravel the presence of the exotic hybrid meson. Since these two amplitudes describe different orbital angular momentum of the π and η mesons, the asymmetry which is sensitive to their interference is an angular asymmetry defined by

$$A(Q^2, y_l, \hat{t}, m_{\pi\eta}) = \frac{\int \cos \theta_{cm} d\sigma^{\pi^0\eta}(Q^2, y_l, \hat{t}, m_{\pi\eta}, \cos \theta_{cm})}{\int d\sigma^{\pi^0\eta}(Q^2, y_l, \hat{t}, m_{\pi\eta}, \cos \theta_{cm})} \quad (2.202)$$

as a weighted integral over polar angle θ_{cm} of the relative momentum of π and η mesons, illustrated in Fig. 2.29.

The angle θ_{cm} can be related to usual ζ variable entering the definition of GDA, as shown in Sec. 2.1.2 with a slight modification when taking into account the different masses for π and η . We refer to Ref. [W13] for details. Our estimation of the asymmetry (2.202) is shown on Fig. 2.30.

Figure 2.29: Typical process describing the electroproduction of a $\pi\eta$ pair.

It vanishes for $m_{\pi\eta} \approx 1.3$ GeV. Besides, one can see from Fig. 2.30 that the first positive extremum is located at $m_{\pi\eta}$ around the mass of a_2 meson while the second negative extremum corresponds to the hybrid meson mass. Note that this angular asymmetry is completely similar to the charge asymmetry which was studied in $\pi^+\pi^-$ electroproduction at HERMES [250].

2.5.5 Exotic hybrid meson production in $\gamma^*\gamma$ collisions

Photon-photon collisions, with one deeply virtual photon, is an excellent tool for the study of different aspects of QCD. The main feature of such processes is that a QCD factorization theorem holds, which separates a hard partonic subprocess involving scattered photons from either a DA describing a transition of a quark-antiquark pair to a meson or a GDA describing the transition of a quark-antiquark pair to two- or three-meson states. In Ref. [W18], we extended our previous study to $\gamma^*\gamma$ collisions with production of both longitudinally and transversally polarised hybrid meson. Note that the positive C parity of the hybrid meson does not allow any contribution from a Bremsstrahlung process. We thus consider the process

$$e(k_1) + e(l_1) \rightarrow e(k_2) + e(l_2) + H(p). \quad (2.203)$$

Specifying a positive C parity two body decay channel, like $\pi^0\eta$, one may equivalently investigate the process

$$e(k_1) + e(l_1) \rightarrow e(k_2) + e(l_2) + \pi(p_\pi) + \eta(p_\eta). \quad (2.204)$$

We calculate the hard amplitude up to the level of twist 3 and thus ignore the contributions of mass terms. The case of hybrid production and its decay products, $\pi\eta$ pair in electron-photon collisions is similar to the electron-proton case, with the important distinction that no unknown generalized parton distribution enters the amplitude, so that the only place where non-perturbative physics enters is the final state DA or generalized distribution amplitudes (GDA). We emphasize the $\pi\eta$ pair production as a promising way for detecting the hybrid meson.

Depending whether the hybrid is seen directly or through its decay mode, one should consider either the factorization through DAs or through GDAs. The corresponding DAs, similar to the one of the ρ -meson (see

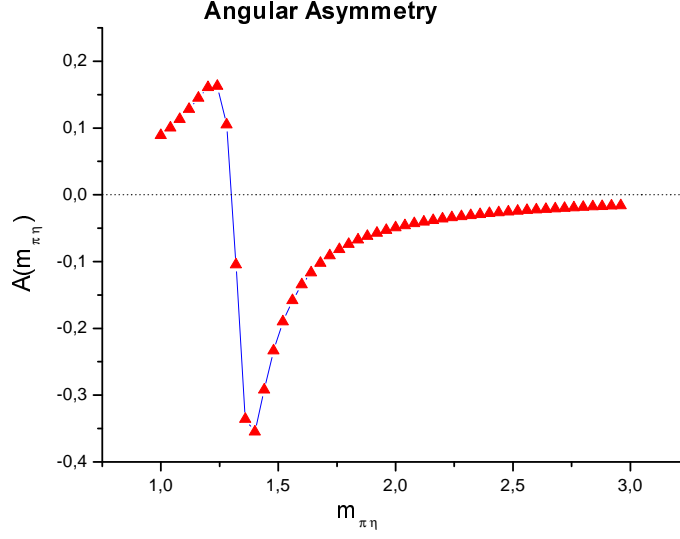


Figure 2.30: The angular asymmetry as a function of $m_{\pi\eta}$.

Sec.1.4.3), are naturally defined as

$$\langle H(p, \lambda) | \bar{\psi}(z) \gamma_\mu [z; -z] \psi(-z) | 0 \rangle = f_H M_H \left[p_\mu e^{(\lambda)} \cdot n \int_0^1 du e^{i(u-\bar{u})p \cdot z} \phi_1^H(u) + e_{\mu T}^{(\lambda)} \int_0^1 du e^{i(u-\bar{u})p \cdot z} \phi_3^H(u) \right] \quad (2.205)$$

for the vector correlator, and

$$\langle H(p, \lambda) | \bar{\psi}(z) \gamma_\mu \gamma_5 [z; -z] \psi(-z) | 0 \rangle = i f_H M_H \varepsilon_{\mu e_T^{(\lambda)} p n} \int_0^1 du e^{i(u-\bar{u})p \cdot z} \phi_A^H(u) \quad (2.206)$$

for the axial correlator. We use the following short notation : $\varepsilon_{skml} = \varepsilon_{\mu_1 \mu_2 \mu_3 \mu_4} s_{\mu_1} k_{\mu_2} m_{\mu_3} l_{\mu_4}$. In eqns (2.205) and (2.206), the polarization vector $e_\mu^{(\lambda)}$ describes the spin state of the hybrid meson. Due to the C -charge invariance, the symmetry properties of these DAs reads

$$\phi_1^H(u) = -\phi_1^H(1-u), \quad \phi_3^H(u) = -\phi_3^H(1-u), \quad \phi_A^H(u) = \phi_A^H(1-u). \quad (2.207)$$

We refer to Ref. [W18] for the definition and study of the corresponding $\pi\eta$ GDAs, with an account of a possible background, modeled by its magnitude K and its phase α .

We investigated the ratio of cross-sections for H production over the π^0 production, proportional to the square of the ratio of transition form factors for $\gamma^* \gamma \rightarrow H$ and $\gamma^* \gamma \rightarrow \pi^0$. As for the usual treatment of a pseudoscalar meson [133], the transition form factor $F_{H\gamma}$ scales like $1/Q^2$ up to logarithmic corrections due to the QCD evolution of the DA. Based on this analysis, we got approximately $R \simeq 40\%$. The effect of twist 3 contribution (treated here à la Wandzura-Wilczek) reduces this ratio below $Q^2 = 4 \text{ GeV}^2$. Still, the effect is not dramatic, and this ratio is still larger than 20 % for $Q^2 = 1 \text{ GeV}^2$. We also studied the $\pi\eta$ production through the cross-section, as well as the angular distribution of the produced particles.

Since lepton beams are easily polarized, we may consider the single spin asymmetry associated with the case where one of the initial lepton is longitudinally polarized while the polarizations of the other one are averaged over. This single spin asymmetry will turn out to give access to the phase difference of leading twist and twist 3 components of the final state GDA.

For that, we consider now the exclusive process where a longitudinally polarized lepton (with helicity h) scatters on an unpolarized photon to produce the lepton and the hybrid meson detected through its decay into a $\pi\eta$ pair. Such a process allows to define an asymmetry which is zero at the leading twist level but receives contributions from the interference of twist 2 and twist 3 amplitudes. This asymmetry is related to the azimuthal angular dependence of the polarized cross section and it is defined as

$$\mathcal{A}_1(s_{e\gamma}, Q^2, W^2; \varphi) = \frac{\int d \cos \theta_{cm} (d\sigma^{(\rightarrow)} - d\sigma^{(\leftarrow)})}{\int d \cos \theta_{cm} (d\sigma^{(\rightarrow)} + d\sigma^{(\leftarrow)})}, \quad (2.208)$$

where we denote by $d\sigma^{(\rightarrow)}$ the differential cross section $d\sigma_{e\gamma \rightarrow e\pi\eta}^{(h=1)}/dW^2 dQ^2 d \cos \theta_{cm} d\varphi$. The angles are defined according to Fig. 2.31. This quantity depends much on the unknown background phase α . On Fig. 2.32,

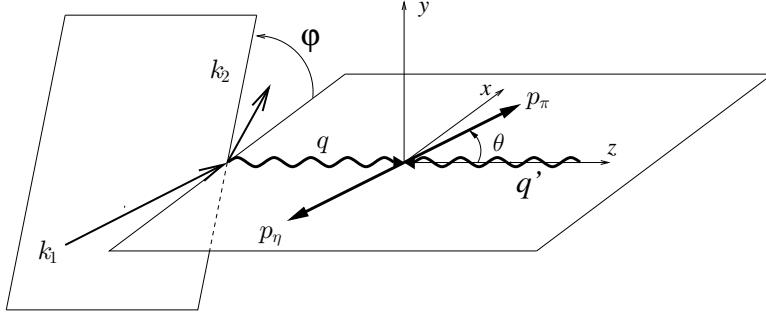


Figure 2.31: Kinematics of the process $e \gamma \rightarrow e \pi \eta$.

we present our result with the choice $\alpha = 0$. See Ref. [W18] for other choices of parameters. The resulting asymmetry is sizeable and should be measurable.

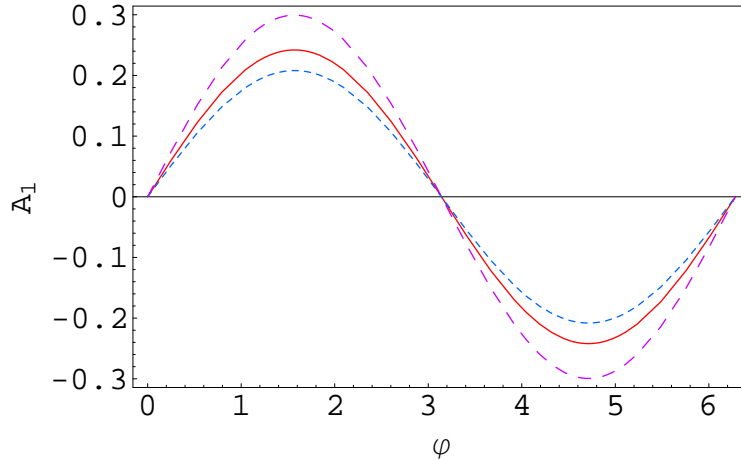


Figure 2.32: The single spin asymmetry \mathcal{A}_1 as function of $\varphi = (0, 2\pi)$. Values of parameters: $W = 1.4 \text{ GeV}$, $Q^2 = 5.0 \text{ GeV}^2$, $s_{e\gamma} = 10 \text{ GeV}^2$, $\alpha = 0$. The solid line corresponds to $K = 0.8$, the short-dashed line to $K = 1.0$, the long-dashed line to $K = 0.5$.

These various theoretical studies are thus very promising. Both in electroproduction mode and in $\gamma^*\gamma$ reactions, we have proven the feasibility of a dedicated experimental search and characterization of a $J^{PC} = 1^{-+}$ hybrid state. This is basically based on the fact that the amplitudes are not suppressed in Q^2 , being dominated by twist 2 contributions.

In particular, if a hybrid meson exists with $J^{PC} = 1^{-+}$ around 1.4 GeV and with a sizeable branching ratio to $\pi - \eta$, much can be learned about it from the experimental observation of $\gamma^*\gamma$ reactions and the precise

study of the $\pi - \eta$ final state. The magnitude of the cross section that we obtain in our model of the $\pi - \eta$ GDA indicates that present detectors at current e^+e^- colliders are able to get good statistics on these reactions, provided the tagging procedure is efficient.

Chapter 3

Light-Cone Collinear Factorization

Based on [W25, W24]

3.1 Introduction

In this chapter, we will extend the collinear factorization which have been discussed in previous chapters at the twist 2 level to situations where higher twist corrections are included. Such an inclusion may improve the description of data at moderate values of the hard scale. More importantly, there are processes which are dominated by twist 3 effects. Such a consistent inclusion of higher twist contributions within collinear factorization is then compulsory.

Indeed, the transversally polarized ρ -meson production does not enter the leading twist controllable case [175, 176] but only the twist 3 more intricate part of the amplitude [160–162, 251]. This is due to the fact that the leading twist distribution amplitude (DA) of a transversally polarized vector meson is chiral-odd, and hence decouples from hard amplitudes at the twist two level, as we have seen in Sec. 1.4.9, even when another chiral-odd quantity is involved [175, 176], unless in reactions with more than two final hadrons [179, 180, W26]. An understanding of the quark-gluon structure of a transversally polarized vector meson is however an important task of hadronic physics if one cares about studying confinement dynamics. This quark gluon structure may be described by distribution amplitudes which we have discussed in the previous chapter. On the experimental side, a continuous effort has been devoted to the exploration of ρ -meson photo and electro-production, from moderate [252–255] to very large energy [256–263]. The kinematical analysis of the final π -meson pair allows then to separate the different helicity amplitudes, hence to measure the transversally polarized ρ meson production amplitude. We will see in Chap. 5 that in particular at HERA, very precise measurements of the whole spin density matrix element have been performed, and that the ρ_T production is by no mean negligible, although non-dominant for deep electroproduction. This thus deserve dedicated studies in terms of QCD.

In the literature there are two approaches to the factorization of the scattering amplitudes in exclusive processes at leading and higher twists. The first approach [161, 162, 251, 264], being the generalization of the Ellis-Furmanski-Petronzio (EFP) method [265–271] to the exclusive processes, deals with the factorization in the momentum space around the dominant light-cone direction. We shall call it the Light-Cone Collinear Factorization (LCCF). On the other hand, there exists a covariant approach in coordinate space successfully applied [135–137] for a systematic description of distribution amplitudes of hadrons carrying different twists. This approach will be called the Covariant Collinear Factorization approach (CCF). Although being quite different and using different distribution amplitudes, both approaches can be applied to the description of the same processes. This fact calls for verification whether these two descriptions are equivalent and lead to the same physical consequences. This can be clarified by establishing a precise vocabulary between objects appearing in the two approaches and by comparing physical results obtained with the help of the two methods.

In this chapter, we will concentrate ourselves on the first point, i.e. on the description of LCCF method and its equivalence with CCF, at twist 3. The arguments presented here will be as much as general as possible, although when needed we will rely on a specific example for illustration, the $\gamma^* \rightarrow \rho_T$ impact factor. We

conjecture that the method is very general and can be extended for other exclusive processes and for higher twist corrections going beyond twist 3. The explicit verification of the equivalence between LCCF and CCF on the specific example of the $\gamma^* \rightarrow \rho_T$ impact factor will be performed, based on a detailed computation, in Chap. 6.

The LCCF method involves a Taylor expansion of the scattering amplitude in the momentum space around the dominant light-cone direction and thus naturally introduces an appropriate set of non-perturbative correlators which encode effects not only of the lowest but also of the higher Fock states of the produced particle. The reduction of the original set of correlators to a set of independent ones is achieved with the help of equations of motion and invariance of the scattering amplitude under rotation on the light-cone.

3.2 Factorization beyond leading twist

Let us start with the most general form of the exclusive amplitude for the hard process $A \rightarrow \rho B$ (where A and B denotes initial and final states in kinematics where a hard scale allows a partonic interpretation) which we are interested in, written in the momentum representation and in axial gauge, as

$$\mathcal{A} = \int d^4\ell \operatorname{tr} \left[H(\ell) \Phi(\ell) \right] + \int d^4\ell_1 d^4\ell_2 \operatorname{tr} \left[H_\mu(\ell_1, \ell_2) \Phi^\mu(\ell_1, \ell_2) \right] + \dots, \quad (3.1)$$

where H and H_μ are the coefficient functions with two parton legs and three parton legs, respectively, as illustrated in Fig. 3.1 on the example of $\gamma^* \rightarrow \rho$ impact factor, which is defined in full length in Sec.4.2. In

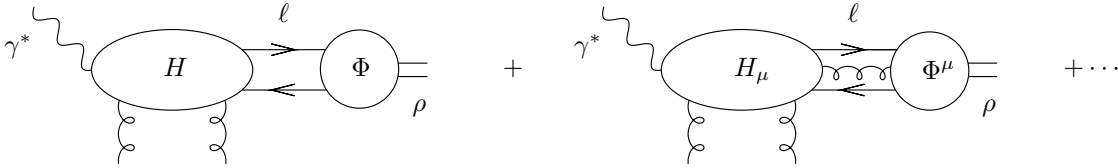


Figure 3.1: 2- and 3-parton correlators attached to a hard scattering amplitude in the example of the $\gamma^* \rightarrow \rho$ impact factor, where vertical lines are hard t -channel gluons in the color singlet state.

(3.1), the soft parts are given by the Fourier-transformed two or three partons correlators which are matrix elements of non-local operators. We consider the leading asymptotics of $1/Q$ expansion, separately for the cases of longitudinally (twist 2) and transversely polarized (twist 3) meson production. The amplitude (3.1) is not factorized yet because the hard and soft parts are related by the four-dimensional integration in the momentum space and by the summation over the Dirac indices.

To factorize the amplitude, we first choose the dominant direction around which we intend to decompose our relevant momenta and we Taylor expand the hard part. Let p and n be the conventionally called “plus” and “minus” light-cone vectors, respectively, normalized as $p \cdot n = 1$. We carry out an expansion of ℓ in the basis defined by the p and n light-cone vectors:

$$\ell_{i\mu} = y_i p_\mu + (\ell_i \cdot p) n_\mu + \ell_{i\mu}^\perp, \quad y_i = \ell_i \cdot n, \quad (3.2)$$

and make the following replacement of the integration measure in (3.1):

$$d^4\ell_i \longrightarrow d^4\ell_i dy_i \delta(y_i - \ell \cdot n). \quad (3.3)$$

Afterwards, the hard part coefficient function $H(\ell)$ has to be decomposed around the dominant “plus” direction:

$$H(\ell) = H(y p) + \left. \frac{\partial H(\ell)}{\partial \ell_\alpha} \right|_{\ell=y p} (\ell - y p)_\alpha + \dots \quad (3.4)$$

where $(\ell - y p)_\alpha \approx \ell_\alpha^\perp$ up to twist 3. One can see that the above-mentioned steps (3.2)-(3.4) do not yet allow us to factorize collinearly the amplitude in the momentum space since the l^\perp dependence of the hard part is an excursion out of the collinear framework. To obtain a factorized amplitude, one performs an integration by parts

to replace ℓ_α^\perp by ∂_α^\perp acting on the soft correlator. This leads to new operators \mathcal{O}^\perp which contain transverse derivatives, such as $\bar{\psi} \partial^\perp \psi$, and thus to the necessity of considering additional DAs $\Phi^\perp(l)$. This procedure accomplishes the factorization of the amplitude in momentum space. Factorization in the Dirac space can be achieved by the Fierz decomposition. For example, in the case of two fermions, one should project out the Dirac matrix $\psi_\alpha(0) \bar{\psi}_\beta(z)$ which appears in the soft part of the amplitude on the relevant Γ matrices, using Eq. (1.30). Thus, after all these stages, the amplitude takes the simple factorized form¹,

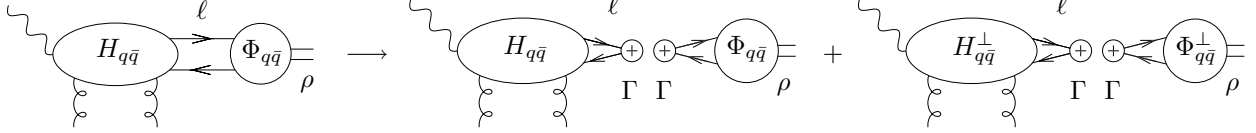


Figure 3.2: Factorization of 2-parton contributions in the example of the $\gamma^* \rightarrow \rho$ impact factor.

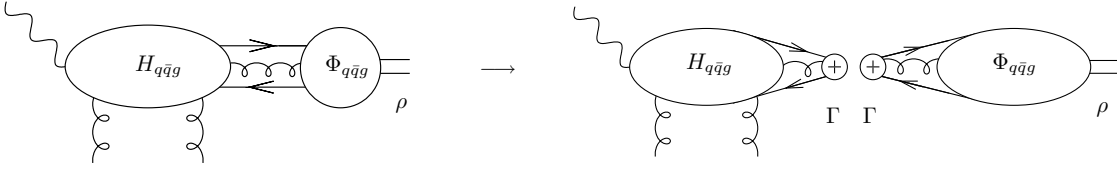


Figure 3.3: Factorization of 3-parton contributions in the example of the $\gamma^* \rightarrow \rho$ impact factor.

$$\mathcal{A} = \int_0^1 dy \text{tr} [H_{q\bar{q}}(y) \Gamma] \Phi_{q\bar{q}}^\Gamma(y) + \int_0^1 dy \text{tr} [H_{q\bar{q}}^\perp(y) \Gamma] \Phi_{q\bar{q}}^{\perp\Gamma}(y) + \int_0^1 dy_1 dy_2 \text{tr} [H_{q\bar{q}g}^\mu(y_1, y_2) \Gamma] \Phi_{q\bar{q}g}^\Gamma(y_1, y_2), \quad (3.5)$$

in which the two first terms in the r.h.s correspond to the two parton contribution and the last one to the three body contribution. This is illustrated symbolically in the example of the $\gamma^* \rightarrow \rho$ impact factor in Fig. 3.2 for 2-parton contributions and in Fig. 3.3 for 3-parton contributions.

Alternatively, combining the two last terms together in order to emphasize the fact they both originate from the Taylor expansion based on the covariant derivative, this factorization can be written as

$$\mathcal{A} = \int_0^1 dy \text{tr} [H(y) \Gamma] \Phi^\Gamma(y) + \int_0^1 dy_1 dy_2 \text{tr} [H^\mu(y_1, y_2) \Gamma] \Phi_\mu^\Gamma(y_1, y_2). \quad (3.6)$$

For definiteness², let us focus on the ρ -meson production case where the soft parts of the amplitude read

$$\begin{aligned} \Phi^\Gamma(y) &= \int_{-\infty}^{+\infty} \frac{d\lambda}{2\pi} e^{-i\lambda y} \langle \rho(p) | \bar{\psi}(\lambda n) \Gamma \psi(0) | 0 \rangle \\ \Phi_\rho^\Gamma(y_1, y_2) &= \int_{-\infty}^{+\infty} \frac{d\lambda_1 d\lambda_2}{4\pi^2} e^{-i\lambda y_1 \lambda_1 - i(y_2 - y_1) \lambda_2} \langle \rho(p) | \bar{\psi}(\lambda_1 n) \Gamma i \overleftrightarrow{D}_\rho^T(\lambda_2 n) \psi(0) | 0 \rangle. \end{aligned} \quad (3.7)$$

where in accordance with Eq. (1.40),

$$i \overleftrightarrow{D}_\mu = i \overrightarrow{\partial}_\mu + g A_\mu. \quad (3.8)$$

Eq.(3.7) supplemented by the appropriate choice of the Fierz matrices defines the set of non-perturbative correlators relevant for the description of the ρ -meson, which we will now discuss.

¹Despite the fact that these formulae are given here up to twist 3, the method can be extended to higher twist contributions.

²In the following, the notations $|\rho\rangle$ or $|V\rangle$ will be used when the specific nature of the vector meson does not matter.

3.3 Parametrizations of vacuum-to-rho-meson matrix elements up to twist 3

In this section, we introduce the parametrizations of the vacuum-to- ρ -meson matrix elements needed when calculating the process of exclusive ρ -production. As a concrete example, we shall below calculate the $\gamma_T^* \rightarrow \rho_T$ impact factor. Since we will follow two different approaches for our calculations, it is instructive to present two ways for parametrizing the corresponding matrix elements.

3.3.1 LCCF parametrization

We insist on the fact that in LCCF approach, the coordinates z_i in the parametrizations have to be proportionnal to the light-cone vector n . This is in contrast to the CCF approach where z lies on the light cone but does not correspond to any fixed light-cone direction. The transverse polarization of the ρ -meson is defined by the conditions (at twist 3, $p_\rho \sim p$)

$$e_T \cdot n = e_T \cdot p = 0, \quad (3.9)$$

i.e. e_T has only a \perp component, while e_L has no \perp component. Now, we introduce the parametrizations of the vacuum-to- ρ -meson matrix elements needed for the calculation, for example, of the $\gamma_T^* \rightarrow \rho_T$ impact factor. Keeping all the terms up to the twist-3 order with the axial (light-like) gauge, $n \cdot A = 0$, the matrix elements of quark-antiquark nonlocal operators can be written in terms of the light-cone basis vectors as (here, $z = \lambda n$)

$$\langle \rho(p_\rho) | \bar{\psi}(z) \gamma_\mu \psi(0) | 0 \rangle \stackrel{\mathcal{F}_1}{=} m_\rho f_\rho [\varphi_1(y) (e^* \cdot n) p_\mu + \varphi_3(y) e_{T\mu}^*], \quad (3.10)$$

$$\langle \rho(p_\rho) | \bar{\psi}(z) \gamma_5 \gamma_\mu \psi(0) | 0 \rangle \stackrel{\mathcal{F}_1}{=} m_\rho f_\rho i \varphi_A(y) \varepsilon_{\mu\alpha\beta\delta} e_T^{*\alpha} p^\beta n^\delta, \quad (3.11)$$

where the corresponding flavour matrix has been omitted³, and where we use $\varepsilon^{0123} = -\varepsilon_{0123} = 1$ and $\gamma_5 = i \gamma^0 \gamma^1 \gamma^2 \gamma^3$. For the sake of conciseness, we denote $\stackrel{\mathcal{F}_1}{=}$ the Fourier transformation with measure

$$\int_0^1 dy \exp[iy p \cdot z], \quad (3.12)$$

where $z = \lambda n$. The momentum fraction y ($\bar{y} \equiv 1 - y$) corresponds to the quark (antiquark). Note that the decomposition over the γ -matrix basis has been taken in the form:

$$-\langle \psi \bar{\psi} \rangle = \frac{1}{4} \langle \bar{\psi} \gamma_\mu \psi \rangle \gamma^\mu + \frac{1}{4} \langle \bar{\psi} \gamma_5 \gamma_\mu \psi \rangle \gamma^\mu \gamma_5 + \dots, \quad (3.13)$$

in such a way that the minus sign in front of the axial term is absorbed into the axial correlators. The matrix elements of the quark-antiquark operators with transverse derivatives are parametrized according to

$$\langle \rho(p_\rho) | \bar{\psi}(z) \gamma_\mu i \overleftrightarrow{\partial}_\alpha^T \psi(0) | 0 \rangle \stackrel{\mathcal{F}_1}{=} m_\rho f_\rho \varphi_1^T(y) p_\mu e_{T\alpha}^* \quad (3.14)$$

$$\langle \rho(p_\rho) | \bar{\psi}(z) \gamma_5 \gamma_\mu i \overleftrightarrow{\partial}_\alpha^T \psi(0) | 0 \rangle \stackrel{\mathcal{F}_1}{=} m_\rho f_\rho i \varphi_A^T(y) p_\mu \varepsilon_{\alpha\lambda\beta\delta} e_T^{*\lambda} p^\beta n^\delta, \quad (3.15)$$

where we introduced $\overleftrightarrow{\partial}_\rho = \frac{1}{2}(\overrightarrow{\partial}_\rho - \overleftarrow{\partial}_\rho)$ which is the standard antisymmetric derivative. The DAs $\varphi_1, \varphi_3, \varphi_A$ satisfies the normalization conditions

$$\int_0^1 \varphi_1(y) = 1, \int_0^1 \varphi_3(y) = 1 \quad \text{and} \quad \int_0^1 (y - \bar{y}) \varphi_A(y) = \frac{1}{2}. \quad (3.16)$$

In the same way, the matrix elements of quark-gluon nonlocal operators can be parametrized as

$$\begin{aligned} \langle \rho(p_\rho) | \bar{\psi}(z_1) \gamma_\mu g A_\alpha^T(z_2) \psi(0) | 0 \rangle &\stackrel{\mathcal{F}_2}{=} m_\rho f_{3\rho}^V B(y_1, y_2; y_g) p_\mu e_{T\alpha}^*, \\ \langle \rho(p_\rho) | \bar{\psi}(z_1) \gamma_5 \gamma_\mu g A_\alpha^T(z_2) \psi(0) | 0 \rangle &\stackrel{\mathcal{F}_2}{=} m_\rho f_{3\rho}^A i D(y_1, y_2; y_g) p_\mu \varepsilon_{\alpha\lambda\beta\delta} e_T^{*\lambda} p^\beta n^\delta, \end{aligned} \quad (3.17)$$

³The normalization in (3.10,3.11) thus corresponds to a meson which would be a one flavour quark-antiquark state $|V\rangle = |f\bar{f}\rangle$, with for example $\langle V(p) | \bar{\psi}_f(z) \gamma_\mu \psi_f(0) | 0 \rangle \stackrel{\mathcal{F}_1}{=} m_V f_V [\dots]$.

where the momentum fractions y_1 , \bar{y}_2 and y_g correspond to the quark, antiquark and gluon, respectively. The symbol $\stackrel{\mathcal{F}_2}{\equiv}$ now stands for (here, $z_i = \lambda_i n$)

$$\int_0^1 dy_1 dy_2 dy_g \delta(y_2 - y_1 - y_g) \exp [iy_1 p \cdot z_1 + iy_g p \cdot z_2]. \quad (3.18)$$

In the *r.h.s.* of (3.17), it is useful to perform the integration over the gluon fraction y_g (which then equals $y_2 - y_1$). Afterwards, the parametrizations (3.17) take the forms:

$$\langle \rho(p_\rho) | \bar{\psi}(z_1) \gamma_\mu g A_\alpha^T(z_2) \psi(0) | 0 \rangle \stackrel{\mathcal{F}_2}{\equiv} m_\rho f_{3\rho}^V B(y_1, y_2) p_\mu e_{T\alpha}^*, \quad (3.19)$$

$$\langle \rho(p_\rho) | \bar{\psi}(z_1) \gamma_5 \gamma_\mu g A_\alpha^T(z_2) \psi(0) | 0 \rangle \stackrel{\mathcal{F}_2}{\equiv} m_\rho f_{3\rho}^A iD(y_1, y_2) p_\mu \varepsilon_{\alpha\lambda\beta\delta} e_T^{\lambda*} p^\beta n^\delta, \quad (3.20)$$

with the symbol $\stackrel{\mathcal{F}_2}{\equiv}$ implying

$$\int_0^1 dy_1 \int_0^1 dy_2 \exp [iy_1 p \cdot z_1 + i(y_2 - y_1) p \cdot z_2]. \quad (3.21)$$

Note that the positivity of the gluon light-cone momentum fraction imposes that quark-gluon parameterizing functions have the form

$$B(y_1, y_2) \stackrel{def}{=} \mathcal{B}(y_1, y_2; y_2 - y_1) \theta(y_1 \leq y_2 \leq 1), \quad D(y_1, y_2) \stackrel{def}{=} \mathcal{D}(y_1, y_2; y_2 - y_1) \theta(y_1 \leq y_2 \leq 1). \quad (3.22)$$

As we already mentioned by writting Eq.(3.6), it is also natural to introduce the following objects:

$$\begin{aligned} \langle \rho(p_\rho) | \bar{\psi}(z_1) \gamma_\mu i \overleftrightarrow{D}_\alpha^T(z_2) \psi(0) | 0 \rangle &\stackrel{\mathcal{F}_2}{\equiv} m_\rho f_\rho \tilde{B}(y_1, y_2) p_\mu e_{T\alpha}^*, \\ \langle \rho(p_\rho) | \bar{\psi}(z_1) \gamma_5 \gamma_\mu i \overleftrightarrow{D}_\alpha^T(z_2) \psi(0) | 0 \rangle &\stackrel{\mathcal{F}_2}{\equiv} m_\rho f_\rho i\tilde{D}(y_1, y_2) p_\mu \varepsilon_{\alpha\lambda\beta\delta} e_T^{\lambda*} p^\beta n^\delta, \end{aligned} \quad (3.23)$$

where these parameterizing functions are now equal to

$$\begin{aligned} \tilde{B}(y_1, y_2) &= \frac{1}{2} \left(\varphi_1^T(y_1) + \varphi_1^T(y_2) \right) \delta(y_1 - y_2) + \zeta_3^V B(y_1, y_2), \\ \tilde{D}(y_1, y_2) &= \frac{1}{2} \left(\varphi_A^T(y_1) + \varphi_A^T(y_2) \right) \delta(y_1 - y_2) + \zeta_3^A D(y_1, y_2), \end{aligned} \quad (3.24)$$

with the dimensionless coupling constants

$$\zeta_3^V = \frac{f_{3\rho}^V}{f_\rho} \quad \text{and} \quad \zeta_3^A = \frac{f_{3\rho}^A}{f_\rho}. \quad (3.25)$$

Note that the function φ_1 corresponds to the twist-2, and functions B and D to the genuine (dynamical) twist-3, while functions φ_3 , φ_A , φ_1^T , φ_A^T (or alternatively \tilde{B} and \tilde{D}) contain both parts: kinematical (à la Wandzura-Wilczek, noted WW) twist-3 and genuine (dynamical) twist-3.

In (3.10)–(3.11), the functions φ_1 , φ_3 , φ_A , φ_1^T and φ_A^T parameterizing the two-particle correlators obey the following symmetry properties:

$$\varphi_1(y) = \varphi_1(1 - y), \quad \varphi_3(y) = \varphi_3(1 - y), \quad \varphi_A(y) = -\varphi_A(1 - y), \quad \varphi_1^T(y) = -\varphi_1^T(1 - y), \quad \varphi_A^T(y) = \varphi_A^T(1 - y). \quad (3.26)$$

These symmetry properties result from G -conjugation (or C -conjugation for neutral mesons). At the same time, the symmetry properties of the functions parameterizing the quark-gluon correlators are:

$$\mathcal{B}(y_1, y_2; y_g) = -\mathcal{B}(1 - y_2, 1 - y_1; y_g), \quad \mathcal{D}(y_1, y_2; y_g) = \mathcal{D}(1 - y_2, 1 - y_1; y_g). \quad (3.27)$$

Notice that, in the case of three-particle functions, G -conjugation involves the replacement: $y_1 \leftrightarrow \bar{y}_2$, while the gluon fraction y_g remains invariant under G -conjugation.

3.3.2 CCF parametrization

We recall and rewrite (doing standard fields transformations) the original CCF parametrizations of the ρ DAs [135–137], which we already introduced in Sec. 1.4.3, adapting them to our case when vector meson is produced in the final state. The formula for the axial-vector correlator reads

$$\langle \rho(p_\rho) | \bar{\psi}(z) [z, 0] \gamma_\mu \gamma_5 \psi(0) | 0 \rangle = \frac{1}{4} f_\rho m_\rho \varepsilon_\mu^{e_T^* p z} \int_0^1 dy e^{iy(p \cdot z)} g_\perp^{(a)}(y), \quad (3.28)$$

where we denote⁴

$$\varepsilon_\mu^{e_T^* p z} = \varepsilon_\mu^{\alpha\beta\gamma} e_{T\alpha}^* p_\beta z_\gamma, \quad (3.29)$$

and where

$$[z_1, z_2] = P \exp \left[ig \int_0^1 dt (z_1 - z_2)_\mu A^\mu(t z_1 + (1-t) z_2) \right] \quad (3.30)$$

is the Wilson line, defined in accordance with the convention (1.40). The transverse vector e_T is orthogonal to the light-cone vectors p and z . Neglecting mass effects, i.e. up to twist 3 level, it is decomposed as follows

$$e_{T\mu} = e_\mu - p_\mu \frac{e \cdot z}{p \cdot z} - z_\mu \frac{e \cdot p}{p \cdot z}, \quad (3.31)$$

where e is the meson polarization vector. Since as we will discuss later n can be arbitrary, and since the concrete definition of n influences the definition of transverse polarization, it is useful to remove the dependence on e_T in correlation functions. For that, we use Eq.(3.31) and rewrite the original CCF parametrization in terms of the full meson polarization vector e . This is already done for the axial-vector correlator (3.28) since due to the properties of fully antisymmetric tensor $\varepsilon_{\mu\nu\alpha\beta}$ one can use in the r.h.s. of (3.28) the full meson polarization vector e instead of e_T .

The definition of 2-parton vector correlator of a ρ -meson can be written in the form

$$\langle \rho(p_\rho) | \bar{\psi}(z) [z, 0] \gamma_\mu \psi(0) | 0 \rangle = f_\rho m_\rho \int_0^1 dy e^{iy(p \cdot z)} \left[p_\mu \frac{e^* \cdot z}{p \cdot z} \phi_\parallel(y) + e_{T\mu}^* g_\perp^{(v)}(y) - z_\mu \frac{m^2}{2} \frac{e^* \cdot z}{(p \cdot z)^2} g_3(y) \right]. \quad (3.32)$$

All distribution amplitudes describing two particle correlators are normalized to unity

$$\int_0^1 dy \left\{ \phi_\parallel, g_\perp^{(a)}, g_\perp^{(v)}, g_3 \right\} (y) = 1. \quad (3.33)$$

Using relations (3.31, 3.33) and integration by parts one can rewrite the vector correlator (3.32) in the form

$$\langle \rho(p_\rho) | \bar{\psi}(z) [z, 0] \gamma_\mu \psi(0) | 0 \rangle = f_\rho m_\rho \int_0^1 dy e^{iy(p \cdot z)} \left[-i p_\mu (e^* \cdot z) h(y) + e_\mu^* g_\perp^{(v)}(y) + iz_\mu \frac{m^2}{2} \frac{e^* \cdot z}{p \cdot z} \bar{h}(y) \right], \quad (3.34)$$

where we introduce the auxiliary functions

$$h(y) = \int_0^y dv \left(\phi_\parallel(v) - g_\perp^{(v)}(v) \right), \quad (3.35)$$

$$\bar{h}(y) = \int_0^y dv \left(g_3(v) - g_\perp^{(v)}(v) \right). \quad (3.36)$$

⁴Note that, as already emphasized, our sign convention for the antisymmetric tensor is $\epsilon^{0123} = 1$, opposite to the one used in Ref. [135–137]. The corresponding sign change is taken here into account.

Note that the r.h.s of (3.34) now only involves the full polarization vector e , as was noted above for the axial correlator. The last term in the r.h.s. of (3.34) contributes to the physical amplitude starting from the twist 4 level only, therefore we will neglect it in the following.

For quark-antiquark-gluon correlators (up to twist 3 level) the parametrizations of Refs. [136, 137] have the forms⁵

$$\langle \rho(p_\rho) | \bar{\psi}(z) [z, t z] \gamma_\alpha g G_{\mu\nu}(t z) [t z, 0] \psi(0) | 0 \rangle = -i p_\alpha [p_\mu e_{\perp\nu}^* - p_\nu e_{\perp\mu}^*] m_\rho f_{3\rho}^V \int D\alpha V(\alpha_1, \alpha_2) e^{i(p \cdot z)(\alpha_1 + t\alpha_g)}, \quad (3.37)$$

$$\langle \rho(p_\rho) | \bar{\psi}(z) [z, t z] \gamma_\alpha \gamma_5 g \tilde{G}_{\mu\nu}(t z) [t z, 0] \psi(0) | 0 \rangle = -p_\alpha [p_\mu e_{\perp\nu}^* - p_\nu e_{\perp\mu}^*] m_\rho f_{3\rho}^A \int D\alpha A(\alpha_1, \alpha_2) e^{i(p \cdot z)(\alpha_1 + t\alpha_g)}, \quad (3.38)$$

where $\alpha_1, \alpha_2, \alpha_g$ correspond to momentum fractions of quark, antiquark and gluon respectively inside the ρ -meson,

$$\int D\alpha = \int_0^1 d\alpha_1 \int_0^1 d\alpha_2 \int_0^1 d\alpha_g \delta(1 - \alpha_1 - \alpha_2 - \alpha_g) \quad (3.39)$$

and $\tilde{G}_{\mu\nu} = -\frac{1}{2} \epsilon_{\mu\nu\alpha\beta} G^{\alpha\beta}$. These three partons DAs are normalized as follows

$$\int D\alpha (\alpha_1 - \alpha_2) V(\alpha_1, \alpha_2) = 1, \quad \int D\alpha A(\alpha_1, \alpha_2) = 1. \quad (3.40)$$

In what follows we will work in the axial gauge $A \cdot n = 0, n^2 = 0$. In this gauge the gluon field can be expressed in terms of field strength as follows

$$A_\alpha(y) = \int_0^\infty d\sigma e^{-\epsilon \sigma} n^\beta G_{\alpha\beta}(y + \sigma n) \quad (3.41)$$

which implies that the $(\bar{q} A q)$ correlators involving the gluon field A reads

$$\langle \rho(p_\rho) | \bar{\psi}(z) \gamma_\mu g A_\alpha(tz) \psi(0) | 0 \rangle = -p_\mu e_{T\alpha}^* m_\rho f_{3\rho}^V \int \frac{D\alpha}{\alpha_g} e^{i(p \cdot z)(\alpha_1 + t\alpha_g)} V(\alpha_1, \alpha_2), \quad (3.42)$$

$$\langle \rho(p_\rho) | \bar{\psi}(z) \gamma_\mu \gamma_5 g A_\alpha(tz) \psi(0) | 0 \rangle = -i p_\mu \frac{\varepsilon_\alpha^{z p e_T^*}}{(p \cdot z)} m_\rho f_{3\rho}^A \int \frac{D\alpha}{\alpha_g} e^{i(p \cdot z)(\alpha_1 + t\alpha_g)} A(\alpha_1, \alpha_2). \quad (3.43)$$

3.4 Equations of motion

The correlators introduced above are not independent, since they are constrained by the QCD equations of motion for the field operators entering them, as we discussed in the previous chapter. In the simplest case of fermionic fields, they follow from the vanishing of matrix elements $\langle (i\hat{D}(0)\psi(0))_\alpha \bar{\psi}_\beta(z) \rangle = 0$ and $\langle \psi_\alpha(0) i(\hat{D}(z)\bar{\psi}(z))_\beta \rangle = 0$ due to the Dirac equation, then projected on different Fierz structure.

Let us start with the QCD equation of motion written for the fermion field $\psi(0)$:

$$\langle i \overrightarrow{\mathcal{D}}(0) \psi(0) \bar{\psi}(z) \rangle = 0, \quad (3.44)$$

where $\langle \dots \rangle$ denote arbitrary hadron states which we here specify as $\langle \rho | \dots | 0 \rangle$. Also, we stress that, in (3.44), the fermion fields ψ and $\bar{\psi}$ should be understood as fields with free Dirac indices. Then, we first focus on the quark-antiquark part of (3.44) which can be written as

$$\int d^4 z e^{-iy p \cdot z - i\bar{y} p \cdot x} \left\{ \langle i \overrightarrow{\mathcal{D}}_L^x \psi(x) \bar{\psi}(z) \rangle + \langle i \overrightarrow{\mathcal{D}}_T^x \psi(x) \bar{\psi}(z) \rangle \right\} \Big|_{x=0}. \quad (3.45)$$

⁵Note that in those definition $f_\rho, f_{3\rho}^V$ and $f_{3\rho}^A$ have dimension of mass. This is agreement with Ref. [137] but differ from Ref. [136] in which $f_{3\rho}^V$ and $f_{3\rho}^A$ have dimension of mass square.

Here, we separate out the longitudinal derivatives from the transverse ones. Working with the longitudinal derivative contribution, we get

$$i\gamma_\rho \int d^4z e^{-iy\rho \cdot z - i\bar{y}\rho \cdot x} \frac{\partial^L}{\partial x_\rho} \langle \psi(x) \bar{\psi}(z) \rangle \Big|_{x=0} = \bar{y} \not{\rho} \int d^4z e^{-iy\rho \cdot z - i\bar{y}\rho \cdot x} \langle \psi(x) \bar{\psi}(z) \rangle \Big|_{x=0}, \quad (3.46)$$

where an integration by parts has been used. Let us now decompose $\langle \psi(x) \bar{\psi}(z) \rangle$ over the γ -basis (the Fierz decomposition):

$$-\langle \psi(x) \bar{\psi}(z) \rangle = \frac{1}{4} \langle \bar{\psi}(z) \gamma_\alpha \psi(x) \rangle \gamma^\alpha + \frac{1}{4} \langle \bar{\psi}(z) \gamma_5 \gamma_\alpha \psi(x) \rangle \gamma^\alpha \gamma_5. \quad (3.47)$$

With (3.47), after the use of the parametrization of the relevant correlators, one gets for the longitudinal derivative contribution (see, (3.46)):

$$\frac{\bar{y}}{4} \not{\rho} \not{\rho}^T \varphi_3(y) + i \frac{\bar{y}}{4} \not{\rho} \not{\rho}^T \gamma_5 \varphi_A(y) = -\frac{i}{4} \sigma_{\rho e^T} \left\{ \bar{y} \varphi_3(y) + \bar{y} \varphi_A(y) \right\}, \quad (3.48)$$

where again we introduced the short-hand notations:

$$\sigma_{\rho e^T} = \sigma_{\alpha\beta} p^\alpha e_T^{*\beta}, \quad a_{T\rho} = \varepsilon_{\rho e^T} p_n. \quad (3.49)$$

We thus have for the longitudinal derivative contribution:

$$\int d^4z e^{-iy\rho \cdot z - i\bar{y}\rho \cdot x} \langle i \vec{\partial}_L \psi(x) \bar{\psi}(z) \rangle \Big|_{x=0} = -\frac{i}{4} \sigma_{\rho e^T} m_\rho f_\rho \left\{ \bar{y} \varphi_3(y) + \bar{y} \varphi_A(y) \right\}. \quad (3.50)$$

While, the correlators with the transverse derivatives in (3.45) can directly be expressed via the corresponding parameterizing functions with the help of (3.14) and (3.15):

$$\int d^4z e^{-iy\rho \cdot z - i\bar{y}\rho \cdot x} \langle i \vec{\partial}_T \psi(x) \bar{\psi}(z) \rangle \Big|_{x=0} = -\frac{i}{4} \sigma_{\rho e^T} m_\rho f_\rho \left\{ \varphi_1^T(y) + \varphi_A^T(y) \right\}. \quad (3.51)$$

Therefore, within the WW approximation (where all genuine twist 3 are disappeared) the equations of motion takes the following simple form:

$$\varphi_+^T(y) = -\bar{y} \varphi_+^{WW}(y), \quad (3.52)$$

where the plus (minus)-combination is defined as

$$\varphi_\pm(y) = \varphi^{\text{“vector”}}(y) \pm \varphi^{\text{“axial”}}(y). \quad (3.53)$$

Let us now take into account the quark-gluon correlators. Using (3.17), one can obtain that

$$-\gamma_\rho \langle A^{T\rho}(0) \psi(0) \bar{\psi}(z) \rangle = \frac{1}{4} \gamma_\rho \left\{ \langle \bar{\psi}(z) \gamma_\alpha A^{T\rho}(0) \psi(0) \rangle \gamma_\alpha + \langle \bar{\psi}(z) \gamma_5 \gamma_\alpha A^{T\rho}(0) \psi(0) \rangle \gamma_\alpha \gamma_5 \right\}, \quad (3.54)$$

where

$$\begin{aligned} \langle \bar{\psi}(z) \gamma_\alpha g A_\rho^T(0) \psi(0) \rangle &= m_\rho f_{3\rho}^V p_\alpha e_{T\rho}^* \int_0^1 dy_1 dy_2 e^{iy_1 p \cdot z} B(y_1, y_2), \\ \langle \bar{\psi}(z) \gamma_5 \gamma_\alpha g A_\rho^T(0) \psi(0) \rangle &= m_\rho f_{3\rho}^A i p_\alpha a_{T\rho} \int_0^1 dy_1 dy_2 e^{iy_1 p \cdot z} D(y_1, y_2). \end{aligned} \quad (3.55)$$

Thus, combining the quark-antiquark and quark-gluon correlators, one derives the following relation:

$$\int_0^1 dx \left(\tilde{B}(y, x) + \tilde{D}(y, x) \right) = -\bar{y} \varphi_+(y), \quad (3.56)$$

where one used the notations (3.24).

In a similar way, we can derive the relation associated with the C -conjugated equation:

$$\langle \psi(0) \bar{\psi}(z) i \overleftarrow{D}(0) \rangle = 0. \quad (3.57)$$

which reads

$$\int_0^1 dx \left(\tilde{B}(x, y) - \tilde{D}(x, y) \right) = y \varphi_-(y). \quad (3.58)$$

Combining the relations (3.56) and (3.58) with the use of (3.24) and (3.53), we obtain

$$\begin{aligned} & \bar{y}_1 \varphi_3(y_1) + \bar{y}_1 \varphi_A(y_1) + \varphi_1^T(y_1) + \varphi_A^T(y_1) \\ &= - \int_0^1 dy_2 \left[\zeta_3^V B(y_1, y_2) + \zeta_3^A D(y_1, y_2) \right] \end{aligned} \quad (3.59)$$

and

$$\begin{aligned} & y_1 \varphi_3(y_1) - y_1 \varphi_A(y_1) - \varphi_1^T(y_1) + \varphi_A^T(y_1) \\ &= - \int_0^1 dy_2 \left[-\zeta_3^V B(y_2, y_1) + \zeta_3^A D(y_2, y_1) \right]. \end{aligned} \quad (3.60)$$

Note that Eq.(3.60) can be obtained by the replacement $y_1 \rightarrow \bar{y}_1$ in (3.59) and the use of symmetry properties (3.26, 3.27).

3.5 Additional set of equations

3.5.1 Light-cone factorization direction arbitrariness

Contrarily to the light-cone vector p related to the out-going meson momentum, the second light-cone vector n (with $p \cdot n = 1$), required for the parametrization of the needed correlators introduced in section 3.3.1 is arbitrary. The physical observables do not depend on the specific choice of n , thus the scattering amplitudes should be n -independent. For any specific process, there is a natural choice for n , which one may denote as n_0 . For instance, in forward $e - p$ collision, the proton momentum defines n_0 . More generally, one may expand an arbitrary choice of n as [161, 251, 265–271]

$$n_\mu = \alpha p_\mu + \beta n_{0\mu} + n_\mu^\perp, \quad (3.61)$$

with the two constraints

$$p \cdot n = 1 \quad \text{and} \quad n^2 = 0, \quad (3.62)$$

which fixes the coefficients $\beta = 1$ and $\alpha = -n_\perp^2/2$. The light-cone vector n is thus parametrized by its transverse components n_\perp .

Let us now analyse the various source of n -dependence. First, it enters the definition of the non-local correlators introduced in Sec.3.3.1 through the light-like separation $z = \lambda n$. These correlators are defined in the axial light-like gauge $n \cdot A = 0$, which allows to get rid of Wilson lines. Second, it determines the notion of transverse polarization of the ρ . Last, n enters the Sudakov decomposition (3.2) which defines the transverse parton momentum involved in the collinear factorization. Note that this notion of parton transverse momentum should not be confused with the notion of transverse momenta of external particles (e.g. in the case of $\gamma^* \rightarrow \rho$ impact factor to be discussed in Chap. 6, entering in $\gamma^* N(p_2) \rightarrow \rho(p) N$ process, the t -channel gluons have a transverse momentum determined within another Sudakov basis defined by the external light-cone momenta $p_1 = p$ and incoming nucleon momentum p_2).

This n -independence principle leads to additional non-trivial constraints between the non-perturbative correlators entering the factorized amplitude. It was crucial for the understanding of inclusive structure functions properties at the twist three level [265–271] and its relevance for some exclusive processes was pointed out in [161, 251]. We show now that this condition expressed at the level of the *full amplitude* of any process can be reduced to a set of conditions involving only the soft correlators. The obtained equations are process independent and do not assume a priori any Wandzura-Wilczek approximation. The strategy for deriving these equations relies on the power of the Ward identities to relate firstly amplitudes with different number of legs and secondly higher order coefficients in the Taylor expansion (3.4) to lower order ones.

In the case of processes involving ρ_T production up to twist 3 level, we will now derive the equations

$$\frac{d}{dy_1} \varphi_1^T(y_1) + \varphi_1(y_1) - \varphi_3(y_1) + \zeta_3^V \int_0^1 \frac{dy_2}{y_2 - y_1} (B(y_1, y_2) + B(y_2, y_1)) = 0, \quad (3.63)$$

$$\frac{d}{dy_1} \varphi_A^T(y_1) - \varphi_A(y_1) + \zeta_3^A \int_0^1 \frac{dy_2}{y_2 - y_1} (D(y_1, y_2) + D(y_2, y_1)) = 0. \quad (3.64)$$

The n -independence of \mathcal{A} for an arbitrary fixed polarization vector e is expressed by the condition

$$\frac{d}{dn_\perp^\mu} \mathcal{A} = 0, \quad (3.65)$$

which we write in the form

$$\frac{d}{dn_\perp^\mu} \mathcal{A} = \frac{\partial n^\alpha}{\partial n_\perp^\mu} \frac{\partial \mathcal{A}}{\partial n^\alpha} + \frac{\partial(e^* \cdot n)}{\partial n_\perp^\mu} \frac{\partial \mathcal{A}}{\partial(e^* \cdot n)} = [-n_\perp^\mu p^\alpha + g_{\perp\mu}^\alpha] \frac{\partial}{\partial n^\alpha} \mathcal{A} + e_{\perp\mu}^* \frac{\partial \mathcal{A}}{\partial(e^* \cdot n)}. \quad (3.66)$$

Let us emphasize the fact that although n fixes the gauge, the hard part does not depend on this gauge fixing vector, as we will show below after the technical derivation of Eqs.(3.63, 3.64). It means that the variation of n only affects the n -dependence related to the definition of transverse momentum ℓ_\perp and of transverse ρ polarization.

We also note that the appearance of the total derivative in Eqs.(3.65, 3.66) may be interpreted as a (vector) analog of the renormalization group (RG) invariance equation when the dependency on the renormalization parameter coming from various sources cancel. One can view this as a RG-like flow in the space of light-cone directions of contributions to the amplitude where the polarization vector plays the role of a beta function.

The scattering amplitude \mathcal{A} receives contributions from the vector correlators, which result into \mathcal{A}^{vector} , and from the axial vector correlators, which lead to \mathcal{A}^{axial} part of \mathcal{A} . Due to different parity properties of the vector and the axial-vector correlators, the condition (3.66) means effectively two separate conditions:

$$\frac{d}{dn_\perp^\mu} \mathcal{A}^{vector} = 0 \quad (3.67)$$

and

$$\frac{d}{dn_\perp^\mu} \mathcal{A}^{axial} = 0. \quad (3.68)$$

The dependence of \mathcal{A} on the vector n_\perp is obtained through the dependence of \mathcal{A} on the full vector n . This dependence on n is different in \mathcal{A}^{axial} and in \mathcal{A}^{vector} parts.

The dependence of \mathcal{A}^{axial} on the vector n enters only through the expression $\varepsilon^{pn\beta\gamma}$ involving the contraction with the momentum p and in which the indices β and γ are contracted with some other vectors. Thus the condition (3.68) is equivalent to

$$\frac{\partial n^\alpha}{\partial n_\perp^\mu} \frac{\partial}{\partial n^\alpha} \mathcal{A}^{axial} = [-n_\perp^\mu p^\alpha + g_{\perp\mu}^\alpha] \frac{\partial}{\partial n^\alpha} \mathcal{A}^{axial} = \frac{\partial}{\partial n_\perp^\mu} \mathcal{A}^{axial} = 0 \quad (3.69)$$

where we took into account the peculiar dependence of \mathcal{A}^{axial} on n discussed above. This will lead at the level of DAs to the equation (3.64).

In the vector part, the dependence with respect to n is identified by rewriting the polarization vector for transversally polarized ρ with the help of the identity

$$e_T^\mu = e^\mu - p^\mu e \cdot n, \quad (3.70)$$

since $e \cdot p = 0$. Thus the dependence of \mathcal{A}^{vector} on the vector n enters only through the scalar product $e^* \cdot n$, and Eq.(3.67) can be written as

$$\frac{d}{dn_\perp^\mu} \mathcal{A}^{vector} = e_T^{*\mu} \frac{\partial}{\partial (e^* \cdot n)} \mathcal{A}^{vector} = 0 \quad (3.71)$$

which results in

$$\frac{\partial}{\partial (e^* \cdot n)} \mathcal{A}^{vector} = 0 \quad (3.72)$$

from which follows Eq.(3.63).

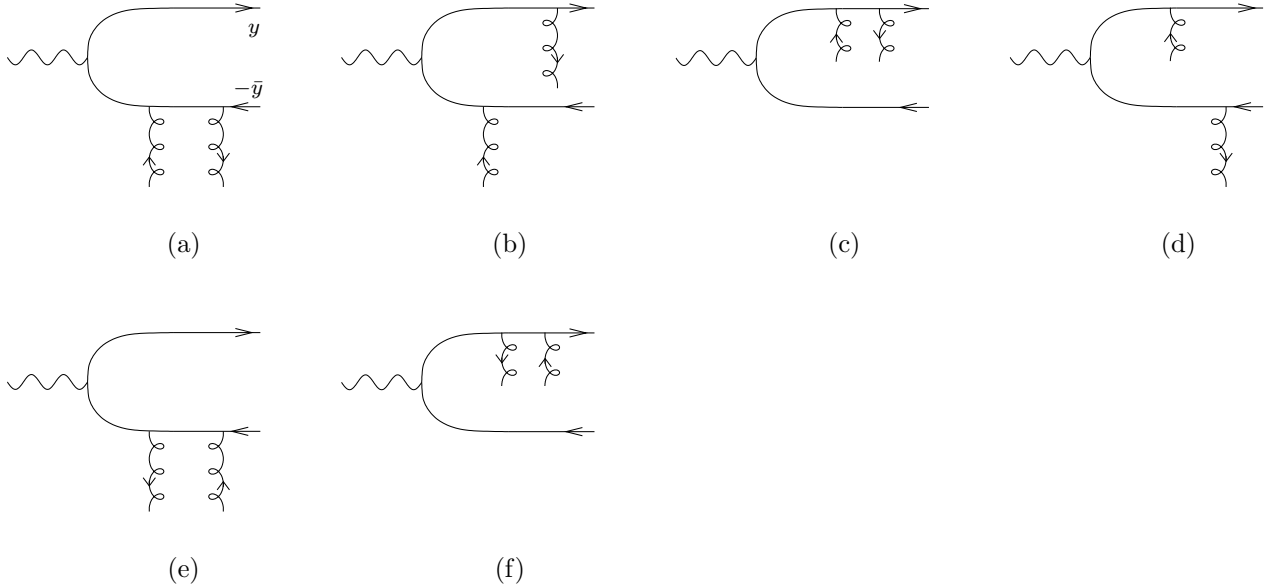


Figure 3.4: The 6 hard diagrams attached to the 2-parton correlators, which contribute to the $\gamma^* \rightarrow \rho$ impact factor, with momentum flux of external line, along p_1 direction. These drawing implicitly assume that the two right-hand side spinor lines are closed on the two possible Fierz structures \not{p} or $\not{p}\gamma^5$.

We will now derive equations (3.63, 3.64) using as a tool the explicit example of the $\gamma^* \rightarrow \rho$ impact factor. We want here to insist on the fact that the proof is independent of the specific process under consideration, and only rely on general arguments based on Ward identities. For the $\gamma^* \rightarrow \rho$ impact factor, which will be computed in details in Chap. 6, one needs to consider 2-parton contributions both without transverse derivative (illustrated by diagrams of Fig. 3.4) and with transverse derivative (see Fig. 3.5), as well as 3-parton contributions (see Figs.3.6, 3.7, 3.8). Note that these drawing implicitly assume that the two right-hand side spinor lines are closed on the the two possible Fierz structures \not{p} or $\not{p}\gamma^5$ involved in the correlators of ρ -meson DAs.

With respect to the usual collinear factorization in t -channel, the only thing which should be kept in mind when considering an impact factor is that the two t -channel gluons are off-shell, with a a non-sense polarisation, i.e. proportional to p_2 . More details about k_T -factorization will be given in Sec. 4.2. This peculiar situation does not play any important role in the following arguments.

In the color space, each of those diagrams can be projected in two parts, characterized by the two Casimir invariants C_F and N_c . The equations (3.63, 3.64) are obtained by considering the consequence of the n -independency on the contribution to the C_F color structure. The n -independency condition applied to the N_c structure is automatically satisfied and does not lead to new constraints, as we have shown in Appendix A of Ref. [24].

We start with the derivation of Eq.(3.63), which corresponds to the vector correlator contributions with C_F invariant. The 3-parton ($q\bar{q}g$) contribution and the 2-parton contribution involving Φ^\perp to \mathcal{A} can be reduced to

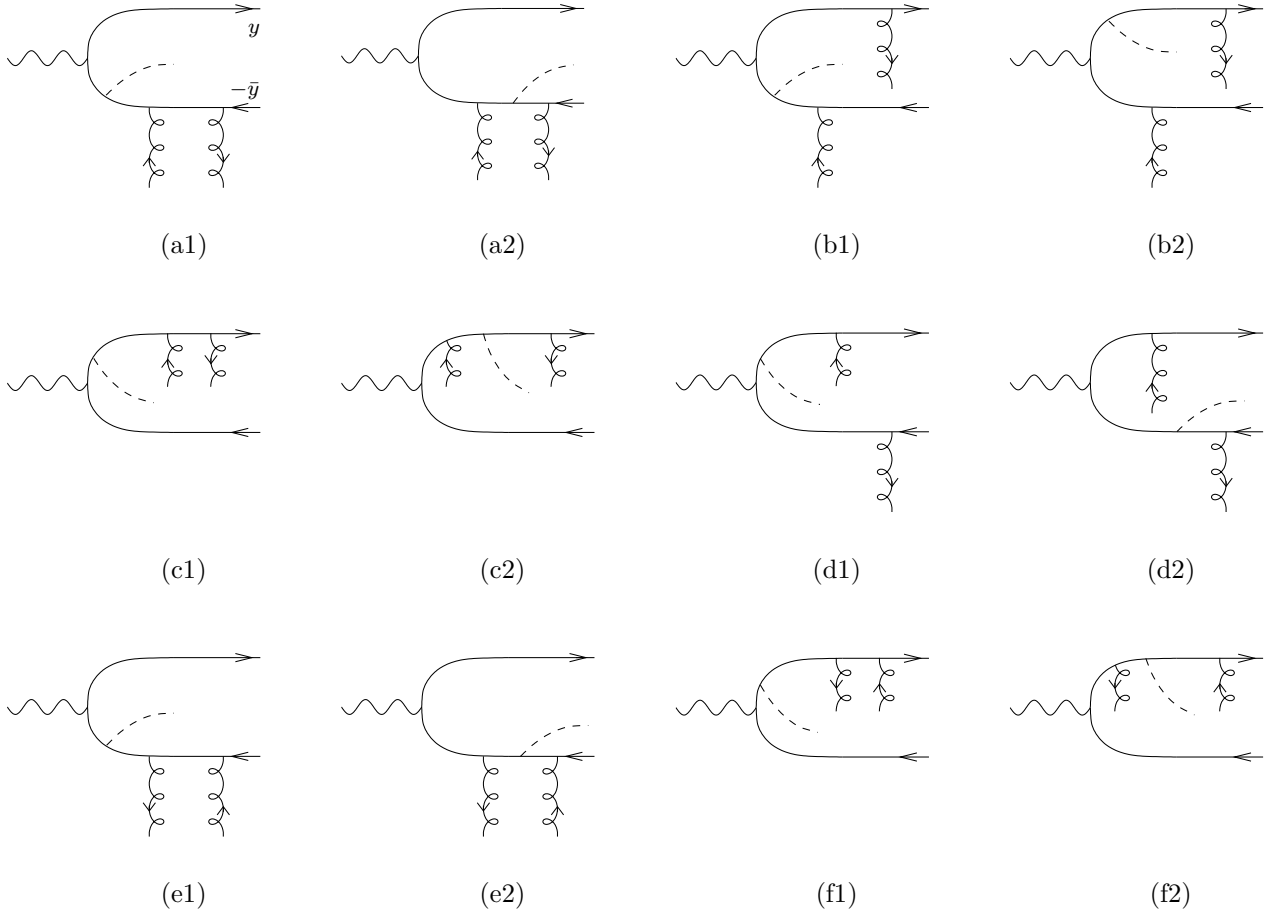


Figure 3.5: The 12 contributions arising from the first derivative of the 6 hard diagrams attached to the 2-parton correlators, which contribute to the $\gamma^* \rightarrow \rho$ impact factor, with momentum flux of external line, along p_1 direction.

the convolution of the leading order hard 2-parton contributions with linear combination of correlators, thanks to the use of the Ward identity.

In the case of the 3-parton vector correlator (3.19), due to (3.70) the dependency on n enters linearly and only through the scalar product $e^* \cdot n$. Thus, the action on the amplitude of the derivative d/dn_\perp involved in (3.72) can be extracted by the replacement $e_\alpha^* \rightarrow -p_\alpha$, which means in practice that the Feynman rule (using conventions of Ref. [98] for computing the T matrix element) $g t^a \gamma^\alpha e_\alpha^*$ entering the coupling of the gluon inside the hard part should be replaced by $-g t^a \gamma^\alpha p_\alpha$. Then, using the Ward identity for the hard part, it reads

$$(y_1 - y_2) \text{tr} [H_{q\bar{q}g}^\rho(y_1, y_2) p_\rho \not{p}] = \text{tr} [H_{q\bar{q}}(y_1) \not{p}] - \text{tr} [H_{q\bar{q}}(y_2) \not{p}] ,$$

which can be seen graphically as

$$\begin{aligned}
 & p_\mu \left[\text{Diagram 1} \right] \\
 = & \frac{1}{y_1 - y_2} \left[\text{Diagram 2} - \text{Diagram 3} \right] \tag{3.73}
 \end{aligned}$$

as we will show below with more details, and will give the last term of r.h.s of Eq.(3.63). The proof can be settled easily relying on a graphical rule in order to use the collinear Ward identity. Indeed within the conventions of [98], the collinear Ward identity can be symbolically written as

$$p_\mu \begin{array}{c} \longrightarrow \\ y_1 p \end{array} \bullet \begin{array}{c} \longrightarrow \\ \gamma^\mu \end{array} \begin{array}{c} \longrightarrow \\ y_2 p \end{array} = \frac{1}{y_2 - y_1} \left[\begin{array}{c} \text{Diagram 4} \\ \text{Diagram 5} \end{array} \right] \tag{3.74}$$

where each fermionic line is a propagator. The wavy lines with double arrows are there in order to fulfill momentum conservation, since the *incoming* momentum is $y_1 p$ while the *outgoing* momentum is $y_2 p$.

Let us consider the 3-parton "*abelian*" diagrams, illustrated in Fig. 3.6. Applying the Ward identity (3.74)

to graphs (aG1) and (aG2) gives

$$\begin{aligned}
 & -(y_2 - y_1)p_\mu \left[\text{Diagram 1} + \text{Diagram 2} \right] \\
 = & \text{Diagram 3} - \text{Diagram 4} \\
 + & \text{Diagram 5} - \text{Diagram 6} \\
 = & \text{Diagram 7} - \text{Diagram 8}, \tag{3.75}
 \end{aligned}$$

where the indicated momentum fractions correspond to flow along the momentum p_1 of the ρ -meson. The last line of Eq.(3.75) has been obtained after cancellation of the first and fourth term in the second equality, and the two remaining diagrams have been relabelled (in the first term of the last line, one does $y_2 - 1 \rightarrow y_1 - 1$ for the outgoing antiquark, and in the second term, one does $y_1 \rightarrow y_2$ for the outgoing quark), as far as the external lines are concerned, after using the fact that this does not change its internal structure.

The same identity applies for each couple of graphs (bG1, bG2), (cG1, cG2), (dG1, dG2), (eG1, eG2) and

(fG1, fG2). This leads to the following identity

$$\begin{aligned}
& - \int_0^1 dy_1 \int_0^1 dy_2 B(y_1, y_2) \\
& \times p_\mu \left[\begin{array}{c} \text{Diagram 1} + \text{Diagram 2} + \text{Diagram 3} + \text{Diagram 4} + \text{Diagram 5} + \text{Diagram 6} \\ \text{Diagram 7} + \text{Diagram 8} + \text{Diagram 9} + \text{Diagram 10} + \text{Diagram 11} + \text{Diagram 12} \end{array} \right] \\
& = \int_0^1 dy_1 \int_0^1 dy_2 \frac{B(y_1, y_2)}{y_2 - y_1} \\
& \times \left\{ \left[\begin{array}{c} \text{Diagram 13} + \text{Diagram 14} + \text{Diagram 15} + \text{Diagram 16} + \text{Diagram 17} + \text{Diagram 18} \\ \text{Diagram 19} + \text{Diagram 20} + \text{Diagram 21} + \text{Diagram 22} + \text{Diagram 23} + \text{Diagram 24} \end{array} \right] - (y_1 \leftrightarrow y_2) \right\} \\
& = \int_0^1 dy_1 \int_0^1 \frac{dy_2}{y_2 - y_1} [B(y_1, y_2) + B(y_2, y_1)] \\
& \times \left[\begin{array}{c} \text{Diagram 25} + \text{Diagram 26} + \text{Diagram 27} + \text{Diagram 28} + \text{Diagram 29} + \text{Diagram 30} \\ \text{Diagram 31} + \text{Diagram 32} + \text{Diagram 33} + \text{Diagram 34} + \text{Diagram 35} + \text{Diagram 36} \end{array} \right] \quad (3.76)
\end{aligned}$$

where the last line is obtained after performing the change of variable $y_1 \leftrightarrow y_2$ in the second term. Note that the hard part given by diagrams inside Eq.(3.76) is convoluted with the last term of Eq.(3.63).

A similar treatment of 2-parton correlators with transverse derivative whose contributions can be viewed as 3-parton processes with vanishing gluon momentum leads to

$$\begin{aligned}
& - \int_0^1 dy_1 \int_0^1 dy_2 \delta(y_1 - y_2) \varphi_1^T(y_1) \\
& \times p_\mu \left[\begin{array}{c} \text{Diagram 37} + \text{Diagram 38} + \text{Diagram 39} + \text{Diagram 40} + \text{Diagram 41} + \text{Diagram 42} \\ \text{Diagram 43} + \text{Diagram 44} + \text{Diagram 45} + \text{Diagram 46} + \text{Diagram 47} + \text{Diagram 48} \end{array} \right] \\
& = \int_0^1 dy_1 \int_0^1 dy_2 \delta(y_1 - y_2) \frac{\varphi_1^T(y_1)}{y_2 - y_1} \\
& \times \left\{ \left[\begin{array}{c} \text{Diagram 49} + \text{Diagram 50} + \text{Diagram 51} + \text{Diagram 52} + \text{Diagram 53} + \text{Diagram 54} \\ \text{Diagram 55} + \text{Diagram 56} + \text{Diagram 57} + \text{Diagram 58} + \text{Diagram 59} + \text{Diagram 60} \end{array} \right] - (y_1 \leftrightarrow y_2) \right\}
\end{aligned}$$

$$\begin{aligned}
&= \int_0^1 dy_1 \frac{d}{dy_1} \varphi_1^T(y_1) \\
&\times \left[\begin{array}{c} \text{Diagram 1} \\ \text{Diagram 2} \\ \text{Diagram 3} \\ \text{Diagram 4} \\ \text{Diagram 5} \\ \text{Diagram 6} \end{array} \right], \quad (3.77)
\end{aligned}$$

where the last line is obtained after integration by part. This leads to the convolution of the first term of the l.h.s of Eq.(3.63) with the $[\dots]$ part in (3.77).

The second term, with φ_1 , of the l.h.s of Eq.(3.63) originates from the 2-parton vector correlator and corresponds to the contribution for the longitudinally polarized ρ with $e_L \sim p$. The third term with φ_3 corresponds to the contribution of the same correlator for the polarization vector of ρ_T written as in Eq.(3.70). To get Eq.(3.63), we used the fact that each individual term obtained above when expressing the n -independency condition involve the *same* 2-parton hard part, convoluted with the Eq.(3.63) through an integration over y_1 . The arguments used above, based on the collinear Ward identity, are clearly independent of the detailed structure of this resulting 2-parton hard part. Therefore, we deduce from this that Eq.(3.63) itself should be satisfied.

A similar treatment for axial correlators leads to Eq.(3.64). To prove this, we start from Eq.(3.69) and we note that the parametrizations of matrix elements of correlators with axial-vector currents (3.15, 3.17, 3.20) involve the quantity

$$p^\mu \varepsilon^\alpha e_T^* p^n \quad (3.78)$$

in which the index α is contracted with the matrix γ^α appearing in the vertex of gluon emission in the hard part and the momentum p^μ is contracted with the Fierz matrix $\gamma_\mu \gamma^5$ corresponding in the hard part to the meson vertex. First let us note that in the expression (3.78) one can replace e_T^* by the full polarization vector e^* , i.e.

$$p^\mu \varepsilon^\alpha e_T^* p^n = p^\mu \varepsilon^\alpha e^* p^n. \quad (3.79)$$

Secondly, the inspection of the quantity (3.78) or (3.79) leads to the conclusion that in order to use the Ward identities in a similar way as it was done in the vector part we need to interchange in (3.78) the indices $\mu \leftrightarrow \alpha$. It is done with the help of the Schouten identity, which for our peculiar case means that

$$p^\mu \varepsilon^\alpha e_T^* p^n = p^\alpha \varepsilon^\mu e_T^* p^n. \quad (3.80)$$

After that, the momentum p^α acts on the gluon vertex in the hard part, so the consequences of the n -independence of the axial part of the impact factor maybe derived in exactly the same way as we did above in the case of vector correlators, since the vector $\varepsilon^\mu e_T^* p^n$ is completely factorized. One then obtains Eq.(3.64) from Eq.(3.63) after the replacements $B \rightarrow D$, $\varphi_3 \rightarrow \varphi_A$, $\varphi_1^T \rightarrow \varphi_A^T$ and $\varphi_1 \rightarrow 0$ since there is no counterpart of the twist 2 DA φ_1 for the axial part.

Since we rely on the n -independency of the amplitude, one may wonder about the effect of the gauge choice, which is fixed by n , on the hard part. The QCD Ward identities require the vanishing of the amplitude in which polarization vector of a gluon is replaced by its momentum provided all other partons are on the mass shell. In the framework of the k_T -factorization (see Sec. 4.2), the t -channel gluons are off the mass-shell. Therefore the replacement of the s -channel gluon polarization vector by its momentum leads to the vanishing of scattering amplitude up to terms proportional to k_\perp^2/s where k_\perp are transverse momenta of t -channel gluons. From the point of view of the t -channel, the gauge invariance of the impact-factor means that it should vanish when the transverse momentum of any t -channel gluon vanishes. To achieve this property it is necessary to include in a consistent way not only DAs with lowest Fock state containing only quarks but also those involving quarks and gluon, as we will show in detail in Chap. 6.

In practice, we here check this invariance by contracting the s -channel emitted gluon vertex in the hard part with the momentum, which in collinear factorization is proportional to the ρ -meson momentum, which leads to simplifications in the use of (collinear) Ward identities.

In order to prove this, one should first project on the various color Casimir structure. In the case of the impact factor (see Chap. 6), this means to distinguish N_c and C_F terms. In this case, C_F terms arise from 2-partons diagrams and from 3-partons diagrams where the emitted gluon is attached to a quark line, while N_c

terms are obtained from 3-partons diagrams where the emitted gluon is attached to a quark line only between 2 t -channel exchanged gluons or from diagrams involving at least one triple gluon vertex.

The method is almost identical with the one used above when deriving the n -independence equations. Consider first the case of hard 3-partons diagrams entering the vector part of Fierz decomposition. We contract the s -channel emitted gluon vertex with its momentum, which is proportional to p_μ . The next step is to use the same method as the one used in Eq.(3.76), except that the DA B is not involved here. One thus finally gets two groups of 6 diagrams (which differ by the labeling of outgoing quarks, one being y_1 and \bar{y}_1 for the quark and antiquark respectively, and the other one being y_2 and \bar{y}_2 for the quark and antiquark respectively). Since we started here from the consideration of the $\gamma_T^* \rightarrow \rho_T$ transition, each of these 6 hard contributions, due to the appearance of the remaining \not{p} from the Fierz structure, thus now encodes the hard part of the transition $\gamma_T^* \rightarrow \rho_L$. This transition vanishes in our kinematics, which leads to the conclusion that this hard part is gauge invariant. The same treatment can be applied to the hard diagrams with derivative insertion displayed in Fig. 3.5, since this insertion corresponds to the peculiar limit of vanishing ‘‘gluon’’ momentum.

The proof for the axial part of the Fierz decomposition goes along the same line. The only difference lays on the appearance of the $\not{p}\gamma^5$ structure, which corresponds to a meson b_1 with quantum numbers $J^{PC} = 1^{+-}$ instead of 1^{--} for ρ , leading finally to the hard part of the transition $\gamma_T^* \rightarrow b_{1L}$ which vanishes in our kinematics.

In the case of contribution proportional to N_c , one can prove that these hard terms are also gauge invariant. This is proven in Appendix A of Ref. [24]. The reason is the same as the one which led to the conclusion that N_c terms do not lead to additional n -independence condition.

Although our implementation of factorization and n -independence condition is illustrated here on the particular example of the impact factor at twist 3, we expect that this procedure is more general and that the above method can be applied for other exclusive processes, for which the key tool is still the collinear Ward identity. This means in particular that each building block (soft and hard part, for each structure which lead to the introduction of a DA) are separately gauge invariant. This fact simplifies dramatically the use of the n -independence principle.

3.5.2 A minimal set of non-perturbative correlators

We now solve the previous equations, namely the two equation of motions (3.59,3.60) and the two equations (3.63,3.64) coming from the n -independence. This effectively reduces the set of 7 DAs to the set of 3 independent DAs φ_1, B, D .

To start with we represent the distributions $\varphi_3(y), \varphi_A(y), \varphi_1^T(y)$ and $\varphi_A^T(y)$ generically denoted as $\varphi(y)$ as the sums

$$\varphi(y) = \varphi^{WW}(y) + \varphi^{gen}(y), \quad \varphi(y) = \varphi_3(y), \varphi_A(y), \varphi_1^T(y), \varphi_A^T(y), \quad (3.81)$$

where $\varphi^{WW}(y)$ and $\varphi^{gen}(y)$ are contributions in the so called Wandzura-Wilczek approximation and the genuine twist-3 contributions, respectively.

The Wandzura-Wilczek contributions are solutions of Eqs. (3.59, 3.60, 3.63, 3.64) with vanishing 3-parton distributions $B(y_1, y_2)$ and $D(y_1, y_2)$, i.e. which satisfy the equations

$$\bar{y}_1 \varphi_3^{WW}(y_1) + \bar{y}_1 \varphi_A^{WW}(y_1) + \varphi_1^T{}^{WW}(y_1) + \varphi_A^T{}^{WW}(y_1) = 0 \quad (3.82)$$

$$y_1 \varphi_3^{WW}(y_1) - y_1 \varphi_A^{WW}(y_1) - \varphi_1^T{}^{WW}(y_1) + \varphi_A^T{}^{WW}(y_1) = 0. \quad (3.83)$$

$$\frac{d}{dy_1} \varphi_1^T{}^{WW}(y_1) = -\varphi_1(y_1) + \varphi_3^{WW}(y_1), \quad \frac{d}{dy_1} \varphi_A^T{}^{WW}(y_1) = \varphi_A^{WW}(y_1). \quad (3.84)$$

By adding and subtracting Eqs. (3.82,3.83) together with the use of Eqs. (3.84) one obtains equations which involve only φ_3^{WW} and φ_A^{WW}

$$\frac{d}{dy_1} \varphi_3^{WW}(y_1) = -(\bar{y}_1 - y_1) \frac{d}{dy_1} \varphi_A^{WW}(y_1), \quad 2\varphi_1(y_1) = \frac{d}{dy_1} \varphi_A^{WW}(y_1) + (\bar{y}_1 - y_1) \frac{d}{dy_1} \varphi_3^{WW}(y_1) \quad (3.85)$$

and which solutions, satisfying the normalization conditions

$$\int_0^1 dy \varphi_3^{WW}(y) = 1 \quad \text{and} \quad \int_0^1 dy \varphi_A^{WW}(y) = 1, \quad (3.86)$$

read

$$\varphi_A^{WW}(y_1) = \frac{1}{2} \left[\int_0^{y_1} \frac{dv}{\bar{v}} \varphi_1(v) - \int_{y_1}^1 \frac{dv}{v} \varphi_1(v) \right], \quad \varphi_3^{WW}(y_1) = \frac{1}{2} \left[\int_0^{y_1} \frac{dv}{\bar{v}} \varphi_1(v) + \int_{y_1}^1 \frac{dv}{v} \varphi_1(v) \right]. \quad (3.87)$$

These expressions and Eqs. (3.82, 3.83) give finally the remaining solutions $\varphi_A^{T WW}$ and $\varphi_1^{T WW}$

$$\varphi_A^{T WW}(y_1) = \frac{1}{2} \left[-\bar{y}_1 \int_0^{y_1} \frac{dv}{\bar{v}} \varphi_1(v) - y_1 \int_{y_1}^1 \frac{dv}{v} \varphi_1(v) \right], \quad \varphi_1^{T WW}(y_1) = \frac{1}{2} \left[-\bar{y}_1 \int_0^{y_1} \frac{dv}{\bar{v}} \varphi_1(v) + y_1 \int_{y_1}^1 \frac{dv}{v} \varphi_1(v) \right]. \quad (3.88)$$

We note that these two WW results (3.87) were obtained in Ref. [272] when considering the transition form factor $B \rightarrow \rho \gamma$. The distributions φ^{gen} carrying the genuine twist-3 contributions satisfy the equations

$$\bar{y}_1 \varphi_3^{gen}(y_1) + \bar{y}_1 \varphi_A^{gen}(y_1) + \varphi_1^{T gen}(y_1) + \varphi_A^{T gen}(y_1) = - \int_0^1 dy_2 [\zeta_3^V B(y_1, y_2) + \zeta_3^A D(y_1, y_2)], \quad (3.89)$$

$$y_1 \varphi_3^{gen}(y_1) - y_1 \varphi_A^{gen}(y_1) - \varphi_1^{T gen}(y_1) + \varphi_A^{T gen}(y_1) = - \int_0^1 dy_2 [-\zeta_3^V B(y_2, y_1) + \zeta_3^A D(y_2, y_1)], \quad (3.90)$$

$$\begin{aligned} \frac{d}{dy_1} \varphi_1^{T gen}(y_1) &= \varphi_3^{gen}(y_1) - \zeta_3^V \int_0^1 \frac{dy_2}{y_2 - y_1} (B(y_1, y_2) + B(y_2, y_1)), \\ \frac{d}{dy_1} \varphi_A^{T gen}(y_1) &= \varphi_A^{gen}(y_1) - \zeta_3^A \int_0^1 \frac{dy_2}{y_2 - y_1} (D(y_1, y_2) + D(y_2, y_1)). \end{aligned} \quad (3.91)$$

Similarly as in the WW case, one can obtain equations without distributions $\varphi^{T gen}$ by adding and subtracting Eqs. (3.89, 3.90) together with the use of (3.91)

$$\begin{aligned} &\frac{d}{dy_1} \varphi_3^{gen}(y_1) + (\bar{y}_1 - y_1) \frac{d}{dy_1} \varphi_A^{gen}(y_1) \\ &= 4 \zeta_3^A \int_0^1 \frac{dy_2}{y_2 - y_1} D^{(+)}(y_1, y_2) - 2 \zeta_3^V \frac{d}{dy_1} \int_0^1 dy_2 B^{(-)}(y_1, y_2) - 2 \zeta_3^A \frac{d}{dy_1} \int_0^1 dy_2 D^{(+)}(y_1, y_2), \end{aligned} \quad (3.92)$$

$$\begin{aligned} &\frac{d}{dy_1} \varphi_A^{gen}(y_1) + (\bar{y}_1 - y_1) \frac{d}{dy_1} \varphi_3^{gen}(y_1) \\ &= 4 \zeta_3^V \int_0^1 \frac{dy_2}{y_2 - y_1} B^{(+)}(y_1, y_2) - 2 \zeta_3^V \frac{d}{dy_1} \int_0^1 dy_2 B^{(+)}(y_1, y_2) - 2 \zeta_3^A \frac{d}{dy_1} \int_0^1 dy_2 D^{(-)}(y_1, y_2), \end{aligned} \quad (3.93)$$

where $O^{(\pm)}(y_1, y_2) = O(y_1, y_2) \pm O(y_2, y_1)$ for $O = B, D$. Let us note that Eq. (3.93) can be obtained from Eq. (3.92) and by the interchange $\varphi_A^{gen} \leftrightarrow \varphi_3^{gen}$ and $B \leftrightarrow D$.

From Eqs. (3.92, 3.93) supplemented by the boundary conditions $\mathcal{B}(y, y) = 0 = \mathcal{D}(y, y)$ (see later in Section

3.6) one gets in a straightforward although somehow tedious way the equation for φ_3^{gen}

$$\begin{aligned} \frac{d}{dy_1} \varphi_3^{gen}(y_1) = & -\frac{1}{2} \left(\frac{1}{y_1} + \frac{1}{\bar{y}_1} \right) \\ & \left\{ \zeta_3^V \left[y_1 \int_{y_1}^1 dy_2 \frac{d}{dy_1} B(y_1, y_2) - \bar{y}_1 \int_0^{y_1} \frac{d}{dy_1} B(y_2, y_1) + (\bar{y}_1 - y_1) \left(\int_{y_1}^1 dy_2 \frac{B(y_1, y_2)}{y_2 - y_1} + \int_0^{y_1} dy_2 \frac{B(y_2, y_1)}{y_2 - y_1} \right) \right] \right. \\ & \left. + \zeta_3^A \left[y_1 \int_{y_1}^1 dy_2 \frac{d}{dy_1} D(y_1, y_2) + \bar{y}_1 \int_0^{y_1} \frac{d}{dy_1} D(y_2, y_1) - \int_{y_1}^1 dy_2 \frac{D(y_1, y_2)}{y_2 - y_1} - \int_0^{y_1} dy_2 \frac{D(y_2, y_1)}{y_2 - y_1} \right] \right\}, \end{aligned} \quad (3.94)$$

which properly normalized solution can be written in the form

$$\varphi_3^{gen}(y) = \frac{1}{2} \left(- \int_y^1 \frac{dy_1}{y_1} + \int_0^1 \frac{dy_1}{\bar{y}_1} \right) \{ \dots \}, \quad (3.95)$$

in which both integrals act on the expression inside $\{ \dots \}$ on the r.h.s of Eq.(3.94). The expression (3.95) can be simplified after changing the order of the nested integrals. After performing this task we obtain that

$$\begin{aligned} \varphi_3^{gen}(y) = & \quad (3.96) \\ & -\frac{1}{2} \int_y^1 \frac{du}{u} \left[\int_0^u dy_2 \frac{d}{du} (\zeta_3^V B - \zeta_3^A D)(y_2, u) - \int_u^1 \frac{dy_2}{y_2 - u} (\zeta_3^V B - \zeta_3^A D)(u, y_2) - \int_0^u \frac{dy_2}{y_2 - u} (\zeta_3^V B - \zeta_3^A D)(y_2, u) \right] \\ & -\frac{1}{2} \int_0^{y_1} \frac{du}{\bar{u}} \left[\int_u^1 dy_2 \frac{d}{du} (\zeta_3^V B + \zeta_3^A D)(u, y_2) - \int_u^1 \frac{dy_2}{y_2 - u} (\zeta_3^V B + \zeta_3^A D)(u, y_2) - \int_0^u \frac{dy_2}{y_2 - u} (\zeta_3^V B + \zeta_3^A D)(y_2, u) \right]. \end{aligned}$$

Finally, the solution for $\varphi_1^{T gen}$ is obtained from the first Eq. (3.91) and (3.96)

$$\varphi_1^{T gen}(y) = \int_0^y du \varphi_3^{gen}(u) - \zeta_3^V \int_0^y dy_1 \int_y^1 dy_2 \frac{B(y_1, y_2)}{y_2 - y_1}. \quad (3.97)$$

The corresponding expressions for $\varphi_A^{gen}(y)$ and $\varphi_A^{T gen}(y)$ are obtained from Eq.(3.96) and (3.97) by the substitutions:

$$\varphi_3^{gen}(y) \xrightarrow{\zeta_3^V B \leftrightarrow \zeta_3^A D} \varphi_A^{gen}(y), \quad (3.98)$$

$$\varphi_1^{T gen}(y) \xrightarrow{\zeta_3^V B \leftrightarrow \zeta_3^A D} \varphi_A^{T gen}(y). \quad (3.99)$$

In conclusion of this section, we explicitly succeeded in representing our results (3.87), (3.88), (3.96), (3.97), (3.98) (3.99) in terms of 3 independent DAs: the twist 2 DA φ_1 and the twist 3 DAs B, D .

3.6 Dictionary

For comparison of expressions (3.19, 3.20) with the definitions (3.42, 3.43) we perform the change of variables $z \rightarrow z_1, tz \rightarrow z_2, \alpha_d \rightarrow y_1$ and $\alpha_u = 1 - y_2$, i.e. $\alpha_g = y_2 - y_1$. It results in the following identification of the 3-parton DAs in LCCF and CCF approaches

$$B(y_1, y_2) = -\frac{V(y_1, 1 - y_2)}{y_2 - y_1} \quad (3.100)$$

$$D(y_1, y_2) = -\frac{A(y_1, 1 - y_2)}{y_2 - y_1}. \quad (3.101)$$

From (3.100, 3.101) and Ref. [136] follows the boundary conditions $B(y, y) = 0 = D(y, y)$.

Taking in Eqs.(3.32, 3.34) the coordinate z along the light-cone vector n , $z = \lambda n$, permits the identification of the vector DAs in Eq.(3.10):

$$\varphi_1(y) = \phi_{\parallel}(y), \quad \varphi_3(y) = g_{\perp}^{(v)}(y), \quad (3.102)$$

and of the axial DA in Eq. (3.11)

$$\varphi_A(y) = -\frac{1}{4} \frac{\partial g_{\perp}^{(a)}(y)}{\partial y}. \quad (3.103)$$

One can also check the validity of Eqs.(3.102, 3.103) directly by the use of our explicit solutions (3.87, 3.96, 3.98) and expressions for $g_{\perp}^{(v)}$ and $g_{\perp}^{(a)}$ given Ref. [136] in terms of ϕ_{\parallel} , V and A DAs. This non trivial check can be done with the help of methods similar to those used in Appendix B of Ref. [W24] elaborated when comparing the results of the calculation of the $\gamma^* \rightarrow \rho_T$ impact factor in LCCF and CCF approaches, which we will discuss in Chap. 6.

We have thus shown how the LCCF method should be used in practice when dealing with hard exclusive processes beyond leading twist. We have shown in detail in the case of a twist 3 dominated process how a non minimal set of DAs should be introduced, and then reduced to a minimal set through Lorentz invariance on the light-cone combined with EOMs. The dictionary between the independent DAs in LCCF and CCF is straightforward, as we have shown in Sec. 3.6. The non-trivial part in LCCF is to express the spurious collection of DAs (here φ_3 , φ_A , φ_1^T , φ_A^T .) in terms of the independent one (here φ_1 , B and D or equivalently ϕ_{\parallel} , V and A) which is chosen to be a basis, and which contains all the non-perturbative information at a given twist. Once this step has been made, the Feynman rules for computing the hard part are straightforward in LCCF. This will be illustrated in details in Chap. 6, through an explicit computation within both methods.

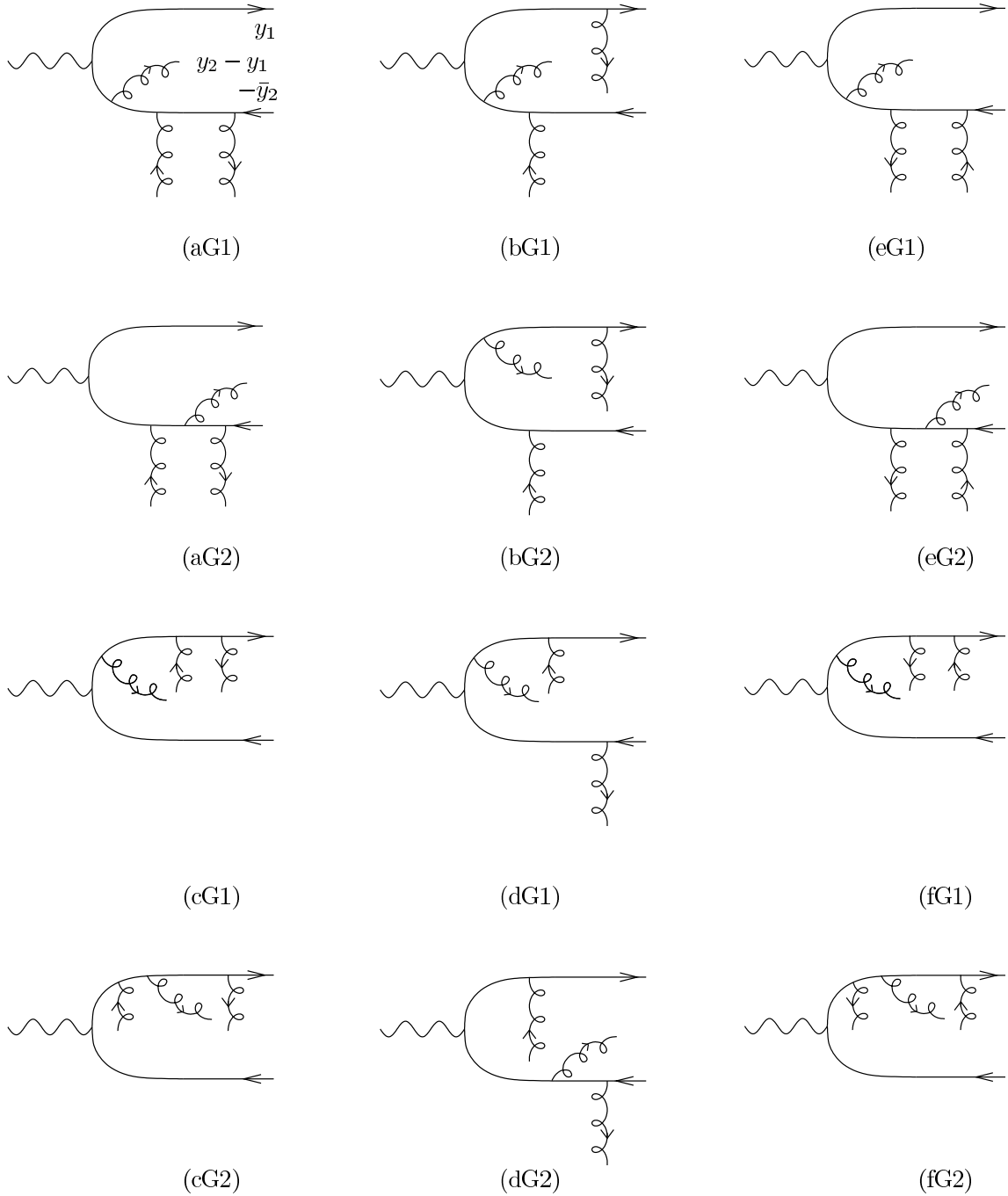


Figure 3.6: The 12 "Abelian" (i.e. without triple gluon vertex) type contributions from the hard scattering amplitude attached to the 3-parton correlators for the $\gamma^* \rightarrow \rho$ impact factor, with momentum flux of external line, along p_1 direction.

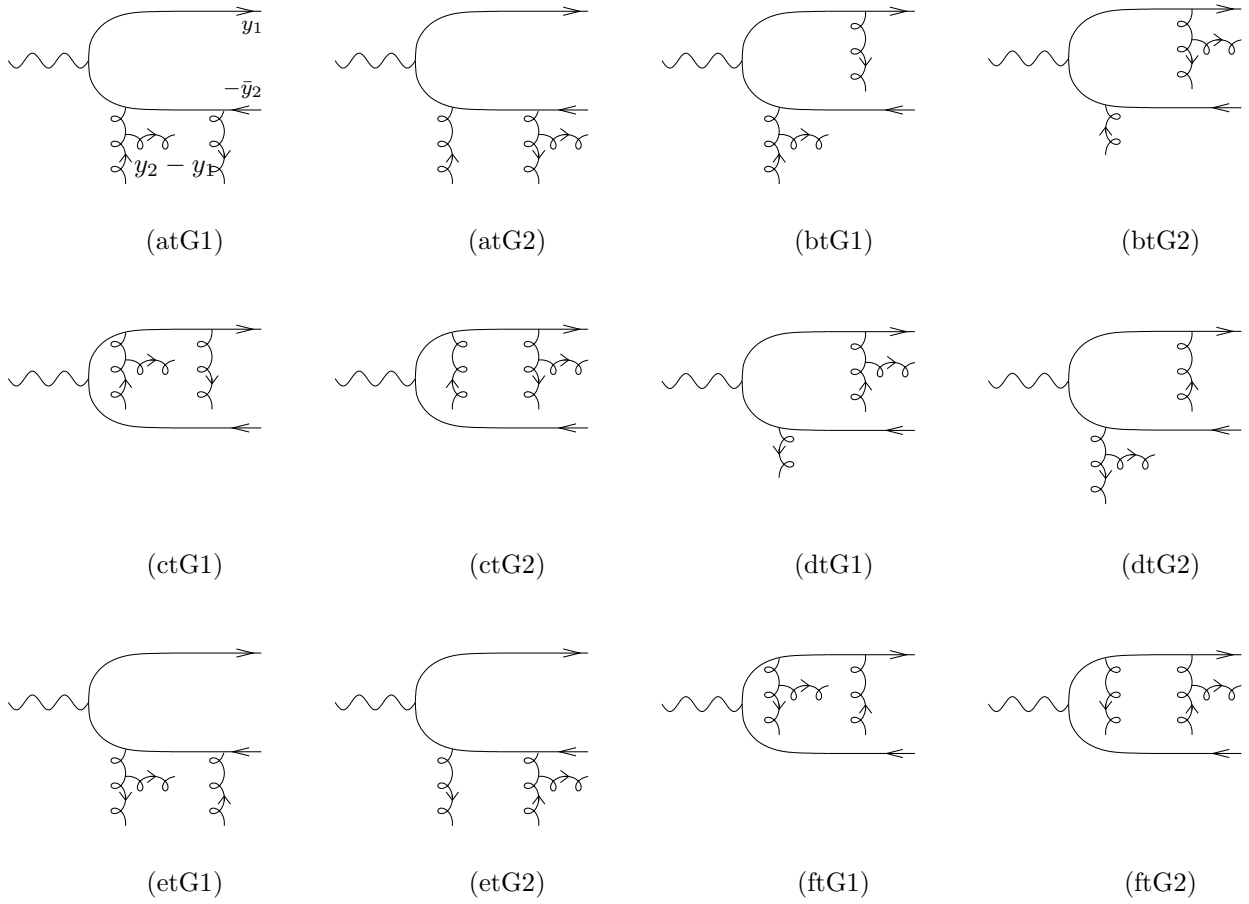


Figure 3.7: The 12 "non-abelian" -(with one triple gluon vertex) contributions from the hard scattering amplitude attached to the 3-parton correlators, for the $\gamma^* \rightarrow \rho$ impact factor, with momentum flux of external line, along p_1 direction.

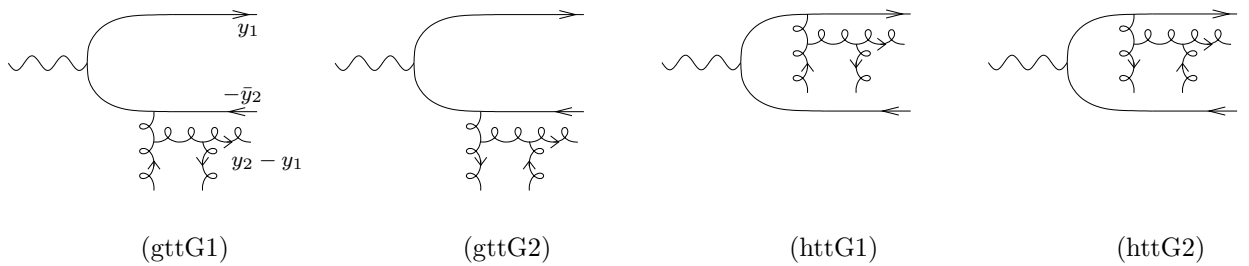


Figure 3.8: The 4 "non-abelian" -(with two triple gluon vertices) contributions from the hard scattering amplitude attached to the 3-parton correlators, for the $\gamma^* \rightarrow \rho$ impact factor, with momentum flux of external line, along p_1 direction.

Part II

QCD in the Regge limit

Chapter 4

Theoretical status

Hadronic reactions at low momentum transfer and high energies are described in the framework of QCD in terms of the dominance of color singlet exchanges corresponding to a few reggeized gluons. The charge conjugation even sector of the t -channel exchanges is understood as the QCD-Pomeron. For more than three decades, tremendous effort have been devoted to the study of QCD in the perturbative Regge limit. In order to use QCD analytically in a controllable manner, that is perturbatively, one should select *semi-hard processes*, for which an hard scale justifies the application of perturbation theory, and at the same time involves a very large center of mass energy with respect to t . In that case, the dynamics of the process can be assumed to be driven by the short distance dynamics of QCD. In this chapter we will recall the theoretical status of QCD in the Regge limit. We will now review the various modern approaches which have been elaborated in order to study QCD in the semi-hard regime. For reviews, see [273–275]. Chap. 5 will be devoted to phenomenological applications.

4.1 LL BFKL Pomeron

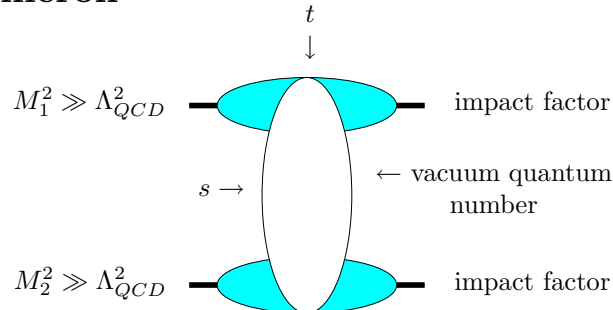


Figure 4.1: Scattering at $s \gg -t$.

At high energy ($s \gg -t$), consider the elastic scattering amplitude of two *IR safe (hard) probes* (Fig. 4.1), following the seminal work of Balitskii, Fadin, Kuraev and Lipatov [2–5]. The t -channel exchanged particles are gluons only, since at large s the scattering amplitude involving N particles of spin σ_i in t -channel behaves as

$$\mathcal{M} \sim s^{\sum_i \sigma_i - N + 1}. \quad (4.1)$$

For the minimal case of two gluon exchange, the amplitude behaves as s , leading to a constant cross-section. This corresponds to the Born contribution. Higher order contributions involving the triple gluon coupling modifies this behaviour. Indeed small values of α_S (perturbation theory applies due to hard scales) can be compensated by large $\ln s$ enhancements, calling for a resummation of $\sum_n (\alpha_S \ln s)^n$ series, illustrated diagrammatically by Fig. 4.2 at the amplitude level.

This results in the effective BFKL ladder [2–5], called Leading Log hard Pomeron as illustrated in Fig. 4.3 (for a pedagogical review, see [275]). Each vertical line is a reggeized gluon, that is a particle with the color and the spin of a gluon, but with a moving angular momentum depending of its off-shellness. Its is build from

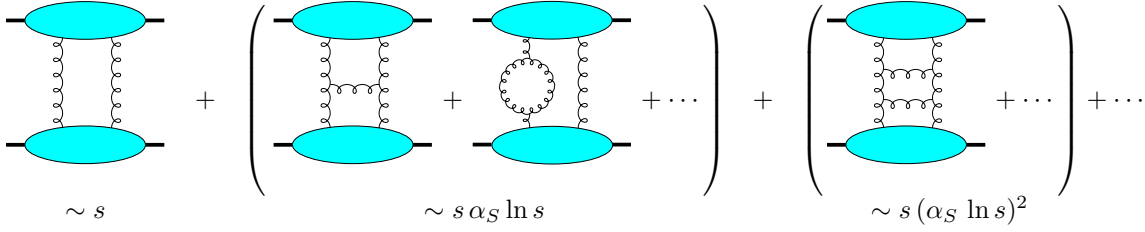


Figure 4.2: Diagrams contributing to the LL resummation.

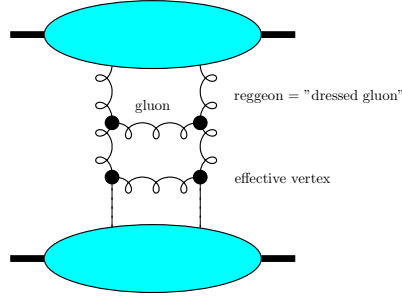


Figure 4.3: Effective BFKL ladder.

the resummation of an infinite set of t -channel gluons. The horizontal lines are ordinary gluons. As illustrated in Fig. 4.4 in the simple case of quark-quark scattering, the effective vertices are the sum of usual Yang-Mills vertex (YM) and of upper (A1, A2) and lower (B1, B2) Bremsstrahlung contributions which can be presented algebraically as a three-gluon vertex.

The resulting t -channel bound state is a QCD realization of the Pomeron, carrying vacuum quantum numbers (color singlet, P and C even). The resulting 4-gluon scattering amplitude satisfies an evolution equation as a function of s , which kernel is constructed from the effective vertex and the reggeon trajectory, called BFKL equation. As we have shown in Ref. [W17], the reggeon trajectory can be obtained by computing the soft part of the Z factor of the gluon field, in a physical gauge. This could in principle be extended to NLLx, NNLLx, etc... The comparison with the higher order NNLLx gluon trajectory result [276] leads to an agreement up to constant terms, which presumably are related to contributions coming from real terms, since the notion of gluon trajectory is non-physical.

The first step in order to solve BFKL equation is to express the amplitude of the process through the inverse Mellin transform with respect to the squared center-of-mass energy s as

$$\mathcal{M}(s, t) = is \int \frac{d\omega}{2\pi i} e^{\omega Y} f_\omega(r^2), \quad (4.2)$$

where $t - t_{min} \sim -r^2$, (r is considered as Euclidean, as is any two-dimensional vector in the following), and Y is the rapidity variable, $Y = \ln(s/s_0)$. In the particular case where $r^2 = 0$, the BFKL Green's function can be easily obtained in momentum space [273, 274]. In this case, denoting k (k') the momentum of the lower (resp. upper) gluon of the 4-gluon Green function, the impact representation for $f_\omega(0)$ reads

$$f_\omega(0) = \frac{1}{2(2\pi)^2} \int \frac{dk^2}{k^3} \frac{dk'^2}{k'^3} \Phi_1^{ab}(k) \Phi_2^{ab}(k') \int_{-\infty}^{\infty} d\nu \frac{1}{\omega - \omega(\nu)} \left(\frac{k^2}{k'^2} \right)^{i\nu}, \quad (4.3)$$

where the integration over angles has been performed. The functions Φ_i^{ab} are the impact factors describing the coupling of the BFKL pomeron to vertex 1 or 2, and a, b are the color indices of the t -exchanged gluons (which form a color singlet). They will be discussed in Sec. 4.2. The function $\omega(\nu)$ is the BFKL characteristic function which is defined by [2-5]

$$\omega(\nu) = \bar{\alpha}_s \chi(\nu), \quad (4.4)$$

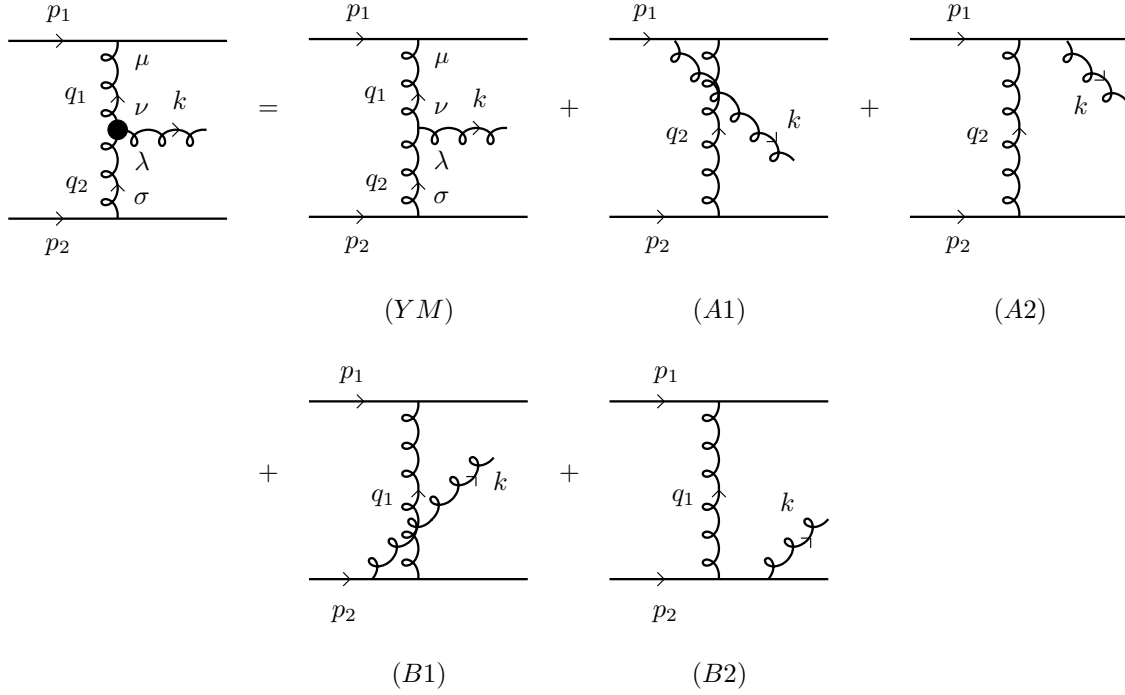


Figure 4.4: Lipatov vertex.

with $\bar{\alpha}_s \equiv \alpha_s N_c / \pi$ and

$$\chi(\nu) = 2\Psi(1) - \Psi\left(\frac{1}{2} + i\nu\right) - \Psi\left(\frac{1}{2} - i\nu\right), \quad \Psi(x) = \Gamma'(x)/\Gamma(x). \quad (4.5)$$

The general solution of the BFKL equation for arbitrary values of t is more involved [277] and will not be discussed in detail here. It can be obtained using the fact that this equation is invariant with respect to global conformal transformations, due to the absence of scale in the LLx approximation [277]. The basis of these solution is then obtain in direct (or coordinate) space using the principal series representation of $SL(2, C)$. It of course reduces to a simple expression at the Born level, which reads,

$$\mathcal{M} = is \int \frac{d^2k}{(2\pi)^2 k^2 (r-k)^2} \Phi_1^{ab}(k, r-k) \Phi_2^{ab}(k, r-k). \quad (4.6)$$

The special case $r^2 = 0$ of Eq. (4.6) can be readily obtained from Eq. (4.3) since after performing $\alpha_s = 0$ the integral over k' can be easily performed.

Using the optical theorem in order to relate the total cross-section to the imaginary part of the forward scattering amplitude, one obtains, when solving the BFKL equation

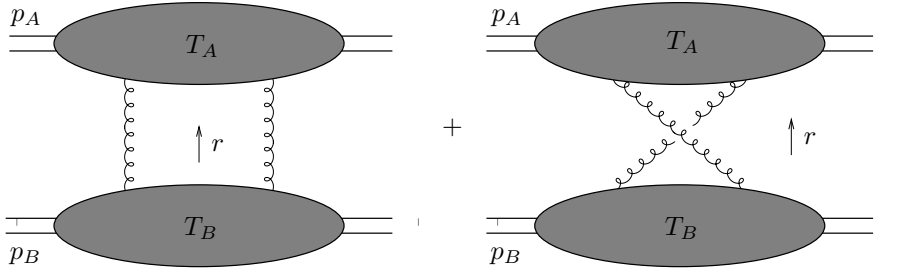
$$\sigma_{tot} \sim s^{\alpha_P(0)-1} \quad (4.7)$$

with $\alpha_P(0) - 1 = C \alpha_S$ ($C > 0$).

Later on, an equivalent approach at large N_c , the *dipole model* due to Nikolaev, Zakharov [278, 279] and to Mueller [280–283], has been developed. Based on the old-fashioned perturbation theory on the light-cone and in the light-cone gauge [77, 78], it provides a very simple and illuminating picture of the BFKL series. Its main ingredient is the soft eikonal emission, which iterates at any order in the planar 't Hooft limit [284, 285]. In this approach, rather than dealing with the scattering amplitude, one computes the soft (but still perturbative) content of a heavy onium wave function, a bound state of quark-antiquark pair (the bounding of the pair has some non-perturbative origin, given for granted and of no interest here). This content is illustrated at the lowest order in Fig. 4.5.



Figure 4.5: One gluon contribution to the onium wave function

Figure 4.6: Amplitude for the process $h_A(p_A) h_B(p_B) \rightarrow h_A(p_A + q) h_B(p_B - q)$ with s and u -channel contributions.

The natural degrees of freedom turn out to be color dipoles, that is color-anticolor pairs. Their density satisfies, when changing the rapidity (or the longitudinal IR cut-off for the softest gluon in the wave function), an evolution equation of Markovian type, because of the absence of interference terms in the large N_c limit, which makes the dipole evolving through a classical cascade.

The equivalence between BFKL and dipole model was proven at the level of diagrams [283], where in particular it was shown that the real contributions to the dipole kernel and to the BFKL one differs, as well as the virtual contributions, while their sum are identical. We proved this equivalence at the level of the $\gamma^*\gamma^* \rightarrow \gamma^*\gamma^*$ impact-parameter b dependent amplitude [W8]. Due to the conformal invariance of the dipole kernel (similar to the one of the BFKL kernel), the contribution of large and small distances requires a similar treatment. This led to a non-trivial large b shape of the amplitude, which we could extract in an analytical way in [W8], correcting the result of Ref. [282], and obtaining an agreement with the result [286] obtained from the numerical Monte Carlo OEDIPUS [287] for the generating dipole-functional.

4.2 k_T factorization

Consider the hard scattering of colorless particles A and B in the large $S = (p_A + p_B)^2$ limit

$$h_A(p_A) h_B(p_B) \rightarrow h_A(p_A + r) h_B(p_B - r) \quad (4.8)$$

The simplest amplitude, which we call Born amplitude (although at low energy some lowest order contribution in powers of α_s may also exist, e.g. the quark-box contribution to the elastic $\gamma^*\gamma^*$ scattering amplitude, or to the exclusive $\gamma^*\gamma^* \rightarrow \rho\rho$ amplitude, which we computed in Sec. 2.4), is given by the diagram shown in Fig 4.6 and involves two t -channel gluons connecting the upper and lower blobs. For the moment, we have focussed on the dynamics responsible for the LL resummation, and did not pay attention to the blobs T_A and T_B . In order to compute a physical scattering process, one should couple the 4-gluons Green function to the hadronic state, as we wrote without justification in Eq.(4.3). This is made by the k_T -factorization [288–294], illustrated in Fig. 4.7 for the process $\gamma^*\gamma^* \rightarrow \gamma^*\gamma^*$ at Born order. As usual, we introduce two light like vectors p_1 and p_2 , satisfying $2p_1 \cdot p_2 = s$. If the two initial states would be massless, these two Sudakov vectors would be chosen in such a way that the upper (lower) photon momentum would be $p_A = p_1$ (resp. $p_B = p_2$). In the case of virtual

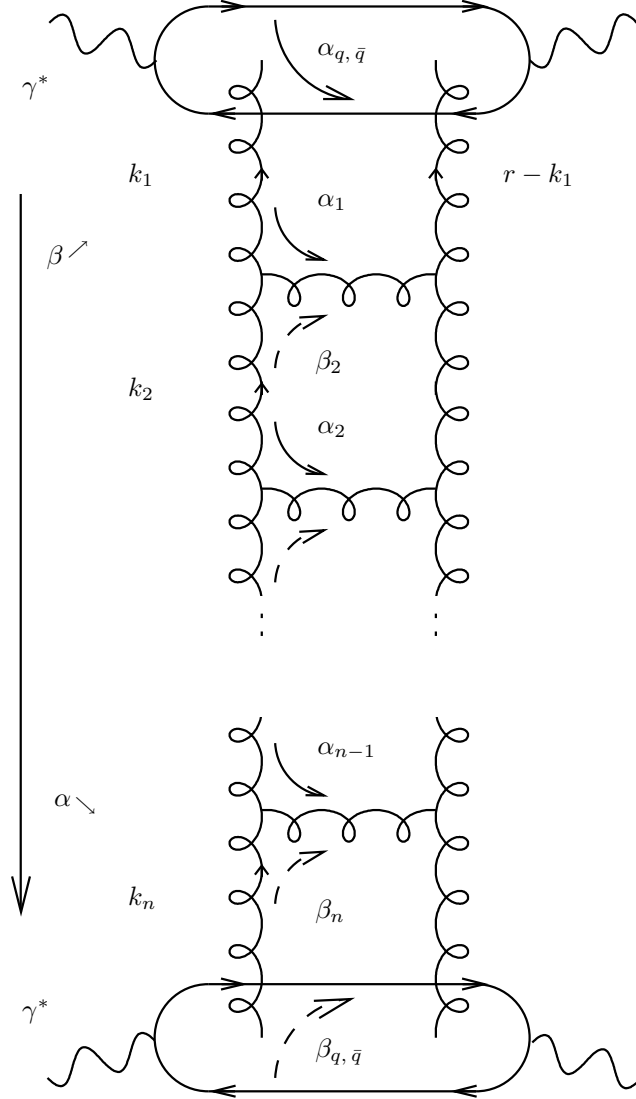


Figure 4.7: k_T factorization, illustrated for the process $\gamma^* \gamma^* \rightarrow \gamma^* \gamma^*$. Continuous arrows shows the flux of α (+) components, while dashed arrows shows the flux of β (-) components.

photons, the upper (lower) photons have an additional small component along p_2 (resp. p_1). Denoting by q_1 (q_2) the momentum of the upper (resp. lower) virtual photon, one can write

$$q_1 = p_1 - \frac{Q_1^2}{s} p_2 \quad \text{and} \quad q_2 = p_2 - \frac{Q_2^2}{s} p_1. \quad (4.9)$$

The idea is now to decompose any vector on p_1 , p_2 and their transverse plane, as we did in Chap. 1 when studying collinear factorization when we used the decomposition (1.10). In particular, any t -channel gluon can be decomposed as

$$k_i = \alpha_i p_1 + \beta_i p_2 + k_{\perp i}. \quad (4.10)$$

In these variables, the integration elements over the various gluon loops read

$$d^4 k_i = \frac{s}{2} d\alpha_i d\beta_i d^2 k_{\perp i}. \quad (4.11)$$

In LL approximation, the chain of gluons satisfies the multiregge-kinematics. It means that the α_i and β_i variables along the chain of gluons are strongly ordered as shown in Fig. 4.7 (this is the phase space responsible

for the large $\ln s$ terms). In the case of NLL, NNLL, ... approximations, this ordering should be extended in the so-called quasi-multiregge kinematics, meaning that these constraints should be fulfilled between each subset of emitted partons (for example, at NLL, two partons can be emitted within the same rapidity). As illustrated for the process $\gamma^*\gamma^* \rightarrow \gamma^*\gamma^*$ in Fig. 4.7, with a typical ladder-type diagram with $n - 1$ rungs, one can thus set $\alpha_1 = 0$ ($\beta_n = 0$) in the upper (resp. lower) blob. This simplifies dramatically the integration over k_1 and k_n since it can be reorganised as an integration over β_1 (α_n) in the upper (resp. lower) blob, the remaining $d\alpha_1$ and $d\beta_n$ being part of the 4-gluons Green function.

The second step in order to justify the k_T factorization formula is to notice that the $g^{\mu\nu}$ tensor of the numerator of the t -channel gluons - in Feynman gauge, with the upper (lower) index denoted μ (resp. ν) - can be safely replaced according to

$$g^{\mu\nu} \rightarrow \frac{2}{s} p_2^\mu p_1^\nu \quad (4.12)$$

in the LL approximation, since other contributions of the tensor can be easily proven to give subleading contributions. The corresponding polarizations

$$\varepsilon_{NS(up)}^\mu = \sqrt{\frac{2}{s}} p_2^\mu \quad \text{and} \quad \varepsilon_{NS(down)}^\nu = \sqrt{\frac{2}{s}} p_1^\nu \quad (4.13)$$

are called *non-sense polarization*, following Gribov. One finally get the k_T -factorization formula (expressed here for the Born order contribution)

$$\mathcal{M} = is \int \frac{d^2 \underline{k}}{(2\pi)^2 \underline{k}^2 (\underline{r} - \underline{k})^2} \Phi^{ab h_A \rightarrow h_A}(\underline{k}, \underline{r} - \underline{k}) \Phi^{ab h_B \rightarrow h_B}(-\underline{k}, -\underline{r} + \underline{k}), \quad (4.14)$$

where Φ^{ab} are *impact factors* defined as

$$\Phi^{ab} = \frac{1}{2} \int \frac{d\beta}{2\pi} \left(S_{\mu\nu}^{h_A g \rightarrow h_A g} p_2^\mu p_2^\nu \frac{2}{s} \right), \quad (4.15)$$

where a sum over color indices a and b is assumed. We emphasize the fact that in the example of $\gamma^* \rightarrow \gamma^*$, impact factors, these impact factors are defined in the kinematical region where virtualities of the photon, Q^2 , and t -channel gluons k_\perp^2 , are of the same order, $Q^2 \sim k_\perp^2$, and much larger than Λ_{QCD}^2 . Let us make here a technical remark on the normalization of the various building blocks introduced here, which varies in the litterature. It is rather conventional to define independently the impact factors as well as the Green function as the sum of s - and u -channel contribution, with the price of an eventual spurious multiplicative factor of 4. We choice to define impact factors by including an additional factor $1/2$ in each of them, in order to compensate this multiplicative factor (and more generally we accompany this sum by a prefactor $1/p!$ in the case of the exchange of p gluons in the t -channel), as shown in Fig. 4.8. To end-up with normalizations, note that the $1/2$ factor arising from the integration (4.11) is included in the 4-gluon Green function, compensating the symmetrical factor 2 due to the fact that both s - and u -channel contributions are identical, since the *signature* of the two-gluon exchange is positive in the example discussed above¹.

It is interesting to note that β variable is related to the s -channel Mandelstam variable for the channel photon(q_1)-gluon(k), through

$$\kappa = (k + q)^2 = \beta s + q^2 + k^2. \quad (4.16)$$

The impact factor can thus be expressed as the integral over the discontinuity of the S matrix element, after closing the β integral around the right-cut, as

$$\Phi = \frac{1}{2s} \int \frac{d\chi}{2\pi} \text{Disc}_\kappa \left(S_{\mu\nu}^{\gamma^* g \rightarrow \gamma^* g} p_2^\mu p_2^\nu \frac{2}{s} \right), \quad (4.17)$$

as illustrated in Fig. 4.9.

In the resummed LL approximation, one should simply replace the Born order Green function $2/(\underline{k}^2 (\underline{r} - \underline{k})^2)$ in (4.14) by the solution of the BFKL equation, since the arguments given above for one gluon loop integration

¹In the case of 3 gluons exchange, both positive and negative signature coexists, corresponding respectively to symmetrical and antisymmetrical contributions with respect to $s \leftrightarrow u$ exchange. They contribute respectively to the Pomeron and Odderon exchange, which we shortly discuss in Sec. 4.3.

Figure 4.8: Combinatoric factors entering the impact representation for the process $h_A(p_A) h_B(p_B) \rightarrow h_A(p_A + r) h_B(p_B - r)$.

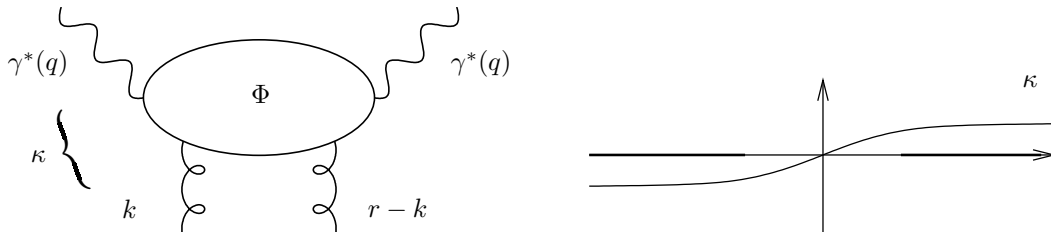


Figure 4.9: The impact factor as a cut amplitude. Left: κ as an s -channel Mandelstam variable. Right: integration path in κ -plane.

generalize straightforwardly in the case of the effective BFKL ladder (which involves an arbitrary number of k_i -loop integrations with α_i and β_i strongly ordered). The impact representation of the scattering amplitude for the reaction (6.1) can then be rewritten as

$$\mathcal{M} = \frac{is}{(2\pi)^2} \int \frac{d^2\mathbf{k}}{k^2} \Phi_1^{ab}(\mathbf{k}, \mathbf{r} - \mathbf{k}) \int \frac{d^2\mathbf{k}'}{k'^2} \Phi_2^{ab}(-\mathbf{k}', -\mathbf{r} + \mathbf{k}') \int_{\delta-i\infty}^{\delta+i\infty} \frac{d\omega}{2\pi i} \left(\frac{s}{s_0}\right)^\omega G_\omega(\mathbf{k}, \mathbf{k}', \mathbf{r}) \quad (4.18)$$

where G_ω is the 4-gluons Green function which obeys the BFKL equation [2–5]. G_ω reduces to

$$G_\omega^{Born} = \frac{1}{\omega} \delta^2(\mathbf{k} - \mathbf{k}') \frac{k^2}{(\mathbf{r} - \mathbf{k})^2} \quad (4.19)$$

within the Born approximation, and (4.18) then reduces to (4.14). Note that in the impact factor representation, the whole s dependency is in the Green function, while the impact factors are s -independent. At Born order, the amplitude is thus linear in s , and through the optical theorem the corresponding total cross-section is a constant when varying s .

The impact factors satisfy peculiar properties for vanishing t -channel momentum. In the large s -limit, although the t -channel gluons are off-shell, neglecting contributions of the order of k^2/s , the QCD Ward identity requires the vanishing of the amplitude when contracting any index of the S matrix element by the momentum of the corresponding out-going gluon, i.e.

$$S_{\mu\nu}^{\gamma^* g \rightarrow \gamma^* g} k^\mu = S_{\mu\nu}^{\gamma^* g \rightarrow \gamma^* g} (r - k)^\nu = 0. \quad (4.20)$$

Since $k = \beta p_2 + k_\perp$ in the multiregge kinematics, the impact factor (4.14), which is proportional to $S_{\mu\nu}^{\gamma^* g \rightarrow \gamma^* g} p_2^\mu p_2^\nu$, is thus also proportional to

$$S_{\mu\nu}^{\gamma^* g \rightarrow \gamma^* g} k_\perp^\mu (r - k)_\perp^\nu \quad (4.21)$$

which vanishes when either k_\perp or $(r - k)_\perp$ goes to zero (the S matrix is not singular in these limits). Thus, the impact factor should vanish when any of the t -channel gluon has a vanishing momentum. Note that we implicitly assume here that the probe is colorless, so that it does not contribute to the Ward identity. This is not satisfied when coupling a Pomeron to a parton in diffractive scattering. This also explains, from the point of view of the Green function, why the IR properties of the BFKL Pomeron are regular in the singlet channel.

4.3 The Odderon

In our presentation of k_T -factorization in the previous section, we encountered the concept of signature. In fact, the dominant contributions to the total cross sections of hadronic reactions are related to the Pomeron (\mathbb{P}) and to the Odderon (\mathbb{O}) exchanges. While the Pomeron exchange having the quantum numbers of the vacuum represents a dominant contribution to the sum of total cross sections for a given hadronic process and its crossing counterpart which is even under crossing, the odderon exchange dominates the difference of these two cross sections, which is odd under the crossing symmetry. Within Regge theory pomeron and odderon are therefore natural partners. The importance of Odderon exchange for the phenomenology of hadronic reactions was noted long ago [295] and was the subject of many investigations (for a review, see Ref. [296]). With the advent of QCD, the theoretical status of the perturbative Odderon followed the development of the analogous description of its Pomeron partner. Within QCD in LLx, the odderon appears as the color singlet exchange of three gluons, which interactions are of a form very similar to the interactions of the two gluons forming the pomeron. It is therefore not surprising that soon after the derivation of the BFKL equation for the pomeron there was derived an analogous Bartels Jaroszewicz Kwiecinski Praszalowicz (BJKP) equation [297–300] for the odderon. We will further consider this equation in Sec. 4.6.1 when discussing higher order corrections in relation with unitarization of QCD.

4.4 LL BFKL Pomeron: limitations

The LLx BFKL Pomeron faces several limitations, inherent to the approximations on which it relies.

First, at LLx the scale s_0 entering in the $Y = \ln s/s_0$ resummation is not fixed, and is somehow arbitrary at this order.

Second, the running of the coupling constant and scale fixing of α_S are not prescribed at LL, since their effect is subleading.

Third, energy-momentum is not conserved in the BFKL approach (this remains at any order: NLLx, NNLLx, ...), while it is naturally implemented through the vanishing of the first moment of the splitting functions, in the usual collinear renormalisation group approach (à la DGLAP [61–64]). Indeed in this standard renormalization group approach, one consider from the very beginning non local matrix elements. The energy-momentum tensor corresponds to their first moment, which is protected against radiative corrections.

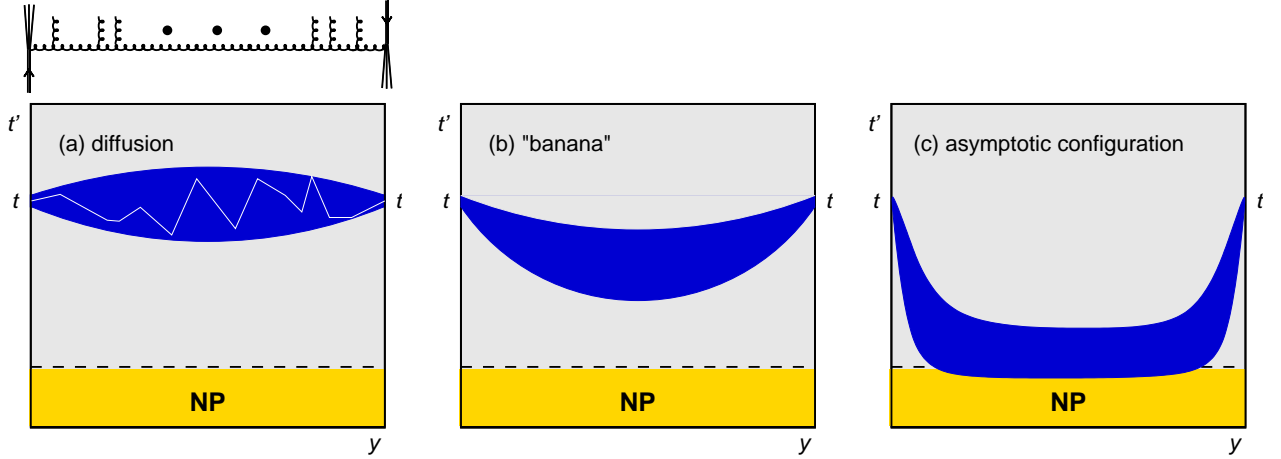


Figure 4.10: Diffusion along the BFKL ladder. Figure from Ref. [301].

Fourth, diffusion along the BFKL ladder spoils the IR safeness of the BFKL Pomeron: at fixed α_S , there is a gaussian diffusion of k_T , with a cigar-like picture [302]. The more s increases, the larger is the broadness. Setting $t = \ln Q^2/\Lambda_{QCD}^2$ (fixed from the probes) and $t' = \ln k^2/\Lambda_{QCD}^2$ ($k^2 \sim -k_T^2 =$ virtuality of an arbitrary exchanged gluon along the chain), the typical width of the cigar is $\Delta t' \sim \sqrt{\alpha_S Y}$ (Fig. 4.10a). The Non-Perturbative domain is touched when $\Delta t' \sim \sqrt{\alpha_S Y} \sim t$. In a simple running implementation, using $\underline{a}(t) = 1/(bt)$ (with $b = \beta_0/(4N_c) = 11/12$ when neglecting quarks in LLx), the border of the cigar touches NP for $Y \sim bt^3$ ($b = 11/12$) while the center of the cigar approaches NP when $Y \sim bt^2$ ("banana structure" of Fig. 4.10b). A more involved treatment of LL BFKL with running coupling, which can qualitatively be more easily understood in a collinear toy model [303], showed [304] that the cigar is "swallowed" by NP in the middle of the ladder (Fig. 4.10c): one faces tunneling when $Y \sim t$, meaning that IR safety is doubtful. Such a behaviour can be interpreted as a transition [301] between a hard Pomeron regime and a soft Pomeron regime [305] à la Donnachie and Landshoff. Unfortunately, this LLx based analysis showed that the window for which the hard Pomeron could be seen is very narrow, if not zero, basically due to a rather large hard energy dependence of the hard BFKL Pomeron. We will see below that there are in fact good reasons, based on higher order corrections (which in practice reduce the value of the \mathbb{P} intercept, in agreement with HERA data), to believe that this is not true and that there exist a range where a BFKL Pomeron (not the LLx one) could be seen.

4.5 Higher order corrections

Higher order corrections to BFKL kernel are known at NLLx order ($\alpha_S \sum_n (\alpha_S \ln s)^n$ series) [276, 306–308], and have been recently extended to the non-forward case [309, 310]. Impact factors are known in some cases at NLLx. The $\gamma^* \rightarrow \gamma^*$ impact factor has been computed at $t = 0$ [311–314] but only partial numerical results have been obtained, which evaluate the effect of real corrections [315]. At the moment, this impact factor is not in a form which could be of simple practical use. The forward jet production vertex has been also evaluated at NLLx [316, 316] and is a building block for Mueller Navelet jets, for which we present in Sec. 5.1.1 a complete NLLx evaluation. Finally, the $\gamma^* \rightarrow \rho$ impact factor in the forward limit has been computed in Ref. [317]) and

was the basis of the first complete NLLx treatment.

The NLLx kernel leads to *very large corrections with respect to LLx*, and dramatically changes the LLx predictions. The NLLx kernel, taken as it is, is larger than the leading order kernel, and for any reasonable value of α_s it is negative; the pomeron intercept becomes less than one for $\alpha_s \gtrsim 0.15$. Furthermore it has two complex conjugate saddle points which can lead to oscillating cross sections. The perturbative expansion of the BFKL kernel is therefore highly unstable and far from converging. See Refs. [318–322] for a discussion of these problems.

The main part of these corrections can be obtained from a physical principle, based on a kinematical constraint along the gluon ladder (which is subleading with respect to LL BFKL) [323–325]. The idea is to take into account properly the fact that in the real part of the BFKL kernel, the virtuality of the t -channel gluons exchanged along the ladder should be dominated by the transverse momentum squared. However it is rather unclear whether this has anything to do with NLL correction: in principle this constraint would be satisfied when including LLx+NLLx+NNLLx+NNNLLx+... This constraint is more related to the improved collinear resummed approaches (see below) for which the vanishing of the first moment of the splitting function is natural.

The above perturbative instabilities occurring at NLLx order clearly require an improved scheme. Either one can use a physical motivation to fix the scale of the coupling²: this is the basis of BLM scheme [158], applied for the $\gamma^*\gamma^*\rightarrow X$ total cross-section [326,327] and for the $\gamma^*\gamma^*\rightarrow\rho\rho$ exclusive process [W16, 328].

Another approach, to which we will refer as the collinear improved NLLx, was initiated by Salam and then by Ciafaloni. This resummed approach is inspired by the compatibility with the usual renormalization group approach³, and in particular with the fact that collinear renormalization group forbid the occurrence of logs of the collinear scale with higher powers than the coupling. For example in the total inclusive process $\gamma^*(Q_1)\gamma^*(Q_2)\rightarrow X$, one includes *both* full DGLAP LLQ for $Q_1 \gg Q_2$ and “anti-DGLAP” LLQ $Q_1 \ll Q_2$, fixes the relation between Y and s in a symmetric way compatible with DGLAP and implement the running of α_s . This approach leads to modified BFKL kernels⁴ $\chi(\gamma, \omega)$ depending on both γ and ω . This form comes about because of a resummation which removes unphysical double logarithms in the DGLAP and “anti-DGLAP” limits where γ is close to 0 or 1 [318], and which resums logarithms from the running of the coupling [319,320,329]. This means that when performing the inverse Mellin transform in Eq.(4.2), the position of the pole in the ω plane is determined by the equation

$$\omega = \bar{\alpha}_s \chi(\gamma, \omega). \quad (4.22)$$

One should note that these constraints do not fix completely the form of the modified BFKL kernel. It only constraint the values of the residues of the double and triple poles at $\gamma = 0$ and $\gamma = 1$. It turns out that the kernel used in the Lund dipole model [324,325], which is an implementation of CCFM equation, leads to a kernel which respect the collinear and anti collinear constraints introduced by Salam, and a reasonable ansatz for higher order correction of the type NNLLx, etc... Note that this ansatz is also equivalent to the improved LLx BFKL kernel based on a kinematical constraint [323]. The implementation of these constraints at full NLLx order is more involved [318–320,329]. We refer to these papers for details of the various scheme which have been proposed. In Sec. 5.1.1, we will use in particular the scheme 3 of Salam when dealing with Mueller Navelet jets at full NLLx order, which we will compare with full NLLx collinear improved resummation. Coming back to the IR diffusion problem discussed in section 4.4, this scheme enlarges the validity of perturbative QCD, leading to a larger domain in which linear perturbative Regge dynamics is expected.

A simplified version [330] of the Salam procedure at fixed α_s results in performing in the LLx BFKL Green function

$$\frac{1}{k^3 k'^3} \int \frac{d\omega}{2\pi i} \int \frac{d\gamma}{2\pi i} \left(\frac{k^2}{k'^2} \right)^{\gamma-1/2} \frac{e^{\omega Y}}{\omega - \omega(\gamma)}$$

the replacement $\omega - \omega(\gamma) \rightarrow \omega - \omega(\gamma, \omega)$. The ω integration is performed through contour closing around the pole at $\omega = \omega(\gamma, \omega)$, and the γ integration is made using the saddle point approximation at large Y . This takes into account the main NLL corrections, as discussed above (within 7 % accuracy), and implement the main effects of the resummed scheme of Salam et al. We will use this simplified LLx implementation in Sec. 7.4.6.

²The running of the coupling constant should be implemented at NLLx, while the scale is fixed starting from NNLLx.

³See Ref. [321] where the basical ideas are explained in a very pedagogical manner.

⁴The discussion is most conveniently performed using the variable $\gamma = \frac{1}{2} + i\nu$ rather than ν .

To end this discussion, let us note that a similar approach based on the compatibility between $\ln 1/x$ and $\ln Q^2$ resummations have been made starting from the $\ln Q^2$ resummation (instead of the $\ln 1/x$ resummation starting point of Salam), after the introduction of a “duality” principle in Ref. [331], which lead to a long series of papers [332–340] based on this idea, including NLLx and running coupling effects. There is now an agreement that the Salam et al. approach is equivalent to this later one.

4.6 Non-linear regime and saturation

Based on very general arguments as analyticity, crossing, causality and the fact that there is a gap in the spectrum of states bounded by the strong force (the pion has a non zero mass), Froissart could establish his bound on the total hadron-hadron cross-section [341], which states that

$$\sigma_{tot} \leq \ln^2 s, \quad (4.23)$$

for asymptotically large s . Unitarity tells that for each impact parameter b , amplitudes should fulfil $T(s, b) < 1$. From the LLx QCD computation of the hard Pomeron exchange (4.7), this bound is clearly violated by perturbation theory, and this remains true at NLLx order. Although strictly speaking valid only for hadronic observables, and not for external virtual states such as γ^* , there is a common belief that it should be satisfied within any reasonable perturbative resummed scheme. This is the starting point of various lines of research, which led to various unitarization and saturation models.

4.6.1 Generalized Leading Log Approximation

The *Generalized Leading Log Approximation*, taking into account any *fixed* number n of t -channel exchanged reggeons, leads to the Bartels, Jaroszewicz, Kwiecinski, Praszalowicz equation [297–300], a 2-dimensional quantum mechanical problem (time $\sim \ln s$) with n sites, where the space is the coordinate space of the t -channel reggeons. This 2-dimensional space can be expressed as the product of an holomorphic and antiholomorphic sector, and the elementary hamiltonian describing the interaction between two reggeons is holomorphically separable [342, 343], which means that

$$H_{ij} = H(z_i, z_j) + H(\bar{z}_i, \bar{z}_j). \quad (4.24)$$

where $z_{i,j}$ and $\bar{z}_{i,j}$ are the holomorphic and antiholomorphic coordinates of the reggeons. These hamiltonians are globally conformal invariant [342, 343], which means that they are invariant under Möbius transforms

$$z_j \longrightarrow z'_j = \frac{az_j + b}{cz_j + d}, \quad \bar{z}_j \longrightarrow \bar{z}'_j = \frac{\bar{a}\bar{z}_j + \bar{b}}{\bar{c}\bar{z}_j + \bar{d}} \quad (4.25)$$

with $ad - bc = \bar{a}\bar{d} - \bar{b}\bar{c} = 1$. This global conformal invariance is an $SL(2, \mathbb{C})$ invariance, to be distinguished from the $SL(2, \mathbb{R})$ encountered within collinear factorization (see Sec. 1.4.5). The whole hamiltonian describing the evolution in rapidity of the n -reggeon state is the sum these hamiltonians

$$\mathcal{H}_n = -\frac{\alpha}{2\pi} \sum_{i>j} H_{ij} t_i^c t_j^c, \quad (4.26)$$

where the generator t_i^c in the adjoint representation acts tensorially in the color space of the Reggeon i . Explicitly, in the space i , $(t^c)_{ab} = -iC_{cab}$.

The two corresponding holomorphic and antiholomorphic hamiltonian do not commute for arbitrary N_c , due to the non-trivial color structure.

In the large N_c limit, this 2-dimensional quantum mechanical problem greatly simplifies. Indeed, in the 't Hooft limit the only remaining structures have the topology of a cylinder in color space, and the holomorphic and antiholomorphic sector decouples. Furthermore, the cylinder topology means that only nearest-neighbour reggeons interact. Thus, the model can be viewed as two one-dimensional Schrödinger equations for n sites, with periodic boundary conditions. It was then shown that these one-dimensional models are *integrable models* in the large N_c limit [343–347]: they are identical to one of the XXX Heisenberg spin chain. This means that one

can construct a set of conserved operators which commutes with themselves and with this hamiltonian, relying on the so-called Yang-Baxter equation. Although it is known to be integrable, the fact that its symmetry group $SL(2, C)$ (arising from the global invariance⁵) is *non-compact* makes the solution non-trivial. The usual integrable models with a symmetry group as $SU(2)$, like the usual XXX Heisenberg spin chain, the Ising model, the Potts model, or the 6-vertex model have been studied in great details in the seventies, and their spectrum have been computed relying on the coordinate Bethe ansatz⁶ or its extension, the Algebraic Bethe ansatz. In the case of non-compact groups, the situation is much harder, and the usual Bethe ansatz cannot be applied directly (it leads to a sub-class of solution which are trivial). A more involved method, the Functionnal Bethe ansatz, was successfully applied and lead to the solution of BJKP for arbitrary n . This means that the energy spectrum could be computed, and thus the intercepts. In the case of n even, the bound states of t -channel reggeons have the quantum numbers of the Pomeron $P=C=+1$, while for n odd, such bound states contribute both to Pomeron and Odderon $P=C=-1$ exchange. For Odderon, $\alpha_0 < 1$ [348–353]. When summing with respect to n , it is expected that the whole series, although divergent, could have a critical behaviour with an Odderon intercept $\alpha_0 = 1$. Howether, these bounds states decouples from Born impact factors. They couple to photon impact factor only through non trivial color states, of multipole type, which are therefore suppressed by $1/N_c^2$ powers.

In contrast, it is possible to exhibit a *critical* solution ($\alpha_0 = 1$) which couples to Born impact factors. These peculiar solutions can be obtained either from the perturbative Regge approach [354] or from the dipole model, as we have shown in Ref. [W11]. Since they have a critical behaviour and couple to the Born impact factors, they provide an interesting model when performing phenomenological studies of the odderon. Recent studies taking into account the effect of the running coupling [355] or including higher BFKL effects (NLL, etc...) within the collinear improved BFKL kernel discussed above [356] lead to an intercept which should remain one at any order.

4.6.2 Extended Generalized Leading Log Approximation and Color Glass Condensate

In comparison with the previous approach, the Extended Generalized Leading Log Approximation [357–361], in which the number of reggeon in t -channel is non conserved, satisfies full unitarity (in all sub-channel) and is an *effective 2-d field theory* realizing the Gribov idea of Reggeon field theory [362] in QCD. A comprehensive and pedagogical review of this approach can be found in Ref. [361].

In the framework of EGLLA, the simplest new building block (with singlet sub-channels) is the triple Pomeron vertex [358–360, 363]. Based on conformal properties allowing to relate this vertex to conformal block of an underlying (still unknown) conformal field theory, and using bootstrap properties, an evaluation of this vertex was possible [364]. This vertex contains two contributions: a planar one, and a non planar one, suppressed by $1/N_c^2$ with respect to the planar one. It turns out that when starting from the dipole side, thus restricting to the planar contribution, and evaluating the corresponding $1 \rightarrow 2$ dipole kernel [365–367], the obtained planar contribution was identical with the planar part of the triple Pomeron vertex of EGLLA.

This planar vertex led to the simplest version of a non-linear extension of the BFKL equation, the Balitski-Kovchegov (BK) equation [368–371], [372, 373], involving *fan-diagrams* (with singlet sub-channels). The Kovchegov approach relies on the Mueller dipole model, starting from the generating functionnal for dipoles. In the Balitski method, the BK equation is a simplified version of his shock-wave approach, an extensive generalization of eikonal methods to QCD.

In these approaches, loops (in terms of Pomerons) corrections are unknown, and obtaining them would be a major step. Another effective field theory approach has been developed separately [374–377], which provides the necessary building block (reggeon-reggeon-gluon and 3-gluons vertices) necessary for the explicit computation of any type of diagram. Despite this fact, the precise relation between this effective theory and the EGLLA has not been clarified, and explicit applications of this effective field theory would be highly desirable.

Third, the multipomeron approach makes contact with AGK cutting rules [378] of pre-QCD. In the large N_c limit, this is the dominant contribution when coupling to Born impact factors (leading with respect to BJKP), and it leads to unitarization [379, 380].

⁵One can show that the Casimir of the conformal group is one of the conserved operators of the model.

⁶One is looking, in the coordinate space x (of n dimension), for solutions which are linear combinations of plane waves of type $e^{ik \cdot x}$.

Fourth, during the last decade, the Color Glass Condensate [381–389] and B-JIMWLK equation were elaborated (for a review, see Ref. [390]). Although technically rather different, they are both based on the idea of emission of soft gluons by classical currents. Gluons carrying longitudinal momenta below a given scale are treated though the usual eikonal emission of a fast moving source. The BFKL equation corresponds to the case where the recoil of the source is neglected. Taking into account these recoil effects leads to non-linearities.

More precisely, these effective field theory are based on the scattering picture of a probe off the field of a source, which is treated through a renormalisation group equation with respect to a longitudinal scale, with an explicit integration out of modes below this scale. The approach of Balitski [368–371] relies on the scattering of Wilson loops and computation of interaction of one loop with the field of the other (related to the eikonal phase approach à la Nachtmann). Note that within the dipole model, a similar approach, based on the computation of the scattering phase of a dipole in the field emitted by a fast moving object (involving color structures as well as multicolor states), was suggested in Ref. [W7]. Recently, this shock wave approach provided an alternative computation of the NLLx BFKL kernel with respect to the usual bootstrap approach.

The BK equation is a simplified version of the B-JIMWLK equation, corresponding to the mean field approximation: one neglect any multi-particle correlation except the two gluon one. There is at the moment no clear one-to-one correspondence between ELLA and CGC, except in the peculiar BK limiting case. Loops (in terms of Pomerons) corrections are also unknown. Toy models in 1+0 dimensions are under development (Reggeon field theory) to understand these corrections.

Starting from the BK equation, Munier and Peschanski exhibited very interesting links between saturation models and statistical physics (reaction-diffusion models of the FKPP class) [391–394]. These models provide a saturation scale $Q_s(Y)$ growing with Y : above this scale the scattering amplitude T is small (color transparency), and below it saturates. See [395] for a recent review. This reduces the contribution of gluons with $k^2 < Q_s^2$ and may solve the IR diffusion problem.

4.6.3 Saturation and geometrical scaling

From the phenomenological side, these developments were considered as rather formal since both BFKL of DGLAP evolution could describe the data, without appealing for non-linear contributions responsible for a saturation of parton growth. A careful analysis of HERA data in fact revealed, when combining x_{Bj} and Q^2 in term of a single variable τ and plotting the $\sigma_{tot}^{\gamma^*p}$ data as a function of this τ that a curve occurred, with almost no spreading [396]. Golec-Biernat and Wüsthoff (GBW) then introduced a dipole model [397, 398] for describing the total γ^*p cross-section [397] as well as diffractive events [398]. The basic idea is to describe the $\gamma^* - p$ interaction at small x_{Bj} as the scattering of a $q\bar{q}$ pair (a dipole, which is also the starting point in Mueller's onium approach), formed long before the scattering off the proton (in a non-symmetric frame where the nucleon is at rest). This initial dipole is characterized by a transverse size r and by a relative fraction of longitudinal momentum carried by the quark and the antiquark. One should then parametrize the dipole-nucleon scattering cross-section. The total cross-section can be expressed as (here $r = |\underline{r}|$)

$$\sigma_{T,L}(x, Q^2) = \int d^2\underline{r} \int_0^1 d\alpha |\Psi_{T,L}(\alpha, \underline{r})|^2 \hat{\sigma}(x, \underline{r}), \quad (4.27)$$

where $\Psi_{T,L}$ is the photon wave function for the transverse (T) and longitudinally polarized (L) photons, which can be expressed in terms of Bessel functions. One then use an effective description of the saturation dynamics, implemented in a simple functional form of the effective dipole cross section $\hat{\sigma}(x, r)$ which describes the interaction of the $q\bar{q}$ dipole with a nucleon:

$$\hat{\sigma}(x, r^2) = \sigma_0 \left\{ 1 - \exp\left(-\frac{r^2}{4R_0^2(x)}\right) \right\}, \quad (4.28)$$

where the x -dependent radius R_0 is given by

$$R_0(x) = \frac{1}{GeV} \left(\frac{x}{x_0}\right)^{\lambda/2}. \quad (4.29)$$

From the fact the squared wave functions are peaked at $r \sim 2/Q$, one gets a usual linear perturbative description in the regime $r \ll R_0$. In that limit the dipole cross-section scales like r^2 , a typical behaviour for color-transparency. This is for example what is obtained when computing the dipole-dipole scattering through a two

gluon exchange (which form just comes out of an eikonal treatment [W8]), when considering a nucleon probe made itself of dipoles. The power-like behaviour of $R_0(x)$ is inspired by the hard Pomeron description of the HERA data in the linear regime, obtained within the Mueller dipole model when dressing by small- x gluon emissions à la BFKL (dipoles in Mueller approach) the initial $q\bar{q}$ dipole.

On the other hand, when r gets larger, of the order of $2R_0$, the cross-section saturates, with for small Q^2 a maximal value which equals σ_0 . The critical saturation line is thus given by $Q = Q_s(x)$ with

$$Q_s(x) = 1/R_0(x). \quad (4.30)$$

To get the geometric scaling prediction, one should note that the non-trivial functional dependency of the γ^* wave function is completely expressed as a shape in the dimensionless variable $\bar{r} \equiv |r|Q$. In this variable, the dipole cross-section (4.28) has now the functional form

$$\hat{\sigma} \left(\frac{Q_s^2(x)}{Q^2} \bar{r}^2 \right) \quad (4.31)$$

after using the saturation scale (4.30). Combining Eqs.(4.31) and (4.27), it is now clear that the functional form of the dipole cross-section (4.28) remains intact after the perturbative dressing due to the γ^* wave function. One can therefore expect the geometric scaling of the total cross-section at small x :

$$\sigma_{tot}^{\gamma^* p \rightarrow X}(x, Q^2) = \sigma_{tot}^{\gamma^* p \rightarrow X}(\tau), \quad \tau = Q^2/Q_s^2(x). \quad (4.32)$$

with $Q_s(x)$ given by

$$Q_s(x) = Q_0 \left(\frac{x}{x_0} \right)^{-\lambda/2}, \quad Q_0 \equiv 1\text{GeV} \quad (4.33)$$

and the parameters $\lambda=0.288$ and $x_0=3.04 \cdot 10^{-4}$. Note that the value of λ is the typical order of magnitude of the Pomeron intercept (minus one) measured at HERA. This saturation model was further extended by including the effect of DGLAP evolution [400]. This can be done by replacing in the dipole cross-section $\hat{\sigma}(x, r^2)$ the elementary r^2 dipole-dipole cross-section valid in the color transparency regime by a more elaborate cross-section which include DGLAP evolution through the gluon density entering the scattering off the dipole.

In Ref. [399], a compilation of all available data [401–405] for F_2 as been used, leading to an almost perfect agreement with geometric scaling, as shown in Fig. 4.11.

This geometrical scaling is the feature of a non-linear evolution, which BK equation can generate. Although strictly speaking geometric scaling does not imply saturation, it is a manifestation of saturation, which is difficult to get without a cross-section which would saturate, and lead to a stronger motivation for studying saturation and unitarization effects in QCD through perturbative approaches.

Another sign of the saturation effect was presented in Ref. [406] were a model, in the spirit of GBW, was constructed inspired by the BK equation, smoothly interpolating between the saturated regime and the linear regime. This model was able to describe the most recent very precise F_2 data [401–403] in the moderate domain of Q^2 , explicitly exhibiting a need for saturation effects at small x and small Q^2 in comparison with a pure linear evolution à la BFKL.

Geometrical scaling can be extended at each impact parameter b , as we have shown in Ref. [W10]. The idea of a b -dependent saturation scale is due to Mueller [407], while a b -dependent S -matrix for dipole-proton scattering was studied for diffractive meson electroproduction in Ref. [408]. We consider here the idealized process of scattering of a dipole of size $1/Q$ off a dipole of size $1/\Lambda$. Λ and Q are fixed momentum scales, which are taken in the perturbative region in the following discussion, and the ordering $Q > \Lambda$ is assumed. We suppose that b is larger than the sizes of the initial-state dipoles: $b \gg 1/Q, 1/\Lambda$. The Mellin representation of the solution of the BFKL equation then reads [W8, 409]

$$\mathcal{A}_d(y, Q, b) = \frac{1}{2} \frac{1}{Q^2 \Lambda^2 b^4} \int \frac{d\gamma}{2i\pi} (1-2\gamma) v(\gamma) (16b^2 Q \Lambda)^{2\gamma} e^{\bar{\alpha}_s y \chi(\gamma)}, \quad (4.34)$$

where as usual the integration goes over a line in the complex plane parallel to the imaginary axis and intersecting the real axis between 0 and 1 and where the function $v(\gamma) = \alpha_s^2 / (16\gamma^2(1-\gamma)^2)$ is the Mellin transform

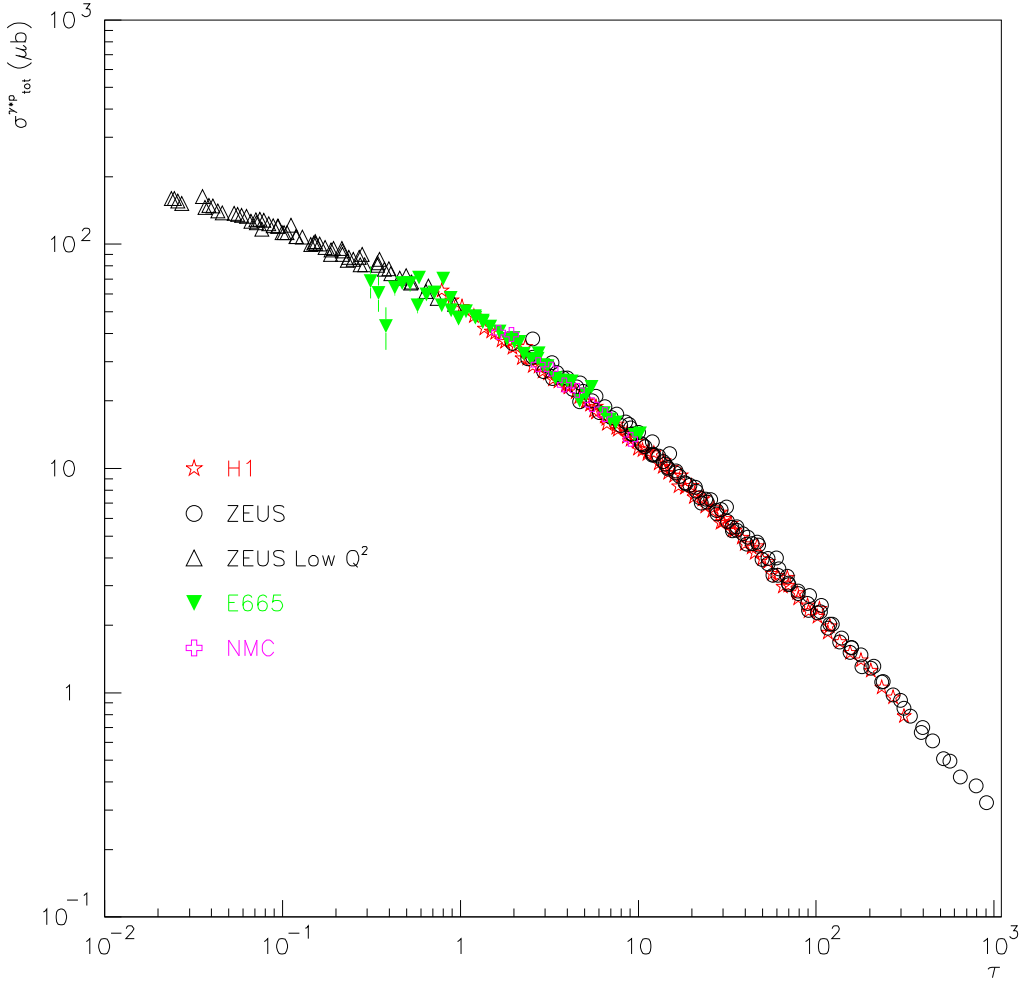


Figure 4.11: $\gamma^* - p$ total cross section based on the whole data set of DIS data in the low- x regime plotted as a function of a single scaling variable $\tau = Q^2/Q_s^2(x)$. Geometrical scaling is the fact that all data follow a single curve, although they depend a priori on to variables: x and Q^2 . Figure from Ref. [399].

of the elementary dipole-dipole elastic amplitude with respect to the ratio of their sizes, with appropriate normalization. Applying the steepest-descent method to the impact parameter dependent amplitude (4.34) gives

$$\mathcal{A}_d(y, Q, b) = \frac{128\pi\alpha_s^2}{(\pi a^2 y)^{3/2}} \log(16b^2 Q \Lambda) \exp \left\{ \omega y - \log(16b^2 Q \Lambda) - \frac{1}{a^2 y} \log^2(16b^2 Q \Lambda) \right\}. \quad (4.35)$$

The saturation scale is then defined by the scale $Q = Q_s$ for which this amplitude is of order 1, the saturation scale Q_s being given by

$$Q_s^2(y, b) = \frac{1}{256\Lambda^2 b^4} \exp(\lambda y). \quad (4.36)$$

In the regime where Q/Q_s is sufficiently close to Λ , the amplitude can then be expressed as a function of Q and Q_s only:

$$\mathcal{A}_d(Q, Q_s(y, b)) = \frac{64\alpha_s^2}{\sqrt{\pi a^2 y_0}} (2\gamma - 1) \left(\frac{Q_s^2(y, b)}{Q^2} \right)^\gamma, \quad (4.37)$$

where the saturation scale now depends on the impact parameter b . Thus we see that the amplitude for each impact parameter is a function of the ratio of the inverse size of the projectile and of the *local* saturation scale.

In fact, the form (4.36) presumably assume to much perturbative control, though the non-perturbative tail is probably important. Including non-perturbative effects, the b dependence of Q_s becomes exponential. This does not change dramatically the conclusion on the possibility of seeing local geometrical scaling in some range in b .

A former analysis [408] has already shown the relevance of impact parameter dependent analysis in the discussion of saturation. There, the S -matrix element for dipole-proton scattering at fixed impact parameter was extracted from diffractive electro-production of vector mesons at HERA. This quantity can be interpreted as a transparency coefficient, and thus quantifies the “blackness” of the proton as seen by the projectile. Such kind of analysis is always model-dependent, since to get the correct normalization of the S -matrix element, one has to rely on an *ad hoc* model for the final-state vector meson. Although it was shown in Ref. [408] that requiring that the initial state be a *longitudinal* photon limits the model-dependence, an estimated uncertainty of 20% was still recognized. However, dependence of the cross section on a scaling variable can be tested in a model-independent way.

The scattering amplitude at fixed impact parameter can be extracted from differential cross sections for high energy quasi-elastic processes by a Fourier transform with respect to the momentum transfer. By quasi-elastic we mean that the initial and final states have the same number of particles. In practice, the process we are thinking of will be diffractive electroproduction of vector mesons.

Let us consider such a quasi-elastic process. Its amplitude \mathcal{A} is related to the differential cross section through the formula

$$\frac{d\sigma}{dt} = \frac{1}{16\pi} |\mathcal{A}(t)|^2, \quad (4.38)$$

where t is the usual Mandelstam variable and all other dependencies have been omitted. At high energies, it is well-known that the scattering amplitude is essentially imaginary. A Fourier transform of the square root of the differential cross section with respect to the two-dimensional momentum transfer then gives the scattering amplitude for a fixed impact parameter. More specifically, one writes

$$\mathcal{A}(b) = \left| \sqrt{\pi} \int_{-\infty}^0 dt J_0(b\sqrt{|t|}) \sqrt{\frac{d\sigma}{dt}} \right|, \quad (4.39)$$

where J_0 is a Bessel function. This is the formula we will use to extract the b -dependent amplitude from the data. In the case of electroproduction of vector mesons, at high energy, the photon splits into a dipole which scatters off the proton before recombining into a meson. This picture is the Fourier conjugate picture of the collinear factorization studied in Chap. 1. According to this picture, the scattering amplitude \mathcal{A} is the convolution of the photon wave function ψ_{γ^*} , the meson wave-function ψ_V and the dipole amplitude \mathcal{A}_d :

$$\mathcal{A}(y, Q, b) = \int d^2r \psi_{\gamma^*}^\dagger(r, Q) \otimes \psi_V(r) \cdot \mathcal{A}_d(y, 1/r, b). \quad (4.40)$$

Due to the fact that the product of the wave functions $\psi_{\gamma^*}^\dagger \otimes \psi_V$ is peaked around a typical dipole size depending only on the external transverse momentum scales, the scaling of the dipole amplitude \mathcal{A}_d (see Eqs.(4.37)) is transmitted to the photon-proton amplitude \mathcal{A}_{e1} . As it is well-known from both empirical tests [410, 411] and experimental [412] studies, the relevant distance scale at the photon-meson vertex is a combination of the photon virtuality Q and of the meson mass M , namely $1/\sqrt{Q^2 + M^2}$ instead of $1/Q$ as in the case of inclusive scattering. We then obtain from Eqs.(4.36), and (4.37) that the amplitude \mathcal{A}_{e1} should be a function of the scaling variable $\tau = (Q^2 + M^2)(x/x_0)^\lambda$ only.

To check this statement, we applied the transformation (4.39) to the HERA data [256, 413] on electroproduction of ρ^0 vector mesons, where the total cross section as well as the logarithmic t -slope B were quoted. The data can then be represented by the parametrization

$$\frac{d\sigma}{dt} = B\sigma \cdot e^{-B|t|}, \quad (4.41)$$

up to $|t|$ of the order of $|t_{\max}| = 1 \text{ GeV}^2$, which corresponds to the range in which data have been collected.

The scattering amplitude at each impact parameter reads

$$\begin{aligned} \mathcal{A}(y, Q, b) &= \sqrt{\pi} \left| \int_{-|t_{\max}|}^0 dt J_0(b\sqrt{|t|}) \sqrt{B\sigma} \cdot e^{-B|t|/2} + \int_{-\infty}^{-|t_{\max}|} dt J_0(b\sqrt{|t|}) \sqrt{\frac{d\sigma}{dt}} \right| \\ &\simeq \sqrt{\pi} \left| \int_{-\infty}^0 dt J_0(b\sqrt{|t|}) \sqrt{B\sigma} \cdot e^{-B|t|/2} \right| = 2\sqrt{\frac{\pi\sigma}{B}} e^{-b^2/2B} . \end{aligned} \quad (4.42)$$

The experimental points range from $Q^2 = 0.47$ to 27 GeV^2 and $W = 23.4$ to 150 GeV . Due to the lack of data for the slope B for all values of Q^2 and W , we assumed

$$B(Q, W) = 0.6 \cdot \left(\frac{14}{(Q^2 + M^2)^{0.26}} + 1 \right) + 4\alpha' \log(W/75) , \quad (4.43)$$

all quantities appearing in the previous formula being expressed in powers of 1 GeV . The parametrization (4.43) at $W = 75 \text{ GeV}$ is taken from [414]. A logarithmic energy dependence has been added according to the Donnachie-Landshoff parametrization for the soft Pomeron. We set the Regge slope α' to the value 0.25 which is measured in hadron-hadron cross sections. The results on Fig.4.12 are consistent with “local” geometric scaling within uncertainties. Although the kinematical range of the data is not very large, scaling is a non-trivial feature since data points of different Q and W overlap.

Further development based on numerical solution of BK equation in the non forward limit [415] or relying on the traveling waves analysis inspired by statistical physics [416] allowed to push further our analysis. In particular an analysis, this time in the t Mandelstam variable, led to a possible local dependency of the scaling variable on t . Comparison with HERA data seemed to support this idea [417].

4.7 Onium-onium scattering as a gold plated experiment: $\gamma^{(*)}\gamma^{(*)}$ at colliders

This theoretical introduction to QCD in the perturbative Regge limit shows explicitly in what kind of physical processes one may have a look to test this peculiar dynamics, and thus to the observables which should be of interest.

First, these observables should be free of IR divergencies, and as less as possible sensitive to the non-perturbative content of QCD. This can be achieved by selecting external or internal probes with transverse sizes $\ll 1/\Lambda_{QCD}$ (*hard* γ^* , *heavy* meson (J/Ψ , Υ), *energetic* forward jets) or by choosing large t in order to provide the hard scale.

Second, they should be governed by the “*soft*” perturbative dynamics of QCD (BFKL) and *not* by its *collinear* dynamics (DGLAP-ERBL): probes should have comparable transverse sizes. One should therefore select semi-hard processes with $s \gg p_{T_i}^2 \gg \Lambda_{QCD}^2$ where $p_{T_i}^2$ are typical transverse scale, all of the same order.

Third, they should allow control of k_T -spreading, that is the transition from linear to non-linear (saturated regime), meaning the possibility of varying s for fixed transverse size of the probes.

Finally, they should give access both to forward (i.e. inclusive) and non-forward (i.e. exclusive processes) dynamics, both testing linear and non-linear regimes.

$\gamma^{(*)}\gamma^{(*)}$ scattering satisfies all these requirements. This type of process, already illustrated in Fig. 4.1, is among the one to be discussed in the next chapter.

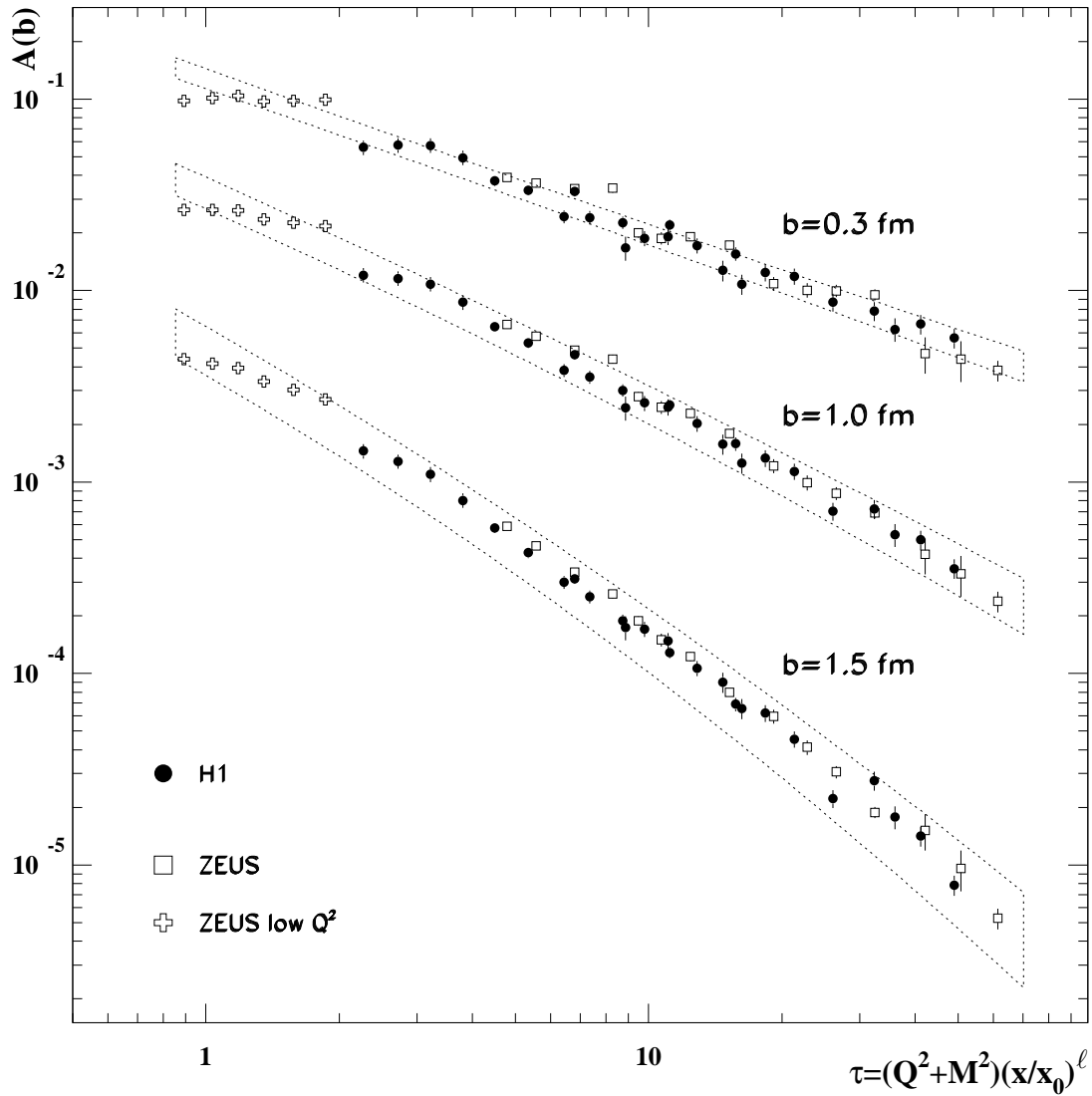


Figure 4.12: Amplitude for 3 different impact parameters as a function of the scaling variable. The dotted contours indicate a rough estimate of the total uncertainty due to experimental error on both the total cross section σ and the slope B , see Ref. [10]. The data points are derived from H1 [413] and ZEUS [256] analysis of diffractive production of ρ^0 mesons. The error bars shown take into account the uncertainty on the measurement of the total cross section only.

Chapter 5

Inclusive and Exclusive tests of BFKL dynamics

Many proposals and tests have been made in order to reveal the dynamics of QCD in the perturbative Regge limit. As we have shown in the previous chapter, the best place for such tests is in principle provided by onium-onium scattering, corresponding to $\gamma^*\gamma^*$ processes at e^+e^- colliders. Nethertheless, many valuable tests can be performed in other colliders, which we will first discuss.

5.1 Hadron-hadron colliders

At high energy hadron colliders like Tevatron or LHC, tests are feasible, when using specific processes involving hard jets in order to justify the applicability of perturbative QCD. Jet reconstruction is by itself a very non-trivial problem, involving jet algorithms (cone and k_t are the most popular one) whose implementation will not discuss here. It will be enough for us to know that a jet can basically be described in terms of its pseudo-rapidity, its transverse energy and its azimuthal angle, which can be related to standard variables of a theoretician [418].

The pseudo-rapidity of a particle is defined by

$$\eta = -\ln \tan \frac{\theta}{2} \quad (5.1)$$

where θ is the angle between the particle momentum \vec{p} and the beam, or equivalently, by trivial trigonometric transformations,

$$\text{ch } \eta = \frac{1}{\sin \theta}. \quad (5.2)$$

This can be equivalently written in terms of the momentum of the particle as

$$\eta = \frac{1}{2} \ln \frac{|\vec{p}| + p_L}{|\vec{p}| - p_L} \quad (5.3)$$

where p_L is the \vec{p} component along the beam axis, as can be seen easily by combining the relation $\tan(\theta/2) = (\sin \theta)/(1 + \cos \theta)$ with $\cos \theta = p_L/|\vec{p}|$. In most practical cases, the mass of the particle can be neglected, and the pseudo-rapidity then equals the rapidity defined by

$$y = \frac{1}{2} \ln \frac{E + p_L}{E - p_L} = \frac{1}{2} \ln \frac{p_+}{p_-}, \quad (5.4)$$

which we already used within our discussion of the BFKL equation. From the fact that Eq.(5.4) is equivalent to

$$\text{th } y = \frac{p_L}{E} \quad (5.5)$$

the name of rapidity is clear, since it equals the usual rapidity used to parametrize the longitudinal boost:

$$(E_T, p_T, 0) \longrightarrow (E, p_T, p_L) \quad (5.6)$$

where $E_T = \sqrt{m^2 + p_T^2}$ (also usually called transverse mass, and denoted m_T in the literature), with the boost

$$E = \cosh \eta E_T \quad (5.7)$$

$$p_L = \sinh \eta E_T. \quad (5.8)$$

One can thus write, from the fact that $\cos \theta = \text{th } \eta$,

$$E_T = E \sin \theta \quad (5.9)$$

$$p_L = |\vec{p}| \text{th } \eta \sim E \cos \theta, \quad (5.10)$$

where the last approximation is valid in the zero mass limit. The relation between “experimentally oriented” variables and “theoretically oriented” variables at the cross-section level is obtained from the straightforward expression of the jacobian, giving

$$\frac{d\sigma}{dE d\theta} = \frac{d\sigma}{dE_T d\eta}. \quad (5.11)$$

Note that the difference in the rapidity of two particles is independent of Lorentz boosts along the beam axis. Indeed, in terms of the light-cone variables

$$p_{\pm} = \frac{1}{\sqrt{2}}(E \pm p_L),$$

a Lorentz transform along the beam axis reads

$$\begin{aligned} p'_+ &= e^{\phi} p_+ \\ p'_- &= e^{-\phi} p_-. \end{aligned} \quad (5.12)$$

Thus, the rapidity transforms as

$$y' = y + \phi \quad (5.13)$$

which shows that the *relative* rapidity is unchanged. In hadron collider physics, the rapidity (or pseudorapidity) is widely used, instead of the polar angle θ , due to the famous rapidity plateau which states that particle production is almost constant as a function of rapidity.

5.1.1 Mueller-Navelet jets

Based on [W27], to be submitted

This test of BFKL is based on the measure for two jets at large p_T (hard scale), such that $s \gg p^2 \gg \Lambda_{\text{QCD}}^2$, separated by a large rapidity $\Delta\eta$, including possible activity between the two observed jets, as illustrated in Fig. 5.1. The idea is to consider two jets of similar p_T in order to minimize the effect of collinear resummation [419]. From a lowest order treatment it is clear that these two jets should be almost back-to-back, in the very forward and very backward regions.

On the other hand, the large value of $\Delta\eta = \ln(s/p^2)$ should exemplify the effect of BFKL dynamics, due to possible emission of gluons between them (thus the Pomeron contributes there at $t = 0$ at the level of the cross-section), leading to enhanced terms which sums up as $\sum(\alpha_s \Delta\eta)^n$ (LL), $\alpha_s \sum(\alpha_s \Delta\eta)^n$ (NLL), etc..., leading to a power-like rise for the cross section. However, to realize this growth as a manifestation of multi-Regge kinematics is very difficult since it is drastically damped by the behavior of the parton distribution functions (PDFs) when $x \rightarrow 1$. A possible way out is to fix the PDFs and to vary the center-of-mass energy of the hadron collider itself, and thereby vary the rapidity difference, $\Delta\eta$, between the two tagged jets. BFKL predicts a behavior of the cross sections of the form $\sigma \sim \exp(\alpha - 1)Y/\sqrt{Y}$ with α being the intercept. The $D0$ collaboration analyzed data taken at the Tevatron $p\bar{p}$ -collider from two periods of measurement at different energies $\sqrt{s} = 630$ and 1800 GeV. The ratio of the two dijet cross-sections measured at these two different energies can then be expected to be almost PDF-independent. From these they extracted an intercept of $1.65 \pm .07$ [420], an higher value than the LL BFKL prediction, which for typical kinematics of $D0$ experiment should rather give an intercept of 1.45. It has been argued [421] that the exact experimental and theoretical definitions of the cross sections disagreed making the interpretation of the results cumbersome. Moreover, this experimental measurement of the intercept only relies on two data points, which is probably not enough to constraint this measure.

Beside the cross section a more exclusive observable within this process drew the attention, namely the azimuthal correlation between these jets [422, 423]. The signal of a BFKL dynamics is a decorrelation of relative azimuthal angle between emitted jets when increasing $\Delta\eta$. Indeed, while a LLQ DGLAP evolution would imply that the two jets would be emitted back-to-back, the fact that more and more (untagged) gluons can be emitted between them when increasing their relative rapidity should lead to a decorrelation of this relative azimuthal angle. Studies were made at LLx [422–424], which overestimates this decorrelation by far. A better agreement with the data [420] could be obtained in the LLx scenario using an event generator which takes into account in a exact way the energy-momentum conservation, which is a subleading effect in pure BFKL approach [425]. On the other hand, the (kinematical) modified LLx BFKL approach [426] (see section 4.5), again based on LLx jet vertices, could also provide some better agreement with the data.

At the same time, an exact fixed NLLQ (α_s^3) Monte Carlo calculation using the program JETRAD [427] lead to a too low estimate of the decorrelation, while the Monte Carlo program HERWIG [428], also based on NLLQ à la DGLAP was in perfect agreement with the data. It should be noted that this last treatment includes some Sudakov resummation effects, which might be important. The inclusion of such effects within a BFKL approach in an open problem which might be of interest for phenomenology.

Starting from first principle from the point of view of Regge and Quasi-multi-Regge kinematics, NLLx [429, 430] and collinear resummed NLLx [431] studies (with LL jet vertices, playing there the role of impact factors) have been performed, improving the situation with respect to pure LLx BFKL, but still leading to a much stronger decorrelation than the one seen by the data. There is at the moment a general belief that the effect of NLLx corrections are important mainly for the Green function, and not for the impact factors. We will show, based on a full NLLx order analysis [W27], that this is not true, and that the inclusion of NLLx jets vertices first stabilizes the cross-section when varying the various parameters (PDFs, renormalization/factorization scale, choice of s_0 scale), leads to a cross-section which has a shape much closer to NLLQ DGLAP type of evolution, and last, that the decorrelation is much weaker, although still rather unstable at this NLLx order treatment. Last, we will investigate the effect of the improved collinear resummation and find a rather minor change in our above conclusions. Technical details of the numerical implementation as well as very detailed curves and tables can be found in Ref. [W27].

Let us briefly give a general picture of the dynamical picture of the process before entering with more detail the full NLLx description which we have obtained. The Mueller–Navelet jets lie at the interface of collinear factorization and BFKL dynamics at a semi-inclusive level (the interface with collinear factorization and BFKL

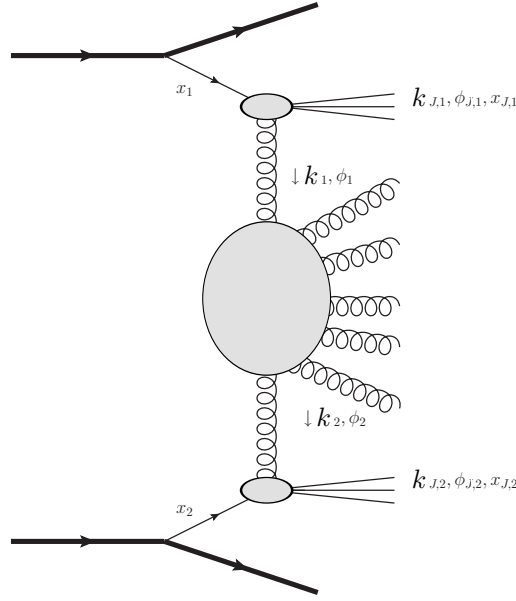


Figure 5.1: kinematics

dynamics within exclusive processes will be studied later in this chapter). The partons emitted from the hadrons carry large longitudinal momentum fractions and, after scattering off each other, they produce the two tagged jets. Due to their large transverse momentum, these jets enforce the partons to be hard and thus to obey collinear factorization. In particular, their scale dependence is governed by the DGLAP evolution equations. Between the jets, on the other hand, we require a large rapidity difference. Therefore, the hadronic cross section factorizes into two usual collinear PDFs convoluted with the partonic cross section, described within the BFKL approach. Thus, from the point of view of the partonic cross section, the incoming partons are treated as on-shell and collinear to the incident hadrons.

LLx calculation

The kinematic setup is schematically shown in Fig. 5.1. The two hadrons collide at a center of mass energy s producing two very forward jets, the transverse momenta of the jets are labeled by Euclidean two dimensional vectors¹ $\mathbf{k}_{J,1}$ and $\mathbf{k}_{J,2}$, while their azimuthal angles are noted as $\phi_{J,1}$ and $\phi_{J,2}$. We will denote the rapidities of the jets by $y_{J,1}$ and $y_{J,2}$.

At any real experiment transverse momenta as well as rapidities are measured within certain intervals. A proper theoretical calculation should take this into account and integrate $|\mathbf{k}_{J,i}|$ and $y_{J,i}$ over the according interval. However, since at the LHC the binning in rapidity and in transverse momentum will be quite narrow [432], we consider the case of fixed rapidities and transverse momenta.

Due to the large longitudinal momentum fractions $x_{J,1}$ and $x_{J,2}$ of the forward jets, collinear factorization holds and the differential cross section can be written as

$$\frac{d\sigma}{d|\mathbf{k}_{J,1}| d|\mathbf{k}_{J,2}| dy_{J,1} dy_{J,2}} = \sum_{a,b} \int_0^1 dx_1 \int_0^1 dx_2 f_a(x_1) f_b(x_2) \frac{d\hat{\sigma}_{ab}}{d|\mathbf{k}_{J,1}| d|\mathbf{k}_{J,2}| dy_{J,1} dy_{J,2}}, \quad (5.14)$$

where $f_{a,b}$ are the standard parton distribution functions (PDFs) of a parton a (b) in the according proton. They depend furthermore on the renormalization scale μ_R and the factorization scale μ_F .

The partonic cross section at lowest order in the collinear factorization approach would just be described by simple two-to-two scattering processes as they are discussed in standard text books. However, the necessary resummation of logarithmically enhanced contributions calls for a description of the partonic cross section in

¹This notation is identical with the notation \underline{k} used in other chapters.

k_T -factorization:

$$\frac{d\hat{\sigma}_{ab}}{d|\mathbf{k}_{J,1}|d|\mathbf{k}_{J,2}|dy_{J,1}dy_{J,2}} = \int d\phi_{J,1}d\phi_{J,2} \int d^2\mathbf{k}_1d^2\mathbf{k}_2 V_a(-\mathbf{k}_1, x_1)G(\mathbf{k}_1, \mathbf{k}_2, \hat{s})V_b(\mathbf{k}_2, x_2), \quad (5.15)$$

where G is the BFKL Green's function depending on $\hat{s} = x_1x_2s$, and the jet vertex V at lowest order reads [316, 433]:

$$V_a^{(0)}(\mathbf{k}, x) = h_a^{(0)}(\mathbf{k})\mathcal{S}_J^{(2)}(\mathbf{k}; x) \quad \text{where} \quad h_a^{(0)}(\mathbf{k}) = \frac{\alpha_s}{\sqrt{2}} \frac{C_{A/F}}{\mathbf{k}^2} \quad (5.16)$$

$$\mathcal{S}_J^{(2)}(\mathbf{k}; x) = \delta\left(1 - \frac{x_J}{x}\right) |\mathbf{k}_J| \delta^{(2)}(\mathbf{k} - \mathbf{k}_J). \quad (5.17)$$

In the definition of $h_a^{(0)}$, $C_A = N_c = 3$ is to be used for initial gluon and $C_F = (N_c^2 - 1)/(2N_c) = 4/3$ for initial quark. Following the notation of Ref. [316, 433], the dependence of V on the jet variables is implicit.

Combining the PDFs with the jet vertices we now write

$$\frac{d\sigma}{d|\mathbf{k}_{J,1}|d|\mathbf{k}_{J,2}|dy_{J,1}dy_{J,2}} = \int d\phi_{J,1}d\phi_{J,2} \int d^2\mathbf{k}_1d^2\mathbf{k}_2 \Phi(\mathbf{k}_{J,1}, x_{J,1}, -\mathbf{k}_1)G(\mathbf{k}_1, \mathbf{k}_2, \hat{s})\Phi(\mathbf{k}_{J,2}, x_{J,2}, \mathbf{k}_2), \quad (5.18)$$

where

$$\Phi(\mathbf{k}_{J,2}, x_{J,2}, \mathbf{k}_2) = \int dx_2 f(x_2) V(\mathbf{k}_2, x_2). \quad (5.19)$$

These Φ are no longer impact factors in the classical sense as they depend, after the convolution in x with the PDF, on the total energy s . In the 'pure' BFKL formula of Eq. (5.15) the longitudinal momentum fractions x_i were just some external parameter and the vertices V would not depend on \hat{s} nor on s .

In respect of the azimuthal decorrelation we want to investigate later, it is useful to define the following coefficients:

$$\mathcal{C}_m \equiv \int d\phi_{J,1}d\phi_{J,2} \cos(m(\phi_{J,1} - \phi_{J,2} - \pi)) \int d^2\mathbf{k}_1d^2\mathbf{k}_2 \Phi(\mathbf{k}_{J,1}, x_{J,1}, -\mathbf{k}_1)G(\mathbf{k}_1, \mathbf{k}_2, \hat{s})\Phi(\mathbf{k}_{J,2}, x_{J,2}, \mathbf{k}_2). \quad (5.20)$$

Knowing these coefficients, one can easily obtain the differential cross section

$$\frac{d\sigma}{d|\mathbf{k}_{J,1}|d|\mathbf{k}_{J,2}|dy_{J,1}dy_{J,2}} = \mathcal{C}_0, \quad (5.21)$$

and the following measure of azimuthal decorrelation

$$\langle \cos(m\varphi) \rangle \equiv \langle \cos(m(\phi_{J,1} - \phi_{J,2} - \pi)) \rangle = \frac{\mathcal{C}_m}{\mathcal{C}_0}. \quad (5.22)$$

By decomposing Φ in terms of the LLx-BFKL eigenfunctions

$$E_{n,\nu}(\mathbf{k}_1) = \frac{1}{\pi\sqrt{2}} (\mathbf{k}_1^2)^{i\nu - \frac{1}{2}} e^{in\phi_1}, \quad (5.23)$$

we can reduce the number of final integrations. To this purpose we define the intermediate coefficients

$$\begin{aligned} \hat{C}_{n_1,\nu_1}^{(1)}(\mathbf{k}_{J,1}, x_{J,1}) &= \int d^2\mathbf{k}_1 \Phi(\mathbf{k}_{J,1}, x_{J,1}, -\mathbf{k}_1) E_{n_1,\nu_1}(\mathbf{k}_1) \\ &= (-1)^{n_1} \int d^2\mathbf{k}' \Phi(\mathbf{k}_{J,1}, x_{J,1}, \mathbf{k}') E_{n_1,\nu_1}(\mathbf{k}') \end{aligned} \quad (5.24)$$

$$\hat{C}_{n_2,\nu_2}^{(2)}(\mathbf{k}_{J,2}, x_{J,2}) = \int d^2\mathbf{k}_2 \Phi(\mathbf{k}_{J,2}, x_{J,2}, \mathbf{k}_2) E_{n_2,\nu_2}^*(\mathbf{k}_2), \quad (5.25)$$

and make use of the following relations between different representations of the BFKL Green's function introducing the – at LLx arbitrary – scale s_0 :

$$G(\mathbf{k}_1, \mathbf{k}_2, \hat{s}) = \int \frac{d\omega}{2\pi i} G_\omega(\mathbf{k}_1, \mathbf{k}_2) \left(\frac{\hat{s}}{s_0} \right)^\omega \quad (5.26)$$

$$\begin{aligned} G_{n_1, n_2, \nu_1, \nu_2; \omega} &= \int d^2\mathbf{k}_1 \int d^2\mathbf{k}_2 E_{n_1, \nu_1}^*(\mathbf{k}_1) G_\omega(\mathbf{k}_1, \mathbf{k}_2) E_{n_2, \nu_2}(\mathbf{k}_2) \\ &= \frac{1}{\omega - \omega(n_1, \nu_1)} \delta_{n_1, n_2} \delta(\nu_1 - \nu_2), \end{aligned} \quad (5.27)$$

where $\omega(n_1, \nu_1)$ is given by the LLx eigenvalue of the BFKL equation, which extends Eq. (4.5) for arbitrary n values, namely

$$\omega(n, \nu) = \bar{\alpha}_s \chi_0 \left(|n|, \frac{1}{2} + i\nu \right) \quad (5.28)$$

$$\chi_0(n, \gamma) = 2\Psi(1) - \Psi\left(\gamma + \frac{n}{2}\right) - \Psi\left(1 - \gamma + \frac{n}{2}\right), \quad (5.29)$$

with $\Psi(x) = \Gamma'(x)/\Gamma(x)$, and $\bar{\alpha}_s = N_c \alpha_s / \pi$ as usual.

With these new definitions we can write Eq. (5.20) as:

$$\begin{aligned} C_m &\equiv \sum_n \int d\nu \int d\phi_{J,1} d\phi_{J,2} \hat{C}_{n,\nu}^{(1)}(\mathbf{k}_{J,1}, x_{J,1}) \left(\frac{\hat{s}}{s_0} \right)^{\omega(n,\nu)} \hat{C}_{n,\nu}^{(2)}(\mathbf{k}_{J,2}, x_{J,2}) \cos(m\varphi) \\ &= (-1)^m \sum_n \int d\nu \left(\frac{\hat{s}}{s_0} \right)^{\omega(n,\nu)} \left[\left(\int d\phi_{J,1} \cos(m\phi_{J,1}) \hat{C}_{n,\nu}^{(1)}(\mathbf{k}_{J,1}, x_{J,1}) \right) \left(\int d\phi_{J,2} \cos(m\phi_{J,2}) \hat{C}_{n,\nu}^{(2)}(\mathbf{k}_{J,2}, x_{J,2}) \right) \right. \\ &\quad \left. + \left(\int d\phi_{J,1} \sin(m\phi_{J,1}) \hat{C}_{n,\nu}^{(1)}(\mathbf{k}_{J,1}, x_{J,1}) \right) \left(\int d\phi_{J,2} \sin(m\phi_{J,2}) \hat{C}_{n,\nu}^{(2)}(\mathbf{k}_{J,2}, x_{J,2}) \right) \right] \end{aligned} \quad (5.30)$$

After a little bit of simple algebra we end up with

$$C_m = (4 - 3\delta_{m,0}) \int d\nu C_{m,\nu}(|\mathbf{k}_{J,1}|, x_{J,1}) C_{m,\nu}^*(|\mathbf{k}_{J,2}|, x_{J,2}) \left(\frac{\hat{s}}{s_0} \right)^{\omega(m,\nu)}. \quad (5.31)$$

Here we have defined

$$C_{m,\nu}(|\mathbf{k}_J|, x_J) = \int d\phi_J d^2\mathbf{k} dx f(x) V(\mathbf{k}, x) E_{m,\nu}(\mathbf{k}) \cos(m\phi_J). \quad (5.32)$$

The origin of the factor $(4 - 3\delta_{m,0})$ in Eq. (5.31) is twofold. Firstly the integration over ϕ_J leads to a $\delta_{m,|n|}$. Secondly when using the addition formula for $\cos(m\varphi)$ to disentangle $\phi_{J,1}$ and $\phi_{J,2}$ also coefficients with sine instead of cosine are generated. While for $m = 0$ they vanish, for $m \neq 0$ they give the same contribution as those with the cosine.

Inserting Eq. (5.16) into Eq. (5.32) we obtain for the LLx Mueller Navelet jet vertices in conformal space

$$C_{m,\nu}^{(\text{LLx})}(|\mathbf{k}_J|, x_J) = \frac{\alpha_s C_{A/F}}{2} (\mathbf{k}_J^2)^{i\nu-1} x_J f_a(x_J) (1 + \delta_{m,0}). \quad (5.33)$$

It is worth to note, that $C_{m,\nu}^{(\text{LLx})}$ depends on m only in a trivial way $(1 + \delta_{m,0})$ such that the azimuthal correlations (5.22) do not depend on the PDFs at all. In the following section we will see, that this changes when one takes into account the NLLx corrections to the jet vertices.

NLLx calculation

The master formulae of the LLx calculation (5.31, 5.32) will also be used for the NLLx calculation. Even though the vertices do not simplify as drastically as in the LLx case, we gain the possibility to calculate for a

limited number of m the coefficients $C_{m,\nu}$ as universal grids in ν . In transverse momentum space one would need a two dimensional grid. Moreover, at NLLx there are some contributions with an additional transverse momentum integration, such that some contributions would be analytic functions in *e.g.* \mathbf{k}_1 while other would be proportional to distributions like $\delta^{(2)}(\mathbf{k}_1 - \mathbf{k}_{J,1})$.

Strong coupling, renormalization scheme and PDFs at NLLx

Based on the $\overline{\text{MS}}$ renormalization scheme, we use the MSTW 2008 PDFs [434] and the two-loop strong coupling in the following form:

$$\alpha_s(\mu_R^2) = \frac{1}{b_0 L} \left(1 + \frac{b_1 \ln L}{b_0^2 L} \right), \quad (5.34)$$

with $L = \ln \mu_R^2 / \Lambda_{\text{QCD}}^2$, and

$$b_0 = \frac{33 - 2N_f}{12\pi}, \quad b_1 = \frac{153 - 19N_f}{24\pi^2}. \quad (5.35)$$

In the following α_s or $\bar{\alpha}_s$ without argument is to be understood as $\alpha_s(\mu_R^2)$ or $\bar{\alpha}_s(\mu_R^2)$ respectively. Since in the MSTW 2008 PDFs μ_R and μ_F are set to be equal, for a consistent calculation we are forced to perform this identification throughout the whole calculation as well.

Jet vertices at NLLx

To calculate the coefficients $C_{m,\nu}$ (5.32) at NLLx level, we take for $V_a(\mathbf{k}, x)$ instead of just the LLx result $V^{(0)}(\mathbf{k}, x)$ (5.16) the full NLLx vertex

$$V_a(\mathbf{k}, x) = V_a^{(0)}(\mathbf{k}, x) + \alpha_s V_a^{(1)}(\mathbf{k}, x). \quad (5.36)$$

The matrix elements needed to calculate the Mueller Navelet jet vertex at next to leading order – namely the partonic $2 \rightarrow 3$ process at tree level and the partonic $2 \rightarrow 2$ process at one loop level – are known since long time. The separation of collinear singularities (to be absorbed by renormalized PDFs) from the BFKL large logarithms in s was performed by Bartels, Vacca and Colferai [316, 433], in terms of a generic and infrared-safe jet algorithm. In this work, we shall apply such procedure to a concrete jet algorithm, namely the cone algorithm, as will be explained below.

We will build on the results obtained in Ref. [316, 433] using their notation as well. In detail, we perform a slightly different collinear subtraction in the terms where an integrated transverse momentum (\mathbf{l}) is rescaled by some longitudinal momentum fraction: we rescale the cutoff parameter $\Lambda = \mu_F$ accordingly. This variant does not change the singular terms, and all the discussion of the arrangement of divergences and subtractions remains unchanged. However the finite part of the subtraction changes such that beside the cutoff functions also the ‘virtual’ part of the vertex changes, *e.g.* the term proportional to $\left(\frac{\ln(1-z)}{1-z} \right)_+$ vanishes completely.²

²We note a misprint in equation (105) of Ref. [316]: in the ‘real’ C_A term the expression $\mathbf{q} - \mathbf{k}$ must be replaced by $\mathbf{q} - z\mathbf{k}$ both in numerator and in the denominator. Just after it, $+ -$ is to be interpreted as $-$.

The final expressions for the NLLx correction to the vertices read:

$$\begin{aligned}
& V_q^{(1)}(\mathbf{k}, x) \\
= & \left[\left(\frac{3}{2} \ln \frac{\mathbf{k}^2}{\Lambda^2} - \frac{15}{4} \right) \frac{C_F}{\pi} + \left(\frac{85}{36} + \frac{\pi^2}{4} \right) \frac{C_A}{\pi} - \frac{5}{18} \frac{N_f}{\pi} - b_0 \ln \frac{\mathbf{k}^2}{\mu^2} \right] V_q^{(0)}(\mathbf{k}, x) \\
& + \int dz \left(\frac{C_F}{\pi} \frac{1-z}{2} + \frac{C_A}{\pi} \frac{z}{2} \right) V_q^{(0)}(\mathbf{k}, xz) \\
& + \frac{C_A}{\pi} \int \frac{d^2 \mathbf{k}'}{\pi} \int dz \left[\frac{1+(1-z)^2}{2z} \right. \\
& \quad \times \left((1-z) \frac{(\mathbf{k}-\mathbf{k}') \cdot ((1-z)\mathbf{k}-\mathbf{k}')}{(\mathbf{k}-\mathbf{k}')^2 ((1-z)\mathbf{k}-\mathbf{k}')^2} h_q^{(0)}(\mathbf{k}') \mathcal{S}_J^{(3)}(\mathbf{k}', \mathbf{k}-\mathbf{k}', xz; x) \right. \\
& \quad \left. \left. - \frac{1}{\mathbf{k}'^2} \Theta(\Lambda^2 - \mathbf{k}'^2) V_q^{(0)}(\mathbf{k}, xz) \right) \right. \\
& \quad \left. - \frac{1}{z(\mathbf{k}-\mathbf{k}')^2} \Theta(|\mathbf{k}-\mathbf{k}'| - z(|\mathbf{k}-\mathbf{k}'| + |\mathbf{k}'|)) V_q^{(0)}(\mathbf{k}', x) \right] \\
& + \frac{C_F}{2\pi} \int dz \frac{1+z^2}{1-z} \int \frac{d^2 \mathbf{l}}{\pi \mathbf{l}^2} \\
& \quad \times \left[\frac{\mathcal{N}C_F}{\mathbf{l}^2 + (\mathbf{1}-\mathbf{k})^2} \left(\mathcal{S}_J^{(3)}(z\mathbf{k} + (1-z)\mathbf{l}, (1-z)(\mathbf{k}-\mathbf{l}), x(1-z); x) \right. \right. \\
& \quad \left. \left. + \mathcal{S}_J^{(3)}(\mathbf{k} - (1-z)\mathbf{l}, (1-z)\mathbf{l}, x(1-z); x) \right) \right. \\
& \quad \left. - \Theta \left(\frac{\Lambda^2}{(1-z)^2} - \mathbf{l}^2 \right) \left(V_q^{(0)}(\mathbf{k}, x) + V_q^{(0)}(\mathbf{k}, xz) \right) \right] \\
& - \frac{2C_F}{\pi} \int dz \left(\frac{1}{1-z} \right) \int \frac{d^2 \mathbf{l}}{\pi \mathbf{l}^2} \left[\frac{\mathcal{N}C_F}{\mathbf{l}^2 + (\mathbf{1}-\mathbf{k})^2} S_J^{(2)}(\mathbf{k}, x) \right. \\
& \quad \left. - \Theta \left(\frac{\Lambda^2}{(1-z)^2} - \mathbf{l}^2 \right) V_q^{(0)}(\mathbf{k}, x) \right], \tag{5.37}
\end{aligned}$$

$$\begin{aligned}
& V_g^{(1)}(\mathbf{k}, x) \\
= & \left[\left(\frac{11}{6} \frac{C_A}{\pi} - \frac{1}{3} \frac{N_f}{\pi} \right) \ln \frac{\mathbf{k}^2}{\Lambda^2} + \left(\frac{\pi^2}{4} - \frac{67}{36} \right) \frac{C_A}{\pi} + \frac{13}{36} \frac{N_f}{\pi} - b_0 \ln \frac{\mathbf{k}^2}{\mu^2} \right] V_g^{(0)}(\mathbf{k}, x) \\
& + \int dz \frac{N_f}{\pi} \frac{C_F}{C_A} z(1-z) V_g^{(0)}(\mathbf{k}, xz) \\
& + \frac{N_f}{\pi} \int \frac{d^2 \mathbf{k}'}{\pi} \int_0^1 dz P_{qg}(z) \left[\frac{h_q^{(0)}(\mathbf{k}')}{(\mathbf{k} - \mathbf{k}')^2 + \mathbf{k}'^2} \mathcal{S}_J^{(3)}(\mathbf{k}', \mathbf{k} - \mathbf{k}', xz; x) \right. \\
& \quad \left. - \frac{1}{\mathbf{k}'^2} \Theta(\Lambda^2 - \mathbf{k}'^2) V_q^{(0)}(\mathbf{k}, xz) \right] \\
& + \frac{N_f}{2\pi} \int \frac{d^2 \mathbf{k}'}{\pi} \int_0^1 dz P_{qg}(z) \frac{\mathcal{N} C_A}{((1-z)\mathbf{k} - \mathbf{k}')^2} \left[z(1-z) \frac{(\mathbf{k} - \mathbf{k}') \cdot \mathbf{k}'}{(\mathbf{k} - \mathbf{k}')^2 \mathbf{k}'^2} \mathcal{S}_J^{(3)}(\mathbf{k}', \mathbf{k} - \mathbf{k}', xz; x) \right. \\
& \quad \left. - \frac{1}{\mathbf{k}^2} \Theta(\Lambda^2 - ((1-z)\mathbf{k} - \mathbf{k}')^2) \mathcal{S}_J^{(2)}(\mathbf{k}, x) \right] \\
& + \frac{C_A}{\pi} \int_0^1 \frac{dz}{1-z} [(1-z)P(1-z)] \int \frac{d^2 \mathbf{l}}{\pi \mathbf{l}^2} \\
& \quad \times \left\{ \frac{\mathcal{N} C_A}{\mathbf{l}^2 + (\mathbf{l} - \mathbf{k})^2} \left[\mathcal{S}_J^{(3)}(z\mathbf{k} + (1-z)\mathbf{l}, (1-z)(\mathbf{k} - \mathbf{l}), x(1-z); x) \right. \right. \\
& \quad \left. \left. + \mathcal{S}_J^{(3)}(\mathbf{k} - (1-z)\mathbf{l}, (1-z)\mathbf{l}, x(1-z); x) \right] \right. \\
& \quad \left. - \Theta \left(\frac{\Lambda^2}{(1-z)^2} - \mathbf{l}^2 \right) \left[V_g^{(0)}(\mathbf{k}, x) + V_g^{(0)}(\mathbf{k}, xz) \right] \right\} \\
& - \frac{2C_A}{\pi} \int_0^1 \frac{dz}{1-z} \int \frac{d^2 \mathbf{l}}{\pi \mathbf{l}^2} \left[\frac{\mathcal{N} C_A}{\mathbf{l}^2 + (\mathbf{l} - \mathbf{k})^2} \mathcal{S}_J^{(2)}(\mathbf{k}, x) - \Theta \left(\frac{\Lambda^2}{(1-z)^2} - \mathbf{l}^2 \right) V_g^{(0)}(\mathbf{k}, x) \right] \\
& + \frac{C_A}{\pi} \int \frac{d^2 \mathbf{k}'}{\pi} \int_0^1 dz \left[P(z) \left((1-z) \frac{(\mathbf{k} - \mathbf{k}') \cdot ((1-z)\mathbf{k} - \mathbf{k}')}{(\mathbf{k} - \mathbf{k}')^2 ((1-z)\mathbf{k} - \mathbf{k}')^2} h_g^{(0)}(\mathbf{k}') \right. \right. \\
& \quad \left. \left. \times \mathcal{S}_J^{(3)}(\mathbf{k}', \mathbf{k} - \mathbf{k}', xz; x) - \frac{1}{\mathbf{k}'^2} \Theta(\Lambda^2 - \mathbf{k}'^2) V_g^{(0)}(\mathbf{k}, xz) \right) \right. \\
& \quad \left. - \frac{1}{z(\mathbf{k} - \mathbf{k}')^2} \Theta(|\mathbf{k} - \mathbf{k}'| - z(|\mathbf{k} - \mathbf{k}'| + |\mathbf{k}'|)) V_g^{(0)}(\mathbf{k}', x) \right]. \tag{5.38}
\end{aligned}$$

Here N_f denotes the number of active quark flavors, $b_0 = (11N_c - 2N_f)/(12\pi)$, and $\mathcal{N} = \alpha_s/\sqrt{2}$. A priori, the factorization scale $\mu_F = \Lambda$ and the renormalization scale $\mu_R = \mu$ are independent of each other even though in the end we will set them equal.

Jet definition

For a concrete calculation of Mueller Navelet jet production one also has to choose a concrete jet algorithm obeying the property of infra-red safety, as required by the general procedure of Refs. [316, 433]. Two of the

most common and mostly used ones are the cone algorithm

$$\begin{aligned} \mathcal{S}_J^{(3,\text{cone})}(\mathbf{k}', \mathbf{k} - \mathbf{k}', xz; x) &= \mathcal{S}_J^{(2)}(\mathbf{k}, x) \Theta \left(\left[\frac{|\mathbf{k} - \mathbf{k}'| + |\mathbf{k}'|}{\max(|\mathbf{k} - \mathbf{k}'|, |\mathbf{k}'|)} R_{\text{cone}} \right]^2 - [\Delta y^2 + \Delta \phi^2] \right) \\ &+ \mathcal{S}_J^{(2)}(\mathbf{k} - \mathbf{k}', xz) \Theta \left([\Delta y^2 + \Delta \phi^2] - \left[\frac{|\mathbf{k} - \mathbf{k}'| + |\mathbf{k}'|}{\max(|\mathbf{k} - \mathbf{k}'|, |\mathbf{k}'|)} R_{\text{cone}} \right]^2 \right) \\ &+ \mathcal{S}_J^{(2)}(\mathbf{k}', x(1-z)) \Theta \left([\Delta y^2 + \Delta \phi^2] - \left[\frac{|\mathbf{k} - \mathbf{k}'| + |\mathbf{k}'|}{\max(|\mathbf{k} - \mathbf{k}'|, |\mathbf{k}'|)} R_{\text{cone}} \right]^2 \right), \end{aligned} \quad (5.39)$$

as it has been adapted for NLLx calculation in Ref. [435], and the k_T algorithm

$$\begin{aligned} \mathcal{S}_J^{(3,k_T)}(\mathbf{k}', \mathbf{k} - \mathbf{k}', xz; x) &= \mathcal{S}_J^{(2)}(\mathbf{k}, x) \Theta(R_{k_T}^2 - [\Delta y^2 + \Delta \phi^2]) \\ &+ \mathcal{S}_J^{(2)}(\mathbf{k} - \mathbf{k}', xz) \Theta([\Delta y^2 + \Delta \phi^2] - R_{k_T}^2) \\ &+ \mathcal{S}_J^{(2)}(\mathbf{k}', x(1-z)) \Theta([\Delta y^2 + \Delta \phi^2] - R_{k_T}^2), \end{aligned} \quad (5.40)$$

where

$$\Delta y = \log \left(\frac{1-z}{z} \frac{|\mathbf{k} - \mathbf{k}'|}{|\mathbf{k}'|} \right), \quad \Delta \phi = \arccos \frac{\mathbf{k}'(\mathbf{k} - \mathbf{k}')}{\sqrt{\mathbf{k}'^2(\mathbf{k} - \mathbf{k}')^2}}. \quad (5.41)$$

In our study we will use the cone algorithm with a cone size of $R_{\text{cone}} = .5$ as it probably will be used in a CMS analysis at the LHC [432].

LL subtraction and s_0

The requirement of a BFKL calculation that the two scattering objects have a similar hard scale is reflected by the fact that in this standard situation of BFKL physics the energy scale s_0 can be written as a product of two energy scales each assigned to one of these scattering objects.

$$s_0 = \sqrt{s_{0,1}s_{0,2}} \quad (5.42)$$

In Ref. [316, 433] the energy scale $s_{0,i}$ (assigned to the Mueller Navelet jet) was chosen as $(|\mathbf{k}_J| + |\mathbf{k}_J - \mathbf{k}|)^2$. While \mathbf{k} is integrated over, it is preferable to let s_0 depend only on external scales. Also $\hat{s} = x_1 x_2 s$ is in fact not an external scale since also the longitudinal momentum fractions x_1 and x_2 are integrated over. Therefore, we want to change to a new s'_0 :

$$s_{0,1} = (|\mathbf{k}_{J,1}| + |\mathbf{k}_{J,1} - \mathbf{k}_1|)^2 \quad \rightarrow \quad s'_{0,1} = \frac{x_1^2}{x_{J,1}^2} \mathbf{k}_{J,1}^2 \quad (5.43)$$

$$s_{0,2} = (|\mathbf{k}_{J,2}| + |\mathbf{k}_{J,2} - \mathbf{k}_2|)^2 \quad \rightarrow \quad s'_{0,2} = \frac{x_2^2}{x_{J,2}^2} \mathbf{k}_{J,2}^2 \quad (5.44)$$

$$\frac{\hat{s}}{s_0} \quad \rightarrow \quad \frac{\hat{s}}{s'_0} = \frac{x_{J,1} x_{J,2} s}{|\mathbf{k}_{J,1}| \cdot |\mathbf{k}_{J,2}|} = e^{y_{J,1} - y_{J,2}} \equiv e^Y, \quad (5.45)$$

where we introduced the rapidities $y_{J,1/2}$ of the Mueller Navelet jets, and their relative rapidity $Y = y_{J,1} - y_{J,2}$.

The energy scale s_0 is a free parameter in the calculation. However, like for the renormalization scale at NLLx level a change of it does not go without consequences. In fact, a change of $s_0 \rightarrow s'_0$ in the Green's function has to be accompanied by an according correction term to the impact factors [436, 437]:

$$\Phi_{\text{NLLx}}(\mathbf{k}_i; s'_{0,i}) = \Phi_{\text{NLLx}}(\mathbf{k}_i; s_{0,i}) + \int d^2\mathbf{k}' \Phi_{\text{LLx}}(\mathbf{k}'_i) \mathcal{K}_{\text{LLx}}(\mathbf{k}'_i, \mathbf{k}_i) \frac{1}{2} \ln \frac{s'_{0,i}}{s_{0,i}}, \quad (5.46)$$

with \mathcal{K}_{LLx} being the LLx BFKL kernel. Due to the Dirac delta distribution $\delta(1 - x_{J,i}/x_i)$ in the jet algorithm inside Φ the ratio of longitudinal momentum fractions in $s'_{0,i}$ reduces to 1 and hence the logarithm in Eq. (5.46) vanishes for $\mathbf{k}'_i = \mathbf{k}_i$ such that only the real part of the kernel contributes.

A subsequent change of $s_{0,i}$ by just a factor λ can be easily performed at the very end because of the use of BFKL eigenfunctions:

$$\begin{aligned}
& C_{m,\nu}(|\mathbf{k}_J|, x_J; s_0'' = \lambda s_0') - C_{m,\nu}(|\mathbf{k}_J|, x_J; s_0') \\
&= \int d\phi_J d^2\mathbf{k} \int d^2\mathbf{k}' dx f(x) V^{(0)}(\mathbf{k}', x) \mathcal{K}(\mathbf{k}', \mathbf{k}) E_{m,\nu}(\mathbf{k}) \cos(m\phi_J) \frac{1}{2} \ln \frac{s_0''}{s_0'} \\
&= \int d\phi_J \int d^2\mathbf{k}' dx f(x) V^{(0)}(\mathbf{k}', x) \bar{\alpha}_s \chi_0 \left(m, \frac{1}{2} + i\nu \right) E_{m,\nu}(\mathbf{k}') \cos(m\phi_J) \frac{1}{2} \ln \lambda \\
&= \bar{\alpha}_s \chi_0 \left(m, \frac{1}{2} + i\nu \right) C_{m,\nu}^{(\text{LLx})}(|\mathbf{k}_J|, x_J) \frac{1}{2} \ln \lambda. \tag{5.47}
\end{aligned}$$

The LLQ subtraction (denoted LL in formula below), *i.e.* the terms multiplied by $\Theta(|\mathbf{k}-\mathbf{k}'|-z(|\mathbf{k}-\mathbf{k}'|+|\mathbf{k}'|))$ in Eqs. (5.37, 5.38), cancels some part in the limit of the additional emission having a big rapidity distance to the jet. In fact, numerically this cancellation works very poorly due to an azimuthal averaging which has been performed for the LLQ subtraction. A significant improvement can be obtained by omitting this averaging and introducing new LLQ subtraction terms

$$V_{\text{q; LL subtraction}}^{(1)} = -\frac{C_A}{\pi^2} \frac{1}{z(\mathbf{k}-\mathbf{k}')^2} \frac{(\mathbf{k}-\mathbf{k}')(\mathbf{k}-\mathbf{k}'-z\mathbf{k}')}{(\mathbf{k}-\mathbf{k}')^2(\mathbf{k}-\mathbf{k}'-z\mathbf{k}')^2} V_{\text{q}}^{(0)}(\mathbf{k}', x) \tag{5.48a}$$

$$V_{\text{g; LL subtraction}}^{(1)} = -\frac{C_A}{\pi^2} \frac{1}{z(\mathbf{k}-\mathbf{k}')^2} \frac{(\mathbf{k}-\mathbf{k}')(\mathbf{k}-\mathbf{k}'-z\mathbf{k}')}{(\mathbf{k}-\mathbf{k}')^2(\mathbf{k}-\mathbf{k}'-z\mathbf{k}')^2} V_{\text{g}}^{(0)}(\mathbf{k}', x). \tag{5.48b}$$

As a consequence $s_{0,i}$ changes from $s_{0,i} = (|\mathbf{k}_{J,i}| + |\mathbf{k}_{J,i} - \mathbf{k}_i|)^2$ to $s_{0,i} = (\mathbf{k}_i - 2\mathbf{k}_{J,i})^2$. It is also possible to use

$$\tilde{V}_{\text{q; LL subtraction}}^{(1)} = -\frac{C_A}{\pi^2} \frac{1}{z(\mathbf{k}-\mathbf{k}')^2} \frac{(\mathbf{k}-\mathbf{k}')(\mathbf{k}-\mathbf{k}'-z\mathbf{k})}{(\mathbf{k}-\mathbf{k}')^2(\mathbf{k}-\mathbf{k}'-z\mathbf{k})^2} V_{\text{q}}^{(0)}(\mathbf{k}', x) \tag{5.49a}$$

$$\tilde{V}_{\text{g; LL subtraction}}^{(1)} = -\frac{C_A}{\pi^2} \frac{1}{z(\mathbf{k}-\mathbf{k}')^2} \frac{(\mathbf{k}-\mathbf{k}')(\mathbf{k}-\mathbf{k}'-z\mathbf{k})}{(\mathbf{k}-\mathbf{k}')^2(\mathbf{k}-\mathbf{k}'-z\mathbf{k})^2} V_{\text{g}}^{(0)}(\mathbf{k}', x), \tag{5.49b}$$

which are slightly inferior concerning the numerical performance but giving a s_0 change from $s_{0,i} = (|\mathbf{k}_{J,i}| + |\mathbf{k}_{J,i} - \mathbf{k}_i|)^2$ to $s_{0,i} = \mathbf{k}_{J,i}^2$.

We have checked that all three possible subtraction terms after combining them with the according correction term (5.46) lead to the same result. For reasons of numerical performance we have chosen Eqs. (5.48).

BFKL Green's function at NLLx

Last but not least, we also have to take the BFKL Green's function at NLLx level. The key to the Green's function is the BFKL kernel at NLLx [307, 308]. While at LLx the BFKL equation is conformal invariant, at NLLx it is not such that in fact the LLx eigenfunctions $E_{n,\nu}$ (5.23) are strictly speaking not eigenfunctions of the NLLx kernel. Nevertheless, the action of the NLLx BFKL kernel on the eigenfunctions has been calculated in Ref. [438]. The status of the $E_{n,\nu}$ being eigenfunctions formally can be saved if one accepts the eigenvalue to become an operator containing a derivative with respect to ν [429, 430, 439]. In combination with the impact factors the derivate acts on the impact factors and effectively leads to a contribution to the eigenvalue which depends on the impact factors [429, 430, 439, 440]:

$$\begin{aligned}
\omega(n, \nu) = & \bar{\alpha}_s \chi_0 \left(|n|, \frac{1}{2} + i\nu \right) + \bar{\alpha}_s^2 \left[\chi_1 \left(|n|, \frac{1}{2} + i\nu \right) \right. \\
& \left. - \frac{\pi b_0}{2N_c} \chi_0 \left(|n|, \frac{1}{2} + i\nu \right) \left\{ -2 \ln \mu_R^2 - i \frac{\partial}{\partial \nu} \ln \frac{C_{n,\nu}(|\mathbf{k}_{J,1}|, x_{J,1})}{C_{n,\nu}(|\mathbf{k}_{J,2}|, x_{J,2})} \right\} \right], \tag{5.50}
\end{aligned}$$

where

$$\begin{aligned}
\chi_1(n, \gamma) = & \mathcal{S}\chi_0(n, \gamma) + \frac{3}{2}\zeta(3) - \frac{\beta_0}{8N_c}\chi_0^2(n, \gamma) \\
& + \frac{1}{4} \left[\psi''\left(\gamma + \frac{n}{2}\right) + \psi''\left(1 - \gamma + \frac{n}{2}\right) - 2\phi(n, \gamma) - 2\phi(n, 1 - \gamma) \right] \\
& - \frac{\pi^2 \cos(\pi\gamma)}{4 \sin^2(\pi\gamma)(1 - 2\gamma)} \left\{ \left[3 + \left(1 + \frac{N_f}{N_c^3}\right) \frac{2 + 3\gamma(1 - \gamma)}{(3 - 2\gamma)(1 + 2\gamma)} \right] \delta_{n,0} \right. \\
& \left. - \left(1 + \frac{N_f}{N_c^3}\right) \frac{\gamma(1 - \gamma)}{2(3 - 2\gamma)(1 + 2\gamma)} \delta_{n,2} \right\}, \tag{5.51}
\end{aligned}$$

with the constant $\mathcal{S} = (4 - \pi^2 + 5\beta_0/N_c)/12$. $\zeta(n) = \sum_{k=1}^{\infty} k^{-n}$ is the Riemann zeta function while the function ϕ reads

$$\begin{aligned}
\phi(n, \gamma) = & \sum_{k=0}^{\infty} \frac{(-1)^{k+1}}{k + \gamma + \frac{n}{2}} \left(\psi'(k + n + 1) - \psi'(k + 1) \right. \\
& \left. + (-1)^{k+1} [\beta'(k + n + 1) + \beta'(k + 1)] + \frac{\psi(k + 1) - \psi(k + n + 1)}{k + \gamma + \frac{n}{2}} \right), \tag{5.52}
\end{aligned}$$

with

$$\beta'(\gamma) = \frac{1}{4} \left[\psi'\left(\frac{1 + \gamma}{2}\right) - \psi'\left(\frac{\gamma}{2}\right) \right]. \tag{5.53}$$

At NLLx accuracy, only the leading order vertex coefficients (5.33) enter in the derivative term of (5.50).

$$-2 \ln \mu_R^2 - i \frac{\partial}{\partial \nu} \ln \frac{C_{n,\nu}^{(\text{LLx})}(|\mathbf{k}_{J,1}|, x_{J,1})}{C_{n,\nu}^{(\text{LLx})}(|\mathbf{k}_{J,2}|, x_{J,2})} = 2 \ln \frac{|\mathbf{k}_{J,1}| \cdot |\mathbf{k}_{J,2}|}{\mu_R^2} \tag{5.54}$$

Collinear improved Green's function

As we shortly explained in Sec. 4.5, there are methods to improve the NLLx BFKL kernel for $n = 0$ by imposing compatibility with the DGLAP equation [61–64] in the collinear limit [318–320, 329]. They are known under the name ω -shift because essentially poles in $\gamma = 1/2 + i\nu$ and $1 - \gamma$ are shifted by $\omega/2$ with some compensation terms ensuring that the result is not changed at fixed order (having in mind that $\omega \sim \bar{\alpha}_s \chi_0$). The different attempts are very similar, and here we use the most transparent method presented in [318]. In fact, based on previous experience [430, 440] we use Scheme 3 of [318]. The new kernel $\bar{\alpha}_s \chi^{(1)}(\gamma, \omega)$ with shifted poles replaces $\bar{\alpha}_s \chi_0(\gamma, 0) + \bar{\alpha}_s^2 \chi_1(\gamma, 0)$ and $\omega(0, \nu)$ is obtained by solving the implicit equation

$$\omega(0, \nu) = \bar{\alpha}_s \chi^{(1)}(\gamma, \omega(0, \nu)) \tag{5.55}$$

for $\omega(n, \nu)$ numerically.

In general the additional ν -derivative term makes it necessary to recalculate the coefficients $d_{1,k}$ (defined in Ref. [318]) but in our case the vertex does not contain any poles in γ nor in $1 - \gamma$ leaving the coefficients $d_{1,k}$ unchanged. This was obtained numerically by using a closed contour in γ -plane around 0 or around 1, and numerically integrate integer powers of γ or $1 - \gamma$ times the vertex. Based on Cauchy formula used here in reverse manner, one can then obtain a numerical evaluation of the residue of arbitrary order, and show that they actually vanish. By introducing an ω dependence in the eigenvalue the pole in (5.27) is no longer a simple one such that residue in fact reads

$$G_{0,0,\nu_1,\nu_2}(\hat{s}) = \left(1 - \frac{\partial \chi^{(1)}(\frac{1}{2} + i\nu_1, \omega)}{\partial \omega} \Big|_{\omega=\omega(0,\nu_1)} \right)^{-1} \left(\frac{\hat{s}}{s_0} \right)^{\omega(0,\nu_1)} \delta(\nu_1 - \nu_2). \tag{5.56}$$

Results

We focus on the symmetric situation $|\mathbf{k}_{J,1}| = |\mathbf{k}_{J,2}|$ and study the two cases $|\mathbf{k}_{J,1}| = 35$ GeV, and $|\mathbf{k}_{J,1}| = 50$ GeV. Due to our method of calculation it is easy to use the coefficient grids of these two cases and combine them to study the asymmetric scenario of $|\mathbf{k}_{J,1}| = 35$ GeV, $|\mathbf{k}_{J,2}| = 50$ GeV (plus the ‘mirrored’ process $|\mathbf{k}_{J,1}| = 50$ GeV, $|\mathbf{k}_{J,2}| = 35$ GeV) even though in so doing one mixes different choices for μ_R . But since α_s only varies by $\sim 4\%$ between 35 GeV and 50 GeV we give the according result as well³.

In all cases we choose the number of active flavors to be five ($N_f = 5$) with $\Lambda_{\text{QCD}} = 221.2$ MeV such that $\alpha_s(M_Z^2) = 0.1176$.

The Monte Carlo integration [441] itself is error-prone. However, as we show in what follows, there are more serious uncertainties due to the renormalization scale μ_R which we choose as $\mu_R = \sqrt{|\mathbf{k}_{J,1}| \cdot |\mathbf{k}_{J,2}|}$. To study the dependence on it we vary μ_R by factors 2 and 1/2 respectively. The same we do for the energy scale $\sqrt{s_0}$.

We investigate the uncertainty rooted in the uncertainty of PDFs formula for asymmetric errors as defined in Eqs. (51,52) of [434] with the eigenvector set ensuring all data sets are described within their 90% confidence level limits.

The symmetric case $|\mathbf{k}_{J,1}| = |\mathbf{k}_{J,2}| = 35$ GeV

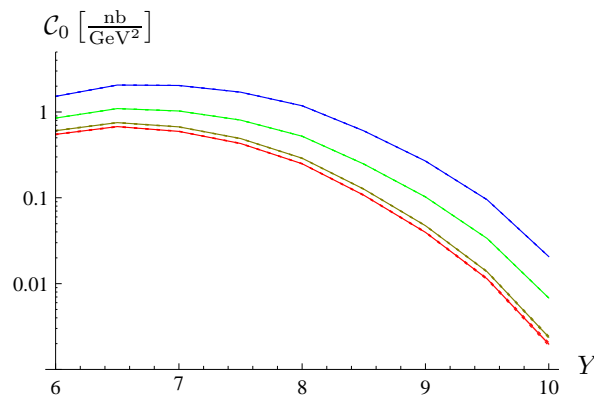


Figure 5.2: Differential cross section in dependence on Y for $|\mathbf{k}_{J,1}| = |\mathbf{k}_{J,2}| = 35$ GeV. Blue shows the pure LLx result, brown the pure NLLx result, green the combination of LLx vertices with the collinear improved NLLx Green’s function, red the full NLLx vertices with the collinear improved NLLx Green’s function. The errors due to the Monte Carlo integration – though hardly visible – are given as error bands.

The first thing to look at is the differential cross section as defined in Eq. (5.21). The result of our calculation is shown in Fig. 5.2. The NLLx correction to the vertices damps the cross section drastically even though the full NLLx BFKL calculation still leads to a larger cross section than standard Monte Carlo generators [432]. The purely numerical error due to the Monte Carlo integration of the NLLx vertices is below 1%. We varied the renormalization and factorization scale by factors 2 and 1/2 to investigate the μ_R dependence. A full scan over this interval is not possible due to the CPU time consumption of the evaluation for a single choice of μ_R . The results are displayed in Fig. 5.3. As one would expect, the full NLLx result depends less on μ_R than the LLx result or the combination of LLx vertices and NLLx Green’s function which was so far state-of-the-art [430,431]. However, after inclusion of the NLLx vertices the μ_R dependence is no longer monotone. Another important energy scale is s_0 introduced by the Mellin transformation from energy to ω space which is necessary to formulate the BFKL equation. Like μ_R it is an artificial scale which in an all order calculation would not affect the result. Indeed, the dependence is reduced when the NLLx corrections to the vertices are taken into account (see Fig. 5.4). The dependence on PDF uncertainties is shown in Fig. 5.5.

The azimuthal decorrelation has often been predicted to be a striking feature of BFKL physics but our inclusion of NLLx vertices shows an enormous correlation in the azimuthal angles shown in Fig. 5.6, rather close from the typical values predicted by LLQ Monte Carlos PYTHIA [442] and HERWIG [428], used for CMS studies [432].

³Detailed tables of our results, for precise comparisons with other approaches, are explicitly provided in Ref. [W27].

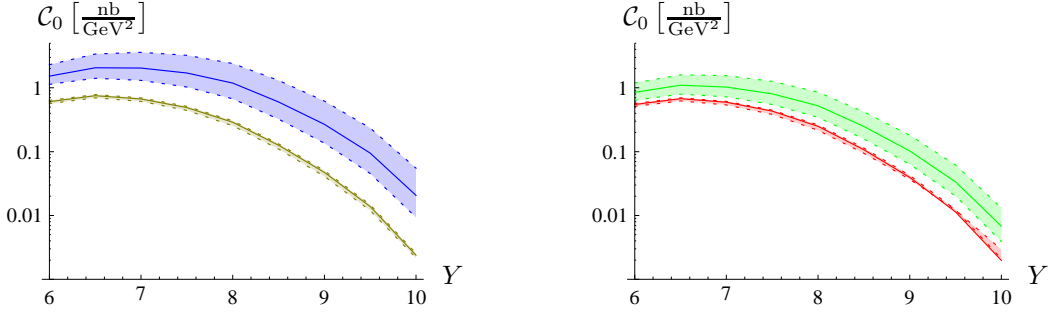


Figure 5.3: Effect of changing $\mu_R = \mu_F$ by factors 2 and 1/2 respectively on the differential cross section in dependence on Y for $|\mathbf{k}_{J,1}| = |\mathbf{k}_{J,2}| = 35$ GeV. Blue shows the pure LLx result, brown the pure NLLx result, green the combination of LLx vertices with the collinear improved NLLx Green's function, red the full NLLx vertices with the collinear improved NLLx Green's function.

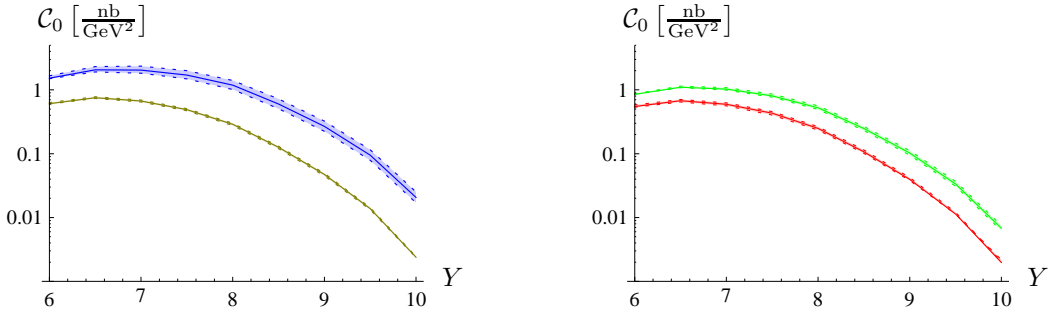


Figure 5.4: Effect of changing $\sqrt{s_0}$ by factors 2 and 1/2 respectively on the differential cross section in dependence on Y for $|\mathbf{k}_{J,1}| = |\mathbf{k}_{J,2}| = 35$ GeV. Blue shows the pure LLx result, brown the pure NLLx result, green the combination of LLx vertices with the collinear improved NLLx Green's function, red the full NLLx vertices with the collinear improved NLLx Green's function.

Note that HERWIG has the tendency to predict more decorrelation, presumably because since it implements more radiations than PYTHIA, it has the phenomenological effect to involve some kind of NLLQ corrections, which enhance the decorrelation. The numeric uncertainties for the calculations including the NLLx vertices is here larger because the coefficients $C_{n,\nu}$ contain an azimuthal integration which in the case of $n = 0$ becomes trivial while for $n = 1$ has to be carried out. Not only is the Y dependence much flatter for the NLLx vertices. But the mean value for $\cos\varphi$ itself is very close to 1. The μ_R dependence (see Fig. 5.7) is puzzling compared to that of just C_0 (see Fig. 5.3) and C_1 (see Fig. 5.13) since the inclusion of the NLLx vertices does not reduce the μ_R dependence. A similar behavior can be observed for the s_0 dependence (see Figs. 5.8 and 5.14). See Ref. [W27] for similar curves for the C_2 coefficient.

Numerically this effect is rooted in the complete vanishing of changes of LLx vertices in ratios C_m/C_n since these changes are not very sensitive on n in case of LLx vertices. In contrast, the NLLx correction – especially the LL subtraction – is very large (and negative) for the $n = 0$ component while of minor significance for $n > 0$. However, comparing the pure LLx with the pure NLLx calculation the relative change in fact is reduced for the NLLx one. For both scales, the curves exceeding 1 belong to smaller scales which seem to be very disfavored in full NLL BFKL calculations as already discussed in [328, 439, 443]. The dependence on the PDFs completely drops out for LLx vertices and also for NLLx vertices it is negligible (see Ref. [W27] for the corresponding figure).

It has been proposed to rather look at ratios C_m/C_n with $m \neq 0 \neq n$ [430] since concerning the Green's

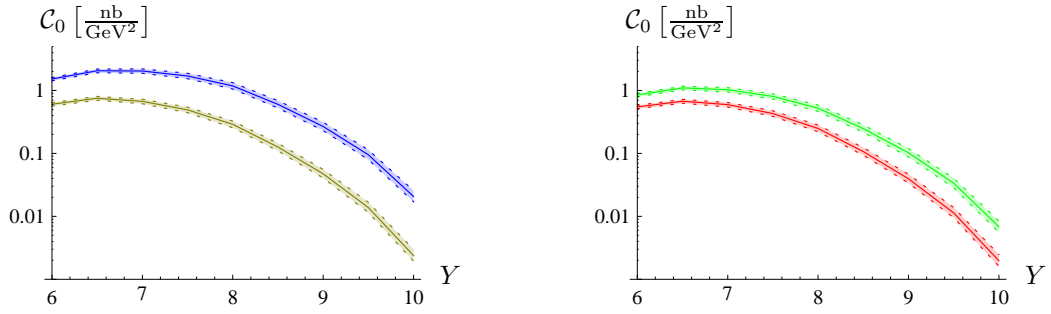


Figure 5.5: Effect of the PDF errors on the differential cross section in dependence on Y for $|\mathbf{k}_{J,1}| = |\mathbf{k}_{J,2}| = 35 \text{ GeV}$. Blue shows the pure LLx result, brown the pure NLLx result, green the combination of LLx vertices with the collinear improved NLLx Green's function, red the full NLLx vertices with the collinear improved NLLx Green's function.

function the largest uncertainty is associated with the $n = 0$ component. This observation is not altered by the inclusion of NLLx vertices (see Fig. 5.12 and Ref. [W27] for the corresponding figures for the $\mu_R = \mu_F, \sqrt{s_0}$ and PDF dependency).

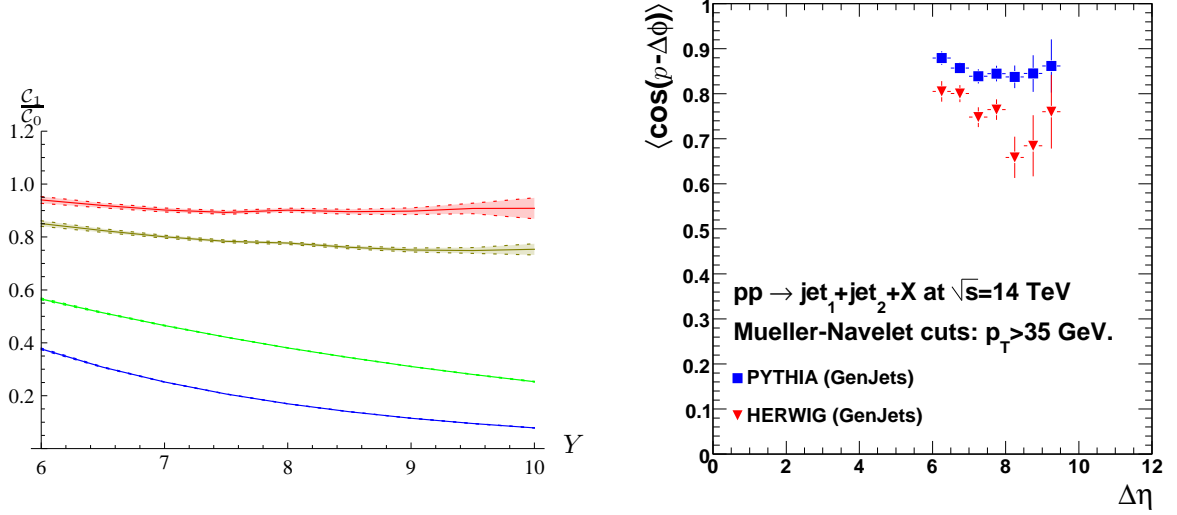


Figure 5.6: Left: $\langle \cos \varphi \rangle$ in dependence on Y for $|\mathbf{k}_{J,1}| = |\mathbf{k}_{J,2}| = 35$ GeV. Blue shows the pure LLx result, brown the pure NLLx result, green the combination of LLx vertices with the collinear improved NLLx Green's function, red the full NLLx vertices with the collinear improved NLLx Green's function. The errors due to the Monte Carlo integration are given as error bands. Right: Monte Carlo results of the CMS Collaboration, based on a LLQ approach. Figure from Ref. [432].

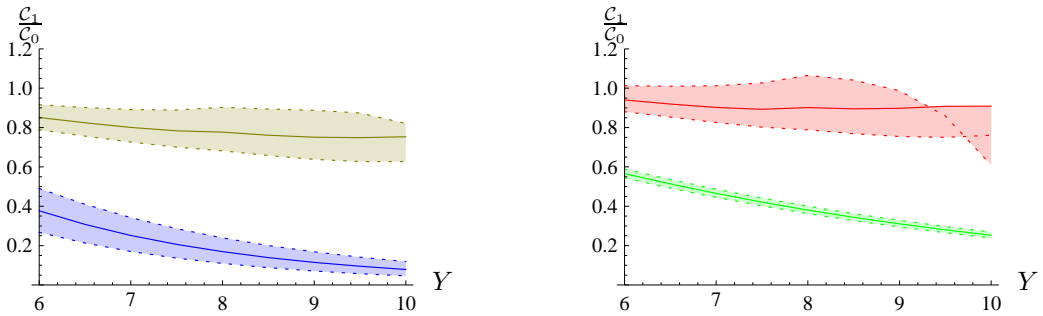


Figure 5.7: Effect of changing $\mu_R = \mu_F$ by factors 2 and 1/2 respectively on $\langle \cos \varphi \rangle$ in dependence on Y for $|\mathbf{k}_{J,1}| = |\mathbf{k}_{J,2}| = 35$ GeV. Blue shows the pure LLx result, brown the pure NLLx result, green the combination of LLx vertices with the collinear improved NLLx Green's function, red the full NLLx vertices with the collinear improved NLLx Green's function.

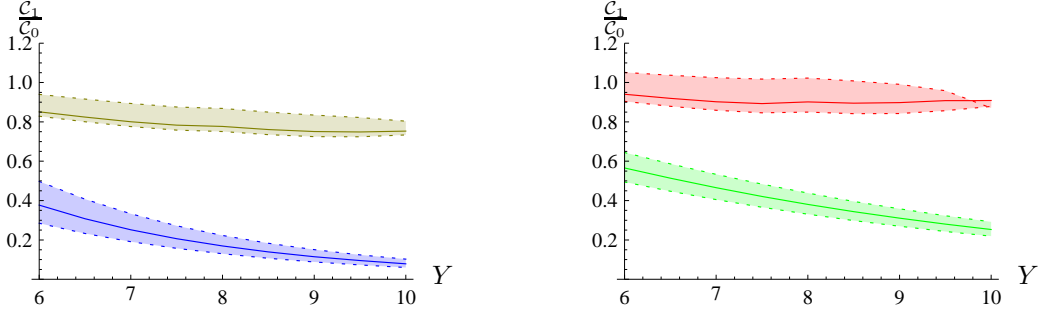


Figure 5.8: Effect of changing $\sqrt{s_0}$ by factors 2 and 1/2 respectively on $\langle \cos \varphi \rangle$ in dependence on Y for $|\mathbf{k}_{J,1}| = |\mathbf{k}_{J,2}| = 35$ GeV. Blue shows the pure LLx result, brown the pure NLLx result, green the combination of LLx vertices with the collinear improved NLLx Green's function, red the full NLLx vertices with the collinear improved NLLx Green's function.

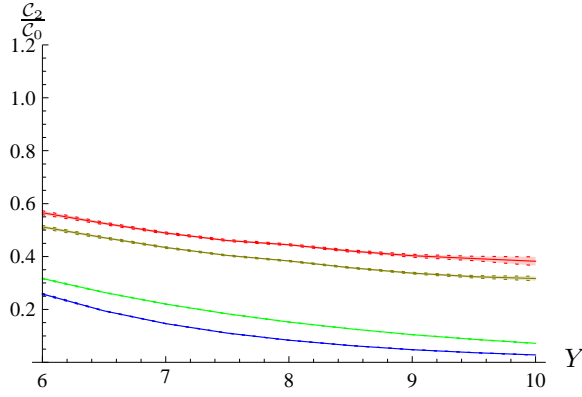


Figure 5.9: $\langle \cos 2\varphi \rangle$ in dependence on Y for $|\mathbf{k}_{J,1}| = |\mathbf{k}_{J,2}| = 35$ GeV. Blue shows the pure LLx result, brown the pure NLLx result, green the combination of LLx vertices with the collinear improved NLLx Green's function, red the full NLLx vertices with the collinear improved NLLx Green's function. The errors due to the Monte Carlo integration – though hardly visible – are given as error bands.

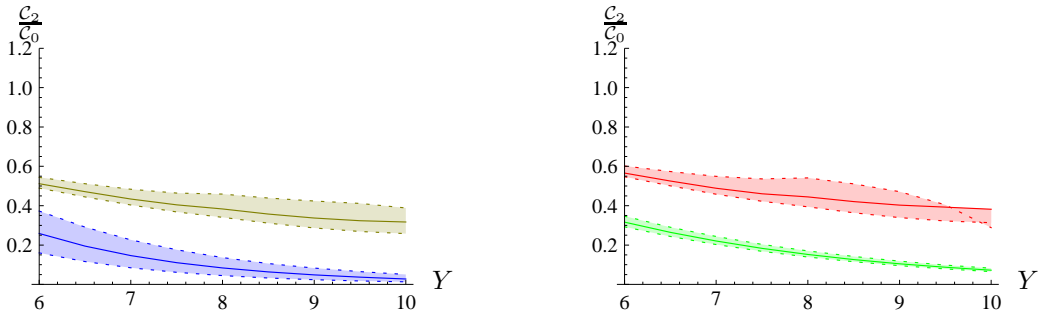


Figure 5.10: Effect of changing $\mu_R = \mu_F$ by factors 2 and 1/2 respectively on $\langle \cos 2\varphi \rangle$ in dependence on Y for $|\mathbf{k}_{J,1}| = |\mathbf{k}_{J,2}| = 35$ GeV. Blue shows the pure LLx result, brown the pure NLLx result, green the combination of LLx vertices with the collinear improved NLLx Green's function, red the full NLLx vertices with the collinear improved NLLx Green's function.

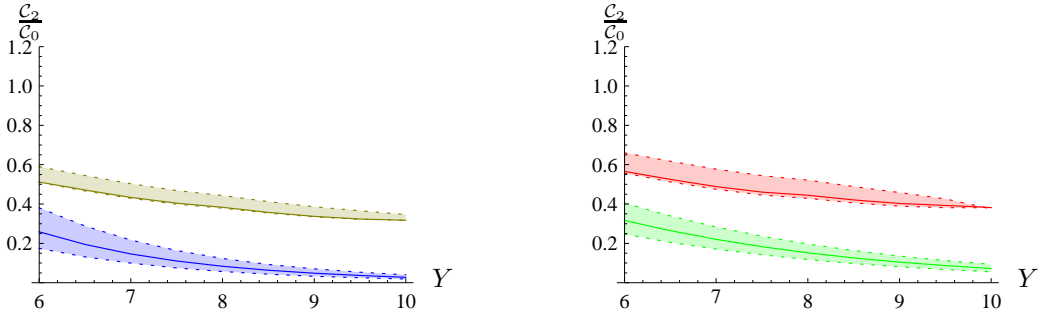


Figure 5.11: Effect of changing $\sqrt{s_0}$ by factors 2 and 1/2 respectively on $\langle \cos 2\varphi \rangle$ in dependence on Y for $|\mathbf{k}_{J,1}| = |\mathbf{k}_{J,2}| = 35$ GeV. Blue shows the pure LLx result, brown the pure NLLx result, green the combination of LLx vertices with the collinear improved NLLx Green's function, red the full NLLx vertices with the collinear improved NLLx Green's function.

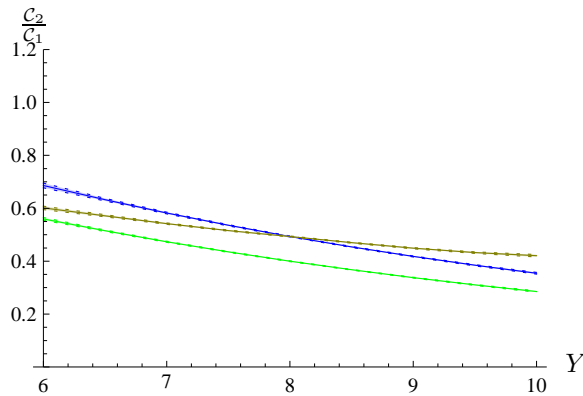


Figure 5.12: $\langle \cos 2\varphi \rangle / \langle \cos \varphi \rangle$ in dependence on Y for $|\mathbf{k}_{J,1}| = |\mathbf{k}_{J,2}| = 35$ GeV. Blue shows the pure LLx result, brown the pure NLLx result, green the combination of LLx vertices with the NLLx Green's function. The errors due to the Monte Carlo integration – though hardly visible – are given as error bands.

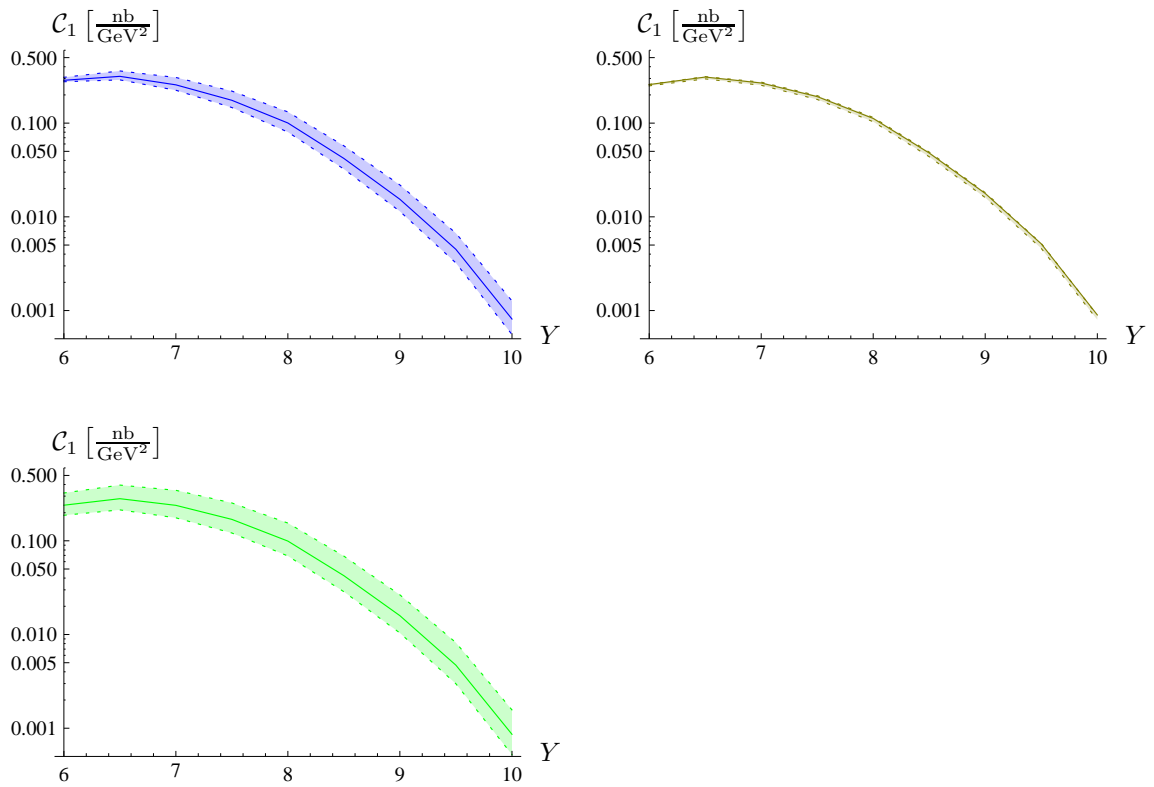


Figure 5.13: Effect of changing $\mu_R = \mu_F$ by factors 2 and 1/2 respectively on the coefficient \mathcal{C}_1 in dependence on Y for $|\mathbf{k}_{J,1}| = |\mathbf{k}_{J,2}| = 35 \text{ GeV}$. Blue shows the pure LLx result, brown the pure NLLx result, green the combination of LLx vertices with the collinear improved NLLx Green's function.

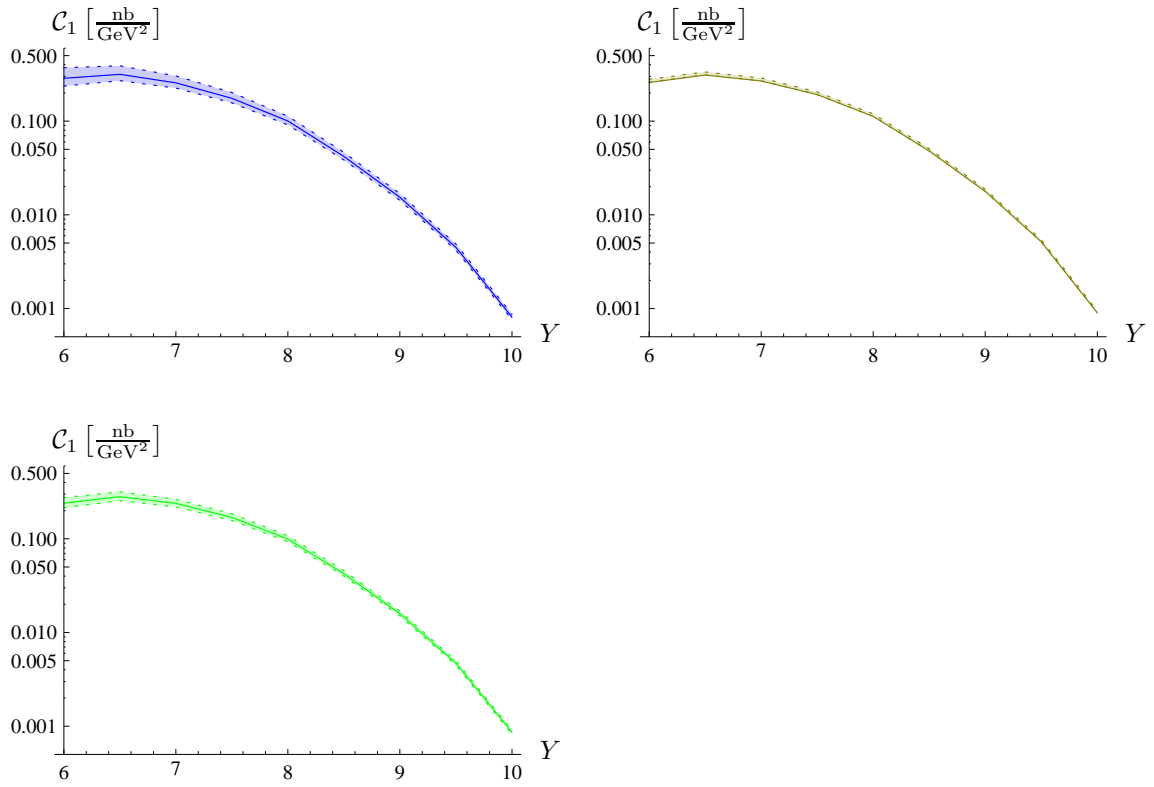


Figure 5.14: Effect of changing $\sqrt{s_0}$ by factors 2 and 1/2 respectively on the coefficient \mathcal{C}_1 in dependence on Y for $|\mathbf{k}_{J,1}| = |\mathbf{k}_{J,2}| = 35 \text{ GeV}$. Blue shows the pure LLx result, brown the pure NLLx result, green the combination of LLx vertices with the collinear improved NLLx Green's function.

The symmetric case $|\mathbf{k}_{J,1}| = |\mathbf{k}_{J,2}| = 50 \text{ GeV}$

Going to larger jet scales, we meet more or less the same advantages and problems as for 35 GeV. The problematic behavior for smaller scales of s_0 and/or μ_R is more dramatic for $|\mathbf{k}_{J,1}| = |\mathbf{k}_{J,2}| = 50 \text{ GeV}$ (see *e.g.* Figs. 5.19, 5.20, 5.22, 5.23). Especially the μ_R dependence (see Fig. 5.19 seems to indicate that already the a priori natural scale $\mu_R = |\mathbf{k}_J|$ is too small. See Ref. [W27] for detailed studies of the PDF dependency of the \mathcal{C}_i coefficients, as well as s_0 and μ_R dependency of the \mathcal{C}_1 and \mathcal{C}_2 coefficients. We note that the stability of $\mathcal{C}_2/\mathcal{C}_1$ is weaker than in the $|\mathbf{k}_{J,1}| = |\mathbf{k}_{J,2}| = 35 \text{ GeV}$ case in the large rapidity range (see Figs. 5.25 and 5.26).

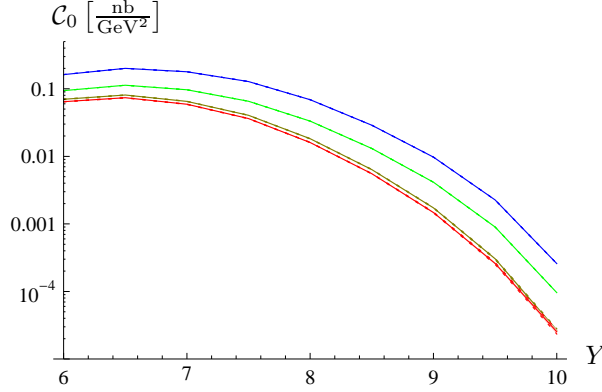


Figure 5.15: Differential cross section in dependence on Y for $|\mathbf{k}_{J,1}| = |\mathbf{k}_{J,2}| = 50 \text{ GeV}$. Blue shows the pure LLx result, brown the pure NLLx result, green the combination of LLx vertices with the collinear improved NLLx Green's function, red the full NLLx vertices with the collinear improved NLLx Green's function. The errors due to the Monte Carlo integration – though hardly visible – are given as error bands.

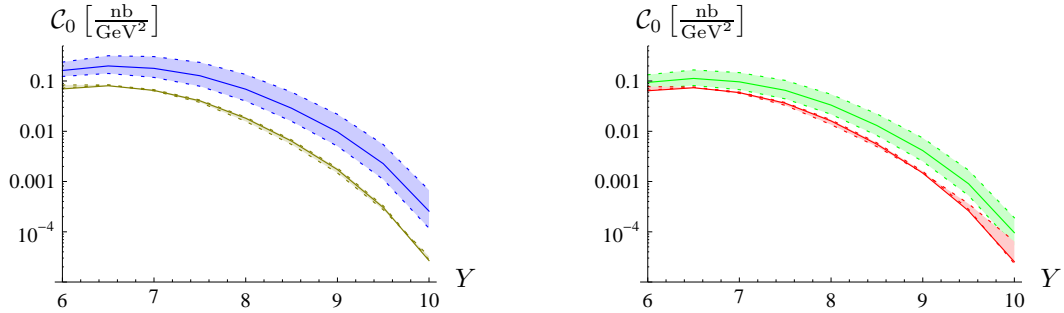


Figure 5.16: Effect of changing $\mu_R = \mu_F$ by factors 2 and 1/2 respectively on the differential cross section in dependence on Y for $|\mathbf{k}_{J,1}| = |\mathbf{k}_{J,2}| = 50 \text{ GeV}$. Blue shows the pure LLx result, brown the pure NLLx result, green the combination of LLx vertices with the collinear improved NLLx Green's function, red the full NLLx vertices with the collinear improved NLLx Green's function.

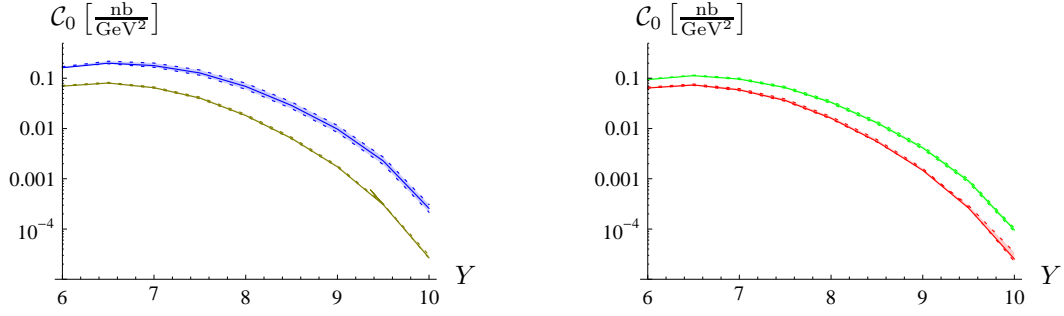


Figure 5.17: Effect of changing $\sqrt{s_0}$ by factors 2 and 1/2 respectively on the differential cross section in dependence on Y for $|\mathbf{k}_{J,1}| = |\mathbf{k}_{J,2}| = 50$ GeV. Blue shows the pure LLx result, brown the pure NLLx result, green the combination of LLx vertices with the collinear improved NLLx Green's function, red the full NLLx vertices with the collinear improved NLLx Green's function.

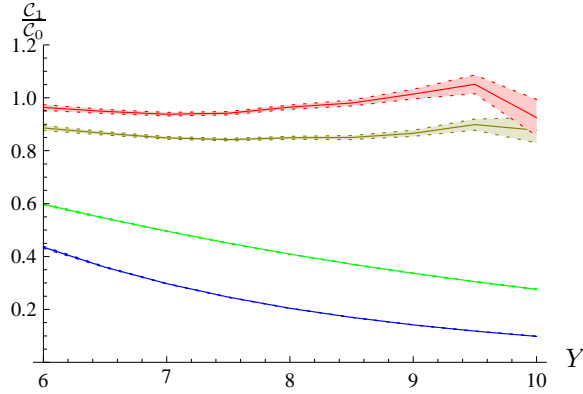


Figure 5.18: $\langle \cos \varphi \rangle$ in dependence on Y for $|\mathbf{k}_{J,1}| = |\mathbf{k}_{J,2}| = 50$ GeV. Blue shows the pure LLx result, brown the pure NLLx result, green the combination of LLx vertices with the collinear improved NLLx Green's function, red the full NLLx vertices with the collinear improved NLLx Green's function. The errors due to the Monte Carlo integration are given as error bands.

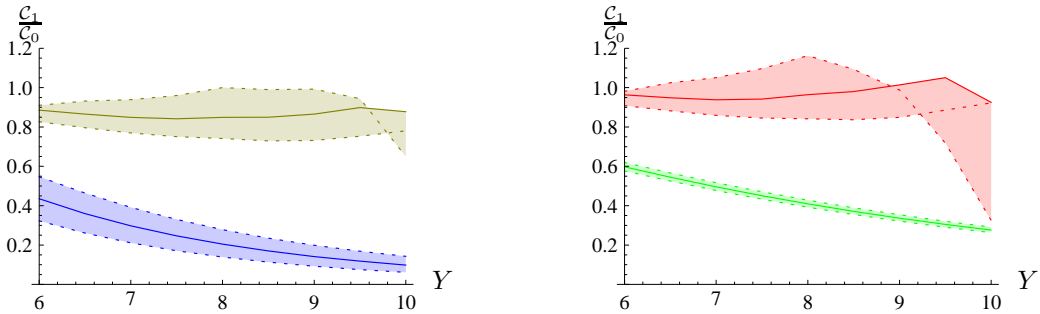


Figure 5.19: Effect of changing $\mu_R = \mu_F$ by factors 2 and 1/2 respectively on $\langle \cos \varphi \rangle$ in dependence on Y for $|\mathbf{k}_{J,1}| = |\mathbf{k}_{J,2}| = 50$ GeV. Blue shows the pure LLx result, brown the pure NLLx result, green the combination of LLx vertices with the collinear improved NLLx Green's function, red the full NLLx vertices with the collinear improved NLLx Green's function.

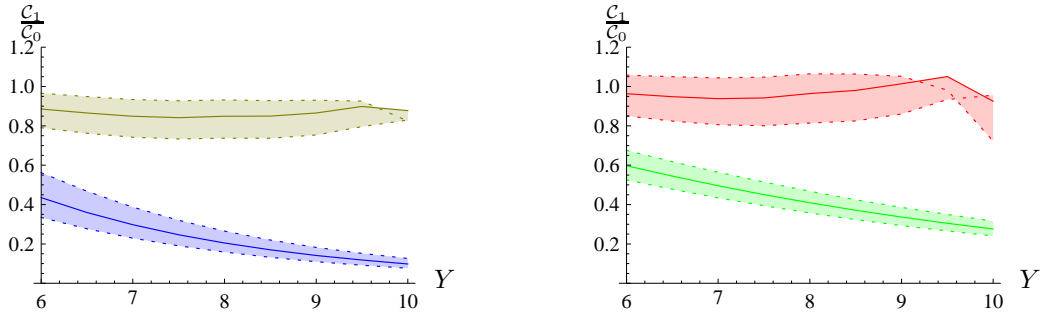


Figure 5.20: Effect of changing $\sqrt{s_0}$ by factors 2 and 1/2 respectively on $\langle \cos \varphi \rangle$ in dependence on Y for $|\mathbf{k}_{J,1}| = |\mathbf{k}_{J,2}| = 50$ GeV. Blue shows the pure LLx result, brown the pure NLLx result, green the combination of LLx vertices with the collinear improved NLLx Green's function, red the full NLLx vertices with the collinear improved NLLx Green's function.

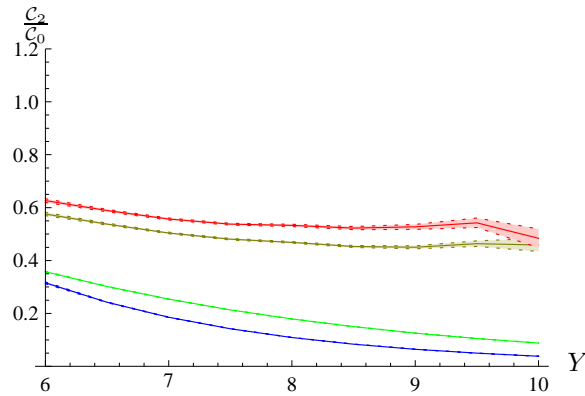


Figure 5.21: $\langle \cos 2\varphi \rangle$ in dependence on Y for $|\mathbf{k}_{J,1}| = |\mathbf{k}_{J,2}| = 50$ GeV. Blue shows the pure LLx result, brown the pure NLLx result, green the combination of LLx vertices with the collinear improved NLLx Green's function, red the full NLLx vertices with the collinear improved NLLx Green's function. The errors due to the Monte Carlo integration – though hardly visible – are given as error bands.

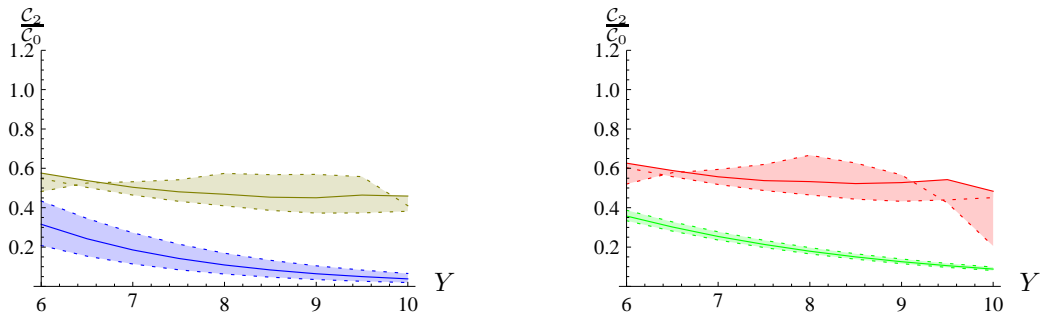


Figure 5.22: Effect of changing $\mu_R = \mu_F$ by factors 2 and 1/2 respectively on $\langle \cos 2\varphi \rangle$ in dependence on Y for $|\mathbf{k}_{J,1}| = |\mathbf{k}_{J,2}| = 50$ GeV. Blue shows the pure LLx result, brown the pure NLLx result, green the combination of LLx vertices with the collinear improved NLLx Green's function, red the full NLLx vertices with the collinear improved NLLx Green's function.

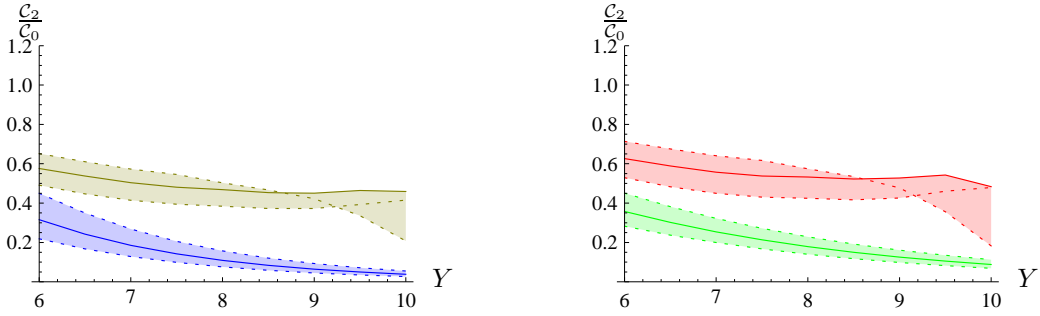


Figure 5.23: Effect of changing $\sqrt{s_0}$ by factors 2 and 1/2 respectively on $\langle \cos 2\varphi \rangle$ in dependence on Y for $|\mathbf{k}_{J,1}| = |\mathbf{k}_{J,2}| = 50$ GeV. Blue shows the pure LLx result, brown the pure NLLx result, green the combination of LLx vertices with the collinear improved NLLx Green's function, red the full NLLx vertices with the collinear improved NLLx Green's function.

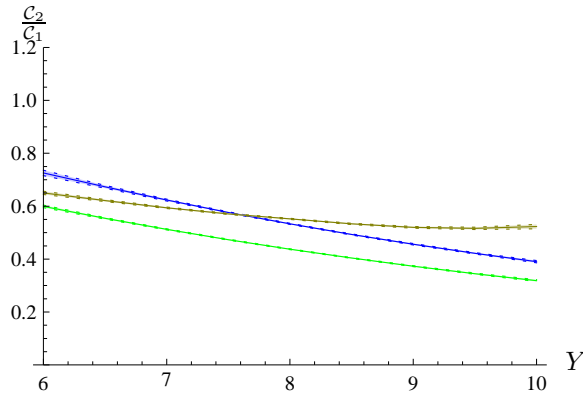


Figure 5.24: $\langle \cos 2\varphi \rangle / \langle \cos \varphi \rangle$ in dependence on Y for $|\mathbf{k}_{J,1}| = |\mathbf{k}_{J,2}| = 50$ GeV. Blue shows the pure LLx result, brown the pure NLLx result, green the combination of LLx vertices with the NLLx Green's function. The errors due to the Monte Carlo integration – though hardly visible – are given as error bands.

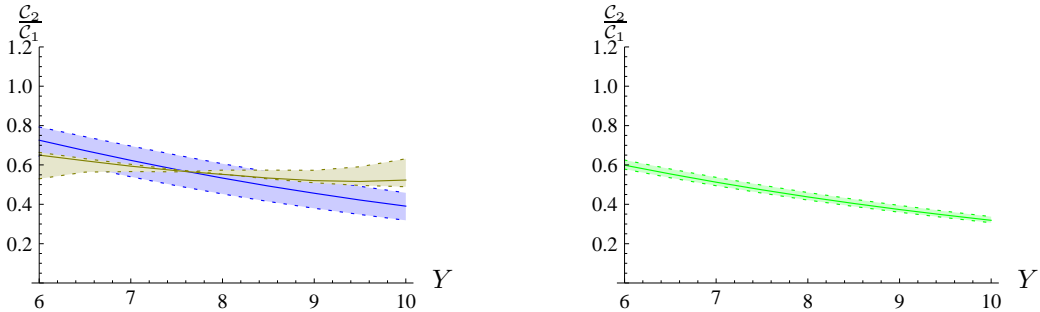


Figure 5.25: Effect of changing $\mu_R = \mu_F$ by factors 2 and 1/2 respectively on $\langle \cos 2\varphi \rangle / \langle \cos \varphi \rangle$ in dependence on Y for $|\mathbf{k}_{J,1}| = |\mathbf{k}_{J,2}| = 50$ GeV. Blue shows the pure LLx result, brown the pure NLLx result, green the combination of LLx vertices with the NLLx Green's function.

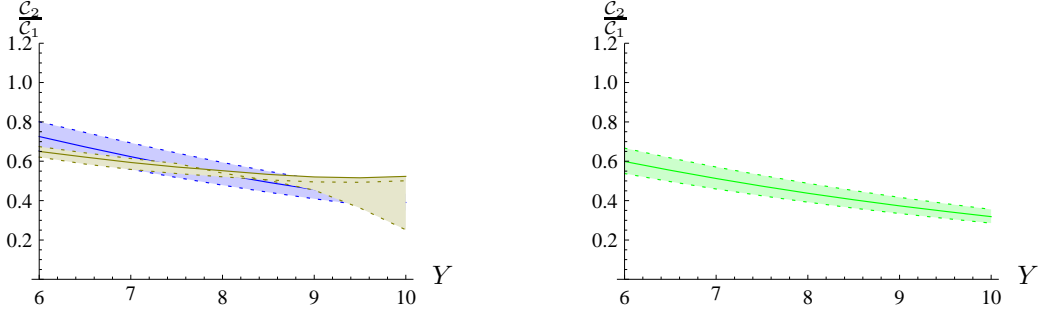


Figure 5.26: Effect of changing $\sqrt{s_0}$ by factors 2 and 1/2 respectively on $\langle \cos 2\varphi \rangle / \langle \cos \varphi \rangle$ in dependence on Y for $|\mathbf{k}_{J,1}| = |\mathbf{k}_{J,2}| = 50$ GeV. Blue shows the pure LLx result, brown the pure NLLx result, green the combination of LLx vertices with the NLLx Green's function.

The asymmetric case $|\mathbf{k}_{J,1}| = 35$ GeV, $|\mathbf{k}_{J,2}| = 50$ GeV

We end up with the consideration of the asymmetric case, which we investigate in order to provide a comparison with NLLQ predictions based on NLLQ predictions [444] obtained through the NLLQ partonic generator DIJET [445]. These prediction are very sensitive to the precise compensation between the real and the virtual contribution, and symmetric cut leads to some kind of Sudakov resummation effects which are not under control at the moment [446], even leading to a negative cross-section for $|\mathbf{k}_{J,1}| = 35$ GeV = $|\mathbf{k}_{J,2}| = 35$ GeV. These prediction are much more stable in the asymmetric configuration. Our own predictions are given in Figs. 5.27, 5.30, 5.33, 5.36.

The sensitivity of our prediction with respect to s_0 , μ_R and PDFs is similar to the two previous symmetrical configurations, as shown in Figs. 5.28, 5.29, 5.31, 5.32, 5.34, 5.35, 5.37, 5.38. See Ref. [W27] for detailed studies of the PDF dependency of the \mathcal{C}_i coefficients, as well as s_0 and μ_R dependency of the \mathcal{C}_1 and \mathcal{C}_2 coefficients.

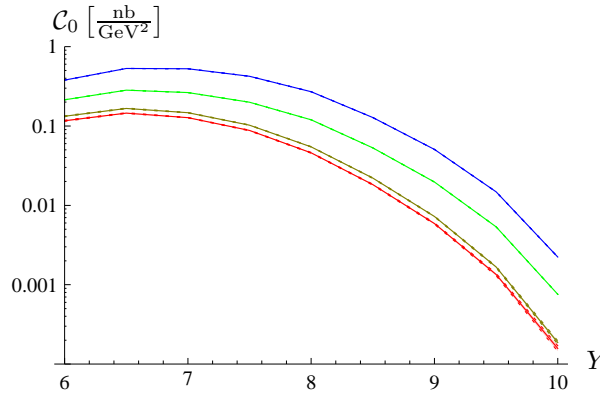


Figure 5.27: Differential cross section in dependence on Y for $|\mathbf{k}_{J,1}| = 35$ GeV, $|\mathbf{k}_{J,2}| = 50$ GeV. Blue shows the pure LLx result, brown the pure NLLx result, green the combination of LLx vertices with the collinear improved NLLx Green's function, red the full NLLx vertices with the collinear improved NLLx Green's function. The errors due to the Monte Carlo integration – though hardly visible – are given as error bands.

We now display a comparison between our prediction and the NLLQ predictions [444], for the cross-section in Fig. 5.39, for the $\langle \cos \varphi \rangle$ dependence in Fig. 5.40 and for the $\langle \cos 2\varphi \rangle$ dependence in Fig. 5.41.

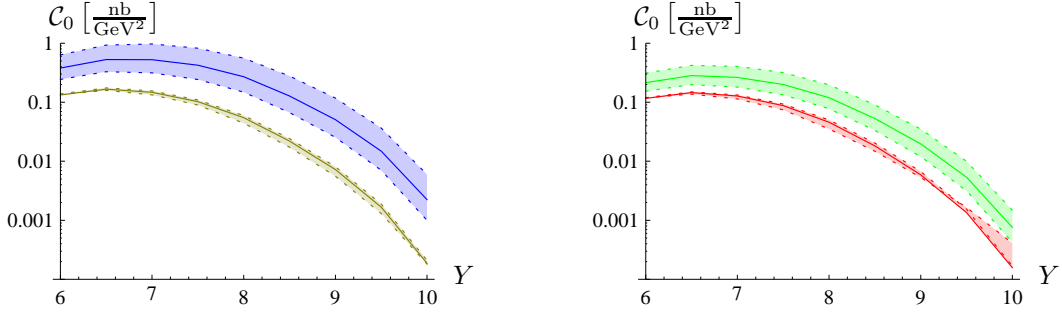


Figure 5.28: Effect of changing $\mu_R = \mu_F$ by factors 2 and 1/2 respectively on the differential cross section in dependence on Y for $|\mathbf{k}_{J,1}| = 35$ GeV, $|\mathbf{k}_{J,2}| = 50$ GeV. Blue shows the pure LLx result, brown the pure NLLx result, green the combination of LLx vertices with the collinear improved NLLx Green's function, red the full NLLx vertices with the collinear improved NLLx Green's function.

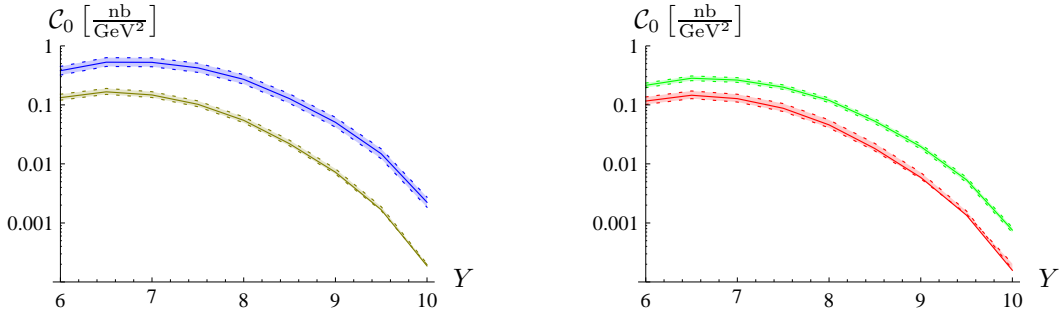


Figure 5.29: Effect of changing $\sqrt{s_0}$ by factors 2 and 1/2 respectively on the differential cross section in dependence on Y for $|\mathbf{k}_{J,1}| = 35$ GeV, $|\mathbf{k}_{J,2}| = 50$ GeV. Blue shows the pure LLx result, brown the pure NLLx result, green the combination of LLx vertices with the collinear improved NLLx Green's function, red the full NLLx vertices with the collinear improved NLLx Green's function.

Conclusions

We have implemented at a full NLLx order the Mueller Navelet jets cross-section as well as their relative azimuthal angle dependency. In contrast to the general belief, the effect of NLLx corrections to the vertex function is very important, of the same order as the one obtained when passing from LLx to NLLx Green function. The importance of NLLx corrections to impact factor observed in the present work is analogous with recent results obtained at NLLx in diffractive double ρ -electroproduction [328, 439]. Interestingly, the full NLLx calculations for $\langle \cos \varphi \rangle$ and $\langle \cos 2\varphi \rangle$ are quite close to a calculation [444] using DIJET [445] which is based on DGLAP dynamics and to a dedicated study [432] using PYTHIA [442] and HERWIG [428]. The uncertainty due to changes in μ_R (and s_0) is drastically reduced for all C_n when one takes into account the NLLx Mueller Navelet vertices. The uncertainty due to PDFs are also very small. As a consequence, our results for the cross-section are very stable.

However, for azimuthal decorrelation the dependence on μ_R (and s_0) is still sizeable. In the case of the NLLx Green's function with collinear improvement one observes that $\langle \cos \varphi \rangle$ can exceed 1 for certain choices of the parameters, in particular for low values of $\mu_R = \mu_F$, taken to be smaller than the “natural” value $\sqrt{|k_{J,1}| |k_{J,2}|}$. One might also think of a collinear improvement of the vertices [329] but the Mueller Navelet vertex for fixed $|\mathbf{k}_J|$ does not contain poles in γ nor $1 - \gamma$, so there is no room for such a treatment. The resummation of soft initial radiation might be of relevance for the azimuthal correlation as well. This is left for further investigations.

At present, there is little experience with the effect of NLLx impact factors. To the best of our knowledge, up

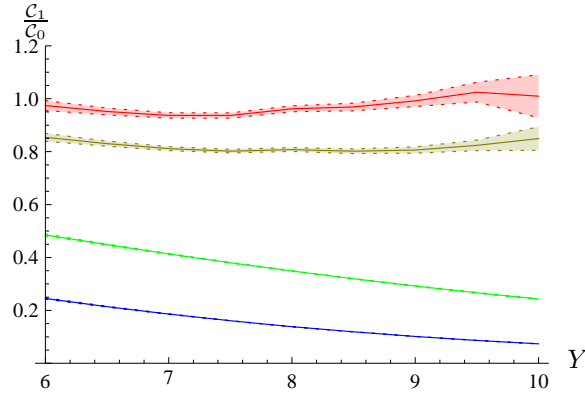


Figure 5.30: $\langle \cos \varphi \rangle$ in dependence on Y for $|\mathbf{k}_{J,1}| = 35$ GeV, $|\mathbf{k}_{J,2}| = 50$ GeV. Blue shows the pure LLx result, brown the pure NLLx result, green the combination of LLx vertices with the collinear improved NLLx Green’s function, red the full NLLx vertices with the collinear improved NLLx Green’s function. The errors due to the Monte Carlo integration are given as error bands.

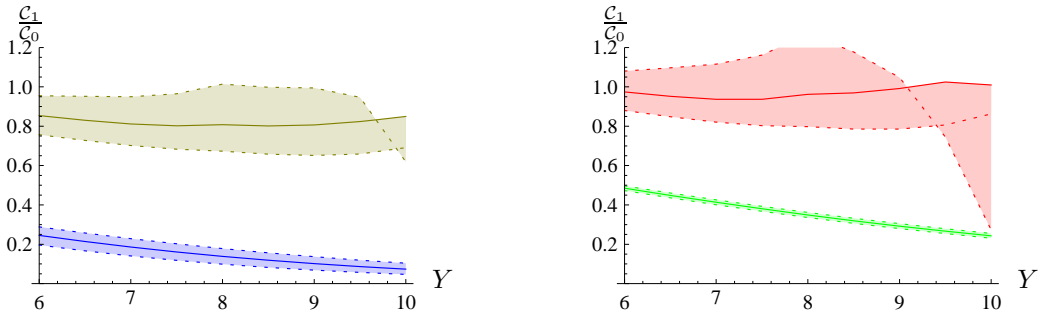


Figure 5.31: Effect of changing $\mu_R = \mu_F$ by factors 2 and 1/2 respectively on $\langle \cos \varphi \rangle$ in dependence on Y for $|\mathbf{k}_{J,1}| = 35$ GeV, $|\mathbf{k}_{J,2}| = 50$ GeV. Blue shows the pure LLx result, brown the pure NLLx result, green the combination of LLx vertices with the collinear improved NLLx Green’s function, red the full NLLx vertices with the collinear improved NLLx Green’s function.

to now, the only full NLLx BFKL calculation existing in the literature is the vector meson production in virtual photon collisions [328, 439, 443], which is very sensitive to NLLx corrections to the impact factor and for which very large values for s_0 and μ_R are preferred. In [443] it has been shown that a collinear improved treatment combined with the application of the principle of minimal sensitivity [153, 154] reduces this large values to more “natural” values. Still, μ_R larger than the “natural” values are favored [443]. In the present case, with such a choice, we get azimuthal correlations which are rather similar with DGLAP dynamics predictions. To conclude, contrarily to the expectation, it thus seems that the azimuthal decorrelation is almost not enhanced by rapidity. This suggest that the study of Mueller-Navelet jets is probably not the best place to exhibit differences between BFKL and DGLAP dynamics.

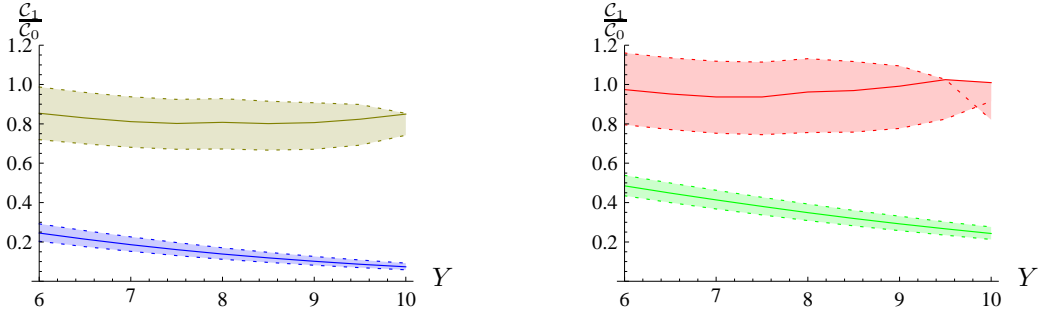


Figure 5.32: Effect of changing $\sqrt{s_0}$ by factors 2 and 1/2 respectively on $\langle \cos \varphi \rangle$ in dependence on Y for $|\mathbf{k}_{J,1}| = 35$ GeV, $|\mathbf{k}_{J,2}| = 50$ GeV. Blue shows the pure LLx result, brown the pure NLLx result, green the combination of LLx vertices with the collinear improved NLLx Green's function, red the full NLLx vertices with the collinear improved NLLx Green's function.

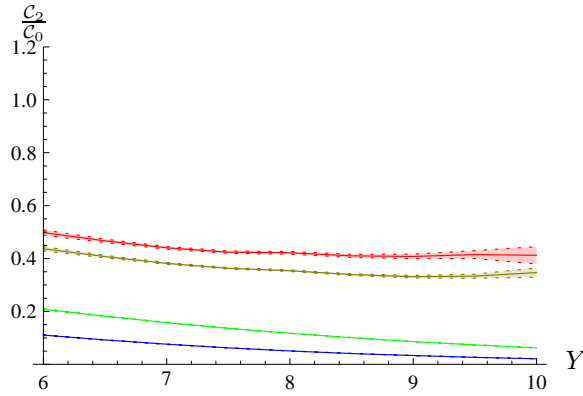


Figure 5.33: $\langle \cos 2\varphi \rangle$ in dependence on Y for $|\mathbf{k}_{J,1}| = 35$ GeV, $|\mathbf{k}_{J,2}| = 50$ GeV. Blue shows the pure LLx result, brown the pure NLLx result, green the combination of LLx vertices with the collinear improved NLLx Green's function, red the full NLLx vertices with the collinear improved NLLx Green's function. The errors due to the Monte Carlo integration – though hardly visible – are given as error bands.

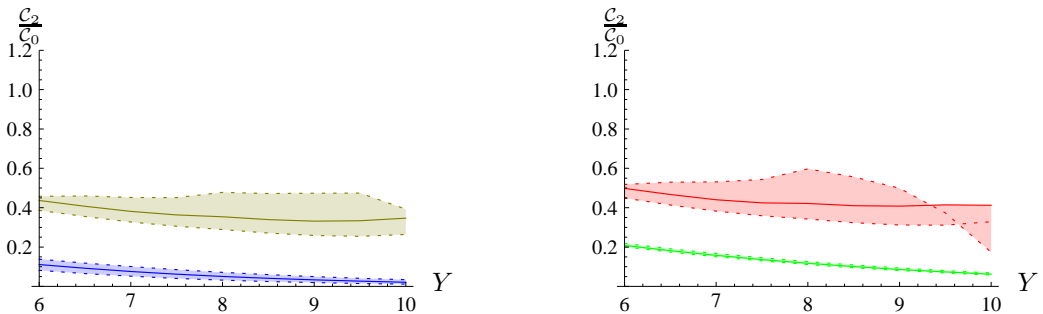


Figure 5.34: Effect of changing $\mu_R = \mu_F$ by factors 2 and 1/2 respectively on $\langle \cos 2\varphi \rangle$ in dependence on Y for $|\mathbf{k}_{J,1}| = 35$ GeV, $|\mathbf{k}_{J,2}| = 50$ GeV. Blue shows the pure LLx result, brown the pure NLLx result, green the combination of LLx vertices with the collinear improved NLLx Green's function, red the full NLLx vertices with the collinear improved NLLx Green's function.

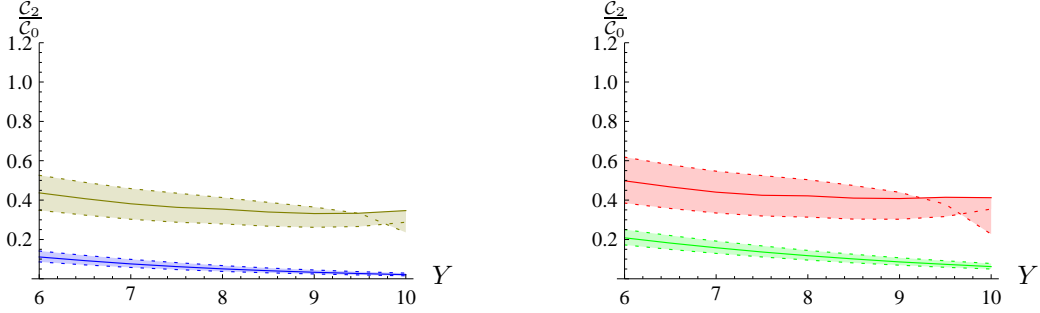


Figure 5.35: Effect of changing $\sqrt{s_0}$ by factors 2 and 1/2 respectively on $\langle \cos 2\varphi \rangle$ in dependence on Y for $|\mathbf{k}_{J,1}| = 35$ GeV, $|\mathbf{k}_{J,2}| = 50$ GeV. Blue shows the pure LLx result, brown the pure NLLx result, green the combination of LLx vertices with the collinear improved NLLx Green's function, red the full NLLx vertices with the collinear improved NLLx Green's function.

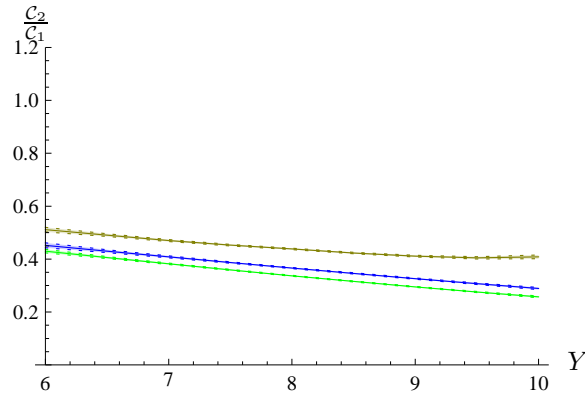


Figure 5.36: $\langle \cos 2\varphi \rangle / \langle \cos \varphi \rangle$ in dependence on Y for $|\mathbf{k}_{J,1}| = 35$ GeV, $|\mathbf{k}_{J,2}| = 50$ GeV. Blue shows the pure LLx result, brown the pure NLLx result, green the combination of LLx vertices with the NLLx Green's function. The errors due to the Monte Carlo integration – though hardly visible – are given as error bands.

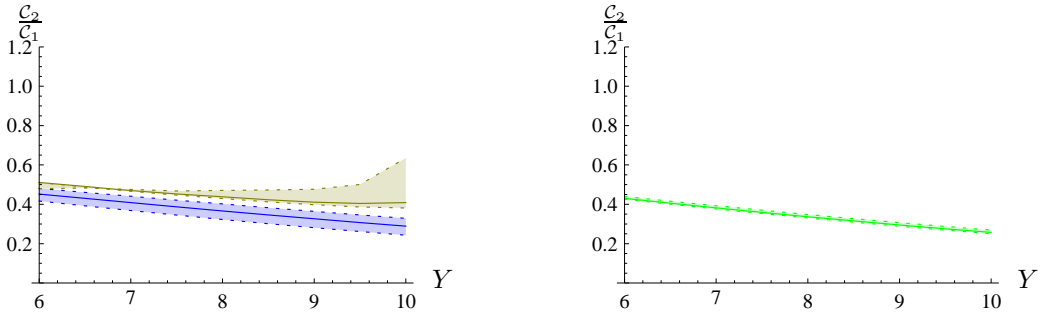


Figure 5.37: Effect of changing $\mu_R = \mu_F$ by factors 2 and 1/2 respectively on $\langle \cos 2\varphi \rangle / \langle \cos \varphi \rangle$ in dependence on Y for $|\mathbf{k}_{J,1}| = 35$ GeV, $|\mathbf{k}_{J,2}| = 50$ GeV. Blue shows the pure LLx result, brown the pure NLLx result, green the combination of LLx vertices with the NLLx Green's function.

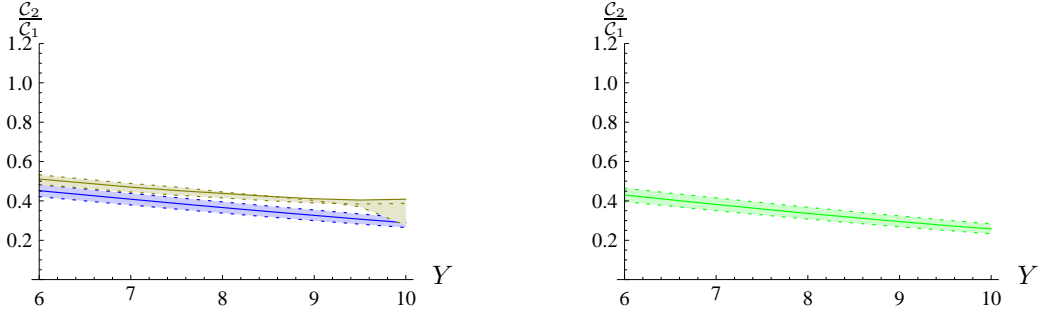


Figure 5.38: Effect of changing $\sqrt{s_0}$ by factors 2 and 1/2 respectively on $\langle \cos 2\varphi \rangle / \langle \cos \varphi \rangle$ in dependence on Y for $|\mathbf{k}_{J,1}| = 35$ GeV, $|\mathbf{k}_{J,2}| = 50$ GeV. Blue shows the pure LLx result, brown the pure NLLx result, green the combination of LLx vertices with the NLLx Green's function.

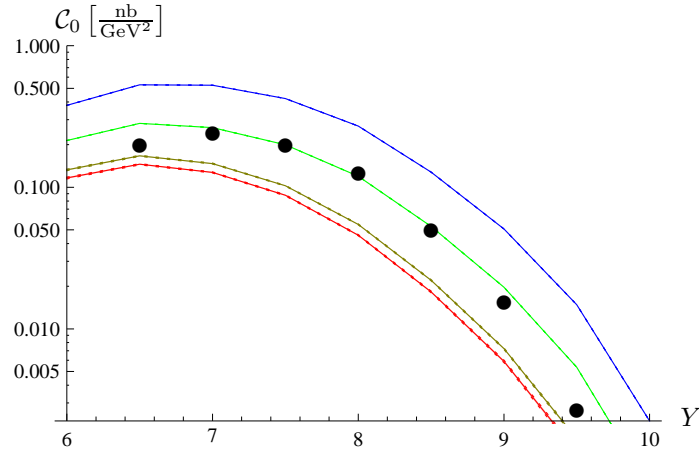


Figure 5.39: Differential cross section in dependence on Y for $|\mathbf{k}_{J,1}| = 35$ GeV, $|\mathbf{k}_{J,2}| = 50$ GeV. Blue shows the pure LLx result, brown the pure NLLx result, green the combination of LLx vertices with the collinear improved NLLx Green's function, red the full NLLx vertices with the collinear improved NLLx Green's function. The errors due to the Monte Carlo integration – though hardly visible – are given as error bands. Dotted points are based on the NLLQ prediction of Ref. [444].

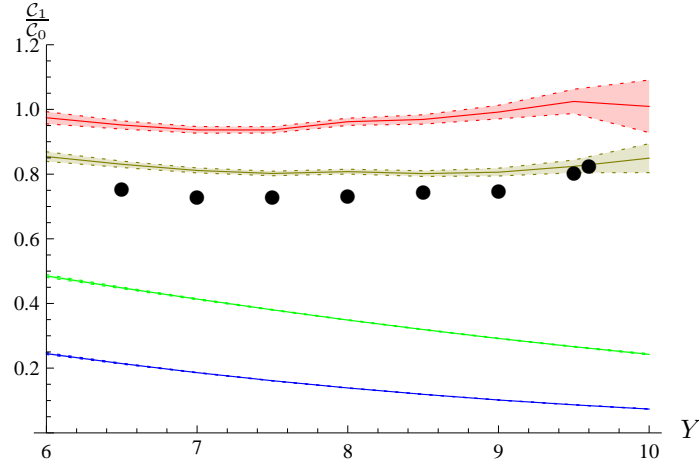


Figure 5.40: $\langle \cos \varphi \rangle$ in dependence on Y for $|\mathbf{k}_{J,1}| = 35$ GeV, $|\mathbf{k}_{J,2}| = 50$ GeV. Blue shows the pure LLx result, brown the pure NLLx result, green the combination of LLx vertices with the collinear improved NLLx Green's function, red the full NLLx vertices with the collinear improved NLLx Green's function. The errors due to the Monte Carlo integration are given as error bands. Dotted points are based on the NLLQ prediction of Ref. [444].

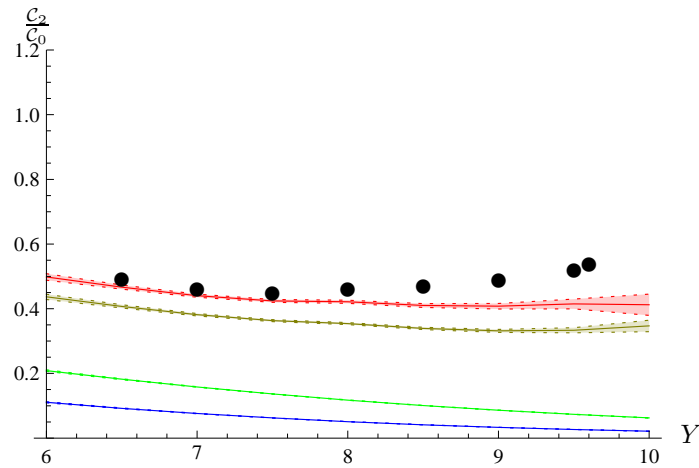


Figure 5.41: $\langle \cos 2\varphi \rangle$ in dependence on Y for $|\mathbf{k}_{J,1}| = 35$ GeV, $|\mathbf{k}_{J,2}| = 50$ GeV. Blue shows the pure LLx result, brown the pure NLLx result, green the combination of LLx vertices with the collinear improved NLLx Green's function, red the full NLLx vertices with the collinear improved NLLx Green's function. The errors due to the Monte Carlo integration – though hardly visible – are given as error bands. Dotted points are based on the NLLQ prediction of Ref. [444].

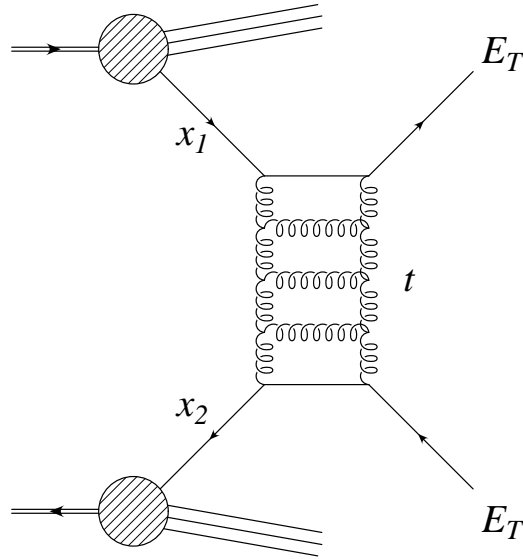


Figure 5.42: Diffractive high energy jet production.

5.1.2 Diffractive high energy double jet production

In a hadron-hadron collision, a jet-gap-jet event is defined by demanding to tag two jets with a high $-E_T \gg \Lambda_{QCD}$ and a large rapidity between them. This is thus a more exclusive process than the Mueller-Navelet one which we have just discussed. Between the gap, the object exchanged in the t -channel is color singlet and carries a large momentum transfer due to the large p_T , and when the rapidity gap is large one can expect the exchange of a hard Pomeron (the hard scale is here provided by t). A non trivial point is due to the fact that the solution of LLx BFKL equation for t arbitrary is given in impact parameter space, which can be written based on the $SL(2, C)$ conformal invariance of the kernel due to absence of scale. However this can be used in practice when the probes are colorless [277], because then the elementary Born two gluon-exchange contribution, which evolves due to BFKL equation, can be written itself in a conformal invariant way. In that case, the impact factor vanishes when the virtuality of the parton goes to zero. This is a direct consequence of gauge invariance of the probe, as we explained in Sec. 4.2. This is clearly not the case when coupling the BFKL Pomeron to partons, which are not colorless. For $t \neq 0$, imposing the conformal invariance of the Born term leads to the appearance of δ terms in momentum space, which have no clear relationship with Feynman diagrams. Mueller-Tang provided a prescription [447] in order to couple BFKL Pomeron solution in that diffractive case, which means basically to remove these δ contributions. This was further studied in Ref. [448], and understood as a deformed representation of the BFKL kernel that can be coupled to colored particles, and for which the bootstrap relation is fulfilled [449].

It turns out that this LLx treatment is not enough to describe the data, measured a Tevatron by CDF [450] and D0 [451] collaborations.

A first try to improve this LLx treatment was attempted in Ref. [452] by also taking into account the soft interactions which in hadron-hadron collisions can destroy the rapidity gap, the so-called gap survival probability. An agreement was only obtained with the BFKL LLx calculation done at fixed coupling constant α_s . However, from the theory side, the importance of NLLx BFKL corrections appeals for a consistent treatment which would include them. In [453], it was shown that a good description of the data could be obtained when some NLLx corrections were numerically taken into account in an effective way, based on the modified LLx BFKL kernel discussed above, but the full NLLx BFKL kernel was still not implemented. A NLLx BFKL treatment including the Salam prescription, but still with a LLx impact factor, has been performed in Ref. [454], leading to a satisfactory description of the data.

5.1.3 High p_T central jet production

High p_T central jet production with a rapidity gap between the protons and the jet has focused much interest, in particular based on the fact that this exclusive process may be an interesting channel for C and P -even Higgs searches. The mechanism is a gluon exchange to which the Higgs couples through a quark loop, with another t -channel gluon exchange to compensate the color exchange [455], modified by possible Pomeron-like enhancement due to the large rapidities between the protons and the Higgs.

Unfortunately, one needs to take into account perturbative Sudakov form factor which are needed to guarantee the exclusiveness of the final state (denoted as T^2 at the level of probability). This can be done at the double-logarithmic level as well as at the NLL level (single logs). Note that this amplitude T plays a crucial role in regulating the loop integral over the gluon momentum to which the Higgs is coupled. Additionally, in hadron-hadron collisions, one should include soft rescattering among the spectators partons, leading to gap survival factors, which cannot be computed perturbatively (denoted as S^2 at the level of probability). When comparing diffractive events at HERA with results from Tevatron, one phenomenologically extract typical values $S^2 \sim 0.1$. See [456] for a review of the various models and proposal in order to see Higgs in diffractive processes. In particular, the exclusive Higgs cross-section is decreased by a factor of $\sim 10^{-4}$ with respect to inclusive production, and the estimated cross-section is $\sigma(pp \rightarrow p + H + p) \simeq 3$ fb, with an uncertainty of two [457], if a tagging of the out-going proton is possible [458]. This idea lead to the FP420 proposal [459] of having silicon tracker and fast-timing detectors in the LHC tunnel at 420 m from the interaction points of the ATLAS and CMS experiments. In this exclusive case, from a $J_z = 0$ selection rule, one can suppress the $b\bar{b}$ background. The H quantum numbers can be reconstructed through the angular distribution of two tagged outgoing protons. The mass measurement may be rather precise (of the order of 1 GeV), when combining a missing mass measurement (with respect to the outgoing protons) and the invariant mass of the $b\bar{b}$ pair produced by the H decay. When including efficiencies, the expected number of Standard Models H events should be around 12. For SUSY Higgs bosons, this diffractive channel might be one of the most interesting for certain regions in the SUSY space parameters [458].

The inclusive production $\sigma(pp \rightarrow X + H + Y)$ is more favorable in terms of cross-sections (although this has the consequence of possible pile-up problems at LHC), but one pay the price of loosing the spin selection rule, and further, no missing mass measurement is possible.

Central inelastic production $pp \rightarrow X + (HX) + Y$ is not interesting from the point of view of Higgs searches.

The need for inclusion of T and S factors explain why the theoretical treatment of Higgs production in diffraction cannot be described in a factorizable manner. See however [460–463] for alternative approaches based on a factorization treatment combined with effective correction factors.

More recently, hard rescattering corrections have been considered, which basically means to take into account effects of the BK type, based on hard triple-Pomeron coupling diagrams. Theoretical studies [464] have shown the importance of such contribution. However, a dedicated phenomenological study [465] for the LHC case shows that this should not affect the prediction for diffractive Higgs production.

In a somehow separate way, exclusive forward jet production in hadron-hadron collision are by themselves interesting for BFKL studies. The basics ingredients are the same as the one needed when studying Mueller-Navelet jets. It relies on the computation of impact factors and Green function at LLx and NLLx order. The effective jet vertex requires a precise definition of the emitted jet (made of one or two s -channel emitted particle at NLLx), and modeling of proton impact factor (the only hard scale is p_T^2 , and a phenomenological ansatz is needed for the \mathbb{P} -proton coupling). Studies have been made combining NLLx Green functions with LLx jet vertex [466, 467]. So far, there exist no complete NLLx treatment. It would be of much interest to investigate the effect of NLLx jet vertex in this approach. From our results for MN jets at full NLLx one may expect a rather dramatic effect.

5.2 HERA

Since the beginning of HERA in 1992, there have been much efforts in order to see the perturbative Regge dynamics. We will mainly discuss here tests which are not completely inclusive, and briefly report on pure DIS studies.

5.2.1 DIS and diffractive DIS

When applying BFKL type of dynamics to DIS, one faces the problem that since Q^2 is the only hard scale, a model for the proton, either in term of coupling or in term of dipole densities is needed [468, W5, W29, 469]. It turns out that BFKL (at $t = 0$) and DGLAP (NNLL) [470] both describe the data [401–403], and the tremendous efforts in order to try to see a need for BFKL dynamics in inclusive data were not conclusive.

Diffractive scattering within the parton model was suggested long ago [471], in $p\bar{p} \rightarrow X\bar{p}$ through an exchange of a Pomeron between the proton and the anti-proton. The experimental signature was expected to be a gap between the \bar{p} remnants and the jets (X state). Extended to HERA, i.e. replacing the \bar{p} by p and p by a γ^* , the same configuration was expected, this time corresponding experimentally to a gap in the detector between the proton remnants and the diffractive final state. Based on simple color counting, one indeed expected to see 10% of diffractive events in DIS. This was clearly seen at HERA for the first time, and measured with very high precision [472–475], being one of the important achievement of HERA experiments. Several models can describe the data.

The first one relies on the idea that the Pomeron has a point-like structure [471], like the proton. Then, inspired by Regge theory, the corresponding *diffractive* structure function is expressed as a sum of two components, a Pomeron-like one (defining a Pomeron Structure Function (PSF)) and a secondary Reggeon component (defining a Reggeon structure function). These Pomeron and Reggeon parton densities then obeys DGLAP evolution. This model is referred as the PSF model. In the second model due to Bartels, Ellis, Kowalski and Wüsthoff (BEKW) [476], the diffractive structure function is described through the coupling of a two-gluon ladder, in the spirit of QCD Pomeron, to 2 ($q\bar{q}$ initiated, for $\gamma_{L,T}^*$) and 3 jets ($q\bar{q}g$ initiated, for γ_T^*) final states. This was studied phenomenologically in Ref. [477]. The third one [409, 478] relies on the QCD dipole model [280–283], i.e. on the BFKL approach. Finally, the DIS diffraction data were studied based on the BGW saturation model, which we presented in Sec. 4.6.3.

We refer to Ref. [479] for a global analysis of ZEUS and H1 HERA data, where it is shown that each of the above four models can describe the whole set of data. The best description is provided by the BEKW and the PSF models.

One can try to combine the whole set of data from DIS with a NLLx BFKL treatment with various resummation scheme à la Salam et al. This provides a model with two parameters [480], which, although leading to a description of the data, is less satisfactory than the LLx BFKL description [W5] with 3 parameters.

5.2.2 Transverse energy flow

Based on the fact that it is very hard to disentangle BFKL type of dynamics from conventional partonic evolution à la DGLAP at a fully inclusive level, it has been suggested to use the fact that BFKL ladders allow for a transverse energy flow E_T which is much larger than in conventional partonic evolution, due to the absence of transverse momentum ordering in the multi-Regge kinematics which is the basis of LLx BFKL [481, 482]. The data [483, 484] were rather conclusive in the small x and moderate Q^2 values, and seemed to favor BFKL dynamics. However, we are not aware of more recent model based on a NLLx studies, in which the quasi-multi-Regge kinematics should be implemented. This may change the expected picture, and it would be interesting to investigate the effect of NLLx contributions for this observable.

5.2.3 Energetic forward jet and π^0 production

The hard forward jet production in DIS, with a rapidity gap between the scattered electron and the jet, is one of the key observable which has been proposed for testing BFKL dynamics [485, 486]. The idea is again to maximize the BFKL effects, while reducing DGLAP resummation through the choice of $k_T^2 \sim Q^2$. Since it is an inclusive observable (there is activity between the jet and the scattered electron), it involve the BFKL LLx Pomeron at $t = 0$. The hard scale of the process is provided by the γ^* virtuality and the jet energy. Early HERA data [488–490] have been compared with DGLAP and BFKL predictions, favoring BFKL evolution, in particular in the region where the virtualities of the jet and of the initial $\gamma^*(Q^2)$ are comparable, but not excluding a more standard partonic evolution. In particular, models including resolved photons (like RAPGAP) could describe the data (for highly virtual jets, one gets access to the partonic content of the virtual photon, which should thus be taken into account) [491, 492].

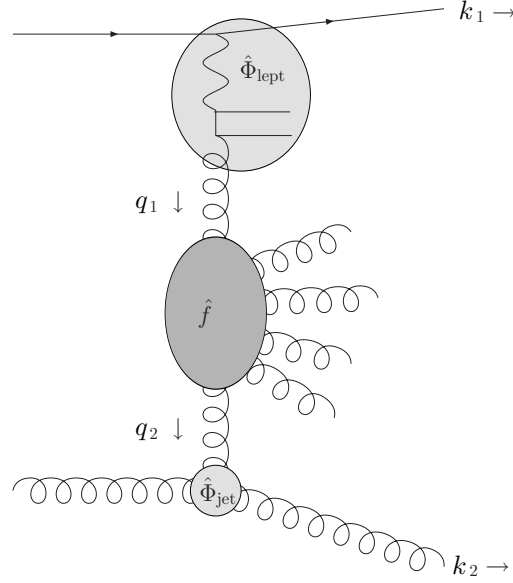


Figure 5.43: Decomposition of the hard partonic cross section in forward jet production. Figure from [487].

Various Monte Carlos have been used for comparison with the most recent data [493, 494]. The CASCADE [495, 496] Monte Carlo is based on the CCFM approach [497–500], which interpolates between BFKL and DGLAP resummations. The CCFM equation is based on angular ordering of the partonic emission and resums the same logs of $1/x$ in the small x limit as the LLx BFKL approach. On the other hand, the Lund dipole model (also called Color Dipole Model (CDM)) [501, 502], which we already mention when discussing the collinear resummed approach à la Salam, is the basis of the ARIADNE Monte Carlo [503].

The situation is the following. For single forward jet, a NLLQ DGLAP approach describes well the data, when combining the direct and resolved photon components [504]. These data are equivalently well described when using the CDM model. Consistently with this Monte Carlo result, approaches based on collinear improved NLLx BFKL leads to a good description of the data for $k_T^2 \sim Q^2$. [505, 506].

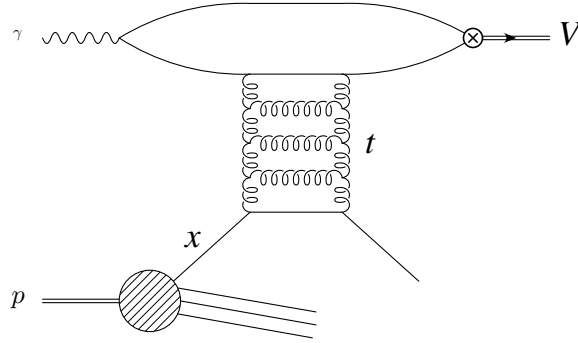
On the other hand, when considering events with *two* forward jets, the NLLQ DGLAP prediction with direct and resolved photon contributions fail to describe the data, while the CDM model, which contains some intrinsically unordered k_T dynamics, specific to perturbative Regge approaches, describes well the data. This might be one of the first sign that data call for a (linear) BFKL type of dynamics, for which partonic approaches fails, at least at the NLLQ level.

Similarly, it has been proposed to study forward photon production [507], by demanding them to be emitted in same hemisphere as the out-going proton (to avoid contamination from the quark-box coupled to the initial virtual photon). These photons could be in principle more reliably measured than forward jets. However, one should isolate them in order to avoid contamination from $\pi^0 \rightarrow \gamma\gamma$ decay. Additionally, due to a $\alpha/(2\pi)$ suppression factor with respect to jet production, the cross-section is much lower. This was studied at LLx BFKL order, giving a strong enhancement with respect to the quark-box contribution. We are not aware of recent studies of that process at NLLx order.

Another observable, of the same type as the one investigated above for Mueller-Navelet jets, has been proposed [508]: the dependence on the azimuthal angle ϕ of the forward jet with respect to the incoming lepton. The lowest order contribution $eq \rightarrow eq$ predicts a back-to-back emission. The $O(\alpha_s)$ corrections, from the partonic processes $e + g \rightarrow e + q\bar{q}$ or $e + q \rightarrow e + q + g$, give a dependency of the type

$$\frac{d\sigma}{d\phi} \sim A + B \cos \phi + C \cos(2\phi). \quad (5.57)$$

$O(\alpha_s^2)$ corrections give a dependency of the same type, but for the B term which vanishes, due to antisymmetry in the polar angle distribution ($\theta \rightarrow \pi - \theta$) of the quark-antiquark pair at the top of the diagram, at the γ^* vertex. At $O(\alpha_s^2)$ these quarks are predominantly produced backwards, i.e they are not tagged as forward jet.

Figure 5.44: Exclusive vector meson production at large t .

After integration over their total phase space the antisymmetric contributions thus cancel out. One thus gets

$$\frac{d\sigma}{d\phi} \sim A' + C' \cos(2\phi) \quad (5.58)$$

with $C' < 0$, thus leading to a maximum at $\phi = \pi/2$. The BFKL ladder is expected to flatten this distribution. This effect has been studied at LLx level in [508] and at NLLx in [487] for the Green function. A full NLLx treatment, including the NLLx jet vertex, in the same spirit as we did for MN jets in Sec. 5.1.1, has not been performed.

5.2.4 Exclusive vector meson production

Hard exclusive vector meson production in the diffractive process $\gamma^{(*)} p \rightarrow V X$ at large s , with a gap in rapidity between the meson and the proton remnants, is enhanced by LLx resummation effects [509, 510]. It is thus a very interesting process to be studied at HERA, since it is an excellent playground in order to understand QCD when combining delicate collinear effects (including possible higher twist contribution) with hard Regge type of dynamics specific to the HERA kinematics. For the same reason, as we will see in the next chapter, ILC will be an ideal place for extending this studies. Much experimental efforts have been devoted to this process by both H1 and ZEUS experiments, with an impressive improvement of the precision, in particular for the measurement of the various spin-density matrix elements [256–261].

Depending on the values of t , the proton would remain almost intact, or would be destroyed by the interaction with the virtual photon. From the theoretical side, a perturbative description is possible when t and/or Q^2 is large, providing the hard scale which justifies factorization. The exclusive $\gamma^* p \rightarrow J/\Psi p$ was the first process to be discussed in this context [511] in the $t = 0$ limit.

On the other hand, at large t , the process $\gamma^{(*)} p \rightarrow V X$ is sensitive to the non-forward structure of the hard Pomeron. The mechanism is then based on the coupling of a Pomeron to an (on-shell) parton extracted from the proton, described by usual PDFs, as illustrated in Fig. 5.44. The approach is thus rather similar to the double exclusive jets production studied above. For the same reason, one need to couple this non-forward Pomeron to the quark or to the gluon in a consistent way, relying on the Mueller-Tang prescription [447]. Many theoretical focussed on the BFKL resummation effects, at LLx order [512], either by iterating the kernel numerically [513] or by taking approximate analytical solution of the non-forward BFKL equation, restricting to the azimuthally symmetric solution $n = 0$ [514]. In these approaches, the coupling to the meson was treated in a non-relativistic way, which means that the quark and antiquark making the meson should equally share the momentum of the meson. This can be justified for heavy mesons like J/Ψ or Υ . In that case, defining the velocity of the quark by v , one can show that $\frac{1}{2}(1-v) \leq x_{1,2} \leq \frac{1}{2}(1+v)$ which gives a support localized at $x_{1,2} \simeq \frac{1}{2}$ in the non-relativistic limit $v \ll 1$ (see for example page 189 of [9]). This does not apply to light-vector meson (ρ, ω, ϕ) for which $v \rightarrow 1$. In that case a more elaborate collinear factorization is needed, leading to the introduction of DAs, as we discussed in Chap. 1.

The first model of diffractive leptonproduction of vector mesons $\gamma^* p \rightarrow V p$ based on QCD factorization involving a DA was presented in the seminal paper [28], in the HERA kinematics, using Q^2 as a hard scale.

It is a LLQ approach in the t -channel, combining meson DA with gluon PDF (at large s skewness was not taken into account and the discussion was restricted to the $t = 0$ case). Emphasize was put on the end-point singularities encountered for transversally polarized meson.

A LLQ model for heavy meson production was then elaborated in [515], introducing a transverse momentum for the quark and antiquark inside the meson, thus going outside of a pure collinear treatment, which lead to the absence of end-point singularities. Results were obtained for the various polarizations of $\gamma^{(*)}$ and V .

Meanwhile, a model was elaborated, which relies on hadron-parton duality, i.e. on the fact that the produced ρ or J/Ψ are seen as resonances in their final multi-hadronic states, with appropriate quantum numbers $J^{PC} = 1^{--}$, and does not use the concept of collinear factorization for the meson production [516–518] (MRT model), and for which therefore the problem of end-point contributions does not exist.

Within the k_T -factorization approach for exclusive processes [519], a full analysis of the polarization effects was performed in [520] for the process $\gamma^* p \rightarrow \rho p$, at large Q^2 . This was done using a dipole description for the γ^* and for the ρ , which was then Fourier transformed to get the impact factor for the $\gamma^* \rightarrow \rho$ transition. The coupling with the proton was treated using a simple model for the proton impact factor, respecting the constraint that it should vanish for vanishing virtuality of the t -channel gluon. Denote as $M_{\lambda_1 \lambda_2}$ the helicity amplitude of the process, where $\lambda_1 = 0, \pm$ is the photon helicity and $\lambda_2 = 0, \pm$ is the vector-meson helicity⁴. The s -channel helicity conservation rule, which we already discussed in Sec. 1.4.7 within a pure collinear approach, was studied within the k_T -factorization [520]. Pure SCHC would mean that $M_{0+} = M_{+0} = M_{+-} = 0$, which is now modified by a possible transfer of orbital momentum from the two t -channel gluons, which is outside of a pure collinear treatment à la ERBL-DGLAP. The obtained results lead to hierarchy:

$$M_{00} > M_{++} > M_{+0} > M_{0+} > M_{+-} \quad (5.59)$$

with the scaling given by

$$\begin{aligned} \frac{M_{+0}}{M_{00}} &\sim \frac{\sqrt{|t|}}{Q} \frac{1}{\sqrt{2}\gamma}, & \frac{M_{++}}{M_{00}} &\sim \frac{\langle M \rangle}{Q} \frac{1+\gamma}{\gamma} & \frac{M_{0+}}{M_{00}} &\sim -\frac{\sqrt{|t|}\langle M \rangle}{Q^2} \frac{\sqrt{2}}{\gamma} \\ \frac{M_{+-}}{M_{00}} &\sim \frac{|t|\langle M \rangle}{Q^3} \frac{2(\gamma+2)}{\gamma} + c \frac{|t|\langle M \rangle}{Q m_\rho^2} \end{aligned} \quad (5.60)$$

where $\langle M \rangle$ is the mean invariant mass of the $q\bar{q}$ dipole, weighted by the ρ light-cone wave function, which is expected to be of the order of the meson mass (except for peculiar configurations for which the dipole may become larger, see below). Eq.(5.60) leads to the hierarchy (5.59) for the gluon anomalous between .5 and .7. No end-point singularity was encountered in this approach, due to the off-shellness of the t -channel exchanged momentum, by an amount of k_T^2 , playing the role of a regulator in comparison with usual GPD or PDF based approaches in which parton are on the mass-shell.

The recent HERA data [260, 261] are in agreement with the above hierarchy, as can be seen for the two dominant transitions in Fig. 5.45. They exhibit the expected twist 2 dominance of the $\gamma_L^* \rightarrow \rho_L$ transition with respect to the the $\gamma_T^* \rightarrow \rho_T$. The $W_{\gamma^* p}^2$ evolution is governed by a Pomeron-like behaviour. A transition is seen in the data, governed by the parameter $Q^2 + M_V^2$, from a DL type of intercept [305] towards a hard Pomeron intercept of the order of 1.3, compatible with inclusive DIS studies. The data for ratio $\sigma_L/\sigma_T = |M_{00}|^2/|M_{11}|^2$ are also consistent with the MRT model [516–518]. This may indicate that this ratio is not very sensitive to the precise form of the ρ wave-function.

It turns out that the data can also be well described by a GPD like evolution, when including a gaussian ansatz for the meson wave function combined with Sudakov resummation effects [171–173]. The effect of saturation in exclusive meson production has been addressed by many authors [397, 398, 406, 408]. See [261, 263] for a comparison between some models including saturation and the most recent data, showing that electroproduction of meson can be described in a dipole model including saturation. Thus, the situation at the moment is rather confusing. There seems to be a need for at least a linear BFKL type of dynamics. However, improved GPD like model can describe the data. Light-meson electroproduction at large W^2 is a very complex process, due to the mixing between several type of dynamics (collinear and Regge-like), combined with various sources of higher twist contribution (from the meson side as well as from the Pomeron side). It is thus very premature to extract any definite conclusion at the moment when comparing the data with the available

⁴One should be aware to the fact that experimentalists usually denote these helicity amplitude by permutting the two indices, see for example Ref. [261].

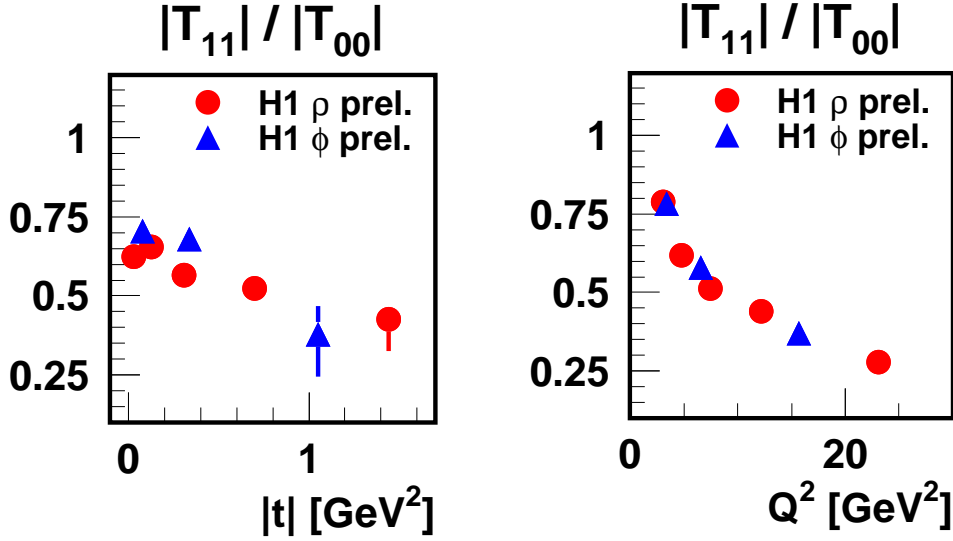


Figure 5.45: H1 data for the ratio of the two dominant transitions in light-meson electroproduction, with the notations $T_{11} = M_{++}$ and $T_{00} = M_{00}$. Figure from X. Janssen (H1) DIS 2008 [262].

models. In Chap. 6, we will study in detail how a consistent twist-3 treatment of ρ -electroproduction (including both 2 and 3-body contributions) can be carried on. We will compute explicitly the $\gamma^* \rho$ impact factor up to twist 3 both within CCF and LCCF methods. This new building block should provide very interesting phenomenological effects for any semi-hard exclusive process.

The photoproduction process $\gamma p \rightarrow \rho X$ has been studied at large t , in Ref. [521], taking into the chiral-odd DA of the photon which can contribute at low values of Q^2 in addition to its chiral-even ponctual coupling. Both chiral odd and chiral even ρ -meson had thus to be considered in order to get a consistent treatment. The authors of Ref. [521] restricted themselves to the WW approximation, therefore only considering 2-partons contributions to the ρ -meson, the twist 3 contributions being generated by pure kinematical effects. Again denoting as $M_{\lambda_1 \lambda_2}$ the helicity amplitude of the process, where $\lambda_1 = \pm$ is the photon helicity and $\lambda_2 = 0, \pm$ is the vector-meson helicity, one obtains the following results from the point of view of end-point singularities: the non-spin flip chiral-even part M_{++}^{even} as well as the single spin-flip chiral-odd part M_{+0}^{odd} and double spin-flip chiral-odd part M_{+-}^{odd} faces end-point singularities, while other contribution are finite. Thus, contrarily to the electroproduction case, it seems that the off-shellness of the t -channel exchanged gluons is not enough to prevent end-point singularities. A detailed analysis with respect to t -scaling however showed that in the phenomenological accessible range, the finite contribution M_{++}^{odd} should dominate with respect to other contributions.

However, one of the problem arising from the t -shape of the data is the fact that they behave like $d\sigma/dt \sim 1/t^3$, while the standard chiral even analysis, confirmed by the analysis of Ref. [521], predict a behaviour like $d\sigma/dt \sim 1/t^4$ for the $T \rightarrow T$ transitions and $d\sigma/dt \sim 1/t^3$ for the $T \rightarrow L$ transition. The addition of a chiral odd contribution does not change this behaviour.

A LLx analysis of the HERA data at the level of differential cross-section $d\sigma/dt$ indicated a need for LLx type of resummation both for heavy and light vector mesons [522, 523]. Note that effect of NLLx simulated by the modified BFKL LLx through the kinematical constraint was found to have quite an important effect, strongly depending on the scale taken for the running coupling. A somehow similar analysis to the one of [521] have been carried on more recently in [524, 525]. The chiral-odd contributions are then obtained by giving a constituent mass to the quark. As is well known, such a term is responsible for chiral-odd transitions. The problem of end-point singularities, which might be a sign for breaking of factorization, has been adressed in this analysis. It was shown that BFKL LLx resummation improves the infrared behaviour, as is usual for BFKL Pomeron. This model leads to a good description of the data at the level of $d\sigma/dt$ within a pure LLx treatment (Fig. 5.46). It however needs a phenomenological adjustment of the s_0 parameter which is needed to define the rapidity and which is not prescribed in LLx, taken there to be a linear combination of m_ρ^2 and t .

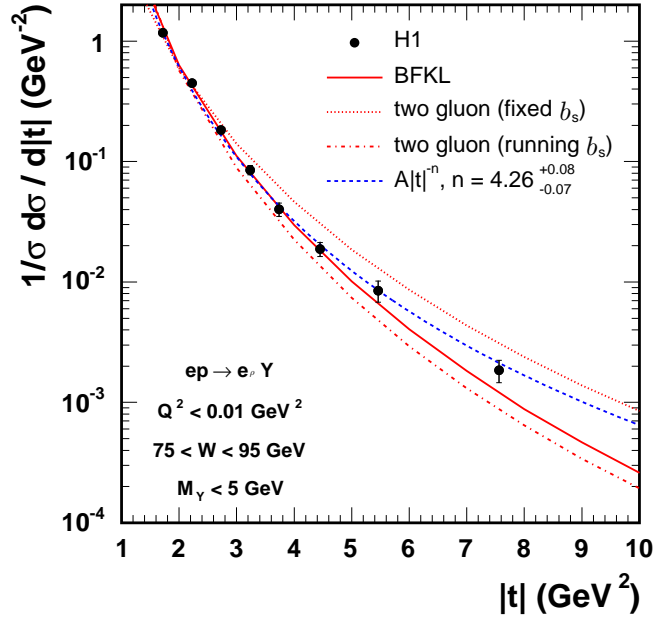


Figure 5.46: Exclusive vector meson production at HERA. Figure from [524].

When distinguishing the ρ_T and ρ_L production amplitude through the measured spin-density matrix element r_{10}^{04} coefficient (which is approximately proportional to $|M_{+0}|^2$), the models of [525] failed in describing the data, getting a contribution with a wrong sign, although one may claim that the experimental value is small.

Another approach, based on a modified meson wave function which goes outside the pure collinear approximation has been developed. In this model, the quark and antiquark can carry transverse momenta with respect to the meson momentum. Their distribution is given by a gaussian distribution

$$\Psi^{V\lambda}(\ell, z) = f_V \frac{V^\lambda(\ell, z, m_V)}{m_V^2} \exp \left[-\frac{|\ell|^2 + m_q^2}{z\bar{z}m_V^2} \right] \quad (5.61)$$

in a similar way as the GPD like approach of [171–173] for meson electroproduction. The form is motivated by QCD sum rules. It is obtained by Borel transformation of the quark propagator coupled to the virtual photon with respect to Q^2 and by substitution of the Borel variable by m_V^2 , where m_V is of the order of the meson mass [526]. This model can be used after Fourier transform in transverse coordinate space to get a dipole formulation of the scattering process. The usual hard contribution is obtained when all propagators involved in the impact factor when coupling the t -channel gluons to the photon are far off-mass shell. In dipole language, it means that the dipole have a small size. However, there are two interesting situations in which this dipole which scatter off the proton can have a large size. The first situation occurs when the longitudinal fraction of the momentum carried by quark or antiquark building the meson vanishes. This potential end-point singularity contribution are regularized by the above ansatz (5.61). Indeed, as shown in [527], the end-point contributions can be resummed at all twist and leads to a finite result. The second situation of large dipole size occurs when the t -channel gluons are attached to 2 different quark lines. In that case, for photoproduction, the quark propagators between a t -channel gluon and the photon can have a momentum which is purely longitudinal, for certain configurations of the hard t -channel gluons. This leads to a typical topology very similar to the upper part of Fig. 1.4 which we shortly discussed in the large angle Landshoff mechanism. Indeed, in this situation both the quark which is part of the dipole coupled to the ρ and the quark which is part of the dipole coupled to the photon have almost zero transverse momentum [528]. This mechanism⁵, combined with a double-logarithmic $\sum(\alpha_s \ln 1/x \ln t)^n$ approximation, leads to a flattening of the t dependency for the non-flip transition amplitude. This could provide an explanation for the similar experimental magnitude of ρ_L and ρ_T photoproduction. It also provides a correct sign for the r_{10}^{04} coefficient.

The diffractive photoproduction of photon has also been studied [519, 529–531], within k_T -factorization in LLx. The amplitude is dominated by non-flip transitions (the flip transition is $1/t$ suppressed with respect to

⁵This model does not include any chiral-odd contribution.

the non-flip transition). The corresponding non-flip transition amplitude is predicted to fall off like $1/t$ at the Born level (two gluon exchange). When taking into account LLx BFKL evolution, the fall off at the level of the cross-section should go much faster than $1/t^2$, basically due to the fact that at the level of the amplitude, the enhancement factor goes like $\exp(12 \ln 2 \alpha_s / \pi \ln W^2 / (-t))$. Even for very unnatural low values of $\alpha_s \sim .14$, it would lead to a cross-section scaling at least like $1/t^{2.8}$. This has been measured by the H1 experiment [532]. Although the W^2 evolution is compatible with a BFKL type of evolution (but statistics prevent from any conclusion, the value of the intercept being not very well constraint), the observed t shape is $1/t^{2.6}$, much less steeper than predicted by LLx.

Before ending this section, we should comment on the fact that we have ignored in the above discussion the effect of the non-forward kinematics, of the GPD type. This question was addressed in [533]. Based on the fact that the QCD evolution is based on splitting of partons, it tends to push partons from large to low value of x when increasing Q^2 . In the low x_{Bj} limit, i.e. low ξ limit, the typical non-diagonal content of GPDs, at a given scale Q^2 for $x \sim \xi$, arises from the evolution of partonic distribution at a low Q_0^2 value with $x \gg \xi$. It thus means that the *intial* partonic content could be described only in terms of usual forward PDFs, leading to a kind of “washing-out” of non-forward effects. This can be quantitatively implemented using the Shuvaev transform [534] which relies on the fact that due to the conformal invariance of LLQ ERBL-DGLAP evolution, known to be diagonalized through Gegenbauer moments, it is possible to recast the study of GPD evolution as the DGLAP evolution of some usual PDFs, if one can find effective forward PDFs whose Mellin moment are equal to Gegenbauer moments of the GPD under study. This problem can be analytically solved, giving an integral transform which relates the GPD with this effective PDF. The detailed study of [533] showed that this “washing-out” effect turns in practice to a multiplicative correction factor, the so-called Shuvaev factor, when passing from PDFs to GPDs at small x_{Bj} , which tends to unity in the typical kinematical range of HERA we are here considering, with a precision of the order of 10%. See however [23] for a review of the limitation of this method.

5.3 $\gamma^* \gamma^*$ at LEP2

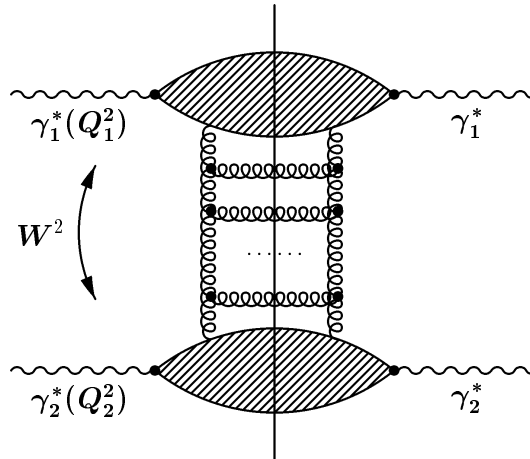


Figure 5.47: The $\gamma^* - \gamma^*$ total cross-section in k_T -factorization. Figure from [535].

The LEP2 available energy ($\sqrt{s_{e^+e^-}} = 183$ to 202 GeV) allowed tests of the total $\gamma^* \gamma^*$ cross-section, thus realizing the idea of onium-onium total cross-section. This process was studied with LLx BFKL [536–538], dipole model [W9, 539], modified LLx BFKL (based on kinematical constraints) [535, 540] (see Fig. 5.48a). A NLLx BFKL was carried on [326, 327] (see Fig. 5.49a), based on a NLLx Green function and a LLx impact factor, with a BLM [158] prescription which had the effect of significantly reduce the NLLx corrections with respects to the LLx Pomeron.

The LEP data [541–544] have been analyzed in view of these models. Fig. 5.48b displays the comparison [540] between OPAL data and modified LLx BFKL (modified by kinematical constraints), including quark box

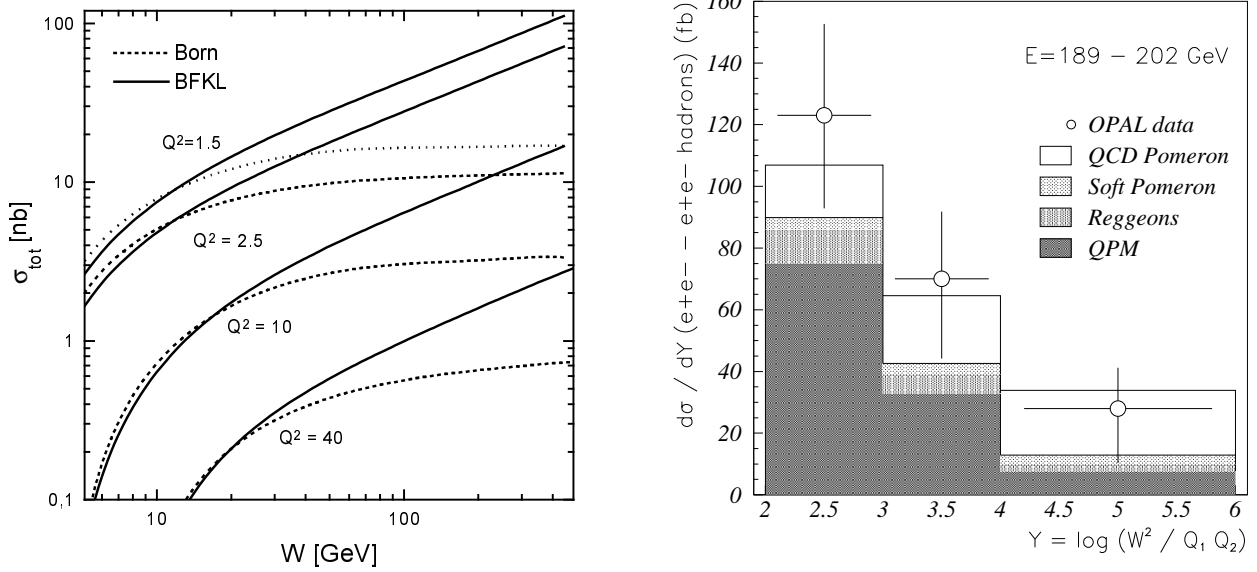


Figure 5.48: a (left): Modified LLx BFKL prediction, with $s_0 = Q^2$ (upper curve) and $s_0 = 4Q^2$ (lower curve) versus Born. b (right): OPAL LEP2 data for $\gamma^*\gamma^*$ total cross-section. versus modified LLx BFKL prediction. Figures from [540].

(simulating usual DGLAP for $Q_1 \sim Q_2$), soft Pomeron and reggeon contributions. A comparison between DELPHI data [541] and the NLLx model of Ref. [327] is given in Fig. 5.49. First, the Born 2 gluon exchange and quark exchange are too small in the large Y set of the data. Second, LLx BFKL is too high (even including quark mass effects, which have an important effect [545]). The scenarios with modified LLx BFKL or NLLx BFKL with BLM scale fixing is plausible, but not needed by the data which could equally well be described by LLQ type of resummations, except in the large rapidity domain, for rapidities larger than 4, where there is presumably a sign of BFKL type of dynamics. Due to the very complicated form of the NLLx $\gamma^* \rightarrow \gamma^*$ impact factor, which is at present not available in a closed ready-to-use form, there have been no complete NLLx study of the $\gamma^*\gamma^*$ total cross-section. Recently, one step further has been made, by adding to the LLx impact factor additional NLLx terms needed to implement the invariance of the full amplitude with respect to s_0 and μ_R dependence [546]. This has been done based on BLM [158] and PMS [153, 154] procedure. This should be contrasted with Ref. [326, 327] where the BLM procedure was implemented at the level of the intercept itself, which is not supposed to be a physical observable. However, it turns out that these two results are compatible, and that this NLLx Green function + LLx improved impact factor also describes the LEP2 data at large rapidity.

However, lack of statistics forbade any definite conclusion, as one can see in Fig. 5.49b, specially for the interesting experimental point at $Y = 5.5$ which has a very large uncertainty. Indeed, the luminosity (617 pb^{-1} for L3, 592.9 pb^{-1} for OPAL, 640 pb^{-1} for ALEPH, 550 pb^{-1} for DELPHI) and the energy were limited. Further, since the cross-section decreases very rapidly when the virtualities of the γ^* increases, low (although still perturbative) values of Q^2 are required, corresponding to out-going leptons very close from the beam pipe. At LEP 2, due to a rather high minimal detection angle, of only 30 mrad, the tagging of out-going leptons did not allow for high counting rates. Including all LEP 2 data, only 491 events at L3, 133 events for OPAL, 891 events for ALEPH were collected. Thus, no definite conclusion could be obtained about a signal of BFKL type of dynamics. This situation would of course change if we would have a high energy and luminosity collider, with dedicated forward detectors. This should be the case at ILC, as we will discuss in Chap. 7.

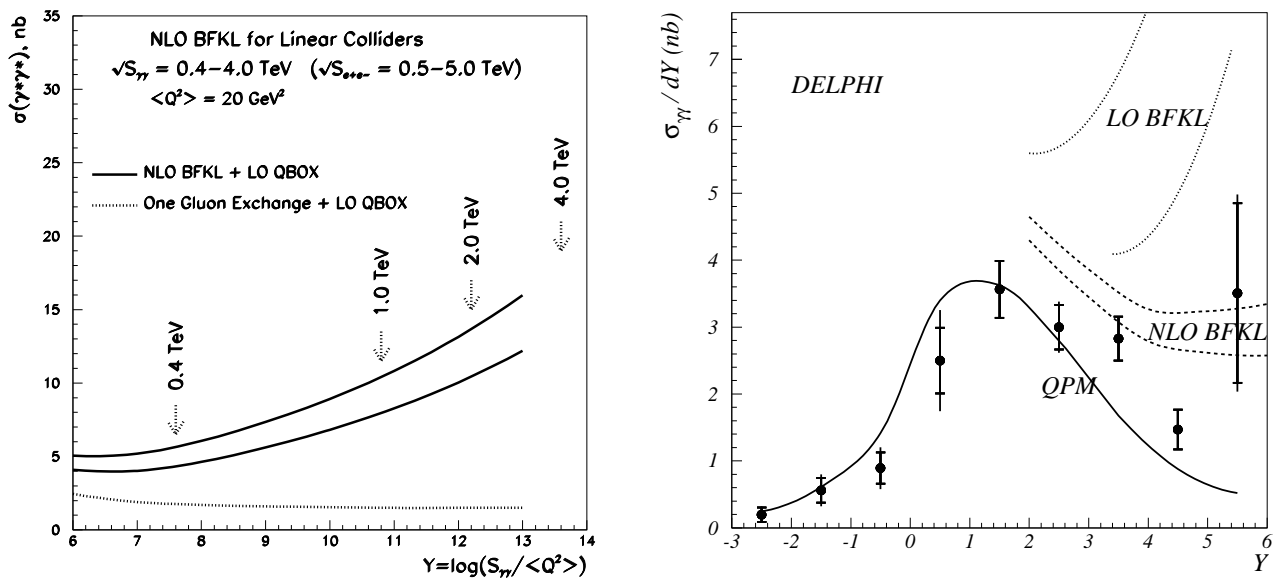


Figure 5.49: a (left): The two solid curves are BLM scale-fixed NLLx BFKL, with $s_0 = Q^2$ (upper curve) and $s_0 = 4Q^2$ (lower curve). The dotted curve is the Born two gluon contribution plus the quark box exchange. Figure from [327]. b (right): DELPHI data, compared with these NLLx predictions, with LLx and with the quark-parton model (QPM), which is included in both NLLx and LLx predictions. Figure from [541].

Chapter 6

Exclusive processes in the Regge limit beyond leading twist

Based on [W24]

As we have seen in Chap. 4, impact factors (including jet vertices) are building blocks of high energy reactions in the k_T -factorization approach. At the moment, several impact factors are known at the LLx level and at twist 2. Some impact factors have been computed at NLLx: the $\gamma^* \rightarrow \gamma^*$ impact factor, which enters the $\gamma^* \rightarrow \gamma^*$ total cross-section, the forward $\gamma^* \rightarrow \rho$ impact factor [317], and the forward jet vertex. We have seen in the specific example of MN jets (see Sec. 5.1.1), which is one of the first complete NLLx treatment that have been carried on [W27] (with the case of forward diffractive $\gamma^* \gamma^* \rightarrow \rho \rho$ production [328, 439, 443]), that these corrections, contrarily to the general belief, can be very important, when passing from a LLx impact factor combined with a NLLx Green function to a NLLx impact factor combined with a NLLx Green function.

Besides this, as we have seen in the previous chapter, the detailed polarization studies for the various $\gamma_{L,T}^* \rightarrow \rho_{L,T}$ transition in ρ -electroproduction extracted from HERA data exhibit two dominant transitions: the dominating twist 2 $\gamma_L^* \rightarrow \rho_L$ and the twist 3 $\gamma_T^* \rightarrow \rho_T$. This later one has been measured and is by no means negligible. From the theory side, we have seen that various models exist. One of their common feature is that they exhibit a huge sensitivity with respect to twist 3 or higher effects (end-point contribution, Landshoff mechanism, chiral-odd contributions...). According to our knowledge, there is at the moment no full-twist 3 computation of any hard exclusive process, and such a computation from first principle might be of importance in order to check whether the data ask for a dynamical twist 3 contribution which would go beyond a pure kinematical twist 3 description à la WW. This could be tested using asymptotical DAs. In the future, this could be used for describing

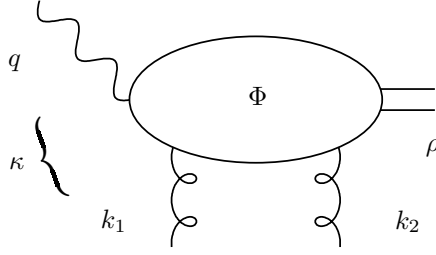
$$\gamma^*(q) + \gamma^*(q') \rightarrow \rho_T(p_1) + \rho(p_2) \quad (6.1)$$

at ILC. In the next chapter, we will study in detail $\gamma_{L,T}^*(q) + \gamma_{L,T}^*(q') \rightarrow \rho_L(p_1) + \rho_L(p_2)$, leaving the phenomenological study of $\gamma^*(q) + \gamma^*(q') \rightarrow \rho_T(p_1) + \rho(p_2)$ for future projects.

On the other hand, as we have seen from the beginning of this manuscript, ρ -exclusive production is an interesting playground for developing and testing theoretical tools, besides any phenomenological question. This was in particular our basic object when exhibiting a picture of factorization at moderate energy involving a TDA and a GDA at twist 2, see Sec. 2.4.

As we have seen in Chap. 3, the application of factorization to the description of an exclusive process beyond leading twist is not straightforward. One of our goal for the present study is to show explicitly, on a specific example at twist 3 level, how the LCCF leads to rather simple practical computations. We will thus now compute in detail the $\gamma_T^* \rightarrow \rho_T$ impact factor up to twist 3. This will be done both within LCCF and CCF approaches, in the forward limit. We will show that these two results are identical, and that they are gauge invariant and free of any end-point singularities [W24, W48, W50, W54, W56].

A perturbative treatment of the process (6.1) is valid within k_T -factorization whenever the virtual photons carry large squared momenta $q^2 = -Q^2$ ($q'^2 = -Q'^2$) $\gg \Lambda_{QCD}^2$, and the Mandelstam variable s obeys the condition $s \gg Q^2, Q'^2, -t \simeq \underline{t}^2$. The hard scale which justifies the applicability of perturbative QCD is set by

Figure 6.1: $\gamma^* \rightarrow \rho$ impact factor.

Q^2 and Q'^2 and/or by t . Neglecting meson masses, one considers for reaction (6.1) the light cone vectors p_1 and p_2 as the vector meson momenta ($2p_1 \cdot p_2 = s$). The virtual photon momentum q then reads as usual

$$q = p_1 - \frac{Q^2}{s} p_2. \quad (6.2)$$

We focus here on the $\gamma^* \rightarrow \rho$ impact factor Φ of the subprocess

$$g(k_1, \varepsilon_1) + \gamma^*(q) \rightarrow g(k_2, \varepsilon_2) + \rho_T(p_1), \quad (6.3)$$

illustrated in Fig. 6.1a. As we have seen in Sec. 4.2, it is the integral of the S -matrix element $\mathcal{S}_\mu^{\gamma^* g \rightarrow \rho_T g}$ with respect to the Sudakov component of the t -channel k momentum along p_2 , or equivalently the integral of the κ -channel discontinuity of the S -matrix element $\mathcal{S}_\mu^{\gamma^* g \rightarrow \rho_T g}$:

$$\Phi^{\gamma^* \rightarrow \rho}(\underline{k}, \underline{r} - \underline{k}) = e^{\gamma^* \mu} \frac{1}{2s} \int_{-\infty}^{+\infty} \frac{d\kappa}{2\pi} \mathcal{S}_\mu^{\gamma^* g \rightarrow \rho g}(\underline{k}, \underline{r} - \underline{k}) = e^{\gamma^* \mu} \frac{1}{2s} \int_0^{+\infty} \frac{d\kappa}{2\pi} \text{Disc}_\kappa \mathcal{S}_\mu^{\gamma^* g \rightarrow \rho g}(\underline{k}, \underline{r} - \underline{k}), \quad (6.4)$$

where $\kappa = (q + k_1)^2$ denotes the Mandelstam variable s for the subprocess (6.3), as illustrated in Fig. 6.1. Note that the two reggeized gluons have so-called non-sense polarizations $\varepsilon_1 = \varepsilon_2^* = p_2 \sqrt{2/s}$. Considering the forward limit for simplicity, the gluon momenta reduce to

$$k_1 = \frac{\kappa + Q^2 + \underline{k}^2}{s} p_2 + k_\perp, \quad k_2 = \frac{\kappa + \underline{k}^2}{s} p_2 + k_\perp, \quad k_1^2 = k_2^2 = k_\perp^2 = -\underline{k}^2. \quad (6.5)$$

Finally, let us note that when writing (6.5) we took an exact kinematics for the fraction of momentum along p_2 . This kinematics naturally extends the usual Regge kinematics in the case where t -channel momentum transfer along p_2 is allowed, which corresponds to the skewed kinematics which is typical of GPD studies. In usual computation of impact factors used in k_T -factorization, one usually makes the approximation that these two fractions are exactly opposite. Here we make such a choice in order to introduce skewedness effects in a correct manner since these terms will contribute at the twist 3 order we are interested in. Note that within k_T -factorization, the description of impact factor for produced hadron described within QCD collinear approach requires a modification of twist counting due to the off-shellness of the t -channel partons. Therefore, when here we say "up to twist 3" we only mean twist counting from the point of view of the collinear factorization of the produced ρ -meson, and not of the whole amplitude, e.g. $\gamma^* p \rightarrow \rho p$ or $\gamma^* \gamma^* \rightarrow \rho p$.

In order to describe the collinear factorization of ρ -production inside the impact factor (6.4), we note that the kinematics of the general approach discussed in Chap. 3 is related to our present kinematics for the impact factor (6.4) by setting $p = p_1$, while a natural choice for n is obtained by setting $n = n_0 = p_2 / (p_1 \cdot p_2)$ (this latter choice for n , though natural, is somehow arbitrary as we discussed in Sec. 3.5.1).

We will now distinguish and make a comparative analysis of two different approaches: LCCF and CCF. We will show that these two results are actually fully equivalent to each other, when using the dictionary of Sec. 3.6.

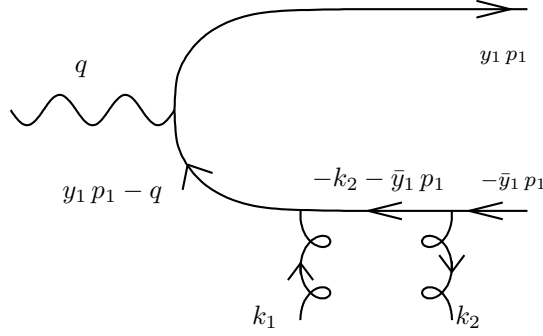


Figure 6.2: The detailed structure of the diagram (a).

6.1 Calculation based on the Light-Cone Collinear Factorization approach

6.1.1 $\gamma_L^* \rightarrow \rho_L$ transition as a recall

Working within the LCCF, we first recall the calculation of the $\gamma_L^* \rightarrow \rho_L$ transition which receives contribution only from the diagrams with quark-antiquark correlators¹. It is given by contributions from the p_μ term of the correlators (3.10) of the twist 2. Higher order corrections would start at twist 4, which is below our accuracy. The computation of the corresponding impact factor is standard [509]. It involves the computation of the 6 diagrams of Fig. 3.4. The longitudinal polarization of the virtual photon reads, in the Sudakov basis,

$$e_{\gamma_L}^\mu = \frac{1}{Q} \left(p_1^\mu + \frac{Q^2}{s} p_2^\mu \right), \quad (6.6)$$

while the momentum of the ρ reads

$$p_\rho^\mu = p_1^\mu + \frac{m_\rho^2}{s} p_2^\mu, \quad (6.7)$$

and the longitudinal polarization of the ρ is

$$e_L^\mu \equiv e_{\rho_L}^\mu = \frac{1}{m_\rho} \left(p_1^\mu - \frac{m_\rho^2}{s} p_2^\mu \right). \quad (6.8)$$

Consider for example the diagram (a) of Fig. 3.4, as illustrated in Fig. 6.2. Computing the corresponding S -matrix element, the corresponding contribution to the impact factor reads

$$\Phi_a = -e_q \frac{1}{4} \frac{2}{s} (-i) f_\rho m_\rho g^2 \frac{\delta^{ab}}{2N_c} \frac{1}{2s} \int_0^1 dy \int \frac{d\kappa}{2\pi} \frac{\text{Tr}[\not{\epsilon}_{\gamma_L}(y \not{p}_1 - \not{q}) \not{p}_2 (\not{k}_2 + \bar{y} \not{p}_1) \not{p}_2 \not{p}_1]}{[(y p_1 - q)^2 + i\eta][(k_2 + \bar{y} p_1)^2 + i\eta]} \varphi_1(y), \quad (6.9)$$

where the factor $1/4$ is reminiscent from the Fierz identity, the factor $2/s$ comes from the normalization of the non-sense polarizations. Finally, the color factor $\frac{\delta^{ab}}{2N_c}$ is due to the fact that when summing over the color of the t -channel gluons, the net color coefficient for $\gamma^* \gamma^* \rightarrow \rho \rho$ should be $(N_c^2 - 1)/(4N_c^2)$ (due a Fierz factor $1/N_c$ when factorizing each of the two ρ DAs). Among the two propagators, only the second one, involving $(k_2 + \bar{y} p_1)^2 + i\eta = \kappa \bar{x} - \underline{k}^2 x + i\eta$ has a pole in κ , contributing when closing the contour below (therefore contributing to the discontinuity). The result is then easily obtained after extracting the corresponding residue. Diagram (c) provide the same contribution, since it can be obtained from (a) by the replacement $x \leftrightarrow \bar{x}$. Diagrams (b) and (d) vanishes for this twist 2 transition. Diagrams contributes only when closing the κ contour

¹Hereafter, except for final results, we perform the computation for a meson which would be a one flavour quark-antiquark state. Its wave function is then restored at the very end.

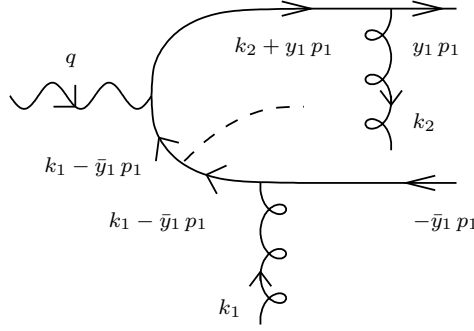


Figure 6.3: The detailed structure of the diagram (b1).

above. Finally, the net result for the $\gamma_L^* \rightarrow \rho_L$ impact factor is, after taking into account the ρ^0 wave function

$$\Phi^{\gamma_L^* \rightarrow \rho_L}(\underline{k}^2) = \frac{2e g^2 f_\rho}{\sqrt{2} Q} \frac{\delta^{ab}}{2N_c} \int_0^1 dy \varphi_1(y) \frac{\underline{k}^2}{y \bar{y} Q^2 + \underline{k}^2}. \quad (6.10)$$

Note that diagrams (a) and (c) of Fig. 3.4 are the only diagrams which contribute when computing the hard part by closing the κ contour below.

6.1.2 $\gamma_T^* \rightarrow \rho_T$ transition

We now concentrate on the $\gamma_T^* \rightarrow \rho_T$ transition, which impact factor will be one of the main results of this paper. The 2-parton contribution contains the terms arising from the diagram Fig. 3.4, where the quark-antiquark correlators have no transverse derivative, and from the diagrams Fig. 3.5, where the quark-antiquark correlators stand with a transverse derivatives. The computation of the diagrams of Fig. 3.4 for the $\gamma_T^* \rightarrow \rho_T$ transition goes along the same line as for the twist 2 $\gamma_L^* \rightarrow \rho_L$ transition discussed above. The practical trick used for computing the contributions of Fig. 3.5 is the Ward identity

$$\frac{\partial}{p_\mu} \longrightarrow \text{---} \text{---} \text{---} = \text{---} \text{---} \bullet \text{---} \text{---} \text{---} \quad \text{where} \quad \text{---} \text{---} \text{---} = \frac{1}{m - \not{p} - i\epsilon}, \quad (6.11)$$

where lines denotes fermionic propagators. This leads to an additional Feynman rule when inserting a derivative. The corresponding insertions are denoted with dashed lines in Fig. 3.5.

Consider for example the diagram (b1) of Fig. 3.5, illustrated in Fig. 6.3. Computing the corresponding S -matrix element for the vector part, the corresponding contribution to the impact factor reads

$$\Phi_{b1}^V = -e_q \frac{1}{4} \frac{2}{s} (-i) g^2 f_\rho m_\rho \frac{\delta^{ab}}{2N_c} \frac{1}{2s} \int_0^1 dy \int \frac{d\kappa}{2\pi} \text{Tr}[\not{\epsilon}_\gamma(k_1 - \bar{y} \not{p}_1) \not{\epsilon}_T^*(k_1 - \bar{y} \not{p}_1) \not{p}_2 \not{p}_1 \not{p}_2(k_2 + y \not{p}_1)] \varphi_3^T(y), \quad (6.12)$$

This part of the impact factor receives (identical) contributions when closing the κ integration contour either from above or from below, which reads

$$\Phi_{b1}^V = -\frac{e_q g^2}{2} f_\rho m_\rho \frac{\delta^{ab}}{2N_c} \int_0^1 dy y \frac{-e_T^* \cdot e_\gamma (y \bar{y} Q^2 + \underline{k}^2) + 2e_T^* \cdot k e_T^* \cdot k (1 - 2y)}{(Q^2 y \bar{y} + \underline{k}^2)^2} \varphi_3^T(y). \quad (6.13)$$

The computation of the axial part is similar (note the $i/4$ factor from Fierz)

$$\Phi_{b1}^A = -e_q \frac{i}{4} \frac{2}{s} (-i) g^2 f_\rho m_\rho \frac{\delta^{ab}}{2N_c} \frac{1}{2s} \int_0^1 dy \int \frac{d\kappa}{2\pi} \text{Tr}[\not{\epsilon}_\gamma(k_1 - \bar{y} \not{p}_1) \gamma_\alpha(k_1 - \bar{y} \not{p}_1) \not{p}_2 \not{p}_1 \gamma_5 \not{p}_2(k_2 + y \not{p}_1)] \epsilon_{e_T^* p m}^\alpha \varphi_3^T(y), \quad (6.14)$$

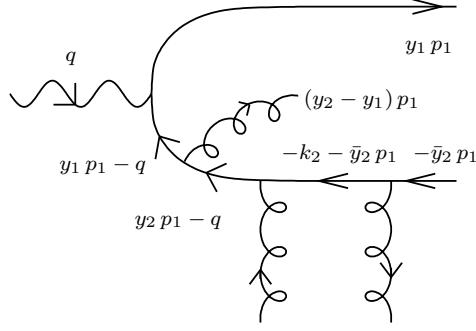


Figure 6.4: The detailed structure of the diagram (aG1).

and leads to

$$\Phi_{b1}^A = -\frac{e_q g^2}{2} f_\rho m_\rho \frac{\delta^{ab}}{2N_c} \int_0^1 dy y \frac{-e_T^* \cdot e_\gamma (y \bar{y} Q^2 - \underline{k}^2) + 2 e_T^* \cdot k e_T^* \cdot k}{(Q^2 y \bar{y} + \underline{k}^2)^2} \varphi_A^T(y). \quad (6.15)$$

The contributions of 3-parton correlators are of two types, the first one being of "abelian" type (without triple gluon vertex, see Fig.3.6) and the second involving non-abelian coupling with one triple gluon vertex (see Fig.3.7) or two (see Fig.3.8). Let us first consider the "abelian" class. They involve two kind of Casimir invariants:

$$\begin{aligned} \frac{1}{N_c} Tr(t^c t^a t^b t^c) &= C_F \frac{\delta^{ab}}{2N_c} \equiv C_a \frac{\delta^{ab}}{2N_c} : (\text{aG1}), (\text{cG1}), (\text{eG1}), (\text{fG1}) \\ \frac{1}{N_c} Tr(t^c t^a t^c t^b) &= \left(C_F - \frac{N_c}{2}\right) \frac{\delta^{ab}}{2N_c} \equiv C_b \frac{\delta^{ab}}{2N_c} : (\text{bG1}), (\text{dG1}), (\text{aG2}), (\text{cG2}), (\text{bG2}), (\text{dG2}), (\text{eG2}), (\text{fG2}), \end{aligned} \quad (6.16)$$

where the $1/N_c$ comes from the Fierz coefficient when factorizing the quark-antiquark state in color space. Again, to illustrate the method, we consider the peculiar diagram (aG1) of Fig.3.6, illustrated in Fig.6.4. The vector contribution reads

$$\begin{aligned} \Phi_{aG1}^V &= -e_q \frac{1}{4} \frac{2}{s} (i) g^2 f_\rho m_\rho \frac{\delta^{ab}}{2N_c} \frac{1}{2s} \int_0^1 dy_1 dy_2 \int \frac{d\kappa}{2\pi} \frac{Tr[\not{\epsilon}_\gamma (y_1 \not{p}_1 - \not{q}) \not{\epsilon}_T^* (y_2 \not{p}_1 - \not{q}) \not{p}_2 (\kappa_2 + \bar{y}_2 \not{p}_1) \not{p}_2 \not{p}_1]}{[(y_1 p_1 - q)^2 + i\eta][(y_2 p_1 - q)^2 + i\eta][(\kappa_2 + \bar{y}_2 p_1)^2 + i\eta]} \\ &\times B(y_1, y_2), \end{aligned} \quad (6.17)$$

and equals

$$\Phi_{aG1}^V = -\frac{e_q g^2}{2} f_\rho m_\rho \frac{\delta^{ab}}{2N_c} \int_0^1 dy_1 dy_2 \frac{e_T^* \cdot e_\gamma}{\bar{y}_1 Q^2} B(y_1, y_2). \quad (6.18)$$

The corresponding axial contribution reads

$$\begin{aligned} \Phi_{aG1}^A &= -e_q \frac{i}{4} \frac{2}{s} (i) g^2 f_\rho m_\rho \frac{\delta^{ab}}{2N_c} \frac{1}{2s} \int_0^1 dy_1 dy_2 \int \frac{d\kappa}{2\pi} \frac{Tr[\not{\epsilon}_\gamma (y_1 \not{p}_1 - \not{q}) \gamma_\alpha (y_2 \not{p}_1 - \not{q}) \not{p}_2 (\kappa_2 + \bar{y}_2 \not{p}_1) \not{p}_2 \not{p}_1]}{[(y_1 p_1 - q)^2 + i\eta][(y_2 p_1 - q)^2 + i\eta][(\kappa_2 + \bar{y}_2 p_1)^2 + i\eta]} \\ &\times \epsilon_{e_T^* p n}^\alpha D(y_1, y_2), \end{aligned} \quad (6.19)$$

and equals

$$\Phi_{aG1}^A = -\frac{e_q g^2}{2} f_\rho m_\rho \frac{\delta^{ab}}{2N_c} \int_0^1 dy_1 dy_2 \frac{e_T^* \cdot e_\gamma}{\bar{y}_1 Q^2} D(y_1, y_2). \quad (6.20)$$

Consider now the "non-abelian" diagrams of Fig.3.7, involving a single triple gluon vertex. They involve two

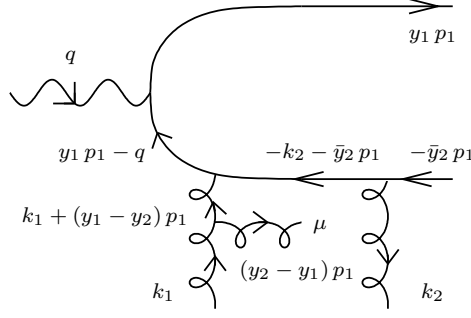


Figure 6.5: The detailed structure of the "non-abelian" (with one triple gluon vertex) diagram (atG1).

kind of color structure:

$$\frac{2}{N_c^2 - 1} (-i) \text{Tr}(t^c t^b t^d) f^{cad} = \frac{N_c}{2} \frac{1}{C_F} \frac{\delta^{ab}}{2 N_c} : (\text{atG1}), (\text{dtG1}), (\text{etG1}), (\text{btG2}), (\text{ctG2}), (\text{ftG2}) \quad (6.21)$$

$$\frac{2}{N_c^2 - 1} (-i) \text{Tr}(t^c t^d t^b) f^{cad} = -\frac{N_c}{2} \frac{1}{C_F} \frac{\delta^{ab}}{2 N_c} : (\text{ctG1}), (\text{btG1}), (\text{ftG1}), (\text{atG2}), (\text{dtG2}), (\text{etG2}),$$

where the $2/(N_c^2 - 1)$ comes from the Fierz coefficient when factorizing the quark-antiquark gluon state in color space. Let us consider the diagram (atG1) of Fig.3.7, illustrated in Fig.6.5. We denote as

$$d^{\nu\rho}(k) = g^{\nu\rho} - \frac{k^\nu n^\rho + k^\rho n^\nu}{k \cdot n} \quad (6.22)$$

the numerator of the gluon propagator in axial gauge, and

$$V_{\mu_1, \mu_2, \mu_3}(k_1, k_2, k_3) = (k_1 - k_2)_{\mu_1} g_{\mu_1 \mu_2} + \dots \quad (6.23)$$

the momentum part of the 3-gluon vertex, where k_i are incoming, labeled in the counter-clockwise direction. The contribution of the diagram (atG1) then reads, for the vector DA,

$$\begin{aligned} \Phi_{\text{atG1}}^V &= -e_q \frac{1}{4} \frac{2}{s} \frac{(-i) N_c}{2 C_F} g^2 m_\rho f_\rho \frac{\delta^{ab}}{2 N_c} \frac{1}{2s} \int_0^1 dy_1 dy_2 \int \frac{d\kappa}{2\pi} \text{Tr}[\not{\epsilon}_\gamma (y_1 \not{p}_1 - \not{q}) \gamma_\nu (\not{k}_2 + \bar{y}_2 \not{p}_1) \not{p}_2 \not{p}_1] \\ &\times \frac{d^{\nu\rho}(k_1 + (y_1 - y_2)p_1) V_{\rho\lambda\alpha}(-k_1 - (y_1 - y_2)p_1, k_1, (y_1 - y_2)p_1)}{[(y_1 p_1 - q)^2 + i\eta][(k_1 + (y_1 - y_2)p_1)^2 + i\eta][(k_2 + \bar{y}_2 p_1)^2 + i\eta]} p_2^\lambda e_T^{*\alpha} e_\gamma^\mu B(y_1, y_2). \end{aligned} \quad (6.24)$$

Note that for this diagram, as well as for all "non-abelian" diagrams, one can easily check that only the $g^{\nu\rho}$ part of (6.22) contributes.

Closing the κ contour above or below gives for the vector DA part of the diagram (atG1) the result

$$\Phi_{\text{atG1}}^V = -\frac{e_q g^2}{2} m_\rho f_\rho \frac{\delta^{ab}}{2 N_c} \frac{N_c}{C_F} \int_0^1 dy_1 dy_2 \frac{(y_1 - y_2) \bar{y}_2}{\bar{y}_1 (\bar{y}_1 \underline{k}^2 + \bar{y}_2 (y_2 - y_1) Q^2)} e_T^{*\alpha} \cdot e_\gamma B(y_1, y_2). \quad (6.25)$$

Similarly, the contribution of the diagram (atG1) reads, for the axial DA,

$$\begin{aligned} \Phi_{\text{atG1}}^A &= -e_q \frac{i}{4} \frac{2}{s} \frac{(-i) N_c}{2 C_F} g^2 m_\rho f_\rho \frac{\delta^{ab}}{2 N_c} \frac{1}{2s} \int_0^1 dy_1 dy_2 \int \frac{d\kappa}{2\pi} \text{Tr}[\not{\epsilon}_\gamma (y_1 \not{p}_1 - \not{q}) \gamma_\nu (\not{k}_2 + \bar{y}_2 \not{p}_1) \not{p}_2 \not{p}_1 \gamma_5] \\ &\times \frac{d^{\nu\rho}(k_1 + (y_1 - y_2)p_1) V_{\rho\lambda\alpha}(-k_1 - (y_1 - y_2)p_1, k_1, (y_1 - y_2)p_1)}{[(y_1 p_1 - q)^2 + i\eta][(k_1 + (y_1 - y_2)p_1)^2 + i\eta][(k_2 + \bar{y}_2 p_1)^2 + i\eta]} p_2^\lambda \epsilon_{e_T^* p n}^\alpha D(y_1, y_2), \end{aligned} \quad (6.26)$$

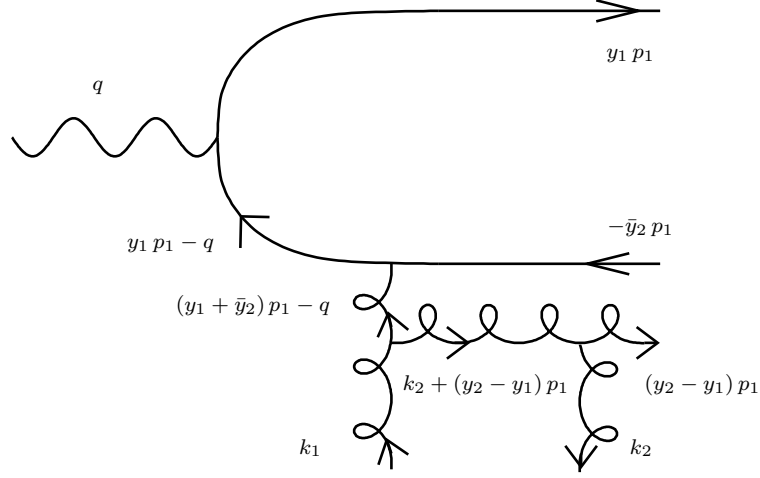


Figure 6.6: The detailed structure of the diagram (gttG1).

and closing the κ contour above or below gives

$$\Phi_{atG1}^A = -\frac{e_q g^2}{2} m_\rho f_\rho \frac{\delta^{ab}}{2 N_c} \frac{N_c}{C_F} \int_0^1 dy_1 dy_2 \frac{(y_1 - y_2) \bar{y}_2}{\bar{y}_1 (\bar{y}_1 \underline{k}^2 + \bar{y}_2 (y_2 - y_1) Q^2)} e_T^* \cdot e_\gamma D(y_1, y_2). \quad (6.27)$$

We consider now the "non-abelian" diagrams of Fig.3.8, involving two triple gluon vertices. They all involve the color structure

$$-\frac{2}{N_c^2 - 1} \text{Tr}[t^c t^d] f^{cea} f^{edb} = \frac{N_c}{C_F} \frac{\delta^{ab}}{2 N_c}. \quad (6.28)$$

For illustration, let us consider the diagram (gttG1) of Fig.3.8, illustrated in Fig.6.6. It reads, for the vector DA,

$$\begin{aligned} \Phi_{gttG1}^V &= -e_q \frac{1}{4} \frac{2(-i)N_c}{s C_F} g^2 m_\rho f_\rho \frac{\delta^{ab}}{2 N_c} \frac{1}{2s} \int_0^1 dy_1 dy_2 \int \frac{d\kappa}{2\pi} \text{Tr}[\not{\epsilon}_\gamma (y_1 \not{p}_1 - \not{q}) \gamma_\nu \not{p}_1] d^{\nu\rho} (-q + (1 + y_1 - y_2) p_1) \\ &\times \frac{V_{\rho\lambda\alpha}(q - (1 + y_1 - y_2) p_1, k_1, -k_2 + (y_1 - y_2) p_1) d^{\alpha\beta}(k_2 + (y_2 - y_1) p_1)}{[(y_1 p_1 - q)^2 + i\eta][(-q + (1 + y_1 - y_2) p_1)^2 + i\eta][(k_2 + (y_2 - y_1) p_1)^2 + i\eta]} \\ &\times V_{\beta\tau\delta}(k_2 + (y_2 - y_1) p_1, -k_2, (y_1 - y_2) p_1) p_2^\lambda p_2^\tau e_T^{*\delta} B(y_1, y_2). \end{aligned} \quad (6.29)$$

It equals, when closing the κ contour below on the single pole coming from the third propagator,

$$\Phi_{gttG1}^V = -\frac{e_q g^2}{2} m_\rho f_\rho \frac{\delta^{ab}}{2 N_c} \frac{N_c}{C_F} \frac{1}{Q^2} \int_0^1 dy_1 dy_2 \frac{B(y_1, y_2)}{\bar{y}_1} e_T^* \cdot e_\gamma. \quad (6.30)$$

The axial DA contribution from the diagram (gttG1) reads

$$\begin{aligned} \Phi_{gttG1}^V &= -e_q \frac{i}{4} \frac{2(-i)N_c}{s C_F} g^2 m_\rho f_\rho \frac{\delta^{ab}}{2 N_c} \frac{1}{2s} \int_0^1 dy_1 dy_2 \int \frac{d\kappa}{2\pi} \text{Tr}[\not{\epsilon}_\gamma (y_1 \not{p}_1 - \not{q}) \gamma_\nu \not{p}_1] \gamma_5] d^{\nu\rho} (-q + (1 + y_1 - y_2) p_1) \\ &\times \frac{V_{\rho\lambda\alpha}(q - (1 + y_1 - y_2) p_1, k_1, -k_2 + (y_1 - y_2) p_1) d^{\alpha\beta}(k_2 + (y_2 - y_1) p_1)}{[(y_1 p_1 - q)^2 + i\eta][(-q + (1 + y_1 - y_2) p_1)^2 + i\eta][(k_2 + (y_2 - y_1) p_1)^2 + i\eta]} \\ &\times V_{\beta\tau\sigma}(k_2 + (y_2 - y_1) p_1, -k_2, (y_1 - y_2) p_1) p_2^\lambda p_2^\tau \epsilon_{\tau\nu\mu}^* B(y_1, y_2). \end{aligned} \quad (6.31)$$

It equals, when closing the κ contour below on the single pole coming from the third propagator,

$$\Phi_{gttG1}^A = -\frac{e_q g^2}{2} m_\rho f_\rho \frac{\delta^{ab}}{2 N_c} \frac{N_c}{C_F} \frac{1}{Q^2} \int_0^1 dy_1 dy_2 \frac{D(y_1, y_2)}{\bar{y}_1} e_T^* \cdot e_\gamma. \quad (6.32)$$

All other diagrams of each class can be computed according to the previous examples.

In order to present now the full result in a compact form, we decompose the result impact factor into spin-non-flip and spin-flip part. The non-flip part is proportional to

$$T_{n.f.} = -(e_\gamma \cdot e_T^*), \quad (6.33)$$

whereas the spin-flip part involves

$$T_f = \frac{(e_\gamma \cdot k_\perp)(e_T^* \cdot k_\perp)}{\underline{k}^2} + \frac{(e_\gamma \cdot e_T^*)}{2}. \quad (6.34)$$

We label the transverse polarizations as²

$$\epsilon^{(+)} \equiv \epsilon^{(R)} = -\frac{i}{\sqrt{2}} [e_1 + i e_2] = -\frac{i}{\sqrt{2}} (0, 1, i, 0), \quad (6.35)$$

$$\epsilon^{(-)} \equiv \epsilon^{(L)} = \frac{i}{\sqrt{2}} [e_1 - i e_2] = \frac{i}{\sqrt{2}} (0, 1, -i, 0). \quad (6.36)$$

They satisfy

$$\epsilon^{(\lambda)*} = \epsilon^{(-\lambda)}. \quad (6.37)$$

and

$$\epsilon^{(+)} \epsilon^{(+)*} = \epsilon^{(+)} \epsilon^{(-)} = -1, \quad \text{and} \quad \epsilon^{(-)} \epsilon^{(-)*} = \epsilon^{(-)} \epsilon^{(+)} = -1. \quad (6.38)$$

In this basis,

$$\epsilon_\mu^{(+)} \epsilon_\nu^{(+)*} + \epsilon_\mu^{(-)} \epsilon_\nu^{(-)*} = \epsilon_\mu^{(+)} \epsilon_\nu^{(-)} + \epsilon_\mu^{(-)} \epsilon_\nu^{(+)} = -g_{\perp \mu\nu}. \quad (6.39)$$

Decomposing the impact factor as the sum of spin-non-flip and spin-flip contributions

$$\Phi_{n.f.}^{\gamma_T^* \rightarrow \rho_T}(\underline{k}^2) = \Phi_{n.f.}^{\gamma_T^* \rightarrow \rho_T}(\underline{k}^2) T_{n.f.} + \Phi_{f.}^{\gamma_T^* \rightarrow \rho_T}(\underline{k}^2) T_f, \quad (6.40)$$

and introducing the notations

$$\alpha = \underline{k}^2 / Q^2 \quad \text{and} \quad C^{ab} = -\frac{e g^2 m_\rho f_\rho}{\sqrt{2} Q^2} \frac{\delta^{ab}}{2 N_c} \quad (6.41)$$

one obtain the following results for the two bodies contribution

$$\begin{aligned} \Phi_{n.f.2}^{\gamma_T^* \rightarrow \rho_T}(\underline{k}^2) &= \frac{C^{ab}}{2} \frac{1}{C_F} C_F \int_0^1 dy_1 \left\{ \frac{(2y_1 - 1) \varphi_1^T(y_1) + 2y_1(1 - y_1) \varphi_3(y_1) + \varphi_A^T(y_1)}{y_1(1 - y_1)} \right. \\ &\quad \left. - \frac{2\alpha(\alpha + 2y_1(1 - y_1))((2y_1 - 1) \varphi_1^T(y_1) + \varphi_A^T(y_1))}{y_1(1 - y_1)(\alpha + y_1(1 - y_1))^2} \right\} \end{aligned} \quad (6.42)$$

and

$$\Phi_{f.2}^{\gamma_T^* \rightarrow \rho_T}(\underline{k}^2) = \frac{C^{ab}}{2} \frac{1}{C_F} C_F \int_0^1 dy_1 \frac{4\alpha}{(\alpha + (1 - y_1)y_1)^2} [(1 - 2y_1) \varphi_1^T(y_1) + \varphi_A^T(y_1)]. \quad (6.43)$$

²Convention of Landau.

The three bodies contribution reads

$$\begin{aligned} \Phi_{n.f.3}^{\gamma_T^* \rightarrow \rho_T}(\underline{k}^2) &= C^{ab} \frac{1}{C_F} \int_0^1 dy_1 \int_0^1 dy_2 \left\{ \frac{y_1 \zeta_3^A D(y_1, y_2)}{\alpha + (1-y_1)y_1} \left(\frac{\alpha(N_c - 2C_F)}{(y_1 - y_2 + 1)\alpha + y_1(1-y_2)} + \frac{\alpha N_c(1-y_1)}{y_2\alpha + y_1(y_2 - y_1)} \right) \right. \\ &\quad - \frac{y_1 \zeta_3^V B(y_1, y_2)}{\alpha + (1-y_1)y_1} \left(\frac{\alpha(2C_F - N_c)(2y_1 - 1)}{(y_1 - y_2 + 1)\alpha + y_1(1-y_2)} + \frac{\alpha N_c(1-y_1)}{y_2\alpha + y_1(y_2 - y_1)} \right) \\ &\quad \left. + (\zeta_3^V B(y_1, y_2) + \zeta_3^A D(y_1, y_2)) \left(\frac{2C_F y_1}{\alpha + (1-y_1)y_1} - \frac{1}{1-y_1} \left[\frac{N_c(1-y_2)(y_1 - y_2)Q^2}{(1-y_1)\alpha + (1-y_2)(y_2 - y_1)} + C_F + N_c \right] \right) \right\} \end{aligned} \quad (6.44)$$

and

$$\begin{aligned} \Phi_{f.3}^{\gamma_T^* \rightarrow \rho_T}(\underline{k}^2) &= \frac{C^{ab}}{2} \frac{1}{C_F} \frac{4\alpha y_1}{\alpha + y_1(1-y_1)} \left(\frac{2C_F - N_c}{\alpha(1+y_1-y_2) + y_1(1-y_2)} - \frac{N_c}{\alpha y_2 + y_1(-y_1 + y_2)} \right) \\ &\quad \times [\zeta_3^A D(y_1, y_2)(1+y_1-y_2) + \zeta_3^V B(y_1, y_2)(1-y_1-y_2)]. \end{aligned} \quad (6.45)$$

The full result for the impact factor reads, after several simplifications due to the use of the equation of motion and the symmetrical properties of 2 and 3-parton correlators, as

$$\begin{aligned} &\Phi_{n.f.}^{\gamma_T^* \rightarrow \rho_T}(\underline{k}^2) \\ &= \frac{C^{ab}}{2} \left\{ -2 \int dy_1 \frac{(\alpha + 2y_1(1-y_1))\alpha}{y_1(1-y_1)(\alpha + y_1(1-y_1))^2} [(2y_1 - 1)\varphi_1^T(y_1) + \varphi_A^T(y_1)] \right. \\ &\quad + 2 \int dy_1 dy_2 [\zeta_3^V B(y_1, y_2) - \zeta_3^A D(y_1, y_2)] \frac{y_1(1-y_1)\alpha}{\alpha + y_1(1-y_1)} \left[\frac{2 - N_c/C_F}{\alpha(y_1 - y_2 + 1) + y_1(1-y_2)} \right. \\ &\quad - \left. \frac{N_c}{C_F} \frac{1}{y_2\alpha + y_1(y_2 - y_1)} \right] - 2 \int dy_1 dy_2 [\zeta_3^V B(y_1, y_2) + \zeta_3^A D(y_1, y_2)] \left[\frac{2 + N_c/C_F}{1-y_1} \right. \\ &\quad + \frac{y_1}{\alpha + y_1(1-y_1)} \left(\frac{(2 - N_c/C_F)y_1\alpha}{\alpha(y_1 - y_2 + 1) + y_1(1-y_2)} - 2 \right) \\ &\quad \left. \left. + \frac{N_c(y_1 - y_2)(1-y_2)}{C_F} \frac{1}{\alpha(1-y_1) + (y_2 - y_1)(1-y_2)} \right] \right\} \end{aligned} \quad (6.46)$$

and

$$\begin{aligned} \Phi_{f.}^{\gamma_T^* \rightarrow \rho_T}(\underline{k}^2) &= \frac{C^{ab}}{2} \left\{ 4 \int dy_1 \frac{\alpha}{(\alpha + y_1(1-y_1))^2} [\varphi_A^T(y_1) - (2y_1 - 1)\varphi_1^T(y_1)] \right. \\ &\quad - 4 \int dy_1 dy_2 \frac{y_1\alpha}{\alpha + y_1(1-y_1)} [\zeta_3^A D(y_1, y_2)(-y_1 + y_2 - 1) + \zeta_3^V B(y_1, y_2)(y_1 + y_2 - 1)] \\ &\quad \left. \times \left[\frac{(2 - N_c/C_F)}{\alpha(y_1 - y_2 + 1) + y_1(1-y_2)} - \frac{N_c}{C_F} \frac{1}{y_2\alpha + y_1(y_2 - y_1)} \right] \right\}. \end{aligned} \quad (6.47)$$

The gauge invariance of the considered impact factor requires a special attention. As we have seen at the end of Sec. 4.2, the $\gamma^* \rightarrow \rho_T$ impact factor is constructed in such a manner that it should vanish when $\underline{k}^2 = 0$, as a consequence of the gauge invariance of the impact factor. From our final formulas (6.46) and (6.47), it is obvious to check that $\Phi_{f.}$ and $\Phi_{n.f.}$ indeed vanish when $\underline{k}^2 = 0$ since $T_{n.f.}$ is a phase for flip transition, which is regular in the $\underline{k}^2 \rightarrow 0$ limit. The vanishing of the "abelian", i.e. proportional to C_F part of (6.46) is particularly subtle since it appears as a consequence of the equations of motions (3.59, 3.60). Because of that some comments can be useful. Let us note that the sum of Eq. (3.59) multiplied by y_1 and of Eq. (3.60) multiplied by \bar{y}_1 takes the form

$$\begin{aligned} &2y_1\bar{y}_1\varphi_3(y_1) + (y_1 - \bar{y}_1)\varphi_1^T(y_1) + \varphi_A^T(y_1) \\ &= -y_1 \int_0^1 dy_2 [\zeta_3^V B(y_1, y_2) + \zeta_3^A D(y_1, y_2)] - \bar{y}_1 \int_0^1 dy_2 [-\zeta_3^V B(y_2, y_1) + \zeta_3^A D(y_2, y_1)], \end{aligned} \quad (6.48)$$

from which, after integration over y_1 of the both sides of (6.48) multiplied by $\frac{1}{y_1\bar{y}_1}$, we derive the equality

$$\int_0^1 \frac{dy_1}{y_1\bar{y}_1} (2y_1\bar{y}_1\varphi_3(y_1) + (y_1 - \bar{y}_1)\varphi_1^T(y_1) + \varphi_A^T(y_1)) = - \int_0^1 dy_1 \int_0^1 dy_2 \frac{2}{\bar{y}_1} [\zeta_3^V B(y_1, y_2) + \zeta_3^A D(y_1, y_2)] . \quad (6.49)$$

Now, by inspecting the expression (6.42) in the limit $\alpha \rightarrow 0$ we see that only the first term in $\{\dots\}$ survives and it has a form of the l.h.s of expression (6.49). Similarly, by inspecting the expression (6.44) in the limit $\alpha \rightarrow 0$ we see, that only the last line of this expression survives in the limit $\alpha \rightarrow 0$ and that the resulting expression coincides with the r.h.s of (6.49). Consequently, the non-vanishing terms cancel out due to the relation (6.49). At the same time, the vanishing of non-abelian ($\sim N_c$) part of (6.44) is the result of direct cancellation of the nonvanishing contributions of the diagrams (bG1), (dG1), (aG2), (cG2), (bG2), (dG2), (eG2), (fG2) of Fig. 3.6 (see Eq.(6.16)) with the corresponding ones coming from diagrams of Fig. 3.7 and Fig. 3.8 containing triple-gluon vertices. Thus, the expression for the $\gamma^* \rightarrow \rho_T$ impact factor has finally a gauge-invariant form only provided the genuine twist 3 contributions have been taken into account, hidden in formula (6.46) when writing $\Phi_{n.f.}$ by the fact that we have used e.o.m., which explicitly relate 2 and 3 particles correlators.

We end up this section with a comment about the problem of end-point singularities. Such singularities does not occur both in WW approximation and in full twist-3 order approximation. First, the flip contribution (6.47) obviously does not have any end-point singularity. The potential end-point singularity for the non-flip contribution (6.46) is spurious since $\varphi_A^T(x_1)$, $\varphi_1^T(x_1)$ vanishes at $x_1 = 0, 1$ (this is enough to justify the regularity of the result in the WW approximation), as well as $B(x_1, x_2)$ and $D(x_1, x_2)$.

6.2 Calculation based on the Covariant Collinear Factorization

We now calculate the impact factor using the CCF parametrization of Ref. [135–137] for vector meson DAs. Let us outline basic ideas behind our calculation. We need to express the impact factor in terms of hard coefficient functions and soft parts parametrized by light-cone matrix elements. The standard technique here is an operator product expansion on the light cone, $z^2 \rightarrow 0$, which naturally gives the leading term in the power counting and leads to the described above factorized structure. Unfortunately we do not have an operator definition for an impact factor, and therefore, we have to rely in our actual calculation on the perturbation theory. The primary complication here is that $z^2 \rightarrow 0$ limit of any single diagram is given in terms of light-cone matrix elements without any Wilson line insertion between the quark and gluon operators, like

$$\langle V(p_V) | \bar{\psi}(z) \gamma_\mu \psi(0) | 0 \rangle \quad \text{and} \quad \langle V(p_V) | \bar{\psi}(z) \gamma_\mu A_\alpha(tz) \psi(0) | 0 \rangle ,$$

we will call conventionally such objects as perturbative correlators. Actually we need to combine together contributions of quark-antiquark and quark-antiquark gluon diagrams in order to obtain a final gauge invariant result.

One should stress that despite working in the axial gauge one can not neglect completely an effect coming from the Wilson lines since the two light cone vectors z and n are not equal to each other and thus, generically, Wilson lines are not equal to unity. Nevertheless in the axial gauge the contribution of each additional parton costs one extra power of $1/Q$, therefore a calculation can be organized in a simple iterative manner expanding the Wilson line. At twist three level it is enough to consider the first two terms of such expansion

$$[z, 0] = 1 + ig \int_0^1 dt z^\alpha A_\alpha(zt) + \mathcal{O}(A^2) . \quad (6.50)$$

For instance, the quark-antiquark vector correlator can be written, for the general case $z^2 \neq 0$, as

$$\langle V(p_V) | \bar{\psi}(z) \gamma_\mu \psi(0) | 0 \rangle = \langle V(p_V) | \bar{\psi}(z) \gamma_\mu [z, 0] \psi(0) | 0 \rangle - ig \int_0^1 dt \langle V(p_V) | \bar{\psi}(z) \gamma_\mu z^\alpha A_\alpha(zt) \psi(0) | 0 \rangle , \quad (6.51)$$

where we formally inserted the Wilson line in the r.h.s and performed its approximate subtraction according to (6.50). Then using relation (3.41), we express the gluon field operator in the second term of (6.51) in terms

of field strength, which gives us the $\langle V(p_V)|\bar{\psi}(z)\gamma_\mu G_{\alpha\beta}(tz)\psi(0)|0\rangle$ correlator. For the later we apply again the procedure of Wilson lines insertion (and its approximate subtraction)

$$\begin{aligned} \langle V(p_V)|\bar{\psi}(y)\gamma_\mu\psi(0)|0\rangle &= \langle V(p_V)|\bar{\psi}(z)\gamma_\mu[z,0]\psi(0)|0\rangle \\ -ig \int_0^1 \int_0^\infty dt d\sigma e^{-\epsilon\sigma} \langle V(p_V)|\bar{\psi}(z)[z,zt+n\sigma]\gamma_\mu z^\alpha n^\beta G_{\alpha\beta}(zt+n\sigma)[zt+n\sigma,0]\psi(0)|0\rangle &+ \dots, \end{aligned} \quad (6.52)$$

where \dots stands for the correlators with more than one gluon field.

Such correlator naturally appears (after Fierz decomposition) in the expression for the impact factor generated by the leading order diagrams of perturbation theory. Now we proceed to the extraction of leading $1/Q$ asymptotic. It is achieved, due to the dimensional counting reasons, by the substitution of the off light-cone correlators by their light-cone limit where $zt+n\sigma \propto z$, $z^2 \rightarrow 0$. In this limit, using the CCF parametrization of Sec. 3.3.2 for the light-cone correlators, one can deduce after some transformations that

$$\begin{aligned} \langle \rho(p_\rho)|\bar{\psi}(z)\gamma_\mu\psi(0)|0\rangle|_{z^2 \rightarrow 0} &= \\ f_\rho m_\rho \left[-i p_\mu (e^* \cdot z) \int_0^1 dy e^{iy(p \cdot z)} (h(y) - \tilde{h}(y)) + e_\mu^* \int_0^1 dy e^{iy(p \cdot z)} g_\perp^{(v)}(z) \right] &+ \dots, \end{aligned} \quad (6.53)$$

where \dots stands for the contributions vanishing at twist 3 level, and

$$\tilde{h}(y) = \zeta_3^V \int_0^y d\alpha_1 \int_0^{\bar{y}} d\alpha_2 \frac{V(\alpha_1, \alpha_2)}{\alpha_g^2}, \quad (6.54)$$

The physical polarization vector satisfies $e \cdot p_\rho = 0$ (or $e \cdot p = 0$ since $p_\rho = p$ up to twist 3). On the other hand, the transversely polarized meson is chosen to be orthogonal to the light-cone vectors fixed by the external kinematics: $e \cdot n_0 = 0$. But one should take into account that the e_T vector defined by (3.31) has a non vanishing scalar product with the vector n_0 ,

$$e_T \cdot n_0 = -\frac{e \cdot z}{p \cdot z}. \quad (6.55)$$

This relation was used to derive (6.53).

Note that the $zt+n\sigma \propto z$ condition means actually that the vector z (which is an internal integration variable for the impact factor) is approaching during this limiting procedure the direction of the light cone vector n , $z \propto n$. One should mention, to avoid any misunderstanding, that it does not mean that we must put, say in Eqs. like (6.53), the $e \cdot z$ scalar product equal to zero. What we actually do when performing the $1/Q$ power expansion is a Taylor expansion of scalar functions $F(p \cdot z, z^2)$, which depend generically on the two variables $p \cdot z$ and z^2 , with respect to the variable z^2 , whereas any scalar product of z with other vectors should remain intact.

Performing a similar sequence of steps we obtain the following result for the axial-vector correlator at the twist 3 level

$$\begin{aligned} \langle \rho(p_\rho)|\bar{\psi}(z)\gamma_\mu\gamma_5\psi(0)|0\rangle|_{z^2 \rightarrow 0} &= \\ \frac{1}{4} f_\rho m_\rho \left[\epsilon_{\mu\alpha\beta\gamma} e^{*\alpha} p^\beta z^\gamma \int_0^1 dy e^{iy(p \cdot z)} (g_\perp^{(a)}(y) - \tilde{g}_\perp^{(a)}(y)) + \epsilon_{\mu\alpha\beta\gamma} e^{*\alpha} p^\beta n^\gamma p \cdot z \int_0^1 dy e^{iy(p \cdot z)} \tilde{g}_\perp^{(a)}(y) \right], \end{aligned} \quad (6.56)$$

with

$$\tilde{g}_\perp^{(a)}(y) = 4 \zeta_3^A \int_0^y d\alpha_1 \int_0^{\bar{y}} d\alpha_2 \frac{A(\alpha_1, \alpha_2)}{\alpha_g^2}. \quad (6.57)$$

Comparing the obtained results (6.53), (6.56) for the perturbative correlators with initial parametrizations (3.34), (3.28) we see that at twist 3-level the net effect of the Wilson line is just some renormalization of the h function in the case of vector correlator, whereas for the axial-vector we obtain in addition to the function g_\perp^a renormalization a new Lorentz structure, the last term in (6.56). Nevertheless, we found that the last term in (6.56) produces at the end a zero contribution to impact factor.

Let us now discuss gluonic diagrams which involves quark-antiquark gluon correlators, like

$$\langle \rho(p_\rho) | \bar{\psi}(z) \gamma_\mu A_\alpha(w) \psi(0) | 0 \rangle.$$

Applying our procedure one can easily show that at twist 3 level

$$\begin{aligned} \langle \rho(p_\rho) | \bar{\psi}(z) \gamma_\mu g A_\alpha(w) \psi(0) | 0 \rangle_{|w \propto z, z^2 \rightarrow 0} &= -m_\rho f_{3\rho}^V p_\mu e_{T\alpha}^* \int D\underline{\alpha} \frac{V(\alpha_1, \alpha_2)}{\alpha_g} e^{i(p \cdot z)\alpha_1 + i(p \cdot w)\alpha_g}, \\ \langle \rho(p_\rho) | \bar{\psi}(z) \gamma_\mu \gamma_5 g A_\alpha(w) \psi(0) | 0 \rangle_{|w \propto z, z^2 \rightarrow 0} &= -i m_\rho f_{3\rho}^A p_\mu \epsilon_{\alpha\beta\gamma\delta} n^\beta p^\gamma e_{T\alpha}^{*\delta} \int D\underline{\alpha} \frac{A(\alpha_1, \alpha_2)}{\alpha_g} e^{i(p \cdot z)\alpha_1 + i(p \cdot w)\alpha_g}, \end{aligned} \quad (6.58)$$

see Eq.(3.42,3.43). Note that the first nontrivial effects induced by the Wilson line insertion start for such perturbative correlators at the level of twist 4 only. Therefore taking into account such 3-partons contributions is quite straightforward: one needs to calculate, projected in accordance with (6.58), diagrams describing the production of collinear on-shell quark-antiquark gluon state. One comment is here in order. Perturbative expansion generates, among others, diagrams where the gluon field is attached not to the internal part of the diagrams but to the "external" quark (or antiquark) lines. Such diagrams, in accordance to the logic of collinear factorization, should be factorized in terms of not 3-parton but 2-parton correlators. Quasi-collinear gluon radiation appears at large distances and corresponding subprocess should be factorized not in the hard coefficient but is included in the soft part of the process, described by the 2-parton quark-antiquark correlator.

The internal variable z (and w) integration can be reduced to the Fourier integrals

$$\int d^4 z e^{i(l \cdot z)} = (2\pi)^4 \delta^4(l), \quad \int d^4 z z_\alpha e^{i(l \cdot z)} = -i(2\pi)^4 \frac{\partial}{\partial l^\alpha} \delta^4(l),$$

where l stays here for some combination of the external and internal momenta³. The corresponding intermediate calculations do not contain principle difficulties both for the case of 2-partons and 3-partons contributions. Note that the contributions computed here have the same hard part as the one of the section 6.1, except for 2-partons contributions with derivatives discussed in that section which have no counterpart here. In what follows, we simply give the final results. Then we will discuss in details an important issue related with the restoration of the gauge invariance for the final result.

We use the notations

$$\alpha = \frac{k^2}{Q^2}, \quad c_f = \frac{N^2}{N^2 - 1}$$

For the 3-parton contributions we obtain the result

$$\Phi^3 = -\frac{e g^2 m_\rho f_\rho}{\sqrt{2} Q^2} \frac{\delta^{ab}}{2N_c} \{ \Phi^{q\bar{q}g}(\alpha) + \Delta\Phi^3 \}, \quad (6.59)$$

with

$$\Delta\Phi^3 = -\frac{T_{n.f.}}{2} \int \frac{Dz}{\bar{z}_1 \bar{z}_2 z_g} \{ \zeta_3^V V(z_1, z_2)(z_1 - z_2) + \zeta_3^A A(z_1, z_2)(\bar{z}_1 + \bar{z}_2) \} \quad (6.60)$$

and

$$\begin{aligned} \Phi^{q\bar{q}g}(\alpha) &= \int Dz \frac{2\alpha}{z_1 z_2 z_g^2} \\ &\times \left\{ (\zeta_3^V V(z_1, z_2) + \zeta_3^A A(z_1, z_2)) T_{n.f.} \left(\frac{(1 - c_f) \bar{z}_g z_1}{\alpha \bar{z}_g + z_1 z_2} - \frac{c_f z_g^2}{\alpha \bar{z}_1 + z_2 z_g} - \frac{(z_2 - \bar{z}_1 c_f) z_1 z_2}{\bar{z}_1 (\alpha + z_1 \bar{z}_1)} - \frac{(z_1 - \bar{z}_2 c_f) \bar{z}_2}{(\alpha + z_2 \bar{z}_2)} \right) \right. \\ &\left. + (\zeta_3^V V(z_1, z_2) - \zeta_3^A A(z_1, z_2)) 2z_1 T_f \left(\frac{(1 - c_f) \bar{z}_g^2}{\alpha \bar{z}_g + z_1 z_2} - \frac{c_f z_g \bar{z}_1}{\alpha \bar{z}_1 + z_2 z_g} - \frac{c_f z_g \bar{z}_2}{\alpha \bar{z}_2 + z_1 z_g} + \frac{c_f \bar{z}_1 - z_2}{\alpha + z_1 \bar{z}_1} + \frac{c_f \bar{z}_2 - z_1}{\alpha + z_2 \bar{z}_2} \right) \right\}, \end{aligned} \quad (6.61)$$

where Dz is defined according to (3.39) and where we have used symmetry properties of gluon distribution amplitudes under the exchange of quark momentum fractions: $V(z_1, z_2) = -V(z_2, z_1)$, $A(z_1, z_2) = A(z_2, z_1)$.

³The subsequent integration over the internal momenta with delta function derivative is done using integration by parts.

Let us discuss now the 2-parton contributions. We obtain

$$\Phi^2 = -\frac{e g^2 m_\rho f_\rho \delta^{ab}}{\sqrt{2} Q^2 2N_c} \{ \Phi^{q\bar{q}}(\alpha) + \Delta\Phi^2 \}, \quad (6.62)$$

with

$$\Phi^{q\bar{q}}(\alpha) = \int_0^1 dz \left\{ T_{n.f.} \Phi^+(z) \frac{\alpha(\alpha + 2z\bar{z})}{z\bar{z}(\alpha + z\bar{z})^2} + T_f \Phi^-(z) \frac{2\alpha}{(\alpha + z\bar{z})^2} \right\}, \quad (6.63)$$

where

$$\Phi^\pm(\alpha) = (2z - 1) [h(z) - \tilde{h}(z)] \pm \frac{g_\perp^{(a)}(z) - \tilde{g}_\perp^{(a)}(z)}{4}, \quad (6.64)$$

whereas for $\Delta\Phi^2$ term we get

$$\Delta\Phi^2 = T_{n.f.} \int_0^1 dz \left\{ g_\perp^{(v)}(z) - \frac{\Phi^+(z)}{2z\bar{z}} \right\}. \quad (6.65)$$

Note that $\Phi^{q\bar{q}}(\alpha)$ and $\Phi^{q\bar{q}g}(\alpha)$ vanish in the limit $\alpha \rightarrow 0$, whereas $\Delta\Phi^2$ and $\Delta\Phi^3$ do not depend on α . Now we need to demonstrate that $\Delta\Phi^2$ and $\Delta\Phi^3$ cancel each other. It guarantees the property of the impact factor, $\Phi(\alpha = 0) = 0$, which is directly related to the gauge invariance.

One can now separate from $\Delta\Phi^2$ the contribution $\Delta\Phi_a^2$ that is due to functions $\tilde{h}(z)$ and $\tilde{g}_\perp^a(z)$, which originates in our method from the Wilson lines insertion procedure,

$$\Delta\Phi^2 = \Delta\Phi_a^2 + \Delta\Phi_b^2, \quad (6.66)$$

where

$$\Delta\Phi_a^2 = T_{n.f.} \int_0^1 \frac{dz}{2z\bar{z}} \left\{ (2z - 1) \tilde{h}(z) + \frac{\tilde{g}_\perp^{(a)}(z)}{4} \right\}. \quad (6.67)$$

To calculate $\Delta\Phi_a^2$, it is convenient to present $\tilde{h}(z)$ and $\tilde{g}_\perp^{(a)}(z)$ in the form

$$\tilde{h}(u) = \zeta_3^V \int_0^1 dt \int Dz \delta(u - z_1 - z_{gt}) \frac{V(z_1, z_2)}{z_g}, \quad \tilde{g}_\perp^{(a)}(z) = 4 \zeta_3^A \int_0^1 dt \int Dz \delta(u - z_1 - z_{gt}) \frac{A(z_1, z_2)}{z_g}.$$

Using this relation one can easily found that

$$\Delta\Phi_a^2 = \frac{T_{n.f.}}{2} \int Dz \left\{ \zeta_3^V \frac{V(z_1, z_2)}{z_g^2} \ln \frac{z_1 \bar{z}_1}{z_2 \bar{z}_2} + \zeta_3^A \frac{A(z_1, z_2)}{z_g^2} \ln \frac{\bar{z}_1 \bar{z}_2}{z_1 z_2} \right\}.$$

The second term in (6.66) can be reduced to the form

$$\Delta\Phi_b^2 = \frac{T_{n.f.}}{2} \int_0^1 dz \{ \ln(z) g^{\uparrow\downarrow}(z) + \ln(\bar{z}) g^{\downarrow\uparrow}(z) \}.$$

where [136]

$$g^{\uparrow\downarrow}(z) = g_\perp^{(v)}(z) + \frac{1}{4} \frac{d}{dz} g_\perp^{(a)}(z), \quad g^{\downarrow\uparrow}(z) = g_\perp^{(v)}(z) - \frac{1}{4} \frac{d}{dz} g_\perp^{(a)}(z).$$

Then, we separate the WW and genuine twist 3 contributions to $\Delta\Phi_b^2$,

$$\Delta\Phi_b^2 = \Delta\Phi_b^{2WW} + \Delta\Phi_b^{2gen},$$

in accordance with

$$g^{\uparrow\downarrow}(z) = g^{\uparrow\downarrow WW}(z) + g^{\uparrow\downarrow gen}(z), \quad g^{\downarrow\uparrow}(z) = g^{\downarrow\uparrow WW}(z) + g^{\downarrow\uparrow gen}(z).$$

Using the explicit expressions for these functions in the WW limit

$$g^{\uparrow\downarrow WW}(z) = \int_z^1 \frac{du}{u} \phi_{\parallel}(u), \quad g^{\downarrow\uparrow WW}(z) = \int_0^z \frac{du}{u} \phi_{\parallel}(u),$$

one can easily find that the WW contribution to $\Delta\Phi_b^2$ vanishes,

$$\Delta\Phi_b^{2WW} = 0.$$

Then, using results of Ref. [136], which allow to express $g^{\uparrow\downarrow gen}(z)$ and $g^{\downarrow\uparrow gen}(z)$ in terms of 3-parton DAs, we found after some transformations that

$$\Delta\Phi_b^{2gen} = \frac{T_{n.f.}}{2} \int Dz \left\{ \zeta_3^V \frac{V(z_1, z_2)}{z_g} \left(\frac{z_1 - z_2}{\bar{z}_1 \bar{z}_2} - \ln \frac{z_1 \bar{z}_1}{z_2 \bar{z}_2} \frac{1}{z_g} \right) + \zeta_3^A \frac{A(z_1, z_2)}{z_g} \left(\frac{\bar{z}_1 + \bar{z}_2}{\bar{z}_1 \bar{z}_2} - \ln \frac{\bar{z}_1 \bar{z}_2}{z_1 z_2} \frac{1}{z_g} \right) \right\}.$$

These results mean that

$$\Delta\Phi^2 = \frac{T_{n.f.}}{2} \int \frac{Dz}{z_g \bar{z}_1 \bar{z}_2} \left\{ \zeta_3^V V(z_1, z_2)(z_1 - z_2) + \zeta_3^A A(z_1, z_2)(\bar{z}_1 + \bar{z}_2) \right\}, \quad (6.68)$$

and thus that the constant terms of 2-parton (6.68) and 3-parton (6.60) contributions cancel each other

$$\Delta\Phi^2 + \Delta\Phi^3 = 0.$$

Finally, the impact factor is given as a sum of two contributions

$$\Phi(\alpha) = -\frac{e g^2 m_\rho f_\rho}{\sqrt{2} Q^2} \frac{\delta^{ab}}{2N_c} \left\{ \Phi^{q\bar{q}}(\alpha) + \Phi^{q\bar{q}g}(\alpha) \right\} \quad (6.69)$$

where $\Phi^{q\bar{q}}(\alpha)$ and $\Phi^{q\bar{q}g}(\alpha)$ are given in eqs. (6.63) and (6.61).

6.3 Comparison of the two computations and discussion

The above results for the $\gamma^* \rightarrow \rho$ impact factor were obtained based on the LCCF and CCF method, and look at first sight very different. As a testing ground of the validity of the dictionary elaborated in section 3.6, it is interesting to show the exact equivalence between the two results. The detailed proof relies on the rewriting of both results in terms of the DAs $\varphi_1 B, D$, and uses the expressions for $g^{\uparrow\downarrow gen}$ and $g^{\downarrow\uparrow gen}$ through V (thus through B) and A (thus through D) as given in Ref. [136]. Since it is rather involved and technical, we do not present the proof here. This is done with whole details in Appendix B of Ref. [W24], where the exact equivalence between the two results is proven.

The above computation has thus explicitly illustrated the efficiency of the LCCF method, which allows us to include in a systematic way higher twist effects, here exemplified on the study of the ρ -meson production up to twist 3 accuracy. Our computation is rather straightforward in LCCF approach, while more involved in CCF. On the other hand, the price to pay in LCCF is that one needs to introduce a set of DAs which are not independent. As explained in Chap. 3, the crucial point in the comparison of these two methods is the use of Lorentz invariance constraints formulated as the n -independence of the scattering amplitude within LCCF method, which allows one to reduce these DAs to a minimal set, when combined with the EOMs.

Our result of course does not preclude the solution of the end-point singularity problem which we already discussed, and which may still require a separate treatment. However, we expect that we could use our result to predict in a way rather independent of the unintegrated gluon distribution in the proton the ratio of the two dominant transitions $\gamma_L^* \rightarrow \rho_L$ and $\gamma_T^* \rightarrow \rho_T$.

To the best of our knowledge, our obtained result is the first complete twist 3 result for an exclusive process -including dynamical genuine twist 3 effects-, here based on k_T -factorization. The first natural extension of the present study would be to consider the non-forward case. This is essentially a matter of technical computations. We do not expect any surprise at that level, but this is clearly needed in order to get a description of the t dependence. In the electroproduction case, this will of course mix with the t -dependence of the coupling of the

Pomeron to the proton, which combines both perturbative (à la BFKL) and non-perturbative origins. Another interesting question would be to consider twist 4 contributions, in particular when using practically the LCCF approach. This again could be studied in this impact factor example. Besides this, we have not considered the effect of ERBL-DGLAP evolution, which, although they are expected to be moderate due to the limited values of Q^2 , might be of practical importance if phenomenology is to be done at an increasing level of precision.

The problem of combining NLLx studies with a twist 3 treatment should also be addressed. This could give a consistent treatment for all kind of transitions in the large s limit, at NLLx level. At the moment, we do not know any example of NLLx description involving higher twist effects. Additionally, the problem of end-point contributions presumably require the inclusion of Sudakov type of effect. The problem of including such effects within k_T -factorization is an open question, even at LLx. Thus, hard ρ -exclusive production will presumably remain a subject of very active research both from the experimental and the theoretical sides.

Chapter 7

Onium-onium scattering in $\gamma^{(*)}\gamma^{(*)}$ colliders

7.1 Sources of photons

The direct $\gamma\gamma$ cross-section (computed through the box diagram) is out of reach experimentally. For example, $\sigma^{\gamma\gamma\rightarrow\gamma\gamma} \sim 10^{-64}(\omega_\gamma/\text{eV})^6\text{cm}^2$, that is 10^{-65}cm^2 for visible light ($\omega \sim 1\text{ eV}$)! This can be circumvented in two ways: photons can be produced either, using the Fermi [547], Weizsäcker [548], Williams [549] idea that the field of a charged particle is a flux of equivalent photon (which are almost real), from a high luminosity collider of charged particle (Ap , pp , e^+p , e^+e^-) or from Compton backscattering to pump the energy of electrons of a storage ring or of a collider in order to produce high luminosity and high energy photons.

7.1.1 Photon colliders: hadron and nucleus colliders

The first option can be realized in hadron and nucleus colliders: to produce high energy $\omega = zE_{Ze}$ photons with high luminosity, the equivalent photon approximation

$$P_{\gamma/Z_e}(z, Q^2) \sim Z^2 \alpha_{em}/(z Q^2)$$

implies that one can use either a high energy (to compensate the $1/z$ pole) and high luminosity hadron collider (LHC, Tevatron), or a heavy nucleus collider (Z^2 then balance the lower luminosity) (RHIC, LHC). At LHC, both modes would give comparable fluxes of photons. Note however that contrarily to a general belief, as we will discuss in Sec. 7.5.4, the hadron-hadron mode provides a higher flux than when replacing hadrons by heavy nucleus. Still, $\gamma\gamma$ events are polluted by pure (soft) hadronic interactions between source of photons, since hadrons or nucleus are sensitive to strong interaction. One needs to select peculiar ultraperipheral events [550–552] for which the typical impact parameter b between hadrons (nucleus) exceeds $1/\Lambda_{QCD}$. Such ultraperipheral collisions of protons or nuclei of high energies constitute a promising new way to study QCD processes initiated by two quasi real photons, since they mimic e^+e^- colliders, which of course do not face any hadronic interactions among themselves, and are thus considered to be very “clean”. Such a selection is possible experimentally with very forward detectors, with (anti)tagging protons: forward detector at CDF (with coming data), LHC detectors (Roman pots) suggested at 420 m (FP420 at cms and ATLAS) and 220 m (RP200 at ATLAS) from the Interaction Point at LHC [459]. These last detectors are very promising for both $\gamma\gamma$ and hadronic diffractive physics (ex: Higgs exclusive production, MSSM, QCD), but they suffer from non trivial problems with fast time trigger (long distance from IP to the detector to be compared with the rate of events at high luminosity). Combining both detectors would increase acceptance. In the high luminosity mode of LHC, it is anyway not clear whether pile-up (occurring when a second scattering occurs during the time of a first scattering) would not prevent studies of ultraperipheral processes. Typically, the integrated luminosity should probably not exceed 1 fb^{-1} in order to avoid pile-up, which reduces significantly the opportunity for dedicated exclusive studies at LHC. The situation would be more favorable in the low luminosity mode.

For some peculiar ultraperipheral processes, it may well be that the tagging of out-going proton could not be feasible. In that case, the distinction with pure strong-interaction processes could be made relying on the

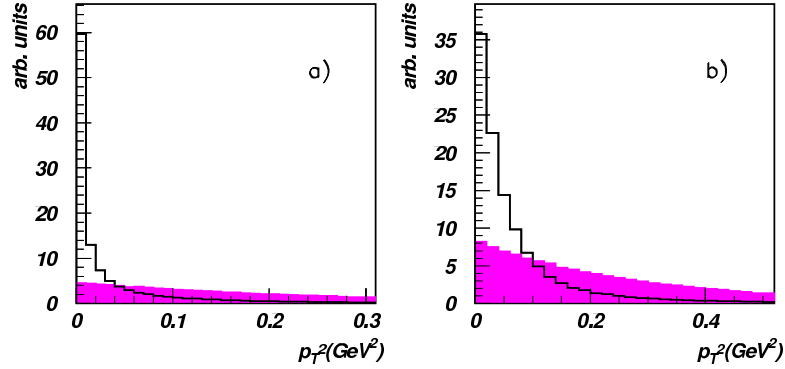


Figure 7.1: Distribution of the transverse momenta squared of the scattered protons for the $\gamma - \gamma$ (empty histogram) and $\mathbb{P} - \mathbb{P}$ (shaded histogram) collision assuming a diffractive slope of $B = 4 \text{ GeV}^{-2}$, without (left) and with (right) smearing by the beam divergence. Figure from Ref. [553].

different low t spectra (Coulomb pole for ultraperipheral processes from the photon mediated processes versus power-like behaviour in QCD mediated events) [553]. For the pure QCD induced processes, instead of a pole behaviour, the shape has a typical $\exp(-Bp_T^2)$ behaviour, with $B \simeq 4 \text{ GeV}^{-2}$. In fact, due to smearing by the beam divergence for the initial running condition at LHC, the distinction is less clear than one could expect, as shown in Fig. 7.1.

Additionally, since the impact parameter b is not directly reconstructed, survival probability [554] have to be taken into account. In the elastic case, it corresponds to the probability of the scattered protons not to dissociate due to the secondary soft interactions rescattering, as we shortly discussed in Sec.5.1.3. This is of course a non-perturbative ingredient which cannot be extracted from first principles. Since the proton impact parameter goes like the inverse of $\sqrt{Q^2}$ (where Q^2 is the photon virtuality), b is much larger than the range of strong interaction. The effect of these survival probabilities is expected to be small for $\gamma\gamma$ induced processes than for $p\gamma$ processes. Still, since the average values of Q^2 get higher when increasing the $\gamma - \gamma$ cms energy, this gap survival probability, close to 100% for two-photon induced processes at moderate energies, decreases when considering $\gamma - \gamma$ processes in the Regge limit.

The above situation should be contrasted with processes involving e^\pm , which are not directly affected by strong interaction. This is the key reason why e^+e^- colliders are the cleanest solution in principle for $\gamma^{(*)}\gamma^{(*)}$ physics, both from a theoretical and from an experimental point of view.

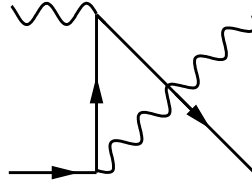
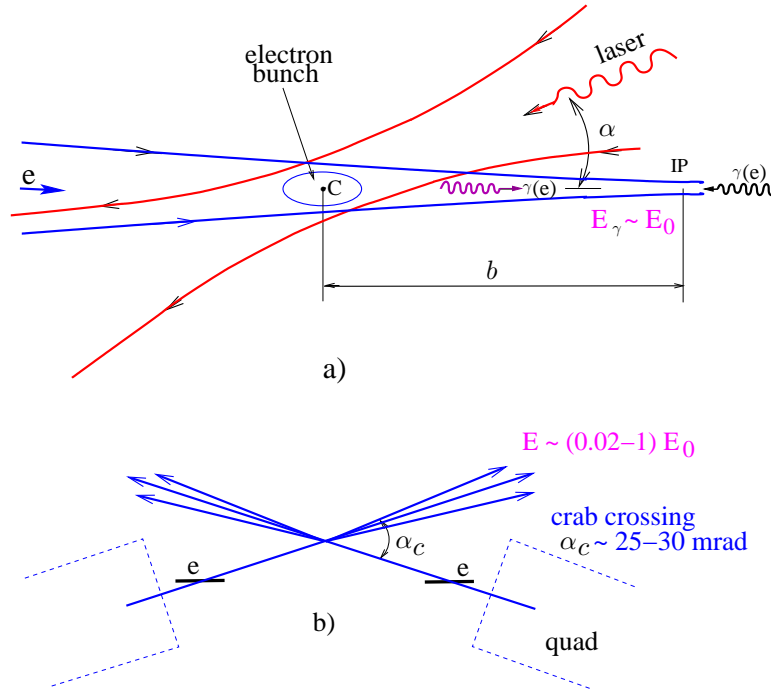
7.1.2 Photon colliders: $e \rightarrow \gamma$ conversion

At e^+e^- colliders, a small number of equivalent photons, of soft spectrum ($dn_\gamma \sim 0.03 d\omega/\omega$), is produced:

$$L_{\gamma\gamma}(W_\gamma/(2E_e) > 0.1) \sim 10^{-2} L_{e^+e^-} \quad \text{and} \quad L_{\gamma\gamma}(W_\gamma/(2E_e) > 0.5) \sim 0.4 \cdot 10^{-3} L_{e^+e^-} .$$

To produce a photon collider, the Novosibirsk group suggested [555–557] to reconsider the use of Compton backscattering of a laser on the high energy electron beam of a collider [558–560]. Due to the u -channel diagram of Fig. 7.2, which has an almost vanishing propagator, the cross-section is peaked in the backward direction. In this direction, almost all the energy of the incoming electron is transferred to the outgoing photon (up to 82 % at ILC 500 GeV). The limit comes from the fact that one does not want to reconvert γ in e^+e^- pairs! The corresponding number of equivalent photons is of the order of 1 if the beam has a small size, with laser flash energy of 1 – 10 J. The photon beam follows the direction of the incoming electron beam with an opening angle of $1/\gamma_e$. Due to the very good focussing of electrons beams expected at ILC, this is the main effect limiting the luminosity in γ mode: the distance b between conversion region and Interaction Point is ~ 1.5 mm, making impossible to use a magnet to deflect the low energy outgoing electron beam.

It has been suggested to use a non zero scattering angle between the two incoming beams to remove them (see Fig. 7.3). In order to compensate the potential lost luminosity with non zero scattering angle, *crab-cross* scattering is studied (the packet is not aligned with the direction of its propagation, like a crab). The luminosity

Figure 7.2: u -channel diagram for Compton scattering.Figure 7.3: $\gamma\gamma/\gamma e$ collider with cross-crab angle. Figure from Ref. [561].

could reach $0.17 L_{e^+e^-}$, a very interesting value since the cross-sections in $\gamma\gamma$ are usually one order of magnitude higher than for e^+e^- . As we already seen when discussing chiral-odd GPDs, the matrix element of the Compton process is helicity-conserving except for the term proportional to the electron mass, which is helicity-flip, and *dominates in the backward region*. This provides a very elegant way of *producing quasi monochromatic photons of maximal energy and given polarization*, by using $2\lambda_e P_c = -1$ ($\lambda_e =$ mean electron helicity and $P_c =$ mean laser photon circular polarization), see Fig. 7.4. Note that the WW distribution is sharply peaked around almost on-shell and soft photons: in γe or $\gamma\gamma$ mode, in order to use perturbative QCD, one needs to provide hard scales, from the outgoing state ($J/\Psi, \dots$) or from large t . Ingoing γ^* hard states are provided only in e^+e^- mode with double tagged outgoing leptons.

7.2 ILC project

The International Linear Collider (ILC) is expected to be a rather expensive project: 1.78 G \$ for site-dependent costs (tunnelling in a specific region, ...) and 4.87 G \$ for shared values of high technology and conventional components. Still, this estimate is comparable to the cost for the Large Hadron Collider (LHC) when including costs for pre-existing facilities. The decision of constructing this collider will be taken depending on the results obtained at LHC, in particular for precision measurement in the Higgs sector and potentially for beyond standard model physics. Still, from the point of view of strong interaction studies, it is a very clean machine, as any e^+e^-

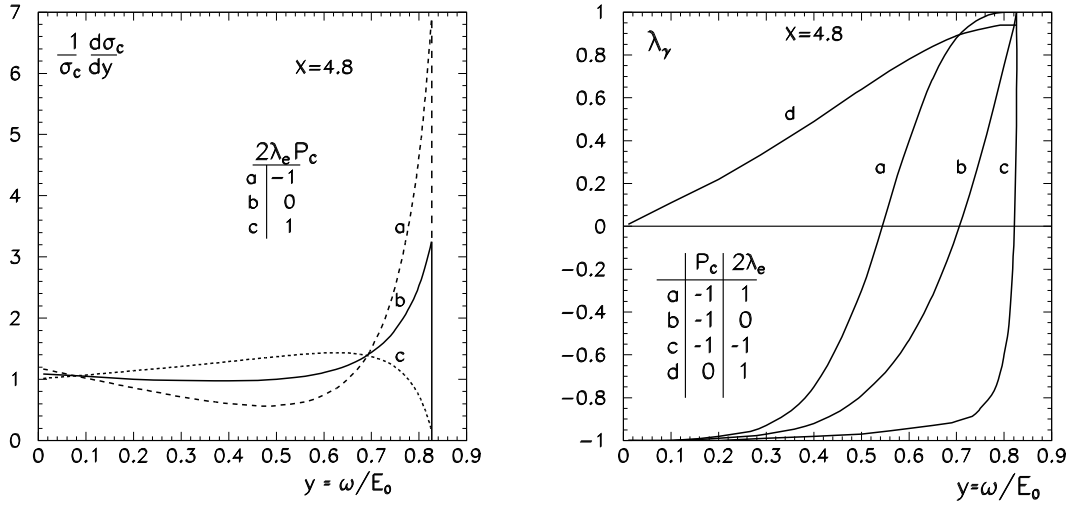


Figure 7.4: Spectrum (left) and average helicity (right) of the Compton-scattered photons. Figure from [562].

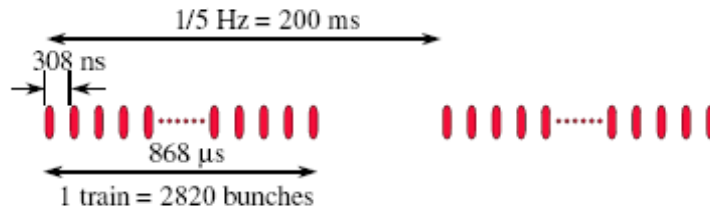


Figure 7.5: Paquet structure for ILC.

collider, in comparison with hadron-hadron colliders. Its high cms energy combined with a high luminosity would open the way to many interesting exclusive channels [563]. It would be very complementary with respect to low energy and high luminosity accelerators like JLab, BEPC-III ...

7.2.1 Reference Design Report for ILC

The design value of $\sqrt{s_{e^+e^-}} = 2E_{lepton}$ should have a nominal value of be 500 GeV, with a luminosity of 125 fb^{-1} per year within 4 years of running, at 500 GeV, with a possible scan in energy between 200 GeV and 500 GeV. An upgrade at 1 TeV, with a luminosity of 1 ab^{-1} within 3 to 4 years is planned. To reach such high luminosities, the paquets should have a rather intricate structure (see Fig. 7.5) [563]. There are non trivial technological problem for extracting the outgoing beam. At the moment, 3 options are considered for the scattering angle: 2 mrad, 14 mrad and 20 mrad, with in each case a hole in the detector at that angle to let the outgoing beam get through toward the beam dump (reducing the acceptance in the forward calorimeter). Crab-cross scattering is needed to get high luminosity. Two interaction regions are highly desirable: one which could be at low crossing-angle, and one compatible with $e\gamma$ and $\gamma\gamma$ physics (through single or double laser Compton backscattering). $\gamma\gamma$ mode leads to the severe constraint that $\alpha_c > 25 \text{ mrad}$ ¹. The mirrors could be placed either inside or outside the detector, depending on the chosen technology, in $e\gamma$ and $\gamma\gamma$ modes, with *almost no space for any forward detector in a cone of 95 mrad* (Fig. 7.6). If the option suggested by Telnov (single detector + single interaction point + single extraction line) would be chosen (this solution without displacement of the detector between 2 interaction points is much cheaper) it could become difficult to make diffractive physics. However, this $\gamma - \gamma$ option is of major importance for many channels, based on the very high cross-section for exclusive processes

¹last quadrupole ($\varnothing = 5\text{cm}$) at 4m from IP and horizontal disruption angle=12.5 mrad, thus $0.125 + 5/400 = 25 \text{ mrad}$.

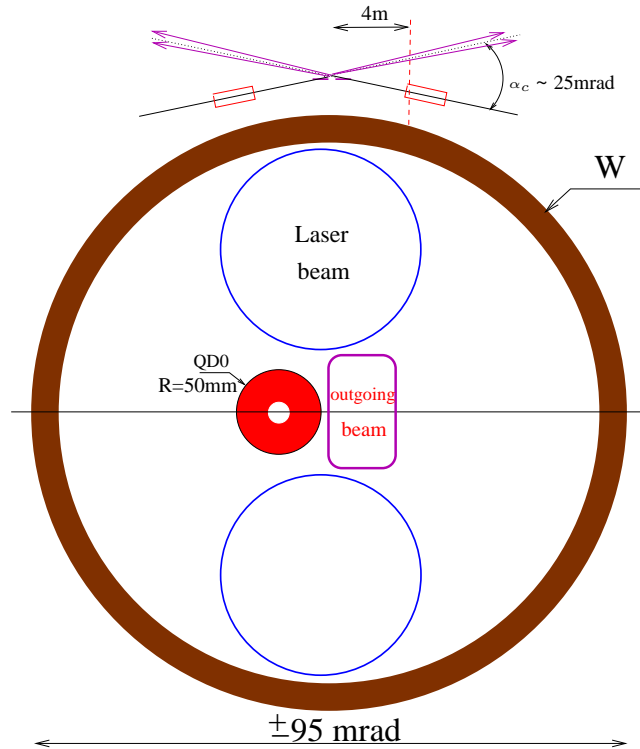


Figure 7.6: Layout of the quad and electron and laser beams at the distance of 4 m from the interaction point. Figure from Ref. [561].

in comparison with e^+e^- mode. A $\gamma-\gamma$ option together with an e^+e^- collider, with two detectors, would be the best solution. Though, for economical reason, a scenario without this initial $\gamma-\gamma$ option has been preferred recently.

7.2.2 Detectors at ILC

There are 4 concepts of detectors at the moment: GLD, Large Detector Concept, Silicon Design Detector Study (Sid) and 4th (sic). Each of them involves a very forward electromagnetic calorimeter for luminosity measurement, with tagging angle for outgoing leptons down to 5 mrad (10 years ago, 20 mrad was almost impossible!). It is ideal for diffractive physics, which cross-sections are sharply peaked in the very forward region. The luminosity is enough to get high statistics, even for exclusive events, as we will illustrate in detail in Sec. 7.4. For example, LDC (see Fig. 7.7) contains a BeamCal, an electromagnetic calorimeter devoted to luminosity measurement, located at 3.65 m from the vertex [564]. The main background is due to beamstrahlung photons, leading to energy deposit in cells close from the beam pipe (see Fig. 7.8). This implies cutting-of the cells for lepton tagging with $E_{min}=100$ GeV, $\theta_{min} = 4$ mrad (and to lower energies for large angles).

7.3 $\gamma^*\gamma^* \rightarrow \text{hadrons total cross-section}$

In comparison to LEP, which we considered in Sec. 5.3, s would be higher, the luminosity would be much higher (a factor $\sim 10^3$), and detectors would give access to events much closer to the beam pipe (LEP: $\theta_{min} \geq 25$ to 30 mrad). One can thus hope to get a much better access to QCD in perturbative Regge limit, since the typical virtualities of the photons will be lower, thus leading to higher cross-sections. To have enough statistics in order to see a BFKL enhancement with respect to conventional partonic at TESLA, it was considered to be important

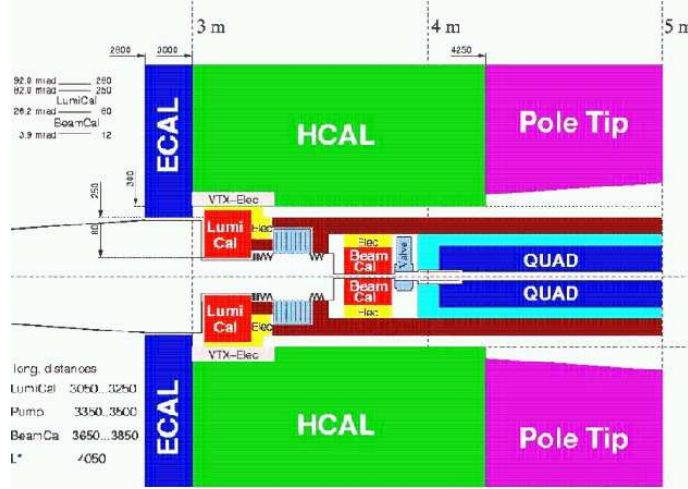


Figure 7.7: LDC detector project.

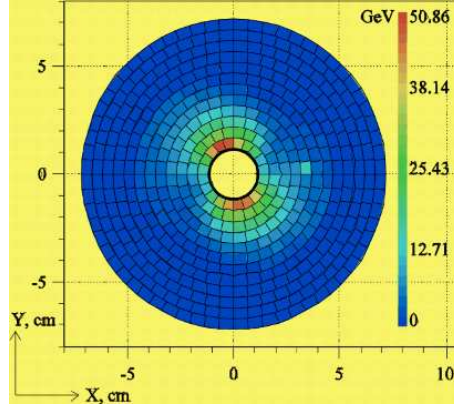


Figure 7.8: Beamstrahlung in BeamCal.

to get access down to $\theta_{min} \simeq 25$ to 20 mrad, as we have shown in [W9]. Probably this could be extended up to 30 mrad due to the expected luminosity (a factor 2 to 3 of luminosity higher than TESLA project, which we considered in [W9]). With detection down to 4 mrad, this is thus not anymore a critical parameter². In a modified LLx BFKL scenario [535], one expects around 10^4 events per year with $\theta_{min} \simeq 10$ mrad.

7.4 The $\gamma^*\gamma^* \rightarrow \rho_L^0 \rho_L^0$ exclusive process

Based on [W15, W16, W20]

In the $\gamma\gamma$ case (e^+e^- without tagging or $\gamma\gamma$ collider option), one can consider any diffractive process of type $\gamma\gamma \rightarrow J/\Psi J/\Psi$ [565, 566] (or other heavy produced state). The hard scale is provided by the charmed quark mass, with an expected number of events for TESLA around $7.4 \cdot 10^4$ (i.e. $9 \cdot 10^4$ with ILC luminosity). The expected efficiency of the detectors at the time of the TESLA project when Ref. [566] appeared, combined with a branching ratio of the order of 6 % in both e^+e^- and $\mu^+\mu^-$ modes lead to an expected number of events of 88, for $\theta_{min} > 20$ mrad. The situation could be much more favorable based on much lower values of the minimum

²Note that within a γe and $\gamma\gamma$ option, the Telnov suggestion would forbid any forward detector below typically 100 mrad.

tagging angles at ILC.

Due to the small detection angle offered by Beamcal, combined with high energy and high luminosity, one can think about the very exclusive process $\gamma^*\gamma^* \rightarrow \rho^0 \rho^0$ from $e^+e^- \rightarrow e^+e^-\rho^0 \rho^0$ with double tagged out-going electrons. In order to avoid any complication due to twist 3 contributions, we will in fact restrict ourselves to the twist-2 dominant ρ_L production, thus considering the process

$$e^+e^- \rightarrow e^+e^-\rho_L^0\rho_L^0. \quad (7.1)$$

We proposed and studied this reaction in [W31, W34, W15, W16, W35, W38 W20, W41, W45] as a test of BFKL dynamics at arbitrary t . The idea is to select events in which two vector mesons are produced with large rapidity gap, through scattering of two highly virtual photons, thus getting access to the kinematical regime in which the perturbative approach is justified. If additionally one selects the events with comparable photon virtualities, the perturbative Regge dynamics of QCD of the BFKL type should dominate with respect to the conventional partonic evolution of DGLAP type. In comparison with the study which we performed in Sec. 2.4, we are thus exploring now a different kinematical region in which the cms energy is parametrically large: this is the lower left corner of the phase-space described in Fig. 2.24. The study of Sec. 2.4 will provide us a partonic à la DGLAP description of the process. One of the question to be adressed will be to find a kinematical region in which such a partonic contribution is suppressed with respect to the gluon exchange contribution à la BFKL.

From a phenomenological point of view, before studying the process in detail, let us note that one can expect measurable counting rates for our reaction, by a rule of thumb comparison with $\gamma\gamma \rightarrow J/\Psi J/\Psi$. Indeed, by crossing, since the typical values of Q_i^2 should be comparable with $m_{J/\Psi}^2$, and since the ρ production will be treated through collinear factorization in a way which make it similar to the γ point-like coupling of $\gamma\gamma \rightarrow J/\Psi J/\Psi$, (the detailed form of the ρ DA does not change dramatically the order of magnitude), the fact that the authors of Ref. [565, 566] got measurable cross-section made us confident before starting detailed study.

The first step is to study in detail the Born order two gluon contribution, in order to prove the feasibility of the experiment. We do this at the level of

$$\gamma_{L,T}^*(q_1) \gamma_{L,T}^*(q_2) \rightarrow \rho_L^0(k_1) \rho_L^0(k_2), \quad (7.2)$$

for arbitrary values of $t = (q_1 - k_1)^2$, with $s \gg -t$. The process is illustrated in Fig. 7.9. Based on our

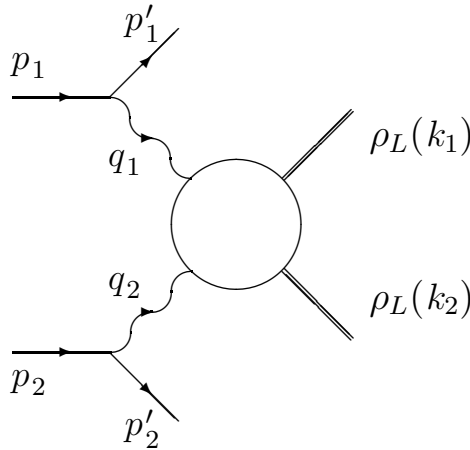


Figure 7.9: Amplitude for the process $e^+e^- \rightarrow e^+e^-\rho_L^0\rho_L^0$.

computation of Chap. 6, this could be extended to the case of ρ_T production. The choice of longitudinal polarizations of both the scattered photons and produced vector mesons which we first adressed in Refs. [W31, W34, W15, W35] was dictated by the fact that this configuration of the lowest twist-2 gives the dominant contribution in the powers of the hard scale Q^2 , when $Q_1^2 \sim Q_2^2 \sim Q^2$, as we have seen in Sec. 1.4.7. We then extended our study for all combinations of polarizations of virtual photons necessary to obtain all helicity amplitudes of the process (7.2) in Refs. [W20, W41, W45].

The study of the BFKL enhancement effects, at LLx and in the collinear improved LLx approach à la Salam, were studied for $t = 0$ in Refs. [W16, W38]. A full NLLx study has been carried at $t = 0$ in Refs. [328, 439] and in the collinear improved NLLx approach in Ref. [443]. We shall comment on the various obtained results at the end of this section. Note that restricting to $t = 0$ automatically selects the longitudinally polarized photon. A dedicate study for arbitrary value of t should thus be performed to get an evaluation of BFKL enhancement effects of the Born order evaluation for all γ^* polarization.

7.4.1 Kinematics

The measurable cross section for the process (7.1) of Fig. 7.9 is related to the amplitude of the process (7.2), illustrated in Fig. 7.10, through the usual flux factors for respectively transversally and longitudinally polarized photons

$$t(y_i) = \frac{1 + (1 - y_i)^2}{2}, \quad l(y_i) = 1 - y_i, \quad (7.3)$$

where y_i ($i = 1, 2$) are the longitudinal momentum fractions of the bremsstrahlung photons with respect to the incoming leptons. This relation reads [221]

$$\begin{aligned} \frac{d\sigma(e^+e^- \rightarrow e^+e^- \rho_L^0 \rho_L^0)}{dy_1 dy_2 dQ_1^2 dQ_2^2} &= \frac{1}{y_1 y_2 Q_1^2 Q_2^2} \left(\frac{\alpha}{\pi}\right)^2 [l(y_1) l(y_2) \sigma(\gamma_L^* \gamma_L^* \rightarrow \rho_L^0 \rho_L^0) + t(y_1) l(y_2) \sigma(\gamma_T^* \gamma_L^* \rightarrow \rho_L^0 \rho_L^0) \\ &+ l(y_1) t(y_2) \sigma(\gamma_L^* \gamma_T^* \rightarrow \rho_L^0 \rho_L^0) + t(y_1) t(y_2) \sigma(\gamma_T^* \gamma_T^* \rightarrow \rho_L^0 \rho_L^0)] . \end{aligned} \quad (7.4)$$

The presence of hard scales Q_i^2 permits us to apply the collinear approximation at each $q\bar{q}\rho$ -meson vertex, and the use of distribution amplitude (DA) for describing the $q\bar{q}$ content of the ρ mesons, as illustrated in Fig. 7.10. The amplitude M_H will be described using the impact representation, valid at high energy, as illustrated in

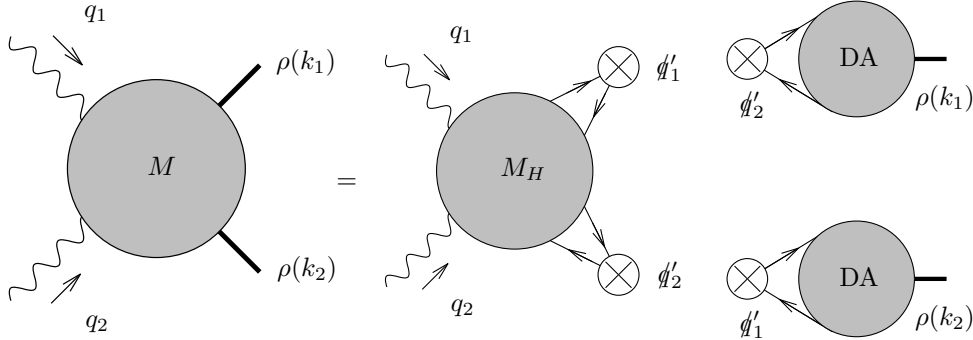


Figure 7.10: The amplitude of the process $\gamma^*(Q_1)\gamma^*(Q_2) \rightarrow \rho_L^0(k_1)\rho_L^0(k_2)$ with the collinear factorization in the $q\bar{q}\rho$ vertex.

Fig. 7.11, except when dealing with the quark exchange which we considered in Sec.2.4.

We introduce two light-like Sudakov vectors q'_1 and q'_2 which form a natural basis for two scattered virtual photons³, which satisfy $2q'_1 \cdot q'_2 \equiv s \sim 2q_1 \cdot q_2$. The usual $s_{\gamma^*\gamma^*}$ is related to the auxiliary useful variable s by $s_{\gamma^*\gamma^*} = s - Q_1^2 - Q_2^2$. The momentum transfer in the t -channel is $r = k_1 - q_1$. In this basis, the incoming photon momenta read

$$q_1 = q'_1 - \frac{Q_1^2}{s} q'_2 \quad \text{and} \quad q_2 = q'_2 - \frac{Q_2^2}{s} q'_1. \quad (7.5)$$

In accordance with (6.6), the polarization vectors of longitudinally polarized photons are, after using (7.5),

$$\epsilon_\mu^{L(1)} = \frac{q_{1\mu}}{Q_1} + \frac{2Q_1}{s} q'_{2\mu} \quad \text{and} \quad \epsilon_\mu^{L(2)} = \frac{q_{2\mu}}{Q_2} + \frac{2Q_2}{s} q'_{1\mu}, \quad (7.6)$$

with $\epsilon_{L(i)}^2 = 1$ and $q_i \cdot \epsilon_{L(i)} = 0$, whereas the polarization vectors of transversally polarized photons are two dimensional transverse vectors satisfying $\epsilon_{T(i)}^2 = -1$ ($i = 1, 2$) and $q_i \cdot \epsilon_{T(i)} = 0$.

³In previous chapters we denoted these light-cone vectors by p_1 and p_2 , but here p_1 and p_2 denote the lepton momenta.

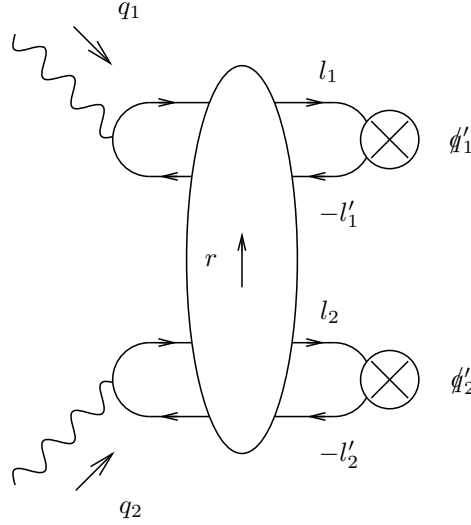


Figure 7.11: The amplitude M_H in the impact representation. The vertical blob symbolizes the interaction of two $q\bar{q}$ dipoles through gluon exchanges at high s .

We label the momentum of the quarks and antiquarks entering the meson wave functions as l_1 and l'_1 for the upper part of the diagram and l_2 and l'_2 for the lower part (see Fig. 7.11).

In the basis (7.5), the vector meson momenta can be expanded in the form

$$\begin{aligned} k_1 &= \alpha(k_1) q'_1 + \frac{\underline{r}^2}{\alpha(k_1) s} q'_2 + r_\perp, \\ k_2 &= \beta(k_2) q'_2 + \frac{\underline{r}^2}{\beta(k_2) s} q'_1 - r_\perp. \end{aligned} \quad (7.7)$$

In the following, we will treat the ρ meson as being massless. α and β are very close to unity, and reads

$$\begin{aligned} \alpha(k_1) &\simeq 1 - \frac{Q_2^2 + \underline{r}^2}{s} + O\left(\frac{1}{s^2}\right), \\ \beta(k_2) &\simeq 1 - \frac{Q_1^2 + \underline{r}^2}{s} + O\left(\frac{1}{s^2}\right), \end{aligned} \quad (7.8)$$

where $\underline{r}^2 = -r_\perp^2$. They will be replaced by 1 in the phenomenological applications of Secs. 7.4.3 and 7.4.4. In this decomposition, it is straightforward to relate $t = r^2$ to \underline{r}^2 through the approximate relation

$$t \sim -\frac{Q_1^2 Q_2^2}{s} - \underline{r}^2 \left(1 + \frac{Q_1^2}{s} + \frac{Q_2^2}{s} + \frac{\underline{r}^2}{s}\right) \quad (7.9)$$

(see [15] for an exact relation). From Eq.(7.9) the threshold for $|t|$ is given by $|t|_{min} = Q_1^2 Q_2^2 / s$, corresponding to $r_\perp = 0$. In the kinematical range we are interested in, the relation (7.9) can be approximated as $\underline{r}^2 = -t$, as usually in the Regge limit.

The links with the e^+e^- process can be made by using the same Sudakov basis for the two incoming leptons:

$$p_1 = \frac{1}{y_1} q'_1 + y_1 \frac{\underline{p}_1^2}{s} q'_2 + p_{\perp 1} \quad \text{and} \quad p_2 = \frac{1}{y_2} q'_2 + y_2 \frac{\underline{p}_2^2}{s} q'_1 + p_{\perp 2}, \quad \text{with} \quad \underline{p}_i^2 = \frac{1-y_i}{y_i^2} Q_i^2. \quad (7.10)$$

Thus, one gets

$$s_{e^+e^-} = \frac{s}{y_1 y_2} \left(1 + \frac{(1-y_1)(1-y_2)Q_1^2 Q_2^2}{s^2}\right) - 2\underline{p}_1 \cdot \underline{p}_2.$$

In the following, since we keep only the dominant s contribution, we use the approximate relation $s_{e^+e^-} \sim s/(y_1 y_2)$.

7.4.2 Impact representation

As we have seen in Sec. 4.2, the impact factor representation of the scattering amplitude for the process (4.8) has the form (see Fig. 7.12)

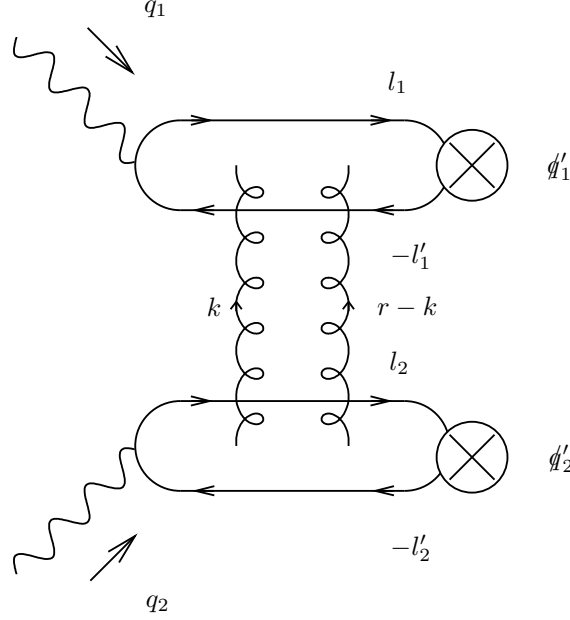


Figure 7.12: Amplitude M_H at Born order. The t -channel gluons are attached to the quark lines in all possible ways.

$$\mathcal{M} = is \int \frac{d^2 \underline{k}}{(2\pi)^2 \underline{k}^2 (\underline{r} - \underline{k})^2} \Phi^{ab} \gamma_{L,T}^*(q_1) \rightarrow \rho_L^0(k_1)(\underline{k}, \underline{r} - \underline{k}) \Phi^{ab} \gamma_{L,T}^*(q_2) \rightarrow \rho_L^0(k_2)(-\underline{k}, -\underline{r} + \underline{k}), \quad (7.11)$$

where $\Phi^{ab} \gamma_{L,T}^*(q_1) \rightarrow \rho_L^0(k_1)(\underline{k}, \underline{r} - \underline{k})$ ($\Phi^{ab} \gamma_{L,T}^*(q_2) \rightarrow \rho_L^0(k_2)(-\underline{k}, -\underline{r} + \underline{k})$) are the impact factors corresponding to the transition of $\gamma_{L,T}^*(q_1) \rightarrow \rho_L^0(k_1)$ ($\gamma_{L,T}^*(q_2) \rightarrow \rho_L^0(k_2)$) via the t -channel exchange of two gluons⁴. The amplitude (7.11) calculated in Born order depends linearly on s (or $s_{\gamma^* \gamma^*}$ when neglecting terms of order Q_i^2/s) as the impact factors are s -independent.

We have recalled in detail in Sec. 6.1.1 how the calculation of the impact factors in the Born approximation is performed. They are obtained by assuming the collinear approximation at each $q\bar{q}\rho$ -meson vertex, which means that projecting the (anti)quark momenta on the Sudakov basis q'_1, q'_2 ,

$$\begin{aligned} l_1 &= z_1 q'_1 + l_{\perp 1} + z_1 r_{\perp} - \frac{(l_{\perp 1} + z_1 r_{\perp})^2}{z_1 s} q'_2, \\ l'_1 &= \bar{z}_1 q'_1 - l_{\perp 1} + \bar{z}_1 r_{\perp} - \frac{(-l_{\perp 1} + \bar{z}_1 r_{\perp})^2}{\bar{z}_1 s} q'_2, \\ l_2 &= z_2 q'_2 + l_{\perp 2} - z_2 r_{\perp} - \frac{(l_{\perp 2} - z_2 r_{\perp})^2}{z_2 s} q'_1, \\ l'_2 &= \bar{z}_2 q'_2 - l_{\perp 2} - \bar{z}_2 r_{\perp} - \frac{(-l_{\perp 2} - \bar{z}_2 r_{\perp})^2}{\bar{z}_2 s} q'_1, \end{aligned} \quad (7.12)$$

we put the relative momentum $l_{i\perp}$ to zero. For longitudinally polarized photons the impact factor reads

$$\Phi^{ab} \gamma_L^*(q_i) \rightarrow \rho_L^0(k_i)(\underline{k}, \underline{r} - \underline{k}) = 4\pi\alpha_s \frac{e}{\sqrt{2}} \frac{\delta^{ab}}{2N_c} Q_i f_{\rho} \alpha(k_i) \int_0^1 dz_i z_i \bar{z}_i \phi(z_i) P_P(z_i, \underline{k}, \underline{r}, \mu_i), \quad (7.13)$$

⁴Note that the normalization used in this manuscript differs by a factor $(2\pi)^2$ in the way the amplitude is written when comparing with Ref. [W20]. This is due to the different normalization $\Phi_{here} = \frac{1}{2\pi} \Phi_{[W20]}$.

where the expression

$$P_P(z_i, \underline{k}, \underline{r}, \mu_i) = \frac{1}{z_i^2 \underline{r}^2 + \mu_i^2} + \frac{1}{\bar{z}_i^2 \underline{r}^2 + \mu_i^2} - \frac{1}{(z_i \underline{r} - \underline{k})^2 + \mu_i^2} - \frac{1}{(\bar{z}_i \underline{r} - \underline{k})^2 + \mu_i^2} \quad (7.14)$$

originates from the impact factor of quark pair production from a longitudinally polarized photon. This expression is the extension to the non-forward case of the formula (6.10), which is obtained by setting $\underline{r} = 0$.

For transversally polarized photons, one obtains

$$\begin{aligned} & \Phi^{ab} \gamma_T^*(q_i) \rightarrow \rho_L^0(k_i)(\underline{k}, \underline{r} - \underline{k}) \\ &= 2\pi\alpha_s \frac{e}{\sqrt{2}} \frac{\delta^{ab}}{2N_c} f_\rho \alpha(k_i) \int_0^1 dz_i (z_i - \bar{z}_i) \phi(z_i) \underline{\epsilon} \cdot \underline{Q}(z_i, \underline{k}, \underline{r}, \mu_i), \end{aligned} \quad (7.15)$$

where

$$\underline{Q}(z_i, \underline{k}, \underline{r}, \mu_i) = \frac{z_i \underline{r}}{z_i^2 \underline{r}^2 + \mu_i^2} - \frac{\bar{z}_i \underline{r}}{\bar{z}_i^2 \underline{r}^2 + \mu_i^2} + \frac{\underline{k} - z_i \underline{r}}{(z_i \underline{r} - \underline{k})^2 + \mu_i^2} - \frac{\underline{k} - \bar{z}_i \underline{r}}{(\bar{z}_i \underline{r} - \underline{k})^2 + \mu_i^2} \quad (7.16)$$

is proportional to the impact factor of quark pair production from a transversally polarized photon.

In the formulae (7.14) and (7.16) and in all this section, we denote $\mu_i^2 = Q_i^2 z_i \bar{z}_i + m^2$, where m is the quark mass. The limit $m \rightarrow 0$ is regular and we will restrict ourselves to the light quark case, taking thus $m = 0$. Both impact factor (7.14) and (7.16) vanish when $\underline{k} \rightarrow 0$ or $\underline{r} - \underline{k} \rightarrow 0$ due to QCD gauge invariance, as we explained in Sec. 4.2.

In the formulae (7.13, 7.15), we have denoted, in order to simplify notations, $\phi \equiv \varphi_1$, which is the twist-2 DA of the produced longitudinally polarized ρ^0 -mesons. For the case with quark q of one flavour it is defined, according to Eq. (1.76), by the matrix element of the non-local, gauge invariant correlator of quark fields on the light-cone, which reduces for ρ_L to

$$\langle 0 | \bar{q}(x) \gamma^\mu q(-x) | \rho_L(p) = \bar{q}q \rangle = f_\rho p^\mu \int_0^1 dz e^{i(2z-1)(px)} \phi(z), \quad (7.17)$$

where the coupling constant is $f_\rho = 216$ MeV and where the gauge links are omitted to simplify the notation. As usual, ϕ is normalized to unity. As in Chap. 6, the amplitudes for production of ρ^0 's are obtained by noting that $|\rho^0\rangle = 1/\sqrt{2}(|\bar{u}u\rangle - |\bar{d}d\rangle)$.

Note that Eq.(7.17) corresponds to the leading twist collinear distribution amplitude. Such an object can be used strictly speaking for asymptotically large Q^2 . In the phenomenological application of sections 7.4.3 and 7.4.4, in order to get measurable cross-sections, the dramatic decrease of the amplitudes with increase of Q_i^2 , combined with the experimental condition of ILC project, requires rather low values of Q_i^2 (of the order of 1 GeV²) for which subleading twist contributions could be significant. This can be taken into account within a more phenomenological approach which incorporates intrinsic k_T quark distribution and which goes beyond standard QCD collinear factorization [170–173], as we discussed in Sec. 1.4.8. We do not consider here these effects and adhere to the usual collinear QCD factorization. We expect that they would not change dramatically the order of magnitude of the cross-section.

Let us label the amplitudes for the scattering process (4.8) through the polarization of the incoming virtual photons as $\mathcal{M}_{\lambda_1 \lambda_2}$. They can be calculated using Eqs.(7.11) and Eqs.(7.13-7.16) supplemented by the choice of the transverse polarization vectors of the photons⁵

$$\underline{\epsilon}^\pm = \frac{1}{\sqrt{2}}(\mp 1, -i) \quad (7.18)$$

and the longitudinal polarization vectors (7.6). For the case $\lambda_1 = \lambda_2 = 0$:

$$\mathcal{M}_{00} = i s C Q_1 Q_2 \int_0^1 dz_1 dz_2 z_1 \bar{z}_1 \phi(z_1) z_2 \bar{z}_2 \phi(z_2) M_{00}(z_1, z_2), \quad (7.19)$$

⁵We use here the same conventions as in Ref. [W20]. These conventions differ by a global factor i with respect to the conventions (6.35) of Chap. 6. This has of course no physical consequence.

with

$$M_{00}(z_1, z_2) = \int \frac{d^2 \underline{k}}{\underline{k}^2 (\underline{r} - \underline{k})^2} P_P(z_1, \underline{k}, \underline{r}, \mu_1) P_P(z_2, -\underline{k}, -\underline{r}, \mu_2); \quad (7.20)$$

for the case $\lambda_2 = +, -$:

$$\mathcal{M}_{0\lambda_2} = i s \frac{C}{2} Q_1 \int_0^1 dz_1 dz_2 z_1 \bar{z}_1 \phi(z_1) (z_2 - \bar{z}_2) \phi(z_2) M_{0\lambda_2}(z_1, z_2), \quad (7.21)$$

with

$$M_{0\lambda_2}(z_1, z_2) = \int \frac{d^2 \underline{k}}{\underline{k}^2 (\underline{r} - \underline{k})^2} P_P(z_1, \underline{k}, \underline{r}, \mu_1) \underline{Q}(z_2, -\underline{k}, -\underline{r}, \mu_2) \cdot \underline{\epsilon}^{\lambda_2}; \quad (7.22)$$

for the case $\lambda_1 = +, -$:

$$\mathcal{M}_{\lambda_1 0} = i s \frac{C}{2} Q_2 \int_0^1 dz_1 dz_2 (z_1 - \bar{z}_1) \phi(z_1) z_2 \bar{z}_2 \phi(z_2) M_{\lambda_1 0}(z_1, z_2), \quad (7.23)$$

with

$$M_{\lambda_1 0}(z_1, z_2) = \int \frac{d^2 \underline{k}}{\underline{k}^2 (\underline{r} - \underline{k})^2} \underline{Q}(z_1, \underline{k}, \underline{r}, \mu_1) \cdot \underline{\epsilon}^{\lambda_1} P_P(z_2, -\underline{k}, -\underline{r}, \mu_2). \quad (7.24)$$

and for the case $\lambda_1 = +, -, \lambda_2 = +, -$:

$$\mathcal{M}_{\lambda_1 \lambda_2} = i s \frac{C}{4} \int_0^1 dz_1 dz_2 (z_1 - \bar{z}_1) \phi(z_1) (z_2 - \bar{z}_2) \phi(z_2) M_{\lambda_1 \lambda_2}(z_1, z_2), \quad (7.25)$$

with

$$M_{\lambda_1 \lambda_2}(z_1, z_2) = \int \frac{d^2 \underline{k}}{\underline{k}^2 (\underline{r} - \underline{k})^2} \underline{Q}(z_1, \underline{k}, \underline{r}, \mu_1) \cdot \underline{\epsilon}^{\lambda_1(1)} \underline{Q}(z_2, -\underline{k}, -\underline{r}, \mu_2) \cdot \underline{\epsilon}^{\lambda_2(2)}. \quad (7.26)$$

Here and in the following, we denote $C = 2\pi \frac{N_c^2 - 1}{N_c^2} \alpha_s^2 \alpha_{em} f_p^2$. In terms of the above amplitudes, the corresponding differential cross-sections can be expressed in the large s limit (neglecting terms of order Q_i^2/s) as

$$\frac{d\sigma^{\gamma_{\lambda_1}^* \gamma_{\lambda_2}^* \rightarrow \rho_L^0 \rho_L^0}}{dt} = \frac{|\mathcal{M}_{\lambda_1 \lambda_2}|^2}{16\pi s^2} \quad (7.27)$$

and it does not depend on s , in accordance to the k_T -factorization in the Born approximation.

7.4.3 Non-forward Born order differential cross-section for $\gamma_{L,T}^* \gamma_{L,T}^* \rightarrow \rho_L^0 \rho_L^0$

Analytical integration in k_T -space through conformal inversion

The k_\perp convolution of the two impact factors with the two t -channel propagators can be rewritten in terms of k_\perp -integral of scalar basic blocs. The most complicated basic blocs are boxes with two massive propagators of different masses, and two massless. This integration is thus non trivial. We developed a powerful method in Ref. [15], inspired by methods used in 2-dimensional conformal theories in coordinate space [567], which we here used in momentum space. This allowed us to perform these integration analytically. The idea is to reduce the number of massless propagator in order to reduce the number of Feynman parameter on which one should integrate. We here illustrate the method on the example of a triangle diagram with one massive propagator and two massless one. The transformation

$$\underline{k} \rightarrow \frac{\underline{K}}{\underline{K}^2}, \quad \underline{r} \rightarrow \frac{\underline{R}}{\underline{R}^2}, \quad m \rightarrow \frac{1}{M} \quad (7.28)$$

reduces the number of propagators and gives

$$\begin{aligned} J_{3m} &= \int \frac{d^2 \underline{k}}{\underline{k}^2 (\underline{k} - \underline{r})^2} \left(\frac{1}{(\underline{k} - \underline{r}a)^2 + m^2} - \frac{1}{\underline{r}^2 + m^2} + (a \leftrightarrow \bar{a}) \right) \\ &= R^2 \int \frac{d^2 \underline{K}}{(\underline{K} - \underline{R})^2} \left(\frac{K^2 R^2}{(\underline{R} - a\underline{K})^2 + \frac{K^2 R^2}{M^2}} - \frac{1}{a^2 r^2 + m^2} + (a \leftrightarrow \bar{a}) \right). \end{aligned} \quad (7.29)$$

After performing the shift of variable $\underline{K} = \underline{R} + \underline{k}'$ and then finally making the inverse transformation

$$\underline{k}' \rightarrow \frac{\underline{k}}{\underline{k}^2}, \quad \underline{R} \rightarrow \frac{\underline{r}}{\underline{r}^2}, \quad M \rightarrow \frac{1}{m}, \quad (7.30)$$

we end up with

$$J_{3m} = \frac{1}{r^2} \int \frac{d^2 \underline{k}}{\underline{k}^2} \left[\frac{(\underline{r} + \underline{k})^2}{(r^2 a^2 + m^2) \left[\left(\underline{k} - \underline{r} \frac{r^2 a \underline{a} - m^2}{r^2 \underline{a}^2 + m^2} \right)^2 + \frac{m^2 r^4}{(r^2 \underline{a}^2 + m^2)^2} \right]} - \frac{1}{a^2 r^2 + m^2} + (a \leftrightarrow \bar{a}) \right]. \quad (7.31)$$

The computation of this integral can now be performed using standard Feynman parameter technique, with now only 2 parameters instead of 3. It turns out that this method was known in 4-dimensions [568], in the case of ladder diagrams⁶.

Analytical results for k_\perp -integrated amplitude $M_{\lambda_1 \lambda_2}$

In this section we summarize the results for the amplitudes $M_{\lambda_1 \lambda_2}$ obtained after performing analytically the k_\perp integrals. In the transverse-transverse (TT) case, the amplitude can be expressed in term of two projection operators in the transverse plane as follows:

$$M_{\lambda_1 \lambda_2}(z_1, z_2) = \left[a(\underline{r}; Q_1, Q_2; z_1, z_2) \left(\delta^{ij} - \frac{r^i r^j}{r^2} \right) + b(\underline{r}; Q_1, Q_2; z_1, z_2) \frac{r^i r^j}{r^2} \right] \epsilon_i^{\lambda_1} \epsilon_j^{\lambda_2}, \quad (7.32)$$

where we denote $\underline{r}^2 = r^2$.

Combining (7.25) and (7.32), and using $|M_{++}|^2 = |M_{--}|^2$, one gets in the case of two photons with the same polarization :

$$|\mathcal{M}_{++}|^2 = s^2 \frac{C^2}{64} \left| \int_0^1 dz_1 dz_2 (z_1 - \bar{z}_1) \phi(z_1) (z_2 - \bar{z}_2) \phi(z_2) (b(\underline{r}; Q_1, Q_2; z_1, z_2) - a(\underline{r}; Q_1, Q_2; z_1, z_2)) \right|^2, \quad (7.33)$$

and analogously for different polarizations :

$$|\mathcal{M}_{+-}|^2 = s^2 \frac{C^2}{64} \left| \int_0^1 dz_1 dz_2 (z_1 - \bar{z}_1) \phi(z_1) (z_2 - \bar{z}_2) \phi(z_2) (b(\underline{r}; Q_1, Q_2; z_1, z_2) + a(\underline{r}; Q_1, Q_2; z_1, z_2)) \right|^2. \quad (7.34)$$

For the longitudinal-transverse (LT) case, restoring the dependency over all variables, one defines from (7.22) and (7.24) the scalar function f

$$M_{0\lambda}(\underline{r}; Q_1, Q_2; z_1, z_2) = f(\underline{r}; Q_1, Q_2; z_1, z_2) \underline{r} \cdot \underline{\epsilon}^\lambda, \quad (7.35)$$

or equivalently

$$M_{\lambda 0}(\underline{r}; Q_1, Q_2; z_1, z_2) = f(\underline{r}; Q_2, Q_1; z_2, z_1) \underline{r} \cdot \underline{\epsilon}^\lambda, \quad (7.36)$$

⁶We thank G. Korchemsky and E. Sokatchev for pointing out to us the existence of this work.

which leads to

$$|\mathcal{M}_{0+}|^2 = |\mathcal{M}_{0-}|^2 = s^2 \frac{C^2}{8} Q_1^2 \underline{r}^2 \left| \int_0^1 dz_1 dz_2 z_1 \bar{z}_1 \phi(z_1) (z_2 - \bar{z}_2) \phi(z_2) f(\underline{r}; Q_1, Q_2; z_1, z_2) \right|^2. \quad (7.37)$$

and analogously for the transverse-longitudinal (TL) case

$$|\mathcal{M}_{+0}|^2 = |\mathcal{M}_{-0}|^2 = s^2 \frac{C^2}{8} Q_2^2 \underline{r}^2 \left| \int_0^1 dz_1 dz_2 z_2 \bar{z}_2 \phi(z_2) (z_1 - \bar{z}_1) \phi(z_1) f(\underline{r}; Q_2, Q_1; z_2, z_1) \right|^2. \quad (7.38)$$

The expressions of $a(\underline{r}; Q_1, Q_2; z_1, z_2)$, $b(\underline{r}; Q_1, Q_2; z_1, z_2)$ and $f(\underline{r}; Q_1, Q_2; z_1, z_2)$ presented as combinations of *finite* standard integrals are given in the Appendix of Ref. [W20].

For the longitudinal-longitudinal (LL) case, it turned out [W15] that (7.19) can be effectively replaced by $\tilde{M}(z_1, z_2)$ whose integral over $z_{1,2}$ with symmetrical DA gives the same result. $\tilde{M}(z_1, z_2)$ reads

$$\begin{aligned} \tilde{M}_{00}(z_1, z_2) = & - \left(\frac{1}{z_1^2 \underline{r}^2 + \mu_1^2} + \frac{1}{\bar{z}_1^2 \underline{r}^2 + \mu_1^2} \right) J_{3\mu_2}(z_2) - \left(\frac{1}{z_2^2 \underline{r}^2 + \mu_2^2} + \frac{1}{\bar{z}_2^2 \underline{r}^2 + \mu_2^2} \right) J_{3\mu_1}(z_1) \\ & + J_{4\mu_1\mu_2}(z_1, z_2) + J_{4\mu_1\mu_2}(\bar{z}_1, z_2). \end{aligned} \quad (7.39)$$

$J_{3\mu}$ and $J_{4\mu_1\mu_2}$ are two dimensional integrals with respectively 3 propagators (1 massive) and 4 propagators (2 massive, with different masses), they are both IR and UV finite. Their expressions are given in the Appendix of Ref. [W20].

Due to the collinear conformal subgroup $SL(2, R)$ invariance discussed in Sec. 1.4.5, the ρ_L^0 distribution amplitude has an expansion in terms of Gegenbauer polynomials of even order which reads

$$\phi(z) = 6z(1-z) \left(1 + \sum_{n=1}^{\infty} a_{2n} C_{2n}^{3/2}(2z-1) \right). \quad (7.40)$$

Except for a short discussion in section 7.4.4, we will restrict ourselves to the asymptotical distribution amplitude corresponding to $a_{2n} = 0$. The effect of taking non zero a_{2n} for $n > 1$ allows us to evaluate the precision of our study.

To complete the evaluation of the amplitude \mathcal{M} , one needs to integrate over the quark momentum fractions z_1 and z_2 in the ρ mesons. For arbitrary values of t , it seems not possible to perform the z_1 and z_2 integrations analytically. We thus do them numerically. We observe the absence of end-point singularity when $z_{1(2)} \rightarrow 0$ or $z_{1(2)} \rightarrow 1$. Indeed, for the longitudinal polarizations involving P_P as defined in Eq.(7.14), the z divergency of type $1/z$, $1/\bar{z}$ is compensated by the $z\bar{z}$ factor when $z \rightarrow 0, 1$, while for transverse polarizations, involving \underline{Q} as defined in Eq.(7.16), there is no singularity since \underline{Q} is itself regular.

For the special case $t = t_{min}$ (where only the LL amplitude is non-vanishing), which will be useful in the discussion of sections 7.4.3 and 7.4.4, the integration over z_i can be performed analytically⁷, with the result [W15]

$$\begin{aligned} \mathcal{M}_{00} = & -is \frac{N_c^2 - 1}{N_c^2} \alpha_s^2 \alpha_{em} f_\rho^2 \frac{9\pi^2}{2} \frac{1}{Q_1^2 Q_2^2} \left[6 \left(R + \frac{1}{R} \right) \ln^2 R + 12 \left(R - \frac{1}{R} \right) \ln R + 12 \left(R + \frac{1}{R} \right) + \left(3R^2 + 2 + \frac{3}{R^2} \right) \right. \\ & \times \left. \left(\ln(1-R) \ln^2 R - \ln(R+1) \ln^2 R - 2\text{Li}_2(-R) \ln R + 2\text{Li}_2(R) \ln R + 2\text{Li}_3(-R) - 2\text{Li}_3(R) \right) \right], \end{aligned} \quad (7.41)$$

where $R = Q_1/Q_2$. When $Q_1 = Q_2$, the expression (7.41) simplifies to

$$\mathcal{M}_{00} = is \frac{N_c^2 - 1}{N_c^2} \alpha_s^2 \alpha_{em} f_\rho^2 \frac{9\pi^2}{Q^4} (14\zeta(3) - 12). \quad (7.42)$$

⁷This non trivial expression was obtained after use of Landen, Euler and Hill relations [569] among Li_2 and Li_3 functions. One needs (see Appendix A.1. of [W15]) in particular to extend analytically the two complex-variable Hill relation for $Li_2(xy)$ in the whole complex plane [570].

On the other hand, in the large $R \gg 1$ typical of a DGLAP-type dynamics, the expression (7.41) reduces to

$$\mathcal{M}_{00} = is \frac{N_c^2 - 1}{N_c^2} \alpha_s^2 \alpha_{em} f_\rho^2 \frac{96\pi^2}{Q_2^4 R^2} \left(\frac{\ln R}{R} - \frac{1}{6R} \right), \quad (7.43)$$

in agreement with the fact that this one loop gluon contribution contributes for a LLQ and a NLLQ term. This result can be obtained directly by imposing from the very beginning the k_\perp ordering typical of parton model. This is shown explicitly in Appendix A.2 of Ref. [15].

Results for differential cross-section

The formulae for $M_{\lambda_1 \lambda_2}$ obtained in Sec. 7.4.3 permit us to evaluate the magnitudes of cross-sections (7.27) of the diffractive double rho production for different helicities of virtual photons. In our estimates we use as a strong coupling constant the three-loop running $\alpha_S(Q_1 Q_2)$ with $\Lambda_{\overline{MS}}^{(4)} = 305$ MeV (see, e.g. [571]).⁸

In Fig. 7.13 we display the t -dependence of the different $\gamma_{L,T}^* \gamma_{L,T}^* \rightarrow \rho_L^0 \rho_L^0$ differential cross-sections for various values of $Q = Q_1 = Q_2$.

We first note the strong decrease of all the cross-sections when $Q_{1,2}^2$ increase. For LL, this follows from an obvious dimensional analysis, since

$$\mathcal{M}_{LL} \propto \frac{s f_\rho^2}{Q^4}$$

(for $Q_1 = Q_2 = Q$), in agreement with (7.42).

Secondly, all the differential cross-sections which involve at least one transverse photon vanish when $t = t_{min}$. It is due to the vanishing of the function \underline{Q} for $\underline{r} = 0$ (see (7.16)). Physically, this fact is related to the s -channel helicity conservation at $t = t_{min}$. Indeed, since the t -channel gluons carry non-sense polarizations, helicity conservation occurs separately in each impact factor.

In Fig. 7.14, we show the shape of the integrands $\overline{M}_{\lambda_1, \lambda_2}$ of the various amplitudes $\mathcal{M}_{\lambda_1 \lambda_2}$ as a function of z_1 and z_2 , as they appear in formulas (7.21, 7.23 and 7.25):

$$\overline{M}_{00} = z_1 \bar{z}_1 \phi(z_1) z_2 \bar{z}_2 \phi(z_2) M_{00}(z_1, z_2), \quad (7.44)$$

and for $\lambda_i = +, -$

$$\overline{M}_{\lambda_1 0} = (z_1 - \bar{z}_1) \phi(z_1) z_2 \bar{z}_2 \phi(z_2) M_{\lambda_1 0}(z_1, z_2), \quad (7.45)$$

$$\overline{M}_{\lambda_1 \lambda_2} = (z_1 - \bar{z}_1) \phi(z_1) (z_2 - \bar{z}_2) \phi(z_2) M_{\lambda_1 \lambda_2}(z_1, z_2). \quad (7.46)$$

$M_{\lambda_1 \lambda_2}(z_1, z_2)$ is symmetric under $(z_i \leftrightarrow \bar{z}_i)$ for a longitudinal polarization $\lambda_i = 0$ (cf. 7.14) and antisymmetric under $(z_i \leftrightarrow \bar{z}_i)$ for a transverse polarization $\lambda_i = +, -$ (cf. 7.16); thus the factors $z_i \bar{z}_i$ for $\lambda_i = 0$ and $z_i - \bar{z}_i$ for $\lambda_i = +, -$ ensure the symmetry of $\overline{M}_{\lambda_1 \lambda_2}$ under $(z_i \leftrightarrow \bar{z}_i)$ as we can see on Fig. 7.14. Because of the ρ_L^0 mesons distribution amplitudes $\phi(z_i)$, $\overline{M}_{\lambda_1 \lambda_2}(z_1, z_2)$ vanishes for any polarization in the end-point region. Consequently the case of a transverse polarization vanishes in the central region $z_i = \bar{z}_i = 1/2$ and also in the end-point region z_i close to 0 or 1, so that it restricts the available z_i phase-space and reduces the resulting differential cross-section, in agreement with the dominance of longitudinal photons (helicity conservation) in the process $\gamma_{L,T}^* \gamma_{L,T}^* \rightarrow \rho_L^0 \rho_L^0$.

The amplitude involving at least one transverse photon has a maximum at low $-t$ value with respect to $Q_1 Q_2$. The Fig. 7.14 corresponds to $-t = 0.16$ GeV² which is a typical value for the region where the cross-sections with transverse photons in Fig. 7.13 are maximal.

A peculiarly characteristic shape appears in the amplitudes with two transverse photons, as shown in bottom panels of Fig. 7.14. When the value of t changes towards t_{min} the peaks become very narrow, as shown in the left panel in Fig. 7.15 for \overline{M}_{+-} . For t very close to t_{min} they are practically concentrated only on the boundary which leads to the vanishing of the amplitude. On the other hand, when the value of t increases and leaves the maximum of cross-sections the peaks in Fig. 7.14 decrease and spread, as shown for \overline{M}_{+-} in the right panel of Fig. 7.15.

⁸Running of α_S is in principle a subleading effect with respect to our treatment. Nevertheless, numerically, as we discuss in sec.7.4.4, the dependence of our predictions for the rates in e^+e^- scattering on a choice of α_s is negligible at Born order, but is more subtle when LLx BFKL corrections are taken into account.

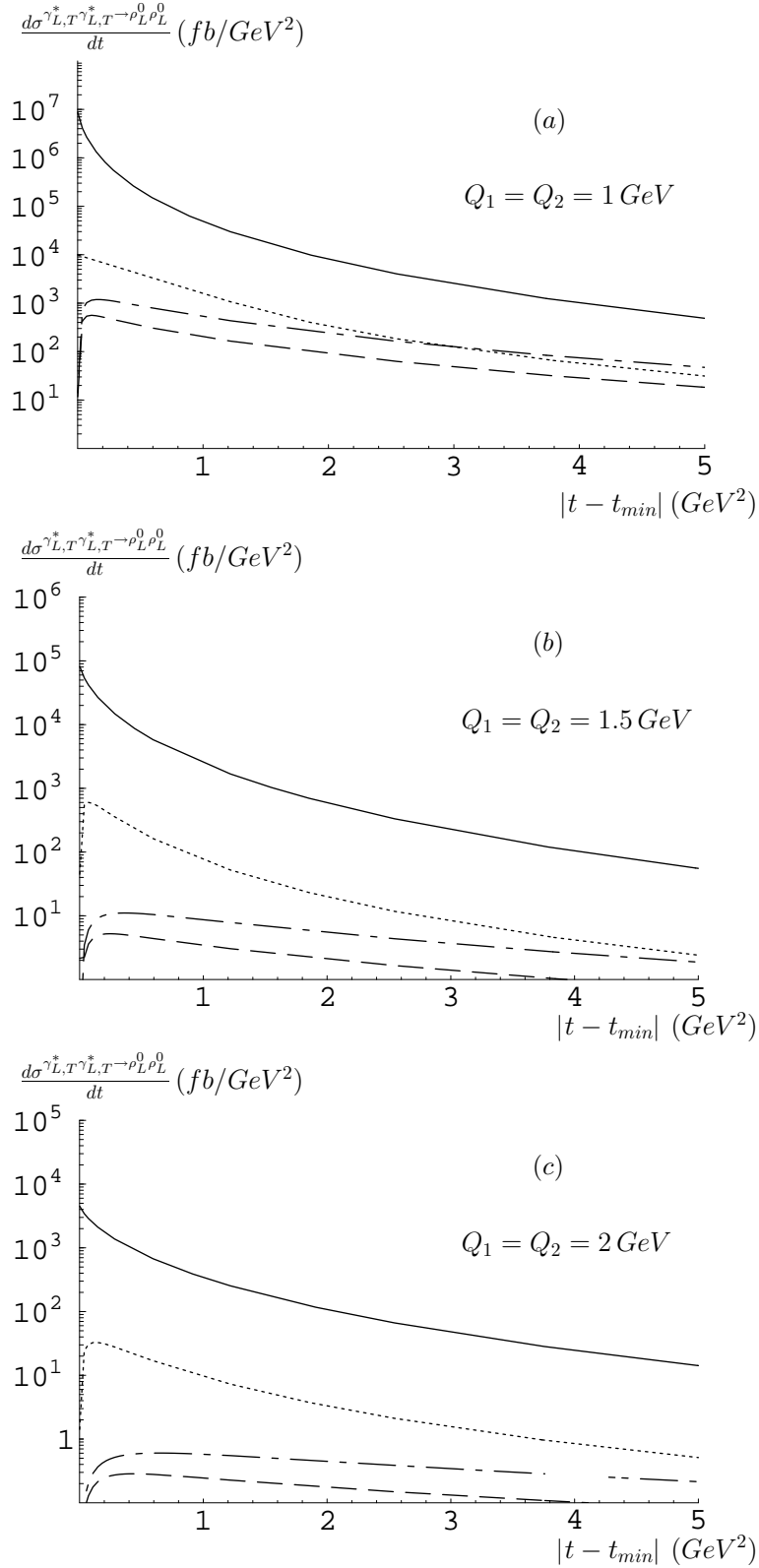


Figure 7.13: Differential cross-sections for the process $\gamma_{L,T}^* \gamma_{L,T}^* \rightarrow \rho_L^0 \rho_L^0$. The solid curve corresponds to the $\gamma_L^* \gamma_L^*$ mode, the dotted one to the $\gamma_T^* \gamma_T^*$ mode, the dashed and the dashed-dotted ones to the $\gamma_T^* \gamma_{T'}^*$ modes with respectively the same $T = T'$ and different $T \neq T'$ transverse polarizations. The different figures (a), (b), (c) correspond to different values of $Q_1 = Q_2$.

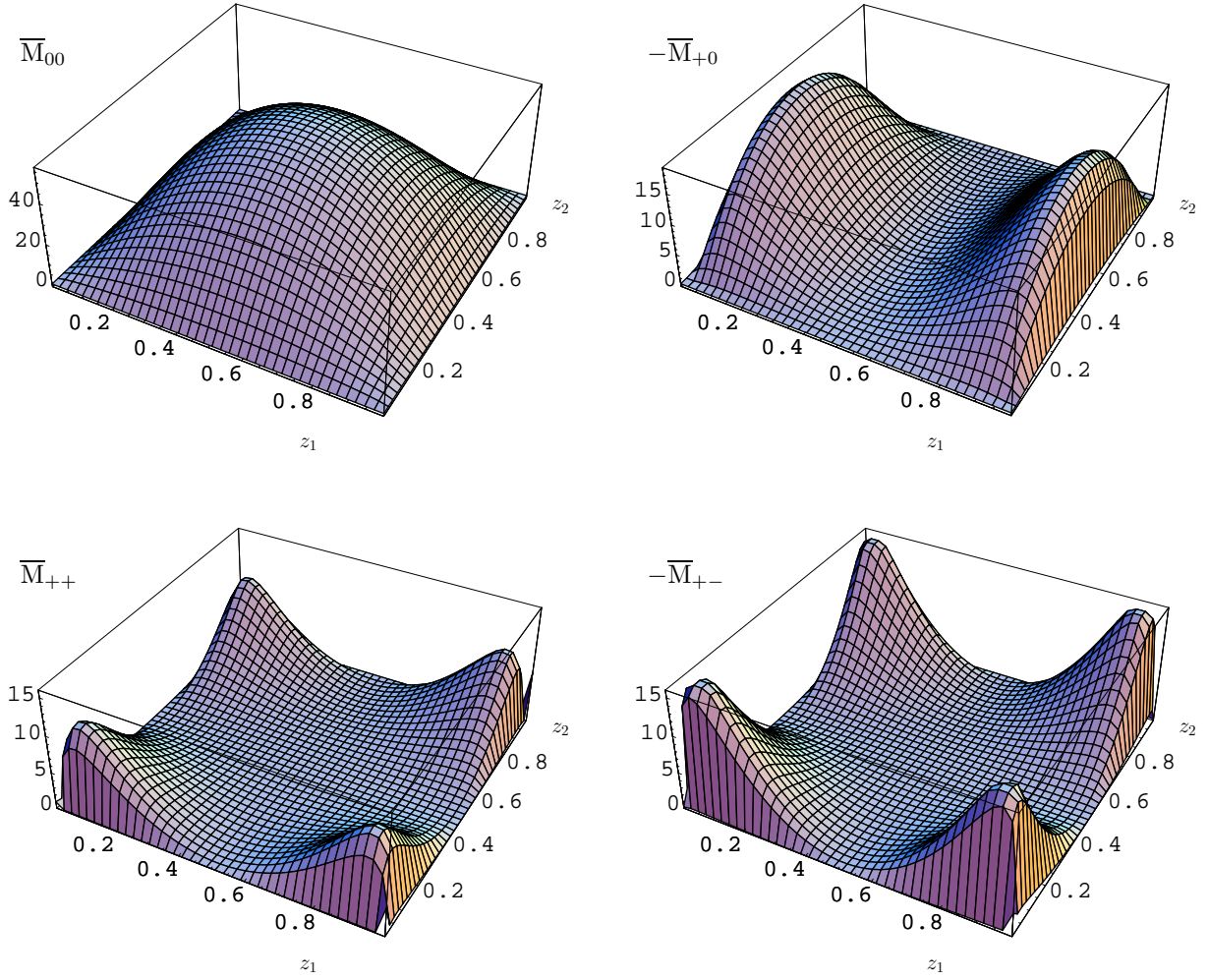


Figure 7.14: Shape of the amplitudes \overline{M}_{00} , $-\overline{M}_{+0}$, \overline{M}_{++} , $-\overline{M}_{+-}$ as functions of z_1 and z_2 , for $-t = 0.16 \text{ GeV}^2$ and $Q_1 = Q_2 = 1 \text{ GeV}$.

In the case of LT polarizations, the shape of the amplitude \overline{M}_{+0} , which contains only one factor $(z_i - \bar{z}_i)$, is shown in the right upper panel of Fig. 7.14. Its comparison with the upper left panel of Fig. 7.14, showing the shape of the \overline{M}_{00} amplitude, leads to the conclusion that \overline{M}_{+0} shares some properties with \overline{M}_{+-} and \overline{M}_{00} . In particular, the presence of a transverse polarization leads to the vanishing of \overline{M}_{+0} at $t = t_{min}$. On the other hand, the presence of a longitudinal polarization increases the cross-section at small values of t . As a consequence of the competition of these two mechanisms, the maximum of the cross-section determined by \overline{M}_{+0} is located closer to t_{min} than in the case of the cross-section given by \overline{M}_{+-} . This is illustrated in Fig. 7.16 which shows the t -dependence of the various differential cross-sections in log-log scale.

Third, in Fig. 7.17, we display the t -dependence of the $\gamma_{L,T}^* \gamma_{L,T}^* \rightarrow \rho_L^0 \rho_L^0$ differential cross-sections for $Q = Q_1 = Q_2 = 1 \text{ GeV}$ up to values of $-t$ much larger than photon virtualities Q_i , where t plays the role of the dominant hard scale in our process. Of course, in such a kinematical region the cross-sections are strongly suppressed in comparison with the small t one. Nevertheless, Fig. 7.17 illustrates the expected fact that the hierarchy of cross-sections is different in two regions: at large t , the $\gamma_T^* \gamma_T^* \rightarrow \rho_L^0 \rho_L^0$ cross-section dominates over the one of $\gamma_L^* \gamma_L^* \rightarrow \rho_L^0 \rho_L^0$, which is the dominant cross-section at small t , since the virtual photons are almost on shell with respect to the large scale given by t .

To conclude this subsection, we note that all the above cross-sections are strongly peaked in the forward cone. The phenomenological predictions obtained in the region of the forward cone will practically dictate the general trends of the integrated cross-sections. This fact is less dangerous than for the real photon case since

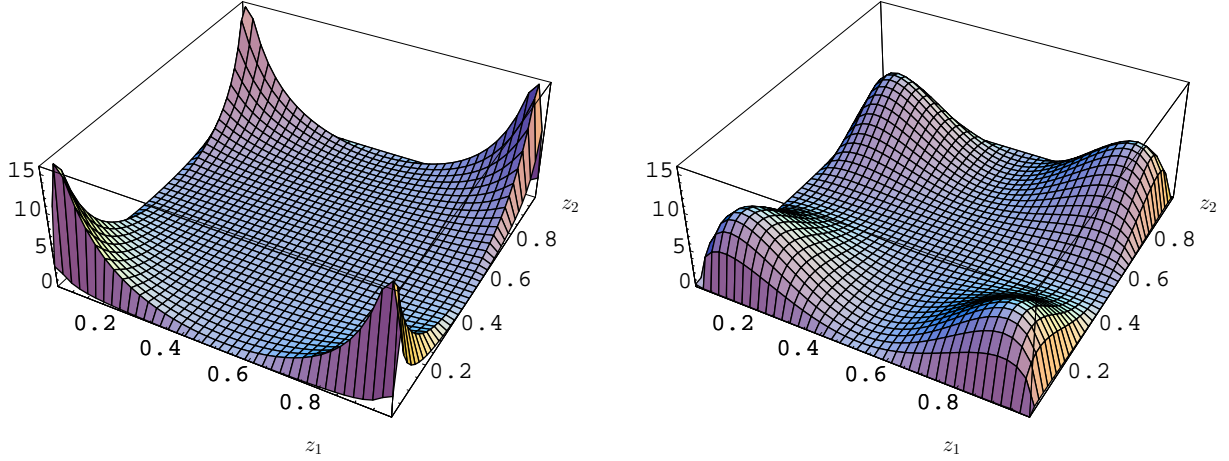


Figure 7.15: Shape of the amplitude $-\overline{M}_{+-}$, for $-t = 0.01 \text{ GeV}^2$ (left) and $-t = 0.8 \text{ GeV}^2$ (right), with $Q_1 = Q_2 = 1 \text{ GeV}$.

the virtual photon is not in the direction of the beam, and thus the outgoing ρ mesons can be tagged. We will come back shortly on this issue. The only difficulty has to do with the tagging of the outgoing lepton, since the cross-section is dominated by small (hard) values of $Q_{1,2}^2$. In this section we did not modify cross-sections by taking into account the virtual photon fluxes, which would amplify both, the dominance of small Q^2 region as well as the small y_i domain, characteristic for very forward outgoing leptons. This is discussed in section 7.4.4. In particular, it will be shown that the differential cross-sections are experimentally visible and seems to be sufficient for the t -dependence to be measured up to a few GeV^2 .

Note also that at this level of calculation there is no s -dependence of the cross-section. It will appear after taking into account triggering effects and/or BFKL evolution.

Quark exchange contribution to the cross-section

The process (4.8) described above involves gluon exchanges which dominate at high energies. However, at lower energy, the process can be described by double quark exchange. This was investigated in Sec. 2.4, in the case $t = t_{min}$. Using the Eqs. (2.131) and (2.132) together with the asymptotical ρ_L^0 distribution amplitude (7.40) one obtains the scattering amplitude for the photons longitudinally polarized

$$\mathcal{M}_{00}^{q\bar{q}} = -40 \pi^2 \frac{N_c^2 - 1}{N_c^2} \frac{\alpha_s \alpha_{em} f_\rho^2}{s} \left[1 + \frac{\left(1 + \frac{Q_1^2}{s} + 2 \frac{Q_1^2 \ln \frac{Q_1^2}{s}}{1 - \frac{Q_1^2}{s}}\right) \left(1 + \frac{Q_2^2}{s} + 2 \frac{Q_2^2 \ln \frac{Q_2^2}{s}}{1 - \frac{Q_2^2}{s}}\right)}{\left(1 - \frac{Q_1^2}{s}\right) \left(1 - \frac{Q_2^2}{s}\right)} \right] \quad (7.47)$$

and for the transversally polarized photons

$$\mathcal{M}_{TT}^{q\bar{q}} = \mathcal{M}_{++}^{q\bar{q}} + \mathcal{M}_{--}^{q\bar{q}} = -40 \pi^2 \frac{N_c^2 - 1}{N_c^2} \frac{\alpha_s \alpha_{em} f_\rho^2}{s} \frac{\left(\frac{7}{2} + \frac{2 \left(1 + \frac{Q_1^2}{s}\right) \ln \frac{Q_1^2}{s}}{1 - \frac{Q_1^2}{s}}\right) \left(\frac{7}{2} + \frac{2 \left(1 + \frac{Q_2^2}{s}\right) \ln \frac{Q_2^2}{s}}{1 - \frac{Q_2^2}{s}}\right) - \frac{1}{4}}{\left(1 - \frac{Q_1^2}{s}\right) \left(1 - \frac{Q_2^2}{s}\right)}. \quad (7.48)$$

In the large s limit, one respectively gets⁹

$$\mathcal{M}_{00}^{q\bar{q}} \simeq -80 \pi^2 \frac{N_c^2 - 1}{N_c^2} \frac{\alpha_s \alpha_{em} f_\rho^2}{s} \quad (7.49)$$

⁹After correcting a misprint in Ref. [W20].

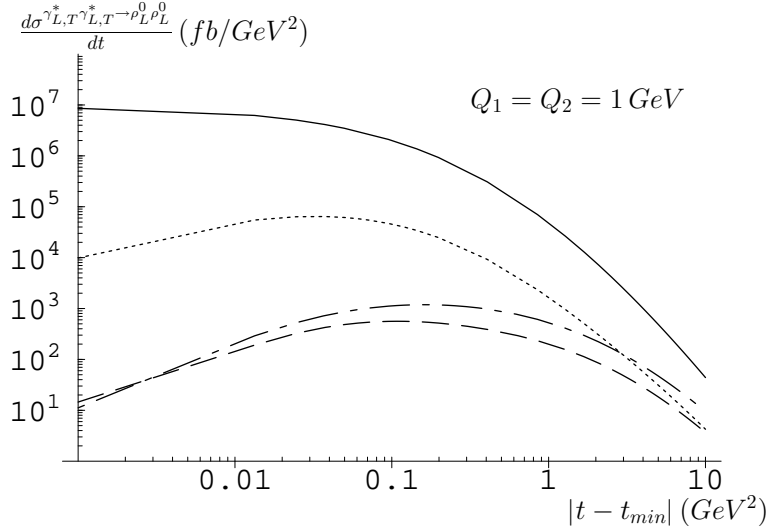


Figure 7.16: Differential cross-sections for the process $\gamma_{L,T}^* \gamma_{L,T}^* \rightarrow \rho_L^0 \rho_L^0$, for small value of t . The solid curve corresponds to the $\gamma_L^* \gamma_L^*$ mode, the dotted one to the $\gamma_L^* \gamma_T^*$ mode, the dashed and the dashed-dotted ones to the $\gamma_T^* \gamma_T^*$ modes with respectively the same $T = T'$ and different $T \neq T'$ transverse polarizations, for $Q_1 = Q_2 = 1 \text{ GeV}$.

and

$$\begin{aligned} \mathcal{M}_{TT}^{q\bar{q}} &\simeq -40 \pi^2 \frac{N_c^2 - 1}{N_c^2} \frac{\alpha_s \alpha_{em} f_\rho^2}{s} \left(4 \ln \frac{Q_1^2}{s} \ln \frac{Q_2^2}{s} + 14 \ln \frac{Q_1 Q_2}{s} + 12 \right) \\ &= -40 \pi^2 \frac{N_c^2 - 1}{N_c^2} \frac{\alpha_s \alpha_{em} f_\rho^2}{s} \left(4 \ln^2 \frac{Q_1 Q_2}{s} + 14 \ln \frac{Q_1 Q_2}{s} - 4 \ln^2 Q_1/Q_2 + 12 \right). \end{aligned} \quad (7.50)$$

Other amplitudes vanish at $t = t_{min}$. These expressions should be compared with the corresponding 2 gluons exchange contributions discussed in the previous sections. The LL amplitude is almost constant around $t = t_{min}$, and given by (7.41). The TT amplitude (7.32) behaves as

$$\mathcal{M}_{TT}^{gg} \simeq -i a \frac{\pi}{2} s \frac{N_c^2 - 1}{N_c^2} \alpha_s^2 \alpha_{em} f_\rho^2 \frac{|t - t_{min}|}{Q_1^3 Q_2^3}, \quad (7.51)$$

where the constant $a = 253.5$ is extracted from a numerical fit.

The Eqs. (7.47 - 7.51) confirm the well known fact that in the Regge limit the two gluon exchange dominates over the double quark exchange, with relative enhancement of s , in accordance with (4.1). In the case of longitudinally polarized photons which does not vanish at t_{min} , and for the same photon virtualities $Q_1^2 = Q_2^2 = Q^2$, let us consider the ratio

$$\mathcal{R}_{LL} = \frac{\mathcal{M}_{00}^{q\bar{q}}}{\mathcal{M}_{00}^{gg}} = \frac{32(Q_u^2 + Q_d^2)}{28 \zeta(3) - 24} \frac{Q^2}{s \alpha_s}. \quad (7.52)$$

For a typical value of $Q^2 = 1 \text{ GeV}^2$, as soon as s ($\simeq s_{\gamma^* \gamma^*}$) is higher than 4 GeV^2 , this ratio is bigger than unity, which at first sight seems to be always the case for ILC. (7.41) would thus completely dominates with respect to (7.47), by several orders of magnitudes. In fact, $s_{\gamma^* \gamma^*}$ can reach such low value as 4 GeV^2 , because of the outgoing energy carried by the outgoing leptons and the strong peak of the Weizsäcker-Williams fluxes at small γ^* energies. We discuss this effect in section 7.4.4 at the level of the $e^+ e^-$ process, after performing the phase-space integration of the differential cross-section at t_{min} . It will be shown that nevertheless the quark contribution is really negligible in almost all the ILC phase space.

In the case of the two gluon contribution with transverse virtual photons (7.51) which vanishes at $t = t_{min}$, its dominance over the corresponding quark contribution (7.48) appears very rapidly when $|t - t_{min}|$ starts to increase, and persists in the whole essential region of the phase space (remember that (7.51) is peaked at $t - t_{min} = k \cdot 0.01 \text{ GeV}^2$ where k is of order 1-10). This dominance will also be discussed in more detail in section 7.4.4 at the level of the $e^+ e^-$ process.

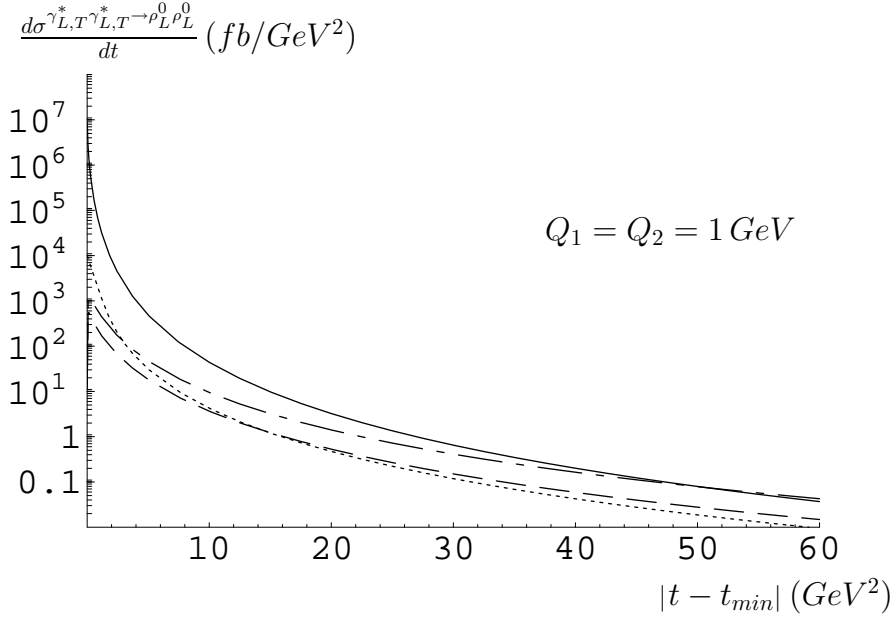


Figure 7.17: Differential cross-sections for the process $\gamma_{L,T}^* \gamma_{L,T}^* \rightarrow \rho_L^0 \rho_L^0$, up to asymptotically large t . The solid curve corresponds to the $\gamma_L^* \gamma_L^*$ mode, the dotted one to the $\gamma_T^* \gamma_T^*$ mode, the dashed and the dashed-dotted ones to the $\gamma_T^* \gamma_T^*$ modes with respectively the same $T = T'$ and different $T \neq T'$ transverse polarizations, for $Q_1 = Q_2 = 1$ GeV.

7.4.4 Non-forward Born order cross-section for $e^+e^- \rightarrow e^+e^- \rho_L^0 \rho_L^0$

Kinematical cuts for the phase-space integration

Our purpose is now to evaluate the cross-section of the process $e^+e^- \rightarrow e^+e^- \rho_L^0 \rho_L^0$ in the planned experimental conditions of the ILC project [563] discussed in Sec. 7.2. The cross-section which takes into account all the kinematical constraints, which are explained below, is given by

$$\frac{d\sigma^{e^+e^- \rightarrow e^+e^- \rho_L^0 \rho_L^0}}{dt} = \int_{Q_{1min}^2}^{Q_{1max}^2} dQ_1^2 \int_{Q_{2min}^2}^{Q_{2max}^2} dQ_2^2 \int_{\epsilon}^{y_{max}} dy_1 \int_{\frac{Q_1 Q_2}{s y_1}}^{y_{max}} dy_2 \frac{d\sigma^{e^+e^- \rightarrow e^+e^- \rho_L^0 \rho_L^0}}{dt dy_1 dy_2 dQ_1^2 dQ_2^2}, \quad (7.53)$$

with $Q_{1min} = 1$ GeV, $Q_{1max} = 4$ GeV, $\epsilon = 10^{-6}$ and $y_{max} = 0.6$. The cross-section (7.53) can be evaluated combining the cross-section formulae (7.4), (7.27) and the results of section 7.4.3 for the helicity scattering amplitudes.

The important feature of the formula (7.53) is that the dominant contribution for the $\gamma^* \gamma^* \rightarrow \rho_L^0 \rho_L^0$ process is strongly peaked at low Q_i . The integration over Q_i , y_i is peaked in the low y_i and Q_i phase space region due to the presence in (7.4) of $1/(y_i Q_i^2)$ factors coming from the Weizsäcker-Williams fluxes, and thus amplifies this effect. We show below that this dominant part of the phase space is accessible experimentally using the BeamCal calorimeter.

The integration domain in (7.53) is fixed by the following considerations. In the laboratory frame, which is also the cms for a linear collider, the standard expression for the momentum fractions which respect to the incoming leptons and for the virtualities of the bremsstrahlung photons are, respectively, given by

$$y_i = \frac{E - E'_i \cos^2(\theta_i/2)}{E} \quad \text{and} \quad Q_i^2 = 4EE'_i \sin^2(\theta_i/2), \quad (7.54)$$

where E is the energy of the beam, while E'_i and θ_i are respectively the energy and the scattering angle of the out-going leptons. At ILC, the foreseen cms energy is $\sqrt{s} = 2E = 500$ GeV. The experimental constraint coming from the minimal detection angle θ_{min} around the beam pipe is given by $\theta_{max} = \pi - \theta_{min} > \theta_i > \theta_{min}$ and leads to the following constraint on y_i

$$y_i > f(Q_i) = 1 - \frac{Q_i^2}{s \tan^2(\theta_{min}/2)}, \quad (7.55)$$

where the constraint on the upper bound of y_i coming from θ_{max} is completely negligible at this cm energy. The condition on the energy of the scattered lepton $E_{max} > E'_i > E_{min}$ results in

$$y_{i\ max} = 1 - \frac{E_{min}}{E} > y_i > 1 - \frac{E_{max}}{E}. \quad (7.56)$$

Moreover we impose that

$$s_{\gamma^*\gamma^*} = y_1 y_2 s > c Q_1 Q_2 \quad (7.57)$$

(where c is an arbitrary constant of the order 1) which is required by the Regge kinematics for which the impact representation is valid. We show below that this constant c can be adjusted to choose bins of data for which also in the case of e^+e^- scattering the contribution with quark exchanges (discussed in Sec. 7.4.3) is completely negligible.

We arbitrarily choose Q_i to be bigger than 1 GeV as it provides the hard scale of the process which legitimates the use of perturbation theory. $Q_{i\ max}$ will be fixed to 4 GeV, since the various amplitudes involved are completely negligible for higher values of virtualities Q_i values (see section 7.4.3). The constraints on $y_{i\ min}$ discussed so far are summarized by conditions

$$y_{1\ min} = \max\left(f(Q_1), 1 - \frac{E_{max}}{E}\right) \text{ and } y_{2\ min} = \max\left(f(Q_2), 1 - \frac{E_{max}}{E}, \frac{c Q_1 Q_2}{s y_1}\right). \quad (7.58)$$

Further simplifications of conditions (7.58) can be done by taking into account that the only condition on the maximal value of energy detection of the scattered leptons comes from kinematics, i.e. $E_{max} = E$, and some specific features of the planned detector.

The BeamCal calorimeter in the very forward region allows in principle to detect particles down to 4 mrad. More precisely, it measures an energy deposit for an angle between 4 mrad and 26 mrad. But this detector is also polluted by the photon beamstrahlung, specially for very small angles (see Fig. 7.8). We assume a non ambiguous identification for particles whose energies are bigger than 100 GeV. More precisely, the efficiency of detection of an electron depends on its energy and becomes less ambiguous when the energy increases. It is above 70 % in the part of the phase space which dominates the cross-section (small y_i , corresponding to $E'_i \simeq E_i$). A precise evaluation of this efficiency would require to set up a Monte Carlo simulation for the beamstrahlung contribution, which is beyond the scope of this paper. This sets the maximal value of y_i to $y_{i\ max} = 1 - \frac{E_{min}}{E} = 0.6$ with $E_{min} = 100$ GeV and $E = 250$ GeV.

Such a big value of E_{min} can be considered as surprisingly high and could lead to a strong reduction of the allowed phase space. In principle one could enlarge the phase space by taking into account particles whose energies E'_i are between 100 GeV and 20 GeV with angles θ_i bigger than 10 mrad (see Fig. 7.8), but the contribution of this domain is negligible (see Fig. 7.18) since the lower bound of y_i (see Eq.(7.58)) prevents us to reach the small values of y_i and Q_i which give the dominant contribution to the cross-section. We safely neglect the contribution of this region of phase space and assume in the following $E_{min} = 100$ GeV and $\theta_{min} = 4$ mrad. Thus, with $\theta_{min} = 4$ mrad and $\sqrt{s} = 500$ GeV, we have $s \tan^2(\theta_{min}/2) = 1 \text{ GeV}^2$, which means that $f(Q) \leq 0$

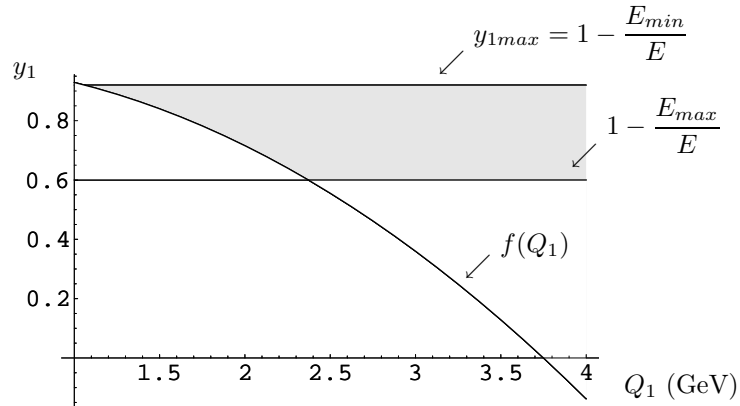


Figure 7.18: y_1 integration domain for $\theta_{min} = 10$ mrad, $E_{min} = 20$ GeV and $E_{max} = 100$ GeV.

for $Q^2 \geq 1\text{GeV}^2$. The relations (7.58), with $E_{max} = E$, reduce to only one condition $y_{2min} = \frac{Q_1 Q_2}{s y_1}$. This has to be supplemented numerically with the condition $y_{1min} = \epsilon$, where ϵ is a numerical cut-off: although, because of the Regge limit condition, we have $y_1 > \frac{Q_1 Q_2}{s y_2} \geq \frac{Q_{1min} Q_{2min}}{s y_{2max}} = 6.610^{-6}$ which thus provides a natural lower cut-off for y_1 , nevertheless we choose $\epsilon = 10^{-6}$ so that it is smaller than the smallest reachable value of y_1 but still non zero. This cut-off has no practical effect, except for avoiding numerical instabilities in the integration code.

The above discussion justifies the various cuts in formula (7.53).

Background in the detector

BeamCal is an electromagnetic calorimeter which cannot distinguish charges of particles. Thus, it is important to check that the cross-sections of any other processes which could lead to final states which can be misidentified with the final state of the process $e^+e^- \rightarrow e^+e^- \rho_L^0 \rho_L^0$ are suppressed. Indeed, the final state of the process $e^+e^- \rightarrow \gamma\gamma \rho_L^0 \rho_L^0$, with photons of the same energy deposit in detector as outgoing leptons, cannot be distinguished with the final state of $e^+e^- \rightarrow e^+e^- \rho_L^0 \rho_L^0$.

We shall argue that the process $e^+e^- \rightarrow \gamma\gamma \rho_L^0 \rho_L^0$ leads to a cross-section which is negligible at ILC. Let us first start with the process $e^+e^- \rightarrow \rho_L^0 \rho_L^0$ illustrated in Fig. 7.19(a), studied in Refs. [572, 573].

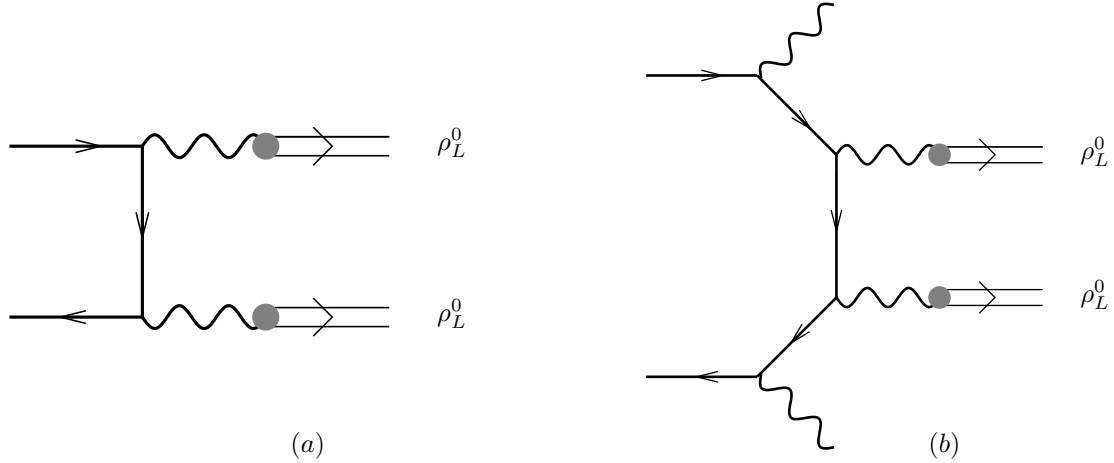


Figure 7.19: Example of Born order diagrams for the process $e^+e^- \rightarrow \rho_L^0 \rho_L^0$ (a) and for the $e^+e^- \rightarrow \gamma\gamma \rho_L^0 \rho_L^0$ process (b).

Its differential cross-section behaves typically like

$$\frac{d\sigma}{dt} \propto \frac{\alpha_{em}^4 f_\rho^4}{s^2 m_\rho^4}, \quad (7.59)$$

with the virtualities of the photons propagators equal to m_ρ^2 . More accurate expressions can be found in [573], if one identifies $g_{V\gamma} = f_\rho m_\rho$.

Now, when considering the competitor process $e^+e^- \rightarrow \gamma\gamma \rho_L^0 \rho_L^0$, that is adding two additional bremsstrahlung photon as in Fig. 7.19(b), we get

$$\frac{d\sigma^{e^+e^- \rightarrow \gamma\gamma \rho_L \rho_L}}{dt dy_1 dy_2 dQ_1^2 dQ_2^2} / \frac{d\sigma^{e^+e^- \rightarrow e^+e^- \rho_L \rho_L}}{dt dy_1 dy_2 dQ_1^2 dQ_2^2} \simeq \frac{\alpha_{em}^2 Q_1^4 Q_2^4}{\alpha_s^4 s^2 m_\rho^4} \quad (7.60)$$

which is suppressed at ILC energies, and would be of comparable order of magnitude only for colliders with cm energy of the order of a few GeV.

Results for cross-section

We now display in Fig. 7.20 the cross-sections $\frac{d\sigma^{e^+e^- \rightarrow e^+e^- \rho_L \rho_L}}{dt}$ as a function of t for the different polarizations, which are plotted after integrating the differential cross-section in (7.53) over the phase space considered previously. We made the following assumptions: we choose the QCD coupling constant to be $\alpha_s(\sqrt{Q_1 Q_2})$ running at

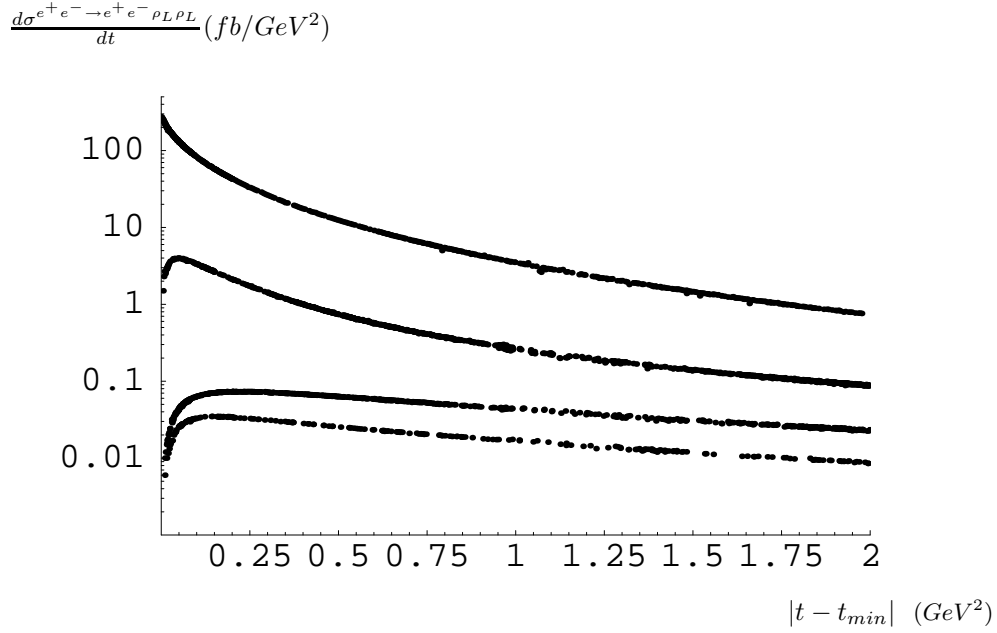


Figure 7.20: Cross-sections for $e^+e^- \rightarrow e^+e^- \rho_L^0 \rho_L^0$ process. Starting from above, we display the cross-sections corresponding to the $\gamma_L^* \gamma_L^*$ mode, to the $\gamma_L^* \gamma_T^*$ modes, to the $\gamma_T^* \gamma_T^*$ modes with different $T \neq T'$ and finally to the $\gamma_T^* \gamma_T^*$ modes with the same $T = T'$.

three loops, the parameter $c = 1$ which enters in the Regge limit condition and the cm energy $\sqrt{s} = 500$ GeV. Fig. 7.20 shows for e^+e^- scattering the same differential cross-sections related to different photon helicities as Fig. 7.13. We see that the shapes of corresponding curves are similar although they lead to quite different values of cross-sections. The cross-sections corresponding to photons with at least one transverse polarization vanish as in the $\gamma^* \gamma^*$ (cf Sec. 7.4.3) case at $t = t_{min}$. Similarly, each of them has a maximum in the very small t region. These maxima are shown more accurately on the log-log plot in Fig. 7.21.

At this point one technical remark is in order. By looking into the upper plot in Fig. 7.21 related to the \mathcal{M}_{00} amplitude, one sees that the points corresponding to nonzero $|t - t_{min}|$ approach smoothly the point on the axis $|t - t_{min}| = 0$. This point $|t - t_{min}| = 0$ is of special interest because it gives the maximum of the total cross-section (since the transverse polarization case vanishes at t_{min}) and then practically dictates the trend of the total cross-section which is strongly peaked in the forward direction (for the longitudinal case) and strongly decreases with t (for all polarizations), as shown already at the level of the $\gamma^* \gamma^*$ cross-sections in Sec. 7.4.3. Due to numerical instabilities, the differential cross-section at $|t - t_{min}| = 0$ must be evaluated in a different way than those for $|t - t_{min}| \neq 0$, i.e. by the use of expression (7.41) in which the integration over z_i was already done in the analytic way. Since Eq.(7.41) involves several polylogarithmic functions its structure of cuts is quite inconvenient for further numerical integration over variables y_i and Q_i . In order to overcome this technical problem it is useful to rewrite (7.41) by the use of Euler identity [569] in the form

$$\begin{aligned} \mathcal{M}_{00} = & -is \frac{N_c^2 - 1}{N_c^2} \alpha_s^2 \alpha_{em} f_\rho^2 \frac{9\pi^2}{2} \frac{1}{Q_1^2 Q_2^2} \left[6 \left(R + \frac{1}{R} \right) \ln^2 R \right. \\ & + 12 \left(R - \frac{1}{R} \right) \ln R + 12 \left(R + \frac{1}{R} \right) + \left(3R^2 + 2 + \frac{3}{R^2} \right) \left(\left(\frac{\pi^2}{6} - \text{Li}_2(1-R) \right) \ln R \right. \\ & \left. \left. - \ln(R+1) \ln^2 R - 2 \text{Li}_2(-R) \ln R + \text{Li}_2(R) \ln R + 2 \text{Li}_3(-R) - 2 \text{Li}_3(R) \right) \right]. \end{aligned} \quad (7.61)$$

since now the imaginary terms only come from $\text{Li}_2(R)$ and $\text{Li}_3(R)$ along their cuts, which cancels among each other analytically. Therefore, one can safely use their real part in a numerical fortran code as defined in standard packages.

The ILC collider is expected to run at a cms nominal energy of 500 GeV, though it might be extended in order to cover a range between 200 GeV and 1 TeV. Because of this possibility, we below discuss how the

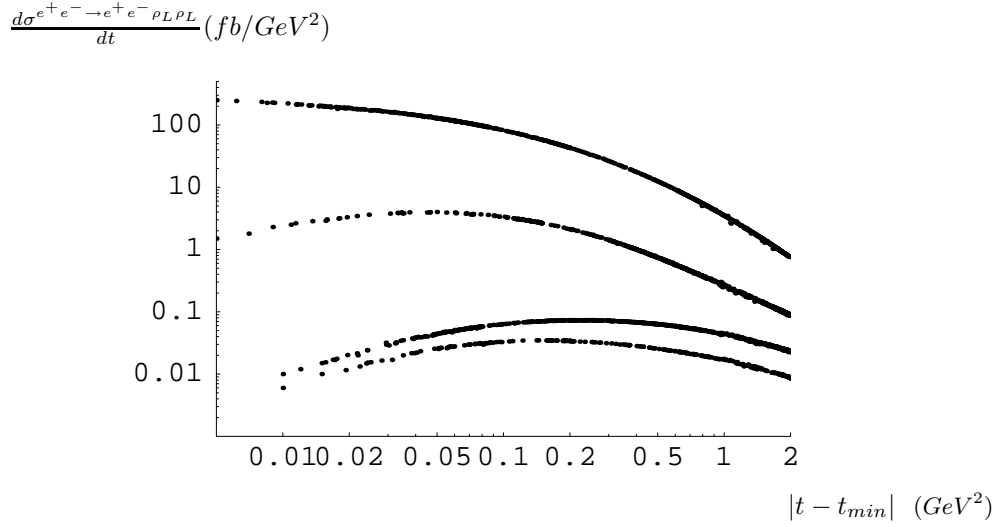


Figure 7.21: Cross-sections for $e^+e^- \rightarrow e^+e^- \rho_L^0 \rho_L^0$ process, in log-log scale. Starting from above, we display the cross-sections corresponding to the $\gamma_L^* \gamma_L^*$ mode, to the $\gamma_L^* \gamma_T^*$ modes, to the $\gamma_T^* \gamma_T^*$ modes with different $T \neq T'$ and finally to the $\gamma_T^* \gamma_T^*$ modes with the same $T = T'$.

change of the energy in cms influences our predictions for the cross-sections measured in the same BeamCal detector. Furthermore, we discuss the effects of our various assumptions on the cross-section $\frac{d\sigma^{e^+e^- \rightarrow e^+e^- \rho_L^0 \rho_L^0}}{dt}$ at the point t_{min} , and consequently on the behaviour of the total cross-section.

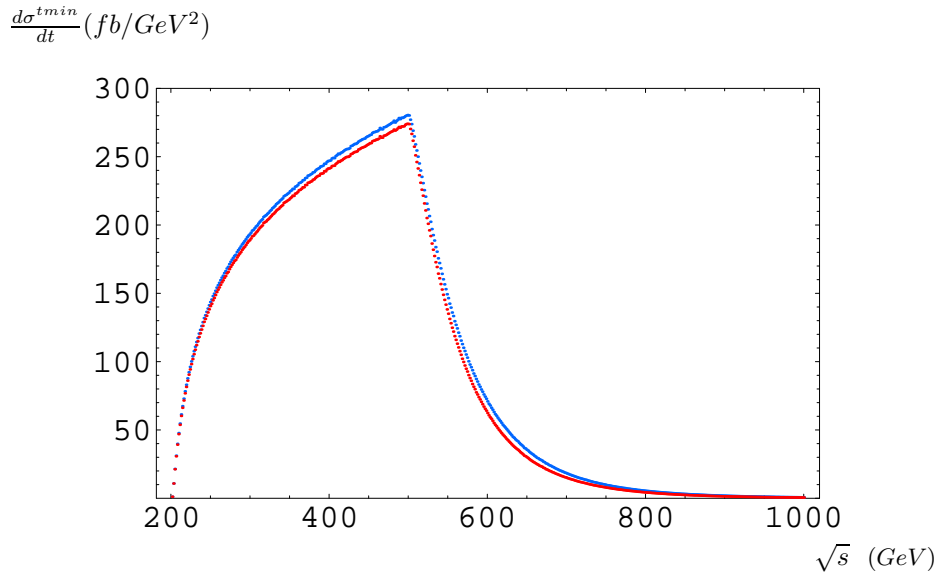


Figure 7.22: Cross-sections for $e^+e^- \rightarrow e^+e^- \rho_L^0 \rho_L^0$ at $t = t_{min}$ for different α_s : the blue and red curves for α_s running respectively at one and three loops, with $c = 1$.

Fig. 7.22 shows the cross-section at t_{min} as a function of the cm energy \sqrt{s} for different choices of strong coupling constant α_s . To see the sensitivity of our predictions to these choices, we plot the cross-section at t_{min} in two cases: the blue curve corresponds to $\alpha_s(\sqrt{Q_1 Q_2})$ running at one loop and the red one to $\alpha_s(\sqrt{Q_1 Q_2})$ running at three loops. The curves in Fig. 7.22 are very close to each other, which leads to a small uncertainty on the total cross-section as we will see in the following.

The shapes of plots in Fig. 7.22 distinguish two different domains: if the planned cm energy range \sqrt{s} is lower

than 500 GeV, the function $f(Q_i)$ (cf. equation (7.55)) appearing as a constraint on the minimum value of y_i in the phase space integration domain does not play any role at $\theta_{min} = 4$ mrad. Thus the cross-section increases with \sqrt{s} between 200 and 500 GeV. Because of the condition we assumed on the minimal value of the energies of the scattered leptons, the y_i integration domain becomes very narrow (cf. equation (7.56)) when \sqrt{s} goes to 200 GeV and leads to a strong decreasing of the cross-section at this cm energy. Note that if \sqrt{s} becomes bigger than 500 GeV, $f(Q_i)$ will cut the small y_i region (which contribute mainly because of the Weizsäcker-Williams photons fluxes) when \sqrt{s} increases. Thus the cross-section falls down between 500 GeV and 1 TeV. This is due to the limitation caused by the minimal detection angle offered by the BeamCal calorimeter, which is thus optimal for our process when $\sqrt{s} = 500$ GeV. This effect on $f(Q_i)$ could be compensated if one could increase the value of Q_i but this would be completely suppressed because of the strong decreasing of the amplitude with Q_i . The above discussion leads also to the conclusion, that although the Born order cross-sections do not depend on s , the triggering effects introduce an s -dependence of the measured cross-sections.

$$\frac{d\sigma^{t_{min}}}{dt} (fb/GeV^2)$$

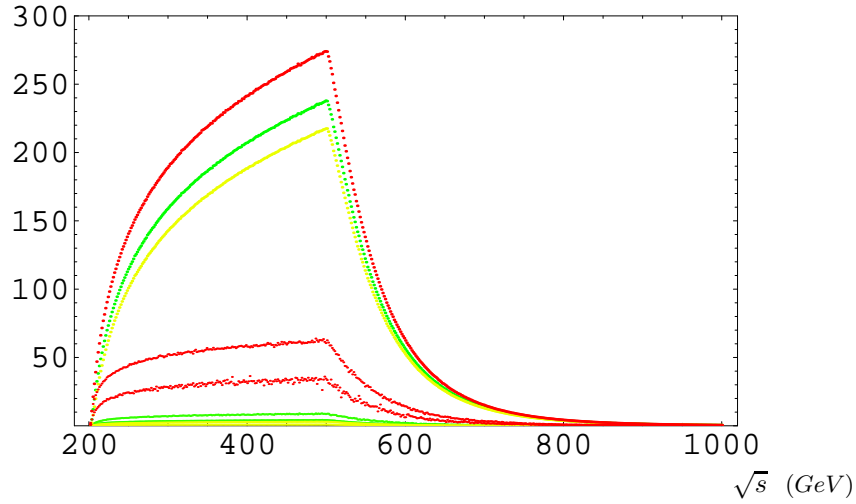


Figure 7.23: Cross-sections for $e^+e^- \rightarrow e^+e^-\rho_L^0\rho_L^0$ at $t = t_{min}$ for different values of the parameter c : the red [black] curves correspond to $c = 1$, the green [dark grey] curves to $c = 2$ and the yellow [light grey] curves to $c = 3$. For each value of c , by decreasing order the curves correspond to gluon-exchange, quark-exchange with longitudinal virtual photons and quark-exchange with transverse virtual photons.

Fig. 7.23 shows the cross-section at t_{min} for different values of the parameter c which enters in the Regge limit condition $s_{\gamma^*\gamma^*} = y_1 y_2 s > c Q_1 Q_2$. The value of the parameter c controls the dominance of gluonic contributions to the scattering amplitude: the increase of c should lead to suppression of quark exchanges. To see that we display the quark contribution in the same bins: we use the usual phase-space for the process $e^+e^- \rightarrow e^+e^-\rho_L^0\rho_L^0$ (cf. Eq.(7.4)) with the expressions of the amplitudes (7.47) and (7.48), and perform their numerical integration on y_i, Q_i with the same cuts as in the two gluon exchange process. For each value of c we plot the three curves corresponding to the two gluon exchange process and the quark exchange processes with longitudinal and transverse virtual photons.

A technical remark is in order when performing this integration numerically. The equation (7.48) is not divergent when $Q_i^2 \rightarrow s$ because this limit is only valid if $s(1 - Q_1^2/s)(1 - Q_2^2/s)$ is finite and positive since this term corresponds in our notation to the cm energy of the virtual photons. In order to avoid numerical instabilities we add the condition $y_1 y_2 s > Q_1^2, Q_2^2$ to the Regge limit condition. We can check that this supplementary constraint does not change our results for the other contributions, namely for the two gluon exchange and the quark exchange with longitudinal virtual photons processes.

As expected, the quark contribution is suppressed when increasing c and becomes completely negligible as soon as c exceeds 2. All above discussion concerned the case $t = t_{min}$ which determines the general trend of the cross-section in the non forward case. Because of that we hope that above conclusions are also valid at the level of the integrated over t cross-section. Thus, we omit below the quark exchanges.

We finally obtain the following results for the total cross-section integrated over t . We shall show three different predictions which differ by the choice of the definition of the coupling constant and by the choice of the value of the parameter c controlling the gluon dominance. First we choose $\alpha_s(\sqrt{Q_1 Q_2})$ running at three loops, the constant $c = 1$, the cms energy $\sqrt{s} = 500$ GeV and we obtain (up to numerical uncertainties):

$$\begin{aligned}\sigma^{LL} &= 32.4 \text{ fb} \\ \sigma^{LT} &= 1.5 \text{ fb} \\ \sigma^{TT} &= 0.2 \text{ fb} \\ \sigma^{Total} &= 34.1 \text{ fb}.\end{aligned}\tag{7.62}$$

With a nominal integrated luminosity of 125 fb^{-1} , this will yield $4.26 \cdot 10^3$ events per year.

Secondly, with the choice of $\alpha_s(\sqrt{Q_1 Q_2})$ running at one loop, the constant $c = 1$ and the cms energy $\sqrt{s} = 500$ GeV, we obtain:

$$\begin{aligned}\sigma^{LL} &= 33.9 \text{ fb} \\ \sigma^{LT} &= 1.5 \text{ fb} \\ \sigma^{TT} &= 0.2 \text{ fb} \\ \sigma^{Total} &= 35.6 \text{ fb}.\end{aligned}\tag{7.63}$$

As expected, we see that the transition from three to one loop changes very little the total cross-section. This result will yield $4.45 \cdot 10^3$ events per year with a nominal integrated luminosity of 125 fb^{-1} .

In the third choice, we choose $\alpha_s(\sqrt{Q_1 Q_2})$ running at three loops, the same cm energy $\sqrt{s} = 500 \text{ GeV}$ and the constant $c = 2$ (for which as previously discussed quark exchanges are completely negligible) and we get:

$$\begin{aligned}\sigma^{LL} &= 28.1 \text{ fb} \\ \sigma^{LT} &= 1.3 \text{ fb} \\ \sigma^{TT} &= 0.2 \text{ fb} \\ \sigma^{Total} &= 29.6 \text{ fb}.\end{aligned}\tag{7.64}$$

This result will yield $3.7 \cdot 10^3$ events per year with a nominal integrated luminosity of 125 fb^{-1} .

Finally, we also consider the same assumptions as the previous ones except for the value of the constant c which is now set to $c = 10$ in order to consider a more drastic Regge limit condition and we obtain:

$$\begin{aligned}\sigma^{LL} &= 19.3 \text{ fb} \\ \sigma^{LT} &= 0.9 \text{ fb} \\ \sigma^{TT} &= 0.11 \text{ fb} \\ \sigma^{Total} &= 20.3 \text{ fb}.\end{aligned}\tag{7.65}$$

This result will yield $2.5 \cdot 10^3$ events per year with a nominal integrated luminosity of 125 fb^{-1} . Thus, this shows that the precise way one implements the restriction of the kinematical phase space to the domain of applicability of the impact representation does not dramatically change the number of events.

All the prediction above were obtained using the asymptotical DA. In order to see the sensitivity of this assumption on our results, we do also the calculation using the DA (7.40) within different models. The choice of the DA of Ref. [574] with $a_2 = -0.1$ and $a_4 = 0$ gives $4.2 \cdot 10^3$ events per year, while the choice of the DA of Ref. [248] with $a_2 = 0.05$ and $a_4 = 0$ gives $4.3 \cdot 10^3$ events per year. In summary, our predictions are quite stable when changing the main parameters characterizing the theoretical uncertainties of our approach.

Let us come back to the detection issue concerning the two ρ^0 's. Each produced ρ^0 has a branching ratio of almost 100 % in the desintegration $\pi^+\pi^-$. Based on the cuts we have used for the tagging of the two out-going electrons, one can try to evaluate whether each of these 4 pions will be detectable, i.e. if they will be not too close from the beam pipe. The angle with respect to the beam pipe of the virtual photon as a function of the angle of the corresponding out-going lepton is $\theta^* \simeq -E'/\sqrt{Q^2 + (E - E')^2} \theta$. Since the cross-section is completely dominated by configurations where $E' \gg \sqrt{Q^2 + (E - E')^2}$, the ρ^0 is far from the beam pipe,

typically 100 mrad. The two emitted pions are a bit boosted in the ρ direction, so they will be seen in a region of the detector where the efficiency should be rather high. In contrast, the $\gamma\gamma \rightarrow J/\Psi J/\Psi$ [565, 566] is much less favorable due to the low 6% branching ratio of $J/\Psi \rightarrow \ell\ell^+$.

We will now study the effect of BFKL enhancement, restricting ourselves to the forward case, thus considering the process

$$\gamma_L^*(q_1) \gamma_L^*(q_2) \rightarrow \rho_L^0(k_1) \rho_L^0(k_2). \quad (7.66)$$

7.4.5 Leading order BFKL resummation effects for the forward $\gamma_L^* \gamma_L^* \rightarrow \rho_L^0 \rho_L^0$ amplitude

General expression

In the BFKL framework, as we saw in Sec. 4.1, writing the amplitude of the process (7.66) through its inverse Mellin transform as

$$\mathcal{M}(s, t) = is \int \frac{d\omega}{2\pi i} e^{\omega Y} f_\omega(r^2), \quad (7.67)$$

and using the forward BFKL solution (4.3) for $f_\omega(0)$, one obtains, after using the expression (6.10) of the forward impact factor¹⁰,

$$\begin{aligned} f_\omega(r^2 = 0) &= 4\pi\alpha_s^2\alpha_{em} \frac{N_c^2 - 1}{N_c^2} f_\rho^2 Q_1 Q_2 \int_0^1 dz_1 z_1 \bar{z}_1 \phi(z_1) \int_0^1 dz_2 z_2 \bar{z}_2 \phi(z_2) \\ &\times \int_{-\infty}^{\infty} d\nu \frac{1}{\omega - \omega(\nu, n)} \left[\int \frac{dk^2}{k^3} \left(\frac{1}{m^2} - \frac{1}{k^2 + \mu_1^2} \right) k^{2i\nu} \right] \left[\int \frac{dk'^2}{k'^3} \left(\frac{1}{m^2} - \frac{1}{k'^2 + \mu_2^2} \right) k'^{-2i\nu} \right]. \end{aligned} \quad (7.68)$$

Let us denote the expressions in the square brackets as $I(z, \nu)$ and $I(z, -\nu)$ respectively. It is straightforward to put the propagators on a common denominator and show that

$$I(z, \nu) = - (m^2)^{-\frac{3}{2}+i\nu} \Gamma\left(\frac{3}{2} - i\nu\right) \Gamma\left(-\frac{1}{2} + i\nu\right) = - (Q_1^2)^{-\frac{3}{2}+i\nu} (z\bar{z})^{-\frac{3}{2}+i\nu} \Gamma\left(\frac{3}{2} - i\nu\right) \Gamma\left(-\frac{1}{2} + i\nu\right). \quad (7.69)$$

Next, the z integrals can also be done. We have

$$\begin{aligned} \int_0^1 dz z \bar{z} \phi(z) I(z, \nu) &= - (Q_1^2)^{-\frac{3}{2}+i\nu} \Gamma\left(\frac{3}{2} - i\nu\right) \Gamma\left(-\frac{1}{2} + i\nu\right) \int_0^1 dz 6 (z\bar{z})^{\frac{1}{2}+i\nu} \\ &= -6\sqrt{\pi} 2^{-2-2i\nu} (Q_1^2)^{-\frac{3}{2}+i\nu} \Gamma\left(\frac{3}{2} - i\nu\right) \Gamma\left(-\frac{1}{2} + i\nu\right) \frac{\Gamma\left(\frac{3}{2} + i\nu\right)}{\Gamma(2 + i\nu)}, \end{aligned} \quad (7.70)$$

since the integral over z is just the definition of the Euler beta function. Finally this yields the Mellin transform

$$\begin{aligned} f_\omega(r^2 = 0) &= 9\pi^2 \alpha_s^2 \alpha_{em} \frac{N_c^2 - 1}{N_c^2} f_\rho^2 Q_1 Q_2 \int_{-\infty}^{\infty} d\nu \frac{1}{\omega - \omega(\nu)} (Q_1^2)^{-3/2+i\nu} (Q_2^2)^{-3/2-i\nu} \\ &\times \frac{\Gamma^2\left(\frac{3}{2} - i\nu\right) \Gamma^2\left(\frac{3}{2} + i\nu\right) \Gamma\left(-\frac{1}{2} - i\nu\right) \Gamma\left(-\frac{1}{2} + i\nu\right)}{\Gamma(2 - i\nu) \Gamma(2 + i\nu)}, \end{aligned} \quad (7.71)$$

which immediately leads to the final result for the amplitude (7.67)

$$\begin{aligned} \mathcal{M}(s, t_{min}, Q_1, Q_2) &= is 9\pi^2 \alpha_s^2 \alpha_{em} \frac{N_c^2 - 1}{N_c^2} f_\rho^2 \frac{1}{(Q_1 Q_2)^2} \int_{-\infty}^{\infty} d\nu e^{\omega(\nu)Y} \left(\frac{Q_1^2}{Q_2^2} \right)^{i\nu} \\ &\times \frac{\Gamma^2\left(\frac{3}{2} - i\nu\right) \Gamma^2\left(\frac{3}{2} + i\nu\right) \Gamma\left(-\frac{1}{2} - i\nu\right) \Gamma\left(-\frac{1}{2} + i\nu\right)}{\Gamma(2 - i\nu) \Gamma(2 + i\nu)}. \end{aligned} \quad (7.72)$$

We define $R \equiv Q_1/Q_2$ and write this as

$$A(s, t_{min}, Q_1, Q_2) = is \frac{N_c^2 - 1}{N_c^2} \frac{9\pi^2 \alpha_s^2 \alpha_{em} f_\rho^2}{(Q_1 Q_2)^2} J(Y, R), \quad (7.73)$$

¹⁰Note that the convention for impact factors differs between [W16], [W20] and this manuscript: $\Phi_{here} = 2\pi\Phi_{[W16]} = \frac{1}{2\pi}\Phi_{[W20]}$.

with

$$J(Y, R) = \int_{-\infty}^{\infty} d\nu e^{\omega(\nu)Y} R^{2i\nu} \frac{\Gamma^2\left(\frac{3}{2} - i\nu\right) \Gamma^2\left(\frac{3}{2} + i\nu\right) \Gamma\left(-\frac{1}{2} - i\nu\right) \Gamma\left(-\frac{1}{2} + i\nu\right)}{\Gamma(2 - i\nu) \Gamma(2 + i\nu)}. \quad (7.74)$$

We now want to evaluate the integral J . We have three possibilities at hand: (i) numerically, (ii) saddle point approximation and (iii) sum over residues of poles of the integrand. The first two methods are used to obtain BFKL results while the last one is used to check the Born limit.

Born limit

A very valuable and non-trivial check on the BFKL result as well as the Born result is the fact that in the limit $Y \rightarrow 0$ (no evolution) or alternatively $\alpha_s \rightarrow 0$ (the gluons in the ladder do not couple to each other) the BFKL amplitude must reduce to the Born level result. We refer to the Appendix of [W16] where we show, using method (iii) for the evaluation of the integral, that our BFKL result (7.72) does indeed reduce to the correct Born level results (7.41) (or equivalently (7.61)) derived in Ref. [W15], first for the special case $R = 1$ and the DGLAP-like limit $R \gg 1$, and finally for the general case $R \neq 1$. Note that the calculations presented in that Appendix are done in a completely different way than in the Born level calculation in Ref. [W15] (there we relied on the computation of k_{\perp} integration for arbitrary t , as explained in Sec. 7.4.3, which were then simplified in the forward limit), so the agreement is very convincing.

Saddle point approximation of the BFKL amplitude

For $R = 1$ the integrand has a saddle point at $\nu = 0$, but the product of Γ -functions that multiplies the exponential is not very broad. This means that the approximation will yield a too large answer. But let us try anyway. The expression multiplying the exponential in the integrand at $\nu = 0$ takes the value $\pi^3/4$, so for the case $Q_1 = Q_2$ we get

$$J(Y, 1) \sim \frac{\pi^3 \sqrt{\pi}}{4} \frac{e^{4 \ln 2 \bar{\alpha}_s Y}}{\sqrt{14 \bar{\alpha}_s \zeta(3) Y}}, \quad Y \gg 1, \quad (7.75)$$

so the BFKL amplitude is

$$A(s, t = t_{min}, Q_1 = Q_2 = Q) \sim i s \pi^5 \sqrt{\pi} \frac{9(N_c^2 - 1) \alpha_s^2 \alpha_{em} f_{\rho}^2}{4N_c^2 Q^4} \frac{e^{4 \ln 2 \bar{\alpha}_s Y}}{\sqrt{14 \bar{\alpha}_s \zeta(3) Y}}. \quad (7.76)$$

However, we can do better than this [W5]. We can keep the general case $Q_1 \neq Q_2$ with $R \equiv Q_1/Q_2$. The integral is then

$$J(Y, R) = \int_{-\infty}^{\infty} d\nu e^{\omega(\nu)Y + 2i\nu \ln R} g\left(\frac{1}{2} + i\nu\right) \quad (7.77)$$

where

$$g(\gamma) \equiv R^{2\gamma} g_1(\gamma) \quad (7.78)$$

with

$$g_1(\gamma) \equiv \frac{\pi^3 \gamma(1 - \gamma)}{\Gamma(5/2 - \gamma) \Gamma(3/2 + \gamma) \sin^3(\pi\gamma)} = \frac{f_1(\gamma)}{\sin^3(\pi\gamma)}. \quad (7.79)$$

Expanding the exponent to second order we see that the saddle point is shifted:

$$\omega(\nu)Y + 2i\nu \ln R \sim \omega(0)Y + 2i \ln R \nu + \frac{\omega''(0)Y}{2} \nu^2 \sim \frac{\omega''(0)Y}{2} \left(\nu + \frac{2i \ln R}{\omega''(0)Y} \right)^2 + \frac{2 \ln^2 R}{\omega''(0)Y} + \omega(0)Y, \quad (7.80)$$

and we can shift the integration variable accordingly to get a Gaussian integral. The result is now

$$J(Y, R) \sim \frac{\pi^3 \sqrt{\pi}}{4} \frac{e^{4 \ln 2 \bar{\alpha}_s Y}}{\sqrt{14 \bar{\alpha}_s \zeta(3) Y}} \exp\left(-\frac{\ln^2 R}{14 \bar{\alpha}_s \zeta(3) Y}\right), \quad Y \gg 1, \quad (7.81)$$

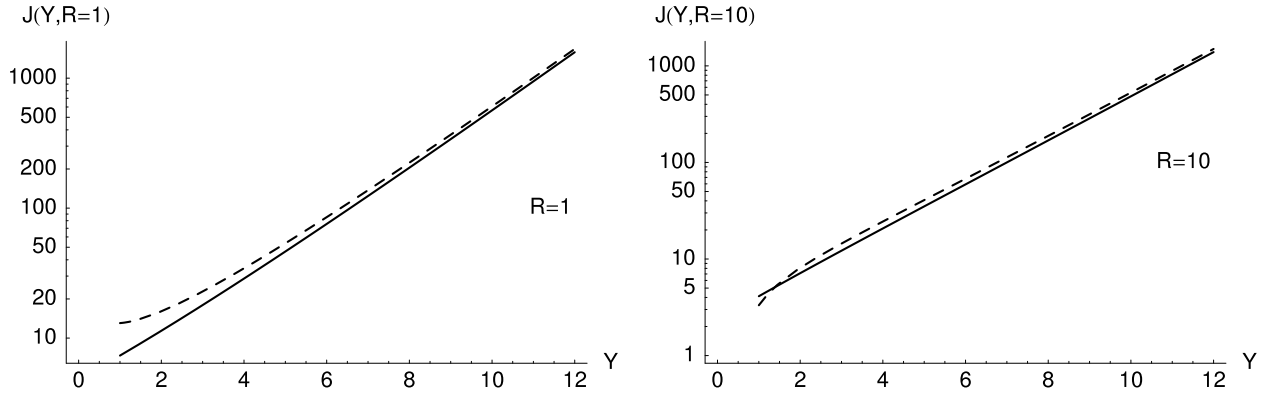


Figure 7.24: Exact numerical result (solid line) and saddle point approximation (dashed) to the integral $J(Y, R)$ for $R = 1$ (left) and $R = 10$ (right).

and

$$A(s, t = t_{min}, Q_1, Q_2) \sim i s \pi^5 \sqrt{\pi} \frac{9(N_c^2 - 1) \alpha_s^2 \alpha_{em} f_\rho^2}{4N_c^2 Q_1^2 Q_2^2} \frac{e^{4 \ln^2 \bar{\alpha}_s Y}}{\sqrt{14 \bar{\alpha}_s \zeta(3) Y}} \exp\left(-\frac{\ln^2 R}{14 \bar{\alpha}_s \zeta(3) Y}\right). \quad (7.82)$$

These approximations can be compared to numerical evaluations of the integral for each value of Y . This is illustrated in Fig. 7.24. We see that the saddle point approximation gives the correct asymptotic behavior for large Y and is less accurate for smaller Y . For $R = 1$ the approximate answer is about 40% too big for $Y \sim 2$ and about 10% too big for $Y \sim 10$. For $R = 10$ the approximation is slightly better. Note that the Linear Collider is likely to test regions with $Y \gtrsim 5$, where the saddle point approximation works relatively well.

Leading order results

In addition to the parameters ρ, f_ρ taken as above in our Born study, one should fix furthermore three parameters in the calculation: α_s in the prefactor, which gives the strength of the coupling of the pomeron to the impact factor; $\bar{\alpha}_s$ in the BFKL exponent, which gives the strength of the coupling of the gluons inside the pomeron; and the energy scale of the rapidity Y . For all cases with a running strong coupling we use a three-loop running $\alpha_s(\mu^2)$ [571] with $\mu^2 = c_\alpha Q_1 Q_2$ as we did in our Born study. Unless otherwise stated, we use this running coupling with $c_\alpha = 1$ in the prefactor of the amplitude.

At LLx accuracy, α_s is a fixed parameter, i.e., it does not run with the gluon momenta in the BFKL ladder. We choose to, however, let it depend on the given Q_1 and Q_2 , which are external to the pomeron but provide a reasonable choice; we thus choose $\bar{\alpha}_s = \frac{N_c}{\pi} \alpha_s(Q_1 Q_2)$. The pomeron intercept is determined by α_s , and it is known to be too large when comparing to HERA data. Our chosen values give quite large pomeron intercepts, but we do not want to artificially suppress the growth by choosing very small values of α_s . Instead we will see in Sec. 7.4.6 that the growth becomes slower when higher order corrections to the BFKL evolution are included.

The rapidity is defined as

$$Y = \ln\left(c_Y \frac{s}{Q_1 Q_2}\right), \quad (7.83)$$

where c_Y is a constant that is not constrained at LLx accuracy. As discussed in [537, 538] this constant is related to the average attained values of $z_{1,2}$ in the process. The authors of [537, 538] chose a very small value $c_Y = 0.01$. We estimate the corresponding effect more conservatively and choose $c_Y = 0.3$ for the cross section predictions shown below (see also [W9]). We will now investigate the sensitivity to these choices. Note that all the results shown here have been obtained by numerical evaluation of the integral over ν and not by the saddle point approximation.

We begin by comparing the energy dependence of the BFKL cross section and the Born cross section. Fig. 7.25a shows the ratio of the differential cross sections $d\sigma/dt|_{t=t_{min}}$ calculated from BFKL and at the Born level, as a function of the rapidity Y for three choices of Q_1 and Q_2 , and for a fixed value $\alpha_s = 0.2$. There

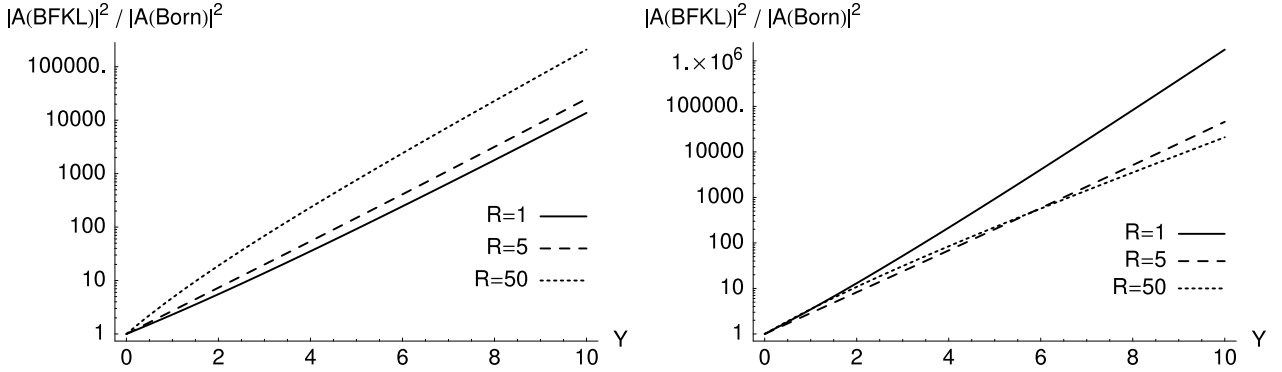


Figure 7.25: a (left): Ratio of the leading order BFKL cross section $\frac{d\sigma}{dt}|_{t=t_{min}}$ to the Born level cross section as a function of the rapidity Y , using $\alpha_s = 0.2$. The solid curve is for $R = Q_1/Q_2 = 1$, the dashed curve is for $R = 5$, and the dotted curve is for $R = 50$. b (right): same ratio with $\alpha_s = \frac{N_c}{\pi}\alpha_s(Q_1, Q_2)$, where Q_2 is fixed at $Q_2 = 2$ GeV and $Q_1 = RQ_2$.

is clearly a strong Y -dependence, as seen from (7.82). Note that all of the Y -dependence of this ratio comes from the BFKL amplitude, since the Born level result is independent of the energy. Fig. 7.25b shows the same plot but using our “standard” choice of $\alpha_s = \frac{N_c}{\pi}\alpha_s(Q_1, Q_2)$. The difference between Figs. 7.25a and 7.25b serves to illustrate the sensitivity to the choice of α_s , and shows that using a Q -dependent coupling for the pomeron decreases the growth with energy for increasing virtualities.

In Fig. 7.26 we show the same ratios as a function of the center-of-mass energy \sqrt{s} for $Q_1 = Q_2 = 2$ GeV in the left plot and for $Q_1 = 10$ GeV, $Q_2 = 2$ GeV in the right plot. The three different curves represent different choices of the energy scale in the definition of Y , corresponding to three different values of the parameter c_Y . This freedom to change the scale introduces an additional uncertainty in the results. In Fig. 7.27 we show the same kind of plot, but varying instead the parameter c_α in the argument of α_s to highlight the uncertainty coming from the choice of scale in α_s . Note that the parameters c_Y and c_α both affect the argument of the BFKL exponential, and thus the energy evolution.

Finally, in Fig. 7.28 we show the ratio as a function of $Q = Q_1 = Q_2$. Thus we see that the BFKL prediction differs from the Born level prediction in all kinematical variables, which allows testing BFKL dynamics experimentally, and possibly fitting the free parameters. However, there are several (very large) uncertainties in the calculated amplitude. This has to be kept in mind when viewing the cross section predictions that will follow.

In Fig. 7.29a we show the differential cross section $d\sigma/dt|_{t=t_{min}}$ as a function of the photon virtuality Q in the symmetric case $R = 1$, i.e. $Q = Q_1 = Q_2$, for three different energies \sqrt{s} , and in Fig. 7.29b we show the same cross section as a function of \sqrt{s} for three different virtualities Q .

These predictions are made with the parameter choices discussed above and contain the corresponding inherent uncertainties. To get some idea of the possible variation in the magnitude of the cross section because of the parameters, we plot in Fig. 7.30 the cross section for $Q = 2$ GeV for the standard parameter choices, and for two extreme versions, one where we choose new parameters $c'_\alpha = 1/2 c_\alpha$, $c'_Y = 2 c_Y$ and one with $c'_\alpha = 2 c_\alpha$, $c'_Y = 1/2 c_Y$. These curves are plotted in gray and should give some indication of the theoretical uncertainty. This clearly calls for an evaluation of NLLx order effects.

7.4.6 Estimation of next to leading order effects

Collinear improved LLx BFKL resummation

The BFKL kernel is known to NLLx accuracy [276, 306–308], as well as the NLLx impact factor for our process [317]. The calculations to obtain the full cross section are difficult, however, and have been performed only recently [328, 439, 443]. At the time of our evaluation of Ref. [W16], it was not yet available. We will explain now how we evaluated higher order effects. To estimate these effects we implement two improvements to the LLx

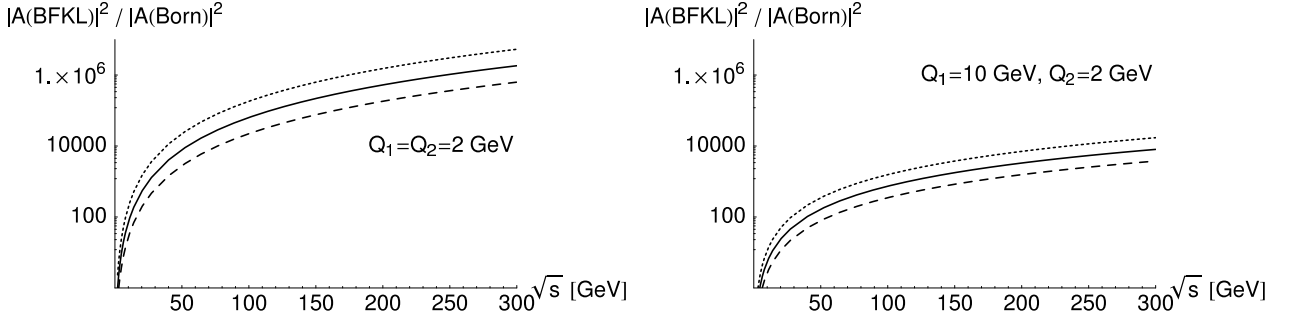


Figure 7.26: Ratio of the leading order BFKL cross section $\left. \frac{d\sigma}{dt} \right|_{t_{min}}$ to the Born level cross section as a function of the center-of-mass energy \sqrt{s} , for $Q_1 = Q_2 = Q = 2$ GeV (left) and $Q_1 = 10$ GeV and $Q_2 = 2$ GeV (right). The different curves in each plot correspond to three different definitions of the rapidity variable, $Y = \ln(c_Y s / (Q_1 Q_2))$. The solid curves are for $c_Y = 1$, dashed curves are for $c_Y = 1/2$, and dotted curves are for $c_Y = 2$. The scale of α_s is given by $c_\alpha = 1$.

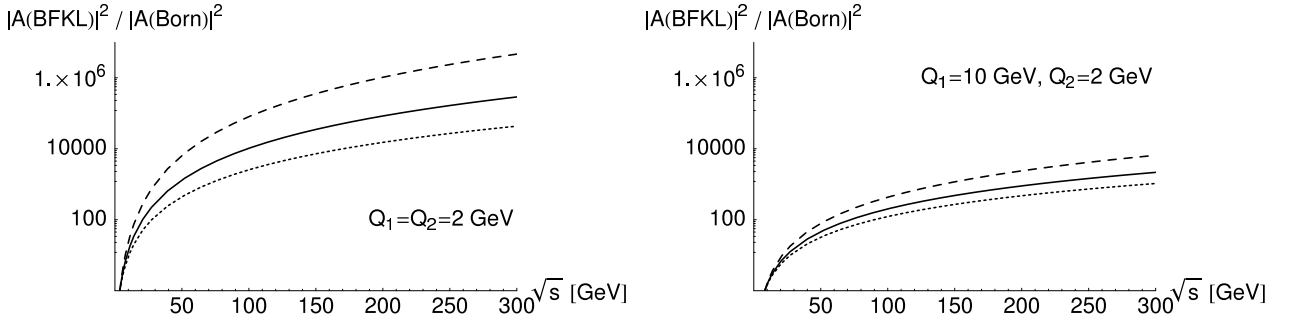


Figure 7.27: Same as Fig. 7.26, but the different curves in each plot correspond instead to three different scale choices in α_s . The solid curves are for $c_\alpha = 1$, dashed curves are for $c_\alpha = 1/2$, and dotted curves are for $c_\alpha = 2$. The scale of Y is given by the standard $c_Y = 0.3$.

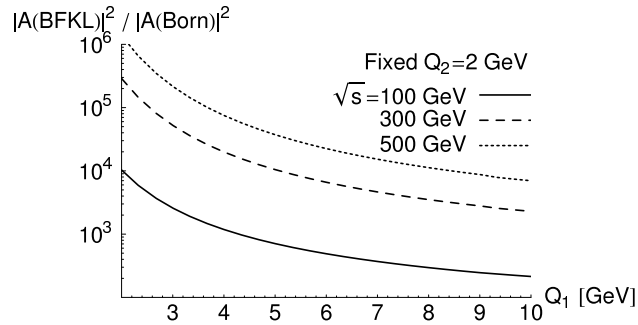


Figure 7.28: Ratio of the leading order BFKL cross section $\left. \frac{d\sigma}{dt} \right|_{t_{min}}$ to the Born level cross section as a function of the virtuality Q_1 for fixed $Q_2 = 2$ GeV, for three different energies \sqrt{s} and standard scale choices c_α, c_Y as defined in the text.

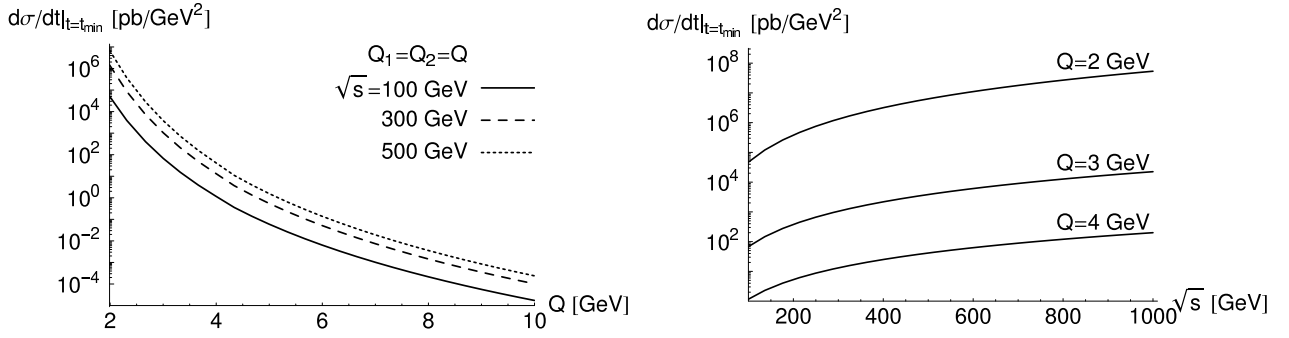


Figure 7.29: a (left): differential cross section $d\sigma/dt|_{t=t_{min}}$ as a function of the photon virtuality $Q = Q_1 = Q_2$ for center-of-mass energies $\sqrt{s} = 100$ GeV, 300 GeV and 500 GeV, with standard scale choices as defined in the text. b (right): differential cross section $d\sigma/dt|_{t=t_{min}}$ as a function of the photon-photon center-of-mass energy \sqrt{s} for photon virtualities $Q = Q_1 = Q_2 = 2$ GeV, 3 GeV and 4 GeV.

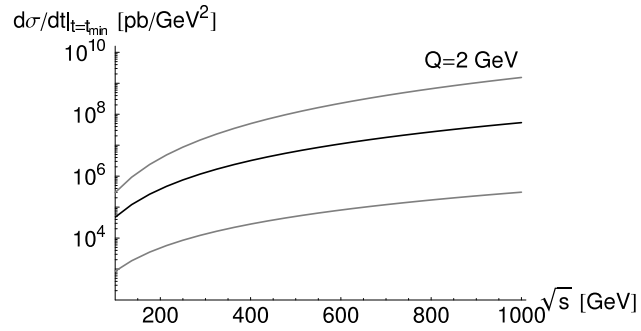


Figure 7.30: Differential cross section $d\sigma/dt|_{t=t_{min}}$ for photon virtuality $Q = Q_1 = Q_2 = 2$ GeV for standard parameters c_α, c_Y (black curve) and for new parameters $c'_\alpha = 1/2 c_\alpha, c'_Y = 2 c_Y$ and $c'_\alpha = 2 c_\alpha, c'_Y = 1/2 c_Y$ (upper resp. lower gray curves).

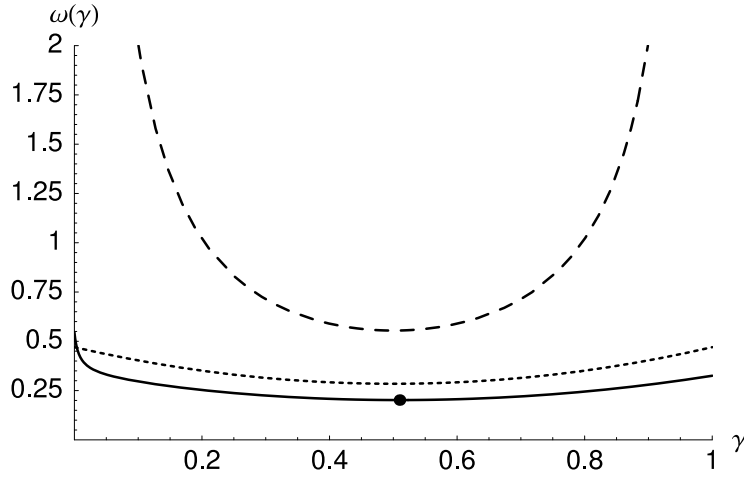


Figure 7.31: The characteristic BFKL functions $\omega_{NLL}(\gamma)$ for the NLL resummed model with $n_f = 3$ (solid line) and $n_f = 0$ (dotted line) and $\omega(\gamma)$ for LLx BFKL (dashed line), for a value of $\bar{\alpha}_s = 0.2$. The dot shows the location of the saddle point of $\omega_{NLL}(n_f = 3)$, $\gamma_s = 0.51$, while $\omega(\gamma)$ and $\omega_{NLL}(n_f = 0)$ have saddle points in $\gamma = 1/2$.

BFKL amplitude. First, we use BLM scale fixing [158] for the running of the coupling in the prefactor. Second, we use a renormalization group resummed BFKL kernel, as will be explained below. We will then compare our estimate of the NLLx effects based on our calculation with the full NLLx evaluation of Ref. [328, 439, 443].

In Ref. [537, 538] it is shown that for the BFKL calculation of the total $\gamma^*\gamma^*$ cross section, the BLM procedure for choosing the scale leads to $\mu^2 = c_\alpha Q_1 Q_2$ with $c_\alpha = e^{-5/3}$, and thus to a larger coupling which will increase the cross section. In the process $\gamma^*p \rightarrow Vp$ at next-to-leading order [575] the correct scale choice was instead found to be $c_\alpha = e^{-1/2}$. The use of the BLM procedure in exclusive processes has been further discussed in [14].

An approximate BLM scale for our process is found by using the NLLx impact factors computed in [317] and neglecting higher order effects in the BFKL kernel. The BLM procedure, choosing the scale such that the terms proportional to β_0 vanish, then leads to the simple choice $c_\alpha = 1$.

We investigate here the effect of higher order corrections described by the LLx collinear resummed approach discussed in Sec. 4.5, which we will denote NLL in this section (although it is based on the LLx kernel). This means that when performing the inverse Mellin transform in Eq.(7.67), the position of the pole in the ω plane is determined by the equation

$$\omega = \bar{\alpha}_s \chi(\gamma, \omega). \quad (7.84)$$

This equation implicitly defines the function $\omega_{NLL}(\gamma)$ that we need to perform the integral $J(Y, R)$ over $\nu = i(1/2 - \gamma)$. We therefore estimate the NLLx BFKL result by using a resummed BFKL kernel in the BFKL exponential, but we keep the LLx form of the solution and the impact factors.

As we explained in Sec. 4.5, the renormalization group (RG) resummed BFKL kernel of Salam [318] and Ciafaloni et al. [319, 320] is actually a resummation of the full NLLx kernel, which removes the problems of this kernel. It is however possible to perform such a resummation of the LLx kernel, which leads to a result that includes a large part of the corrections coming from the NLLx kernel. One such model, based on the general idea of the approach of [318–320] (more specifically Scheme 4 of [318]), was recently proposed by Khoze et al. [330]. This approach uses a fixed strong coupling in the BFKL kernel which is essential for the approach here. A running coupling in the BFKL kernel radically changes the properties of the solutions, and it is no longer possible to evaluate the ω integral by a simple residue. Therefore we do not pursue it here, although it may be attempted along the lines of [480].

We make one modification to the approach of [330]: they use an asymmetric scale choice in the definition of the rapidity (see [318–320] for a discussion) which was appropriate for their problem under study, but our process is more suited for a symmetric scale choice and we therefore perform the necessary modification. The

characteristic function is then expressed as

$$\chi(\gamma, \omega) = \chi_0(\gamma) + \bar{\alpha}_s \chi_1(\gamma, \omega) \quad (7.85)$$

where $\chi_0(\gamma) \equiv \chi(\gamma)$ is the usual BFKL function (4.5). The correction piece $\chi_1(\gamma, \omega)$ is given by

$$\bar{\alpha}_s \chi_1(\gamma, \omega) = \frac{1 + \omega A_1(\omega)}{\gamma + \frac{\omega}{2}} - \frac{1}{\gamma} + \frac{1 + \omega A_1(\omega)}{1 - \gamma + \frac{\omega}{2}} - \frac{1}{1 - \gamma} - \omega \chi_0^{\text{ht}}(\gamma), \quad (7.86)$$

where χ_0^{ht} is the higher twist part of χ_0 ,

$$\chi_0^{\text{ht}}(\gamma) = \chi_0(\gamma) - \frac{1}{\gamma} - \frac{1}{1 - \gamma} = 2\psi(1) - \psi(1 + \gamma) - \psi(2 - \gamma). \quad (7.87)$$

$A_1(\omega)$ is obtained from the Mellin transform of the DGLAP splitting function P_{gg} by

$$\frac{1}{2N_c} P_{gg}(\omega) = \frac{1}{\omega} + A_1(\omega) \quad (7.88)$$

with

$$A_1(\omega) = -\frac{11}{12} - \frac{n_f}{18} + \left(\frac{67}{36} - \frac{\pi^2}{6} \right) \omega + \mathcal{O}(\omega^2). \quad (7.89)$$

We will in the following throw away any terms proportional to ω and only keep singular and constant terms. For $n_f = 0$ we then have $A_1(\omega) \simeq -11/12$. It is possible to account for quark loops for $n_f > 0$ by replacing [330]

$$A_1(\omega) \rightarrow A_1(\omega) + n_f \left[\frac{\bar{\alpha}_s}{4N_c^2} \frac{1}{\gamma} P_{gq}(\omega) P_{qg}(\omega) - \frac{1}{3} \right] \simeq -\frac{11}{12} - \frac{7n_f}{18} + \frac{C_F \bar{\alpha}_s n_f}{6N_c^2 \gamma} \left(\frac{1}{\omega} - \frac{11}{6} \right). \quad (7.90)$$

The characteristic kernel $\omega_{NLL}(\gamma)$ obtained by solving (7.84) with $\chi(\gamma, \omega)$ given by (7.85) is shown both for $n_f = 3$ and $n_f = 0$ in Fig. 7.31 together with the LLx BFKL kernel. An important feature of the kernel (7.84) is that for $n_f = 0$ it has no pole at $\gamma = 0$. The pole reappears when including the quark loops as shown above. It is also clear that for the resummed kernel both the pomeron intercept and the second derivative at the saddle point are reduced.

To compute the cross section using this model we need to make use of Eq.(7.84) in performing the integral over ν . This is possible to do purely numerically, by solving the equation (7.84) explicitly for each given value of γ when performing the integral numerically. However, we may obtain some more insight into the properties of the NLLx corrections by instead performing the integral by the saddle point method as in Section 7.4.5. We expect the accuracy of the saddle point method to be similar to the LLx calculation. For the saddle point calculation we need only compute the position of the saddle point (γ_s, ω_s) , where $\omega_s \equiv \omega_{NLL}(\gamma_s)$, and the particular value $\omega_s'' \equiv \omega_{NLL}''(\gamma_s)$. These can be obtained explicitly in terms of the partial derivatives of the function $\chi(\gamma, \omega)$ as follows. The chain rule gives

$$\frac{d\omega_{NLL}(\gamma)}{d\gamma} = \bar{\alpha}_s \left(\frac{\partial \chi(\gamma, \omega)}{\partial \gamma} + \frac{\partial \chi(\gamma, \omega)}{\partial \omega} \frac{d\omega_{NLL}(\gamma)}{d\gamma} \right) \quad (7.91)$$

so that the saddle point condition gives

$$\left. \frac{d\omega_{NLL}(\gamma)}{d\gamma} \right|_{\gamma=\gamma_s} = 0 \quad \Rightarrow \quad \left. \frac{\partial \chi(\gamma, \omega_s)}{\partial \gamma} \right|_{\gamma=\gamma_s} = 0. \quad (7.92)$$

We then obtain the second derivative of $\omega_{NLL}(\gamma)$ (using the saddle point condition)

$$\omega_s'' = \left. \frac{d^2 \omega_{NLL}(\gamma)}{d\gamma^2} \right|_{\gamma=\gamma_s} = \frac{\bar{\alpha}_s \left. \frac{\partial^2 \chi(\gamma, \omega_s)}{\partial \gamma^2} \right|_{\gamma=\gamma_s}}{1 - \alpha_s \left. \frac{\partial \chi(\gamma_s, \omega)}{\partial \omega} \right|_{\omega=\omega_s}}. \quad (7.93)$$

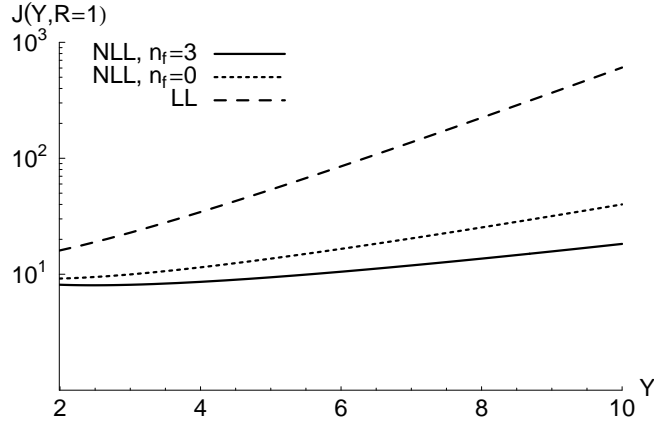


Figure 7.32: Saddle point approximation of the integral $J(Y, R = 1)$ for LLx BFKL and for the LLx corrected kernel.

Finally, to find the saddle point values γ_s, ω_s we must simultaneously solve the equations

$$\begin{cases} \left. \frac{\partial \chi(\gamma, \omega_s)}{\partial \gamma} \right|_{\gamma=\gamma_s} = 0, \\ \omega_s = \alpha_s \chi(\gamma_s, \omega_s). \end{cases} \quad (7.94)$$

The symmetric scale choice with $n_f = 0$ gives a kernel symmetric under $\gamma \rightarrow 1 - \gamma$, so that the saddle point is always located at $\gamma_s = 1/2$. This does not hold for an asymmetric kernel obtained either by the asymmetric scale choice, or, as here, by the inclusion of $n_f > 0$ effects. The saddle point values γ_s, ω_s must then be determined separately for each value of α_s .

The residue obtained by the integral over ω using the ω -dependent kernel is different from the LLx case; we have

$$\text{Res}_{\omega=\omega_s} \frac{e^{\omega Y}}{\omega - \alpha_s \chi(\gamma_s, \omega)} = \frac{e^{\omega_s Y}}{1 - \dot{\omega}_s} \quad (7.95)$$

where we defined the third constant

$$\dot{\omega}_s \equiv \alpha_s \left. \frac{\partial \chi(\gamma_s, \omega)}{\partial \omega} \right|_{\omega=\omega_s}. \quad (7.96)$$

The saddle point evaluation of the integral $J_{NLL}(Y, R)$ now gives

$$A^{NLL}(s, t = t_{min}, Q_1, Q_2) \sim i s \pi^5 \sqrt{2\pi} \frac{9(N_c^2 - 1)}{4N_c^2} \frac{\alpha_s^2 \alpha_{em} f_\rho^2}{Q_1^2 Q_2^2} \frac{e^{\omega_s Y}}{\sqrt{\omega_s'' Y}} \frac{\exp\left(-\frac{2 \ln^2 R}{\omega_s'' Y}\right)}{1 - \dot{\omega}_s}. \quad (7.97)$$

We show the difference between the energy evolution of the LLx kernel and the resummed LLx kernel in Fig. 7.32. This plot shows the integral $J(Y, R = 1)$ for LLx and improved LLx for a fixed value $\alpha_s = 0.2$. The growth with rapidity is strongly reduced by the NLLx effects, and the diffusion pattern is also changed. This is quantified by the pomeron intercept $\alpha_{\mathbb{P}} = \omega_s$, which is reduced from $\alpha_{\mathbb{P}} = 0.55$ to $\alpha_{\mathbb{P}} = 0.20$, and by the second derivative ω_s'' of the kernel, which decreases from $\omega_s'' = 28\bar{\alpha}_s 2\zeta(3) \simeq 6.73$ at the LLx level to $\omega_s'' \simeq 1.02$ using the improved LLx approximation.¹¹ The overall normalization is also affected by the factor $1/(1 - \dot{\omega}_s)$, where in this case $\dot{\omega}_s \simeq -1.51$.

The complete cross section prediction from the LLx modified amplitudes with BLM scale choice is shown in Fig. 7.33 as a function of the energy. The dashed line shows the LLx BFKL result for comparison.

¹¹Note that these values of ω_s and ω_s'' depend on the value of α_s , so care has to be taken to determine them correctly when using formula (7.97).

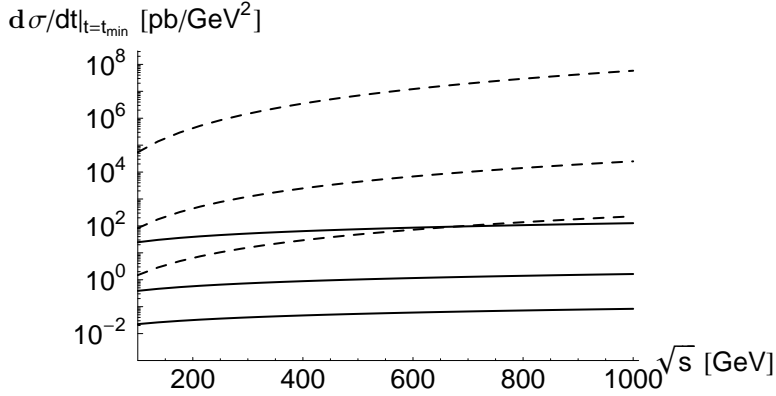


Figure 7.33: Cross section for LLx BFKL (dashed lines) and for the LLx corrected kernel (“NLL”)(solid lines), using $c_Y = 0.3$ and the BLM scale choice $c_\alpha = 1$, for the three cases $Q = Q_1 = Q_2 = 2$ GeV, 3 GeV and 4 GeV (from top to bottom in the plot).

Forward $e^+e^- \rightarrow e^+e^- \rho_L^0 \rho_L^0$ differential cross-section with BFKL evolution

We consider below only the point $t = t_{min}$ and we first consider the leading order BFKL evolution, discussed in Sec. 7.4.5. Of course such an estimate should be taken with great caution since it is well known that LLx BFKL overestimates the magnitude of corrections.

$$\frac{d\sigma^{t_{min}}}{dt} (fb/GeV^2)$$

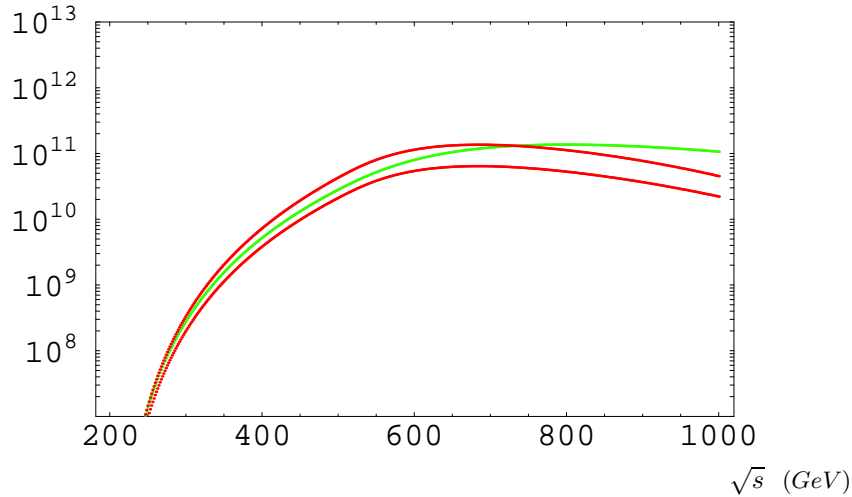


Figure 7.34: Cross-sections for $e^+e^- \rightarrow e^+e^- \rho_L^0 \rho_L^0$ with LLx BFKL evolution at $t = t_{min}$ for different α_s : the upper and lower red curves for α_s running respectively at one and three loops and the green one (the middle curve) for $\alpha_s = 0.46$.

In Fig. 7.34 we show the corresponding cross-section at t_{min} as a function of \sqrt{s} , for different choices of α_s : we considered α_s running at one and three loops (red curves) as in the previous discussion for the two gluon exchange and we also used a fixed value of α_s (green curve) corresponding to the three loops running coupling constant at a typical virtuality $Q = 1.1$ GeV. We have used the expression (7.82) of the LLx BFKL amplitude, with the rapidity $Y = \ln(\frac{c' s y_1 y_2}{Q_1 Q_2})$, $\alpha_s = \frac{N_c}{\pi} \alpha_s(\sqrt{Q_1 Q_2})$. The plots in Fig. 7.34 are obtained by assuming that the constant c' in Eq.(7.82), which at LLx is arbitrary and of order 1, is chosen to be 1. The factor $\exp(4 \ln 2 \bar{\alpha}_s Y)$ explains the enhancement of the sensitivity to the choice of α_s compared to the one in

the Born two gluon exchange case, since $4 \ln 2 Y$ takes big values for ILC rapidities Y . For the same reasons as discussed earlier in this section, the function $f(Q_i)$ does not appear for \sqrt{s} lower than 500 GeV; the LLx BFKL cross-section then grows exponentially with s in this domain. The effect of $f(Q)$ starting from 500 GeV gives an inflexion point of the curves and a maximum beyond 500 GeV; then the curves decrease until 1TeV.

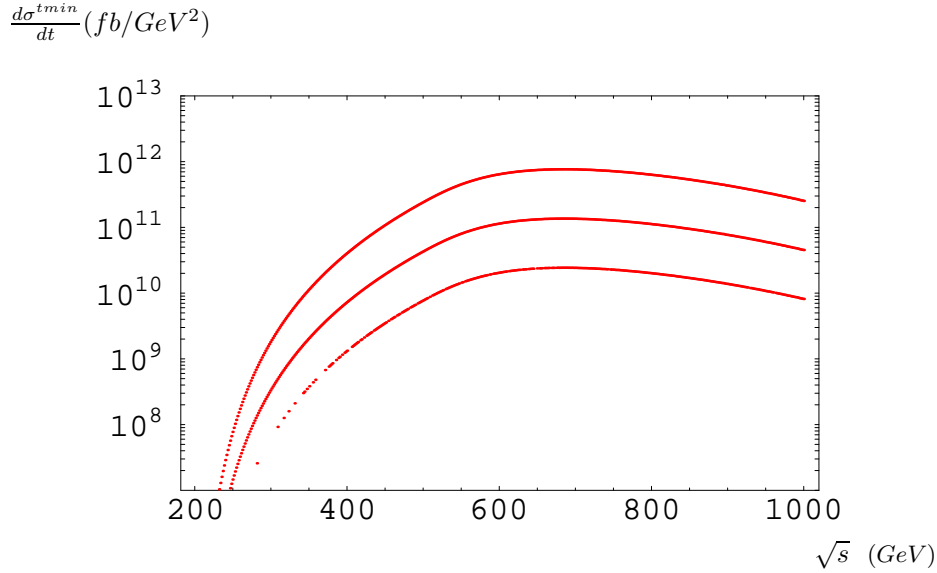


Figure 7.35: LO BFKL cross-section for $e^+e^- \rightarrow e^+e^- \rho_L^0 \rho_L^0$ at $t = t_{min}$ for different values of the parameter c' : by decreasing order, the curves correspond to $c' = 2$, $c' = 1$ and $c' = 0.5$. c is fixed to be equal to 1.

The effect of varying the parameter c' in the BFKL prediction is illustrated in Fig. 7.35. As expected, it has a strong effect in the order of magnitude of the differential cross-section, since the rapidity is very high and thus leads to a large value of the factor $\exp(4 \ln 2 \bar{\alpha}_s Y)$, which is highly sensitive to the precise definition of the rapidity.

Such a dramatic enhancement of the cross-section as well as these uncertainty are clearly non-physical, due to a large Pomeron intercept, in view of HERA result as well as based on our evaluation of higher order corrections of the in Sec.7.4.6 at the level of the $\gamma_L^* \gamma_L^* \rightarrow \rho_L^0 \rho_L^0$ sub-process.

Based on our study of Sec.7.4.6 for higher order corrections, we now display our prediction [W45] at the level of the forward $e^+e^- \rightarrow e^+e^- \rho_L^0 \rho_L^0$ process. In the approach of Sec.7.4.6 we must find the solutions (the improved LLx Pomeron intercept and the anomalous dimension) of the set of the two coupled equations (7.94). Although this approach uses a fixed strong coupling, we reconstruct in ω_s and γ_s a scale dependence by fitting with polynomials of Q_i a large range of solutions obtained for various values of $\alpha_s(\sqrt{Q_1 Q_2})$. Our results are now much less sensitive to the various theoretical assumptions than the ones obtained at LLx accuracy. Having integrated over the accessible phase space of this reaction at ILC, we compare in Fig. 7.36 the curves at Born order (green) with the (red) one obtained after collinear improved LLx BFKL resummation. The experimental cut imposed by the resolution of the electromagnetic calorimeter BeamCal is responsible for the fall of the cross-sections with \sqrt{s} increasing from 500 GeV. This improved LLx evolution gives an enhancement of the Born approximation by a factor 4.5, which allows us to definitively conclude of the measurability of the BFKL evolution for this process at ILC. We finally mention that increasing the collider energy from 500 GeV to 1 TeV will probably lead to a transition between the linear and the saturated regime ($Q_{sat} \sim 1.4$ GeV for $\sqrt{s} = 1$ TeV).

7.4.7 Summary and discussion

The diffractive production of a meson pair is one of the gold plated processes which permit clean studies of the BFKL dynamics at ILC. Our first motivation was thus to show the feasibility of the experiment. In the Born approximation, we estimated the cross-section for production of ρ_L^0 -meson pairs in the e^+e^- collisions occurring

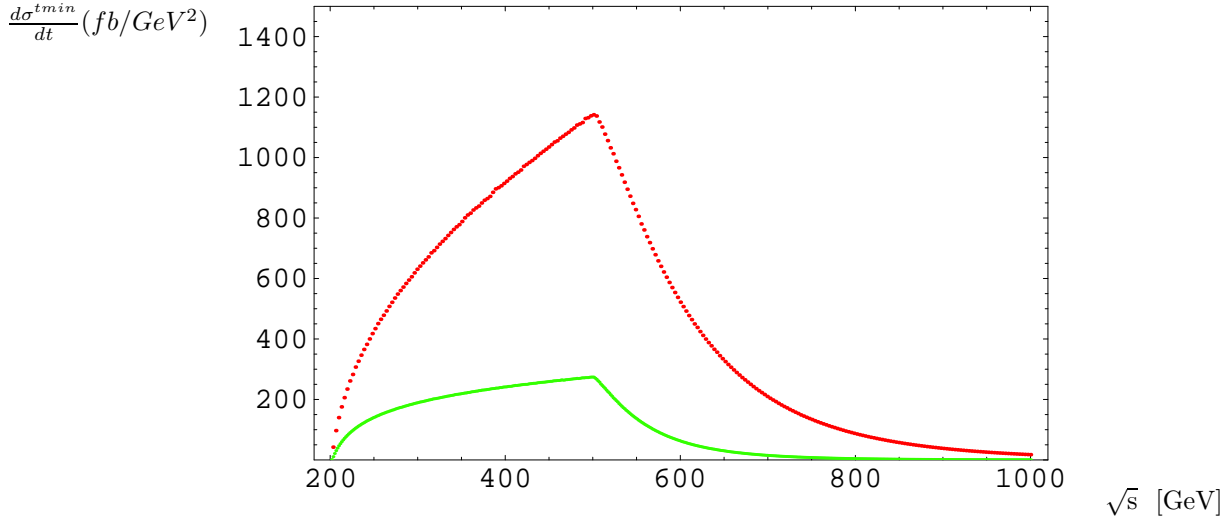


Figure 7.36: Cross-sections at $t = t_{min}$ for $e^+e^- \rightarrow e^+e^- \rho_L^0 \rho_L^0$ with collinear improved BFKL evolution (red curve) and at Born order (green curve).

in the kinematical conditions of future ILC. For this aim, we first calculated all γ^* -helicity contributions in the Born two gluon exchange approximation, in a mostly analytic way, by the use of techniques developed in Ref. [W15]. Having done, we calculated the cross-section for the electroproduction of ρ_L^0 -meson pairs which takes into account kinematical cuts imposed by the LDC design project for the BeamCal detector. By assuming a nominal value of the integrated luminosity, we predict (in the numerical analysis of cross-sections) a production of at least $4 \cdot 10^3$ meson pairs per year, a value which is sufficiently large to ensure a reliable data analysis. These results are stable with respect to our various discussed theoretical uncertainties.

In a controllable manner, by imposing appropriate cuts (7.57), one can get rid of the DGLAP type of contributions (quark exchange) computed in Sec. 2.4, with still high counting rates.

We discussed a possible background process in the BeamCal detector which can identify in a misleading way an outgoing lepton with a photon. We predict that the cross-section for such a background process is negligibly small at ILC energies.

The study of pure LLx leads to an unrealistic enhancement, with very huge uncertainty due to the very high value of the intercept. Our evaluation of the higher order correction through collinear improved LLx BFKL evolution widely reduces both this enhancement and uncertainties, which is essential to make precise predictions. We then obtain an enhancement factor of the order of 4.5

The above discussion about BFKL enhancement was restricted to the forward case $t = t_{min}$. In the non-forward case, the phase space region with small t values dominates the cross-sections. The obtained hierarchy between cross sections in Born approximation for different photon polarizations will presumably still be valid when including BFKL evolution at any order of resummation (LLx, NLLx, etc...). Indeed the argument given in Sec. 7.4.3 for Born order and on which this hierarchy is based, only relies on the s -channel helicity conservation. Technically, it is based on the impact representation which is valid beyond Born and/or LLx approximation.

The full NLLx cross-section, with both impact factors and BFKL kernel computed in the NLLx accuracy, has been carried out at $t = 0$ in [328, 439]. The effect coming from the inclusion of the NLLx impact factors is large, comparable with the effects due to the NLLx correction to the Green function. These NLLx corrections to the impact factors reduces the cross-section. In this study, the values of s_0 and for the scale of the coupling were obtained based on PMS [153, 154], BLM [158] and FAC [155–157] principles. They lead to unnatural high values for these two parameters. At the level of the $\gamma_L^* \gamma_L^* \rightarrow \rho_L^0 \rho_L^0$ sub-process, the obtained prediction of Ref. [328] is displayed in Fig. 7.37, and compared with our collinear improved LLx results¹². We obtain a rather good agreement between the two predictions. However, one cannot deduce any definite conclusion from such a comparison. Indeed, a recent study [443] based on a collinear improved NLLx Green function combined with NLLx impact factors shows that the unnatural choice of the renormalization scale μ_R in the non collinear improved NLLx Green function treatment of Refs. [328, 439] is affected by this collinear improved

¹²Fig. 7.37 differs from the comparison shown in Fig. 8 of Ref. [328] due a numerical mistake in the first version of our paper [W16], corrected in Ref. [W45].

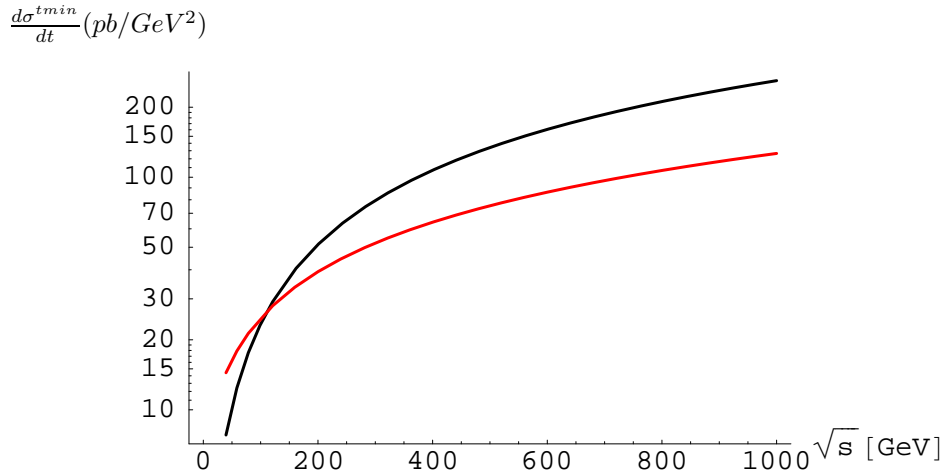


Figure 7.37: Cross-sections at $t = t_{min}$ for $\gamma^*\gamma^* \rightarrow \rho_L^0 \rho_L^0$ with full NLL BFKL evolution (black) [328] and (this work) collinear improved BFKL evolution (red) for $Q_1 = Q_2 = 2\text{GeV}$ and three quark flavors.

NLLx treatment: the application of PMS to the amplitude leads to μ_R values which are still a bit higher than the natural scale $\sqrt{Q_1 Q_2}$, (of the order of $4\sqrt{Q_1 Q_2}$, but not anymore of the order of $10\sqrt{Q_1 Q_2}$). The same conclusion holds for the choice of the scale s_0 which tends to be of the order of the natural scale $Q_1 Q_2$. This is thus consistent with what we obtained in our study of MN jets in Sec. 5.1.1, in particular in relation with the fact that a choice of μ_R a bit higher than the natural scale $k_1 k_2$ leads us to more consistent results for the azimuthal dependency. On the other hand, these lower scales lead to a rather large enhancement of the cross-section with respect to the NLLx evaluation of Refs. [328, 439], of the order of 2 for $Y = 10$, thus giving an enhancement with respect to our collinear improved LLx prediction of a factor up to 4 for $Y = 10$. Clearly, there is still some room for predicting more precisely the counting rates.

In conclusion, the important message of these studies is the clear feasibility of the experiment, and the rather high expected enhancement based on BFKL type of dynamics. However, based on our experience on MN jets and other observables which were considered for a long time to be good tests for BFKL dynamics, definite conclusion could be obtained only when comparing with LLQ and presumably NLLQ DGLAP type of predictions, which are expected to be much lower, but had not been evaluated completely so far (the only available result in this spirit is the lowest order quark exchange contribution, which we evaluated in Sec. 2.4, and the $\ln Q_1/Q_2$ LLQ DGLAP correction (7.42)). This exclusive diffractive reaction may as anticipated become the best tool to investigate the perturbative picture of the hard Pomeron.

7.5 Hard Pomeron-Odderon interference effects in the production of $\pi^+\pi^-$ pairs in high energy $\gamma\gamma$ collisions

Based on [W23]

7.5.1 Introduction

As we saw in Sec. 4.3, from the theoretical point of view the Pomeron should have a C -odd partner, the Odderon. The need for the Odderon contribution [576], in particular to understand the different behaviors of pp and $p\bar{p}$ elastic cross sections [577], is quite generally accepted. Indeed, t -dependence of the elastic pp data at the ISR show a dip for $|t| \simeq 1.3 \text{ GeV}^2$ while the $p\bar{p}$ smoothly decrease at that t , which can be interpreted as a sign of an Odderon contribution, since $\sigma_{p\bar{p}} - \sigma_{pp}$ is sensitive to a C -odd contribution, as illustrated in Fig. 7.38. However, this is the only evidence we have, depending on only a single small set of data. The Odderon has never been

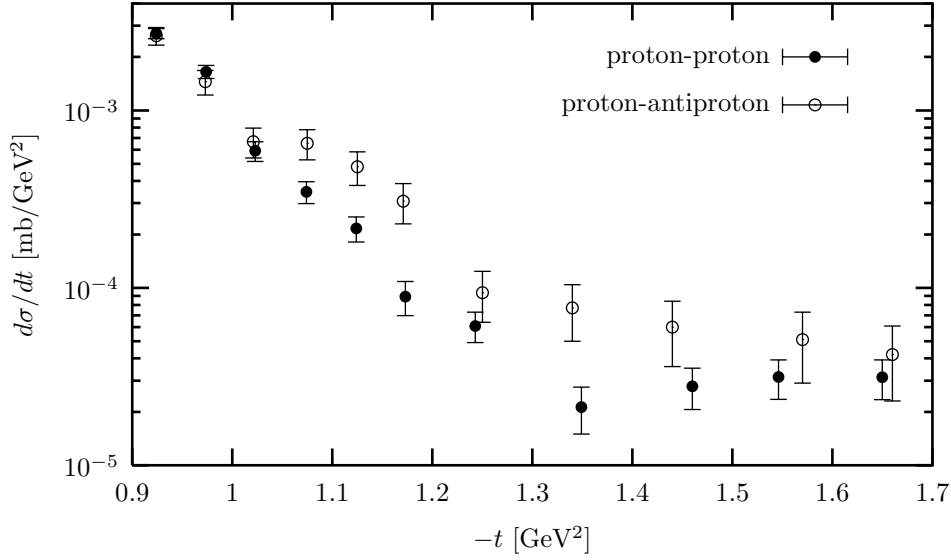


Figure 7.38: Differential cross section for elastic pp and $p\bar{p}$ scattering in the dip region for $\sqrt{s} = 53$ GeV; data taken from [577]. Figure from [296].

seen in the perturbative regime, where it can be described (at lowest order) by the exchange of three gluons in a color singlet state.

Studies of specific channels where the Odderon contribution is expected to be singled out have turned out to be very disappointing, in particular for exclusive photoproduction of π^0 [578], but new channels have recently been proposed. A first possibility is to consider the reaction $\gamma^*\gamma^* \rightarrow \eta_c\eta_c$ [579], which could be tested at ILC. However the expected cross-section is very small. A second recent proposition relies on the exclusive production of a heavy vector meson $C = -$ like J/Ψ or Υ in pp and $p\bar{p}$ collision, through Pomeron-Odderon and Pomeron-photon fusion [580]. Still, in all of these attempts the main difficulty relies on the presumably low value of the Odderon coupling with hadronic states.

Thus, due to its small exchange amplitude one should rather consider observables where Odderon effects are present at the amplitude level – and not at the squared amplitude level. This leads to another strategy to reveal the Odderon, first initiated in Ref. [581], based on observables *linear* in the Odderon amplitude, through interference with the Pomeron amplitude. In Ref. [581], it has been proposed to look for the Odderon in open $c\bar{c}$ diffractive photoproduction, through the asymmetry in the fractional energy of charm versus anticharm jets, which is sensitive to the interference between \mathbb{O} and \mathbb{P} .

This approach has been extended to the diffractive photoproduction of pion pairs [582, 583] and to the diffractive electroproduction of pion pairs [584, 585] since the $\pi^+\pi^-$ -state does not have any definite charge parity and therefore both Pomeron and Odderon exchanges may contribute to the production amplitude.

We now present our results [W23] on such an observable in the hard regime, a charge asymmetry in the production of two $\pi^+\pi^-$ pairs in photon-photon collisions, which could be tested at LHC, and more presumably at ILC. We thus consider the process

$$\gamma(q, \varepsilon) \gamma(q', \varepsilon') \rightarrow \pi^+(p_+) \pi^-(p_-) \pi^+(p'_+) \pi^-(p'_-), \quad (7.98)$$

where ε and ε' are the initial photon polarization vectors, see Fig. 7.39. We have in mind the ultraperipheral collisions of protons or nuclei of high energies, like at LHC, as discussed in Sec. 7.1.1, as well as $\gamma - \gamma$ collision in a photon collider or in an $e^+ - e^-$ collider like ILC.

At high energy the application of pQCD for the calculation of a part of this process is justified by the presence of a hard scale: the momentum transfer $t = (q - p_+ - p_-)^2$ from an initial photon to a final pion pair, $-t$ being of the order of a few GeV². The amplitude of this process may be calculated within k_T -factorization, as the convolution of two impact factors representing the photon to pion pair transitions and a two or three

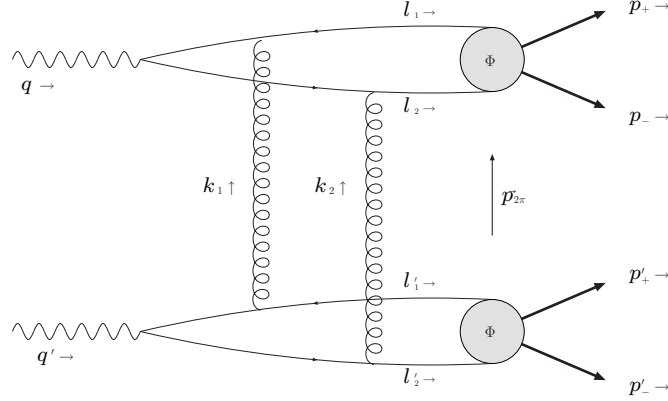


Figure 7.39: Kinematics of the reaction $\gamma\gamma \rightarrow \pi^+\pi^- \pi^+\pi^-$ in a sample Feynman diagram of the two gluon exchange process.

gluon exchange. The impact factors themselves include the convolution of a perturbatively calculable hard part with a non-perturbative input, the two pion GDA which parametrize the quark-antiquark to hadron transition. Since the $\pi^+\pi^-$ system is not a charge parity eigenstate, the GDA includes two charge parity components and allows for a study of the corresponding interference term. The relevant GDA is here just given by the light cone wave function of the two pion system [202].

7.5.2 Kinematics

Let us first specify the kinematics of the process under study, namely the photon-photon scattering as stated in Eq. (7.98). As usual, we decompose all particle momenta using the Sudakov light-like momenta p_1, p_2 with $s = 2 p_1 \cdot p_2$. The initial photon momenta are written as

$$q^\mu = p_1^\mu, \quad q'^\mu = p_2^\mu, \quad (7.99)$$

The momenta of the two pion systems are given by

$$\begin{aligned} p_{2\pi}^\mu &= \left(1 - \frac{p_{2\pi}^2}{s}\right) p_1^\mu + \frac{m_{2\pi}^2 + p_{2\pi}^2}{s} p_2^\mu + p_{2\pi\perp}^\mu \\ p'_{2\pi}^\mu &= \left(1 - \frac{p'_{2\pi}{}^2}{s}\right) p_2^\mu + \frac{m'_{2\pi}{}^2 + p'_{2\pi}{}^2}{s} p_1^\mu + p'_{2\pi\perp}^\mu. \end{aligned} \quad (7.100)$$

The (massless) quark momentum ℓ_1 and antiquark momentum ℓ_2 inside the upper loop before the formation of the two pion system are parametrized as

$$\ell_1^\mu = z p_1^\mu + \frac{(\underline{\ell} + z \underline{p}_{2\pi})^2}{zs} p_2^\mu + (\ell_\perp + z p_{2\pi\perp})^\mu, \quad (7.101)$$

$$\ell_2^\mu = \bar{z} p_1^\mu + \frac{(-\underline{\ell} + \bar{z} \underline{p}_{2\pi})^2}{\bar{z}s} p_2^\mu + (-\ell_\perp + \bar{z} p_{2\pi\perp})^\mu, \quad (7.102)$$

where $2\underline{\ell}$ is the relative transverse momentum of the quarks forming the two pion system, up to small corrections of the order $p_{2\pi}^2/s$. As discussed in Sec. 2.1.1, in the collinear approximation the two pion formation factorizes through a GDA, and we put $\underline{\ell} = 0$ in the hard amplitude.

In a similar way as in (7.101), (7.102), and following the analysis introduced in Sec. 2.1.2, we parametrize the momenta of the produced pions as

$$p_+^\mu = \zeta p_1^\mu + \frac{m_\pi^2 + (\underline{p} + \zeta \underline{p}_{2\pi})^2}{\zeta s} p_2^\mu + (p_\perp + \zeta p_{2\pi\perp})^\mu, \quad (7.103)$$

$$p_-^\mu = \bar{\zeta} p_1^\mu + \frac{m_\pi^2 + (-\underline{p} + \bar{\zeta} \underline{p}_{2\pi})^2}{\bar{\zeta} s} p_2^\mu + (-p_\perp + \bar{\zeta} p_{2\pi\perp})^\mu, \quad (7.104)$$

where $2\underline{p}$ is now their relative transverse momentum, $\zeta = \frac{p_2 \cdot p_+}{p_2 \cdot p_{2\pi}}$ is the fraction of the longitudinal momentum $p_{2\pi}$ carried by the produced π^+ , and $\bar{\zeta} = 1 - \zeta$.

According to (2.63), the variable ζ is related to the polar angle θ which is defined in the rest frame of the pion pair by

$$\beta \cos \theta = 2\zeta - 1, \quad \beta \equiv \sqrt{1 - \frac{4m_\pi^2}{m_{2\pi}^2}}. \quad (7.105)$$

Since the ‘‘longitudinal part’’ of the two pion wave function depends only on the angle θ and does not depend on the azimuthal decay angle ϕ (in the same rest frame of the pair), we focus on the calculation of charge asymmetries expressed in terms of θ (see below). Similar expressions as Eqs. (7.101-7.105) are used for the lower quark loop. Since we are interested in photon interactions in ultraperipheral collisions of hadrons, the photons are quasi real and hence predominantly transversely polarized. The polarization vectors of the photons are written as in Eq. (7.18), i.e.

$$\underline{\epsilon}^\pm = \frac{1}{\sqrt{2}}(\mp 1, -i). \quad (7.106)$$

We will consider spin averaged cross sections since hadron colliders do not produce polarized photon beams.

7.5.3 Scattering amplitudes

In the high energy limit ($s \gg |t|$) we are investigating, we will rely on the impact representation (4.14) of the amplitude, which factorizes into impact factors convoluted over the two-dimensional transverse momenta of the t -channel gluons.

For the Pomeron exchange, which corresponds in the Born approximation of QCD to the exchange of two gluons in a color singlet state, see Fig. 7.39, the impact representation has the form

$$\mathcal{M}_{\mathbb{P}} = i s \int \frac{d^2 \underline{k}_1 d^2 \underline{k}_2 \delta^{(2)}(\underline{k}_1 + \underline{k}_2 - \underline{p}_{2\pi})}{(2\pi)^2 \underline{k}_1^2 \underline{k}_2^2} \Phi_{\mathbb{P}}^{\gamma T}(\underline{k}_1, \underline{k}_2) \cdot \Phi_{\mathbb{P}}^{\gamma T}(\underline{k}_1, \underline{k}_2), \quad (7.107)$$

where $\Phi_{\mathbb{P}}^{\gamma T}(\underline{k}_1, \underline{k}_2)$ is the impact factor for the transition $\gamma_T \rightarrow \pi^+ \pi^-$ via Pomeron exchange.

The corresponding representation for the Odderon exchange, *i.e.* the exchange of three gluons in a color singlet state, is given by the formula

$$\mathcal{M}_{\mathbb{O}} = \frac{8\pi^2 s}{3!} \int \frac{d^2 \underline{k}_1 d^2 \underline{k}_2 d^2 \underline{k}_3 \delta^{(2)}(\underline{k}_1 + \underline{k}_2 + \underline{k}_3 - \underline{p}_{2\pi})}{(2\pi)^6 \underline{k}_1^2 \underline{k}_2^2 \underline{k}_3^2} \Phi_{\mathbb{O}}^{\gamma T}(\underline{k}_1, \underline{k}_2, \underline{k}_3) \cdot \Phi_{\mathbb{O}}^{\gamma T}(\underline{k}_1, \underline{k}_2, \underline{k}_3), \quad (7.108)$$

where $\Phi_{\mathbb{O}}^{\gamma T}(\underline{k}_1, \underline{k}_2, \underline{k}_3)$ is the impact factor for the transition $\gamma_T \rightarrow \pi^+ \pi^-$ via Odderon exchange. The impact factors are calculated by the use of the standard methods of twist 2 factorization, which we illustrated in Sec. 6.1.1. See e.g. Ref. [586] and references therein for the Odderon case.

Impact factors for $\gamma \rightarrow \pi^+ \pi^-$

The leading order calculation in pQCD of the impact factors gives¹³

$$\Phi_{\mathbb{P}}^{\gamma T}(\vec{k}_1, \vec{k}_2) = \frac{i e g^2 \delta^{ab}}{4 N_C} \int_0^1 dz (z - \bar{z}) \underline{\epsilon}^T \cdot \underline{Q}_{\mathbb{P}}(\underline{k}_1, \underline{k}_2) \Phi^{I=1}(z, \zeta, m_{2\pi}^2), \quad (7.109)$$

where the vector $\underline{Q}_{\mathbb{P}}(\underline{k}_1, \underline{k}_2)$ is defined according to (7.16) by¹⁴

$$\underline{Q}_{\mathbb{P}}(\underline{k}_1, \underline{k}_2) = \frac{z \underline{p}_{2\pi}}{z^2 \underline{p}_{2\pi}^2 + \mu^2} - \frac{\bar{z} \underline{p}_{2\pi}}{\bar{z}^2 \underline{p}_{2\pi}^2 + \mu^2} + \frac{\underline{k}_1 - z \underline{p}_{2\pi}}{(\underline{k}_1 - z \underline{p}_{2\pi})^2 + \mu^2} - \frac{\underline{k}_1 - \bar{z} \underline{p}_{2\pi}}{(\underline{k}_1 - \bar{z} \underline{p}_{2\pi})^2 + \mu^2}. \quad (7.110)$$

¹³The definition of impact factor used in this manuscript differs by a factor $-i$ with respect to the one of [W23]: $\Phi_{here} = i \Phi_{[W23]}$. This explains the additional $-$ sign in front of Eq. (10) in [W23] in comparison with the present Eq. (7.107).

¹⁴We use here slightly different notations with respect to (7.16) in order to single out both momenta of t -channel gluons and not their relative momenta. We do the same for $\underline{Q}_{\mathbb{O}}(\underline{k}_1, \underline{k}_2, \underline{k}_3)$.

The calculation of the Odderon exchange contribution gives

$$\Phi_{\mathbb{O}}^{\gamma T}(\underline{k}_1, \underline{k}_2, \underline{k}_3) = \frac{i e g^3 d^{abc}}{8 N_C} \int_0^1 dz (z - \bar{z}) \underline{\epsilon}^T \cdot \underline{Q}_{\mathbb{O}}(\underline{k}_1, \underline{k}_2, \underline{k}_3) \frac{1}{3} \Phi^{I=0}(z, \zeta, m_{2\pi}^2), \quad (7.111)$$

where we have used the definition

$$\underline{Q}_{\mathbb{O}}(\underline{k}_1, \underline{k}_2, \underline{k}_3) = \frac{z \underline{p}_{2\pi}}{z^2 \underline{p}_{2\pi}^2 + \mu^2} + \frac{\bar{z} \underline{p}_{2\pi}}{\bar{z}^2 \underline{p}_{2\pi}^2 + \mu^2} + \sum_{i=1}^3 \left(\frac{\underline{k}_i - z \underline{p}_{2\pi}}{(\underline{k}_i - z \underline{p}_{2\pi})^2 + \mu^2} + \frac{\underline{k}_i - \bar{z} \underline{p}_{2\pi}}{(\underline{k}_i - \bar{z} \underline{p}_{2\pi})^2 + \mu^2} \right). \quad (7.112)$$

Generalized two pion distribution amplitudes

A crucial point of the present study is the choice of an appropriate two pion GDA which includes the full strong interaction related to the production of the two pion system. Various models for this GDA have been proposed in Refs. [202, 584, 585, 587, 588].

Based on an expansion of the GDA in Gegenbauer polynomials $C_n^m(2z-1)$ and in Legendre polynomials $P_l(2\zeta-1)$ as discussed in Sec. 2.1.2, and keeping only the two first terms according to Eq. (2.55) for the $I=1$ contribution and similarly for the first term for the $I=0$ one, we write

$$\Phi^{I=1}(z, \zeta, m_{2\pi}) = 6z\bar{z}\beta f_1(m_{2\pi}) \cos \theta, \quad (7.113)$$

$$\Phi^{I=0}(z, \zeta, m_{2\pi}) = 5z\bar{z}(z - \bar{z}) \left[-\frac{3 - \beta^2}{2} f_0(m_{2\pi}) + \beta^2 f_2(m_{2\pi}) P_2(\cos \theta) \right], \quad (7.114)$$

where $f_1(m_{2\pi})$ can be identified with the electromagnetic pion form factor $F_\pi(m_{2\pi})$. For our calculation we use the following F_π -parametrization inspired by Ref. [589]

$$f_1(m_{2\pi}) = F_\pi(m_{2\pi}) = \frac{1}{1+b} BW_\rho(m_{2\pi}^2) \frac{1 + a BW_\omega(m_{2\pi}^2)}{1+a}, \quad (7.115)$$

with

$$BW_\rho(m_{2\pi}^2) = \frac{m_\rho^2}{m_\rho^2 - m_{2\pi}^2 - i m_{2\pi} \Gamma_\rho(m_{2\pi}^2)} \quad (7.116)$$

$$\Gamma_\rho(m_{2\pi}^2) = \Gamma_\rho \frac{m_\rho^2}{m_{2\pi}^2} \left(\frac{m_{2\pi}^2 - 4m_\pi^2}{m_\rho^2 - 4m_\pi^2} \right)^{3/2} \quad (7.117)$$

$$BW_\omega(m_{2\pi}^2) = \frac{m_\omega^2}{m_\omega^2 - m_{2\pi}^2 - i m_{2\pi} \Gamma_\omega}. \quad (7.118)$$

As masses and widths we use $m_\rho = 775.49$ MeV, $\Gamma_\rho = 146.2$ MeV, $m_\omega = 782.65$ MeV, $\Gamma_\omega = 8.49$ MeV [590]. We fit the remaining free parameters to the data compiled in Ref. [591] obtaining $a = 1.78 \cdot 10^{-3}$ and $b = -0.154$. Including a hypothetical radial excitation or the ρ , the ρ' resonance, as originally used in Ref. [589], gives a significant better fit to the data at large $m_{2\pi}$ but has only a small effect on the asymmetry which is the main object of our studies.

For the $I=0$ component we use different models. The first model follows Ref. [584] and reads

$$f_{0/2}(m_{2\pi}) = e^{i\delta_{0/2}(m_{2\pi})} |BW_{f_{0/2}}(m_{2\pi}^2)|. \quad (7.119)$$

The phase shifts $\delta_{0/2}$ are those from the elastic $\pi^+\pi^-$ scattering, for which we use the parametrization of Ref. [592] below and that of Ref. [593] above the $K\bar{K}$ threshold. $|BW_{f_{0/2}}(m_{2\pi}^2)|$ is the modulus of the Breit-Wigner amplitudes

$$BW_{f_{0/2}}(m_{2\pi}^2) = \frac{m_{f_{0/2}}^2}{m_{f_{0/2}}^2 - m_{2\pi}^2 - i m_{f_{0/2}} \Gamma_{f_{0/2}}}, \quad (7.120)$$

with $m_{f_0} = 980$ MeV, $\Gamma_{f_0} = 40 - 100$ MeV, $m_{f_2} = 1275.1$ MeV, $\Gamma_{f_2} = 185$ MeV [590].

In the second model – elaborated in Ref. [588] – the functions $f_{0/2}$ are the corresponding Omnès functions for S – and D –waves constructed by dispersion relations from the phase shifts of the elastic pion scattering:

$$f_l(m_{2\pi}) = \exp\left(\pi I_l + \frac{m_{2\pi}^2}{\pi} \int_{4m_\pi^2}^{\infty} ds \frac{\delta_l(s)}{s^2(s - m_{2\pi}^2 - i\varepsilon)}\right), \quad \text{with} \quad I_l = \frac{1}{\pi} \int_{4m_\pi^2}^{\infty} ds \frac{\delta_l(s)}{s^2}. \quad (7.121)$$

The assumption that the phases of the GDA equal those of the elastic scattering loses its solid base beyond the $K\bar{K}$ threshold. As discussed in Refs. [588, 594] it might well be that the actual phases of the GDA are closer to the phases of the corresponding \mathcal{T} matrix elements $\frac{\eta e^{2i\delta_l} - 1}{2i}$. The third model for the $I = 0$ component of the GDA takes this into account by using the technique of model 2 with these phases $\delta_{\mathcal{T},l}$ of the \mathcal{T} matrix elements.

While the first and the second model give quite compatible results, model three differs from them significantly. The most striking difference is the absence of pronounced f_0 resonance effects in model 3. In fact, measurements at HERMES [250] do not observe a resonance effect at the f_0 -mass even though a confirmation by an independent experiment would be desirable. From the same measurements at HERMES one can draw the conclusion that using $\delta_{T,2}$ and δ_2 for the f_2 region are both compatible with data [588]. Having this in mind, we consider also a fourth model – a mixed description with the f_0 contribution from model 3 and the f_2 contribution from model 2.

Photon exchange amplitude

The photon has the same C -parity as the Odderon. Therefore, its exchange between the two quark-antiquark systems can mimic an Odderon exchange. The according amplitude is straightforward to calculate and reads

$$\mathcal{M}_\gamma = \frac{s}{2t} \Phi_\gamma^{\gamma T} \cdot \Phi_\gamma^{\gamma T}, \quad (7.122)$$

with

$$\Phi_\gamma^{\gamma T} = \frac{e^2}{2} \int_0^1 dz (z - \bar{z}) \underline{\epsilon}^T \cdot \underline{p}_{2\pi} \left(\frac{z}{\mu^2 + z^2 \underline{p}_{2\pi}^2} + \frac{\bar{z}}{\mu^2 + \bar{z}^2 \underline{p}_{2\pi}^2} \right) \Phi^{I=0}(z, \zeta, m_{2\pi}^2). \quad (7.123)$$

In our concrete process the photon exchange amplitude amounts to the order of 10% of the Odderon exchange amplitude. Although we do not neglect this contribution, it is clear that the asymmetry described in the following section is driven by the Odderon/ Pomeron-interference.

7.5.4 Charge asymmetries and rates

Charge asymmetry and $\mathbb{P} - \mathbb{O}$ interference

The key to obtain an observable which linearly depends on the Odderon amplitude $\mathcal{M}_\mathbb{O}$ is the orthogonality of the C -even GDA (entering $\mathcal{M}_\mathbb{O}$) and the C -odd one (entering the Pomeron amplitude $\mathcal{M}_\mathbb{P}$) in the space of Legendre polynomials in $\cos\theta$. As a consequence, in the total cross section the interference term completely vanishes. In contrast only the interference term survives, when the amplitude squared is multiplied by $\cos\theta$ before the angular integration which corresponds to selecting the charge asymmetric contribution. The asymmetry we are interested in is defined as

$$\begin{aligned} A(t, m_{2\pi}^2, m_{2\pi}^{\prime 2}) &= \frac{\int \cos\theta \cos\theta' d\sigma(t, m_{2\pi}^2, m_{2\pi}^{\prime 2}, \theta, \theta')}{\int d\sigma(t, m_{2\pi}^2, m_{2\pi}^{\prime 2}, \theta, \theta')} \\ &= \frac{\int_{-1}^1 d\cos\theta \int_{-1}^1 d\cos\theta' 2\cos\theta \cos\theta' \operatorname{Re}[\mathcal{M}_\mathbb{P}(\mathcal{M}_\mathbb{O} + \mathcal{M}_\gamma)^*]}{\int_{-1}^1 d\cos\theta \int_{-1}^1 d\cos\theta' [|\mathcal{M}_\mathbb{P}|^2 + |\mathcal{M}_\mathbb{O} + \mathcal{M}_\gamma|^2]}. \end{aligned} \quad (7.124)$$

The obtained landscape as a function of the two invariant masses is not particularly illuminating and would be difficult to measure. To reduce the complexity, we integrate over the invariant mass of one of the two pion

systems to obtain

$$\begin{aligned} \hat{A}(t, m_{2\pi}^2; m_{\min}^2, m_{\max}^2) &= \frac{\int_{m_{\min}^2}^{m_{\max}^2} dm_{2\pi}^{\prime 2} \int \cos \theta \cos \theta' d\sigma(t, m_{2\pi}^2, m_{2\pi}^{\prime 2}, \theta, \theta')}{\int_{m_{\min}^2}^{m_{\max}^2} dm_{2\pi}^{\prime 2} \int d\sigma(t, m_{2\pi}^2, m_{2\pi}^{\prime 2}, \theta, \theta')} \\ &= \frac{\int_{m_{\min}^2}^{m_{\max}^2} dm_{2\pi}^{\prime 2} \int_{-1}^1 d\cos \theta \int_{-1}^1 d\cos \theta' 2 \cos \theta \cos \theta' \operatorname{Re} [\mathcal{M}_{\mathbb{P}}(\mathcal{M}_{\mathbb{O}} + \mathcal{M}_{\gamma})^*]}{\int_{m_{\min}^2}^{m_{\max}^2} dm_{2\pi}^{\prime 2} \int_{-1}^1 d\cos \theta \int_{-1}^1 d\cos \theta' [|\mathcal{M}_{\mathbb{P}}|^2 + |\mathcal{M}_{\mathbb{O}} + \mathcal{M}_{\gamma}|^2]}. \end{aligned} \quad (7.125)$$

Let us note that since the two pion pairs are always in the same C -parity state, because of $C = +$ parity of the initial $\gamma\gamma$ state, it is necessary to keep in Eq. (7.125) the integration weight $\cos \theta'$. Without this weight the single charge asymmetry would vanish. The deviations from this vanishing of the asymmetry may serve as a measure of experimental uncertainties.

Numerical evaluation

Considering an analytic calculation of the matrix element in Eq. (7.108), it turns out that it would require the calculation of two dimensional two-loop box diagrams, whose off-shellness for all external legs is different. The techniques developed in Refs. [568, W15, W20] which rely on the transformation (7.28) can not be applied here due to the very elaborated topology of the most complicated diagrams involved (square box with one additional diagonal line), illustrated in Fig. 7.40. As far as we know, such a diagram has not been evaluated in

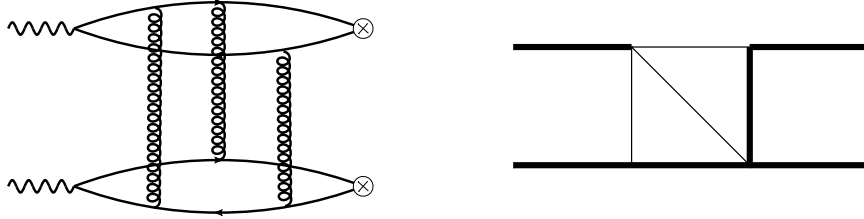


Figure 7.40: Left: most complicated Feynman diagram which need to be evaluated. Right: corresponding scalar-reduced contribution. Thick lines are off-shell lines, while thin lines are massless lines.

the literature. Instead we rely on a numerical evaluation by Monte Carlo methods. In particular we make use of a modified version of VEGAS as it is provided by the CUBA library [441]. The result for the asymmetry \hat{A} at $t = -1 \text{ GeV}^2$ (resp. $t = -2 \text{ GeV}^2$) is shown in Fig. 7.41 (resp. Fig. 7.42). Since our framework is only justified for $m_{2\pi}^2 < -t$, (in fact strictly speaking, one even needs $m_{2\pi}^2 \ll -t$), we keep $m_{2\pi}$ below 1 GeV (resp 1.4 GeV). In each case, we present the expected asymmetry with the GDAs parametrized as discussed above.

Asymmetry in ultraperipheral collisions

In order to evaluate the feasibility of the Odderon search, we need to supplement the calculation of the asymmetry with rate estimates in ultraperipheral collisions at hadron colliders. This rate depends on the Pomeron dominated photon-photon cross section and on the equivalent photon flux. The total photon-photon cross section falls off rapidly with increasing $|t|$ (see Fig. 7.43). Therefore, the integration mainly depends on the lower limit of $|t|$ -integration (t_{\min}). Already for $t_{\min} = -1 \text{ GeV}^2$ we find $\sigma_{\gamma\gamma} = 1.1 \text{ pb}$.

Although in Ref. [550] it is claimed that the photon flux is best for medium-weight ions, and especially superior to that of protons, this is in fact not true. To obtain Fig. 6 of Ref. [550] the effective $\gamma\gamma$ luminosity has been calculated for protons and ions by the Monte Carlo program TPHIC [595] which is based on the Fermi-Weizsäcker-Williams method [547–549] with the additional condition of non-overlapping ions [596, 597], but the authors used a quite small luminosity for proton-proton collisions at the LHC ($14\,000 \text{ mb}^{-1}\text{s}^{-1}$ instead of the official design luminosity $10^7 \text{ mb}^{-1}\text{s}^{-1}$ [598, 599]). Very unfortunately, the identical figure is reprinted in Ref. [551] while a non consistent p-p luminosity of $10^7 \text{ mb}^{-1}\text{s}^{-1}$ is cited.

As already was shown by Cahn and Jackson [597], the $\gamma\gamma$ luminosity in case of ions can be expressed in terms of a universal function $\xi(z)$, where $z = MR \approx 5.665A^{4/3}$ with M being the mass and R the radius of the

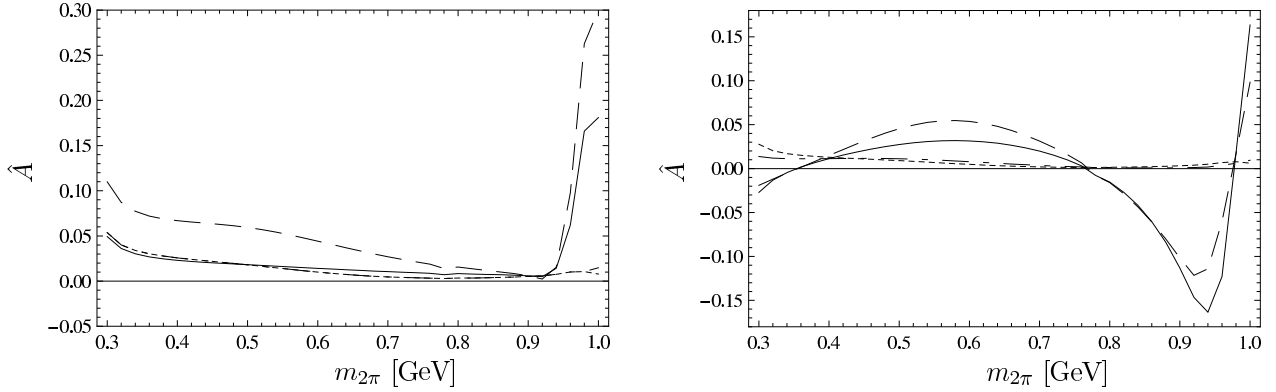


Figure 7.41: Asymmetry \hat{A} at $t = -1 \text{ GeV}^2$ for model 1 (solid), 2 (dashed), 3 (dotted), and 4 (dash-dotted) – model 3 and 4 are nearly on top of each other. Left column has $m_{\min} = .3 \text{ GeV}$ and $m_{\max} = m_\rho$, while right column has $m_{\min} = m_\rho$ and $m_{\max} = 1 \text{ GeV}$.

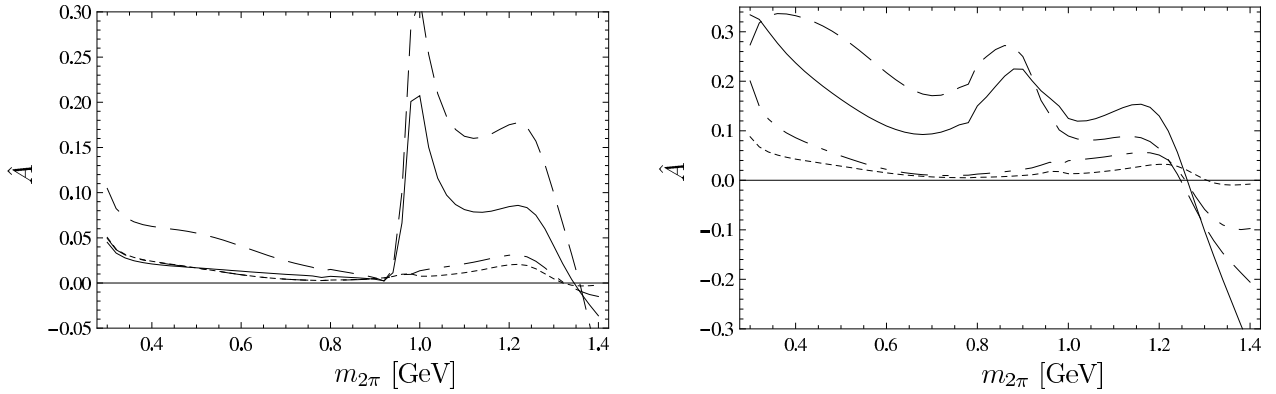


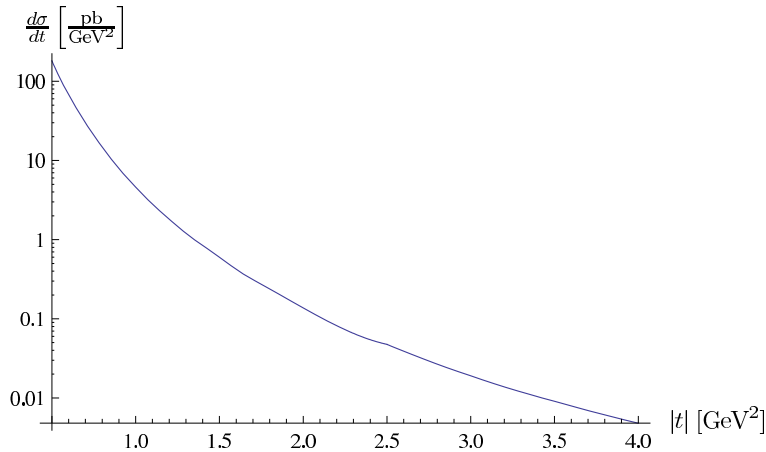
Figure 7.42: Asymmetry \hat{A} at $t = -2 \text{ GeV}^2$ for model 1 (solid), 2 (dashed), 3 (dotted), and 4 (dash-dotted). Left column has $m_{\min} = .3 \text{ GeV}$ and $m_{\max} = m_\rho$, while right column has $m_{\min} = m_{f_0}$ and $m_{\max} = 1.4 \text{ GeV}$.

ion, and a prefactor proportional to Z^4 . Since the luminosity for ions at the LHC decreases roughly as Z^{-4} , the prefactor's Z dependence is more or less compensated and only the universal function ξ remains which is exponentially decreasing with z . Hence, lighter projectiles provide a larger effective $\gamma\gamma$ luminosity, with the protons offering the highest luminosity.

Therefore, we provide a corrected overview over the various effective $\gamma\gamma$ luminosities in Fig. 7.44. For the different ion scenarios that are discussed in Ref. [600] we use the parametrization of Ref. [597] which relies on the Fermi-Weizsäcker-Williams method [547–549] with the additional condition of non-overlapping ions [596, 597]. For protons usually a calculation based on the proton electric dipole form factor $F_E(Q^2) = 1/(1 + \frac{Q^2}{0.71 \text{ GeV}^2})$ in combination with the Weizsäcker-Williams method is used, as it can be found in Ref. [601]. In Ref. [602] a slightly improved version is given, which lowers the photon flux. An inclusion of the corresponding magnetic dipole moment [603] would lead to a flux between those both. For this reason, we use the formulas given in Ref. [601] and Ref. [602] for the case of proton-proton collisions. We also provide the results for the proton treated as a heavy ion because it might be that the non-overlap condition – reducing the flux – is of importance [602], even if such a procedure does not include the proton form factor. We consider such a lower result as a conservative lower estimate. Since the luminosity factors will cancel in the asymmetry, this uncertainty does not affect our conclusions on the Odderon effects. For comparison, we provide also the effective $\gamma\gamma$ luminosities at the intended ILC where the design luminosity for e^+e^- collisions is $2 \cdot 10^{34} \text{ cm}^{-2}\text{s}^{-1}$ [604]¹⁵.

As shown in Fig. 7.44, the effective $\gamma\gamma$ luminosity decreases rapidly with increasing energy. Since our

¹⁵In the calculation of the equivalent photon spectrum [221] we used $q_{\max} = 100 \text{ GeV}$.

Figure 7.43: t -dependence of photon-photon cross section.

intermediate hard scale t is quite small, we are not forced to consider extremely large photon-photon energies. The only condition on the minimal photon-photon energy (s_{\min}) is $s_{\min} \gg |t|$ to ensure the validity of high energy factorization into two separated pion systems. Hence, a s_{\min} of 400 GeV^2 could be already enough. The effect of varying s_{\min} is displayed in Fig. 7.45.

For pp collisions, the rates are high and even for $t_{\min} = -2 \text{ GeV}^2$ sizable. Although heavy ions would offer the possibility to trigger on ultraperipheral collisions by detecting neutrons from giant dipole resonances (GDR) in the Zero Degree Calorimeters, the rates that can be read off from Fig. 7.45 are rather low. Only for medium-weight ions there might be the possibility to measure the process. The best compromise may be Oxygen-Oxygen collisions, which is by no means the priority of the heavy ion physics community.

In hadron-hadron collisions the process of interest could as well be connected by Pomerons to the colliding hadrons. Indeed, in contrast to electromagnetic processes which have been proposed to be studied in ultraperipheral collisions, pions are produced by pure QCD processes as well. In that case one would have to deal with the unknown hadron-Pomeron and Pomeron-Pomeron-two-pion couplings. Therefore, we consider that process as background. This circumstance would make heavy ions preferable because of the different scaling of Pomeron and photon coupling when changing from proton to nuclei scattering. However, experimentally such a background can be suppressed by refusing events with a total p_T larger than some small cut-off. Indeed, the $\gamma\gamma$ events dominates, due to the photon propagator singularities, when each of the transverse momentum is small, which on the average is satisfied when the *total* transverse momentum of our four pion system is imposed to be small. Unfortunately, in practice, it is not easy to demonstrate quantitatively that one can separate these two processes by just relying on the fact that ultraperipheral processes are strongly peaked at low t , contrarily to the flatter dependence of the Pomeron induced ones [553], as we discussed in Sec. 7.1.1.

Additionally, although photon fluxes are important in pp collisions at the designed LHC luminosity ($10^{34} \text{ cm}^{-2}\text{s}^{-1}$), data collected under these conditions will suffer from the pile up of events, which will prevent an analysis of the process considered here from being performed. At lower luminosity, rates may be marginally sufficient for values of $-t \approx 1 \text{ GeV}^2$, but designing a trigger strategy to record interesting events seems very difficult: typical triggers on high p_T mesons demand a minimum p_T of a few GeV, which is incompatible with such low values of $-t$ and the corresponding limit of $m_{2\pi} < \sqrt{-t}$. It could be marginally be achieved within a dedicated study of a few days of run at low luminosity.

One may think about the effect of BFKL type enhancement. Indeed, this would increase the total cross section, which varies like $|\mathcal{M}_{\mathbb{P}}|^2$ but at the same time diminish the asymmetry $\sim \mathcal{M}_{\mathbb{O}}/\mathcal{M}_{\mathbb{P}}$, since the Odderon including BJKP evolution [297–300], as discussed in Sec. 4.6.1, has a smaller intercept, which is presumably equal to unity [354, W11, 355, 356], than the Pomeron one. Our Born order estimate should be corrected by BFKL effects which can be estimated semi-phenomenologically from HERA data, in which the intercept is of the order of $\alpha_{\mathbb{P}} \simeq 1.3$. This leads for $\sqrt{s_{\min}} = 20 \text{ GeV}$ to an increase of ~ 6 for the counting rates and to a slight decrease of the asymmetry $\sim \mathcal{M}_{\mathbb{O}}/\mathcal{M}_{\mathbb{P}}$. This effect is thus not enough to increase dramatically the counting rates in the low luminosity run of LHC.

In contrast, an electron-positron collider such as the projected ILC would be the ideal environment to

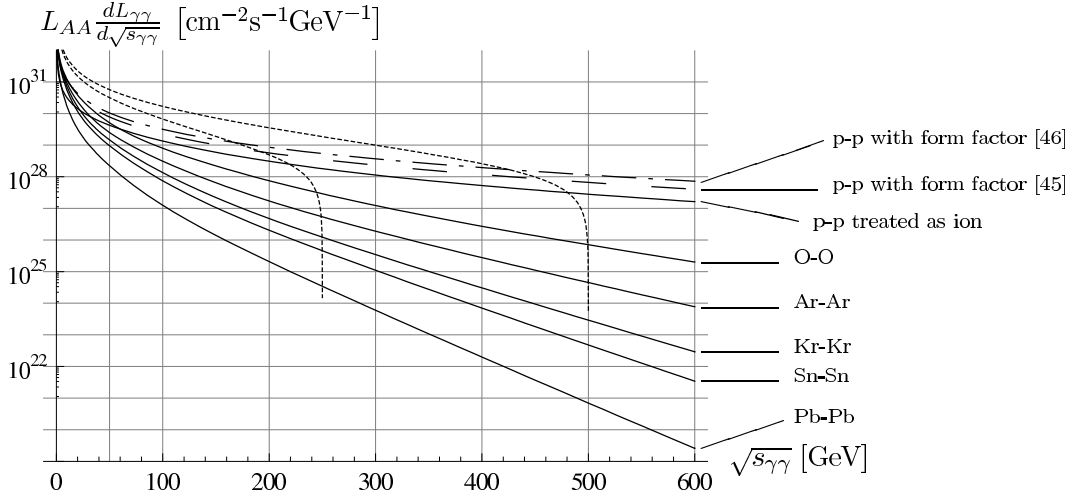


Figure 7.44: Effective $\gamma\gamma$ luminosities for the collision of p-p based on Ref. [601] (dash-dotted) and Ref. [602] (dashed). The results using the parametrization of Ref. [597] for ions are given by solid lines for p-p, $O_{16}^8-O_{16}^8$, $Ar_{40}^{18}-Ar_{40}^{18}$, $Kr_{84}^{36}-Kr_{84}^{36}$, $Sn_{120}^{50}-Sn_{120}^{50}$, $Pb_{208}^{82}-Pb_{208}^{82}$ from top to bottom. For ions we used the average luminosities as given in Ref. [600], for proton we used $L_{pp} = 10^{34} \text{ cm}^{-2}\text{s}^{-1}$. For comparison also effective $\gamma\gamma$ luminosities at the ILC are given for $\sqrt{s_{e^+e^-}} = 250 \text{ GeV}$ and $\sqrt{s_{e^+e^-}} = 500 \text{ GeV}$ (both as dotted lines).

study the process under consideration. Photon photon collisions are indeed the dominant processes there and the background from strong interactions would be completely absent in an e^+e^- collider. As we saw in Sec. 7.1.2, an e^+e^- collider, via Compton-back-scattering, could work as a very effective $\gamma\gamma$ collider. At the ILC [604] for a nominal electron beam energy of 250 GeV the luminosity for photon-photon collisions would be $3.5 \cdot 10^{33} \text{ cm}^{-2}\text{s}^{-1}$ [561] for the high energy photons (energy fraction at least 80% of the maximal possible energy fraction) or even higher, if optimized for photon-photon collisions [605]. As Fig. 7.44 reveals, even running in the electron-positron mode the effective $\gamma\gamma$ luminosity is slightly larger than at the LHC. Additionally, at ILC no pile up phenomenon can blur the picture of a scattering event in comparison with LHC at the same luminosity. For these reasons, the ILC would provide an ideal environment to study the process of interest.

Maybe an alternative, which we did not study, is a large energy electron ion collider in its ultraperipheral mode.

7.5.5 Summary and prospects

We have investigated in real photon-photon collision the production of two $\pi^+\pi^-$ -pairs well separated in rapidity. Due to the non fixed C -parity of these pairs, beside a Pomeron exchange an Odderon exchange is possible as well. We have calculated both contributions in a perturbative approach – justified by t providing the hard scale – where the only soft building blocks needed are the GDAs of the pion pairs. We have shown that a charge asymmetry in the polar angle θ (defined in the rest frame of the pion pairs) is linearly dependent on the Odderon amplitude and moreover is sizable but GDA-model dependent.

In fact, the predicted asymmetry depends much on the two pion GDAs, which are still not really known. The unfavorable situation would be the scenario supported by HERMES measurements of two pion electroproduction [250], which disfavor models with a strong f_0 coupling to the $\pi^+\pi^-$ state. We however think that higher statistics data, which may come from a JLab experiment at 6 or 12 GeV, are definitely needed before one can trust a definite model of the GDAs. Because two pion deep electroproduction in the low energy domain is dominated by quark exchanges, this test of the GDA models is independent of any Odderon search. This looks like a prerequisite to a trustable extraction of the Odderon signal – or of an upper bound on Odderon exchange amplitudes – from ultraperipheral collisions.

Recently the BaBar experiment reported a new measurement of the reaction $\gamma^*\gamma \rightarrow \pi^0$ up to photon virtualities squared of 40 GeV^2 [606]. In this study, the reaction $\gamma^*\gamma \rightarrow \pi^0\pi^0$ was investigated in the $f_0(980)$ and $f_2(1270)$ resonance regions as a potential background for the study of the π^0 transition form factor. This

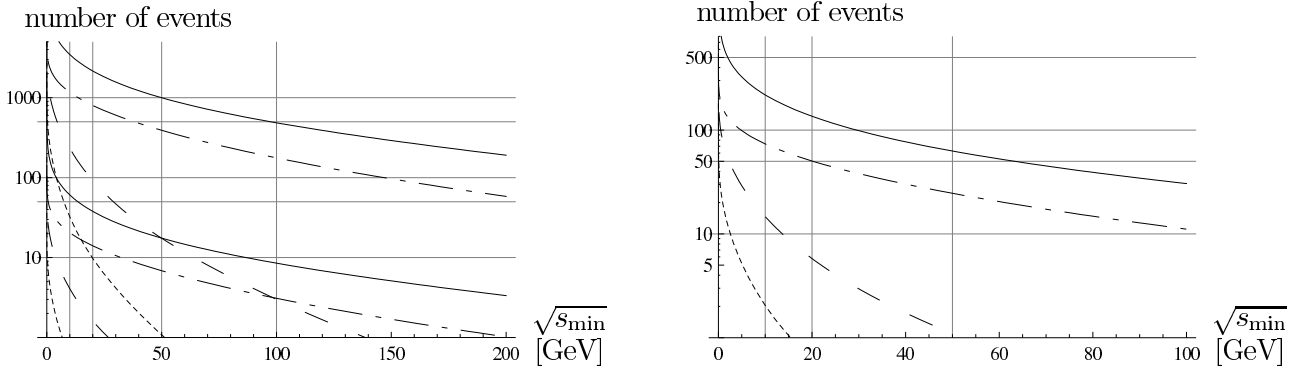


Figure 7.45: Rate of production of two pion pairs in ultraperipheral collisions in dependence on the lower cut s_{\min} given in ‘events per month’ in case of ions, and ‘events per six months’ in case of protons which in both cases correspond to one year of running of LHC. The l.h.s. plot shows the rate for $t_{\min} = -1 \text{ GeV}^2$, the r.h.s. that for $t_{\min} = -2 \text{ GeV}^2$. The solid line displays the result for p-p collision using Ref. [601], the dashed-dotted that for protons treated as heavy ions, the dashed one that for Ar-Ar collisions, and the dotted line that for Pb-Pb collisions. On the left figure, also the much smaller rates coming from the Odderon exchange are shown (with the same dashing).

low- W^2 kinematical region should soon be analysed in the framework of two-meson GDAs.

A first positive indication for a favorable scenario appeared recently. Indeed, CLAS experiment at JLab has recently reported on studies of the reaction $\gamma p \rightarrow p \pi^+ \pi^-$, in the photon energy range 3.0 – 3.8 GeV and momentum transfer range $0.4 < -t < 1.0 \text{ GeV}^2$. Besides the dominant contribution of the $\rho(770)$ meson, CLAS found evidence [607] for the $f_0(980)$ and the $f_2(1270)$. If this is confirmed, this would be very positive for $\mathbb{P} - \mathbb{O}$ interference, since it would select scenarios 1 or 2, for which the interference effect is much higher.

These results are signs that there is a hope to get experimental informations on GDAs, which are at the moment very poor and confusing, in a rather short time. This will settle the question of the adequate model to be used, in particular for the Odderon observable we have discussed.

In conclusion, our proposal to discover the perturbative Odderon through asymmetries in the production of two pion pairs in ultraperipheral collisions at the LHC seems to have a hard time to win over quite severe experimental constraints. However, we believe that the concept is viable, and could be used at ILC.

Conclusion

QCD have reached a degree of maturity in many domains, in particular for PDFs which are now measured and whose evolution is now understood from first principles in a very wide range in x_{Bj} and Q^2 , with an impressive precision. This is one the main achievement of HERA experiments. Meanwhile, the understanding of QCD for more and more exclusive observables has also reached a certain degree of maturity. Data for DVCS and hard electroproduction are now coming more and more, and one can expect the emergence of a rather comprehensive picture of GPDs and related quantities within a decade, with a reasonable degree of precision. All these results have been based on very fruitful interplays between theory and experiment at medium and large energy.

Much of our understanding of QCD at medium energies relies on the collinear factorization, which gave a single framework when dealing with hard exclusive processes. The recent development lead to the introduction of various off-diagonal non-perturbative correlators. It is not an overstatement to stress that this activity is very likely to shed light on the confinement dynamics of QCD through the detailed understanding of the quark and gluon structure of hadrons.

Starting from extension of the conventional PDFs to the GPDs, its has been realized that many observables and thus experiments could be used in order to understand QCD, though the introduction of GDAs, TDAs... In particular, it proved its efficiency in describing the more and more DVCS data which are now coming.

From the theory side, the number of processes for which there is a full understanding of factorization from first principles is very small, basically reducing to DVCS and hard electroproduction of longitudinally polarized mesons. For other processes, factorization is plagued by end-point contributions, which require a special treatment for which there is at the moment no single framework. On top of Sudakov contributions, it has been proposed to consider transverse momentum dependent partonic distributions. This leads at the moment to many developments from the theory side. Despite the complications and new playground it introduces, it is at the moment not clear how such objects will participate in a coherent way to the picture of hard exclusive processes.

Still, the number of experiments in which efforts have been devoted to the study of hard exclusive process as a mainstream is rather small, and it is only recently that high luminosity B-factories started to exploit their high potential for studying exclusive processes, which should lead to a first understanding of GDAs, which is at the moment rather poor from phenomenological side.

After more than three decades of theoretical developments after the seminal papers of BFKL, the understanding of QCD in the particular Regge limit is still uncomplete. There are at the moment several approaches which coexist when dealing with unitarity corrections. This has suggested many fruitful developments in various domains like integrable models, statistical physics, perturbative approaches to non-linear dense systems... Except the special limit of the BK equation, which sums up diagrams which are equivalently obtained from EGGLA, dipole model, QCD shock waves and JIMWLK, there is however no clear comprehension of the relations between these various approaches. Important progresses were made concerning the generic ultra-asymptotic behaviour of scattering amplitudes, based on statistical mechanics methods, in particular using reaction-diffusion equations with noise, which takes into account in an effective way (unknown) higher order QCD corrections. However, starting from first principle, there is at the moment no practical realization of these equations outside of low dimension toys models, and we are far from having a tractable complete theory which could be used at physical energies.

From the phenomenological side, saturations models implements the main features of linear DGLAP and BFKL evolutions, in the color transparency regime, combined with a functional form which realizes saturation. They can now successfully describes the data in the whole HERA range, implementing the main features of partonic distributions in the high density region which any LHC experiment will face, with a very small number

of fitted parameters.

In the linear regime at small- x , studies of higher order corrections lead to the conclusion that the LLx BFKL resummation predicts a Pomeron intercept which is by far too steep, a fact which was meanwhile confirmed by HERA, Tevatron (and LEP) experiments. Various studies have also shown that there is some room to see a linear Regge evolution, not modified by saturation effects, for which NLLx resummation corrections are important and presumably much more in agreement with data. This requires the implementation of additional procedures, to evaluate the effects of higher order corrections and have a compatibility with usual renormalization group predictions. Recent results have shown that the NLLx corrections to impact factors are by no means negligible, and should be included when computed, in order to get reliable predictions. At the moment, despite tremendous efforts both from theoretical and from experimental sides, signals of BFKL linear evolution are rather weak. This is even worse for the elusive Odderon, for which any attempt to catch it failed until now. On one hand, the example of MN jets may be a hint that new coming consistent NLLx BFKL type of descriptions are becoming stable and should be competitive with DGLAP treatments, in a rather large range of phase space. On the other hand, this latter example also provides an explicit case where “natural” observables for revealing the peculiar small- x dynamics with respect to fixed order treatments can be much modified when including NLLx corrections, and become rather close from the fixed order predictions. Finding observables which are stable with respect to NLLx corrections *and* differs significantly with NLLQ prediction thus remains in our opinion a still open task, which might be achieved when considering exclusive final states.

When considering specific exclusive final states, we have shown that a rather coherent picture emerges at small- x , which can incorporate the effect of twist beyond the usual twist 2 description. We hope that the tools we have developed based on LCCF factorization will in the near future provide an efficient way for describing other exclusive processes. Studies of small- x physics at the moment focussed mainly on the gluonic Green function. This was also the essence of the dipole model, where the elementary gluonic degree of freedom is replaced by color dipoles. Only very few investigations of exclusive processes, when based on dipole models, focused on the higher twist corrections when coupled to a final state starting from first principle. We believe that our momentum space treatment beyond twist 2 could be implemented within the dipole model, i.e. in coordinate space.

QCD in the perturbative Regge limit leads naturally to the introduction of unintegrated k_T parton (gluons) distribution involved in the impact representation of high-energy scattering amplitude. On the other hand, such unintegrated distributions were introduced in another context, in relation with spin-physics on which we almost did not elaborate in this manuscript, in particular for transverse spin effects. Indeed, starting from the single transverse spin asymmetries à la Collins [608] or à la Sivers [609, 610], one gets access to the number density of unpolarized partons with intrinsic transverse fixed momentum [611, 612] inside a transversally polarized proton. It would be of much interest to have a single picture for such unintegrated partonic distributions, which appeared naturally in these two very different contexts [613, 614], as well as in k_T -dependent parton showers, which are of much interest of Monte Carlo in jet physics at small- x , and thus presumably for LHC which will be dominated by multi-particle final states. On the other hand, due to the recent developments within processes involving helicity flip GPDs, it may well be that the notion of transverse momentum dependent GPDs should require special attention.

To end up, let us hope that the future ILC project will be built. As any e^+e^- collider, it is a very clean machine. Based on its expected luminosity and on the new kind of detector facilities which are under development, its potentialities in $\gamma^{(*)}\gamma^{(*)}$ are very great and it would be a fantastic tool both for clean experiments beyond the standard model as well as for any kind of QCD studies, in particular for exclusive processes whose rates are too low to be studied at the moment. Besides, lower energy machines with high luminosity like B -factories, existing or planned, like the super- B factory, are very interesting from the point of view of QCD (spectroscopy e.g. exotic states, DAs, GDAs, ...). Let us hope that such possibilities will be taken into account by the whole community, in particular when designing detectors.

Abbreviations and notations used

PDF: Parton Distribution Function

DGLAP: Dokshitzer, Gribov, Lipatov, Altarelli, Parisi (equation)

BFKL: Balitskii, Fadin, Kuraev, Lipatov (equation)

LLx: Leading Logarithmic approximation in $\ln 1/x$ or $\ln s$

NLLx: Next Leading Logarithmic approximation in $\ln 1/x$ or $\ln s$

LLQ: Leading Logarithmic approximation in $\ln Q^2$ or any collinear logarithm

NLLQ: Next Leading Logarithmic approximation in $\ln Q^2$

DVCS: Deep Virtual Compton Scattering

DDVCS: Double Deeply Virtual Compton Scattering

TCS: Timelike Compton Scattering

DA: Distribution Amplitude

GDA: Generalized Distribution Amplitude

GPD: Generalized Parton Distribution

OPE: Operator Product Expansion

CMS: Center of Mass System

CCFM: Ciafaloni Catani Fiorani Marchesini

MN: Mueller Navelet (jets)

SCHC: s -channel helicity conservation

WW: Wandzura-Wilczek (approximation)

LCCF: light-cone collinear factorization

CCF: covariant collinear factorization

EOM: equation of motion

BLM: Brodsky Lepage Mackenzie

PMS: principle of minimal sensitivity

MRT: Martin, Ryskin, Teubner (model for electroproduction of mesons)

GBW: Golec-Biernat, Wüsthoff (model for saturation)

PSF: Pomeron Structure Function (for diffractive DIS)

BEKW: Bartels, Ellis, Kowalski, Wüsthoff (model for diffraction)

pQCD: perturbative QCD

\mathbb{P} : Pomeron

\mathbb{O} : Odderon

$$\bar{z} = 1 - z$$

\underline{k} , \mathbf{k} , \vec{k}_t are two-dimensional euclidean vector

k_{\perp} is a four-dimensional minkowskian vector, with thus $k_{\perp}^2 = -\underline{k}^2 = -\mathbf{k}^2$

\vec{k} is the euclidean part of the four-dimensional vector k

Part III

Bibliography

Personnal publications

(reference ending with an asterisk are the main material of this manuscript)

Published papers

- [W1] E.Buffenoir et S.Wallon, *The correlation length of the Potts model at the first-order transition point*, J. Phys. A: Math. Gen. **26** (1993) 3045-3062.
- [W2] H.Navelet, R.Peschanski et S.Wallon, *On the singular behaviour of structure function at low x* , Mod. Phys. Lett. **A9** (1994) 3393-3402.
- [W3] R.Peschanski et S.Wallon, *Unified QCD evolution equations and the dominant behaviour of structure functions at low x* , Phys. Lett. **B349** (1995) 357-362.
- [W4] Z.Maassarani et S.Wallon, *Barter Equation for the QCD Odderon*, J. Phys. A: Math. Gen. **28** (1995) 6423-6434.
- [W5] H. Navelet, R. Peschanski, Ch. Royon et S. Wallon, *Proton structure functions in the dipole picture of BFKL dynamics*, Phys. Lett. **B385** (1996) 357-364.
- [W6] H. Navelet, R. Peschanski, Ch. Royon, L. Schoeffel et S. Wallon, *On the origin of the rise of F_2 at small x* , Mod. Phys. Lett. **A12** (1997) 887-897.
- [W7] Y. Kovchegov, A.H. Mueller et S. Wallon, *Unitarity Corrections and High Field Strengths in High Energy Hard Collisions*, Nucl. Phys. **B507** (1997) 367-378.
- [W8] H. Navelet et S. Wallon, *Onium-Onium scattering at fixed impact parameter: exact equivalence between the color dipole model and the BFKL Pomeron*, Nucl. Phys. **B522** (1998) 237-281.
- [W9] M. Boonekamp, A. De Roeck, Ch. Royon et S. Wallon, *$\gamma^* - \gamma^*$ total cross-section in the dipole picture of BFKL dynamics*, Nucl.Phys. B555 (1999) 540-564.
- [W10] S. Munier et S. Wallon, *Geometric scaling in exclusive processes*, Eur.Phys.J.C30 (2003) 359-365. [arXiv:hep-ph/0303211].
- [W11] Y. V. Kovchegov, L. Szymanowski et S. Wallon, *Perturbative Odderon in the dipole model*, Phys.Lett.B586 (2004) 267-281.
- [W12] I.V. Anikin, B. Pire, L. Szymanowski, O.V. Teryaev et S. Wallon, *Deep Electroproduction of exotic hybrid mesons*, Phys.Rev.D70 (2004) 011501. *
- [W13] I.V. Anikin, B. Pire, L. Szymanowski, O.V. Teryaev et S. Wallon, *Exotic hybrid mesons in hard electroproduction*, Phys.Rev.D71 (2005) 034021, [arXiv:hep-ph/0411407]. *
- [W14] I.V. Anikin, B. Pire, L. Szymanowski, O.V. Teryaev et S. Wallon, *On BLM scale fixing in exclusive processes*, Eur.Phys.J.C42 (2005) 163-168, [arXiv:hep-ph/0411408]. *
- [W15] B. Pire, L. Szymanowski et S. Wallon, *Double diffractive ρ -production in e^+e^- -collisions*, Eur.Phys.J.C44 (2005) 545-558, [arXiv:hep-ph/0507038]. *
- [W16] R. Enberg, B. Pire, L. Szymanowski et S. Wallon, *BFKL resummation effects in $\gamma^*\gamma^* \rightarrow \rho\rho$* , Eur.Phys.J.C45 (2006) 759-769 [Erratum-ibid. C **51** (2007) 1015]. *
- [W17] A. Shuvaev et S. Wallon, *High energy evolution of soft gluon cascades*, Eur.Phys.J.C46 (2006) 135-145. Eur. Phys. J. C **46** (2006) 135.
- [W18] I.V. Anikin, B. Pire, L. Szymanowski, O.V. Teryaev et S. Wallon, *On exotic hybrid meson production in $\gamma^*\gamma$ collision*, Eur.Phys.J.C47 (2006) 71-79. *

- [W19] B. Pire, M. Segond, L. Szymanowski et S. Wallon, *QCD factorisation in $\gamma^*\gamma^* \rightarrow \rho_L\rho_L$* , Phys.Lett.B639 (2006) 642-651. [arXiv:hep-ph/0605320]. *
- [W20] M. Segond, L. Szymanowski et S. Wallon, *Diffraction production of two $\rho_0(L)$ mesons in e^+e^- collisions*, Eur. Phys. J. C **52** (2007) 93-112. [arXiv:hep-ph/0703166]. *
- [W21] B. Pire, C. Roiesnel, L. Szymanowski and S. Wallon, *On AdS/QCD correspondence and the partonic picture of deep inelastic scattering*, Phys. Lett. B **670**, 84-90 (2008).
- [W22] M. E. Beiyad, B. Pire, L. Szymanowski and S. Wallon, *Diphoton Generalized Distribution Amplitudes*, Phys. Rev. D **78**, 034009 (2008). *
- [W23] B. Pire, F. Schwennsen, L. Szymanowski and S. Wallon, *Hard Pomeron-Odderon interference effects in the production of $\pi^+\pi^-$ pairs in high energy gamma-gamma collisions at the LHC*, Phys. Rev. D **78** (2008) 094009. *

Accepted papers

- [W24] I. V. Anikin, D. Y. Ivanov, B. Pire, L. Szymanowski and S. Wallon, *QCD factorization of exclusive processes beyond leading twist: $\gamma^*T \rightarrow \rho T$ impact factor with twist three accuracy*, accepted for publication by Nucl. Phys. B, arXiv:0909.4090 [hep-ph]. *
- [W25] I. V. Anikin, D. Y. Ivanov, B. Pire, L. Szymanowski and S. Wallon, *On the description of exclusive processes beyond the leading twist approximation*, accepted for publication by Phys. Lett. B, arXiv:0903.4797 [hep-ph]. *

Papers in preparation

- [W26] M. E. Beiyad, B. Pire, M. Segond, L. Szymanowski and S. Wallon, *Photoproduction of a Transverse Meson Vector and Transversity Generalized Parton Distribution*. *
- [W27] D. Colferai, L. Szymanowski, F. Schwennsen and S. Wallon, *Mueller-Navelet jets: a full Next-to-Leading Order BFKL treatment*. *

Conference proceedings

- [W28] S.Wallon, *Unified QCD evolution equations for quarks and gluons*, proceedings of DIS 95, April 1995, Paris, ed J. F. Laporte and Y. Sirois, editions de l'Ecole Polytechnique, 269-271, [arXiv:hep-ph/9509295].
- [W29] S. Wallon, *QCD dipole predictions for quark singlet, gluon and F_L/F_T distributions at HERA*, proceedings Moriond 1996, preprint SPhT T96/048, [arXiv:hep-ph/9610332].
- [W30] S. Wallon, *The equivalence between the color dipole model and the BFKL Pomeron at leading order*, proceedings of the Madrid workshop on small-x physics, "Madrid 1997, Low x Physics" 37-46 [arXiv:hep-ph/9712509].
- [W31] B. Pire, L. Szymanowski et S. Wallon, *Hard Exclusive QCD Processes at the Linear Collider*, International Conference on Linear Colliders, LCWS 04, 19-23 avril 2004, Paris, Editions de L'Ecole Polytechnique, vol.I, 335-340 [arXiv:hep-ph/0410108].
- [W32] I.V. Anikin, B. Pire, L. Szymanowski, O.V. Teryaev et S. Wallon, *$\pi\eta$ Pair Hard Electroproduction and Exotic Hybrid Mesons*, Baryon 2004, 25-29 octobre 2004, Palaiseau, Nucl.Phys.A 755 (2005) 561-564 [arXiv:hep-ph/0501119].
- [W33] I.V. Anikin, B. Pire, L. Szymanowski, O.V. Teryaev et S. Wallon, *Hard Electroproduction of Hybrid Mesons*, Symmetries and Spin, 5-10 juillet 2004, Prague, Czechoslovak Journal of Physics, Vol 55 (2005), A229-A234, suppl. A [arXiv:hep-ph/0608199].
- [W34] B. Pire, L. Szymanowski et S. Wallon, *$\gamma^*\gamma^* \rightarrow \rho\rho$ at very high energy*, Baryon 2004, 25-29 octobre 2004, Palaiseau, Nucl.Phys.A 755 (2005) 626-629 [arXiv:hep-ph/0501155].
- [W35] B. Pire, L. Szymanowski et S. Wallon, *Born order study of $\gamma^*\gamma^* \rightarrow \rho\rho$ at very high energy*, 11th International Conference on Elastic and Diffractive Scattering: Towards High Energy Frontiers, 15-20 mai 2005, Blois, arXiv:hep-ph/0509149.
- [W36] I.V. Anikin, B. Pire, L. Szymanowski, O.V. Teryaev et S. Wallon, *Hard production of exotic hybrid mesons*, 11th International Conference on Elastic and Diffractive Scattering: Towards High Energy Frontiers, 15-20 mai 2005, Blois, arXiv:hep-ph/0509245.
- [W37] I.V. Anikin, B. Pire, L. Szymanowski, O.V. Teryaev et S. Wallon, *Probing the partonic structure of exotic particle in hard electroproduction*, Joint Meeting Heidelberg-Liege-Paris-Rostock, Liege, Belgium, 16-18 décembre 2004, Spa, AIP Conf.Proc.775:51-60 (2005), [arXiv:hep-ph/0510030].
- [W38] R. Enberg, B. Pire, L. Szymanowski et S. Wallon, *Hard Pomeron in exclusive meson production at ILC*, Photon2005, 31

- août-4 septembre 2005, Varsovie, Acta Phys. Polon.B37:847-852 (2006), [arXiv:hep-ph/0511144].
- [W39] I.V. Anikin, O.V. Teryaev, B. Pire, L. Szymanowski, S. Wallon, *Recent and future experimental evidences for exotic mesons in hard reactions*, ICHEP 06, 26 juillet - 2 août 2006, Moscou arXiv:hep-ph/0610177.
- [W40] B. Pire, M. Segond, L. Szymanowski et S. Wallon, *Production of rho0(L) meson pair in gamma* gamma* collisions*, Diffraction 2006, 5-10 septembre 2006, Milos Island, PoS **DIFF2006** (2006) 034, [arXiv:hep-ph/0611092].
- [W41] M. Segond, L. Szymanowski et S. Wallon, *BFKL resummation effects in exclusive production of rho meson pairs at the ILC*, International Conference on Linear Colliders (LCWS07 and ILC07), Hambourg, 30 mai - 3 juin 2007, *Hambourg 2007, LCWS/ILC 2007* 352-355, arXiv:0709.3252 [hep-ph].
- [W42] S. Wallon, *Perturbative QCD in the Regge limit: Prospects at ILC*, 12th International Conference on Elastic and Diffractive Scattering: Forward Physics and QCD, Hambourg, DESY, 21-25 mai 2007, Published in *Hambourg 2007, Blois07, Forward physics and QCD* 360-370, arXiv:0710.0833 [hep-ph].
- [W43] S. Wallon, B. Pire, M. Segond and L. Szymanowski, *Studying QCD factorizations in exclusive $\gamma^*\gamma^* \rightarrow \rho_L^0\rho_L^0$* , 12th International Conference on Elastic and Diffractive Scattering: Forward Physics and QCD, Hambourg, DESY, 21-25 mai 2007, Published in *Hambourg 2007, Blois07, Forward physics and QCD* 69-74, arXiv:0710.0838 [hep-ph].
- [W44] B. Pire, M. Segond, L. Szymanowski and S. Wallon, *QCD Factorizations in Exclusive $\gamma^*\gamma^* \rightarrow \rho_L^0\rho_L^0$* , Photon 2007, Paris, 9-13 juillet 2007, Nucl. Phys. Proc. Suppl. **184**(2008) 224, [arXiv:0710.4413 [hep-ph]].
- [W45] M. Segond, L. Szymanowski and S. Wallon, *A test of the BFKL resummation at ILC*, proceedings of the School on QCD, low-x physics, saturation and diffraction, Copanello Calabria, Italy, July 1-14 2007, Acta Phys. Polon. B **39** (2008) 2577, arXiv:0802.4128 [hep-ph].
- [W46] M. E. Beiyad, B. Pire, L. Szymanowski and S. Wallon, *Two Photon Distribution Amplitudes*, proceedings of the workshop HLPW08, Spa, March 6-8, 2008, AIP Conf. Proc. **1038** (2008) 305-310, [arXiv:0806.1375 [hep-ph]].
- [W47] B. Pire, L. Szymanowski, F. Schwennsen and S. Wallon, *Pomeron-Odderon interference in production of $\pi^+\pi^-$ pairs in ultraperipheral collisions*, proceedings of Diffraction 2008: International Workshop on Diffraction in High-Energy Physics, La Londe-les-Maures, France, September 9-14, 2008, AIP Conf. Proc. **1105** (2009) 377-380, [arXiv:0811.0255 [hep-ph]].
- [W48] I. V. Anikin, D. Y. Ivanov, B. Pire, L. Szymanowski and S. Wallon, *$\gamma^* \rightarrow \rho_T$ impact factor with twist three accuracy*, proceedings of Diffraction 2008: International Workshop on Diffraction in High-Energy Physics, La Londe-les-Maures, France, September 9-14, 2008, AIP Conf. Proc. **1105** (2009) 390, [arXiv:0811.2394 [hep-ph]].
- [W49] M. E. Beiyad, S. Friot, B. Pire, L. Szymanowski and S. Wallon, *Probing photon structure in DVCS on a photon target*, proceedings of PANIC 08, Eilat, Istraël, November 9-14, 2008, arXiv:0901.1792 [hep-ph].
- [W50] I.V. Anikin, D.Yu. Ivanov, B. Pire, L. Szymanowski, S. Wallon, *QCD factorization beyond leading twist in exclusive rho(T) meson production*, proceedings of Cracow Epiphany Conference on Hadronic Interactions at the Dawn of the LHC, Cracow, Poland, 5-7 Jan 2009, arXiv:0904.1482 [hep-ph].
- [W51] B. Pire, F. Schwennsen, L. Szymanowski and S. Wallon, *Pomeron Odderon interference in production of $\pi^+\pi^-$ pairs at LHC*, proceedings of 17th International Workshop on Deep-Inelastic Scattering and Related Subjects (DIS 2009), Madrid, Spain, 26-30 Apr 2009, arXiv:0906.5512 [hep-ph].
- [W52] B. Pire, F. Schwennsen, L. Szymanowski and S. Wallon, *Looking for the Odderon in photon collisions*, proceedings of Photon 09, DESY, 11-15 May 2009, arXiv:0908.1475 [hep-ph].
- [W53] B. Pire, F. Schwennsen, L. Szymanowski and S. Wallon, *Pomeron Odderon interference in production of two $\pi^+\pi^-$ pairs at LHC and ILC*, Proceedings of EPS conference Krakow, 16-22 July 2009, arXiv:0909.3450 [hep-ph].
- [W54] I. V. Anikin, D. Y. Ivanov, B. Pire, L. Szymanowski and S. Wallon, *Hard diffractive processes and non-perturbative matrix elements beyond leading twist: rhoT-meson production*, proceedings of the 10th Workshop on non-perturbative QCD, Paris, 8-12 June 2009, arXiv:0909.4042 [hep-ph].
- [W55] S. Wallon, *Hard exclusive processes: theoretical status*, proceedings of Photon 09, DESY, 11-15 May 2009, arXiv:0909.4052 [hep-ph].
- [W56] I. V. Anikin, D. Y. Ivanov, B. Pire, L. Szymanowski and S. Wallon, *QCD factorization beyond leading twist in exclusive processes: rhoT-meson production*, Proceedings of EPS conference, Krakow, 16-22 July 2009, arXiv:0909.4038 [hep-ph].
- [W57] M. E. Beiyad, B. Pire, M. Segond, L. Szymanowski and S. Wallon, *Transversity Generalized Parton Distributions from gamma N to pi rhot N' with a Large pi rhot Invariant Mass*, proceedings of the XIII Workshop On High Energy Spin Physics Dubna Spin 2009, arXiv:0911.2611 [hep-ph].

Technical reports

- [W58] J. A. Aguilar-Saavedra *et al.* [ECFA/DESY LC Physics Working Group], *TESLA Technical Design Report Part III: Physics at an e^+e^- Linear Collider*
- [W59] J. Roche *et al.*, *Measurements of the electron-helicity dependent cross sections of deeply virtual Compton scattering with CEBAF at 12-GeV* [arXiv:nucl-ex/0609015].
- [W60] A. Djouadi, J. Lykken, K. Moenig, Y. Okada, M. Oreglia, S. Yamashita, et al, International Linear Collider Reference Design Report Volume 2: PHYSICS AT THE ILC, arXiv:0709.1893 [hep-ph].
- [W61] J. Brau *et al.* [ILC Collaboration], *ILC Reference Design Report Volume 1 - Executive Summary*, arXiv:0712.1950 [physics.acc-ph].
- [W62] T. Behnke *et al.* [ILC Collaboration], *ILC Reference Design Report Volume 4 - Detectors*, arXiv:0712.2356 [physics.ins-det].

- [1] X.-D. Ji, *Gauge invariant decomposition of nucleon spin*, *Phys. Rev. Lett.* **78** (1997) 610–613, [[hep-ph/9603249](#)].
- [2] V. S. Fadin, E. A. Kuraev, and L. N. Lipatov, *On the Pomeron singularity in Asymptotically Free Theories*, *Phys. Lett.* **B60** (1975) 50–52.
- [3] E. A. Kuraev, L. N. Lipatov, and V. S. Fadin, *Multi - Reggeon Processes in the Yang-Mills Theory*, *Sov. Phys. JETP* **44** (1976) 443–450.
- [4] E. A. Kuraev, L. N. Lipatov, and V. S. Fadin, *The Pomeron Singularity in Nonabelian Gauge Theories*, *Sov. Phys. JETP* **45** (1977) 199–204.
- [5] I. I. Balitsky and L. N. Lipatov, *The Pomeron Singularity in Quantum Chromodynamics*, *Sov. J. Nucl. Phys.* **28** (1978) 822–829.
- [6] L. V. Gribov, E. M. Levin, and M. G. Ryskin, *Semihard Processes in QCD*, *Phys. Rept.* **100** (1983) 1–150.
- [7] S. J. Brodsky and G. R. Farrar, *Scaling Laws at Large Transverse Momentum*, *Phys. Rev. Lett.* **31** (1973) 1153–1156.
- [8] S. J. Brodsky and G. R. Farrar, *Scaling Laws for Large Momentum Transfer Processes*, *Phys. Rev.* **D11** (1975) 1309.
- [9] V. L. Chernyak and A. R. Zhitnitsky, *Asymptotic Behavior of Exclusive Processes in QCD*, *Phys. Rept.* **112** (1984) 173.
- [10] S. J. Brodsky and G. P. Lepage, *Large Angle Two Photon Exclusive Channels in Quantum Chromodynamics*, *Phys. Rev.* **D24** (1981) 1808.
- [11] P. V. Landshoff, *Model for elastic scattering at wide angle*, *Phys. Rev.* **D10** (1974) 1024–1030.
- [12] R. J. Eden, P. V. Landshoff, D. I. Olive, and J. Polkinghorne, *The analytic S-matrix*. Cambridge University Press.
- [13] P. V. Landshoff and D. J. Pritchard, *Higher order QCD corrections to exclusive processes: The multiple scattering mechanism*, *Zeit. Phys.* **C6** (1980) 69.
- [14] A. H. Mueller, *Perturbative QCD at high-energies*, *Phys. Rept.* **73** (1981) 237.
- [15] A. S. Carroll *et. al.*, *Nuclear Transparency to Large Angle p p Elastic Scattering*, *Phys. Rev. Lett.* **61** (1988) 1698–1701.
- [16] J. P. Ralston and B. Pire, *Oscillatory scale breaking and the chromo - Coulomb phase shift*, *Phys. Rev. Lett.* **49** (1982) 1605.
- [17] B. Pire and J. P. Ralston, *Fixed angle elastic scattering and the chromo - Coulomb phase shift*, *Phys. Lett.* **B117** (1982) 233.
- [18] J. P. Ralston and B. Pire, *Fluctuating Proton Size and Oscillating Nuclear Transparency*, *Phys. Rev. Lett.* **61** (1988) 1823.
- [19] G. R. Farrar, G. Sterman, and H. yi Zhang, *Absence of Sudakov factors in large angle photoproduction and Compton scattering*, *Phys. Rev. Lett.* **62** (1989) 2229.
- [20] J. C. Collins and D. E. Soper, *The Theorems of Perturbative QCD*, *Ann. Rev. Nucl. Part. Sci.* **37** (1987) 383–409.
- [21] P. A. M. Guichon and M. Vanderhaeghen, *Virtual Compton scattering off the nucleon*, *Prog. Part. Nucl. Phys.* **41** (1998) 125–190, [[hep-ph/9806305](#)].
- [22] K. Goeke, M. V. Polyakov, and M. Vanderhaeghen, *Hard Exclusive Reactions and the Structure of Hadrons*, *Prog. Part. Nucl. Phys.* **47** (2001) 401–515, [[hep-ph/0106012](#)].
- [23] M. Diehl, *Generalized parton distributions*, *Phys. Rept.* **388** (2003) 41–277, [[hep-ph/0307382](#)].
- [24] A. V. Belitsky and A. V. Radyushkin, *Unraveling hadron structure with generalized parton distributions*, *Phys. Rept.* **418** (2005) 1–387, [[hep-ph/0504030](#)].

- [25] S. Boffi and B. Pasquini, *Generalized parton distributions and the structure of the nucleon*, *Riv. Nuovo Cim.* **30** (2007) 387, [[arXiv:0711.2625](#)].
- [26] V. D. Burkert and M. Diehl, *Generalized parton distributions*, . In *Close, Frank (ed.) et al.: Electromagnetic interactions and hadronic structure* 359-423.
- [27] M. Guidal, *Generalized Parton Distributions and deep virtual Compton scattering*, *Prog. Part. Nucl. Phys.* **61** (2008) 89–105.
- [28] S. J. Brodsky, L. Frankfurt, J. F. Gunion, A. H. Mueller, and M. Strikman, *Diffractive leptonproduction of vector mesons in QCD*, *Phys. Rev.* **D50** (1994) 3134–3144, [[hep-ph/9402283](#)].
- [29] M. Diehl, T. Gousset, B. Pire, and J. P. Ralston, *Testing the handbag contribution to exclusive virtual Compton scattering*, *Phys. Lett.* **B411** (1997) 193–202, [[hep-ph/9706344](#)].
- [30] **H1** Collaboration, C. Adloff *et. al.*, *Measurement of deeply virtual Compton scattering at HERA*, *Phys. Lett.* **B517** (2001) 47–58, [[hep-ex/0107005](#)].
- [31] **H1** Collaboration, A. Aktas *et. al.*, *Measurement of deeply virtual Compton scattering at HERA*, *Eur. Phys. J.* **C44** (2005) 1–11, [[hep-ex/0505061](#)].
- [32] **ZEUS** Collaboration, S. Chekanov *et. al.*, *Measurement of deeply virtual Compton scattering at HERA*, *Phys. Lett.* **B573** (2003) 46–62, [[hep-ex/0305028](#)].
- [33] **HERMES** Collaboration, A. Airapetian *et. al.*, *Measurement of the beam spin azimuthal asymmetry associated with deeply-virtual Compton scattering*, *Phys. Rev. Lett.* **87** (2001) 182001, [[hep-ex/0106068](#)].
- [34] **HERMES** Collaboration, F. Ellinghaus, *Beam-charge asymmetry associated with DVCS at HERMES*, *Nucl. Phys.* **A711** (2002) 171–174, [[hep-ex/0207029](#)].
- [35] **HERMES** Collaboration, A. Airapetian *et. al.*, *The Beam–Charge Azimuthal Asymmetry and Deeply Virtual Compton Scattering*, *Phys. Rev.* **D75** (2007) 011103, [[hep-ex/0605108](#)].
- [36] **Jefferson Lab Hall A** Collaboration, C. Munoz Camacho *et. al.*, *Scaling tests of the cross section for deeply virtual Compton scattering*, *Phys. Rev. Lett.* **97** (2006) 262002, [[nucl-ex/0607029](#)].
- [37] **CLAS** Collaboration, S. Stepanyan *et. al.*, *First observation of exclusive deeply virtual Compton scattering in polarized electron beam asymmetry measurements*, *Phys. Rev. Lett.* **87** (2001) 182002, [[hep-ex/0107043](#)].
- [38] **CLAS** Collaboration, S. Chen *et. al.*, *Measurement of deeply virtual Compton scattering with a polarized proton target*, *Phys. Rev. Lett.* **97** (2006) 072002, [[hep-ex/0605012](#)].
- [39] **CLAS** Collaboration, F. X. Girod *et. al.*, *Deeply Virtual Compton Scattering Beam-Spin Asymmetries*, *Phys. Rev. Lett.* **100** (2008) 162002, [[arXiv:0711.4805](#)].
- [40] **CLAS** Collaboration, R. De Masi *et. al.*, *Beam spin asymmetry in deep and exclusive pi0 electroproduction*, *Phys. Rev.* **C77** (2008) 042201, [[arXiv:0711.4736](#)].
- [41] N. d’Hose, *Prospects for GPD measurements with COMPASS at CERN, St. Andrews (Hadron physics)* (2004) 379–390.
- [42] L. Schoeffel, *Generalised parton distributions at HERA and prospects for COMPASS*, *Phys. Lett.* **B658** (2007) 33–39, [[arXiv:0706.3488](#)].
- [43] L. Schoeffel, *Advances in diffraction of subnuclear waves*, [arXiv:0908.3287](#).
- [44] A. V. Radyushkin, *Scaling Limit of Deeply Virtual Compton Scattering*, *Phys. Lett.* **B380** (1996) 417–425, [[hep-ph/9604317](#)].
- [45] A. V. Radyushkin, *Asymmetric gluon distributions and hard diffractive electroproduction*, *Phys. Lett.* **B385** (1996) 333–342, [[hep-ph/9605431](#)].
- [46] C. Itzykson and J. Zuber, *Quantum field theory*. McGraw-Hill New York, 1985.
- [47] M. C. Bergere and J. B. Zuber, *Renormalization of feynman amplitudes and parametric integral representation*,

- Commun. Math. Phys.* **35** (1974) 113–140.
- [48] A. V. Efremov and A. V. Radyushkin, *Factorization and Asymptotical Behavior of Pion Form-Factor in QCD*, *Phys. Lett.* **B94** (1980) 245–250.
- [49] A. V. Radyushkin, *Alpha representation and spectral properties of multiparton functions*, *Theor. Math. Phys.* **61** (1985) 1144.
- [50] A. V. Radyushkin, *On spectral properties of parton correlation functions and multiparton wave functions*, *Phys. Lett.* **B131** (1983) 179.
- [51] A. V. Radyushkin, *Nonforward parton distributions*, *Phys. Rev.* **D56** (1997) 5524–5557, [[hep-ph/9704207](#)].
- [52] J. C. Collins, L. Frankfurt, and M. Strikman, *Factorization for hard exclusive electroproduction of mesons in QCD*, *Phys. Rev.* **D56** (1997) 2982–3006, [[hep-ph/9611433](#)].
- [53] L. D. Landau, *On analytic properties of vertex parts in quantum field theory*, *Nucl. Phys.* **13** (1959) 181–192.
- [54] S. Coleman and R. E. Norton, *Singularities in the physical region*, *Nuovo Cim.* **38** (1965) 438–442.
- [55] X.-D. Ji and J. Osborne, *One-loop corrections and all order factorization in deeply virtual Compton scattering*, *Phys. Rev.* **D58** (1998) 094018, [[hep-ph/9801260](#)].
- [56] J. C. Collins and A. Freund, *Proof of factorization for deeply virtual Compton scattering in QCD*, *Phys. Rev.* **D59** (1999) 074009, [[hep-ph/9801262](#)].
- [57] N. H. Christ, B. Hasslacher, and A. H. Mueller, *Light cone behavior of perturbation theory*, *Phys. Rev.* **D6** (1972) 3543.
- [58] D. J. Gross and F. Wilczek, *Asymptotically Free Gauge Theories. 1*, *Phys. Rev.* **D8** (1973) 3633–3652.
- [59] H. Georgi and H. D. Politzer, *Electroproduction scaling in an asymptotically free theory of strong interactions*, *Phys. Rev.* **D9** (1974) 416–420.
- [60] D. J. Gross and F. Wilczek, *Asymptotically free gauge theories. 2*, *Phys. Rev.* **D9** (1974) 980–993.
- [61] V. N. Gribov and L. N. Lipatov, *Deep inelastic $e p$ scattering in perturbation theory*, *Sov. J. Nucl. Phys.* **15** (1972) 438–450.
- [62] L. N. Lipatov, *The parton model and perturbation theory*, *Sov. J. Nucl. Phys.* **20** (1975) 94–102.
- [63] G. Altarelli and G. Parisi, *Asymptotic freedom in parton language*, *Nucl. Phys.* **B126** (1977) 298.
- [64] Y. L. Dokshitzer, *Calculation of the Structure Functions for Deep Inelastic Scattering and $e^+ e^-$ Annihilation by Perturbation Theory in Quantum Chromodynamics*, *Sov. Phys. JETP* **46** (1977) 641–653.
- [65] G. R. Farrar and D. R. Jackson, *The Pion Form-Factor*, *Phys. Rev. Lett.* **43** (1979) 246.
- [66] G. P. Lepage and S. J. Brodsky, *Exclusive Processes in Quantum Chromodynamics: Evolution Equations for Hadronic Wave Functions and the Form-Factors of Mesons*, *Phys. Lett.* **B87** (1979) 359–365.
- [67] S. A. Anikin and O. I. Zavyalov, *Short Distance and Light Cone Expansions for Products of Currents*, *Annals Phys.* **116** (1978) 135–166.
- [68] B. Geyer, D. Robaschik, M. Bordag, and J. Horejsi, *Nonlocal light cone expansions and evolution equations*, *Z. Phys.* **C26** (1985) 591–600.
- [69] O. I. Zavyalov, *Renormalized Quantum Field Theory*. Kluwer Academic Publishers.
- [70] I. I. Balitsky and V. M. Braun, *Nonlocal operator expansion for structure functions of $e^+ e^-$ annihilation*, *Phys. Lett.* **B222** (1989) 123–131.
- [71] I. I. Balitsky and V. M. Braun, *The Nonlocal operator expansion for inclusive particle production in $e^+ e^-$ annihilation*, *Nucl. Phys.* **B361** (1991) 93–140.
- [72] D. Mueller, D. Robaschik, B. Geyer, F. M. Dittes, and J. Horejsi, *Wave functions, evolution equations and*

- evolution kernels from light-ray operators of QCD*, *Fortschr. Phys.* **42** (1994) 101, [[hep-ph/9812448](#)].
- [73] P. Cvitanović, *Group theory: birdtracks, Lie's, and exceptional groups*. Princeton University Press, 2008.
- [74] X.-D. Ji, *Off-forward parton distributions*, *J. Phys.* **G24** (1998) 1181–1205, [[hep-ph/9807358](#)].
- [75] K. J. Golec-Biernat and A. D. Martin, *Off-diagonal parton distributions and their evolution*, *Phys. Rev.* **D59** (1999) 014029, [[hep-ph/9807497](#)].
- [76] M. Diehl, T. Feldmann, R. Jakob, and P. Kroll, *The overlap representation of skewed quark and gluon distributions*, *Nucl. Phys.* **B596** (2001) 33–65, [[hep-ph/0009255](#)].
- [77] J. B. Kogut and D. E. Soper, *Quantum Electrodynamics in the Infinite Momentum Frame*, *Phys. Rev.* **D1** (1970) 2901–2913.
- [78] J. D. Bjorken, J. B. Kogut, and D. E. Soper, *Quantum Electrodynamics at Infinite Momentum: Scattering from an External Field*, *Phys. Rev.* **D3** (1971) 1382.
- [79] S. J. Brodsky and G. P. Lepage, *Exclusive processes in Quantum Chromodynamics*, *Adv. Ser. Direct. High Energy Phys.* **5** (1989) 93–240.
- [80] S. J. Brodsky, H.-C. Pauli, and S. S. Pinsky, *Quantum Chromodynamics and Other Field Theories on the Light Cone*, *Phys. Rept.* **301** (1998) 299–486, [[hep-ph/9705477](#)].
- [81] M. Diehl, *Generalized parton distributions with helicity flip*, *Eur. Phys. J.* **C19** (2001) 485–492, [[hep-ph/0101335](#)].
- [82] P. Hoodbhoy and X.-D. Ji, *Helicity-flip off-forward parton distributions of the nucleon*, *Phys. Rev.* **D58** (1998) 054006, [[hep-ph/9801369](#)].
- [83] V. Barone, A. Drago, and P. G. Ratcliffe, *Transverse polarisation of quarks in hadrons*, *Phys. Rept.* **359** (2002) 1–168, [[hep-ph/0104283](#)].
- [84] M. Anselmino, *Transversity*, [hep-ph/0512140](#).
- [85] J. P. Ralston and D. E. Soper, *Production of Dimuons from High-Energy Polarized Proton Proton Collisions*, *Nucl. Phys.* **B152** (1979) 109.
- [86] X. Artru and M. Mekhfi, *Transversely Polarized Parton Densities, their Evolution and their Measurement*, *Z. Phys.* **C45** (1990) 669.
- [87] R. L. Jaffe and X.-D. Ji, *Chiral odd parton distributions and polarized Drell-Yan*, *Phys. Rev. Lett.* **67** (1991) 552–555.
- [88] R. L. Jaffe and X.-D. Ji, *Chiral odd parton distributions and Drell-Yan processes*, *Nucl. Phys.* **B375** (1992) 527–560.
- [89] J. L. Cortes, B. Pire, and J. P. Ralston, *Measuring the transverse polarization of quarks in the proton*, *Z. Phys.* **C55** (1992) 409–416.
- [90] X.-D. Ji, *Probing the nucleon's transversity distribution in polarized $p p$, p anti- p , and πp collisions*, *Phys. Lett.* **B284** (1992) 137–143.
- [91] B. Pire and J. P. Ralston, *Single spin asymmetries in the Drell-Yan process*, *Phys. Rev.* **D28** (1983) 260.
- [92] J. C. Collins, S. F. Heppelmann, and G. A. Ladinsky, *Measuring transversity densities in singly polarized hadron hadron and lepton - hadron collisions*, *Nucl. Phys.* **B420** (1994) 565–582, [[hep-ph/9305309](#)].
- [93] R. L. Jaffe, X. min Jin, and J. Tang, *Interference Fragmentation Functions and the Nucleon's Transversity*, *Phys. Rev. Lett.* **80** (1998) 1166–1169, [[hep-ph/9709322](#)].
- [94] A. Bianconi, S. Boffi, R. Jakob, and M. Radici, *Two-hadron interference fragmentation functions. I: General framework*, *Phys. Rev.* **D62** (2000) 034008, [[hep-ph/9907475](#)].
- [95] A. Bianconi, S. Boffi, R. Jakob, and M. Radici, *Two-hadron interference fragmentation functions. II: A model calculation*, *Phys. Rev.* **D62** (2000) 034009, [[hep-ph/9907488](#)].

- [96] **HERMES** Collaboration, A. Airapetian *et. al.*, *Single-spin asymmetries in semi-inclusive deep-inelastic scattering on a transversely polarized hydrogen target*, *Phys. Rev. Lett.* **94** (2005) 012002, [[hep-ex/0408013](#)].
- [97] **COMPASS** Collaboration, H. Wollny, *Transversity Signal in two Hadron Pair Production in COMPASS*, [arXiv:0907.0961](#).
- [98] Y. L. Dokshitzer, D. Diakonov, and S. I. Troian, *Hard Processes in Quantum Chromodynamics*, *Phys. Rept.* **58** (1980) 269–395.
- [99] D. Bailin, A. Love, and D. V. Nanopoulos, *Approach to asymptotic freedom in neutrino production and electroproduction*, *Lett. Nuovo Cim.* **9S2** (1974) 501–505.
- [100] M. Bordag and D. Robaschik, *The Altarelli-Parisi equations as renormalization group equations for the coefficients of the nonlocal light cone expansion*, *Theor. Math. Phys.* **49** (1982) 1063.
- [101] M. Bordag, L. Kaschluhn, G. Petrov, and D. Robaschik, *Nonlocal operators in light cone expansion of QCD*, *Sov. J. Nucl. Phys.* **37** (1983) 112.
- [102] T. Braunschweig, J. Horejsi, and D. Robaschik, *Nonlocal light cone expansion and its applications to Deep Inelastic Scattering processes*, *Z. Phys.* **C23** (1984) 19.
- [103] T. Braunschweig, B. Geyer, and D. Robaschik, *Anomalous dimensions of flavor singlet light cone operators*, *Annalen Phys.* **44** (1987) 403–411.
- [104] I. I. Balitsky, *String operator expansion of the t product of two currents near the light cone*, *Phys. Lett.* **B124** (1983) 230–236.
- [105] I. I. Balitsky and V. M. Braun, *Evolution Equations for QCD String Operators*, *Nucl. Phys.* **B311** (1989) 541–584.
- [106] A. P. Bukhvostov, E. A. Kuraev, and L. N. Lipatov, *Deep Inelastic electron Scattering by a Polarized Target in Quantum Chromodynamics*, *JETP Lett.* **37** (1983) 482–486.
- [107] A. P. Bukhvostov, G. V. Frolov, L. N. Lipatov, and E. A. Kuraev, *Evolution Equations for Quasi-Partonic Operators*, *Nucl. Phys.* **B258** (1985) 601–646.
- [108] F. M. Dittes, D. Mueller, D. Robaschik, B. Geyer, and J. Horejsi, *The Altarelli-Parisi Kernel as Asymptotic Limit of an Extended Brodsky-Lepage Kernel*, *Phys. Lett.* **B209** (1988) 325–329.
- [109] X.-D. Ji, *Deeply-virtual Compton scattering*, *Phys. Rev.* **D55** (1997) 7114–7125, [[hep-ph/9609381](#)].
- [110] L. Frankfurt, A. Freund, V. Guzey, and M. Strikman, *Nondiagonal parton distributions in the leading logarithmic approximation*, *Phys. Lett.* **B418** (1998) 345–354, [[hep-ph/9703449](#)].
- [111] I. I. Balitsky and A. V. Radyushkin, *Light-ray evolution equations and leading-twist parton helicity-dependent nonforward distributions*, *Phys. Lett.* **B413** (1997) 114–121, [[hep-ph/9706410](#)].
- [112] J. Blumlein, B. Geyer, and D. Robaschik, *On the evolution kernels of twist 2 light-ray operators for unpolarized and polarized deep inelastic scattering*, *Phys. Lett.* **B406** (1997) 161–170, [[hep-ph/9705264](#)].
- [113] J. Blumlein, B. Geyer, and D. Robaschik, *The virtual Compton amplitude in the generalized Bjorken region: Twist-2 contributions*, *Nucl. Phys.* **B560** (1999) 283–344, [[hep-ph/9903520](#)].
- [114] A. V. Radyushkin, *Double distributions and evolution equations*, *Phys. Rev.* **D59** (1999) 014030, [[hep-ph/9805342](#)].
- [115] F. M. Dittes and A. V. Radyushkin, *Two loop contribution to the evolution of the pion wave function*, *Phys. Lett.* **B134** (1984) 359–362.
- [116] M. H. Sarmadi, *The asymptotic pion form-factor beyond the leading order*, *Phys. Lett.* **B143** (1984) 471.
- [117] G. R. Katz, *Two loop Feynman gauge calculation of the meson nonsinglet evolution potential*, *Phys. Rev.* **D31** (1985) 652.
- [118] S. V. Mikhailov and A. V. Radyushkin, *Evolution kernels in QCD: Two loop calculation in Feynman gauge*, *Nucl.*

- Phys.* **B254** (1985) 89.
- [119] E. G. Floratos, D. A. Ross, and C. T. Sachrajda, *Higher Order Effects in Asymptotically Free Gauge Theories: The Anomalous Dimensions of Wilson Operators*, *Nucl. Phys.* **B129** (1977) 66–88.
- [120] E. G. Floratos, D. A. Ross, and C. T. Sachrajda, *Higher Order Effects in Asymptotically Free Gauge Theories. 2. Flavor Singlet Wilson Operators and Coefficient Functions*, *Nucl. Phys.* **B152** (1979) 493.
- [121] G. Curci, W. Furmanski, and R. Petronzio, *Evolution of Parton Densities Beyond Leading Order: The Nonsinglet Case*, *Nucl. Phys.* **B175** (1980) 27.
- [122] A. V. Belitsky and D. Mueller, *Next-to-leading order evolution of twist-two conformal operators: The abelian case*, *Nucl. Phys.* **B527** (1998) 207–234, [[hep-ph/9802411](#)].
- [123] A. V. Belitsky and D. Mueller, *Broken conformal invariance and spectrum of anomalous dimensions in QCD*, *Nucl. Phys.* **B537** (1999) 397–442, [[hep-ph/9804379](#)].
- [124] A. V. Belitsky, D. Mueller, L. Niedermeier, and A. Schafer, *Evolution of non-forward parton distributions in next-to-leading order: Singlet sector*, *Nucl. Phys.* **B546** (1999) 279–298, [[hep-ph/9810275](#)].
- [125] A. V. Belitsky, D. Mueller, and A. Freund, *Reconstruction of non-forward evolution kernels*, *Phys. Lett.* **B461** (1999) 270–279, [[hep-ph/9904477](#)].
- [126] A. V. Belitsky and D. Mueller, *Exclusive evolution kernels in two-loop order: Parity even sector*, *Phys. Lett.* **B464** (1999) 249–256, [[hep-ph/9906409](#)].
- [127] A. V. Belitsky, A. Freund, and D. Mueller, *Evolution kernels of skewed parton distributions: Method and two-loop results*, *Nucl. Phys.* **B574** (2000) 347–406, [[hep-ph/9912379](#)].
- [128] B. Melic, D. Mueller, and K. Passek-Kumericki, *Next-to-next-to-leading prediction for the photon-to-pion transition form factor*, *Phys. Rev.* **D68** (2003) 014013, [[hep-ph/0212346](#)].
- [129] V. L. Chernyak and A. R. Zhitnitsky, *Asymptotic Behavior of Hadron Form-Factors in Quark Model. (In Russian)*, *JETP Lett.* **25** (1977) 510.
- [130] V. L. Chernyak, A. R. Zhitnitsky, and V. G. Serbo, *Asymptotic hadronic form-factors in quantum chromodynamics*, *JETP Lett.* **26** (1977) 594–597.
- [131] V. L. Chernyak, V. G. Serbo, and A. R. Zhitnitsky, *Calculation of asymptotics of the pion electromagnetic form-factor in the QCD perturbation theory. (in russian)*, *Sov. J. Nucl. Phys.* **31** (1980) 552–558.
- [132] V. L. Chernyak and A. R. Zhitnitsky, *Asymptotics of Hadronic Form-Factors in the Quantum Chromodynamics. (In Russian)*, *Sov. J. Nucl. Phys.* **31** (1980) 544–552.
- [133] G. P. Lepage and S. J. Brodsky, *Exclusive Processes in Perturbative Quantum Chromodynamics*, *Phys. Rev.* **D22** (1980) 2157.
- [134] L. Frankfurt, W. Koepf, and M. Strikman, *Hard diffractive electroproduction of vector mesons in QCD*, *Phys. Rev.* **D54** (1996) 3194–3215, [[hep-ph/9509311](#)].
- [135] P. Ball and V. M. Braun, *The ρ Meson Light-Cone Distribution Amplitudes of Leading Twist Revisited*, *Phys. Rev.* **D54** (1996) 2182–2193, [[hep-ph/9602323](#)].
- [136] P. Ball, V. M. Braun, Y. Koike, and K. Tanaka, *Higher twist distribution amplitudes of vector mesons in QCD: Formalism and twist three distributions*, *Nucl. Phys.* **B529** (1998) 323–382, [[hep-ph/9802299](#)].
- [137] P. Ball and V. M. Braun, *Higher twist distribution amplitudes of vector mesons in QCD: Twist-4 distributions and meson mass corrections*, *Nucl. Phys.* **B543** (1999) 201–238, [[hep-ph/9810475](#)].
- [138] P. Ball, *Theoretical update of pseudoscalar meson distribution amplitudes of higher twist: The nonsinglet case*, *JHEP* **01** (1999) 010, [[hep-ph/9812375](#)].
- [139] I. I. Balitsky, V. M. Braun, and A. V. Kolesnichenko, *Radiative Decay $\Sigma^+ \rightarrow p \gamma$ in Quantum Chromodynamics*, *Nucl. Phys.* **B312** (1989) 509–550.

- [140] V. M. Braun and I. E. Filyanov, *Conformal invariance and pion wave functions of nonleading twist*, *Z. Phys.* **C48** (1990) 239–248.
- [141] V. M. Braun, G. P. Korchemsky, and D. Mueller, *The uses of conformal symmetry in QCD*, *Prog. Part. Nucl. Phys.* **51** (2003) 311–398, [[hep-ph/0306057](#)].
- [142] T. Ohrndorf, *Constraints from conformal covariance on the mixing of operators of lowest twist*, *Nucl. Phys.* **B198** (1982) 26.
- [143] V. L. Chernyak, A. R. Zhitnitsky, and I. R. Zhitnitsky, *Wave functions of the mesons containing s, c, b quarks*, *Sov. J. Nucl. Phys.* **38** (1983) 775.
- [144] M. A. Shifman, A. I. Vainshtein, and V. I. Zakharov, *QCD and Resonance Physics. Sum Rules*, *Nucl. Phys.* **B147** (1979) 385–447.
- [145] V. L. Chernyak and A. R. Zhitnitsky, *Exclusive Decays of Heavy Mesons*, *Nucl. Phys.* **B201** (1982) 492.
- [146] B. L. Ioffe and A. V. Smilga, *Pion Form-Factor at Intermediate Momentum Transfer in QCD*, *Phys. Lett.* **B114** (1982) 353.
- [147] V. A. Nesterenko and A. V. Radyushkin, *Sum Rules and Pion Form-Factor in QCD*, *Phys. Lett.* **B115** (1982) 410.
- [148] A. P. Bakulev and S. V. Mikhailov, *Lattice measurements of nonlocal quark condensates, vacuum correlation length, and pion distribution amplitude in QCD*, *Phys. Rev.* **D65** (2002) 114511, [[hep-ph/0203046](#)].
- [149] L. Del Debbio, *Pion distribution amplitude from the lattice*, *Few Body Syst.* **36** (2005) 77–82.
- [150] V. M. Braun *et al.*, *Moments of pseudoscalar meson distribution amplitudes from the lattice*, *Phys. Rev.* **D74** (2006) 074501, [[hep-lat/0606012](#)].
- [151] A. V. Radyushkin, *Shape of Pion Distribution Amplitude*, [arXiv:0906.0323](#).
- [152] D. Renner, *Status and prospects for the calculation of hadron structure from lattice QCD*, in *Lattice 09*, 2009.
- [153] P. M. Stevenson, *Resolution of the Renormalization Scheme Ambiguity in Perturbative QCD*, *Phys. Lett.* **B100** (1981) 61.
- [154] P. M. Stevenson, *Optimized Perturbation Theory*, *Phys. Rev.* **D23** (1981) 2916.
- [155] G. Grunberg, *Renormalization Group Improved Perturbative QCD*, *Phys. Lett.* **B95** (1980) 70.
- [156] G. Grunberg, *Renormalization group improved predictions for quarkonium decay*, *Phys. Lett.* **B114** (1982) 271.
- [157] G. Grunberg, *Renormalization Scheme Independent QCD and QED: The Method of Effective Charges*, *Phys. Rev.* **D29** (1984) 2315.
- [158] S. J. Brodsky, G. P. Lepage, and P. B. Mackenzie, *On the Elimination of Scale Ambiguities in Perturbative Quantum Chromodynamics*, *Phys. Rev.* **D28** (1983) 228.
- [159] B. Melic, B. Nizic, and K. Passek, *A note on the factorization scale independence of the pQCD predictions for exclusive processes*, *Eur. Phys. J.* **C36** (2004) 453–458, [[hep-ph/0107311](#)].
- [160] L. Mankiewicz and G. Piller, *Comments on exclusive electroproduction of transversely polarized vector mesons*, *Phys. Rev.* **D61** (2000) 074013, [[hep-ph/9905287](#)].
- [161] I. V. Anikin and O. V. Teryaev, *Genuine twist 3 in exclusive electroproduction of transversely polarized vector mesons*, *Phys. Lett.* **B554** (2003) 51–63, [[hep-ph/0211028](#)].
- [162] I. V. Anikin and O. V. Teryaev, *Non-factorized genuine twist 3 in exclusive electro- production of vector mesons*, *Nucl. Phys.* **A711** (2002) 199–202, [[hep-ph/0208126](#)].
- [163] H. nan Li and G. Sterman, *The Perturbative pion form-factor with Sudakov suppression*, *Nucl. Phys.* **B381** (1992) 129–140.
- [164] J. Botts and G. Sterman, *Hard Elastic Scattering in QCD: Leading Behavior*, *Nucl. Phys.* **B325** (1989) 62.

- [165] I. V. Musatov and A. V. Radyushkin, *Transverse momentum and Sudakov effects in exclusive QCD processes: $\gamma^* \gamma \pi^0$ form factor*, *Phys. Rev.* **D56** (1997) 2713–2735, [[hep-ph/9702443](#)].
- [166] S. Descotes-Genon and C. T. Sachrajda, *Sudakov effects in $B \rightarrow \pi l \nu/l$ form factors*, *Nucl. Phys.* **B625** (2002) 239–278, [[hep-ph/0109260](#)].
- [167] R. Jakob and P. Kroll, *The Pion form-factor: Sudakov suppressions and intrinsic transverse momentum*, *Phys. Lett.* **B315** (1993) 463–470, [[hep-ph/9306259](#)].
- [168] R. Jakob, P. Kroll, and M. Raulfs, *Meson - photon transition form-factors*, *J. Phys.* **G22** (1996) 45–58, [[hep-ph/9410304](#)].
- [169] P. Kroll and M. Raulfs, *The π gamma transition form factor and the pion wave function*, *Phys. Lett.* **B387** (1996) 848–854, [[hep-ph/9605264](#)].
- [170] M. Vanderhaeghen, P. A. M. Guichon, and M. Guidal, *Deeply virtual electroproduction of photons and mesons on the nucleon: Leading order amplitudes and power corrections*, *Phys. Rev.* **D60** (1999) 094017, [[hep-ph/9905372](#)].
- [171] S. V. Goloskokov and P. Kroll, *Vector meson electroproduction at small Bjorken- x and generalized parton distributions*, *Eur. Phys. J.* **C42** (2005) 281–301, [[hep-ph/0501242](#)].
- [172] S. V. Goloskokov and P. Kroll, *The longitudinal cross section of vector meson electroproduction*, *Eur. Phys. J.* **C50** (2007) 829–842, [[hep-ph/0611290](#)].
- [173] S. V. Goloskokov and P. Kroll, *The role of the quark and gluon GPDs in hard vector-meson electroproduction*, *Eur. Phys. J.* **C53** (2008) 367–384, [[/08.3569](#)].
- [174] B. Pire and L. Szymanowski, *Probing the nucleon's transversity and the photon's distribution amplitude in lepton pair photoproduction*, *Phys. Rev. Lett.* **103** (2009) 072002, [[/05.1258](#)].
- [175] M. Diehl, T. Gousset, and B. Pire, *Exclusive electroproduction of vector mesons and transversity distributions*, *Phys. Rev.* **D59** (1999) 034023, [[hep-ph/9808479](#)].
- [176] J. C. Collins and M. Diehl, *Transversity distribution does not contribute to hard exclusive electroproduction of mesons*, *Phys. Rev.* **D61** (2000) 114015, [[hep-ph/9907498](#)].
- [177] S. Ahmad, G. R. Goldstein, and S. Liuti, *Nucleon Tensor Charge from Exclusive π^0 Electroproduction*, *Phys. Rev.* **D79** (2009) 054014, [[/05.3568](#)].
- [178] S. V. Goloskokov and P. Kroll, *An attempt to understand exclusive π^+ electroproduction*, [[/06.0460](#)].
- [179] D. Y. Ivanov, B. Pire, L. Szymanowski, and O. V. Teryaev, *Probing chiral-odd GPD's in diffractive electroproduction of two vector mesons*, *Phys. Lett.* **B550** (2002) 65–76, [[hep-ph/0209300](#)].
- [180] R. Enberg, B. Pire, and L. Szymanowski, *Transversity GPD in photo- and electroproduction of two vector mesons*, *Eur. Phys. J.* **C47** (2006) 87–94, [[hep-ph/0601138](#)].
- [181] S. Kumano, M. Strikman, and K. Sudoh, *Novel two-to-three hard hadronic processes and possible studies of generalized parton distributions at hadron facilities*, *Phys. Rev.* **D80** (2009) 074003, [[/05.1453](#)].
- [182] S. Scopetta, *Model study of generalized parton distributions with helicity flip*, *Phys. Rev.* **D72** (2005) 117502, [[hep-ph/0509287](#)].
- [183] B. Pasquini, M. Pincetti, and S. Boffi, *Chiral-odd generalized parton distributions in constituent quark models*, *Phys. Rev.* **D72** (2005) 094029, [[hep-ph/0510376](#)].
- [184] M. Pincetti, B. Pasquini, and S. Boffi, *Chiral-Odd Generalized Parton Distributions and Transversity in Light-Front Constituent Quark Models*, *Czech. J. Phys.* **56** (2006) F229–F236, [[hep-ph/0610051](#)].
- [185] M. Wakamatsu, *Chiral-odd GPDs, transversity decomposition of angular momentum, and tensor charges of the nucleon*, *Phys. Rev.* **D79** (2009) 014033, [[arXiv:0811.4196](#)].
- [186] D. Chakrabarti, R. Manohar, and A. Mukherjee, *Chiral odd GPDs in transverse and longitudinal impact parameter spaces*, *Phys. Rev.* **D79** (2009) 034006, [[arXiv:0811.0521](#)].

- [187] QCDSF Collaboration, M. Gockeler *et al.*, *Quark helicity flip generalized parton distributions from two-flavor lattice QCD*, *Phys. Lett.* **B627** (2005) 113–123, [[hep-lat/0507001](#)].
- [188] QCDSF Collaboration, M. Gockeler *et al.*, *Transverse spin structure of the nucleon from lattice QCD simulations*, *Phys. Rev. Lett.* **98** (2007) 222001, [[hep-lat/0612032](#)].
- [189] E. R. Berger, M. Diehl, and B. Pire, *Timelike Compton scattering: Exclusive photoproduction of lepton pairs*, *Eur. Phys. J.* **C23** (2002) 675–689, [[hep-ph/0110062](#)].
- [190] S. J. Brodsky and F. J. Llanes-Estrada, *Renormalization scale-fixing for complex scattering amplitudes*, *Eur. Phys. J.* **C46** (2006) 751, [[hep-ph/0512247](#)].
- [191] L. Mankiewicz, G. Piller, and T. Weigl, *Hard lepton production of charged vector mesons*, *Phys. Rev.* **D59** (1999) 017501, [[hep-ph/9712508](#)].
- [192] M. Burkardt, *Impact parameter dependent parton distributions and off-forward parton distributions for $\zeta \rightarrow 0$* , *Phys. Rev.* **D62** (2000) 071503, [[hep-ph/0005108](#)].
- [193] J. P. Ralston and B. Pire, *Femto-photography of protons to nuclei with deeply virtual Compton scattering*, *Phys. Rev.* **D66** (2002) 111501, [[hep-ph/0110075](#)].
- [194] M. Diehl, *Generalized parton distributions in impact parameter space*, *Eur. Phys. J.* **C25** (2002) 223–232, [[hep-ph/0205208](#)].
- [195] M. Burkardt, *Transverse deformation of parton distributions and transversity decomposition of angular momentum*, *Phys. Rev.* **D72** (2005) 094020, [[hep-ph/0505189](#)].
- [196] M. Diehl and P. Hagler, *Spin densities in the transverse plane and generalized transversity distributions*, *Eur. Phys. J.* **C44** (2005) 87–101, [[hep-ph/0504175](#)].
- [197] A. Mukherjee, D. Chakrabarti, and R. Manohar, *Chiral Odd Generalized Parton Distributions in Position Space*, *AIP Conf. Proc.* **1149** (2009) 533–538, [[/02.1461](#)].
- [198] M. Anselmino *et al.*, *Transversity and Collins functions from SIDIS and e^+e^- data*, *Phys. Rev.* **D75** (2007) 054032, [[hep-ph/0701006](#)].
- [199] M. Gluck, E. Reya, M. Stratmann, and W. Vogelsang, *Models for the polarized parton distributions of the nucleon*, *Phys. Rev.* **D63** (2001) 094005, [[hep-ph/0011215](#)].
- [200] M. Gluck, E. Reya, and A. Vogt, *Dynamical parton distributions revisited*, *Eur. Phys. J.* **C5** (1998) 461–470, [[hep-ph/9806404](#)].
- [201] M. Diehl, T. Gousset, B. Pire, and O. Teryaev, *Probing partonic structure in $\gamma^* \gamma \rightarrow \pi \pi$ near threshold*, *Phys. Rev. Lett.* **81** (1998) 1782–1785, [[hep-ph/9805380](#)].
- [202] M. Diehl, T. Gousset, and B. Pire, *Exclusive production of pion pairs in $\gamma^* \gamma$ collisions at large Q^{*2}* , *Phys. Rev.* **D62** (2000) 073014, [[hep-ph/0003233](#)].
- [203] M. V. Polyakov, *Hard exclusive electroproduction of two pions and their resonances*, *Nucl. Phys.* **B555** (1999) 231, [[hep-ph/9809483](#)].
- [204] M. K. Chase, *The Q^{*2} evolution of flavor singlet wave functions in QCD*, *Nucl. Phys.* **B174** (1980) 109–122.
- [205] V. N. Baier and A. G. Grozin, *Meson wave functions with two gluon states*, *Nucl. Phys.* **B192** (1981) 476–488.
- [206] Y. L. Dokshitzer, *private communication*, .
- [207] J. M. Cornwall and G. Tiktopoulos, *Infrared Behavior of Nonabelian Gauge Theories*, *Phys. Rev.* **D13** (1976) 3370.
- [208] G. P. Lepage and S. J. Brodsky, *Exclusive Processes in Quantum Chromodynamics: The Form-Factors of Baryons at Large Momentum Transfer*, *Phys. Rev. Lett.* **43** (1979) 545–549.
- [209] I. Gradshteyn and I. Ryzhik, *Table of Integrals, Series and Products*. 1980.

- [210] B. Pire and O. V. Teryaev, *Single spin asymmetries in $\gamma^* \gamma \rightarrow \pi \pi \pi$ at large Q^{*2}* , *Phys. Lett.* **B496** (2000) 76–82, [[hep-ph/0007014](#)].
- [211] Y. Y. Balitsky, V. M. Braun, and A. V. Kolesnichenko, *The decay $\Sigma^+ \rightarrow p \gamma$ in QCD: Bilocal corrections in a variable magnetic field and the photon wave functions*, *Sov. J. Nucl. Phys.* **48** (1988) 348–357.
- [212] P. Ball, V. M. Braun, and N. Kivel, *Photon distribution amplitudes in QCD*, *Nucl. Phys.* **B649** (2003) 263–296, [[hep-ph/0207307](#)].
- [213] V. A. Novikov, M. A. Shifman, A. I. Vainshtein, and V. I. Zakharov, *Calculations in External Fields in Quantum Chromodynamics. Technical Review*, *Fortschr. Phys.* **32** (1984) 585.
- [214] V. M. Braun, S. Gottwald, D. Y. Ivanov, A. Schafer, and L. Szymanowski, *Exclusive photoproduction of hard dijets and magnetic susceptibility of QCD vacuum*, *Phys. Rev. Lett.* **89** (2002) 172001, [[hep-ph/0206305](#)].
- [215] M. Klasen, *Theory of hard photoproduction*, *Rev. Mod. Phys.* **74** (2002) 1221–1282, [[hep-ph/0206169](#)].
- [216] E. Witten, *Anomalous Cross-Section for Photon - Photon Scattering in Gauge Theories*, *Nucl. Phys.* **B120** (1977) 189–202.
- [217] S. Friot, B. Pire, and L. Szymanowski, *Deeply virtual Compton scattering on a photon and generalized parton distributions in the photon*, *Phys. Lett.* **B645** (2007) 153–160, [[hep-ph/0611176](#)].
- [218] B. Pire and L. Szymanowski, *Impact representation of generalized distribution amplitudes*, *Phys. Lett.* **B556** (2003) 129–134, [[hep-ph/0212296](#)].
- [219] I. V. Anikin, B. Pire, and O. V. Teryaev, *On $\gamma^* \gamma$ production of two ρ^0 mesons*, *Phys. Rev.* **D69** (2004) 014018, [[hep-ph/0307059](#)].
- [220] I. V. Anikin, B. Pire, and O. V. Teryaev, *Search for isotensor exotic meson and twist 4 contribution to $\gamma^* \gamma \rightarrow \rho \rho$* , *Phys. Lett.* **B626** (2005) 86–94, [[hep-ph/0506277](#)].
- [221] V. M. Budnev, I. F. Ginzburg, G. V. Meledin, and V. G. Serbo, *The Two photon particle production mechanism. Physical problems. Applications. Equivalent photon approximation*, *Phys. Rept.* **15** (1974) 181–281.
- [222] J. Bjorken, S. Drell, and P. Kahn, *Relativistic quantum fields*, vol. 34. 1966.
- [223] C. T. Hill and G. G. Ross, *QCD prediction for the structure functions of the photon*, *Nucl. Phys.* **B148** (1979) 373.
- [224] R. J. DeWitt, L. M. Jones, J. D. Sullivan, D. E. Willen, and J. H. W. Wyld, *Anomalous Components of the Photon Structure Functions*, *Phys. Rev.* **D19** (1979) 2046.
- [225] B. Pire and L. Szymanowski, *Hadron annihilation into two photons and backward VCS in the scaling regime of QCD*, *Phys. Rev.* **D71** (2005) 111501, [[hep-ph/0411387](#)].
- [226] B. Pire and L. Szymanowski, *QCD analysis of $\bar{p} N \rightarrow \gamma^* \pi$ in the scaling limit*, *Phys. Lett.* **B622** (2005) 83–92, [[hep-ph/0504255](#)].
- [227] **JLab Hall A** Collaboration, G. Laveissiere *et. al.*, *Photon electroproduction from hydrogen at backward angles and momentum transfer squared of $Q^2 = 1.0 \text{ GeV}^2$* , *Phys. Rev.* **C79** (2009) 015201, [[hep-ex/0406062](#)].
- [228] J. P. Lansberg, B. Pire, and L. Szymanowski, *Hard exclusive electroproduction of a pion in the backward region*, *Phys. Rev.* **D75** (2007) 074004, [[hep-ph/0701125](#)].
- [229] **The PANDA** Collaboration, M. F. M. Lutz, B. Pire, O. Scholten, and R. Timmermans, *Physics Performance Report for PANDA: Strong Interaction Studies with Antiprotons*, [arXiv:0903.3905](#).
- [230] J. P. Lansberg, B. Pire, and L. Szymanowski, *Production of a pion in association with a high- Q^2 dilepton pair in antiproton-proton annihilation at GSI- FAIR*, *Phys. Rev.* **D76** (2007) 111502, [[arXiv:0710.1267](#)].
- [231] J. P. Lansberg, B. Pire, and L. Szymanowski, *Exclusive meson pair production in $\gamma^* \gamma$ scattering at small momentum transfer*, *Phys. Rev.* **D73** (2006) 074014, [[hep-ph/0602195](#)].
- [232] M. Diehl, T. Feldmann, P. Kroll, and C. Vogt, *The perturbative limit of the two-pion light-cone distribution*

- amplitude, *Phys. Rev.* **D61** (2000) 074029, [[hep-ph/9912364](#)].
- [233] S. Mandelstam, *Quantum electrodynamics without potentials*, *Ann. Phys.* **19** (1962) 1–24.
- [234] F. E. Close and P. R. Page, *The Photoproduction of hybrid mesons from CEBAF to HERA*, *Phys. Rev.* **D52** (1995) 1706–1709, [[hep-ph/9412301](#)].
- [235] T. Barnes, F. E. Close, and E. S. Swanson, *Hybrid and conventional mesons in the flux tube model: Numerical studies and their phenomenological implications*, *Phys. Rev.* **D52** (1995) 5242–5256, [[hep-ph/9501405](#)].
- [236] S. Godfrey, *The phenomenology of glueball and hybrid mesons*, [hep-ph/0211464](#).
- [237] S. Godfrey and J. Napolitano, *Light meson spectroscopy*, *Rev. Mod. Phys.* **71** (1999) 1411–1462, [[hep-ph/9811410](#)].
- [238] F. E. Close and J. J. Dudek, *Electroweak production of hybrid mesons in a flux-tube simulation of lattice QCD*, *Phys. Rev. Lett.* **91** (2003) 142001, [[hep-ph/0304243](#)].
- [239] F. E. Close and J. J. Dudek, *Hybrid meson production by electromagnetic and weak interactions in a flux-tube simulation of lattice QCD*, *Phys. Rev.* **D69** (2004) 034010, [[hep-ph/0308098](#)].
- [240] C. Bernard *et al.*, *Lattice calculation of 1-+ hybrid mesons with improved Kogut-Susskind fermions*, *Phys. Rev.* **D68** (2003) 074505, [[hep-lat/0301024](#)].
- [241] **E852** Collaboration, D. R. Thompson *et al.*, *Evidence for exotic meson production in the reaction $\pi^- p \rightarrow \eta \pi^- p$ at 18-GeV/c*, *Phys. Rev. Lett.* **79** (1997) 1630–1633, [[hep-ex/9705011](#)].
- [242] **E852** Collaboration, G. S. Adams *et al.*, *Observation of a new $J(PC) = 1-+$ exotic state in the reaction $\pi^- p \rightarrow \pi^+ \pi^- \pi^- p$ at 18-GeV/c*, *Phys. Rev. Lett.* **81** (1998) 5760–5763.
- [243] R. L. Jaffe, K. Johnson, and Z. Ryzak, *Qualitative features of the glueball spectrum*, *Ann. Phys.* **168** (1986) 344.
- [244] G. S. Bali, *QCD forces and heavy quark bound states*, *Phys. Rept.* **343** (2001) 1–136, [[hep-ph/0001312](#)].
- [245] A. V. Kolesnichenko, *Second moments of quark and gluon distribution functions in a proton calculated making use of the QCD sum rules. (in russian)*, *Yad. Fiz.* **39** (1984) 1527–1544.
- [246] I. I. Balitsky, D. Diakonov, and A. V. Yung, *Exotic mesons with $J(PC) = (1-+)$ from QCD sum rules*, *Phys. Lett.* **B112** (1982) 71–75.
- [247] I. I. Balitsky, D. Diakonov, and A. V. Yung, *Exotic mesons with $J(PC) = 1(-+)$, strange and nonstrange*, *Z. Phys.* **C33** (1986) 265–273.
- [248] A. P. Bakulev and S. V. Mikhailov, *The rho meson and related meson wave functions in QCD sum rules with nonlocal condensates*, *Phys. Lett.* **B436** (1998) 351–362, [[hep-ph/9803298](#)].
- [249] D. V. Shirkov and I. L. Solovtsov, *Analytic model for the QCD running coupling with universal $\alpha(s)$ -bar(0) value*, *Phys. Rev. Lett.* **79** (1997) 1209–1212, [[hep-ph/9704333](#)].
- [250] **HERMES** Collaboration, A. Airapetian *et al.*, *Hard exclusive electroproduction of $\pi^+ \pi^-$ pairs*, *Phys. Lett.* **B599** (2004) 212–222, [[hep-ex/0406052](#)].
- [251] I. V. Anikin and O. V. Teryaev, *Wandzura-Wilczek approximation from generalized rotational invariance*, *Phys. Lett.* **B509** (2001) 95–105, [[hep-ph/0102209](#)].
- [252] **CLAS** Collaboration, S. A. Morrow *et al.*, *Exclusive ρ^0 electroproduction on the proton at CLAS*, *Eur. Phys. J.* **A39** (2009) 5–31, [[arXiv:0807.3834](#)].
- [253] **COMPASS** Collaboration, V. Y. Alexakhin *et al.*, *Double spin asymmetry in exclusive ρ^0 muoproduction at COMPASS*, *Eur. Phys. J.* **C52** (2007) 255–265, [[arXiv:0704.1863](#)].
- [254] **HERMES** Collaboration, A. Airapetian *et al.*, *Spin Density Matrix Elements in Exclusive ρ^0 Electroproduction on 1H and 2H Targets at 27.5 GeV Beam Energy*, *Eur. Phys. J.* **C62** (2009) 659–695, [[arXiv:0901.0701](#)].
- [255] **HERMES** Collaboration, A. Borissov, *Spin density matrix elements from ρ^0 and ϕ meson electroproduction*

at HERMES, *AIP Conf. Proc.* **1105** (2009) 19–23.

- [256] **ZEUS** Collaboration, J. Breitweg *et. al.*, *Exclusive electroproduction of ρ^0 and j/ψ mesons at HERA*, *Eur. Phys. J. C* **6** (1999) 603–627, [[hep-ex/9808020](#)].
- [257] **ZEUS** Collaboration, J. Breitweg *et. al.*, *Measurement of diffractive photoproduction of vector mesons at large momentum transfer at HERA*, *Eur. Phys. J. C* **14** (2000) 213–238, [[hep-ex/9910038](#)].
- [258] **ZEUS** Collaboration, S. Chekanov *et. al.*, *Measurement of proton dissociative diffractive photoproduction of vector mesons at large momentum transfer at HERA*, *Eur. Phys. J. C* **26** (2003) 389–409, [[hep-ex/0205081](#)].
- [259] **ZEUS** Collaboration, J. Breitweg *et. al.*, *Measurement of the spin-density matrix elements in exclusive electroproduction of ρ^0 mesons at HERA*, *Eur. Phys. J. C* **12** (2000) 393–410, [[hep-ex/9908026](#)].
- [260] **ZEUS** Collaboration, S. Chekanov *et. al.*, *Exclusive ρ^0 production in deep inelastic scattering at HERA*, *PMC Phys. A* **1** (2007) 6, [[arXiv:0708.1478](#)].
- [261] A. Bruni, X. Janssen, and P. Marage, *Exclusive Vector Meson Production and Deeply Virtual Compton Scattering at HERA*, [arXiv:0812.0539](#).
- [262] **H1** Collaboration, X. Janssen, *Diffractive electroproduction of rho and phi mesons at h1*, . Prepared for 16th International Workshop on Deep Inelastic Scattering and Related Subjects (DIS 2008), London, England, 7-11 Apr 2008.
- [263] A. Levy, *Exclusive vector meson electroproduction at HERA*, [arXiv:0711.0737](#).
- [264] I. V. Anikin, B. Pire, and O. V. Teryaev, *On the gauge invariance of the DVCS amplitude*, *Phys. Rev.* **D62** (2000) 071501, [[hep-ph/0003203](#)].
- [265] A. V. Efremov and O. V. Teryaev, *On spin effects in Quantum Chromodynamics*, *Sov. J. Nucl. Phys.* **36** (1982) 140.
- [266] E. V. Shuryak and A. I. Vainshtein, *Theory of Power Corrections to Deep Inelastic Scattering in Quantum Chromodynamics. 1. Q^{*2} Effects*, *Nucl. Phys.* **B199** (1982) 451.
- [267] E. V. Shuryak and A. I. Vainshtein, *Theory of Power Corrections to Deep Inelastic Scattering in Quantum Chromodynamics. 2. Q^{*4} Effects: Polarized Target*, *Nucl. Phys.* **B201** (1982) 141.
- [268] R. K. Ellis, W. Furmanski, and R. Petronzio, *Unraveling Higher Twists*, *Nucl. Phys.* **B212** (1983) 29.
- [269] A. V. Efremov and O. V. Teryaev, *The transversal polarization in Quantum Chromodynamics*, *Sov. J. Nucl. Phys.* **39** (1984) 962.
- [270] O. V. Teryaev, *Twist - three in proton nucleon single spin asymmetries*, [hep-ph/0102296](#).
- [271] A. V. Radyushkin and C. Weiss, *Kinematical twist-3 effects in DVCS as a quark spin rotation*, *Phys. Rev.* **D64** (2001) 097504, [[hep-ph/0106059](#)].
- [272] A. Ali, V. M. Braun, and H. Simma, *Exclusive radiative B decays in the light cone QCD sum rule approach*, *Z. Phys.* **C63** (1994) 437–454, [[hep-ph/9401277](#)].
- [273] L. N. Lipatov, *Pomeron in Quantum Chromodynamics*, *Adv. Ser. Direct. High Energy Phys.* **5** (1989) 411–489.
- [274] L. N. Lipatov, *Small-x physics in perturbative QCD*, *Phys. Rept.* **286** (1997) 131–198, [[hep-ph/9610276](#)].
- [275] J. R. Forshaw and D. A. Ross, *Quantum chromodynamics and the pomeron*, *Cambridge Lect. Notes Phys.* **9** (1997) 1–248.
- [276] V. S. Fadin, R. Fiore, and M. I. Kotsky, *Gluon Regge trajectory in the two-loop approximation*, *Phys. Lett.* **B387** (1996) 593–602, [[hep-ph/9605357](#)].
- [277] L. N. Lipatov, *The Bare Pomeron in Quantum Chromodynamics*, *Sov. Phys. JETP* **63** (1986) 904–912.
- [278] N. N. Nikolaev and B. G. Zakharov, *Colour transparency and scaling properties of nuclear shadowing in deep inelastic scattering*, *Z. Phys.* **C49** (1991) 607–618.

- [279] N. N. Nikolaev, B. G. Zakharov, and V. R. Zoller, *The Spectrum and solutions of the generalized BFKL equation for total cross-section*, *Phys. Lett.* **B328** (1994) 486–494, [[hep-th/9401052](#)].
- [280] A. H. Mueller, *Soft gluons in the infinite momentum wave function and the BFKL pomeron*, *Nucl. Phys.* **B415** (1994) 373–385.
- [281] A. H. Mueller and B. Patel, *Single and double BFKL pomeron exchange and a dipole picture of high-energy hard processes*, *Nucl. Phys.* **B425** (1994) 471–488, [[hep-ph/9403256](#)].
- [282] A. H. Mueller, *Unitarity and the BFKL pomeron*, *Nucl. Phys.* **B437** (1995) 107–126, [[hep-ph/9408245](#)].
- [283] Z. Chen and A. H. Mueller, *The Dipole picture of high-energy scattering, the BFKL equation and many gluon compound states*, *Nucl. Phys.* **B451** (1995) 579–604.
- [284] G. 't Hooft, *A planar diagram theory for strong interactions*, *Nucl. Phys.* **B72** (1974) 461.
- [285] G. 't Hooft, *Planar diagram field theories*, . Presented at Summer School 'Progress in Gauge Field Theory', Cargese, France, Sep 1-15, 1983.
- [286] G. P. Salam, *Studies of Unitarity at Small x Using the Dipole Formulation*, *Nucl. Phys.* **B461** (1996) 512–538, [[hep-ph/9509353](#)].
- [287] G. P. Salam, *OEDIPUS: Onium evolution, dipole interaction and perturbative unitarisation simulation*, *Comput. Phys. Commun.* **105** (1997) 62–76, [[hep-ph/9601220](#)].
- [288] H. Cheng and T. T. Wu, *Photon-photon scattering close to the forward direction*, *Phys. Rev.* **D1** (1970) 3414–3415.
- [289] G. Frolov and L. Lipatov *Sov. J. Nucl. Phys.* **13** (1971) 333.
- [290] V. Gribov, G. Frolov, and L. Lipatov *Yad. Fiz.* **12** (1971) 994.
- [291] S. Catani, M. Ciafaloni, and F. Hautmann, *Gluon contributions to small x heavy flavor production*, *Phys. Lett.* **B242** (1990) 97.
- [292] S. Catani, M. Ciafaloni, and F. Hautmann, *High-energy factorization and small x heavy flavor production*, *Nucl. Phys.* **B366** (1991) 135–188.
- [293] J. C. Collins and R. K. Ellis, *Heavy quark production in very high-energy hadron collisions*, *Nucl. Phys.* **B360** (1991) 3–30.
- [294] E. M. Levin, M. G. Ryskin, Y. M. Shabelski, and A. G. Shuvaev, *Heavy quark production in semihard nucleon interactions*, *Sov. J. Nucl. Phys.* **53** (1991) 657.
- [295] L. Lukaszuk and B. Nicolescu, *A Possible interpretation of $p p$ rising total cross- sections*, *Nuovo Cim. Lett.* **8** (1973) 405–413.
- [296] C. Ewerz, *The Odderon in quantum chromodynamics*, [hep-ph/0306137](#).
- [297] J. Bartels, *High-Energy Behavior in a Nonabelian Gauge Theory. 1. $T(n \rightarrow m)$ in the Leading Log Normal S Approximation*, *Nucl. Phys.* **B151** (1979) 293.
- [298] J. Bartels, *High-Energy Behavior in a Nonabelian Gauge Theory. 2. First Approximation*, *Nucl. Phys.* **B175** (1980) 365.
- [299] T. Jaroszewicz, *Infrared Divergences and Regge Behavior in QCD*, *Acta Phys. Polon.* **B11** (1980) 965.
- [300] J. Kwiecinski and M. Praszalowicz, *Three Gluon Integral Equation and Odd c Singlet Regge Singularities in QCD*, *Phys. Lett.* **B94** (1980) 413.
- [301] M. Ciafaloni, D. Colferai, G. P. Salam, and A. M. Stasto, *Expanding running coupling effects in the hard pomeron*, *Phys. Rev.* **D66** (2002) 054014, [[hep-ph/0204282](#)].
- [302] J. Bartels and H. Lotter, *A Note on the BFKL pomeron and the 'hot spot' cross- section*, *Phys. Lett.* **B309** (1993) 400–408.

- [303] M. Ciafaloni, D. Colferai, and G. P. Salam, *A collinear model for small- x physics*, *JHEP* **10** (1999) 017, [[hep-ph/9907409](#)].
- [304] M. Ciafaloni, D. Colferai, G. P. Salam, and A. M. Stasto, *Tunneling transition to the pomeron regime*, *Phys. Lett.* **B541** (2002) 314–326, [[hep-ph/0204287](#)].
- [305] A. Donnachie and P. V. Landshoff, *Total cross-sections*, *Phys. Lett.* **B296** (1992) 227–232, [[hep-ph/9209205](#)].
- [306] G. Camici and M. Ciafaloni, *Irreducible part of the next-to-leading BFKL kernel*, *Phys. Lett.* **B412** (1997) 396–406, [[hep-ph/9707390](#)].
- [307] M. Ciafaloni and G. Camici, *Energy scale(s) and next-to-leading BFKL equation*, *Phys. Lett.* **B430** (1998) 349–354, [[hep-ph/9803389](#)].
- [308] V. S. Fadin and L. N. Lipatov, *BFKL pomeron in the next-to-leading approximation*, *Phys. Lett.* **B429** (1998) 127–134, [[hep-ph/9802290](#)].
- [309] V. S. Fadin and R. Fiore, *Non-forward BFKL pomeron at next-to-leading order*, *Phys. Lett.* **B610** (2005) 61–66, [[hep-ph/0412386](#)].
- [310] V. S. Fadin and R. Fiore, *Non-forward NLO BFKL kernel*, *Phys. Rev.* **D72** (2005) 014018, [[hep-ph/0502045](#)].
- [311] J. Bartels, S. Gieseke, and C. F. Qiao, *The $(\gamma^* \rightarrow q \text{ anti-}q)$ Reggeon vertex in next-to-leading order QCD*, *Phys. Rev.* **D63** (2001) 056014, [[hep-ph/0009102](#)].
- [312] J. Bartels, S. Gieseke, and A. Kyrieleis, *The process $\gamma(L)^* + q \rightarrow (q \text{ anti-}q g) + q$: Real corrections to the virtual photon impact factor*, *Phys. Rev.* **D65** (2002) 014006, [[hep-ph/0107152](#)].
- [313] J. Bartels, D. Colferai, S. Gieseke, and A. Kyrieleis, *NLO corrections to the photon impact factor: Combining real and virtual corrections*, *Phys. Rev.* **D66** (2002) 094017, [[hep-ph/0208130](#)].
- [314] V. S. Fadin, D. Y. Ivanov, and M. I. Kotsky, *On the calculation of the NLO virtual photon impact factor. ((V))*, *Nucl. Phys.* **B658** (2003) 156–174, [[hep-ph/0210406](#)].
- [315] J. Bartels and A. Kyrieleis, *NLO corrections to the γ^* impact factor: First numerical results for the real corrections to $\gamma^*(L)$* , *Phys. Rev.* **D70** (2004) 114003, [[hep-ph/0407051](#)].
- [316] J. Bartels, D. Colferai, and G. P. Vacca, *The NLO jet vertex for Mueller-Navelet and forward jets: The quark part*, *Eur. Phys. J.* **C24** (2002) 83–99, [[hep-ph/0112283](#)].
- [317] D. Y. Ivanov, M. I. Kotsky, and A. Papa, *The impact factor for the virtual photon to light vector meson transition*, *Eur. Phys. J.* **C38** (2004) 195–213, [[hep-ph/0405297](#)].
- [318] G. P. Salam, *A resummation of large sub-leading corrections at small x* , *JHEP* **07** (1998) 019, [[hep-ph/9806482](#)].
- [319] M. Ciafaloni and D. Colferai, *The BFKL equation at next-to-leading level and beyond*, *Phys. Lett.* **B452** (1999) 372–378, [[hep-ph/9812366](#)].
- [320] M. Ciafaloni, D. Colferai, and G. P. Salam, *Renormalization group improved small- x equation*, *Phys. Rev.* **D60** (1999) 114036, [[hep-ph/9905566](#)].
- [321] G. P. Salam, *An introduction to leading and next-to-leading BFKL*, *Acta Phys. Polon.* **B30** (1999) 3679–3705, [[hep-ph/9910492](#)].
- [322] J. R. Andersen, *A closer look at the analysis of NLL BFKL*, *AIP Conf. Proc.* **792** (2005) 726–732, [[hep-ph/0507215](#)].
- [323] J. Kwiecinski, A. D. Martin, and P. J. Sutton, *Constraints on gluon evolution at small x* , *Z. Phys.* **C71** (1996) 585–594, [[hep-ph/9602320](#)].
- [324] B. Andersson, G. Gustafson, H. Kharraziha, and J. Samuelsson, *Structure Functions and General Final State Properties in the Linked Dipole Chain Model*, *Z. Phys.* **C71** (1996) 613–624.
- [325] B. Andersson, G. Gustafson, and J. Samuelsson, *The Linked dipole chain model for DIS*, *Nucl. Phys.* **B467** (1996) 443–478.

- [326] S. J. Brodsky, V. S. Fadin, V. T. Kim, L. N. Lipatov, and G. B. Pivovarov, *The QCD pomeron with optimal renormalization*, *JETP Lett.* **70** (1999) 155–160, [[hep-ph/9901229](#)].
- [327] S. J. Brodsky, V. S. Fadin, V. T. Kim, L. N. Lipatov, and G. B. Pivovarov, *High-energy QCD asymptotics of photon photon collisions*, *JETP Lett.* **76** (2002) 249–252, [[hep-ph/0207297](#)].
- [328] D. Y. Ivanov and A. Papa, *Electroproduction of two light vector mesons in next-to-leading BFKL: Study of systematic effects*, *Eur. Phys. J.* **C49** (2007) 947–955, [[hep-ph/0610042](#)].
- [329] M. Ciafaloni, D. Colferai, G. P. Salam, and A. M. Stasto, *Renormalisation group improved small- x Green's function*, *Phys. Rev.* **D68** (2003) 114003, [[hep-ph/0307188](#)].
- [330] V. A. Khoze, A. D. Martin, M. G. Ryskin, and W. J. Stirling, *The spread of the gluon $k(t)$ -distribution and the determination of the saturation scale at hadron colliders in resummed NLL BFKL*, *Phys. Rev.* **D70** (2004) 074013, [[hep-ph/0406135](#)].
- [331] R. D. Ball and S. Forte, *Asymptotically free partons at high energy*, *Phys. Lett.* **B405** (1997) 317–326, [[hep-ph/9703417](#)].
- [332] R. D. Ball and S. Forte, *The small x behaviour of Altarelli-Parisi splitting functions*, *Phys. Lett.* **B465** (1999) 271–281, [[hep-ph/9906222](#)].
- [333] G. Altarelli, R. D. Ball, and S. Forte, *Small- x resummation and HERA structure function data*, *Nucl. Phys.* **B599** (2001) 383–423, [[hep-ph/0011270](#)].
- [334] G. Altarelli, R. D. Ball, and S. Forte, *Resummation of singlet parton evolution at small x* , *Nucl. Phys.* **B575** (2000) 313–329, [[hep-ph/9911273](#)].
- [335] G. Altarelli, R. D. Ball, and S. Forte, *Factorization and resummation of small x scaling violations with running coupling*, *Nucl. Phys.* **B621** (2002) 359–387, [[hep-ph/0109178](#)].
- [336] G. Altarelli, R. D. Ball, and S. Forte, *An anomalous dimension for small x evolution*, *Nucl. Phys.* **B674** (2003) 459–483, [[hep-ph/0306156](#)].
- [337] G. Altarelli, R. D. Ball, and S. Forte, *Perturbatively stable resummed small x evolution kernels*, *Nucl. Phys.* **B742** (2006) 1–40, [[hep-ph/0512237](#)].
- [338] R. D. Ball and S. Forte, *All order running coupling BFKL evolution from GLAP (and vice-versa)*, *Nucl. Phys.* **B742** (2006) 158–175, [[hep-ph/0601049](#)].
- [339] S. Marzani, R. D. Ball, P. Falgari, and S. Forte, *BFKL at Next-to-Next-to-Leading Order*, *Nucl. Phys.* **B783** (2007) 143–175, [[/04.2404](#)].
- [340] G. Altarelli, R. D. Ball, and S. Forte, *Small x Resummation with Quarks: Deep-Inelastic Scattering*, *Nucl. Phys.* **B799** (2008) 199–240, [[/02.0032](#)].
- [341] M. Froissart, *Asymptotic behavior and subtractions in the Mandelstam representation*, *Phys. Rev.* **123** (1961) 1053–1057.
- [342] L. N. Lipatov, *Pomeron and odderon in QCD and a two-dimensional conformal field theory*, *Phys. Lett.* **B251** (1990) 284–287.
- [343] L. N. Lipatov, *High-energy asymptotics of multicolor QCD and two-dimensional conformal field theories*, *Phys. Lett.* **B309** (1993) 394–396.
- [344] L. N. Lipatov, *High-energy asymptotics of multicolor QCD and exactly solvable lattice models*, [hep-th/9311037](#).
- [345] L. N. Lipatov, *Asymptotic behavior of multicolor QCD at high energies in connection with exactly solvable spin models*, *JETP Lett.* **59** (1994) 596–599.
- [346] L. D. Faddeev and G. P. Korchemsky, *High-energy QCD as a completely integrable model*, *Phys. Lett.* **B342** (1995) 311–322, [[hep-th/9404173](#)].
- [347] G. P. Korchemsky, *Bethe ansatz for QCD pomeron*, *Nucl. Phys.* **B443** (1995) 255–304, [[hep-ph/9501232](#)].

- [348] R. A. Janik and J. Wosiek, *Solution of the odderon problem*, *Phys. Rev. Lett.* **82** (1999) 1092–1095, [[hep-th/9802100](#)].
- [349] G. P. Korchemsky, J. Kotanski, and A. N. Manashov, *Compound states of reggeized gluons in multi-colour QCD as ground states of noncompact Heisenberg magnet*, *Phys. Rev. Lett.* **88** (2002) 122002, [[hep-ph/0111185](#)].
- [350] S. E. Derkachov, G. P. Korchemsky, and A. N. Manashov, *Noncompact Heisenberg spin magnets from high-energy QCD. I: Baxter Q-operator and separation of variables*, *Nucl. Phys.* **B617** (2001) 375–440, [[hep-th/0107193](#)].
- [351] S. E. Derkachov, G. P. Korchemsky, J. Kotanski, and A. N. Manashov, *Noncompact Heisenberg spin magnets from high-energy QCD. II: Quantization conditions and energy spectrum*, *Nucl. Phys.* **B645** (2002) 237–297, [[hep-th/0204124](#)].
- [352] H. J. De Vega and L. N. Lipatov, *Interaction of Reggeized gluons in the Baxter-Sklyanin representation*, *Phys. Rev.* **D64** (2001) 114019, [[hep-ph/0107225](#)].
- [353] H. J. de Vega and L. N. Lipatov, *Exact resolution of the Baxter equation for reggeized gluon interactions*, *Phys. Rev.* **D66** (2002) 074013, [[hep-ph/0204245](#)].
- [354] J. Bartels, L. N. Lipatov, and G. P. Vacca, *A New Odderon Solution in Perturbative QCD*, *Phys. Lett.* **B477** (2000) 178–186, [[hep-ph/9912423](#)].
- [355] M. A. Braun, *Odderon with a running coupling constant*, *Eur. Phys. J.* **C53** (2008) 59–63, [[/07.2314](#)].
- [356] A. M. Stasto, *Small x resummation and the Odderon*, *Phys. Lett.* **B679** (2009) 288–292, [[/04.4124](#)].
- [357] J. Bartels, *High-energy behavior in a nonabelian gauge theory. 3. multiple discontinuities and particle \rightarrow multi-reggeon vertices*, . DESY-91-074.
- [358] J. Bartels, *Unitarity corrections to the Lipatov pomeron and the small x region in deep inelastic scattering in QCD*, *Phys. Lett.* **B298** (1993) 204–210.
- [359] J. Bartels, *Unitarity corrections to the Lipatov pomeron and the four gluon operator in deep inelastic scattering in QCD*, *Z. Phys.* **C60** (1993) 471–488.
- [360] J. Bartels and M. Wusthoff, *The Triple Regge limit of diffractive dissociation in deep inelastic scattering*, *Z. Phys.* **C66** (1995) 157–180.
- [361] J. Bartels and C. Ewerz, *Unitarity corrections in high-energy QCD*, *JHEP* **09** (1999) 026, [[hep-ph/9908454](#)].
- [362] V. N. Gribov, *A reggeon diagram technique*, *Sov. Phys. JETP* **26** (1968) 414–422.
- [363] J. Bartels, L. N. Lipatov, and M. Wusthoff, *Conformal Invariance of the Transition Vertex $2 \rightarrow 4$ gluons*, *Nucl. Phys.* **B464** (1996) 298–318, [[hep-ph/9509303](#)].
- [364] G. P. Korchemsky, *Conformal bootstrap for the BFKL pomeron*, *Nucl. Phys.* **B550** (1999) 397–423, [[hep-ph/9711277](#)].
- [365] R. B. Peschanski, *Dual Shapiro-Virasoro amplitudes in the QCD dipole picture*, *Phys. Lett.* **B409** (1997) 491–498, [[hep-ph/9704342](#)].
- [366] A. Bialas, H. Navelet, and R. B. Peschanski, *The QCD triple pomeron coupling from string amplitudes*, *Phys. Rev.* **D57** (1998) 6585–6589, [[hep-ph/9711442](#)].
- [367] A. Bialas, H. Navelet, and R. B. Peschanski, *High-mass diffraction in the QCD dipole picture*, *Phys. Lett.* **B427** (1998) 147–154, [[hep-ph/9711236](#)].
- [368] I. Balitsky, *Operator expansion for high-energy scattering*, *Nucl. Phys.* **B463** (1996) 99–160, [[hep-ph/9509348](#)].
- [369] I. Balitsky, *Factorization for high-energy scattering*, *Phys. Rev. Lett.* **81** (1998) 2024–2027, [[hep-ph/9807434](#)].
- [370] I. Balitsky, *Factorization and high-energy effective action*, *Phys. Rev.* **D60** (1999) 014020, [[hep-ph/9812311](#)].
- [371] I. Balitsky, *Effective field theory for the small- x evolution*, *Phys. Lett.* **B518** (2001) 235–242, [[hep-ph/0105334](#)].
- [372] Y. V. Kovchegov, *Small- x F_2 structure function of a nucleus including multiple pomeron exchanges*, *Phys. Rev.*

- D60** (1999) 034008, [[hep-ph/9901281](#)].
- [373] Y. V. Kovchegov, *Unitarization of the BFKL pomeron on a nucleus*, *Phys. Rev.* **D61** (2000) 074018, [[hep-ph/9905214](#)].
- [374] R. Kirschner, L. N. Lipatov, and L. Szymanowski, *Effective action for multi - Regge processes in QCD*, *Nucl. Phys.* **B425** (1994) 579–594, [[hep-th/9402010](#)].
- [375] R. Kirschner, L. N. Lipatov, and L. Szymanowski, *Symmetry properties of the effective action for high-energy scattering in QCD*, *Phys. Rev.* **D51** (1995) 838–855, [[hep-th/9403082](#)].
- [376] L. N. Lipatov, *Gauge invariant effective action for high-energy processes in QCD*, *Nucl. Phys.* **B452** (1995) 369–400, [[hep-ph/9502308](#)].
- [377] E. N. Antonov, L. N. Lipatov, E. A. Kuraev, and I. O. Cherednikov, *Feynman rules for effective Regge action*, *Nucl. Phys.* **B721** (2005) 111–135, [[hep-ph/0411185](#)].
- [378] V. A. Abramovsky, V. N. Gribov, and O. V. Kancheli, *Character of inclusive spectra and fluctuations produced in inelastic processes by multi - Pomeron exchange*, *Yad. Fiz.* **18** (1973) 595–616.
- [379] J. Bartels and M. G. Ryskin, *The space-time picture of the wee partons and the AGK cutting rules in perturbative QCD*, *Z. Phys.* **C76** (1997) 241–255, [[hep-ph/9612226](#)].
- [380] J. Bartels, M. Salvadore, and G. P. Vacca, *AGK cutting rules and multiple scattering in hadronic collisions*, *Eur. Phys. J.* **C42** (2005) 53–71, [[hep-ph/0503049](#)].
- [381] J. Jalilian-Marian, A. Kovner, A. Leonidov, and H. Weigert, *The Wilson renormalization group for low x physics: Towards the high density regime*, *Phys. Rev.* **D59** (1999) 014014, [[hep-ph/9706377](#)].
- [382] J. Jalilian-Marian, A. Kovner, and H. Weigert, *The Wilson renormalization group for low x physics: Gluon evolution at finite parton density*, *Phys. Rev.* **D59** (1999) 014015, [[hep-ph/9709432](#)].
- [383] J. Jalilian-Marian, A. Kovner, A. Leonidov, and H. Weigert, *The BFKL equation from the Wilson renormalization group*, *Nucl. Phys.* **B504** (1997) 415–431, [[hep-ph/9701284](#)].
- [384] J. Jalilian-Marian, A. Kovner, A. Leonidov, and H. Weigert, *Unitarization of gluon distribution in the doubly logarithmic regime at high density*, *Phys. Rev.* **D59** (1999) 034007, [[hep-ph/9807462](#)].
- [385] A. Kovner, J. G. Milhano, and H. Weigert, *Relating different approaches to nonlinear QCD evolution at finite gluon density*, *Phys. Rev.* **D62** (2000) 114005, [[hep-ph/0004014](#)].
- [386] E. Iancu, A. Leonidov, and L. D. McLerran, *Nonlinear gluon evolution in the color glass condensate. I*, *Nucl. Phys.* **A692** (2001) 583–645, [[hep-ph/0011241](#)].
- [387] E. Iancu, A. Leonidov, and L. D. McLerran, *The renormalization group equation for the color glass condensate*, *Phys. Lett.* **B510** (2001) 133–144, [[hep-ph/0102009](#)].
- [388] E. Ferreira, E. Iancu, A. Leonidov, and L. McLerran, *Nonlinear gluon evolution in the color glass condensate. II*, *Nucl. Phys.* **A703** (2002) 489–538, [[hep-ph/0109115](#)].
- [389] H. Weigert, *Unitarity at small Bjorken x* , *Nucl. Phys.* **A703** (2002) 823–860, [[hep-ph/0004044](#)].
- [390] E. Iancu, A. Leonidov, and L. McLerran, *The colour glass condensate: An introduction*, [hep-ph/0202270](#).
- [391] S. Munier and R. B. Peschanski, *Geometric scaling as traveling waves*, *Phys. Rev. Lett.* **91** (2003) 232001, [[hep-ph/0309177](#)].
- [392] S. Munier and R. B. Peschanski, *Traveling wave fronts and the transition to saturation*, *Phys. Rev.* **D69** (2004) 034008, [[hep-ph/0310357](#)].
- [393] S. Munier and R. B. Peschanski, *Universality and tree structure of high energy QCD*, *Phys. Rev.* **D70** (2004) 077503, [[hep-ph/0401215](#)].
- [394] E. Iancu, A. H. Mueller, and S. Munier, *Universal behavior of QCD amplitudes at high energy from general tools of statistical physics*, *Phys. Lett.* **B606** (2005) 342–350, [[hep-ph/0410018](#)].

- [395] S. Munier, *Quantum chromodynamics at high energy and statistical physics*, *Phys. Rept.* **473** (2009) 1–49, [[arXiv:0901.2823](#)].
- [396] A. M. Stasto, K. J. Golec-Biernat, and J. Kwiecinski, *Geometric scaling for the total gamma* p cross-section in the low x region*, *Phys. Rev. Lett.* **86** (2001) 596–599, [[hep-ph/0007192](#)].
- [397] K. J. Golec-Biernat and M. Wusthoff, *Saturation effects in deep inelastic scattering at low q**2 and its implications on diffraction*, *Phys. Rev.* **D59** (1999) 014017, [[hep-ph/9807513](#)].
- [398] K. J. Golec-Biernat and M. Wusthoff, *Saturation in diffractive deep inelastic scattering*, *Phys. Rev.* **D60** (1999) 114023, [[hep-ph/9903358](#)].
- [399] C. Marquet and L. Schoeffel, *Geometric scaling in diffractive deep inelastic scattering*, *Phys. Lett.* **B639** (2006) 471–477, [[hep-ph/0606079](#)].
- [400] J. Bartels, K. J. Golec-Biernat, and H. Kowalski, *A modification of the saturation model: DGLAP evolution*, *Phys. Rev.* **D66** (2002) 014001, [[hep-ph/0203258](#)].
- [401] **H1** Collaboration, C. Adloff *et. al.*, *Deep-inelastic inclusive e p scattering at low x and a determination of alpha(s)*, *Eur. Phys. J.* **C21** (2001) 33–61, [[hep-ex/0012053](#)].
- [402] **ZEUS** Collaboration, J. Breitweg *et. al.*, *Measurement of the proton structure function F2 at very low Q**2 at HERA*, *Phys. Lett.* **B487** (2000) 53–73, [[hep-ex/0005018](#)].
- [403] **ZEUS** Collaboration, S. Chekanov *et. al.*, *Measurement of the neutral current cross section and F2 structure function for deep inelastic e+ p scattering at HERA*, *Eur. Phys. J.* **C21** (2001) 443–471, [[hep-ex/0105090](#)].
- [404] **E665** Collaboration, M. R. Adams *et. al.*, *Proton and deuteron structure functions in muon scattering at 470-GeV*, *Phys. Rev.* **D54** (1996) 3006–3056.
- [405] **New Muon** Collaboration, M. Arneodo *et. al.*, *Measurement of the proton and deuteron structure functions, F2(p) and F2(d), and of the ratio sigma(L)/sigma(T)*, *Nucl. Phys.* **B483** (1997) 3–43, [[hep-ph/9610231](#)].
- [406] E. Iancu, K. Itakura, and S. Munier, *Saturation and BFKL dynamics in the HERA data at small x*, *Phys. Lett.* **B590** (2004) 199–208, [[hep-ph/0310338](#)].
- [407] A. H. Mueller, *Small x Behavior and Parton Saturation: A QCD Model*, *Nucl. Phys.* **B335** (1990) 115.
- [408] S. Munier, A. M. Stasto, and A. H. Mueller, *Impact parameter dependent S-matrix for dipole proton scattering from diffractive meson electroproduction*, *Nucl. Phys.* **B603** (2001) 427–445, [[hep-ph/0102291](#)].
- [409] S. Munier, R. B. Peschanski, and C. Royon, *Hard diffraction at HERA in the dipole model of BFKL dynamics*, *Nucl. Phys.* **B534** (1998) 297–317, [[hep-ph/9807488](#)].
- [410] J. Nemchik, N. N. Nikolaev, and B. G. Zakharov, *Scanning the BFKL pomeron in elastic production of vector mesons at HERA*, *Phys. Lett.* **B341** (1994) 228–237, [[hep-ph/9405355](#)].
- [411] J. Nemchik, N. N. Nikolaev, E. Predazzi, and B. G. Zakharov, *Color dipole phenomenology of diffractive electroproduction of light vector mesons at HERA*, *Z. Phys.* **C75** (1997) 71–87, [[hep-ph/9605231](#)].
- [412] P. Marage, *Diffraction at HERA*, [hep-ph/0104196](#).
- [413] **H1** Collaboration, C. Adloff *et. al.*, *Elastic electroproduction of rho mesons at HERA*, *Eur. Phys. J.* **C13** (2000) 371–396, [[hep-ex/9902019](#)].
- [414] A. C. Caldwell and M. S. Soares, *Vector meson production in the Golec-Biernat Wuesthoff model*, *Nucl. Phys.* **A696** (2001) 125–137, [[hep-ph/0101085](#)].
- [415] K. J. Golec-Biernat and A. M. Stasto, *On solutions of the Balitsky-Kovchegov equation with impact parameter*, *Nucl. Phys.* **B668** (2003) 345–363, [[hep-ph/0306279](#)].
- [416] C. Marquet, R. B. Peschanski, and G. Soyez, *Traveling waves and geometric scaling at non-zero momentum transfer*, *Nucl. Phys.* **A756** (2005) 399–418, [[hep-ph/0502020](#)].
- [417] C. Marquet, R. B. Peschanski, and G. Soyez, *Exclusive vector meson production at HERA from QCD with*

- saturation, *Phys. Rev.* **D76** (2007) 034011, [[hep-ph/0702171](#)].
- [418] J. C. Collins, *Light cone variables, rapidity and all that*, [hep-ph/9705393](#).
- [419] A. H. Mueller and H. Navelet, *An Inclusive Minijet Cross-Section and the Bare Pomeron in QCD*, *Nucl. Phys.* **B282** (1987) 727.
- [420] **D0** Collaboration, B. Abbott *et al.*, *Probing BFKL dynamics in the dijet cross section at large rapidity intervals in $p\bar{p}$ collisions at $\sqrt{s} = 1800$ GeV and 630-GeV*, *Phys. Rev. Lett.* **84** (2000) 5722–5727, [[hep-ex/9912032](#)].
- [421] J. R. Andersen, V. D. Duca, S. Frixione, C. R. Schmidt, and W. J. Stirling, *Mueller-Navelet jets at hadron colliders*, *JHEP* **02** (2001) 007, [[hep-ph/0101180](#)].
- [422] V. Del Duca and C. R. Schmidt, *Dijet production at large rapidity intervals*, *Phys. Rev.* **D49** (1994) 4510–4516, [[hep-ph/9311290](#)].
- [423] W. J. Stirling, *Production of jet pairs at large relative rapidity in hadron hadron collisions as a probe of the perturbative Pomeron*, *Nucl. Phys.* **B423** (1994) 56–79, [[hep-ph/9401266](#)].
- [424] V. Del Duca and C. R. Schmidt, *BFKL versus $O(\alpha_s^{**3})$ corrections to large rapidity dijet production*, *Phys. Rev.* **D51** (1995) 2150–2158, [[hep-ph/9407359](#)].
- [425] L. H. Orr and W. J. Stirling, *Dijet production at hadron hadron colliders in the BFKL approach*, *Phys. Rev.* **D56** (1997) 5875–5884, [[hep-ph/9706529](#)].
- [426] J. Kwiecinski, A. D. Martin, L. Motyka, and J. Outhwaite, *Azimuthal decorrelation of forward and backward jets at the Tevatron*, *Phys. Lett.* **B514** (2001) 355–360, [[hep-ph/0105039](#)].
- [427] W. T. Giele, E. W. N. Glover, and D. A. Kosower, *Higher order corrections to jet cross-sections in hadron colliders*, *Nucl. Phys.* **B403** (1993) 633–670, [[hep-ph/9302225](#)].
- [428] G. Marchesini *et al.*, *HERWIG: A Monte Carlo event generator for simulating hadron emission reactions with interfering gluons. Version 5.1 - April 1991*, *Comput. Phys. Commun.* **67** (1992) 465–508.
- [429] A. S. Vera, *The Effect of NLO conformal spins in azimuthal angle decorrelation of jet pairs*, *Nucl. Phys.* **B746** (2006) 1–14, [[hep-ph/0602250](#)].
- [430] A. S. Vera and F. Schwennsen, *The azimuthal decorrelation of jets widely separated in rapidity as a test of the BFKL kernel*, *Nucl. Phys.* **B776** (2007) 170–186, [[hep-ph/0702158](#)].
- [431] C. Marquet and C. Royon, *Azimuthal decorrelation of Mueller-Navelet jets at the Tevatron and the LHC*, *Phys. Rev.* **D79** (2009) 034028, [[arXiv:0704.3409](#)].
- [432] **CMS** Collaboration, S. Cerci and D. d’Enterria, *Low- x QCD studies with forward jets in proton-proton collisions at $\sqrt{s} = 14$ TeV in CMS*, *AIP Conf. Proc.* **1105** (2009) 28–32, [[arXiv:0812.2665](#)].
- [433] J. Bartels, D. Colferai, and G. P. Vacca, *The NLO jet vertex for Mueller-Navelet and forward jets: The gluon part*, *Eur. Phys. J.* **C29** (2003) 235–249, [[hep-ph/0206290](#)].
- [434] A. D. Martin, W. J. Stirling, R. S. Thorne, and G. Watt, *Parton distributions for the LHC*, *Eur. Phys. J.* **C63** (2009) 189–285, [[arXiv:0901.0002](#)].
- [435] S. D. Ellis, Z. Kunszt, and D. E. Soper, *The One Jet Inclusive Cross-Section at Order α_s^{**3} . 1. Gluons Only*, *Phys. Rev.* **D40** (1989) 2188.
- [436] V. S. Fadin, *BFKL news*, [hep-ph/9807528](#).
- [437] V. S. Fadin and A. D. Martin, *Infrared safety of impact factors for colorless particle interactions*, *Phys. Rev.* **D60** (1999) 114008, [[hep-ph/9904505](#)].
- [438] A. V. Kotikov and L. N. Lipatov, *NLO corrections to the BFKL equation in QCD and in supersymmetric gauge theories*, *Nucl. Phys.* **B582** (2000) 19–43, [[hep-ph/0004008](#)].
- [439] D. Y. Ivanov and A. Papa, *Electroproduction of two light vector mesons in the next- to-leading approximation*, *Nucl. Phys.* **B732** (2006) 183–199, [[hep-ph/0508162](#)].

- [440] F. Schwennsen, *Phenomenology of jet physics in the BFKL formalism at NLO*, [hep-ph/0703198](#).
- [441] T. Hahn, *CUBA: A library for multidimensional numerical integration*, *Comput. Phys. Commun.* **168** (2005) 78–95, [[hep-ph/0404043](#)].
- [442] T. Sjostrand, S. Mrenna, and P. Skands, *PYTHIA 6.4 Physics and Manual*, *JHEP* **05** (2006) 026, [[hep-ph/0603175](#)].
- [443] F. Caporale, A. Papa, and A. S. Vera, *Collinear improvement of the BFKL kernel in the electroproduction of two light vector mesons*, *Eur. Phys. J.* **C53** (2008) 525–532, [[/07.4100](#)].
- [444] M. Fontannaz, *Dijet azimuthal correlations in hadron-hadron collisions at high energy*, *LPT-Orsay/09-86* (2009).
- [445] P. Aurenche, R. Basu, and M. Fontannaz, *Jet-jet and hadron-jet correlations in hadro- and electro- production*, *Eur. Phys. J.* **C57** (2008) 681–688, [[arXiv:0807.2133](#)].
- [446] M. Fontannaz, J. P. Guillet, and G. Heinrich, *Is a large intrinsic $k(T)$ needed to describe photon + jet photoproduction at HERA?*, *Eur. Phys. J.* **C22** (2001) 303–315, [[hep-ph/0107262](#)].
- [447] A. H. Mueller and W.-K. Tang, *High-energy parton-parton elastic scattering in QCD*, *Phys. Lett.* **B284** (1992) 123–126.
- [448] J. Bartels, J. R. Forshaw, H. Lotter, L. N. Lipatov, M. G. Ryskin, and M. Wusthoff, *How does the BFKL pomeron couple to quarks?*, *Phys. Lett.* **B348** (1995) 589–596, [[hep-ph/9501204](#)].
- [449] J. Bartels, L. N. Lipatov, M. Salvadore, and G. P. Vacca, *Deformed spectral representation of the BFKL kernel and the bootstrap for gluon reggeization*, *Nucl. Phys.* **B726** (2005) 53–74, [[hep-ph/0506235](#)].
- [450] **CDF** Collaboration, F. Abe *et. al.*, *Dijet production by color-singlet exchange at the Fermilab Tevatron*, *Phys. Rev. Lett.* **80** (1998) 1156–1161.
- [451] **D0** Collaboration, B. Abbott *et. al.*, *Probing hard color-singlet exchange in $p\bar{p}$ collisions at $\sqrt{s} = 630$ GeV and 1800 GeV*, *Phys. Lett.* **B440** (1998) 189–202, [[hep-ex/9809016](#)].
- [452] B. Cox, J. R. Forshaw, and L. Lonnblad, *Hard color singlet exchange at the Tevatron*, *JHEP* **10** (1999) 023, [[hep-ph/9908464](#)].
- [453] R. Enberg, G. Ingelman, and L. Motyka, *Hard colour singlet exchange and gaps between jets at the Tevatron*, *Phys. Lett.* **B524** (2002) 273–282, [[hep-ph/0111090](#)].
- [454] F. Chevallier, O. Kepka, C. Marquet, and C. Royon, *Gaps between jets at hadron colliders in the next-to- leading BFKL framework*, *Phys. Rev.* **D79** (2009) 094019, [[arXiv:0903.4598](#)].
- [455] A. Bialas and P. V. Landshoff, *Higgs production in $p p$ collisions by double Pomeron exchange*, *Phys. Lett.* **B256** (1991) 540–546.
- [456] V. A. Khoze, A. D. Martin, and M. G. Ryskin, *Diffraction Higgs production: Myths and reality*, *Eur. Phys. J.* **C26** (2002) 229–236, [[hep-ph/0207313](#)].
- [457] A. De Roeck, V. A. Khoze, A. D. Martin, R. Orava, and M. G. Ryskin, *Ways to detect a light Higgs boson at the LHC*, *Eur. Phys. J.* **C25** (2002) 391–403, [[hep-ph/0207042](#)].
- [458] A. B. Kaidalov, V. A. Khoze, A. D. Martin, and M. G. Ryskin, *Extending the study of the Higgs sector at the LHC by proton tagging*, *Eur. Phys. J.* **C33** (2004) 261–271, [[hep-ph/0311023](#)].
- [459] **FP420 R and D** Collaboration, M. G. Albrow *et. al.*, *The FP420 R&D Project: Higgs and New Physics with forward protons at the LHC*, *JINST* **4** (2009) T10001, [[arXiv:0806.0302](#)].
- [460] B. Cox, J. R. Forshaw, and B. Heinemann, *Double diffractive Higgs and di-photon production at the Tevatron and LHC*, *Phys. Lett.* **B540** (2002) 263–268, [[hep-ph/0110173](#)].
- [461] M. Boonekamp, R. B. Peschanski, and C. Royon, *Inclusive Higgs boson and dijet production via double pomeron exchange*, *Phys. Rev. Lett.* **87** (2001) 251806, [[hep-ph/0107113](#)].
- [462] M. Boonekamp, A. D. Roeck, R. B. Peschanski, and C. Royon, *Higgs boson production via double pomeron*

- exchange at the LHC, *Acta Phys. Polon.* **B33** (2002) 3485–3490, [[hep-ph/0205332](#)].
- [463] R. B. Appleby and J. R. Forshaw, *Diffraction dijet production*, *Phys. Lett.* **B541** (2002) 108–114, [[hep-ph/0111077](#)].
- [464] J. Bartels, S. Bondarenko, K. Kutak, and L. Motyka, *Exclusive Higgs boson production at the LHC: Hard rescattering corrections*, *Phys. Rev.* **D73** (2006) 093004, [[hep-ph/0601128](#)].
- [465] V. A. Khoze, A. D. Martin, and M. G. Ryskin, *On the role of hard rescattering in exclusive diffractive Higgs production*, *JHEP* **05** (2006) 036, [[hep-ph/0602247](#)].
- [466] D. Ostrovsky, *NLO correction to one-particle inclusive production at high energies*, *Phys. Rev.* **D62** (2000) 054028, [[hep-ph/9912258](#)].
- [467] J. Bartels, A. S. Vera, and F. Schwennsen, *NLO inclusive jet production in $k(T)$ -factorization*, *JHEP* **11** (2006) 051, [[hep-ph/0608154](#)].
- [468] A. J. Askew, K. J. Golec-Biernat, J. Kwiecinski, A. D. Martin, and P. J. Sutton, *Implications of scaling violations of F_2 at HERA for perturbative QCD*, *Phys. Lett.* **B325** (1994) 212–218, [[hep-ph/9311376](#)].
- [469] S. Munier and R. B. Peschanski, *High energy factorization predictions for the charm structure function $F_2(c)$ at HERA*, *Nucl. Phys.* **B524** (1998) 377–393, [[hep-ph/9802230](#)].
- [470] A. D. Martin, W. J. Stirling, R. S. Thorne, and G. Watt, *Update of parton distributions at NNLO*, *Phys. Lett.* **B652** (2007) 292–299, [[arXiv:0706.0459](#)].
- [471] G. Ingelman and P. E. Schlein, *Jet Structure in High Mass Diffractive Scattering*, *Phys. Lett.* **B152** (1985) 256.
- [472] **H1** Collaboration, A. Aktas *et al.*, *Measurement and QCD analysis of the diffractive deep- inelastic scattering cross-section at HERA*, *Eur. Phys. J.* **C48** (2006) 715–748, [[hep-ex/0606004](#)].
- [473] **H1** Collaboration, A. Aktas *et al.*, *Diffractive deep-inelastic scattering with a leading proton at HERA*, *Eur. Phys. J.* **C48** (2006) 749–766, [[hep-ex/0606003](#)].
- [474] **ZEUS** Collaboration, S. Chekanov *et al.*, *Study of deep inelastic inclusive and diffractive scattering with the ZEUS forward plug calorimeter*, *Nucl. Phys.* **B713** (2005) 3–80, [[hep-ex/0501060](#)].
- [475] **ZEUS** Collaboration, S. Chekanov *et al.*, *Dissociation of virtual photons in events with a leading proton at HERA*, *Eur. Phys. J.* **C38** (2004) 43–67, [[hep-ex/0408009](#)].
- [476] J. Bartels, J. R. Ellis, H. Kowalski, and M. Wusthoff, *An analysis of diffraction in deep-inelastic scattering*, *Eur. Phys. J.* **C7** (1999) 443–458, [[hep-ph/9803497](#)].
- [477] J. Bartels and C. Royon, *A parametrisation of the inclusive diffractive cross section at HERA*, *Mod. Phys. Lett.* **A14** (1999) 1583–1598, [[hep-ph/9809344](#)].
- [478] A. Bialas, R. B. Peschanski, and C. Royon, *Towards a unified description of total and diffractive structure functions at HERA in the QCD dipole picture*, *Phys. Rev.* **D57** (1998) 6899–6905, [[hep-ph/9712216](#)].
- [479] C. Royon, L. Schoeffel, S. Sapeta, R. B. Peschanski, and E. Sauvan, *A global analysis of inclusive diffractive cross sections at HERA*, *Nucl. Phys.* **B781** (2007) 1–31, [[hep-ph/0609291](#)].
- [480] R. B. Peschanski, C. Royon, and L. Schoeffel, *Confronting next-leading BFKL kernels with proton structure function data*, *Nucl. Phys.* **B716** (2005) 401–420, [[hep-ph/0411338](#)].
- [481] J. Kwiecinski, A. D. Martin, P. J. Sutton, and K. J. Golec-Biernat, *QCD predictions for the transverse energy flow in deep inelastic scattering in the HERA small x regime*, *Phys. Rev.* **D50** (1994) 217–225, [[hep-ph/9403292](#)].
- [482] K. J. Golec-Biernat, J. Kwiecinski, A. D. Martin, and P. J. Sutton, *Transverse energy flow at HERA*, *Phys. Lett.* **B335** (1994) 220–225, [[hep-ph/9405400](#)].
- [483] **H1** Collaboration, C. Adloff *et al.*, *Measurement of charged particle transverse momentum spectra in deep inelastic scattering*, *Nucl. Phys.* **B485** (1997) 3–24, [[hep-ex/9610006](#)].
- [484] **H1** Collaboration, C. Adloff *et al.*, *Measurements of transverse energy flow in deep inelastic- scattering at*

- HERA, *Eur. Phys. J.* **C12** (2000) 595–607, [[hep-ex/9907027](#)].
- [485] A. H. Mueller, *Parton distributions at very small x values*, *Nucl. Phys. Proc. Suppl.* **18C** (1991) 125–132.
- [486] A. H. Mueller, *Jets at LEP and HERA*, *J. Phys.* **G17** (1991) 1443–1454.
- [487] A. Sabio Vera and F. Schwennsen, *Azimuthal decorrelation of forward jets in Deep Inelastic Scattering*, *Phys. Rev.* **D77** (2008) 014001, [[arXiv:0708.0549](#)].
- [488] **H1** Collaboration, S. Aid *et. al.*, *Transverse energy and forward jet production in the low x regime at HERA*, *Phys. Lett.* **B356** (1995) 118–128, [[hep-ex/9506012](#)].
- [489] **ZEUS** Collaboration, J. Breitweg *et. al.*, *Forward jet production in deep inelastic scattering at HERA*, *Eur. Phys. J.* **C6** (1999) 239–252, [[hep-ex/9805016](#)].
- [490] **H1** Collaboration, C. Adloff *et. al.*, *Forward jet and particle production at HERA*, *Nucl. Phys.* **B538** (1999) 3–22, [[hep-ex/9809028](#)].
- [491] H. Jung, *Hard diffractive scattering in high-energy $e p$ collisions and the Monte Carlo generator RAPGAP*, *Comp. Phys. Commun.* **86** (1995) 147–161.
- [492] *RAPGAP*, <http://projects.hepforge.org/rapgap/>.
- [493] **H1** Collaboration, A. Aktas *et. al.*, *Forward jet production in deep inelastic scattering at HERA*, *Eur. Phys. J.* **C46** (2006) 27–42, [[hep-ex/0508055](#)].
- [494] **ZEUS** Collaboration, S. Chekanov *et. al.*, *Forward-jet production in deep inelastic ep scattering at HERA*, *Eur. Phys. J.* **C52** (2007) 515–530, [[arXiv:0707.3093](#)].
- [495] H. Jung and G. P. Salam, *Hadronic final state predictions from CCFM: The hadron- level Monte Carlo generator CASCADE*, *Eur. Phys. J.* **C19** (2001) 351–360, [[hep-ph/0012143](#)].
- [496] H. Jung, *The CCFM Monte Carlo generator CASCADE*, *Comput. Phys. Commun.* **143** (2002) 100–111, [[hep-ph/0109102](#)].
- [497] M. Ciafaloni, *Coherence Effects in Initial Jets at Small q^{*2} / s* , *Nucl. Phys.* **B296** (1988) 49.
- [498] S. Catani, F. Fiorani, and G. Marchesini, *QCD Coherence in Initial State Radiation*, *Phys. Lett.* **B234** (1990) 339.
- [499] S. Catani, F. Fiorani, and G. Marchesini, *Small x behavior of initial state radiation in perturbative QCD*, *Nucl. Phys.* **B336** (1990) 18.
- [500] G. Marchesini, *QCD coherence in the structure function and associated distributions at small x* , *Nucl. Phys.* **B445** (1995) 49–80, [[hep-ph/9412327](#)].
- [501] B. Andersson, G. Gustafson, L. Lonnblad, and U. Pettersson, *Coherence Effects in Deep Inelastic Scattering*, *Z. Phys.* **C43** (1989) 625.
- [502] L. Lonnblad, *Rapidity gaps and other final state properties in the color dipole model for deep inelastic scattering*, *Z. Phys.* **C65** (1995) 285–292.
- [503] L. Lonnblad, *ARIADNE version 4: A Program for simulation of QCD cascades implementing the color dipole model*, *Comput. Phys. Commun.* **71** (1992) 15–31.
- [504] P. Aurenche, R. Basu, M. Fontannaz, and R. M. Godbole, *Deep inelastic scattering and forward π^0 production at NLO*, *Eur. Phys. J.* **C42** (2005) 43–52, [[hep-ph/0504008](#)].
- [505] O. Kepka, C. Royon, C. Marquet, and R. B. Peschanski, *Next-leading BFKL effects in forward-jet production at HERA*, *Phys. Lett.* **B655** (2007) 236–240, [[hep-ph/0609299](#)].
- [506] O. Kepka, C. Royon, C. Marquet, and R. B. Peschanski, *Next-to-leading BFKL phenomenology of forward-jet cross sections at HERA*, *Eur. Phys. J.* **C55** (2008) 259–272, [[hep-ph/0612261](#)].
- [507] J. Kwiecinski, S. C. Lang, and A. D. Martin, *Deep inelastic events containing a forward photon as a probe of*

- small x dynamics*, *Phys. Rev.* **D54** (1996) 1874–1880, [[hep-ph/9603361](#)].
- [508] J. Bartels, V. D. Duca, and M. Wusthoff, *Azimuthal dependence of forward-jet production in DIS in the high-energy limit*, *Z. Phys.* **C76** (1997) 75–79, [[hep-ph/9610450](#)].
- [509] I. F. Ginzburg, S. L. Panfil, and V. G. Serbo, *Possibility of the experimental investigation of the QCD Pomeron in semihard processes at the gamma gamma collisions*, *Nucl. Phys.* **B284** (1987) 685–705.
- [510] I. F. Ginzburg, S. L. Panfil, and V. G. Serbo, *The semihard processes gamma gamma \rightarrow Psi X, gamma gamma \rightarrow Psi Psi, gamma gamma \rightarrow rho Psi*, *Nucl. Phys.* **B296** (1988) 569–581.
- [511] M. G. Ryskin, *Diffraction J / psi electroproduction in LLA QCD*, *Z. Phys.* **C57** (1993) 89–92.
- [512] D. Y. Ivanov, *Diffraction light vector meson production at large momentum transfers*, *Phys. Rev.* **D53** (1996) 3564–3572, [[hep-ph/9508319](#)].
- [513] J. R. Forshaw and M. G. Ryskin, *Diffraction vector meson production at large momentum transfer*, *Z. Phys.* **C68** (1995) 137–148, [[hep-ph/9501376](#)].
- [514] J. Bartels, J. R. Forshaw, H. Lotter, and M. Wusthoff, *Diffraction Production of Vector Mesons at Large t*, *Phys. Lett.* **B375** (1996) 301–309, [[hep-ph/9601201](#)].
- [515] L. Frankfurt, W. Koepf, and M. Strikman, *Diffraction heavy quarkonium photo- and electroproduction in QCD*, *Phys. Rev.* **D57** (1998) 512–526, [[hep-ph/9702216](#)].
- [516] A. D. Martin, M. G. Ryskin, and T. Teubner, *The QCD description of diffraction rho meson electroproduction*, *Phys. Rev.* **D55** (1997) 4329–4337, [[hep-ph/9609448](#)].
- [517] A. D. Martin, M. G. Ryskin, and T. Teubner, *Diffraction electroproduction of rho meson excitations*, *Phys. Rev.* **D56** (1997) 3007–3010, [[hep-ph/9701366](#)].
- [518] A. D. Martin, M. G. Ryskin, and T. Teubner, *Q**2 dependence of diffraction vector meson electroproduction*, *Phys. Rev.* **D62** (2000) 014022, [[hep-ph/9912551](#)].
- [519] I. F. Ginzburg and D. Y. Ivanov, *The q 2 dependence of the hard diffraction photoproduction of vector meson or photon and the range of pQCD validity*, *Phys. Rev.* **D54** (1996) 5523–5535, [[hep-ph/9604437](#)].
- [520] D. Y. Ivanov and R. Kirschner, *Polarization in diffraction electroproduction of light vector mesons*, *Phys. Rev.* **D58** (1998) 114026, [[hep-ph/9807324](#)].
- [521] D. Y. Ivanov, R. Kirschner, A. Schafer, and L. Szymanowski, *The light vector meson photoproduction at large t*, *Phys. Lett.* **B478** (2000) 101–113, [[hep-ph/0001255](#)].
- [522] J. R. Forshaw and G. Poludniowski, *Vector meson photoproduction at high-t and comparison to HERA data*, *Eur. Phys. J.* **C26** (2003) 411–415, [[hep-ph/0107068](#)].
- [523] R. Enberg, L. Motyka, and G. Poludniowski, *Diffraction heavy vector meson production from the BFKL equation*, *Eur. Phys. J.* **C26** (2002) 219–228, [[hep-ph/0207027](#)].
- [524] R. Enberg, J. R. Forshaw, L. Motyka, and G. Poludniowski, *Vector meson photoproduction from the BFKL equation. I: Theory*, *JHEP* **09** (2003) 008, [[hep-ph/0306232](#)].
- [525] G. G. Poludniowski, R. Enberg, J. R. Forshaw, and L. Motyka, *Vector meson photoproduction from the BFKL equation. II: Phenomenology*, *JHEP* **12** (2003) 002, [[hep-ph/0311017](#)].
- [526] I. I. Balitsky and L. N. Lipatov, *Calculation of meson meson interaction cross-section in Quantum Chromodynamics. (in Russian)*, *JETP Lett.* **30** (1979) 355.
- [527] A. Ivanov and R. Kirschner, *Electroproduction of vector mesons: Factorization of end- point contributions*, *Eur. Phys. J.* **C29** (2003) 353–364, [[hep-ph/0301182](#)].
- [528] A. Ivanov and R. Kirschner, *Diffraction large transferred momentum photoproduction of vector mesons*, *Eur. Phys. J.* **C36** (2004) 43–48, [[hep-ph/0311077](#)].
- [529] D. Y. Ivanov and M. Wusthoff, *Hard diffraction photon proton scattering at large t*, *Eur. Phys. J.* **C8** (1999)

- 107–114, [[hep-ph/9808455](#)].
- [530] N. G. Evanson and J. R. Forshaw, *Diffractive photon production in gamma p and gamma gamma interactions*, *Phys. Rev.* **D60** (1999) 034016, [[hep-ph/9902481](#)].
- [531] B. E. Cox and J. R. Forshaw, *Diffractive production of high-p(T) photons at HERA*, *J. Phys.* **G26** (2000) 702–706, [[hep-ph/9912486](#)].
- [532] **H1** Collaboration, F. D. Aaron *et. al.*, *Measurement of Diffractive Scattering of Photons with Large Momentum Transfer at HERA*, *Phys. Lett.* **B672** (2009) 219–226, [[arXiv:0810.3096](#)].
- [533] A. G. Shuvaev, K. J. Golec-Biernat, A. D. Martin, and M. G. Ryskin, *Off-diagonal distributions fixed by diagonal partons at small x and xi*, *Phys. Rev.* **D60** (1999) 014015, [[hep-ph/9902410](#)].
- [534] A. Shuvaev, *Solution of the off-forward leading logarithmic evolution equation based on the Gegenbauer moments inversion*, *Phys. Rev.* **D60** (1999) 116005, [[hep-ph/9902318](#)].
- [535] J. Kwiecinski and L. Motyka, *Probing the QCD pomeron in doubly tagged e+ e- collisions*, *Phys. Lett.* **B462** (1999) 203–210, [[hep-ph/9905567](#)].
- [536] J. Bartels, A. D. Roeck, and H. Lotter, *The gamma* gamma* total cross section and the BFKL pomeron at e+ e- colliders*, *Phys. Lett.* **B389** (1996) 742–748, [[hep-ph/9608401](#)].
- [537] S. J. Brodsky, F. Hautmann, and D. E. Soper, *Probing the QCD pomeron in e+ e- collisions*, *Phys. Rev. Lett.* **78** (1997) 803–806, [[hep-ph/9610260](#)].
- [538] S. J. Brodsky, F. Hautmann, and D. E. Soper, *Virtual photon scattering at high energies as a probe of the short distance pomeron*, *Phys. Rev.* **D56** (1997) 6957–6979, [[hep-ph/9706427](#)].
- [539] A. Bialas, W. Czyz, and W. Florkowski, *Total gamma* gamma* cross section and the BFKL pomeron*, *Eur. Phys. J.* **C2** (1998) 683–689, [[hep-ph/9705470](#)].
- [540] J. Kwiecinski and L. Motyka, *Theoretical description of the total gamma* gamma* cross-section and its confrontation with the LEP data on doubly tagged e+ e- events*, *Eur. Phys. J.* **C18** (2000) 343–351, [[hep-ph/0010029](#)].
- [541] **DELPHI** Collaboration, J. Abdallah *et. al.*, *Study of double-tagged gamma gamma events at LEP II*, *Eur. Phys. J.* **C46** (2006) 559–568, [[hep-ex/0604039](#)].
- [542] **OPAL** Collaboration, G. Abbiendi *et. al.*, *Measurement of the hadronic cross-section for the scattering of two virtual photons at LEP*, *Eur. Phys. J.* **C24** (2002) 17–31, [[hep-ex/0110006](#)].
- [543] **L3** Collaboration, P. Achard *et. al.*, *Double tag events in two photon collisions at LEP*, *Phys. Lett.* **B531** (2002) 39–51, [[hep-ex/0111012](#)].
- [544] **ALEPH** Collaboration, A. Heister *et. al.*, *Study of hadronic final states from double tagged gamma gamma events at LEP*, [[hep-ex/0305107](#)].
- [545] J. Bartels, C. Ewerz, and R. Staritzbichler, *Effect of the charm quark mass on the BFKL gamma* gamma* total cross section at LEP*, *Phys. Lett.* **B492** (2000) 56–62, [[hep-ph/0004029](#)].
- [546] F. Caporale, D. Y. Ivanov, and A. Papa, *BFKL resummation effects in the gamma* gamma* total hadronic cross section*, *Eur. Phys. J.* **C58** (2008) 1–7, [[arXiv:0807.3231](#)].
- [547] E. Fermi, *On the Theory of the impact between atoms and electrically charged particles*, *Z. Phys.* **29** (1924) 315–327.
- [548] C. F. von Weizsacker, *Radiation emitted in collisions of very fast electrons*, *Z. Phys.* **88** (1934) 612–625.
- [549] E. J. Williams, *Nature of the high-energy particles of penetrating radiation and status of ionization and radiation formulae*, *Phys. Rev.* **45** (1934) 729–730.
- [550] G. Baur, K. Hencken, D. Trautmann, S. Sadovsky, and Y. Kharlov, *Coherent gamma gamma and gamma A interactions in very peripheral collisions at relativistic ion colliders*, *Phys. Rept.* **364** (2002) 359–450, [[hep-ph/0112211](#)].

- [551] K. Hencken *et al.*, *The Physics of Ultraperipheral Collisions at the LHC*, *Phys. Rept.* **458** (2008) 1–171, [[arXiv:0706.3356](#)].
- [552] **ALICE** Collaboration, R. Schicker, *The ALICE detector and trigger strategy for diffractive and electromagnetic processes*, *Nucl. Phys. Proc. Suppl.* **179-180** (2008) 196–201, [[arXiv:0807.1472](#)].
- [553] K. Piotrkowski, *Tagging two-photon production at the LHC*, *Phys. Rev.* **D63** (2001) 071502, [[hep-ex/0009065](#)].
- [554] V. A. Khoze, A. D. Martin, and M. G. Ryskin, *Can the Higgs be seen in rapidity gap events at the Tevatron or the LHC?*, *Eur. Phys. J.* **C14** (2000) 525–534, [[hep-ph/0002072](#)].
- [555] I. F. Ginzburg, G. L. Kotkin, V. G. Serbo, and V. I. Telnov, *Production of High-Energy Colliding gamma gamma and gamma e Beams with a High Luminosity at Vlepp Accelerators*, *JETP Lett.* **34** (1981) 491–495.
- [556] I. F. Ginzburg, G. L. Kotkin, V. G. Serbo, and V. I. Telnov, *Colliding gamma e and gamma gamma Beams Based on the Single Pass Accelerators (of Vlepp Type)*, *Nucl. Instr. Meth.* **205** (1983) 47–68.
- [557] I. F. Ginzburg, G. L. Kotkin, S. L. Panfil, V. G. Serbo, and V. I. Telnov, *Colliding gamma e and gamma gamma Beams Based on the Single Pass e+ e- Accelerators. 2. Polarization Effects. Monochromatization Improvement*, *Nucl. Instr. Meth.* **A219** (1984) 5–24.
- [558] F. R. Arutyunian and V. A. Tumanian *Phys. Lett.* **4** (1963) 176.
- [559] F. R. Arutyunian, I. I. Goldman, and V. A. Tumanian *Zh. Eksp. Teor. Fiz. (USSR)* **45** (1963) 312.
- [560] R. H. Milburn, *Electron scattering by an intense polarized photon field*, *Phys. Rev. Lett.* **10** (1963) 75–77.
- [561] V. I. Telnov, *Physics options at the ILC. GG6 summary at Snowmass2005*, *ECONF C0508141* (2005) PLEN0020, [[physics/0512048](#)].
- [562] V. I. Telnov, *Photon colliders: The first 25 years*, *Acta Phys. Polon.* **B37** (2006) 633–656, [[physics/0602172](#)].
- [563] *Basic Conceptual Design Report*, <http://www.linearcollider.org>.
- [564] *LDC outline document*, <http://www.ilcldc.org>.
- [565] J. Kwiecinski and L. Motyka, *Diffractive J/psi production in high energy gamma gamma collisions as a probe of the QCD pomeron*, *Phys. Lett.* **B438** (1998) 203–210, [[hep-ph/9806260](#)].
- [566] J. Kwiecinski, L. Motyka, and A. D. Roeck, *The QCD pomeron at TESLA: Motivation and exclusive J/psi production*, [hep-ph/0001180](#).
- [567] A. N. Vasil'ev, *The Field Theoretic Renormalization Group in Critical Behavior theory and Stochastic Dynamics*. CRC Press, 2004.
- [568] D. J. Broadhurst, *Summation of an infinite series of ladder diagrams*, *Phys. Lett.* **B307** (1993) 132–139.
- [569] L. Lewin, *Polylogarithms and Associated Functions*. North-Holland, New York, 1981.
- [570] S. Wallon, *Hill and Abel relations for Li_2 extended to the whole complex plane*, unpublished.
- [571] S. Bethke, *Determination of the QCD coupling α_s* , *J. Phys.* **G26** (2000) R27, [[hep-ex/0004021](#)].
- [572] M. Davier, M. E. Peskin, and A. Snyder, *Two-photon exchange model for production of neutral meson pairs in e+ e- annihilation*, [hep-ph/0606155](#).
- [573] G. T. Bodwin, E. Braaten, J. Lee, and C. Yu, *Exclusive two-vector-meson production from e+ e- annihilation*, *Phys. Rev.* **D74** (2006) 074014, [[hep-ph/0608200](#)].
- [574] B. Clerbaux and M. V. Polyakov, *Partonic structure of pi and rho mesons from data on hard exclusive production of two pions off nucleon*, *Nucl. Phys.* **A679** (2000) 185–195, [[hep-ph/0001332](#)].
- [575] D. Y. Ivanov, L. Szymanowski, and G. Krasnikov, *Vector meson electroproduction at next-to-leading order*, *JETP Lett.* **80** (2004) 226–230, [[hep-ph/0407207](#)].
- [576] H. G. Dosch, C. Ewerz, and V. Schatz, *The odderon in high energy elastic p p scattering*, *Eur. Phys. J.* **C24**

- (2002) 561–571, [[hep-ph/0201294](#)].
- [577] A. Breakstone *et. al.*, *A measurement of anti-p p and p p elastic scattering in the dip region at $s^{**}(1/2) = 53\text{-gev}$* , *Phys. Rev. Lett.* **54** (1985) 2180.
- [578] **H1** Collaboration, J. Olsson, *Search for odderon induced contributions to exclusive meson photoproduction at HERA*, [hep-ex/0112012](#).
- [579] S. Braunewell and C. Ewerz, *The perturbative odderon in quasidiffractive photon photon scattering*, *Phys. Rev.* **D70** (2004) 014021, [[hep-ph/0403197](#)].
- [580] A. Bzdak, L. Motyka, L. Szymanowski, and J. R. Cudell, *Exclusive J/ψ and v hadroproduction and the QCD odderon*, *Phys. Rev.* **D75** (2007) 094023, [[hep-ph/0702134](#)].
- [581] S. J. Brodsky, J. Rathsman, and C. Merino, *Odderon-pomeron interference*, *Phys. Lett.* **B461** (1999) 114–122, [[hep-ph/9904280](#)].
- [582] I. F. Ginzburg, I. P. Ivanov, and N. N. Nikolaev, *Possible odderon discovery via observation of charge asymmetry in the diffractive $\pi^+\pi^-$ production at HERA*, *Eur. Phys. J. direct* **C5** (2003) 02, [[hep-ph/0207345](#)].
- [583] I. F. Ginzburg, I. P. Ivanov, and N. N. Nikolaev, *Possibility of the odderon discovery via observation of charge asymmetry in the diffractive $\pi^+\pi^-$ production at herA*, *Eur. Phys. J.* **C32S1** (2003) 23–40.
- [584] P. Hagler, B. Pire, L. Szymanowski, and O. V. Teryaev, *Hunting the QCD-odderon in hard diffractive electroproduction of two pions*, *Phys. Lett.* **B535** (2002) 117–126, [[hep-ph/0202231](#)].
- [585] P. Hagler, B. Pire, L. Szymanowski, and O. V. Teryaev, *Pomeron odderon interference effects in electroproduction of two pions*, *Eur. Phys. J.* **C26** (2002) 261–270, [[hep-ph/0207224](#)].
- [586] I. F. Ginzburg and D. Y. Ivanov, *Semihard production of neutral pseudoscalar and tensor mesons in photon-photon collisions*, *Nucl. Phys.* **B388** (1992) 376–390.
- [587] D. Y. Ivanov, M. Diehl, A. Schaefer, and N. Warkentin, *Electroproduction of pion pairs*, *PoS DIFF2006* (2006) 032, [[hep-ph/0611138](#)].
- [588] N. Warkentin, M. Diehl, D. Y. Ivanov, and A. Schafer, *Exclusive electroproduction of pion pairs*, *Eur. Phys. J.* **A32** (2007) 273–291, [[hep-ph/0703148](#)].
- [589] J. H. Kuhn and A. Santamaria, *Tau decays to pions*, *Z. Phys.* **C48** (1990) 445–452.
- [590] **Particle Data Group** Collaboration, C. Amsler *et. al.*, *Review of particle physics*, *Phys. Lett.* **B667** (2008) 1.
- [591] L. M. Barkov *et. al.*, *Electromagnetic Pion Form-Factor in the Timelike Region*, *Nucl. Phys.* **B256** (1985) 365–384.
- [592] J. R. Pelaez and F. J. Yndurain, *The pion pion scattering amplitude*, *Phys. Rev.* **D71** (2005) 074016, [[hep-ph/0411334](#)].
- [593] R. Kaminski, J. R. Pelaez, and F. J. Yndurain, *The pion pion scattering amplitude. II: Improved analysis above anti-K K threshold*, *Phys. Rev.* **D74** (2006) 014001, [[hep-ph/0603170](#)].
- [594] B. Ananthanarayan, I. Caprini, G. Colangelo, J. Gasser, and H. Leutwyler, *Scalar form factors of light mesons*, *Phys. Lett.* **B602** (2004) 218–225, [[hep-ph/0409222](#)].
- [595] K. Hencken, Y. V. Kharlov, G. V. Khaustov, S. A. Sadovsky, and V. D. Samoylenko, *TPHIC, event generator of two photon interactions in heavy ion collisions*, . IFVE-96-38.
- [596] G. Baur and L. G. F. Filho, *Coherent particle production at relativistic heavy ion colliders including strong absorption effects*, *Nucl. Phys.* **A518** (1990) 786–800.
- [597] R. N. Cahn and J. D. Jackson, *Realistic equivalent photon yields in heavy ion collisions*, *Phys. Rev.* **D42** (1990) 3690–3695.
- [598] J. Bossler *et. al.*, *LHC beam instrumentation: Conceptual design report*, . CERN-LHC-PROJECT-REPORT-370.

- [599] O. S. Bruning *et al.*, *LHC design report. Vol. I: The LHC main ring*, . CERN-2004-003-V-1.
- [600] D. Brandt, *Review of the LHC ion programme*, . CERN-LHC-PROJECT-REPORT-450.
- [601] M. Drees and D. Zeppenfeld, *Production of supersymmetric particles in elastic $e p$ collisions*, *Phys. Rev.* **D39** (1989) 2536.
- [602] J. Nystrand, *Electromagnetic interactions in nucleus nucleus and proton proton collisions*, *Nucl. Phys.* **A752** (2005) 470–479, [[hep-ph/0412096](#)].
- [603] B. A. Kniehl, *Elastic $e p$ scattering and the Weizsacker-Williams approximation*, *Phys. Lett.* **B254** (1991) 267–273.
- [604] e. . James Brau *et al.*, *International Linear Collider reference design report. 1: Executive summary. 2: Physics at the ILC. 3: Accelerator. 4: Detectors*, . ILC-REPORT-2007-001.
- [605] V. I. Telnov, *The photon collider at ILC: Status, parameters and technical problems*, *Acta Phys. Polon.* **B37** (2006) 1049–1072, [[physics/0604108](#)].
- [606] **The BABAR** Collaboration, B. Aubert *et al.*, *Measurement of the $\gamma \gamma^* \rightarrow \pi^0$ transition form factor*, *Phys. Rev.* **D80** (2009) 052002, [[arXiv:0905.4778](#)].
- [607] **CLAS** Collaboration, M. Battaglieri *et al.*, *Photoproduction of $\pi^+\pi^-$ meson pairs on the proton*, *Phys. Rev.* **D80** (2009) 072005, [[arXiv:0907.1021](#)].
- [608] J. C. Collins, *Fragmentation of transversely polarized quarks probed in transverse momentum distributions*, *Nucl. Phys.* **B396** (1993) 161–182, [[hep-ph/9208213](#)].
- [609] D. W. Sivers, *Single Spin Production Asymmetries from the Hard Scattering of Point-Like Constituents*, *Phys. Rev.* **D41** (1990) 83.
- [610] D. W. Sivers, *Hard scattering scaling laws for single spin production asymmetries*, *Phys. Rev.* **D43** (1991) 261–263.
- [611] J. C. Collins, *What exactly is a parton density?*, *Acta Phys. Polon.* **B34** (2003) 3103, [[hep-ph/0304122](#)].
- [612] X.-D. Ji, J.-P. Ma, and F. Yuan, *QCD factorization for semi-inclusive deep-inelastic scattering at low transverse momentum*, *Phys. Rev.* **D71** (2005) 034005, [[hep-ph/0404183](#)].
- [613] F. Hautmann, *Multi-particle production and TMD distributions*, . In *Hamburg 2008, Multiparticle dynamics (ISMD08)* 284-290.
- [614] F. Hautmann, *Unintegrated parton distributions and applications to jet physics*, *Acta Phys. Polon.* **B40** (2009) 2139–2163.